Universities of Glasgow and Strathclyde

Department of Naval Architecture and Marine Engineering

TIME DOMAIN MATHEMATICAL MODEL FOR SIX-DEGREE-OF-FREEDOM MOTION IN A WAVE

by

Joonyun Kang

A thesis submitted in fulfilment of the requirements

for the degree of Doctor of Philosophy

August 2009

This thesis is the result of the author's original research. It has been composed by the author and has not been previously submitted for examination which has lead to the award of a degree.

Abstract

To assess the behaviour of a ship in a seaway, this thesis presents the development of an integrated mathematical model describing a six-degree-of-freedom motion of a ship in a wave. This integrated mathematical model is developed with its fundamental base on both traditional seakeeping and manoeuvring theories and thus obtaining of hydrodynamic data sets as well as formulation of force component are needed in a theoretical manner.

To obtain the hydrodynamic data sets, theoretical formulations and numerical implementations are carried out for a ship travelling in a wave. The theoretical formulation of three-dimensional potential flow leads boundary integral equations over mean wetted body surface with three-dimensional translating pulsating Green function. For numerical implementation Constant Panel Method and Higher-Order Panel Method are introduced as distribution technique of source singularities over the idealised body surface and compared for the estimation of hydrodynamic data set of Wigley and Todd Series 60. Mean second-order wave forces are formulated based on the solution of first-order problem and obtained by direct pressure integration over mean wetted body surface. The effects of forward speed and wave heading on the drift force and added resistance are investigated and compare with experimental data.

An integrated mathematical model for manoeuvring motion is further developed with functional form of memory effect represented by convolution integrals of impulse response function to describe arbitrary ship motion in a seaway. For validation of developed numerical tool, benchmark tests have been performed for the prediction of large amplitude ship motion in following seas. Standard manoeuvring tests, turning circle and zig-zag manoeuvres, are presented to demonstrate the wave effects on the manoeuvring performance. The capability of numerical tool has been extended to the prediction of highly non-linear behaviours of parametric rolling phenomenon in longitudinal wave with reasonable accuracy.

Acknowledgements

I would like to express my sincere gratitude to Professor Dracos Vassalos, Director of Ship Stability Research Centre, for his supervision to make this research possible and for his kind help with regard to obtaining financial support through the Scholarship of Strathclyde University and the Overseas Research Student award.

I would like to appreciate support and advice from Dr. B.S. Lee and Professor K.P. Rhee during the long course of study.

I wish to express my sincere thanks to the colleagues of the Ship Stability Research Centre and the staffs of Department and for their assistances and friendship.

I am deeply indebted to my parents for their continuous encouragement and support throughout my entire life. I would like to appreciate my wife Hwa Young for love, and my daughter Seungwon for making this work sweet by just being part of my life.

Table of Contents

List of Figures

List of Tables

Nomenclature

B	Characteristic breadth of a body
C_B	Block coefficient of the body
C_w	Coefficient of waterplane area
F_N	Froude number
g	Acceleration of gravity
$\overline{GM}_L$	Metacentric height in longitudinal direction
$\overline{GM}_T$	Metacentric height in transverse direction
i, j, k	Unit vector in x, y, z directions respectively
I_{xx}, I_{yy}, I_{zz}	Mass moment of inertia
$I_{xy}, I_{yx}, \ldots, I_{zx}$	Product of mass moment of inertia
$\overline{KG}$	Vertical position of centre of gravity form keel line
k_0	Wave number ($=2\pi/\lambda$)
k_{xx}, k_{yy}, k_{zz}	Radius of gyration
L	Characteristic length of a body
LCB	Longitudinal distance of the centre of buoyancy from midship
m	Mass of a body
n	Unit normal vector
r	Position vector of a body surface
T	Characteristic draught of a body
U, U_0	Mean forward speed of a body
(x_G, y_G, z_G)	Centre of gravity
(x_B, y_B, z_B)	Centre of buoyancy
$(x_F, y_F, 0)$	Centre of floatation
β	Angle between incident wave and ship's heading ($\beta = 180°$ for head sea and $\beta = 0°$ for following sea)

λ	Wavelength of incident wave
ρ	Density of the fluid
ω_0	Frequency of incident wave
ω , ω_e	Encounter frequency
ζ_0	Amplitude of incident wave
∇	Differential operator or displacement of a body
∇^2	Laplace' operator

[Seakeeping]

A_{jk}	Added mass in j-th direction due to k-th mode of motion
B_{jk}	Damping coefficient in j-th direction due to k-th mode of motion
C_{jk}	Hydrostatic restoring coefficient in j-th direction due to k-th mode of motion
$E_1(\cdot)$	Exponential integral
$F_j^{(1)}, F_j^{(2)}$	First- and second-order hydrodynamic force in j-th direction
F_j^{EX}	Wave exciting force in j-th direction
F_j^{FK}, F_j^{D}	Froude-Krylov and diffraction force in j-th direction
F_j^{HS}	Hydrostatic restoring force in j-th direction
F_j^{R}	Radiation force in j-th direction
$\mathbf{F}^{(1)}, \mathbf{M}^{(1)}$	First-order external force and moment vector
$\mathbf{F}^{(2)}, \mathbf{M}^{(2)}$	Second-order external force and moment vector
$G(p,q)$	Green function
$H(p,q)$	Wave function in Green function
H_{ij}	Influence coefficient matrix
L_F	Intersection line between the body surface and the free surface
m_j	Component of m-terms in the j-th mode
M_i	Weight function of a higher-order panel

M_{ij}	Inertia coefficient of a body
$M_j^{(2)}$	First-order hydrodynamic moment in j-th direction
n_j	Component of normal vector in the j-th mode
N_i	Shape function of a higher-order panel
$\overline{S}_B, S_B$	Mean and exact wetted body surface
S_{ij}	Waterplane integral
S_∞	Control boundary surface at far-field
$\mathbf{W}$	Velocity field of steady flow
$\mathbf{x}_0$	Position vector defined in $O-X_0Y_0Z_0$
$\mathbf{x}$	Position vector defined in $o-xyz$
$\mathbf{x}'$	Position vector defined in $A-x'y'z'$
$\boldsymbol{\alpha}$	Local oscillatory vector
$\boldsymbol{\delta}=(\xi_1,\xi_2,\xi_3)$	Unsteady translational displacement vector
ε	Perturbation parameter
Φ	Velocity potential of the fluid domain
$\bar{\Phi}, \tilde{\Phi}$	Velocity potential of steady and unsteady flow
$\bar{\phi}$	Steady perturbation potential
ϕ_0, ϕ_7	Incident wave and diffraction potential
ϕ_j	Radiation potential in j-th mode of motion
τ	Non-dimensional frequency
σ	Source strength
$\boldsymbol{\Omega}=(\xi_4,\xi_5,\xi_6)$	Unsteady rotational displacement vector
ξ_j	Motion response in j-th mode
$\bar{\xi}_j$	Complex amplitude of motion in j-th mode
$\zeta, \bar{\zeta}$	Free surface elevation due to unsteady and steady flow
$\zeta_r^{(1)}$	First-order relative wave elevation

[Manoeuvring]

$A(\infty)$	Infinity value of added mass
$B(\infty)$	Infinity value of damping coefficient
F_W	Wave force
F_{HS} , F_{FK}	Hydrostatic and Froude-Krylov force
F_{Diff} , F_{Add}	Diffraction force and added resistance
F_H , F_M	Hull force due to memory effect and manoeuvring force
F_P , F_R	Propeller and rudder force
$h(\tau)$	Impulse response function
$\mathbf{I}_A$	Moment of inertia matrix
K , M , N	External moment in roll, pitch and yaw respectively
N_v , $N_{v\|v\|}$, N_r , $N_{r\|r\|}$,...	Manoeuvring derivatives in yaw
u , v , w	Velocity in surge, sway and heave respectively
$\dot{u}$, $\dot{v}$, $\dot{w}$	Acceleration in surge, sway and heave respectively
p , q , r	Angular velocity in roll, pitch and yaw respectively
$\dot{p}$, $\dot{q}$, $\dot{r}$	Angular acceleration in roll, pitch and yaw respectively
$\mathbf{T}_1$, $\mathbf{T}_2$	Transformation matrix
$\mathbf{v}$	Translation velocity
X , Y , Z	External force in surge, sway and heave respectively
y_v , y_p , y_r	Impulse response function in sway
Y_v , $Y_{v\|v\|}$, Y_r , $Y_{r\|r\|}$,...	Manoeuvring derivative in sway
$Y_{\dot{v}}(\omega)$,..., $Y_r(\omega)$	Frequency dependent hull force derivative in sway
δ	Rudder angle
$\boldsymbol{\omega}$, $\dot{\boldsymbol{\omega}}$	Angular velocity and acceleration vector

Chapter 1. Introduction

1.1 Preamble

Any ship is built with specific purpose of carrying men and/or cargo and mission to accomplish upon the sea environments and consequently it should possess some basic characteristics for successful operations. It should be able to advance with sufficient speed, be strong enough to withstand the rigours of heavy weather and wave impact, and manoeuvre at open sea as well as restricted waters. Many of these features can be understood in the basis of ship dynamics, on which the main interests lie in the behaviour of a floating ship in the sea.

Although it is possible to produce a floating ship only with a basic knowledge of hydrostatics in calm water, ships rarely sail in such a favourable environment. There exist waves, which are the main source of ship motion in a seaway and affect the performance of a ship considerably. Furthermore the motion of a ship in a seaway, whether caused by waves or by its own manoeuvres, can affect its stability and more generally its safety. Since the beginning of shipbuilding history, different types of ships have faced dangerous situations in the rough weather of seas, often resulted in tragic consequences; therefore, the success of ship design depends ultimately on its performance in a seaway. Unfortunately, however, the prediction of ship behaviour in an actual seaway is such a complex problem that the naval architects are usually forced to select the ship particulars and hull form on the basis of calm water performance without much consideration of the sea and weather conditions prevailing over the route on which the ship is to operate.

In order to understand general behaviour of floating structures, diverse fields of technology is required with knowledge not only of fluid mechanics but also of solid

mechanics, control theory, as well as statistics. Here our attention shall be solely devoted to the hydrodynamic aspect, emphasizing those unique to this field as opposed to the other engineering disciplines where fluid mechanics is applicable. For the research of ship behaviour in a seaway, there are still various kinds of applications of hydrodynamics to naval architecture, which involve many separate or common topics and range over a broad level of sophistication.

For example, propellers, rudders, anti-rolling fins, yacht keels, and sails can be treated and understood together since they are fundamentally related to hydrofoils or lifting surfaces. Similarly, the motions of unsteady ship, buoy, or platform in waves and the manoeuvring of ship or submarine in non-straight paths can be analysed, to some extent, from the same basic equations of motion. In fact, however, separation and lifting effects of fluid generally play very important role in the manoeuvring problem, while the ship motions due to waves are not significantly affected by viscosity or vorticity. The degree of sophistication varies from empirical design to theoretical research. Faced with the choice between empirical design information and theoretical approach, compromise might be required to provide the necessary background for an intelligent evaluation and application of a given problem.

As a one possible approach, theoretical investigation of the problem to determine the motions of a ship consists of describing the simple expressions of external disturbances in the seaway and determining the ship motions for such environments. The benefits offered by theoretical studies are as follow:

- General information regarding the relevant characteristics of the ship behaviour in a seaway.
- A prediction of the motion in any presumed seaway.
- An insight into the acceptable values of motions, accelerations, and so on.
- Assessment of the average performance quality.
- Basic ideas regarding stabilisation to reduce motion and actuation to control it.
- Guidelines for model tests and full-scale trials.

In the theoretical approach the motion of the fluid around the ship is generally defined at each point in time and space by a kinematic description of the velocity vector of the fluid particles. This unknown velocity is related to the forces acting on the body by means of Newton's equations, which yields a system of ordinary differential equations. The resultant system of governing equations is the Navier-Stokes equations, supplemented by the continuity equation expressing conservation of fluid mass. In principle, one can solve these equations, subject to boundary conditions on the boundary surfaces of the fluid. If this procedure could actually be carried out, it would be possible to calculate desired answers for arbitrary values of the Reynolds number and Froude number. In practice, however, it has not been possible to solve the Navier-Stokes equations exactly, except for a few cases involving very simple geometries that at first glance have no relation to the shape of marine vehicle.

1.2 Seakeeping

In recent years, greater attention has been paid to the seakeeping performance of a ship due to a number of factors: increasing interest on the high-speed passenger vessels, demand for passenger comfort on board, greater pressure from regulatory organisations and the broader public for safer vessels, great advancement in computer capacity, and developments in prediction and analysis technology. The birth of modern seakeeping analysis was in the mid-20th century as demonstrated by the landmark researches of Ursell (1949). Combined with the availability of high performance computer in the late 20th century, refinements of analysis methods and mathematical techniques have been continued and made routine seakeeping analysis possible in the early design stage.

Seakeeping analysis has taken a very poor second place in preliminary hydrodynamic design for the majority of merchant vessels since it is much more difficult problem compared with that of calm water resistance when higher accuracy is required. This might be particularly true if the seakeeping performance is addressed relatively late in the design spiral by means of expensive model tests. Furthermore, seakeeping characteristics of a vessel depends on so many interrelating factors that it is virtually impossible to predict the change of performance, which is caused by the variations of design factors, without detailed analysis. This is because the evaluation depends not only on the design factors but also on the wave conditions and the criteria against which the vessel is being assessed. Thanks to, however, the great improvement of analysis tools, which are ideal for preliminary design, a large number of design candidates may be easily and quickly examined and compared.

Ships sailing in a sea experience a variety of forces, which result in structural loading and motion responses, due to the various weather and wave environments. In order for ships to be designed to fulfil their designated function such as transportation of passenger and cargoes safely and economically in the ocean, it is of great importance to evaluate their performance at the early stage of design. The relative importance on

the various aspects of ship performance in a seaway varies from design to design, depending on the required operation. The following general issues should be investigated to evaluate seakeeping performance in a seaway when designing seaworthy ships:

- Speed loss and reduction in a seaway: 'involuntary' speed loss due to added resistance in waves and 'voluntary' speed reduction to avoid excessive motions, loads, etc.
- Structural design of the ship with respect to wave loads in seaways.
- Motion response: excessive motions are undesirable since they may impair stability and cause discomfort to the crew and passenger, and damage to the cargo.
- Safety and stability, e.g. capsizing, large roll motions and accelerations, slamming, wave impact on superstructures or deck cargo.
- Shipping and spraying of green water, causing equipment breakdown and degradation of liability.
- Operational limits due to external disturbances, e.g. severe weather condition

Most issues involved with seakeeping performance can be further specified in terms of motion responses in a seaway since ship motions influence unfavourably the seaworthiness of a vessel. Excessive ship motion may occasionally lead to the following consequences:

- Decreasing the forward speed of the vessel resulting from the increase in the resistance of the water.
- Flooding of the deck, due to burying the sides or ends of the vessel under the surface of a wave
- Capsizing of the ship as a result of excessive inclination in rolling
- Damage to the hull or to individual structures on the vessel resulting from the additional forces associated with the motions
- Disturbing the operation of the ship and shifting of poorly secured or non-cohesive cargo as a result of the inclination of the vessel.

- Seasickness, i.e. motion sickness resulting from the pitching and rolling of a ship in a seaway
- Other extreme motions e.g. parametric rolling and motions due to high speed

These various problems encountered with respect to ship motion in a seaway might be investigated in four different ways:

- Directly, as with full-scale trials after launch.
- Experimentally, by means of model tests in controlled environments.
- Analytically, i.e. on a theoretical basis.
- Empirically, through statistical observations.

Many naval architects working in assessment of seakeeping quality have developed methods to predict the behaviour of ship to varying degrees of success over the past century by theoretical and experimental means. For the purpose of predicting the seakeeping quality of a ship, the first idealisation should be done by representation of the natural seaway as superposition of many regular harmonic waves. Physical modelling of a given problem is then followed by establishment of mathematical model so that accessible solution can be acquired. The motion of a vessel in ship hydrodynamics can be expressed by means of equations of motion based on the law of conservation of linear and angular momentum. Numerical computation or experimental measurement, where the ship reactions and external forces are obtained, is carried out in these harmonic waves. This procedure assumes that the reaction of one wave on the ship is not changed by the simultaneous occurrence of another wave. One consequence of the assumed independence of the individual wave reactions is that all reactions of the ship are proportional to wave height. This is called linearisation with respect to wave height and is valid for small wave heights for almost all ship reactions. This procedure is often applied also for seaways with large waves. However, in these cases it can only give rough estimates requiring proper corrections.

One of the major difficulties in the theoretical approach is the non-linearities. There are non-linearities associated with the fluid in the form of viscosity and the velocity squared terms in the pressure equations. The free surface causes non-linear behaviour due to the nature of the free surface boundary conditions and the non-linear behaviour of incident waves. Finally the body geometry causes often causes non-linear hydrostatic restoring forces and non-linear behaviour at the intersection lines between body and free surface. The computations become considerably more expensive if this simplification is not made. Non-linear computations are usually necessary for the treatment of extreme motions e.g. capsizing and broaching phenomenon in the following seas. The only good news is that because of forward speed ships tend to be long and slender with smooth variations along their length. This geometric feature of typical ships is the basis of many approximations that have allowed a significant amount progress until a recent date.

1.3 Manoeuvring

Regarding the progression history of ship hydrodynamics, high performances of resistance and propulsion system are mainly interested in the early days, whilst little attention had been paid to assessment of the manoeuvring performance. After the Oil Shock in the 1970's ship-owners started to build ULCC (Ultra Large Crude Oil Carrier) and extreme situations due to unexpected poor manoeuvrability have often happened. A primary reason has been the lack of manoeuvring performance standards for the ship designer to design to, and/or regulatory authorities to enforce. Consequently some types of ships have been built with very poor manoeuvring qualities that have resulted in marine casualties and pollution. Designers have relied on the ship handling abilities of human operators to compensate for any deficiencies in inherent manoeuvring qualities of the hull. After the oil spill accident of Exxon Valdez in 1990, regulating of ship manoeuvrability has been enforced in order to avoid marine casualties by a ship with poor manoeuvring qualities and protect the sea from pollution and the manoeuvring requirement has become a standard part of the contract between yard and ship-owner.

As a movement to secure and enforce minimum requirements of manoeuvring qualities, the resolution A.751(18), Interim Standards for Ship Manoeuvrability, was first adapted in the Assembly of International Maritime Organization (IMO) in 1993 (IMO Interim Standards). Subsequent discussions on the amendment of the Interim Standards have finally led to the adoption of resolution MSC.137(76), Standards for Ship Manoeuvrability, in the Maritime Safety Committee in 2002 (IMO Standards). Governments are invited to encourage those responsible for the design, construction, repair and operation of ships to apply the IMO Standards to ships constructed on or after 1st January 2004.

The implementation of manoeuvring standards will ensure that ships are designed to a uniform standard, so that an undue burden is not imposed on ship handlers in trying to compensate for deficiencies in inherent ship manoeuvrability. IMO regulations

specify minimum requirements for all ships, but ship-owners may introduce additional or more severe requirements for certain types of ships, e.g. tugs, ferries, exploration ships. Selected quality measures of ship manoeuvrability, which are addressed by the IMO Standards, can be described by the following main characteristics:

- *Inherent dynamic stability*: A ship is dynamically stable on a straight course if it, after a small disturbance, soon will settle on a new straight course without any corrective rudder. The resultant deviation from the original heading will depend on the degree of inherent stability and on the magnitude and duration of the disturbance.

- *Course-keeping ability*: The course-keeping quality is a measure of the ability of the steered ship to maintain a straight path in a predetermined course direction without excessive oscillations of rudder or heading. In most cases, reasonable course control is still possible where there exists an inherent dynamic instability of limited magnitude.

- *Initial turning/course-changing ability*: The initial turning ability is defined by the change-of-heading response to a moderate helm, in terms of heading deviation per unit distance sailed (the P number) or in terms of the distance covered before realizing a certain heading deviation (such as the "time to second execute" demonstrated when entering the zig-zag manoeuvre).

- *Yaw checking ability*: The yaw checking ability of the ship is a measure of the response to counter-rudder applied in a certain state of turning, such as the heading overshoot reached before the yawing tendency has been cancelled by the counter-rudder in a standard zig-zag manoeuvre.

- *Turning ability*: Turning ability is the measure of the ability to turn the ship using hard-over rudder. The result being a minimum "advance at 90° change of

heading" and "tactical diameter" defined by the "transfer at 180° change of heading". Analysis of the final turning diameter is of additional interest.

- *Stopping ability*: Stopping ability is measured by the "track reach" and "time to dead in water" realized in a stop engine-full astern manoeuvre performed after a steady approach at full test speed. Lateral deviations are also of interest, but they are very sensitive to initial conditions and wind disturbances.

Deriving from this background, a great deal of research studies have been carried out to evaluate the manoeuvring performance of a ship by means of theoretical or experimental methods. This conventional manoeuvring theory, however, often presumes calm water environments due to the complex influence of ocean waves on the manoeuvring performance. With the increased number of high speed marine vehicles recently, the effect of ocean wave on the behaviour of a ship has become more important. Furthermore the operations of ships in close proximity to one another and in restricted waters could be good examples where the influence of wave is put forward.

To investigate how the behaviour of the ship is influenced by the existence of ocean wave, a new mathematical model describing the manoeuvring motion of ocean-going ship needs to be developed. This manoeuvring mathematical model should be capable of describing general six-degree-of-freedom motion in a seaway as well as conventional motions of manoeuvring and seakeeping in specific situations. Therefore new mathematical model needs to incorporate with the elements of traditional seakeeping and manoeuvring, in which integration of conventional methods is required to implement standard manoeuvring tests in a wave. Because both manoeuvring and seakeeping theories concern time-dependent ship motions, the main difficulty in both fields is to determine the fluid forces on the hull due to the ship motion. Although they have many other similarities between each other, they also possess many differences, which must be considered in the formulation of integrated model, as follow:

- Contrary to seakeeping, manoeuvring is often investigated in restricted water, e.g. shallow and usually calm channels.
- Linear relations between velocities and forces are reasonably accepted for many applications in seakeeping; most recent manoeuvring models have non-linear formulation.
- Seakeeping is mostly investigated in the frequency domain and partly in the time domain; manoeuvring calculations usually performed in the time domain simulations.
- For coordinate system, in seakeeping equations of motion are written in an inertial coordinate system; in manoeuvring simulations a body-fixed coordinate system is used.
- For fluids forces, viscosity is usually assumed to be of minor importance in seakeeping computations; the free surface is often neglected in manoeuvring simulations. Ideally, both free surface and viscous effects should be considered for both seakeeping and manoeuvring.

Since the motion of a ship in a seaway is arbitrary, the formulation of the fluid actions exerted on the ship is very complicated by the so-called memory effect of the fluid motion and therefore representation of fluid force using convolution terms is essential. Employment of the frequency dependent hydrodynamic coefficients also allows the combination between seakeeping and manoeuvring motions on the basis of comparison between two theories.

Because the main intention of the present study is to develop a six-degree-of-freedom mathematical model with frequency dependent coefficients, incorporating memory effects in waves, so the major emphases are lied on the formulation and validation of a mathematical model which would allow a meaningful integration of conventional manoeuvring and seakeeping theories in the prediction of extreme ship motions.

1.4 Structure of the Thesis

This thesis is structured in eleven chapters. A brief outline of the contents of each chapter is given as follow:

- Chapter 1, *Introduction*, provides the background to the research described in this thesis.

- Chapter 2, *Aims of the Thesis*, states the overall aim and specific objectives that constitute the focus of the research presented in this thesis.

- Chapter 3, *Critical Review*, presents the previous researches in understanding the behaviour of a ship in waves and relevant theoretical and experimental studies carried out. It paves the way for introducing the key elements of approach adopted in Chapter 4.

- Chapter 4, *Approach Adopted*, outlines the elements of approach adopted as fundamental idea that details the development of following chapters.

- Chapter 5, *Formulation of Three-Dimensional Potential Flow*, describes the theoretical formulation of three-dimensional potential flow, which forms the basis of the Boundary Value Problem and leads to the simplified radiation and diffraction problems using linearisation of boundary conditions.

- Chapter 6, *Numerical Implementation of Green Function Method*, details the methodology to get the solution of discretised integral equations over mean wetted body surface using different source distribution techniques.

- Chapter 7, *Hydrodynamic Forces and Ship Motions*, demonstrates the applicability of the developed methods focusing on the hydrodynamic coefficients, wave forces and motion responses.

- Chapter 8, *A Manoeuvring Mathematical Model in Waves*, describes the development of integrated mathematical model for general manoeuvring simulation of a vessel in waves and demonstrates the effects of waves on the manoeuvring motion in a seaway.

- Chapter 9, *Benchmark Study on Parametric Rolling,* presents extensive range of investigation of parametric roll phenomenon and comparison with experiment data to show the capability of numerical model for high amplitude roll motion.

- Chapter 10, *Discussion*, contains an account of the contribution of the thesis to the research field, critically discusses the outcome of the study in terms of the objectives stated in Chapter 2, draws the difficulties encountered during the research and, based upon the discussion, provides recommendations for future research.

- Chapter 11, *Conclusions*, summarises the main conclusions of the research presented in the thesis.

The details about the numerical models and techniques are given in Appendices along with the references used in the literature review and other chapters. The logical sequence and interrelations among the chapters of the thesis are illustrated in Figure 1.1.

The research to be presented in the thesis is founded on the hypothesis that the inherent problem of wave load exerted on a ship in a seaway makes it difficult to assess the ship motion performance using the individual method initially originated from traditional seakeeping and manoeuvring theories. In this respect, this thesis develops a mathematical model and simulation tool that analyse and predict the ship motion performance considering the wave effects. Its applicability is demonstrated by performing a number of case studies, in which various wave conditions are specified.

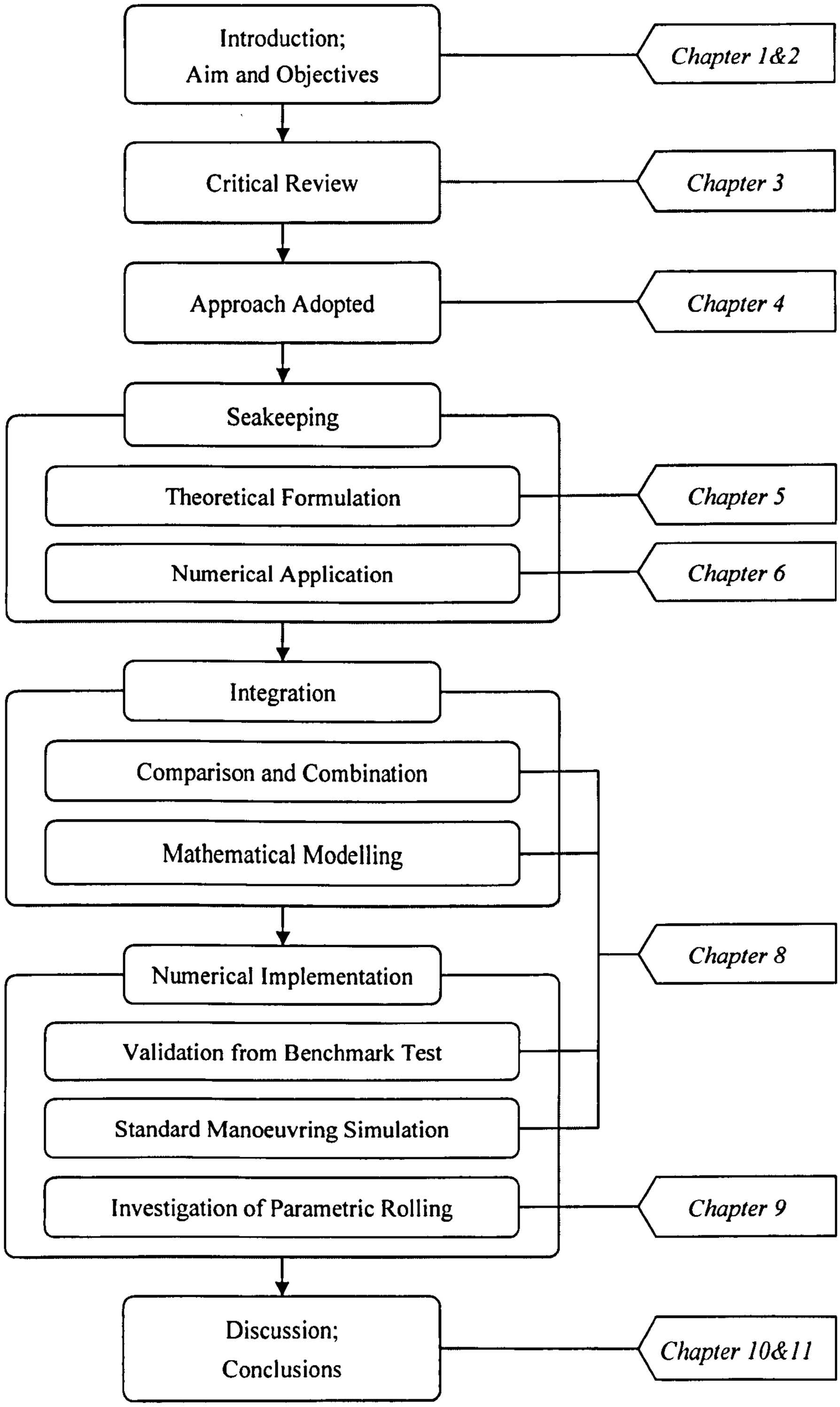

Figure 1.1 Structure of the thesis

1.5 Concluding Remarks

In this introductory chapter the considerations that led to the undertaking of this research have been put forward. The main problem identified, which will be examined in detail in the following chapters, is the lack of technology developed to deal with the problem of a ship manoeuvring motion solely in a wave. In this respect, this thesis will focus on aspects relevant to development of mathematical model and numerical tool for the six-degree-of-freedom motion simulation of a vessel in a seaway.

Chapter 2. Aims of the Thesis

The main aim of this thesis is to develop an integrated six-degree-of-freedom mathematical model for the manoeuvring motion of a ship in a seaway. In the first place it is to develop and validate numerical tools to calculate hydrodynamic coefficients and forces based on recent seakeeping theory. Next is to formulate the equations of motion to describe ship behaviour using hydrodynamic coefficients calculated in the seakeeping theory. The specific objectives can be outlined as follows:

- To carry out critical reviews of theoretical researches on the seakeeping and manoeuvring performance assessment.
- To develop and validate numerical tools, which can calculate hydrodynamic coefficients and wave forces with three-dimensional Green function approach in frequency domain.
- To expand wave forces up to second-order in order to investigate drift effects.

- To formulate a fully six-degree-of-freedom mathematical model describing general ship behaviour in random seaway.
- To take into account the memory effects of fluid force exerted on the hull surface.
- To validate the integrated model by comparison with manoeuvring model experiment in various wave conditions
- To investigate the effects of wave on standard manoeuvring tests.
- To demonstrate the capability of integrated mathematical model for highly non-linear motion like parametric rolling.

Chapter 3. Critical Review

3.1 Preamble

The main objective of this chapter is to review the theoretical and experimental researches on the seakeeping and manoeuvring performance of a ship in a wave and efforts to develop numerical tools to provide the basis for the simulation of manoeuvring motion in a seaway.

The beginning of Chapter 3 attempts critical reviews on the existing theoretical methods to predict the behaviour of ship in a seaway. The in-depth consideration of each method regarding general seakeeping problem concludes with the identification of their capabilities and appropriateness of the approach adopted. Relevant numerical techniques and methods will be critically reviewed regarding specific research issues in the following sections.

Then some important issues to develop the mathematical formulation of manoeuvring motion in a wave will be addressed and reviewed in the following section. The empirical methods employed in the conventional manoeuvring theory as well as relatively recent theoretical method to consider the wave effects on ship motions will be discussed.

3.2 Seakeeping Theory

For many years great attention has been paid to the seakeeping characteristics of a vessel due to a number of factors: fast development of high-speed passenger vessels, increasing demand for passenger comfort, great pressure from regulatory bodies and the broader public request for safety measures, deployment of highly sophisticated systems on smaller naval vessels, staggering advancement in desktop computer capacity, and development in prediction and analysis tools. Because of the presence of the inherent hydrodynamic and geometrical non-linearities of a ship as well as complicated sea environments, the demands for more sophisticated technologies in the seakeeping analysis, have never stopped in both industry and research fields. In what follows, developments of the theoretical approaches for seakeeping analysis and corresponding research issues are described according to the kinds of calculation methods with the potential flow assumption.

Strip method, which is originally based on two-dimensional linear potential flow in the frequency domain, has been used for engineering purposes, because they are very fast and efficient in terms of computational efforts. However, in recent years, attentions tend to be focused on three-dimensional effects and non-linearities in irregular waves and thus three-dimensional Green function methods in the frequency and time domains have been widely applied to both the zero and forward speed problems in connection with the panel method, which discretise the body surface into a finite number of elements. Meanwhile, to overcome the limitations in the time-domain Green function method dealing with only the linearised free-surface condition, Rankine panel method has been developed since the late 1980's. Details of each approach to predict ship motion in a seaway are reviewed in the following sections.

3.2.1 Two-dimensional method

The slenderness of a ship's geometrical shape (i.e. its dominant length compared with breadth and draught, and gradual changes of cross-section along the longitudinal direction) has motivated the simplification of three-dimensional effect of the flow. For small $\partial/\partial x(U/\omega)$, one would find that the change of flow velocity in the transverse direction is much greater than that in longitudinal direction and consequently the flow field in any cross-section might be approximated by the two-dimensional flow in that strip. This has led to so-called 'slender body theory' or 'strip theory', which simplify the complicated three-dimensional problem by the integration of individual two-dimensional strips along the ship length.

In order to obtain good results from strip method applied for the free floating bodies in waves, it is essential to have accurate method to solve the two-dimensional problem, which is mathematically defined as mixed boundary value problem. The two most popular methods to solve this problem are Frank Close-Fit method (Frank, 1967) and multi-pole method (Ursell, 1949). The multi-pole method was first developed by Ursell (1949). He employed source and symmetric multi-pole expansions to solve the heave motion of a half immersed circular cylinder in deep water. Conformal mapping is performed for the transformation of sections with non-circular shape to semi-circle and Lewis-form is often used as the most common mapping function (Lewis, 1929). Frank (1967) used the source distribution technique to solve two-dimensional problem by dividing the ship section into a series of straight-line segments, which is referred to as the Frank Close-Fit method. The main advantage of Frank's method is that a more accurate description of any ship section can be achieved than Lewis form. It can accurately handle rapid change of hull shape such as bulbous bow and stern sections, but it is troubled by irregular frequency. These results of two-dimensional computations have laid groundwork for the development of strip theory.

The first strip theory for ship motions in regular waves was developed by Grim (1953) to solve the problem for two-parameter Lewis form cylinders by conformal mapping onto a circle by using a variation of the Ursell method. Korvin-Kroukovsky and Jacobs (1957) calculated the heave and pitch motions of a vessel in head seas. They assumed that the hydrodynamics associated with the ship could be represented by a series of two-dimensional strips. The two-dimensional boundary value problem to obtain the hydrodynamic coefficients and excitations was then solved for each strip. Although interaction effects between the different strips along the ship's length are not accounted for, their pioneering work has led to wide application of strip theory in ship motion calculation.

Ogilvie and Tuck (1969) performed a mathematically rigorous analysis using slender body theory and developed 'Rational Strip Theory'. Their analysis revealed additional contribution of the forward speed to the cross coupling coefficients involving integrals of the square of potential over the free surface. The complete forms of Ogilvie and Tuck coefficients are superior in mathematical viewpoint, but their practical value is open to debate. In spite of the work of Ogilvie and Tuck (1969), certain aspects of the strip theory remain unsatisfactory from the rational standpoint. The principal questions concern the validity of the solution at low frequency and the emergence of forward speed effects only as higher order corrections. From the underlying assumptions, it is clear that the strip theory is invalid at low frequency of encounter.

The strip theory developed by Salvesen et al. (1970) is not as rigorous as the Ogilvie and Tuck's approach, but their study has become generally accepted by the designers related to marine hydrodynamics since it has been most widely used with respect to seakeeping calculations for traditional ships. They adopted the slender body assumption with a symmetric perturbation expansion to make consistent simplification for the three-dimensional boundary problems. The predictions of heave-pitch motions, vertical wave loads in various heading angles and sway-roll motions in beam seas were found to give good agreement with model tests for high frequencies and moderate Froude number.

Theory	Applicable region
Strip Theory	(2)
Rational Strip Theory	(2), (3)
High-Speed Strip Theory	(2), (3), (4)
Unified Theory	(1), (2)

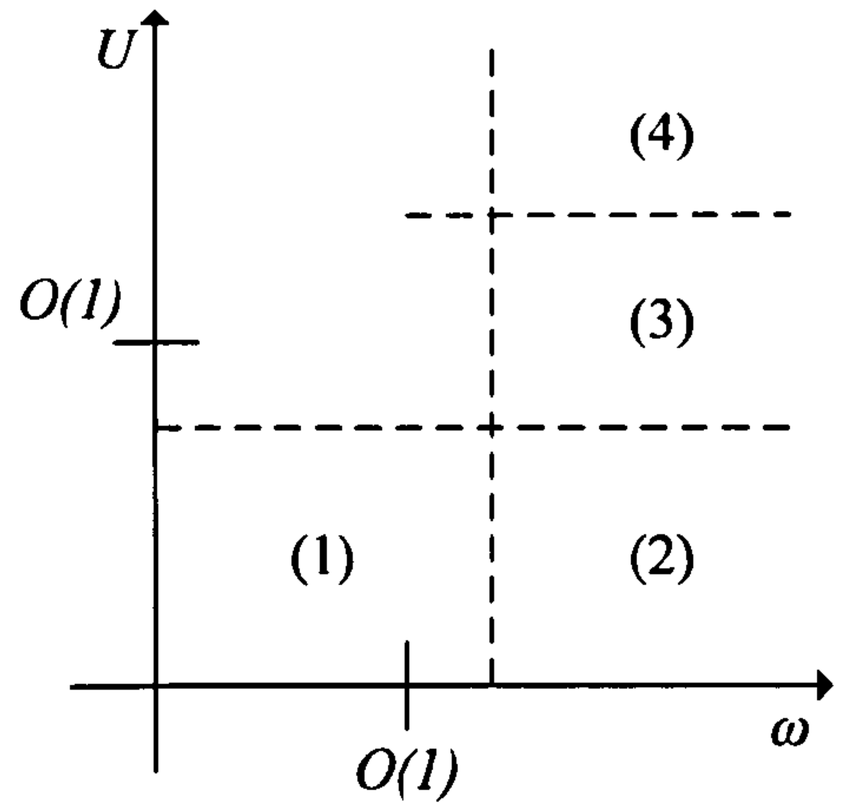

Figure 3.1 Order of parameters valid for various theories (Kashiwagi et al., 1994)

The limit of application to the low frequencies has in principle been overcome by the 'Unified Theory'. The Unified theories of Newman (1978) and Newman & Sclavounos (1980) take into account wave interaction between cross section along the hull. At low frequencies, the unified theory approaches the ordinary slender body theory and yields terms that involve longitudinal interferences between sections, while these interferences disappear at high frequencies and the results become identical to the strip theory. From a rational point of view, unified theory represents an improved slender body theory.

By applying modifications to the slender body theory, several researchers proposed a new approach to solve the ship motion problem. The order of parameters (forward speed and wave frequency) valid for various slender body theories and their applicable regions are compared in Figure 3.1. The review of these slender body theories was also presented with discussions on their accuracy and comparisons with experimental data.

Figure 3.2 shows the comparisons of added mass and damping coefficients predicted by unified theory and effects of forward speed on the hydrodynamic coefficients are well noticed. The model used in the experiment was a mathematical hull form ($L/B = 8$) and its cross sections can be expressed with Lewis form (Kashiwagi et al., 1994).

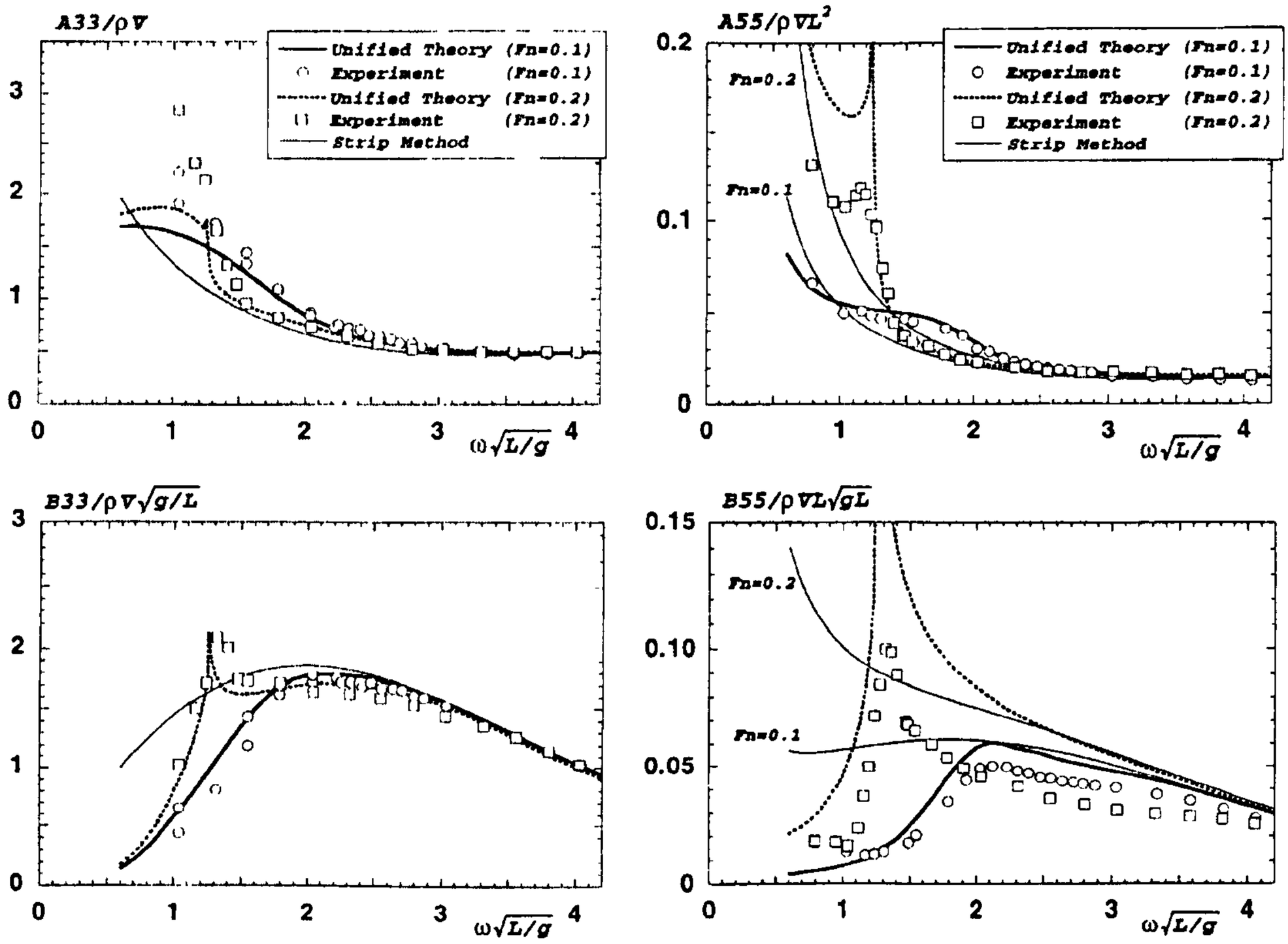

Figure 3.2 Added mass and damping coefficients in heave and pitch of a mathematical ship model at Froude number 0.1 and 0.2 (Kashiwagi et al., 1994)

For non-slender ships the application of the different slender body theories and strip theories are questionable in the prediction of their seakeeping abilities. These vessels require the solution of the full three-dimensional problem. In addition to its obvious value in the determination of seakeeping qualities of non-slender ships, the development of three-dimensional theory is also essential to the validation of the different slender body approximations.

3.2.2 Three-dimensional method

The development of the three-dimensional method to solve the motion of a ship in waves was highly motivated by the offshore engineering in the early 1970's since the large platform structures operate in zero or low speed ranges and require accurate determination of the diffraction forces. This resulted in the development of so-called three-dimensional singularity distribution method through the distribution of pulsating singularities in terms of sources or dipoles with known frequency, satisfying the linear free surface boundary condition. The body boundary condition is then used to determine the unknown strengths of the singularities. Imposing the body boundary condition led to a Fredholm integral equation of the second kind, and thus this method was called 'Boundary Integral Method'. Examples of these methods were established by Faltinsen & Michelson (1974) and Garrison (1978) although they are limited to the zero forward speed.

By the early 1970's the Neumann-Kelvin approach for a ship travelling at a steady forward speed was starting to be used (Brard, 1972). In the Neumann-Kelvin problem the kinematic condition and the constant pressure condition on the free surface condition are linearised, while the kinematic condition on the body boundary condition is satisfied exactly over the mean position of body surface. The traditional approach to solving the Neumann-Kelvin problem is also to use boundary integral method in which the solution is formulated in terms of integrals of fundamental singularities over the surface surrounding the fluid domain. However, by combining the fundamental singularities with other analytic functions, it is possible to develop 'Green functions' that satisfy all the boundary conditions of the problem except on the body surface. Consequently the governing integral equation need only be solved on the body surface.

Meanwhile Hess and Smith (1967) pioneered 'Boundary Element Method' for flows without a free surface. Using a source distribution technique, body surface is discretised into a finite number of flat quadrilaterals in which the source strength is

assumed to be constant. Satisfying the body boundary condition at the centre of each quadrilateral (also called node, control, or collocation point) resulted in a system of linear equations for the unknown source strengths. The velocity and pressure at each quadrilateral can be determined by solving the source strengths. The flat quadrilaterals often called panels and now the term 'panel method' has come to mean any solution technique in which the body surface or other surfaces of the domain have been discretised.

3.2.2.1 Green function

For the zero forward speed case, the three-dimensional panel method using the free surface Green function has been established as a reliable and efficient numerical tool for routine use. However, for the nonzero forward speed case, the corresponding free surface Green function in the frequency domain involves a number of numerical difficulties which hinder the Green function from being practicable in panel methods. In fact, numerous studies have been done on the free-surface Green function at forward speed and generic tools to predict the unsteady motion of a ship with proper considerations of forward speed and encounter frequency due to existence of wave have been developed in the past three decades.

As a pioneering work to solve the three-dimensional hydrodynamic problem in frequency domain for a ship advancing with forward speed in a seaway, Chang (1977) first applied the Green function of the pulsating-translating source given by Wehausen and Laiton (1960) to solve the hydrodynamic problem considering the forward speed. The numerical method in the evaluation of the Green function includes the direct computation of double integrals expressing three-dimensional flow induced by the translating pulsating source. However, it is very time-consuming since the oscillatory behaviour of the integrand may require smaller time step in the numerical integration.

Attempts to establish alternative and more efficient formulations of the complicated Green function have been made by several researchers. A main focus of the approach is to reformulate the double integral in terms of a single integral involving the exponential integral. Bessho (1977) derived the Green function expressed by a genuine single integral in the sense that its integrands are all elementary functions while the integration must be done along a path in the complex plane. Inglis and Price (1981) replaced the double integral term belonging to the principal value formulation in the Green function by single integral involving the exponential integral. The principal value integral was evaluated along a ray in the complex plane so that the oscillatory behaviour of the integrand vanished. Guevel and Bougis (1982) also used the modified exponential integral to reduce the double integral and this formulation involves the time dependent terms. Wu and Eatock Taylor (1987) derived an alternative form of Green function, which leads to a single integral, involving complex exponential integral which is well behaved throughout the range of integration. Exploiting the increasing computer resources in the early 1990's, some practical applications of the three-dimensional Green functions have been carried out by Hoff (1990), Chan (1990), Iwashita & Ohkusu (1992), Ba & Guilbaud (1995), Chen (1999), Boin et al. (2003), and Nobless & Yang (2004). Three different numerical schemes can be divided in terms of the calculation methods of Green function.

Iwashita and Ohkusu (1992) employed the 'steepest descent method' used in Bessho (1977) and performed the integration in complex plane. This is accomplished by deforming the integration path, in order to maintain a constant imaginary part of the integrand (suppressing any oscillation of the integrands) and a decreasing real part. Main part of their study is to find numerically a path on which the integrands do not oscillate and rapidly approach zero. Once this steepest descent path is found, integration is straightforward, and the accuracy of results is controlled without difficulty.

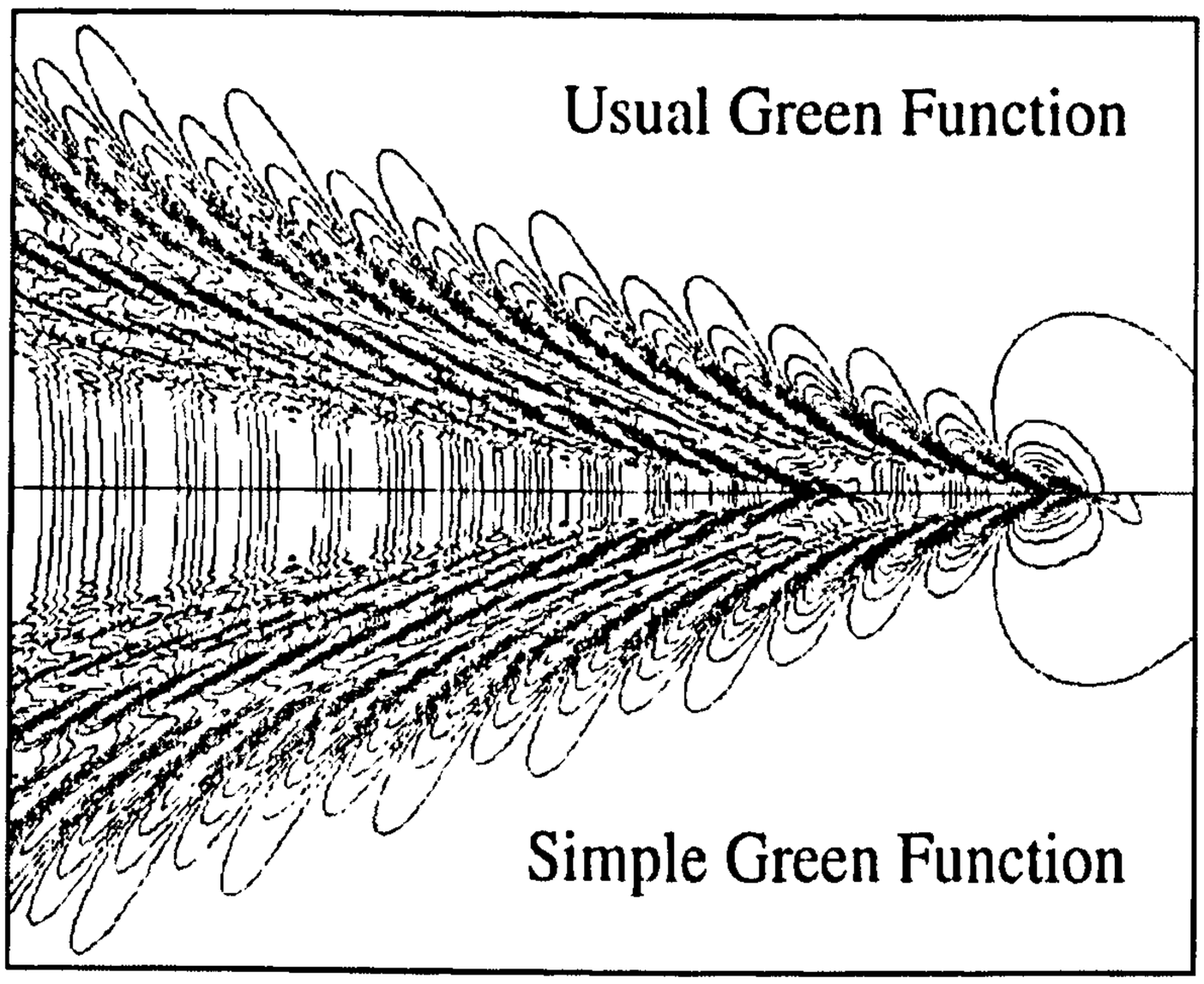

Figure 3.3 Wave system of steady flow generated by a source-sink pair (Noblesse and Yang, 2004)

The method of Guevel and Bougis (1982) was further developed by Ba & Guilbaud (1995) and Boin et al. (2003) to match computer calculations and to calculate the unsteady lifting effects in a vortex-lattice method in the frequency domain. This approach proves advantageous because of a simple integral in the Fourier plane instead of a double one in the complex plane in the steepest descent method. The lifting effects lead to integrations of the second derivatives of the Green function, which have not been previously performed, although the use of the complex integral function is expensive in computation time.

The Green function derived by Chen (1999) and Noblesse and Yang (2004) is expressed as a sum of local-flow components defined by four elementary Rankine sources and three wave components, which represent distinct wave systems generated by a pulsating source advancing at constant speed. This new Green function satisfies the radiation condition and the linearised free surface boundary condition in the far-field but only approximately in the near-field. This feature can be advantageous in taking account of near-field effects in the free-surface boundary condition due to the steady disturbance of a ship. Thus, the Green function is considerably simpler than the free-surface Green function which has been used in the

literatures on wave diffraction-radiation with forward speed. Using their decomposition method, Chen and Noblesse (1998) proposed the 'Super Green functions'. These formulations appear to be quite efficient, especially considering computation time, but they are in part simpler and in part more complicated. Chen and Wu (2001) studied the numerical difficulties in computing the Green function.

For purposes of comparison between Green functions developed in many literatures, the steady flow generated by a point source and a point sink advancing at constant speed U in calm water is considered in Figure 3.3. The source and the sink are slightly submerged below the free surface. The point source and sink are located at $(0.5, 0, -0.02)L$ and $(-0.5, 0, -0.02)L$, respectively. The non-dimensional strength $q = Q/(UL)^2$ of the source-sink pair is taken equal to 0.001 and the Froude number is chosen equal to 0.3. The velocity potentials evaluated using the usual Green function and the simple one of Noblesse and Yang (2004) of the flow generated by the source-sink pair at the free surface plane is illustrated in the upper and lower halves of Figure 3.3. The differences between two formulations vanish in the far-field and are relatively moderate in the near-field.

3.2.2.2 Panel method

Since the slender body theory reviewed in the previous section is based on the concept of idealising the hull by strips, major disadvantage of this method is its inability to treat the three-dimensional effects adequately. Removal of the limitations of slender body theory and consideration of three-dimensional description of body surface enable the interaction effects between various parts of the hull and fluid actions to be suitably treated. The discretisation of hull surface using finite numbers of quadrilateral panels, as proposed by Hess and Smith (1967), can be alternatively applied to the problems of ship motions. Since the Green function approach can also provide a reasonable approximation for many practical purposes, the panel method in connection with the singularity distribution over the discretised elements has been widely used to predict the steady and unsteady motions of a ship in waves. This

approach for fully three-dimensional formulation for the unsteady problem in the frequency domain was initiated by Chang (1977). Since the problem of unsteady motion can be treated in both frequency and time domains, separate reviews are to follow.

The formulation of the ship motion problem follows linear potential theory practise, which separates the steady and unsteady motion problem and solves them individually. However, the interactions of steady and unsteady motions have influence on the body boundary condition for the unsteady motion problem. Therefore two formulations are possible; in the first formulation, the steady motion problem is solved and used to form the body boundary condition for the unsteady motion problem. In the second, the perturbation of the flow caused by the steady motion is neglected and the unsteady problem is solved directly. Inglis and Price (1982a, 1982b) have presented calculations of both formulations. The calculation results of hydrodynamic coefficient, wave loading and motion response for Series 60 with Froude number 0.2 and 0.3 are presented and compared extensively with experimental data including a discussion of the distribution of the coefficients along the length of the hull.

Since early 1980's vigorous efforts were made by many researchers to develop rational mathematical method for predicting wave-induced motion and wave force acting on a ship. These efforts are strongly connected with the efficient and fast evaluation of the free surface Green function adopted in three-dimensional panel method. Typical studies can be found in Guevel & Bougis (1982), Wu & Eatock Taylor (1989), and Iwashita & Ohkusu (1992) with individual formulation of Green function presented. The solution of boundary integral equation was obtained using Constant Panel Method, which assumes the unknown strength of singularity distributed on each panel to be constant.

In order to solve the linear hydrodynamic problem of a ship advancing with a forward speed, Ann et al. (1995) employed a Higher-Order Panel Method to solve the integral equation adopting free surface Green function. The hull surface is

discretised with four-point cubic elements, while nine-point quadrilateral elements are used for the distribution of singularity over the idealised hull surface. Linear hydrodynamic data are obtained and compared with the experimental data for Series 60 travelling in regular waves.

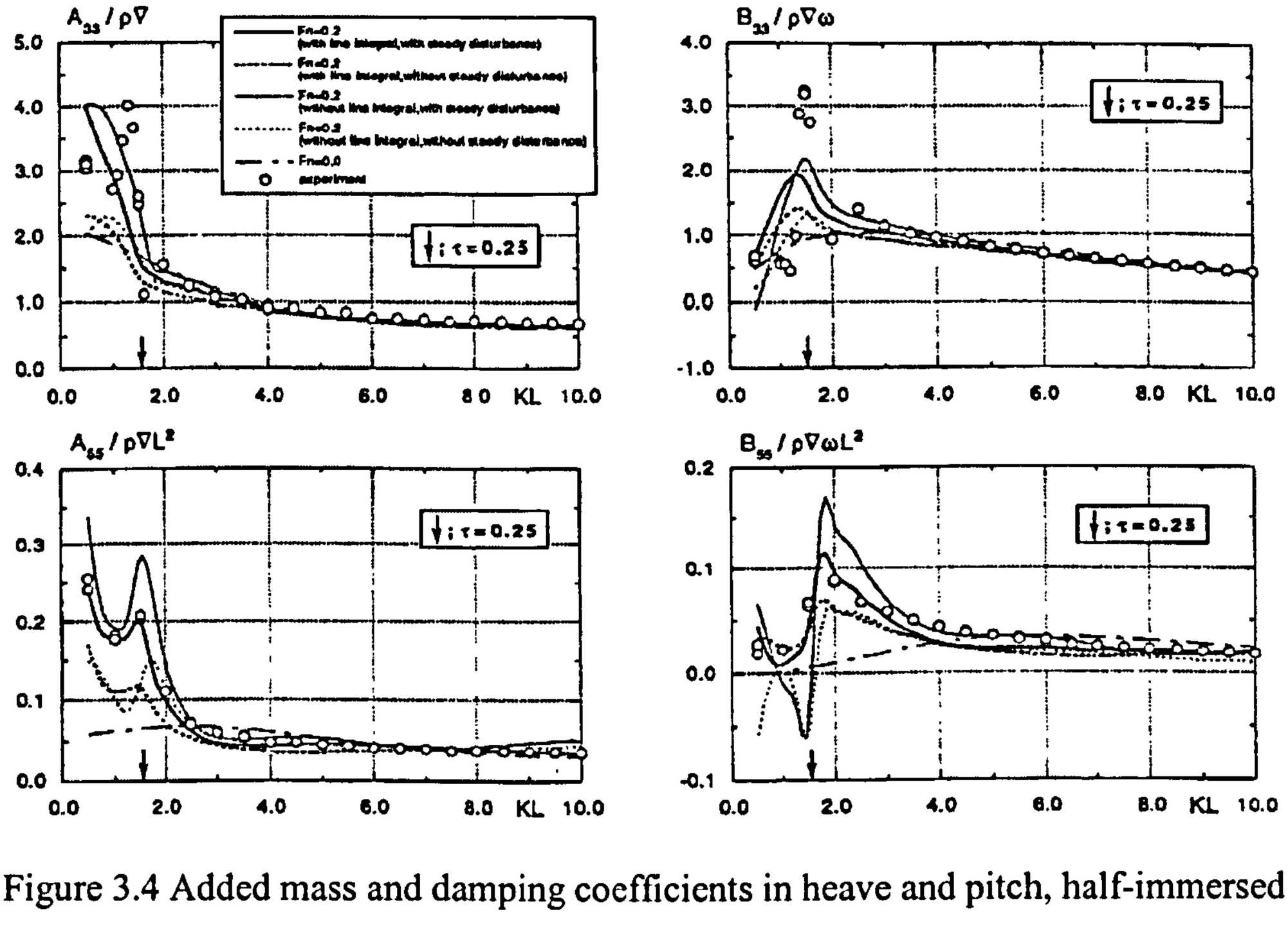

Figure 3.4 Added mass and damping coefficients in heave and pitch, half-immersed prolate spheroid at Froude number 0.0 and 0.2 (Kashiwagi et al., 1994)

Du et al. (2000) carried out an extensive theoretical validation of numerical technique on the speed and frequency dependent solutions associated with seakeeping characteristics of surface piercing vessels travelling in waves. Two alternate theoretical models of Green function in the formulation and numerical scheme are employed and the three-dimensional linear seakeeping problem is addressed in the frequency domain. Each formulation was applied to calculate the hydrodynamic data of Series 60 and high speed mono-hull forms at various Froude numbers. The effects of speed and frequency dependence are discussed and a preliminary study into their influences on the occurrence of irregular frequencies in the numerical schemes is presented.

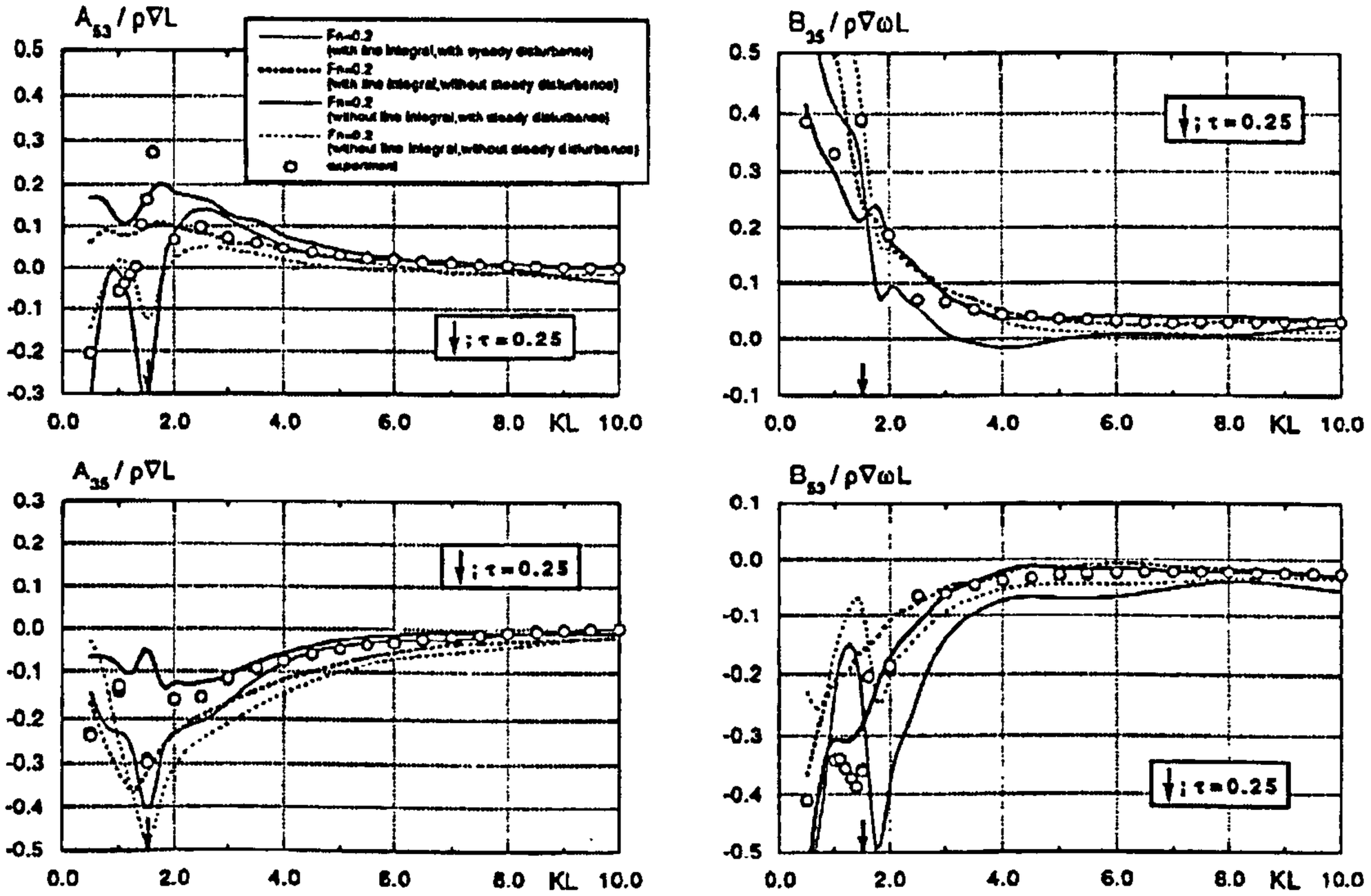

Figure 3.5 Coupled added mass and damping coefficients in heave and pitch, half-immersed prolate spheroid at Froude number 0.0 and 0.2 (Kashiwagi et al., 1994)

Maury et al. (2003) presented a numerical and experimental study of the radiation flow about ships advancing in waves. They used panel methods using two different expressions of the free surface Green function: the single-integral expression of Bessho (1977) and conventional expression with exponential integral used in Guevel and Bougis (1982). The former form of Green function is calculated with steepest descent method and a Simpson adaptive method is applied to evaluate the latter. It is shown that waterline integral term has strong damping effect on the irregular frequencies by showing the increases in amplitudes of irregular frequencies without waterline integrals. Predicted results were compared to test results for Series 60 models of different block coefficients.

Added mass and damping coefficients of a half-immersed prolate spheroid ($L/B = 5$) predicted by three-dimensional Green function method are illustrated in Figure 3.4 and Figure 3.5. It is easily noticed that the inclusion of the waterline integral term in the integral equation and the consideration of steady flow disturbance play an important role in the unsteady flow field. Their effects on the

hydrodynamic coefficients increase dramatically in the region when $\tau < 0.25$. More detailed review on the critical frequency τ will be discussed later. A comparison of heave and pitch exciting forces for the Series 60 and NPL mono-hull travelling in head waves is shown in Figure 3.6. In these figures, agreement between two different formulation of Green function (methods A and B) is extremely close for all of the speeds and frequencies and the effect of forward speed on the wave exciting forces is clearly visible.

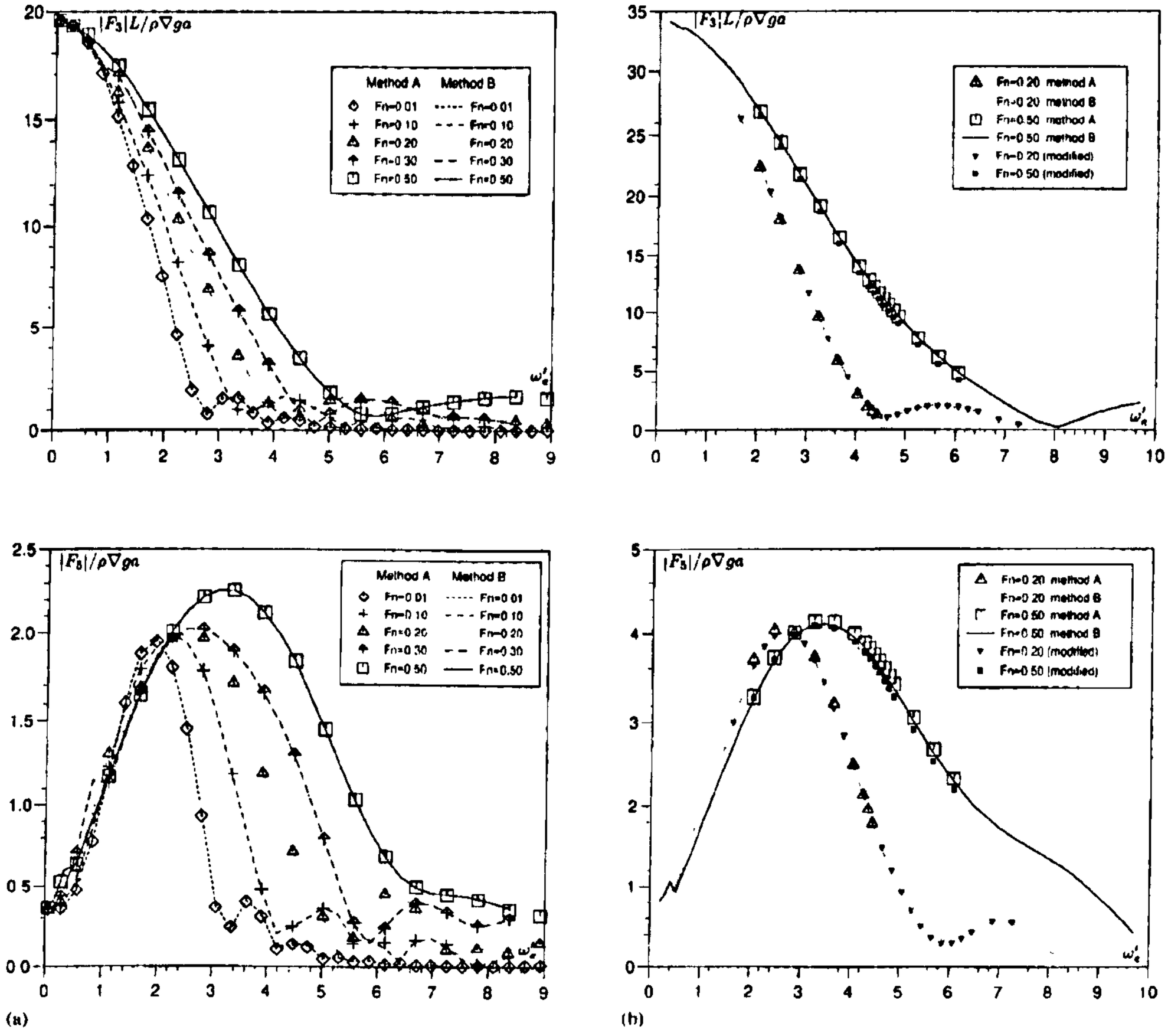

Figure 3.6 Predicted wave exciting forces in heave and pitch for (a) Series 60 hull and (b) the NPL mono-hull form (Du et al., 2000)

3.2.3 Rankine panel method

In the methods employing the Green function of the translating pulsating source in the frequency domain, the unknown singularities are distributed on the hull surface only since the Green function is satisfying the Laplace equation, the linearised free surface condition and radiation condition. Through a number of studies done up to date, it has been shown that the free surface Green function can be computed very accurately over the whole calculation domain. However, some numerical difficulties seem to still exist in solving the integral equations for the source strength or the velocity potential itself on the wetted surface of a ship. In particular, there must be a precise numerical cancellation between the singularities from the line-integral term along the waterline and from the surface-integral term in close proximity to the free surface, but probably this numerical cancellation is not achieved to the level of satisfactory accuracy.

For purpose of avoiding the mathematical complexity inherent in the Green function, much simpler Green function can be introduced, which is called Rankine source. If the Green function of the Rankine source is used, the singularities must be distributed on both hull and free surface since the Rankine source does not satisfy the linearised free surface condition. This permits the enforcement of a wide range of linear, higher-order or fully non-linear free surface conditions irrespective of the time dependence of the underlying flow. There are several variations in this method depending on the way of satisfying the radiation condition at infinity and the time-marching schemes for the free surface condition and the equations of ship motions as described in the review by Sclavounos (1996).

The basis for the development of three-dimensional boundary equation methods using the Rankine source singularity was given by Gadd (1976) and Dawson (1977), who presented a three-dimensional panel method for the steady ship resistance problem. In their methods, the hull and free surface around the vessel were discretised using flat quadrilateral panels. On each panel a Rankine source

singularity was assumed with an unknown constant strength. Using Green's integral formulation the flow problem was formulated and the unknown singularity strength distribution could be solved following the appropriate body boundary conditions. The full free surface modelling method uses the standard double-body linearization technique, originally formulated by Gadd (1976), where the flow past a double-body model in an infinite fluid is calculated prior to performing the full free-surface calculation. This approach was improved by Dawson (1977) by imposing the condition that wave disturbances can only advect in the downstream direction and hence provides a realistic and unique solution to the free-surface wave problem.

Application of the Rankine panel method to the complete three-dimensional steady and time harmonic potential flow past ships advancing with a forward speed was quite successfully introduced by Nakos and Sclavounos (1990) in frequency domain. King et al. (1988) performed seakeeping calculations with forward speed by using the Rankine panel method in the time domain. Since Rankine panel method is versatile in that it can deal with different kinds of free surface conditions that may include non-linear terms, Rankine panel method has been applied so many hydrodynamic research field, e.g. linear or non-linear interactions between ship and wave, high speed vessel and added resistance in waves, in both frequency and time domains. The current state-of-the-art of research activities in the field of Rankine panel method have been reviewed completely in Beck and Reed (2001) and the Report of the Seakeeping Committee of the 24th ITTC (2005).

The standard discretisation of hull and free surface used in Rankine panel method is illustrated in Figure 3.7, where the border of numerical beach is also shown. Corresponding boundary conditions are then enforced to each panel with the consideration of radiation condition in the far field. The discretisation of free surface is further characterised by two parameters, the panel aspect ratio α and the grid Froude number F_h,

$$\alpha = \frac{h_x}{h_y} \qquad \text{and} \qquad F_h = \frac{U}{\sqrt{g h_x}} \tag{3.1}$$

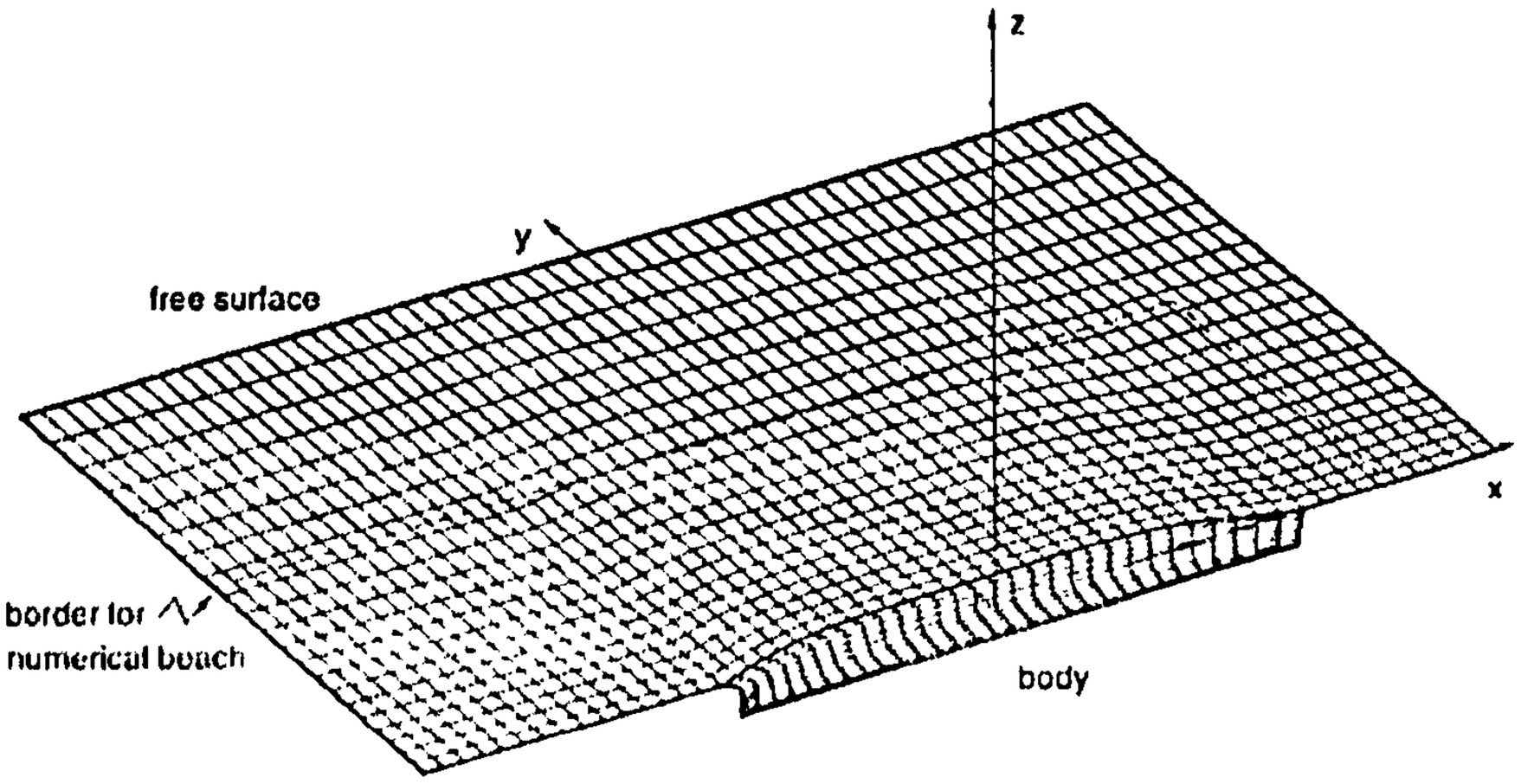

Figure 3.7 Ship hull and free surface discretisation (Ohkusu, 1996)

where h_x and h_y are the panel dimensions in longitudinal and transverse directions respectively. A certain stability criteria that restrict the choice of the corresponding parameters should be met to ensure the convergence of numerical scheme.

3.2.4 Time domain approach

An alternative approach to solve hydrodynamic problem in frequency domain is performing the calculations in the time domain. For the linear problem, the results of frequency and time domains are related by the Fourier transform. The time domain calculation requires the evaluation of convolution integrals over all previous time steps and this, therefore, takes both computational time and memory. For the zero speed case, the frequency domain approach requires less computational efforts than the time domain one due to the convolution integrals, although the evaluation of free surface Green function in both domains requires approximately the same computational time. However, in the case of forward speed, the time domain approach may offer possible advantages, since the Green function applied in the time domain retains its relative simple form regardless of the forward speed compared to the Green function in frequency domain. In the frequency domain, the forward speed Green function is much more complex, requiring greatly increased computer time.

The application of the time domain approach to the three-dimensional body case selecting the free stream as the basis flow for linearisation was presented by Liapis and Beck (1985) for the radiation problem using the impulsive input. The extension of the radiation problem to diffraction problem was developed by King (1987) who used an impulsive wave to obtain the appropriate incident wave boundary condition, considering the body waves as the input to the linear system directly in the time domain. King et al. (1988) employed a non-impulsive input to obtain hydrodynamics coefficients for zero and forward speed cases, but the wave elevation cannot be computed by this approach. Bingham et al. (1993) used a transient free surface Green function to solve the linearised ship motion problem for a ship travelling with steady forward speed through quasi-random incident waves. A technique for extending the impulse response function by asymptotic continuation was presented to reduce the required length of the computations.

The time-domain approach is advantageous to study non-linear problems even in the framework of the free surface Green function method. The levels of approximations technique in treating non-linear characteristics might be various and the simplest one could be that the Froude-Krylov and restoring forces are computed exactly while retaining the radiation and diffraction forces as linear. This approximation can account for dominant non-linearities in large-amplitude motions of a ship without increasing the computation time as compared to the linear formulation (Sen, 2002).

The so-called 'body-exact' formulation for the radiation and diffraction problems is the next higher level of approximation for non-linearities. In this formulation, the transient free-surface Green function is used and the body boundary condition is satisfied on the instantaneous exact wetted surface of the hull while retaining the linearised free-surface boundary condition. Therefore, the computation time in the body-exact formulation is dramatically increased as compared with the linear problem. Since this body-exact problem becomes a time variant system, the solutions of frequency and time domains are not simply related by Fourier Transforms any more and the hydrodynamic forces acting on a vessel undergoing sinusoidal motion are not sinusoidal either. Numerical application of body exact formulation for the

large amplitude motion of a surface piercing body was presented by Lin and Yue (1990). Their calculation results include linear and large motion coefficients and diffraction forces with and without forward speed and the non-linear effects associated with the changing wetted hull are illustrated.

An attempt to develop robust numerical codes in both frequency and time domains has been made since 1980's and the results of both domains were compared with experimental measurements for verification and validation of the codes; WAMIT and SWAN1 developed in frequency domain and LAMP and SWAN2 in time domain. The underlying numerical approach employed in both SWAN codes is a three-dimensional Rankine panel method for potential flows and more details of each numerical code are well explained in the review of Beck et al. (1997). Figure 3.8 and Figure 3.9 show the comparisons of hydrodynamic coefficients predicted by SWAN1 (frequency domain) and SWAN2 (time domain) with the experimental data. The agreement between SWAN's and experiments is generally good, confirming the consistency of the SWAN predictions and their performance relative to experiments.

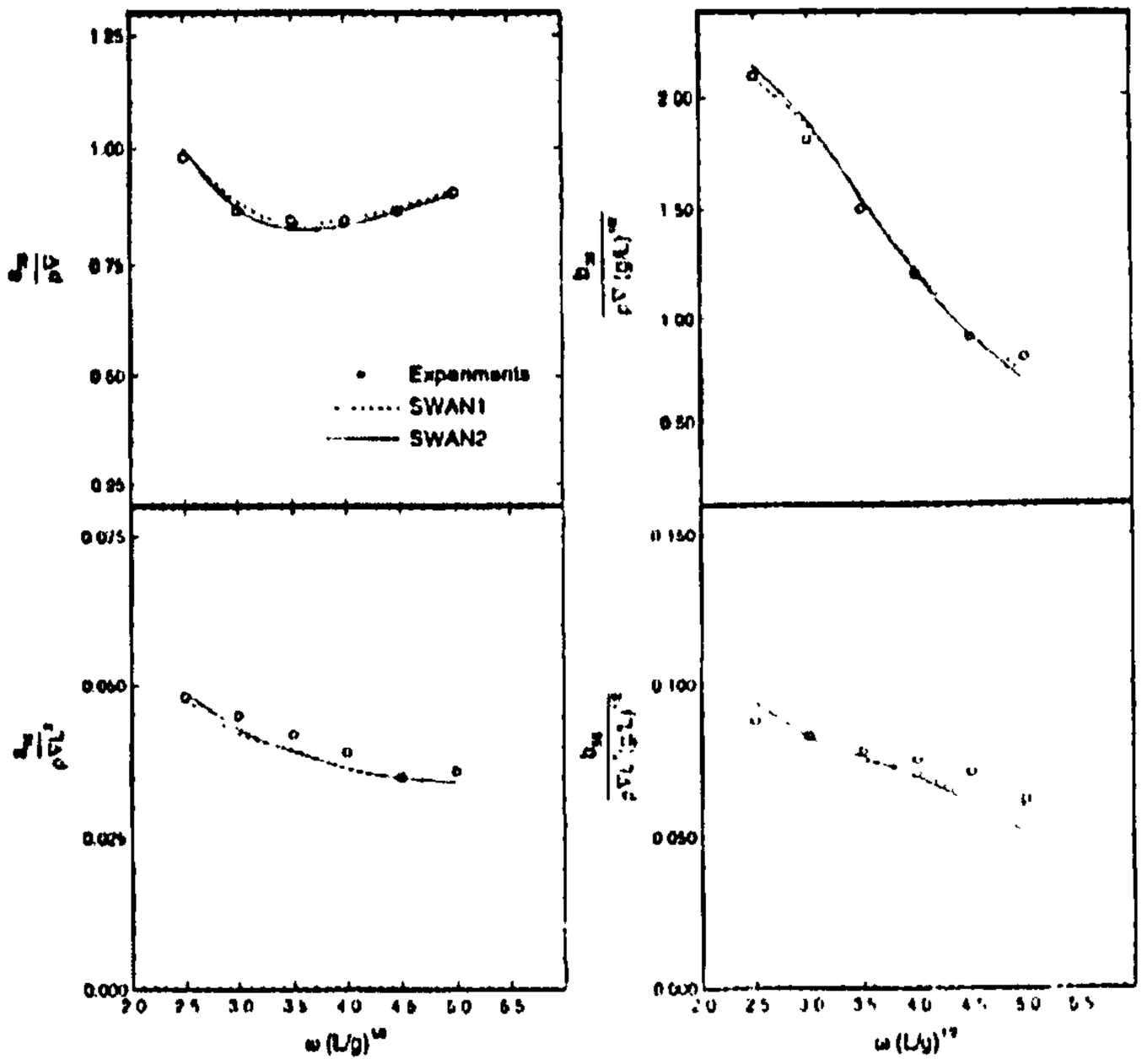

Figure 3.8 Non-dimensional hydrodynamic coefficients for Todd Series 60 at Froude number 0.2 (Sclavounos, 1996)

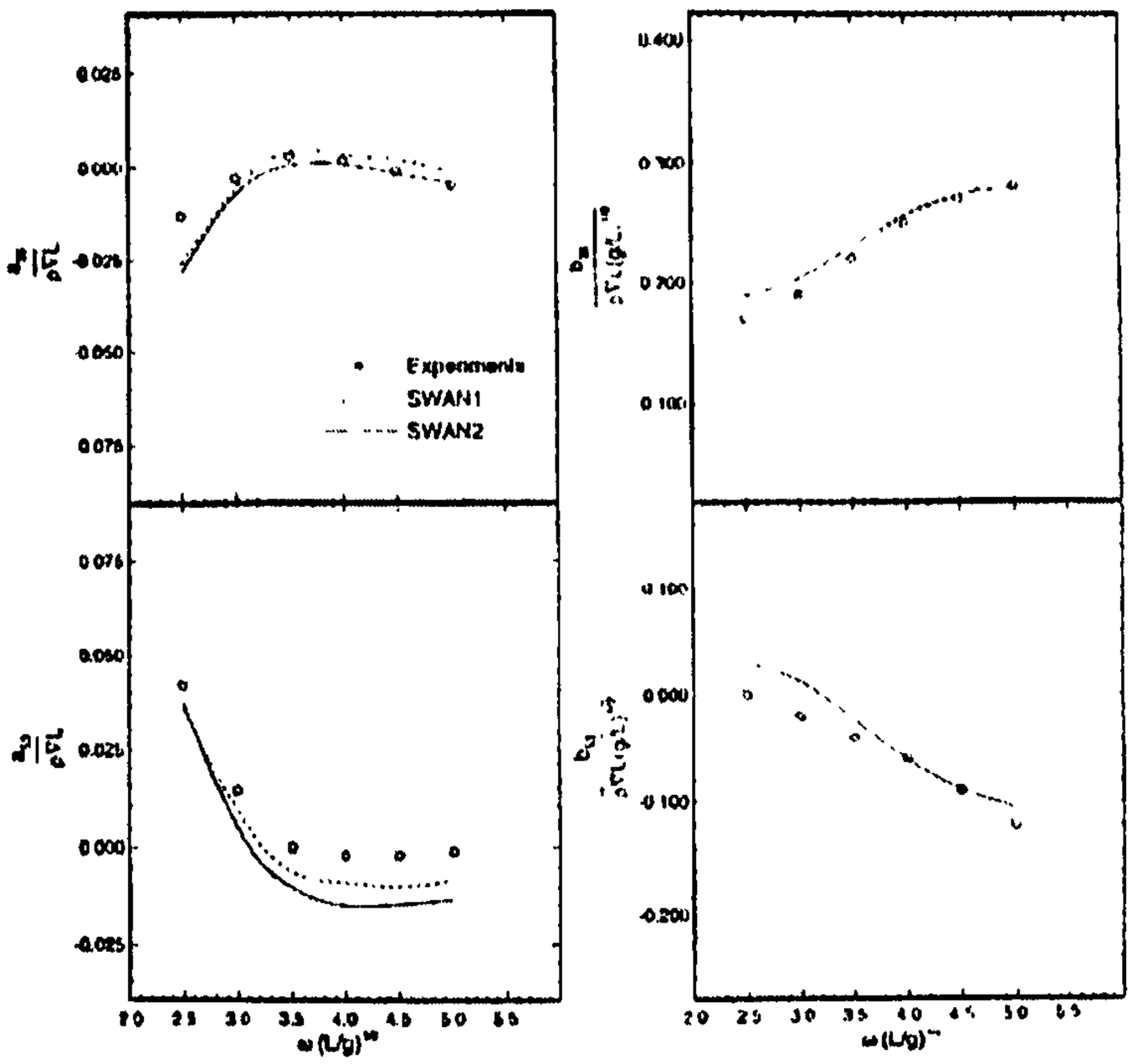

Figure 3.9 Non-dimensional coupled hydrodynamic coefficients for Todd Series 60 at Froude number 0.2 (Sclavounos, 1996)

Similarly, Vassalos et al. (2000) developed computer programs to predict the hydrodynamic loads and responses of high speed craft in the frequency and time domain approaches adopting the free surface Green's functions. Based on a comparative study between the two approaches they suggested the suitability of each approach concerning accuracy of predictions and general applicability to solving high-speed related problems.

3.2.5 Research issues

3.2.5.1 Drift force and added resistance

The hydrodynamic forces acting on a body exposed to the action of the surrounding fluid can be separated into oscillatory and non-oscillatory components. The oscillatory force component cause motions which are proportional to the wave amplitude and the problem regarding these forces and motions are referred to as the first-order theory. The non-oscillatory force component arises from various non-linear effects of the fluid action and is of at least second-order with respect to the wave amplitude. The first-order component shows a zero mean value over a period, while the second-order term is expressed time-averaged constant value in the regular waves or slow-varying random waves. This second-order component is often referred to as the well-known steady drift force and historically drift forces have been of much more interest due to their importance in the design of offshore structures and their moorings.

There are two ways of obtaining the steady second-order drift force. The first one is so-called near-field method using direct pressure integration over the wetted body surface. This method has advantage that the local values of the force can be obtained, which may lead to a better physical insight into the phenomenon. Alternatively the horizontal component of drift force can be obtained from momentum relation of the control volume in the far-field. This far-field method has mathematical and numerical advantages, since the integrals are evaluated at a vertical control surface far away from the body.

Watanabe (1938) and Havelock (1942) first confirmed the existence of drift force in the analysis of the interaction between wave system and ship motion and laid the basis for a mathematical formulation. Maruo (1960) first derived complete expressions for the horizontal surge and sway drift forces acting on a ship at zero speed and Newman (1967) further extended Maruo's expressions to include the yaw

drift moment using the slender body assumptions. Both Maruo (1960) and Newman (1967) used the far-field momentum approach and the expressions of drift forces are given in terms of Kochin functions.

Faltinsen and Michelsen (1974) modified Newman's formulation in connection with the three-dimensional pulsating source distribution technique and extended the formulation to the case of zero forward speed at finite water depth. The results of computations compared with the experimental data for the mean horizontal force on a box shaped floating body showed good agreement but no drift moments result were produced.

Lin & Reed (1976) presented the most complete derivation of the far-field expression for the mean second-order forces on a ship advancing in oblique waves. In their results the second-order steady forces are expressed in terms of Kochin functions but they were not able to express the second-order steady moment in a form suitable for numerical calculations.

Although the far-field method requires less computational effort in the evaluation of mean second-order forces in the horizontal plane, it possesses difficulties in predicting those in the vertical plane. Pinkster & van Oortmersen (1977) computed the mean second-order wave force on a stationary free floating barge in regular waves using the complete near-field method. The drift force was calculated by means of direct pressure integration on the hull surface as derived from first-order potential, which is obtained using the three-dimensional singularity distribution technique. The theoretical results appear to show good agreement with experimental data.

In the case of forward speed problem Faltinsen et al. (1980) employed the two-dimensional pulsating source technique associated with the near-field method to calculate the added resistance of a ship in oblique waves. Their results agreed well with the measured data for three Series 60 ships and a container ship in head waves but under-estimated that of the container ship in bow oblique waves.

Most studies on the drift force during 1980's were concentrated to the theories based on the frequency domain rather than time domain. This restricts the theories to the linear equations and harmonic functions, which are not realistic, since sea wave are not harmonic, especially not in the vicinity of a ship. Thus Prins and Hermans (1994) studied the non-linear equations in the time domain in order to obtain a realistic prediction of the drift force acting on a sphere floating with forward speed. Due to the increasing burdens arising from computational capacities required, they solved, however, linear equations of motion in the time domain.

The longitudinal drift force acting on a ship advancing in waves can be applicable to the prediction of the added resistance, which is important for the overall fuel economy of the ship in a seaway. Added resistance in waves is regarded as the mean increase in resistance force resulting from radiation of energy away from a ship operating in a seaway. A dominant component of added resistance is an additional force to the wave-making resistance due to the disturbance caused by the interactions between ship and fluid domain. Thus, in linear theory, added resistance is the steady second-order force resulting from radiation of energy contained in the first-order radiation and diffraction waves.

Strom-Tejsen et al. (1973) provided basic principles that summarise the early work in added resistance and drew general conclusions concerning the nature of added resistance; 1) The added resistance is proportional to the square of the wave height. 2) The added resistance in a seaway is independent of calm water resistance. 3) The added resistance would depend on the motions and their phase relationship to the wave field. Using various hull forms, e.g. destroyer, high speed and five Series 60 parent hulls with different block coefficients, model experiments to determine added resistance in regular and irregular waves are carried out. The measurement data were compared with theoretical methods, most of which relate added resistance to a phase lag between incident waves and ship motions.

Lin and Reed (1976) adopted the method of momentum conservation theory to obtain second-order steady sway force using stationary phase method. Kashiwagi

(1992) further extends the momentum approach of Lin and Reed (1976) to include the mean second-order yaw moment, avoiding the repeated use of the stationary phase method. These formulations involve far-field representation of the wave field and are analogous to the measurement and prediction of steady wave resistance in calm water. Such approaches to added resistance prediction were necessary in the days when strip theory were the only means of predicting ship motions.

Figure 3.10 shows the comparison of added resistance evaluated by the far-field method and measurement data in a towing tank test with the hull form of a container ship in regular head waves. In the numerical calculations, the peak value is due to the peak of heave and pitch motions, which were calculated by the strip theory. Agreements of the prediction and measurement are fairly good, but some discrepancy is observed in the low wavelength region.

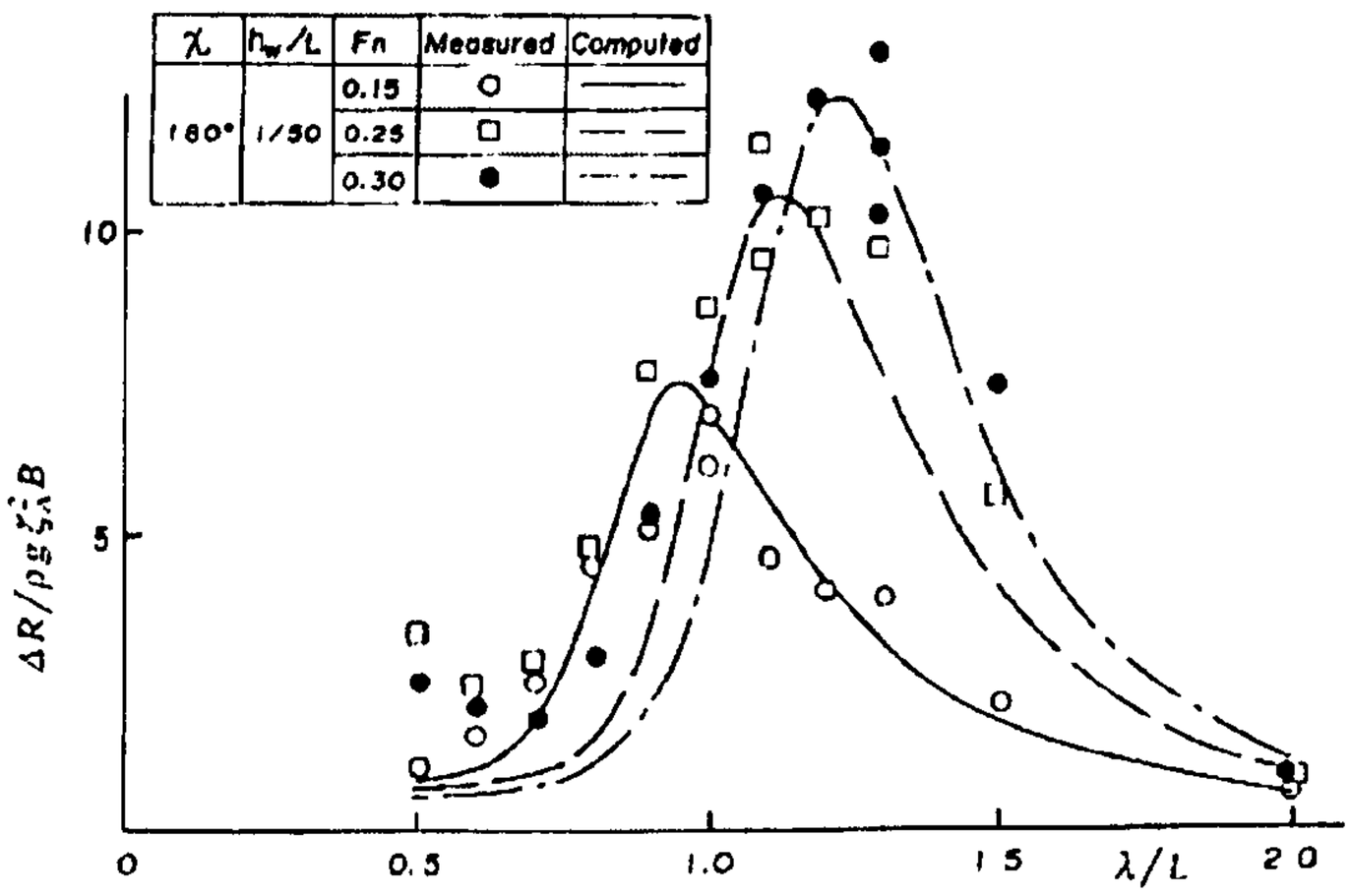

Figure 3.10 Added resistance of container ship (Ohkusu, 1996)

With the advent of three-dimensional methods for the prediction of seakeeping performance, it has become feasible to predict added resistance by means of direct pressure integration over a hull surface. Hermans and Huijsmans (1987) formulated the expression for mean drift force applying Taylor series expansion to the pressure in the mean position of the hull surface. The final expression is identical to that of Pinkster (1977) and is further decomposed into four contributions to the total mean drift force. The second-order drift force is expressed with respect to the first-order

terms like wave elevation, velocity field, motion and force, and second-order potential terms yield no contribution to the drift force.

A brief review on the theory of added resistance and its historic development are given by Ohkusu (1996) and recent state-of-the-art researches are available in the reports of the Loads and Responses Committee of the 22nd ITTC (1999) and 23rd ITTC (2002) and the report of the Seakeeping Committee of the 24th ITTC (2005).

3.2.5.2 Critical frequency at $\tau = 1/4$

One of primary difficulties arising in the three-dimensional panel method adopting free surface Green function is the existence of critical frequency at $\tau = \omega U / g = 1/4$, where ω denotes the encounter frequency, U the forward speed of a ship, and g the acceleration of gravity. The wave propagation due to a translating pulsating source shows that there is a mechanism to propagate wave energy from the ship at the critical frequency. Above the critical frequency $\tau > 1/4$, there are two components in the wave system that both travel downstream with respect to the corresponding reference frame. Below the critical frequency $\tau < 1/4$, three components travel downstream, while one component propagates upstream that travels faster than ship. At the critical point $\tau = 1/4$, there exist two components that act as standing waves with the same speed and direction of the ship and another two more waves that travel downstream allowing energy to radiate away. For many years it has been speculated that at the critical point the wave energy was trapped near the ship and that the motions would blow up due to the unbounded energy.

The motion generated by a body of nonzero volume, oscillating or exposed to an incoming wave, may be found by using a distribution of sources located at the body surface. Since a single source is unbounded at $\tau = 1/4$, it was long believed that the solution of the linear seakeeping problem in the vicinity of this critical frequency is singular. Grue and Palm (1985) found, however, that the motion and physical forces are bounded as $\tau \to 1/4$ for a submerged two-dimensional circular cylinder. Liu and

Yue (1993) showed that the motion at $\tau = 1/4$ is bounded for a submerged two-dimensional body of arbitrary form, provided that the body has a nonzero cross sectional area or the body intersecting the free surface has a finite waterplane area. Then the solution of Grue and Palm (1985) was extended to a floating two-dimensional bodies and three-dimensional submerged bodies.

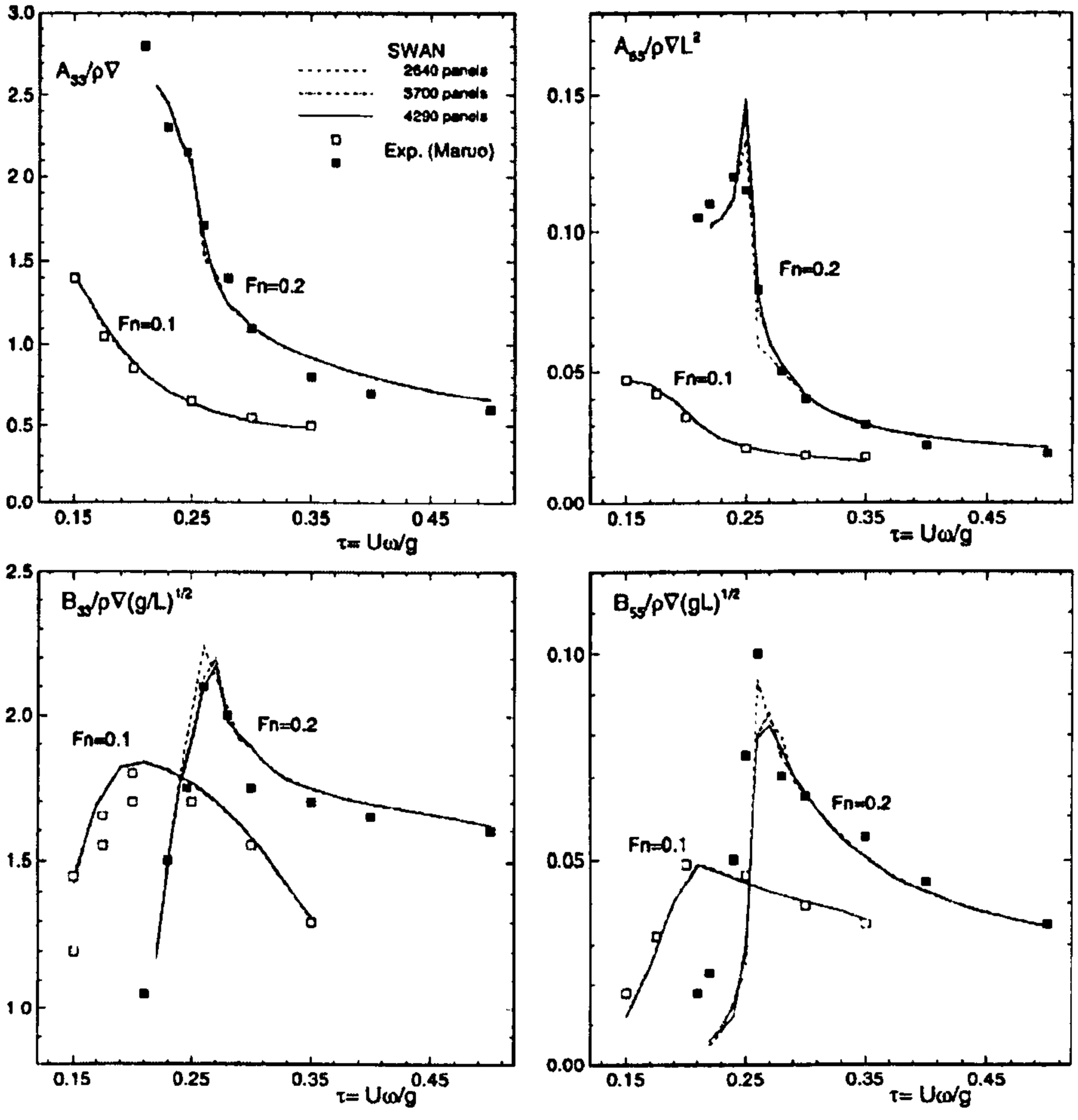

Figure 3.11 Added mass and damping coefficients for a Lewis hull in heave and pitch at Froude numbers 0.1 and 0.2 for three grid densities (Kring, 1998)

In order to demonstrate that a bounded and physically relevant solution exists at the critical point, Kring (1998) used a Rankine panel method in the time domain for the linear seakeeping problem of realistic ship. After addressing the issues of numerical stability and domain sensitivity, numerical convergence was demonstrated with different grid densities and Froude numbers. Difficulties in obtaining the

convergence for both long wavelengths, requiring a large domain size, and short wavelengths, requiring a fine grid resolution, were explained. The spatial convergence of heave and pitch added mass and damping coefficients are illustrated in Figure 3.11.While there are two well defined peaks in the damping coefficients for both heave and pitch, neither of these occurs exactly at $\tau = 1/4$ since there is no reason to expect the maximum value at the critical frequency. The sharp peak in pitch added mass does not represent an unbounded solution but converged to a specific and finite value.

Using free surface Green function of radiation-diffraction problem in the frequency domain, Chen et al. (2000) demonstrated similar finite peak values in the added mass and damping coefficients at $\tau = 1/4$ for both a submerged sphere and a Wigley hull form. Although the hydrodynamic coefficients vary sharply for τ crossing the critical point, it was confirmed that the values are not singular but does have a finite value at $\tau = 1/4$.

3.2.5.3 Validation of seakeeping numerical method

Numerical schemes based on the seakeeping potential theory often play an increasingly important role in predicting hydrodynamic performance of ships in the waves. There are, however, significant differences between the hydrodynamic coefficients at forward speed from theoretical predictions, for example these disagreements can be observed even in the simple mathematical model of Wigley hull form. Also these discrepancies often occur when non-linearities or viscous effects play a role. Furthermore, in the case of regular wave transfer functions, there exists sometimes a considerable disagreement between predictions and experiments, that is, the estimated value of the predictions does not agree with the measurement by an amount that is apparently greater than acceptable experimental scatter. It is obvious that these experimental scatter and bias between estimations and measurements will hold for the resultant motions as well.

Since the first interest of present study lies in the establishment of accurate numerical method to obtain hydrodynamic data set, e.g. hydrodynamic added mass, damping coefficients, wave force as well as motion response, it is required to assess how to prove validity of the outcomes of adopted numerical schemes. Such an attempt has been made first in the 19th ITTC (1990) and recently the Loads and Responses Committee of 23rd ITTC (2002) adopted a Procedure on the validation of seakeeping theories. Its purpose is to provide a preliminary guideline on the validation of two- or three-dimensional seakeeping computer codes for calculating the potential coefficients, wave-induced loads and motions of floating structures and displacement ships in regular waves in the frequency domain.

ITTC Recommended Procedures 7.5-02-07-02.4 for Validation of Seakeeping Computer Codes in the Frequency Domain

A clear distinction has been made between the verification and the validation of a seakeeping computer code:

- **Verification** of a computer code means to check that the code is actually a correct presentation of the mathematical model that forms the basis for it. It establishes that the code written echoes the intended operations and procedures necessary to fulfil or complete the required intended tasks. It means the code in itself is correct.

- **Validation** is the demonstration that the mathematical model of the verified computer code is an adequate representation of the physical reality. It establishes the applicability and integrity of the code developed.

Thus, validation is a much broader activity, which includes verification and comparison with benchmark experimental results. The validation process should provide estimates of suitable metrics that are indicative of the processes involved and

lead to estimates that are compatible with other means of measuring the selected metrics.

Most of the validation process provided in the literatures involves comparisons of linear frequency domain quantities like added mass, damping coefficients and motion responses with experimentally measured data. Any seakeeping code should pass the preliminary examination of these hydrodynamic data set obtained in the numerical calculations. Any mistakes in the numerical scheme result in an improper design which is critical in the ship operation and might last the lifetime of the ship. Meanwhile the model-scale experiments, which are often required for the validation process, are time-consuming and very expensive. When full-scale data is required, the costs can be increased even further. Therefore, great deal of care should be taken in the development of both numerical and experimental approaches for the successful validation work.

To obtain even better results during the implementation of validation, Ohkusu (1998) argued that advanced theory and method in the subject of hydrodynamics must be tested on 'hydrodynamic' experiment rather than the ship motion experiment or the global force experiment. He claimed that integrated quantities, such as global wave loads and response amplitude operators, do not identify the deficiencies in a theoretical formulation and that they combine many factors that can hide errors in both the experiments and theory. Hydrodynamic experiment was detailed as an experiment to understand the basic hydrodynamics of the ship-wave interaction, e.g. measurement of the hydrodynamic pressure distributed on the hull surface or measurement of local wave field around the ship. However, requirements of the experiments will be much more complicated and cost longer time as well as very sophisticated equipments.

3.3 Manoeuvring Theory

The recent increase of interests on the marine safety and casualty resulted in the adoption of regulation on ship manoeuvrability towards performance-based standards As for the Standards for Ship Manoeuvrability adopted by the IMO, the following three points may be very important issues for the mandatory application of the Standards; 1) prediction of manoeuvring performance at the initial design stage, 2) correction of loading condition to the manoeuvrability in the sea trial and 3) correction of environmental disturbances, e.g. wind, wave and current, to the manoeuvrability also in the sea trial.

Although the Manoeuvring Standards require sea trial to be carried out in calm environment, that is to say, in deep unrestricted water, below Beaufort wind scale 5 and sea state 4, and under uniform current, the external forces due to environmental disturbances are inevitable at actual sea. In these conditions, it is very difficult to understand real inherent ship manoeuvrability by the external disturbances, accordingly it is demanded to develop the correction method for the environmental disturbances as in the aforementioned third issue. However, researches of wave effects on manoeuvring performance are not as numerous as those on wind and current effects on manoeuvring motion and trajectory. In order to estimate the effect of external forces on manoeuvring motion correctly, researches for studying wave effect on manoeuvring motion as well as traditional manoeuvring issues will be investigated.

3.3.1 Memory effect

The conventional representation of fluid forces acting on the ship travelling in a seaway was generally determined by the small parasitic motion from a prescribed steady motion and was often expressed as resultant forces with respect to the centre of gravity. It is commonly assumed that the fluid forces at any instant can be

determined by the perturbation of the steady reference motion at that instant. It is the basis of subsequent assumption of 'quasi-steady' flow, on which so-called 'slow motion' derivative is defined. Therefore it has been demonstrated that a frequency dependence of the hydrodynamic forces is not very important in the conventional calm water manoeuvres and simplified mathematical model based on Taylor series expansion is justified. With the concept of linear theory and Taylor expansion, Abkowitz (1964) expressed the fluid forces in the equations of motion with the linear constant coefficients, which are proportional to the motions, e.g. displacement, velocity and acceleration.

Although the slow motion derivatives with constant values are used widely in the stability analysis and control theory, it is often criticised that they does not give accurate prediction of ship motion and their use in linear theory is valid only when the amplitude of parasitic motion is small. When the manoeuvring motion of a ship in a seaway is of interest, the influence of the frequency on forces becomes significant. Moreover the previous motions could play an important role partly in determining the current exciting forces exerted in the confused fluid since the manoeuvring motion of a ship in a seaway has an arbitrary form, which is not prescribed. It has been shown that the fluid forces are dependent on the motion history of a ship in a seaway and it is often referred as 'memory effect' of a fluid action, which is mainly associated with the wave on a free surface due to the unsteady motion of a ship and vortex shedding from the oscillating ship.

In a pioneering study, Cummins (1962) discussed the this memory effect on the ship hydrodynamics and showed that the hydrodynamic forces arising from transient ship motion can be represented by means of convolution integral over the entire time history of the motion. The principles introduced by the author have led to important developments, both theoretically and experimentally.

In the series of theoretical and experimental investigations, Bishop et al. (1973a) examined the functional representation of fluid forces in terms of memory effect and demonstrated making allowance for memory effect without loss of linearity. In the

successive studies Bishop et al. (1973b, 1973c) further applied the theory to oscillatory ship model testing with the Planar Motion Mechanism (PMM), and the analysis of directional stability and control, where only gentle manoeuvres can be described analytically under the conventional assumptions of quasi-steady flow. The fluid forces used in the equations of motion consist of two parts; one is due to the instantaneous state of motion and the other is due to the past history of the motion.

Perez y Perez (1974) expressed the motions of a ship in waves as linear responses to arbitrary exciting forces by means of convolution integral, where frequency independent non-linearities are considered to be part of the arbitrary forces. This method is used in the numerical simulation of sway, roll and yaw motions incorporated with the non-linearities associated with rudder-induced force.

Fujino (1975) also derived the equations of manoeuvring motion by use of impulse response function from frequency dependent hydrodynamic coefficients, which are referred to as 'stability derivatives', instead of constant manoeuvring coefficients. Also the equations of motion were derived by taking 'casualty' into consideration. From this investigation of impulse response function, it has been clarified that usual manoeuvring motion of a ship depends remarkably on the characteristics in the very low range of frequency.

Scragg (1977, 1979) made a comparison of the error in the manoeuvring predictions between linearised equations of motion with and without memory effects. After incorporating certain improvements into the impulse-response technique for the determination of hydrodynamic coefficients, experiments were conducted to measure a complete set of the coefficients. It was concluded that the impulse technique requires substantially fewer experiments than the regular-motion technique to obtain same results and regular-motion technique is incapable of evaluating the stability derivatives at very low frequencies. It was also determined that the significant errors occurred only during the initial phase of the manoeuvring, and that memory effects could be safely ignored for most deepwater manoeuvring problems.

Guo (1981) developed a non-linear theory of ship manoeuvring, based upon the hydrodynamics of arbitrary small motions superimposed upon a constant forward speed. The primary aim of the analysis was to establish the form of the second-order terms in the equations for manoeuvring by allowing only surging, swaying and yawing. The various potentials were found as solutions of integral equations constructed using time-dependent Green function and they exhibit, therefore, memory effects. Then the complete rigid body equations of motion were adjoined, resulting in a set of integro-differential equations. Numerical calculations for the determination of the kernel functions and coefficients were carried out in both time and frequency domain. Calculation results of the numerical model against the experimental data for Series 60 ship showed generally satisfactory agreement. However, viscous and lifting surface effects caused by the manoeuvring motions were not considered.

Loeser (1982) presented the usefulness of impulse response procedure as an experimental tool to determine the stability derivatives. The impulse response procedure was developed into a fast, versatile and accurate procedure for evaluating the linear hydrodynamic properties of a ship hull. The accuracy of the procedure was improved by least-square analysis of multiple impulses and the frequency range was extended to the zero frequency limit, where comparison was made with the similar results from regular motion tests. The effects of shallow water on ship manoeuvring were also demonstrated with different hull forms, Froude numbers and water depths and numerical computation of ship manoeuvres in shallow water was illustrated using the experimentally determined motion derivatives.

Bailey et al. (1998) proposed a practical hybrid approach, which fuses experimental manoeuvring data at low frequencies with theoretical seakeeping data at higher frequencies through identification of the relationship between seakeeping and manoeuvring hydrodynamic terms. The resulting frequency domain data can then be used to calculate an impulse response function, which includes the frequency dependence as well as some of the low frequency viscous characteristics. The frequency domain theoretical seakeeping data, calculated with reference to a set of

equilibrium axes, are first transformed to the body fixed axes used in manoeuvring. The quantitative differences between the theoretical and experimental damping data are then assumed to be due to viscous contributions at low frequencies. Addition of a simple ramp to the theoretical damping data, the zero frequency value chosen to bring the theoretical data into agreement with experimental values and the upper frequency taken to be the point at which the frequency domain data becomes a constant, has been demonstrated to show closer agreement between theoretically determined terms and experimental values over an extended frequency range.

Lee (2000) derived linear integro-differential sway-yaw equations with rudder deflection in regular waves and calculated the maneuvering motion of Todd Series 60 model. Also the indirect method using Fourier transformation was adopted to obtain the impulse responses of radiation and wave exciting forces. The differences between the integro-differential equation and the ordinary differential equation were discussed by comparing the response of a typical manoeuvre like the 10°-10° zig-zag test. The calculation was, however, restricted to a model which has good directional stability and ordinary hull form, and the effect of varying encounter angle during non-linear manoeuvring motion, such as turning manoeuvre in waves, was neglected.

Ballard et al. (2003) presented a time domain mathematical model for the prediction of heave and pitch motions in regular waves. In the linear model, the fluid forces acting on a vessel were expressed in terms of convolution integrals, thus accounting for fluid memory effects. The required impulse response functions were obtained from transform of frequency domain data evaluated using a three-dimensional potential analysis. Non-linear incident wave (Froude-Krylov excitation) and restoring force contributions were included in the mathematical model referenced to a body-fixed axis system. Predictions obtained this partly non-linear model were compared to both linear predictions and experimental results for two merchant ship hull forms.

3.3.2 Coordinates system

The motion of a ship at sea, or a body moving in a fluid, is allowed to move in all the six-degree-of-freedom, i.e. translation along three orthogonal axes and rotating about each of three axes. It is, therefore, necessary to choose an axis system to reference these motions with which the equations of motion are formulated, and the choice should be one which is most convenient for the development of the motion analysis (Abkowitz, 1964).

The traditional approach to the dynamics of manoeuvring, in which a ship is assumed to be rigid, involves the use of 'body-fixed axis' system. Abkowitz (1964) derived the equations of motion for a rigid body with six-degree-of-freedom to body axis and discussed their applications to ship dynamics. For the location of origin in the axis system, two cases were presented. One was the centre of gravity and the other was some arbitrary point within the body. Bishop and Parkinson (1969) demonstrated the effect of origin position on the oscillatory coefficients in the equations of motion since the centre of gravity of a real ship does not always coincide with that of prototype model in the experiment.

An 'equilibrium axis' system translates in a constant speed and often referred to as inertial coordinate system. The motions are defined by reference to equilibrium axis, which does not perform the unsteady motion. When used in the ship dynamics, the origin is normally taken to lie at a known longitudinal position on the centreline of the ship, e.g. midship. Formulations of wave force and ship motion in the axis systems of same orientation can simplify description of given problem and make equilibrium axis system obvious choice of the development of seakeeping theory (see, for example, see Beck et al., 1989).

Although the possession of two distinct approaches of describing ship motion introduces no difficulties of a fundamental nature, both techniques have some advantages and disadvantages. Moreover it is sometimes necessary to adapt

numerical or experimental results obtained using one of the two types of axes for use with the other. Bishop and Price (1981) compared the formulation of each axis system and developed their relationship. By formulating the dynamics of a ship undergoing a particular motion, firstly with reference to a body-fixed axis system and secondly with equilibrium axis system, the transformations between two axes systems are examined to adapt hydrodynamic data.

Hamamoto and Kim (1993) proposed a new coordinate system, referred to as 'Horizontal Body Axes' for describing the manoeuvring motion of a ship in waves. They used this new coordinate system to find equations of motion in a reasonable combination and use the formulas with respect to the hydrodynamic forces, which had been developed in the field of manoeuvrability, stability and seakeeping. Froude-Krylov forces and hydrodynamic forces are evaluated with respect to new coordinate system. Although theoretical comparisons were given between the new axis system and the existing systems, it did not present the effect of the new axis system in the numerical simulations.

Hamamoto and Kim (1993) carried out the time domain simulations for turning and zig-zag trial of a ship in waves. They aimed to find equations of motion in a reasonable combination of the manoeuvring motions in horizontal plane, rolling motion in lateral plane and seakeeping motion in vertical plane using aforementioned new coordinate system.

3.3.3 Combined model

Ship manoeuvrability can be significantly affected by the immediate environment such as wind, waves and current. Environment forces can cause reduced course-keeping stability or complete loss of the ability to maintain a desired course. They can also cause increased resistance to the forward motion of a ship, with consequent demand for additional power to achieve a given speed. Therefore it is important to simulate the behaviour of a ship manoeuvring in rough weather including the effect of wind, current and waves for the prediction of the ship's handling ability and for correcting trials for environmental conditions. Also in many other situations the effects of the environment conditions should be included for the assessment of manoeuvring performance, e.g. investigation of operability criteria, simulator studies and training in rough weather.

Traditional manoeuvring theory, however, has been developed on the strong basis of calm water environment with some exceptional considerations of wind and current (Martin, 1980), and it is unable to explain many aspects arising from the interactions between encountered wave and ship hull during manoeuvring motion in a seaway. Therefore motion of a ship in extreme seas, and in particular, dangerous situations that it is likely to face have been among the major subjects of ship hydrodynamic field. The dynamic characteristics of phenomena and complex mathematical notions concerning the simulation of such motions attracted a large number of researchers and a great amount of experience and knowledge has been gained through experimental and theoretical studies. Many simulation models and experimental methods at the early studies are, however, limited in their applicability by constraints or assumptions concerning, for example, wave direction, small wave amplitude, limited degrees of freedom or harmonic motion. To overcome such restrictions imposed on the early studies, numerical models have been developed to incorporate conventional manoeuvring and seakeeping theories (de Kat & Paulling, 1989; Zafer & Vassalos, 2003). While particular attention was paid to the ship behaviour and its simulation in the prescribed following and quartering seas from the viewpoint of

operation and safety of a vessel, similar attempts have been made to describe more generalised manoeuvring motions in regular waves and random seas.

Rydill (1959) extended linear equations for the unsteered motion of a ship in calm water to the unsteered motion in regular waves, using the Froude hypothesis to evaluate the wave excitation. The unsteered motion in regular waves is then investigated as a first step in the treatment of the steered motion and with a view to applying the results to the motion of models in manoeuvring tank. Finally the unsteered and steered motions in irregular long-crested waves simulating fairly severe sea conditions were investigated to establish the order of the mean angular deviation from course indicated by the linear theory and to demonstrate the efficacy of the control system with a filter in reducing the high frequency components of the rudder movement. However, it was concluded that the linear treatment did not adequately demonstrate the traditional difficulty of steering in following seas.

McCreight (1986) developed a six-degree-of-freedom time domain model for predicting the motions of ship manoeuvring in waves and wind, including wave induced motions. He combined the full non-linear calm water manoeuvring equations of motions with wave effects derived from the linear ship motion theory. Through the use of system identification techniques, added mass and damping data were approximated by the use of extended state space.

de Kat and Paulling (1989) developed a numerical model to determine the large amplitude motion of a steered vessel subjected to severe wave condition, including that may lead to capsizing. The various force components that occur in the large amplitude equations of motion were examined; potential force are based on an extension of linear theory, with the exception that integration of the incident wave pressure giving the Froude-Krylov force is performed over the total instantaneous wetted body surface, and first-order memory effects are considered. Additional non-linear viscous forces due to relative motion between body and fluid are modelled empirically. Good agreement was found between predicted motions and

experimental results, both for capsizing and non-capsizing conditions in following and quartering seas.

Ottosson and Bystrom (1991) developed a numerical tool which can analyse the time domain manoeuvring performance of merchant and naval ships in calm water and in waves. The theoretical method adopted combined the manoeuvring and seakeeping mathematical models, using the superposition principle and interaction effects such as the influence of wave-generated water particle velocities on the manoeuvring hydrodynamic forces, or influence of rudder-induced forces in ship motions in waves. Furthermore, the fact that the wave-induced forces were simulated in time domain provided solid ground for good representation of the couplings between sway-roll-yaw, including the non-linear effects. However, the hydrodynamic forces representing the manoeuvring motions, i.e. low frequency forces, were calculated conventionally as on calm water and did not include the effects generated by the change of the instantaneous shape of the immersed hull in the wave.

Westlake et al. (2000) investigated the motion responses of displacement mono-hulls in oblique regular waves with hydrodynamic coefficients obtained from conformal mapping scheme. To overcome the weakness arising from conventional assumption of strip theory, the relative position of the body induced by the incident wave are considered and coupled equations of motion in five-degree-of-freedom are employed. Subsequently, the wave forces on actual underwater part of the hull are calculated together with the geometric, hydrostatic and hydrodynamic properties on the time stepping scheme. Comparisons with the results of traditional strip method confirmed significant improvements through the coupling mechanism and mapping procedures.

Bailey et al. (1998, 2002) established a "unified mathematical model" which is an attempt to merge seakeeping theory with manoeuvring models in the form of a time simulation. They demonstrated that linear manoeuvring and seakeeping performances can be investigated using a six-degree-of-freedom mathematical model, which combines the knowledge of impulse response functions form linear seakeeping theory with traditional manoeuvring equations of motion. In their

previous study, the traditional manoeuvring derivative Y_r was approximated as follows (Bailey et al., 1998)

$$Y_r(\omega) = -B_{26}(\omega) - \bar{U}A_{22}(\omega) \tag{3.2}$$

where $B_{26}(\omega)$ and $A_{22}(\omega)$ are frequency dependent sway-yaw damping and sway added mass coefficient, respectively. Convolution integral was used to model the first-order linear manoeuvring derivatives and Froude-Krylov forces were calculated at the instantaneous water surface around the hull using quadrilateral panel elements and summing contributions of the fluid actions on each panel. The theory was validated against seakeeping theory on a straight course in waves and against a calm water manoeuvring model for a turning circle and zig-zag manoeuvres with a Mariner type ship.

Figure 3.12 illustrates the predicted path of a turning circle manoeuvre in waves of varying wavelength and of 1.0m amplitude with the orientation of ship presented at intervals of 50 seconds and roll motion excluded. As the ship proceeds around the circle, the encounter frequency changes continuously and this influences the position of the ship in the wave and the instantaneous wetted surface. Compared with the calm water results, the path is more elliptical in shape and is of greater diameter at large wavelength ($\lambda/L = 1.0$), while turning diameters become similar to calm water result and drifted distances to the wave propagation are also reduced at smaller wavelengths ($\lambda/L = 0.5, 0.25$).

Artyszuk (2003) formulated the wave forces to be included in the ship manoeuvring mathematical model. A current state-of-the-art in this subject is thoroughly investigated in the aspects of data availability and validity and the impact of first-order wave force was briefly characterised. A strong effect of the second-order force was proved through a simulation of turning test in regular wave.

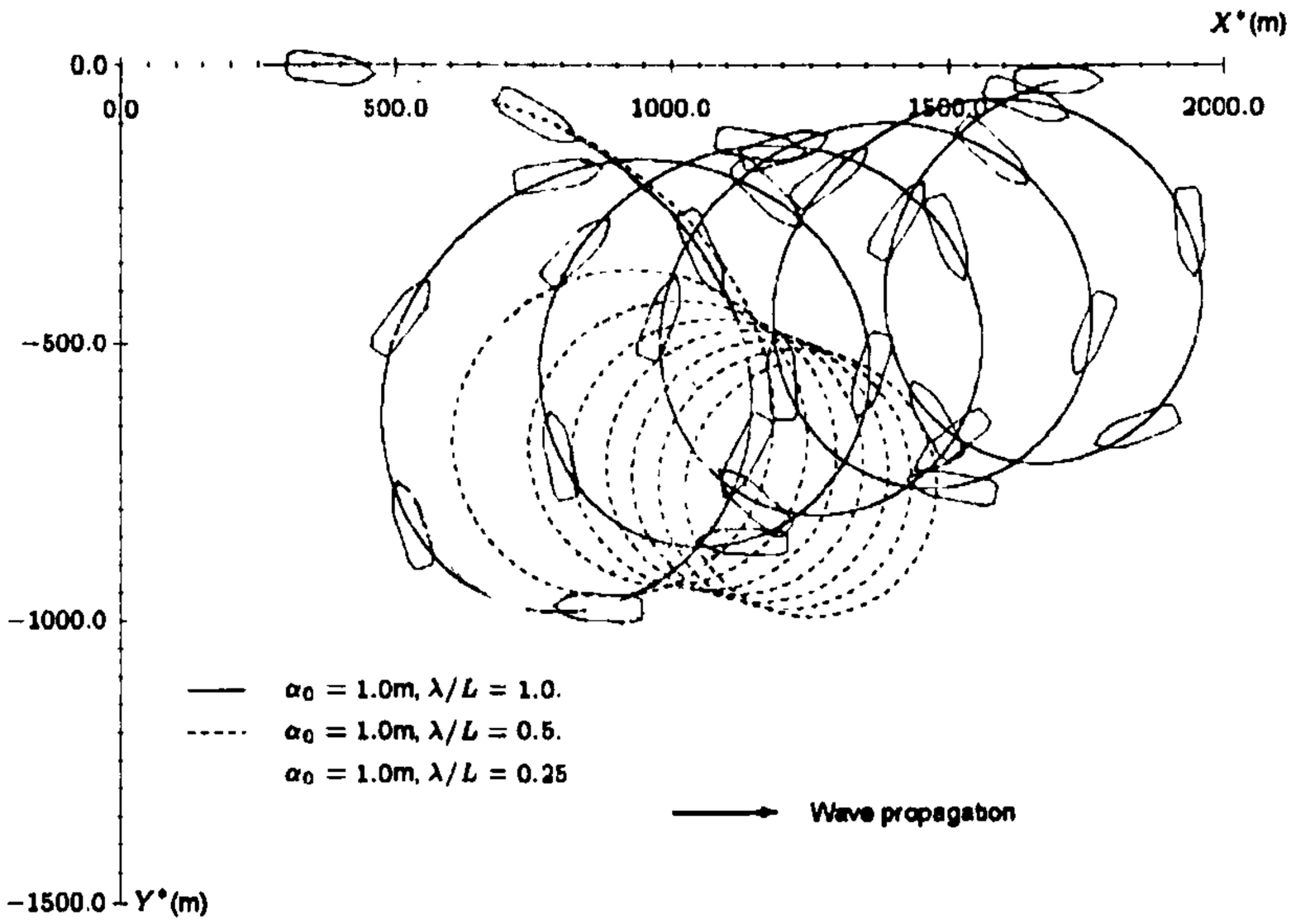

Figure 3.12 Turing circle manoeuvre of Mariner ship (Bailey et al., 2002)

Ueno et al. (2001) proposed calculation method of steady horizontal wave drift force due to short waves acting on ships in manoeuvring motion. The effects of manoeuvring motion on steady drift force are taken into consideration by treating the action of non-uniform flow around a ship upon deformed wave field. Later, Ueno et al. (2003) carried out a free running model test using a VLCC model ship in regular waves with various wave conditions. In 35° turning test in waves, drifting speed, drifting direction, average yaw rate, oblique angle and ship speed ratio during turning motion were obtained. First and second overshoot angles of zig-zag test in waves were measured, and stopping distance and final state heading angle were also shown as functions of wavelength and initial ship heading to waves. All measurement data were compared with those obtained from calm water tests of full loading and ballast conditions. Effects of wavelength and initial heading angle to waves together with the effect of loading condition upon manoeuvring motion were discussed based on these measured data. An example of theoretical calculation for manoeuvring motion of the model ship in wave was provided for further discussion.

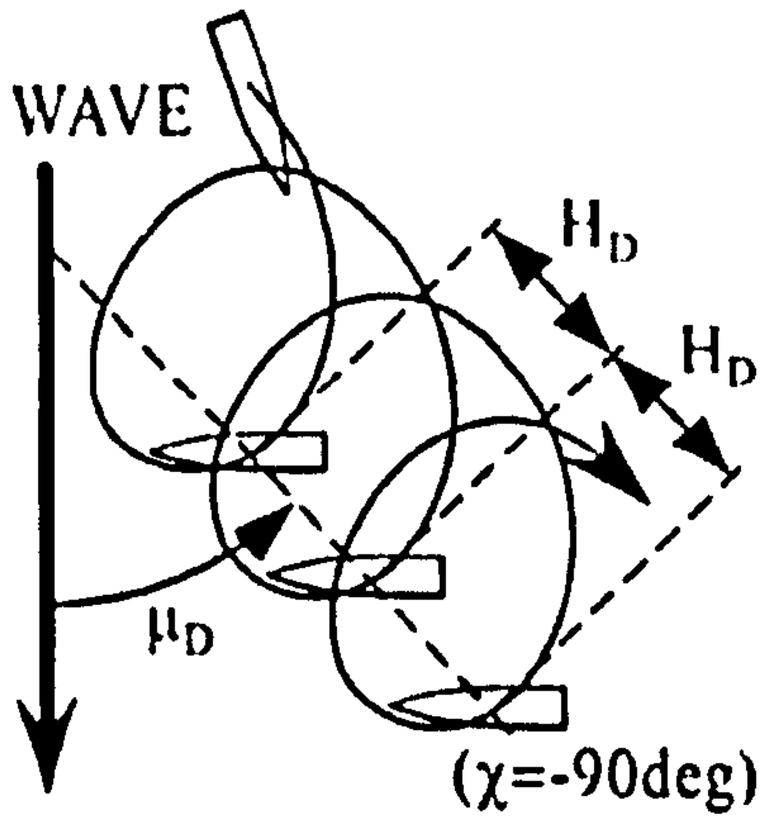

Figure 3.13 Definitions of drifting distance and drifting direction in turning test (Ueno et al., 2003)

Figure 3.13 illustrates the definitions of drifting distance H_D and drifting direction μ_D used in Ueno's study. Drifting distance H_D is defined as distance between successive ship positions in which wave encounter angle χ is equal to -90°. Drifting direction is defined as offset angle from wave propagating direction to moving direction of positions of a ship in which wave encounter angle χ is equal to -90°.

Figure 3.14 shows an example of 35° turning test in wave of 0.4 wavelength ratio. Wave drift forces are calculated using Ueno's method. Although large differences of drifting distance and direction are observed in the trajectory of the turning test, time histories of yaw rate, ship speed, oblique angle and heading angle explain qualitative similarity to the measured data. This comparison implies that improvement is required for practical application of Ueno's method to predict wave drift forces correctly.

Zafer and Vassalos (2003) presented the formulation of the proposed new set of motion equations and the associated terms in the equations together with a solution procedure. A fully non-linear coupled six-degree-of-freedom numerical model was developed with frequency dependent coefficients incorporating memory effects in waves with a new axis system that allows straightforward combination between seakeeping and manoeuvring models whilst accounting for extreme motions. Comparisons of a fishing vessel and container ship were made to investigate the advantage of new axis system and memory effect with respect to heading angle.

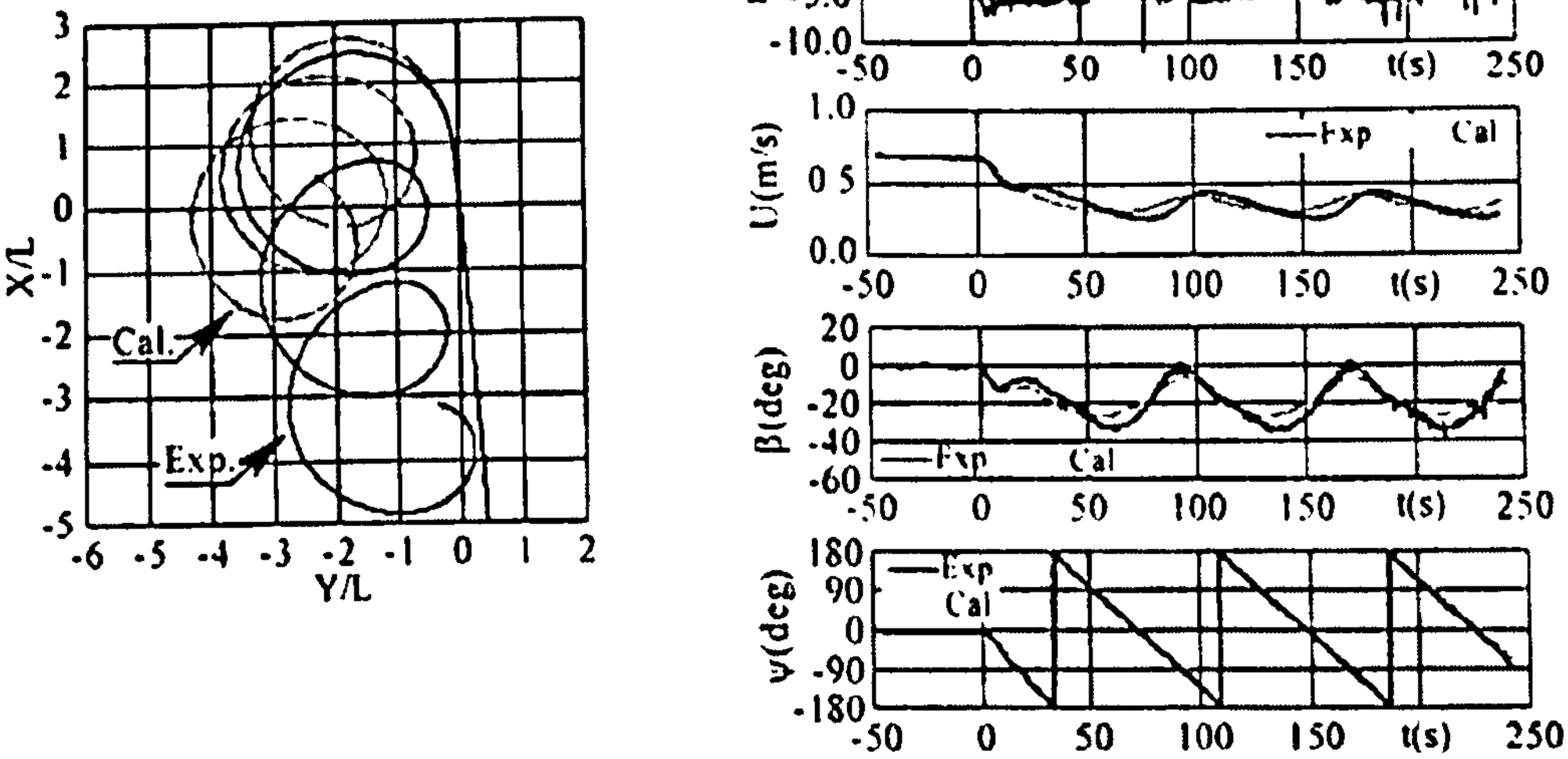

Figure 3.14 Trajectory and time history of ship motion in 35° turning test in wave of 0.4 wavelength ratio in full load condition (Ueno et al., 2003)

Fang et al. (2005) developed a simplified six-degree-of-freedom mathematical model encompassing calm water manoeuvring and traditional seakeeping theories to simulate the ship turning circle test in regular waves. Horizontal body axes system was employed to present equations of manoeuvring motion in waves. All corresponding hydrodynamic forces and coefficients for seakeeping were assumed to be time varying and calculated by strip theory. For simplification, the added mass and damping coefficients were calculated based on the variation of encounter frequency in the constant draft of calm water. The non-linear mathematical model was validated for simulating the turning circle of a containership in sea trial conditions.

3.3.4 Database method

In order to provide the manoeuvring quality of a new ship design, traditionally model experiments have been widely used for the measurement of force acting on either captive or free running model test. Unfortunately manoeuvring model experiments are confined to some prejudices, i.e. these are expensive and highly time-consuming. Actually a large effort is required when the identification of a complete set of all linear and non-linear coefficients in the equations of motion is demanded, for example an input of simulator for various operations.

One alternative to the expensive model tests is the application of computational method, which widely known as Computational Fluid Dynamics (CFD). Although CFD method has been rapidly improved during the last decade some improvements are still required due to some inevitable and relatively high cost processes, e.g. grid generation. The computational times and capacity needed to obtain certain convergence are not small.

The manoeuvring derivatives can be obtained by aforementioned model tests or CFD. At the initial design stage, however, a quick application will be demanded to assess the ship manoeuvring performance. From these points of view, more economically efficient alternative is to use empirical regression formulas, which have been presented by several researchers for the linear and non-linear manoeuvring derivatives used in the sway and yaw equations of motion. This empirical prediction method are simply applicable for various types of ship and very useful in accounting for the effect of principal dimension and the changes of propeller and rudder specifications in manoeuvring predictions even at the early design stage.

A brief review about database method for the prediction of manoeuvring derivatives is as follows. Wagner-Smitt (1970, 1971) examined values of the velocity derivatives measured by means of a PMM tests. In a similar study, Norrbin (1971) analysed a number of experimental measurements of the velocity derivatives. Inoue et al. (1981)

carried out rotating arm tests, which covered a wide range of hull forms at various load conditions including trim and attempted a correlation of the velocity derivatives with hull form parameters. Clarke et al. (1983) presented empirical formulas for the linear acceleration and velocity dependent manoeuvring derivatives from a basis of hull geometry. Kijima et al. (1990) suggested the approximate formulas for estimating the hydrodynamic forces acting on ship in any loading conditions as follow,

$$\begin{aligned} Y'_\beta &= \frac{1}{2}\pi k + 1.4C_B B/L \\ Y'_r - \left(m' + m'_x\right) &= -1.5C_B B/L \\ N'_\beta &= k \\ N'_r &= -0.54k + k^2 \end{aligned} \tag{3.3}$$

where $k = 2d/L$. Kijima (1990) also suggested corresponding expressions in a trimmed condition with the non-dimensional trim parameter, $\tau'(=\tau/d_m)$, where τ is trim quantity and d_m is mean draught.

Almost all of the papers mentioned so far used regression analysis of measurement data obtained from captive model experiments and employed global hull parameters for set of predictor variables, e.g. C_B, L/d, B/d, etc. and combination of these. In the 1990's, it was realised that the shape of aft body has a significant influence on the overall manoeuvring performance and yaw stability, particularly for the container vessels whose aft hull forms were drastically changed from the propulsion consideration.. To express characteristics of aft hull shape Mori (1995) proposed prediction formulas with additional four parameters: e_a and e'_a for fullness of aft run, σ_a aft sections fullness metric, and K form factor.

Fujino (1996) and Kose et al. (1996) showed for a few, mainly full-bodied ships that new formulas using the parameter σ_a improve the accuracy of estimations. Kijima et al. (2000) revised the original expressions of Kijima et al. (1990) and again presented

approximate formulas particularly for aiming the difference of stern hull shape. The formulas of whole linear and non-linear coefficients of sway and yaw equations are obtained from database involved with 15 kinds of ships and their 48 loading conditions.

Meanwhile the linear manoeuvring derivatives have become important because of the demand of the course stability prediction in the IMO Standards. Because the linear derivatives are strongly affected by the stern hull form particularly for full ships, many researches have been concentrated for better expression of them.

3.4 Concluding Remarks

The behaviour of ships in a seaway has been an important subject as the motions and loads have a strong impact on the safety, economics and operational performance of a vessel. With the rapid changes of ship hull forms and increase of service speed, the prediction of performance even in the early design stage becomes more important. Moreover, as the importance of safety and reliability increases the need for accurate prediction of motion behaviour in a seaway becomes essential in the development of theoretical method. Although the developments of fully non-linear hydrodynamic methods have been attempted in the past, their practical application is still a difficult task. Linear prediction tools in combination with non-linear effects benefit from the viewpoint of easy assessment techniques, like the seakeeping assessment in the frequency domain.

Current, state-of-the-art time domain numerical approaches for manoeuvring simulation in a seaway now employ non-linear six-degree-of-freedom mathematical models incorporating memory effects by adopting the impulse response function representation. The hydrodynamic coefficients and wave-induced force in the manoeuvring model can be obtained from the hydrodynamic data set in the seakeeping calculations. New axis systems might be introduced for the transformation of the coefficients obtained and conventional manoeuvring derivatives still play an important role to account for the non-linear viscous effect, which is neglected in potential theory.

Deriving from this background, it is now required to have a coupled non-linear six-degree-of-freedom model with frequency dependent coefficients, incorporating memory effects in random waves. To secure the reliability of the hydrodynamic data set, successful development of three-dimensional panel method should be put in the first place. The mathematical model would also be enhanced by providing straightforward combination of seakeeping and manoeuvring theories accounting for general motions. An outline of the approach will follow in the next Chapter.

Chapter 4. Approach Adopted

4.1 Background

There are two conventional theories on the performance assessment of a ship travelling with forward speed in a seaway: seakeeping and manoeuvring. Although they have many similarities in the point that both theories describe behaviour of a ship, they have been studied and developed separately in the conventional researches.

Seakeeping theory is mainly focused on the assessment of operation of a ship at a specific speed and heading in a sinusoidal regular or irregular wave. To solve the responses and forces of a ship numerically to the wave disturbance, it is general to use potential theory with the assumption of inviscid and irrotational fluid flow around body surface. The fluid actions are expressed in terms of hydrodynamic added mass and damping coefficients and wave excitations depending on wave frequency or encounter frequency.

Conventional manoeuvring theory is, however, associated with mainly horizontal plane motions of a ship, i.e. sway and yaw, which are restricted in calm water and its coupling effects on the vertical plane motions, i.e. heave and pitch, are often neglected. Because of this presumed basis, the manoeuvring derivatives are generally found using extrapolation from the data obtained in PMM tests. Moreover manoeuvring theory is restricted to an assessment of the stability of a vessel from a prescribed reference motion, i.e. turning circle or zig-zag manoeuvres, without taking into account the dynamic conditions of a ship and influences of random wave.

To evaluate the response of a ship in a wave, an integrated mathematical model is developed in the theoretical manner. This integrated model has its fundamental base

on both manoeuvring and seakeeping theory and thus it is required to convert hydrodynamic data sets in the one theory to those in the other theory. In the present project hydrodynamic coefficients are calculated in the numerical tools based on seakeeping theory and they are converted to impulse response functions for integrated mathematical model.

- Following above understanding, the approach to develop an integrated mathematical model contains three major steps.
  - Development of numerical tools based on seakeeping theory
  - Development of integrated mathematical model for a general six-degree-of-freedom motion in a wave
  - Validation of established mathematical model

4.2 Development of Seakeeping Theory

As seen from aforementioned background, it is important to develop reliable numerical tools to ensure the hydrodynamic coefficients and wave forces. The method adopted in this chapter is based on the formulation of the seakeeping problem in frequency domain, in order to find fluid forces exerted on a ship in a regular wave.

The theoretical formulation starts with the derivation of the governing equations for the boundary value problem of potential flow and it leads to linearised radiation and diffraction problems. Solutions of two problems are obtained by solving integral equations over the mean wetted hull surfaces with distribution of a three-dimensional Green function.

The Green function representing a translating pulsating source singularity with forward speed is distributed in either quadrilateral panel of constant strength or high-order panel with variable strength and calculated over the discretised body surface, which represents the hull form. Since the original form of Green function contains double integrals, which are very complicated and time-consuming to calculate, they are changed to single integrals in terms of exponential integrals. Throughout this approach the speed and frequency dependent hydrodynamic coefficients, wave forces and motion response amplitudes can be calculated.

For validation of the numerical code, Wigley hull and Todd Series 60 model with block coefficient 0.7, which have been widely used in a hydrodynamic field, are chosen and the calculation results of hydrodynamic added mass, damping coefficients, wave exciting forces and motion responses are compared with the ones from published numerical results and experimental measurements.

Further investigation to calculate second-order forces is carried out. The "near-field" method is adopted to find mean second-order forces by direct pressure integration

over mean wetted hull surface. It is possible to express second-order forces with first-order velocity potential and its derivatives without solving the second-order potential problem. Numerical calculations of barge and Todd Series 60 ship are presented and investigations of the influences of ship heading on the wave drift forces are demonstrated.

Although a ship motion in a wave can be assumed to be dependent on its frequency and heading angle, it is difficult to calculate these frequency dependent hydrodynamic forces, except for Froude-Krylov force term, in the time domain calculation. Therefore the mathematical model to be developed for general ship motion in a seaway has its background partly in the seakeeping theory to enable the use of frequency dependent hydrodynamic data sets. Once the hydrodynamic data sets, e.g. added mass and damping coefficients, first-order wave exciting force and mean second-order force are estimated successfully in the present approach, these will be vital input for the integrated mathematical model to be formulated in the next approach.

4.3 Development of Integrated Manoeuvring Model

As a second step of approach, integrated mathematical model for the motion of a ship in a seaway is formulated. Since the coordinate systems in both manoeuvring and seakeeping theories are different, adequate coordinate system should be chosen and axis transform between two theories should be included. Space-fixed and upright body-fixed coordinates systems are utilised to express the motion of a ship.

Added mass and damping coefficients are compared with manoeuvring derivatives, which are also frequency dependent, using axis transformation to space-fixed coordinates and their relationship is identified. External forces in the equations of motion are composed of hull, wave excitation, propeller and rudder forces. Hull forces are expressed in terms of convolution integrals with impulse response function representation, where it is possible to describe arbitrary motion and consider memory effects of fluid action. Kernel functions can be calculated by inverse Fourier Transform using either added mass or damping coefficients.

Numerical implementation to solve the equations of motion is developed and time domain simulation using a fourth-order Runge-Kutta method is performed. Impulse response function calculated from either added mass or damping coefficients are compared. Proposed mathematical model is first validated by comparison with experiment data performed in various test environments. Standard manoeuvring test like turning circle and zig-zag manoeuvres are performed and investigation of wave effects is made by comparing with the results obtained by traditional calm water manoeuvring test.

Chapter 5. Formulation of Three-Dimensional Potential Flow

5.1 Preamble

To predict the behaviour of a ships sailing at sea, this chapter begins with the description of three-dimensional flow around a rigid body, which forms the basis for the computation of a boundary value problem. The formulation of the given problem will be developed for a ship travelling with or without forward speed. The flow field will be described as a well-known potential flow with the assumptions of ideal fluid, e.g. inviscid and irrotational fluid, and then the velocity field can be expressed in terms of the gradient of an unknown velocity potential, which satisfies Laplace's equation. Since the velocity potential should also satisfy the exact boundary conditions prescribed in the fluid domain, this leads to a non-linear problem, in which an analytical solution is hardly available. Therefore, a theoretical formulation of the boundary value problem will be carried out by means of a simplification method of the complex non-linear problem. To obtain the velocity potential, further development of boundary integral equation adopting three-dimensional free surface Green function method will be followed.

5.2 Coordinate systems

In order to describe flow field and motions of a ship translating with a constant forward speed, it is required to define three different coordinate systems as shown in Figure 5.1. All these are right-handed orthogonal coordinate systems and either fixed to a relevant point or moving with constant speed.

The space-fixed coordinate system $O-X_0Y_0Z_0$ is fixed to the earth with the origin at any location. The X_0 axis is normally set in the initial direction of ship's forward speed. The Z_0 axis is vertically upward and the X_0Y_0 plane is usually coincident with the undisturbed free surface. This space-fixed coordinate system can be also used to define incident wave and express free surface boundary condition.

The steady moving system $o-xyz$ translates on the calm water level with the same constant velocity of the ship in the positive X_0 direction, and is referred to as inertial coordinate system. The x axis coincides with X_0 axis and the z axis points vertically upward again. The xy plane is also aligned with the calm water level. Therefore transformation from space-fixed coordinate system $O-X_0Y_0Z_0$ to moving coordinate system $o-xyz$ is given by linear relation as

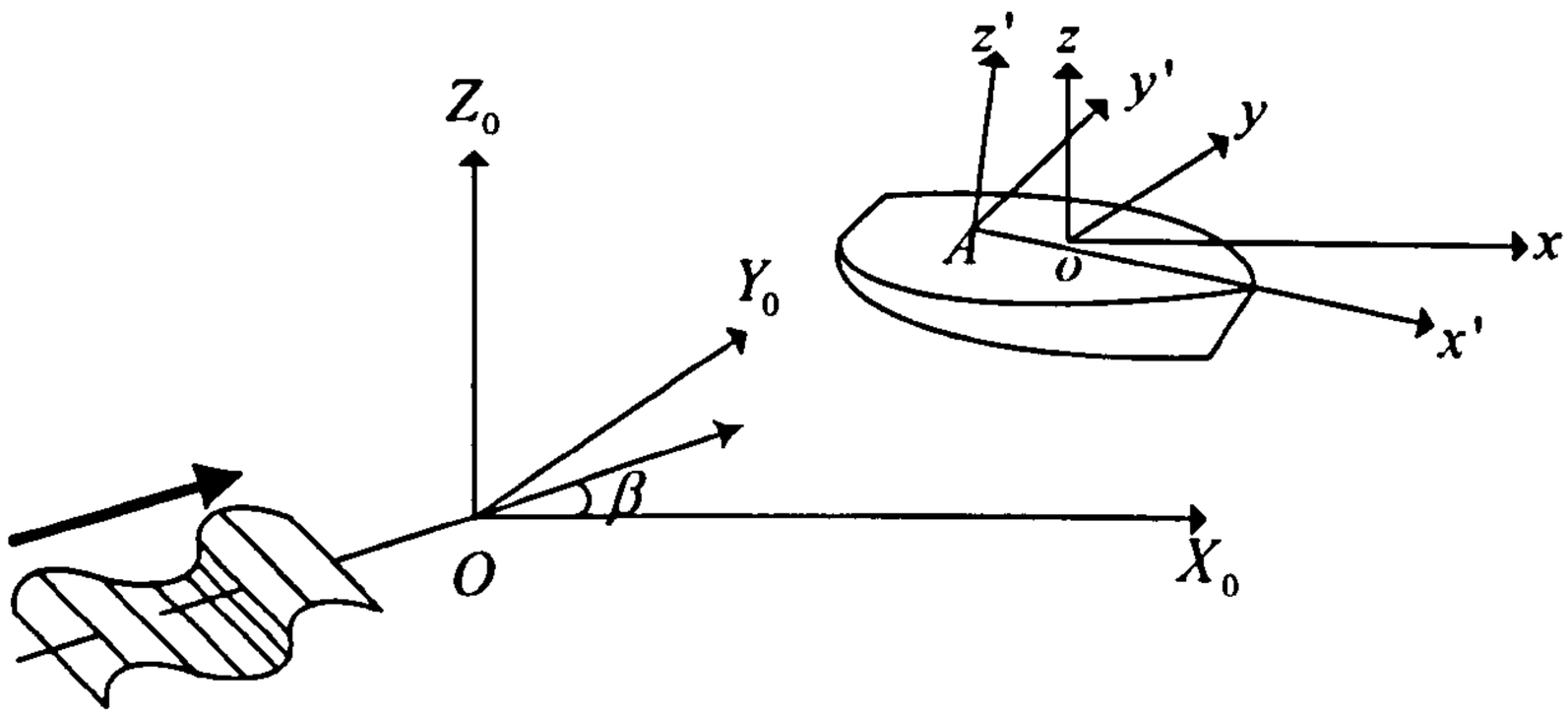

Figure 5.1 Coordinate systems

$$\mathbf{x} = (x, y, z) = (X_0 - Ut, Y_0, Z_0) \tag{5.1}$$

The body-fixed coordinate system $A - x'y'z'$ is fixed with ship with the assumption that hull form of the ship has port/starboard symmetry plane and the $x'z'$ plane is plane of that symmetry. The $x'y'$ plane is coincident with the ship's calm waterplane with positive x' axis pointing to bow, y' axis to port and z' axis upward. The origin is therefore located in the intersection line of centre plane and calm waterplane and often chosen amidships.

The motions of the ship are determined by the orientation of body-fixed coordinate system $A - x'y'z'$ relative to the inertial coordinate system $o - xyz$. Consequently these motions are described in the inertial coordinate system $o - xyz$ and have six degrees of freedom. The six components with complex amplitude ξ_j are referred as surge, sway and heave for translation and roll, pitch and yaw for rotation respectively as shown in Figure 5.2.

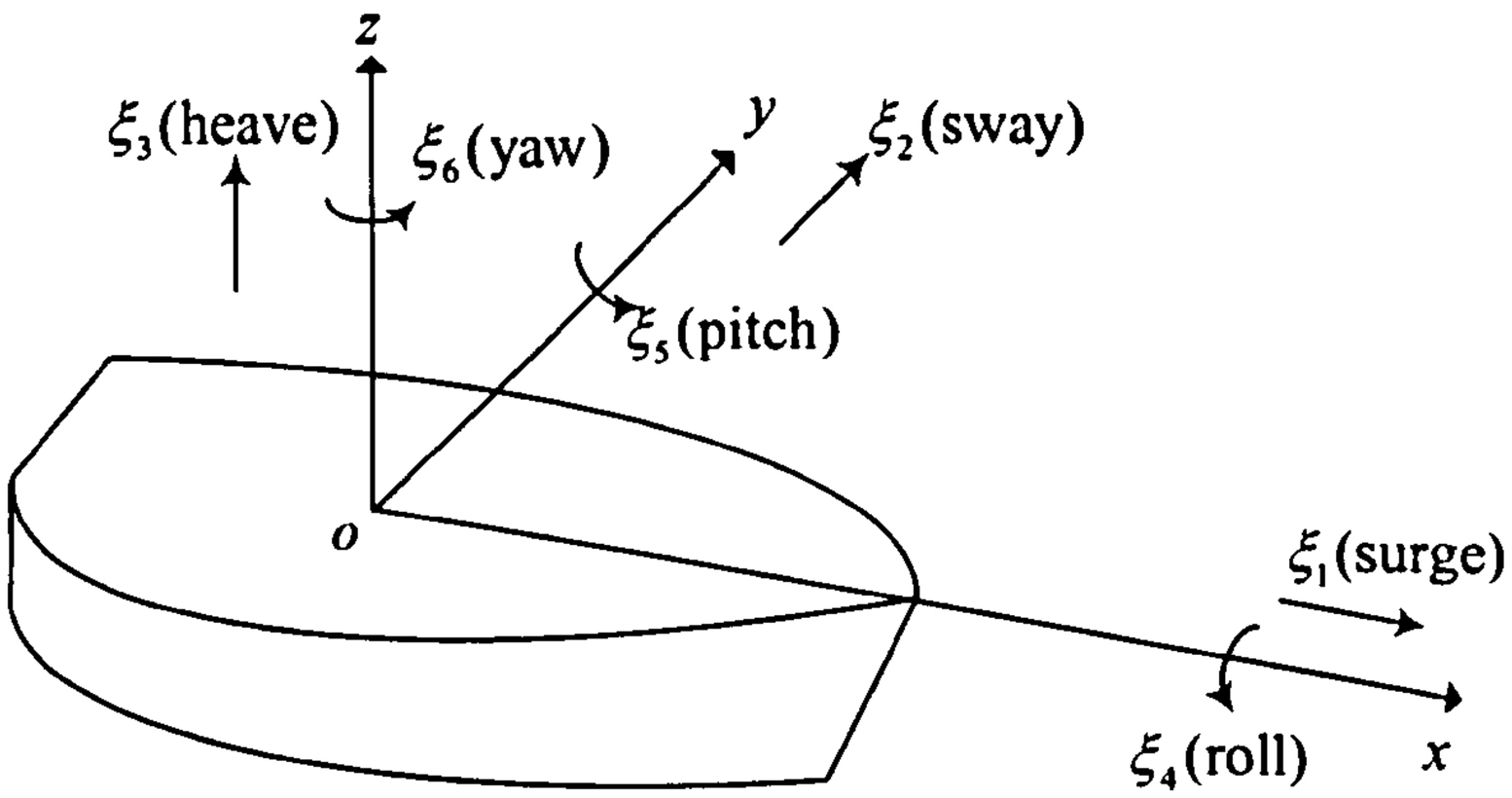

Figure 5.2 Definition of body motions in six degrees of freedom

5.3 Boundary Value Problem

5.3.1 Formulation of the boundary value problem

This section deals with the flow of ideal fluid, that is, fluids which are inviscid and incompressible. The results with this assumption are therefore limited to flow fields in which viscous effects of the fluid are negligible and compressibility of the fluid is unimportant. The mathematical simplification, which results from neglecting viscous and compressible effects, is great and consequently the topic of ideal fluid is mathematically the best understood. And any phenomena which are predicted by the governing equations will be due to the inertia of the fluid.

Since the fluid is assumed to be ideal, the equation of mass conservation can be expressed without density terms due to incompressible property. The equation of momentum conservation for an inviscid fluid is reduced to the Euler equation. That is, the governing equations of the velocity and pressure fields for an ideal fluid are

Continuity equation:

$$\nabla \mathbf{u} = 0 \tag{5.2}$$

Euler equation:

$$\frac{\partial \mathbf{u}}{\partial t} + (\mathbf{u} \cdot \nabla)\mathbf{u} = -\frac{1}{\rho}\nabla p + \mathbf{f} \tag{5.3}$$

where $\mathbf{u}$ is velocity vector, ρ is density of the fluid, p is pressure and $\mathbf{f}$ is body force vector.

If the flow of an ideal fluid around a body originates in an irrotational flow, such as uniform flow, for example, the flow will remain irrotational even near the body. That is, the vorticity of the fluid is zero everywhere in the fluid. Then, since the vorticity

is the curl of velocity vector, the condition of irrotationality will be satisfied identically by choosing velocity vector as follows

$$\mathbf{u} = \nabla \Phi \tag{5.4}$$

The scalar function Φ is called the velocity potential, and the flow fields which are represented in the form of equation (5.4) are frequently referred to as potential flow. In order to find the equation which the velocity potential satisfies, the expression given in equation (5.4) is substituted into the continuity equation given in equation (5.2) to give

Laplace's equation:

$$\nabla^2 \Phi = 0 \tag{5.5}$$

The main advantage of introducing the concept of velocity potential from irrotational flow is that the problem is reduced to a scalar problem rather than a vector field problem. Once the velocity potential is solved from the governing equation of motion, the velocity field can be determined by taking the gradient of the velocity potential. Thus by solving equation (5.5) and utilising equation (5.4), the velocity field can be established without directly using equation of motion given in equation (5.2). Solving Laplace's equation for the velocity potential determines the velocity field only and to obtain pressure distribution across the fluid domain direct use of momentum equation should be made. Instead of using Euler equation given in equation (5.3), its integrated form which is referred to as Bernoulli equation, will be used. So the pressure field can be determined from following equation

Bernoulli equation:

$$p - p_a = -\rho\left(\frac{\partial \Phi}{\partial t} + \frac{1}{2}\nabla \Phi \cdot \nabla \Phi + gz\right) \tag{5.6}$$

From foregoing, it is evident that a simpler form of the governing equations exists for potential flow.

5.3.2 Boundary conditions

Since Laplace's equation has many solutions due to its elliptic type, appropriate boundary conditions should be prescribed in the fluid domain to obtain exact solution of a given problem. For a free floating body in an infinite extent of the fluid, the boundaries enclosing the fluid consist of the free surface, the sea bottom, the control surface at far field and the wetted hull surface, see Figure 5.3. On each of these boundaries, a proper condition should be imposed to ensure a unique solution of the Laplace's equation.

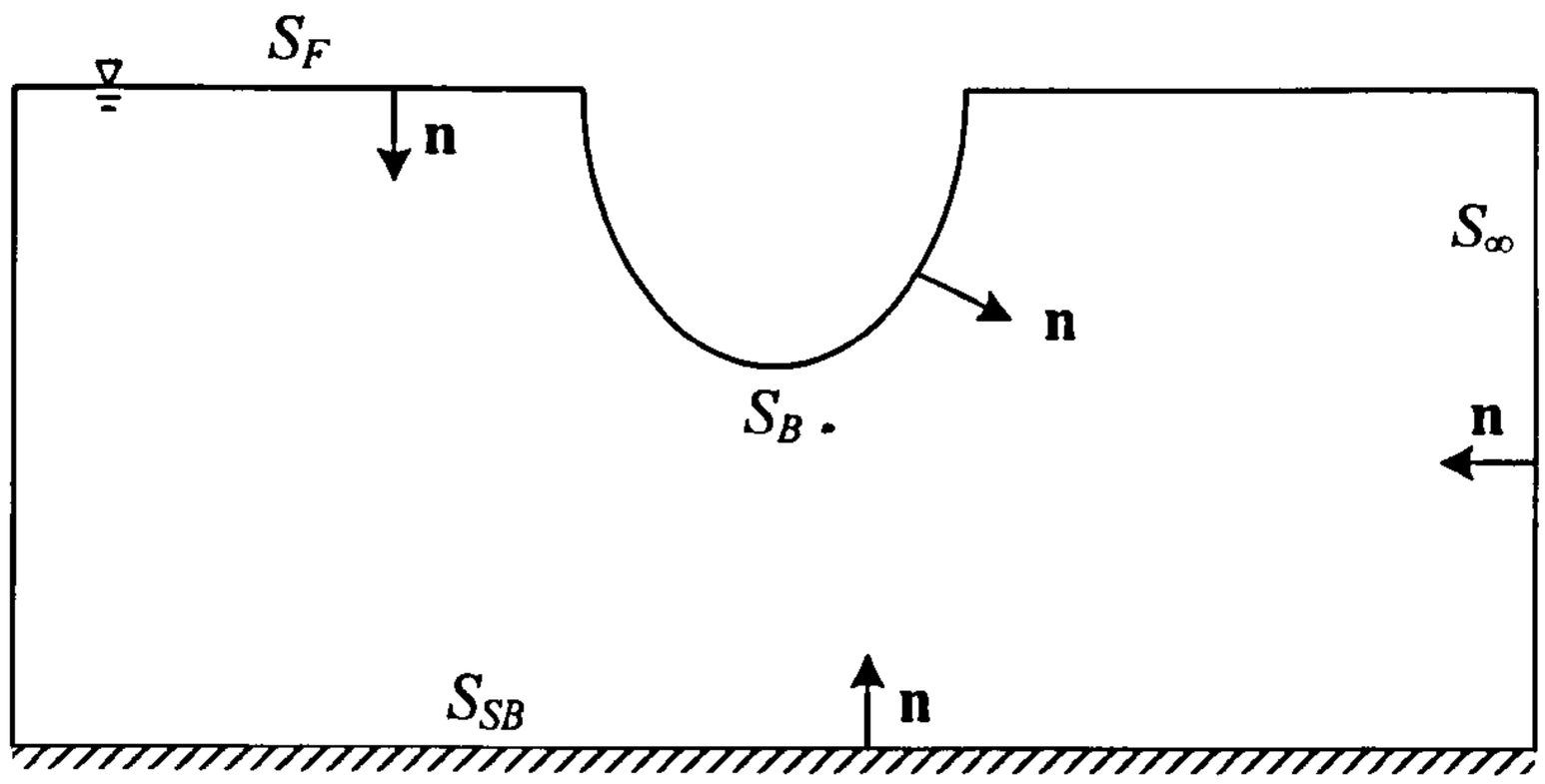

Figure 5.3 Boundaries in the fluid domain

5.3.2.1 Free surface boundary condition

Any point of the free surface can be defined by its elevation and time in the space-fixed coordinate system $O - X_0 Y_0 Z_0$ as

$$Z_0 = \zeta(X_0, Y_0; t) \tag{5.7}$$

The kinematic and dynamic conditions must be satisfied on the free surface defined in equation (5.7). The kinematic boundary condition requires that the normal velocities of the fluid particle and of the free surface are equal and tangential velocity

is zero. The dynamic boundary condition specifies the pressure on the free surface to be equal to the atmospheric pressure, which can be obtained from Bernoulli equation. Thus the kinematic and dynamic boundary conditions can be expressed as

Kinematic boundary condition:

$$\frac{D}{Dt}(\zeta - Z_0) = 0 \qquad \text{on } Z_0 = \zeta \tag{5.8}$$

Dynamic boundary condition:

$$\Phi_t + \frac{1}{2}\nabla\Phi\cdot\nabla\Phi + gZ_0 = 0 \qquad \text{on } Z_0 = \zeta \tag{5.9}$$

where the substantial derivative $D/Dt = \partial/\partial t + \mathbf{u}\cdot\nabla$ is defined in the space-fixed coordinate system and the pressure in the Bernoulli equation has been taken as zero without loss of generality.

Since equation (5.9) hols on the free surface for all time, its substantial derivative can be set equal to zero. This gives an alternative boundary condition for the velocity potential.

$$\Phi_{tt} + g\Phi_{Z_0} + 2\nabla\Phi\cdot\nabla\Phi_t + \frac{1}{2}\nabla\Phi\cdot\nabla(\nabla\Phi\cdot\nabla\Phi) = 0 \quad \text{on } Z_0 = \zeta \tag{5.10}$$

Since this free surface boundary condition is highly non-linear due to its quadratic form and the free surface is not known a priori, it is quite difficult to constitute a practical tool to calculate exact solution. Therefore a simplified free surface boundary condition should be formulated by means of linearization in order to cancel higher-order terms.

5.3.2.2 Body boundary condition

Since the boundary enclosing ship's hull surface is already known, only kinematic boundary condition is required. On the submerged portion of the ship's hull surface S_B, the normal velocity is equal to that of the adjacent fluid. This boundary condition implies that the fluid does not penetrate the body boundary and that there are no gaps between the fluid and the body boundary. The appropriate body boundary condition can be expressed as follows

$$(\mathbf{u}_s - \mathbf{u}) \cdot \mathbf{n} = 0 \qquad \text{on } S_B \tag{5.11}$$

where $\mathbf{u}_s$ is the local velocity of the ship's wetted surface. The unit normal vector $\mathbf{n}$ is defined to point into the fluid domain as shown in Figure 5.3.

5.3.2.3 Sea bottom condition

Since the fluid disturbances decay exponentially with water depth, the infinite depth sea bottom condition requires simply that the velocity potential and its derivatives vanish,

$$\frac{\partial \Phi}{\partial n} = \frac{\partial \Phi}{\partial z} = 0 \qquad \text{at } z \to -\infty \tag{5.12}$$

5.3.2.4 Radiation condition

Although the boundary conditions on all the physical boundaries, i.e. the free surface, body surface and sea bottom, have been prescribed, it is not sufficient enough to ensure a unique solution to the problems imposed to the unbounded fluid domain. Using a fictitious boundary surface S_∞, which extends from sea bottom to the free

surface at infinity, so-called radiation condition can be described to represent a physical phenomenon of energy vanishment at infinity.

For example, the fluid motion produced by an oscillating body without forward speed are outgoing waves in all horizontal directions and vanishes at infinity. The generated wave must be a progressing wave moving away from the source of disturbance at infinity. For the case of Kelvin waves due to a body with a steady forward speed in calm water, the wave disturbance is generated downstream only. For an unsteady flow due to an oscillatory motion of the body moving with constant speed in waves, the radiation condition is much complicated. This is because the propagation of surface waves generated by the interaction of the body motions and incident wave depends on two parameters, i.e. the forward speed and the frequency of oscillation. The steady waves (Kelvin waves) due to the forward motion interact with the unsteady waves generated by the diffraction of the incident waves and the radiated waves, the resultant waves can propagate upstream at certain condition. Although the nature of the unsteady flows is complicated, it is assumed that the potential Φ vanished at infinity excluding incident wave potential.

$$\Phi \propto \frac{1}{\sqrt{r}} e^{-ikr} \qquad \text{at } r \to \infty \qquad (5.13)$$

5.4 Simplification of Non-linear Problem

In the foregoing section, we have formulated the boundary value problem to solve the velocity potential, which satisfies Laplace equations as well as prescribed boundary conditions like the free surface boundary condition, sea bottom boundary condition, body boundary condition and radiation condition. The boundary value problem is exact as long as the fluid domain is assumed to be ideal flow. It is quite difficult, however, to solve this problem exactly because the free surface boundary condition is highly non-linear and the elevation of free surface ζ is not known a priori. Moreover the body boundary condition should be satisfied on the exact wetted surface of the oscillating body, which interacts with the free surface and there are unresolved question regarding the form of radiation condition. Therefore, in order to solve the non-linear problem, further simplification should be made through linearisation of the problem.

When the amplitude of the incident wave is assumed to be small compared to the wavelength and the slope of the wave is smaller than unity, it is possible to linearise the given equations. The assumption of small amplitude can be accepted for the linearization purpose to simplify complicated problems. Once the small amplitude of incident wave is assumed, all of the motion response of the body, diffraction wave and radiation wave, which are created by the incident wave, can be considered to be of small amplitude as well. Then the linearisation in the given problem means simply that all second order terms in the foregoing boundary conditions are assumed to be sufficiently small enough to be neglected and principles of superposition can be applied.

Through linearisation the flow field may be divided by steady and unsteady flow due to forward and oscillatory motions of a body. Steady flow field is mainly due to the forward motion of the body in calm water whereas unsteady flow field is caused by incident waves, diffraction waves and radiation waves by the presence and the

motion of the body in the steady field. Thus velocity potential Φ can be rewritten in the form

$$\Phi(\mathbf{x}_0,t) = \Phi(x+Ut,y,z,t) = \bar{\Phi}(\mathbf{x}) + \tilde{\Phi}(\mathbf{x},t) \tag{5.14}$$

where $\bar{\Phi}$ and $\tilde{\Phi}$ denote steady and unsteady velocity potential respectively. Each velocity potential must satisfy the Laplace's equation

$$\begin{aligned} \nabla^2\bar{\Phi}(\mathbf{x}) &= 0 \\ \nabla^2\tilde{\Phi}(\mathbf{x},t) &= 0 \end{aligned} \tag{5.15}$$

5.4.1 Free surface boundary condition

The free surface boundary condition given in equation (5.10) can be rewritten with linearised expression as

$$\Phi_{tt} + g\Phi_{Z_0} = 0 \qquad \text{on } Z_0 = 0 \tag{5.16}$$

It should be noted that this condition is imposed on the mean position of the free surface, since the difference between the value of Φ or its derivatives on $Z_0 = \zeta$ and $Z_0 = 0$ is a second order quantity.

On the other hand, time derivative of potential in the inertial coordinate system can be redefined with Lorentz transformation as follow

$$\Phi_t = \frac{\partial}{\partial t}\Phi(x_0 - Ut, y_0, z_0, t) = \left(\frac{\partial}{\partial t} - U\frac{\partial}{\partial x}\right)\Phi(x,y,z,t) \tag{5.17}$$

Transforming the linear free surface boundary condition in equation (5.16) gives

$$\Phi_{tt} - 2U\Phi_{xt} + U^2\Phi_{xx} + g\Phi_z = 0 \qquad \text{on } z = 0 \tag{5.18}$$

For a steady flow, the velocity potential $\bar{\Phi}$ due to the steady forward motion of the body is

$$\bar{\Phi}(\mathbf{x}) = -Ux + \bar{\phi}(\mathbf{x}) \tag{5.19}$$

where $\bar{\phi}$ is the steady perturbation potential. The velocity field of the steady flow $\mathbf{W}$ relative to the steady translating frame $o - xyz$ is

$$\mathbf{W}(\mathbf{x}) = \nabla\bar{\Phi} = \nabla(-Ux + \bar{\phi}) \tag{5.20}$$

Substituting equation (5.19) into (5.18) and using $\bar{\Phi}_t = 0$ yield linear free surface boundary condition for steady flow as

$$U^2\bar{\phi}_{xx} + g\bar{\phi}_z = 0 \qquad \text{on } z = 0 \tag{5.21}$$

The steady free surface elevation can be obtained from dynamic free surface boundary condition

$$\left(\frac{\partial}{\partial t} - U\frac{\partial}{\partial x}\right)\bar{\phi} + \frac{1}{2}\nabla\bar{\phi}\cdot\nabla\bar{\phi} + gz = 0 \qquad \text{on } z = \bar{\zeta} \tag{5.22}$$

Rearranging equation (5.22) and substituting $\bar{\phi} = \bar{\Phi} + Ux$ yield

$$\begin{aligned}\bar{\zeta} &= -\frac{1}{2g}\left(\nabla\bar{\Phi}\cdot\nabla\bar{\Phi} - U^2\right) \\ &= -\frac{1}{2g}\left(W^2 - U^2\right)\end{aligned} \qquad \text{on } z = \bar{\zeta} \tag{5.23}$$

For unsteady flow, the free surface boundary condition can be obtained by substituting equation (5.14) into (5.10) and retaining only first order terms as follows

$$\tilde{\Phi}_{tt} + g(\nabla\bar{\Phi}_z + \nabla\tilde{\Phi}_z) + 2\nabla\bar{\Phi}\cdot\nabla\tilde{\Phi}_t + \frac{1}{2}\nabla\bar{\Phi}\cdot\nabla(\nabla\bar{\Phi}\cdot\nabla\bar{\Phi})$$
$$+\nabla\bar{\Phi}\cdot\nabla(\nabla\bar{\Phi}\cdot\nabla\tilde{\Phi}) + \frac{1}{2}\nabla\tilde{\Phi}\cdot\nabla(\nabla\bar{\Phi}\cdot\nabla\bar{\Phi}) = 0$$
$$\text{on } z = \zeta \qquad (5.24)$$

The unsteady free surface elevation can be calculated by similar process of steady case

$$\zeta = -\frac{1}{g}\left[\tilde{\Phi}_t + \frac{1}{2}\left(\nabla\bar{\Phi}\cdot\nabla\bar{\Phi} - U^2\right) + \nabla\bar{\Phi}\cdot\nabla\tilde{\Phi}\right] \qquad \text{on } z = \zeta \qquad (5.25)$$

In order to solve the difference $(\zeta - \bar{\zeta})$, Taylor series expansion about steady elevation $z = \bar{\zeta}$ is applied to equation (5.25) as follows

$$\zeta = \bar{\zeta} - \frac{1}{g}\left[\tilde{\Phi}_t + \nabla\bar{\Phi}\cdot\nabla\tilde{\Phi}\right]_{z=\bar{\zeta}} - \frac{1}{g}(\zeta - \bar{\zeta})(\nabla\bar{\Phi}\cdot\nabla\bar{\Phi}_z)_{z=\bar{\zeta}} \qquad (5.26)$$

Rearranging above gives

$$\zeta - \bar{\zeta} = (\tilde{\Phi}_t + \nabla\bar{\Phi}\cdot\nabla\tilde{\Phi})/(g + \nabla\bar{\Phi}\cdot\nabla\bar{\Phi}_z) \qquad \text{on } z = \bar{\zeta} \qquad (5.27)$$

A similar process can be carried out to expand free surface boundary condition given in equation (5.24) from unsteady position ζ to steady position $\bar{\zeta}$. Applying Taylor series expansion to equation (5.24) about $z = \bar{\zeta}$ gives first order free surface boundary condition as follows

$$\tilde{\Phi}_{tt} + 2\nabla\bar{\Phi}\cdot\nabla\tilde{\Phi}_t + \nabla\bar{\Phi}\cdot\nabla(\nabla\bar{\Phi}\cdot\nabla\tilde{\Phi}) + \frac{1}{2}\nabla\tilde{\Phi}\cdot\nabla(\nabla\bar{\Phi}\cdot\nabla\bar{\Phi}) + g\nabla\tilde{\Phi}_z$$

$$-(\tilde{\Phi}_t + \nabla\bar{\Phi}\cdot\nabla\tilde{\Phi})\left[\frac{1}{2}\frac{\partial}{\partial z}\left\{\nabla\bar{\Phi}\cdot\nabla(\nabla\bar{\Phi}\cdot\nabla\bar{\Phi})\right\} + g\bar{\Phi}_{zz}\right]/(g + \nabla\bar{\Phi}\cdot\nabla\bar{\Phi}_z) = 0$$

$$\text{on } z = \bar{\zeta} \qquad (5.28)$$

Once the solution of steady flow problem is obtained, it makes equation (5.28) a linear free surface boundary condition for unsteady flow problem. Thus the unsteady velocity potential $\tilde{\Phi}$ is governed by equation (5.28), which is association with steady velocity potential $\bar{\Phi}$. Exact solution of equation (5.28) is, however, still very difficult to be evaluated because of its complexity, so further simplification should be made. One reasonable method applicable to reduce above expression is to assuming the amplitude of perturbation potential in steady flow to be small. Then all the terms related to the steady perturbation potential become higher-order, and thus can be neglected in the free surface boundary condition. Consequently the steady velocity vector $\mathbf{W}$ can be assumed as

$$\mathbf{W} = \nabla\bar{\Phi} = (-U, 0, 0) \qquad (5.29)$$

Then equation (5.28) reduces to

$$\tilde{\Phi}_{tt} - 2U\tilde{\Phi}_{xt} + U^2\tilde{\Phi}_{xx} + g\tilde{\Phi}_z = 0 \qquad \text{on } z = 0 \qquad (5.30)$$

or

$$\left(\frac{\partial}{\partial t} - U\frac{\partial}{\partial x}\right)^2\tilde{\Phi} + g\tilde{\Phi}_z = 0 \qquad \text{on } z = 0 \qquad (5.31)$$

where linear free surface boundary condition given in equation (5.31) is in the same form with equation (5.18).

5.4.2 Body boundary condition

Now we have simplified the free surface boundary condition in order to solve the boundary value problem more practically. Nevertheless, there exists another difficulty in solving given problem since the body boundary condition given in equation (5.11) should be satisfied on the oscillating surface S_B exactly. Therefore, further simplification of the given problem will be focused on the linearisation of the body boundary condition.

For the steady flow the body boundary condition on the steady surface $\overline{S}_B$ is known as

$$\mathbf{W} \cdot \mathbf{n} = 0 \qquad \text{on } \overline{S}_B \tag{5.32}$$

Before considering the unsteady case, we might consider the local oscillatory vector $\boldsymbol{\alpha}$ at the body surface S_B, which is defined by the fluctuation of the body-fixed coordinate system $A - x'y'z'$ relative to the inertial coordinate system $o - xyz$ as

$$\begin{aligned} \boldsymbol{\alpha} &= \mathbf{x} - \mathbf{x}' \\ &= \boldsymbol{\delta} + \boldsymbol{\Omega} \times \mathbf{x}' \end{aligned} \tag{5.33}$$

where $\mathbf{x}'$ is the position vector of body surface S_B relative to body-fixed coordinate system $A - x'y'z'$. $\boldsymbol{\delta} = (\xi_1, \xi_2, \xi_3)$ and $\boldsymbol{\Omega} = (\xi_4, \xi_5, \xi_6)$ are the unsteady translational and rotational displacement vectors respectively.

Consequently local velocity vector $\mathbf{u}_s$ can be expressed time derivative of local oscillatory vector $\mathbf{u}_s$ as follows

$$\mathbf{u}_s = \dot{\boldsymbol{\alpha}} \qquad \text{on } S_B \tag{5.34}$$

Now the body boundary condition given in equation (5.11) can be rewritten as

$$\tilde{\Phi}_n = \dot{\boldsymbol{\alpha}} \cdot \mathbf{n} - \mathbf{W} \cdot \mathbf{n} \qquad \text{on } S_B \tag{5.35}$$

Foregoing equation (5.35) can be further expanded from exact surface S_B to mean wetted surface $\bar{S}_B$, since the order of second term in the right hand side is $\mathbf{W} \cdot \mathbf{n} = O(1)$ and its difference of value on each boundary surface is $O(\alpha)$. Following Newman (1978), the two first order contributions to $\mathbf{W} \cdot \mathbf{n}$ come from the rotation of the body-fixed coordinate system, and from the gradient of the steady flow field. Expanding up to first order gives

$$[\mathbf{W} \cdot \mathbf{n}]_{S_B} = [\{\mathbf{W} - \boldsymbol{\Omega} \times \mathbf{W} + (\boldsymbol{\alpha} \cdot \nabla)\mathbf{W}\} \cdot \mathbf{n}]_{\bar{S}_B} \quad \text{on } S_B,\ \bar{S}_B \tag{5.36}$$

Substituting equation (5.36) into equation (5.35) and invoking steady boundary condition in equation (5.32), it follows that

$$\tilde{\Phi}_n = [\dot{\boldsymbol{\alpha}} + \boldsymbol{\Omega} \times \mathbf{W} - (\boldsymbol{\alpha} \cdot \nabla)\mathbf{W}] \cdot \mathbf{n} \qquad \text{on } S_B,\ \bar{S}_B \tag{5.37}$$

An alternative expression to equation (5.37) can be derived from equations (5.33) by using following vector identity

$$(\mathbf{W} \cdot \nabla)\boldsymbol{\alpha} = (\mathbf{W} \cdot \nabla)\boldsymbol{\delta} + [(\mathbf{W} \cdot \nabla)\boldsymbol{\Omega}] \times \mathbf{x}' + \boldsymbol{\Omega} \times [(\mathbf{W} \cdot \nabla)\mathbf{x}'] \tag{5.38}$$

The first two terms in the right hand side of equation (5.38) are zero because both $\boldsymbol{\delta}$ and $\boldsymbol{\Omega}$ are independent of the spatial coordinate. Then equation (5.38) reduces to

$$(\mathbf{W} \cdot \nabla)\boldsymbol{\alpha} = \boldsymbol{\Omega} \times \mathbf{W} \tag{5.39}$$

Thus equation (5.37) can be rewritten as follows

$$\tilde{\Phi}_n = [\dot{\boldsymbol{\alpha}} + (\mathbf{W} \cdot \nabla)\boldsymbol{\alpha} - (\boldsymbol{\alpha} \cdot \nabla)\mathbf{W}] \cdot \mathbf{n} \qquad \text{on } S_B,\ \bar{S}_B \tag{5.40}$$

The first two terms in the right hand side of equation (5.40) mean the rate of change of local oscillatory displacement $\boldsymbol{\alpha}$ in a reference frame moving with the steady flow. Equation (5.40) can be further simplified by use of following vector identity

$$\nabla \times (\boldsymbol{\alpha} \times \mathbf{W}) = (\mathbf{W} \cdot \nabla)\boldsymbol{\alpha} - (\boldsymbol{\alpha} \cdot \nabla)\mathbf{W} + \boldsymbol{\alpha}(\nabla \cdot \mathbf{W}) - \mathbf{W}(\nabla \cdot \boldsymbol{\alpha}) \qquad (5.41)$$

Since $\mathbf{W}$ and $\boldsymbol{\alpha}$ have zero divergence, i.e. $\nabla \cdot \boldsymbol{\alpha} = 0$ and $\nabla \cdot \mathbf{W} = 0$, the last two terms on the right hand side of equation (5.41) are identical to zero. Hence, equation (5.40) can be rewritten as

$$\tilde{\Phi}_n = [\dot{\boldsymbol{\alpha}} + \nabla \times (\boldsymbol{\alpha} \times \mathbf{W})] \cdot \mathbf{n} \qquad \text{on } S_B,\ \bar{S}_B \qquad (5.42)$$

The boundary condition given in equation (5.42) is originally derived by Timman and Newman (1962). Obviously the boundary condition given in either equation (5.40) or equation (5.42) contains the effects from interactions between steady and unsteady flow and these effects make the problem very complex. Once again the assumption used in the case of free surface boundary condition can be applied for further simplification. If the steady perturbation potential is assumed to be small enough to be negligible, equation (5.29) for the steady velocity vector can be adopted. Then equation (5.40) can be expressed as

$$\begin{aligned} \tilde{\Phi}_n &= \left[\left(\frac{\partial}{\partial t} - U\frac{\partial}{\partial x}\right)\boldsymbol{\alpha}\right] \cdot \mathbf{n} \\ &= [\dot{\boldsymbol{\alpha}} - U(\boldsymbol{\Omega} \times \mathbf{i})] \cdot \mathbf{n} \end{aligned} \qquad (5.43)$$

where the second term $(\boldsymbol{\Omega} \times \mathbf{i})$ can be interpreted as an angle of attack due to pitch and yaw.

5.4.3 Decomposition of velocity potential

In the foregoing section, total potential Φ has been separated into steady potential $\bar{\Phi}$ due to straight forward motion and unsteady potential $\tilde{\Phi}$ due to oscillatory motion. The steady potential was further divided by uniform stream part and perturbation potential. Under the assumption of small amplitude of incident waves, the relevant free surface and body boundary conditions of the boundary value problem were linearised in simplified forms.

The unsteady potential can be also decomposed by linear components due to the incident wave, scattered disturbance of incident wave and six-degree-of-freedom motions of the ship. The wave disturbance is called as diffraction wave and the wave generated by the ship motion is called as radiation wave. Since the incident wave will be assumed to be sinusoidal and harmonic with small amplitude, the relevant diffraction and radiation waves can be also regarded to be regular harmonic wave.

Thus the unsteady velocity potential $\tilde{\Phi}$ can be decomposed as

$$\tilde{\Phi}(\mathbf{x},t) = \left[\phi_0 + \phi_7 + \sum_{j=1}^{6} \bar{\xi}_j \phi_j \right] e^{i\omega_e t} \tag{5.44}$$

where ϕ_0 is the incident wave potential, ϕ_7 the diffraction potential and ϕ_j the radiation potential in the j-th mode of ship motion with a complex amplitude $\bar{\xi}_j$. ω_e denotes encounter frequency between oscillating ship moving with forward speed U and the incident wave.

The incident wave potential, which satisfies Laplace equation (5.15), free surface boundary condition (5.30) and sea bottom boundary condition (5.12) for infinite depth, can be expressed as

$$\phi_0 = \frac{ig\zeta_0}{\omega_0} \exp[k_0 z - ik_0(x\cos\beta - y\sin\beta)] \tag{5.45}$$

where ζ_0 : amplitude of incident wave

ω_0 : frequency of incident wave

k_0 : wave number ($=2\pi/\lambda$)

β : angle between incident wave and ship's heading

($\beta = 180°$ for head sea and $\beta = 0°$ for following sea)

The encounter frequency can be calculated as

$$\omega_e = |\omega_0 - Uk_0 \cos\beta| \tag{5.46}$$

where wave number k_0 is given by dispersion relation for infinite depth as follows

$$k = \frac{\omega_0^2}{g} \tag{5.47}$$

The diffraction wave generated by the disturbance of incident wave as if the ship is restrained to the body-fixed coordinate system $A - x'y'z'$. In the diffraction problem, therefore, there is no motion produced by the incident wave, i.e. $\xi_j = 0$ and $\alpha = 0$. Then the body boundary condition given in equation (5.40) for the diffraction problem is reduced to

$$\frac{\partial}{\partial n}(\phi_0 + \phi_7) = 0 \qquad \text{on } \bar{S}_B \tag{5.48}$$

In the case of radiation problem, the wave is generated by the motion of the ship in the j-th mode without considering incident wave. The behaviour of ship motion is same as forced oscillation in the calm water and thus the incident wave and diffraction potential does not exist, i.e. $\phi_0 = 0$ and $\phi_7 = 0$. The body boundary condition given in equation (5.40) for the radiation problem can be reduced to

$$\frac{\partial \phi_j}{\partial n} = i\omega_e n_j + U m_j \qquad \text{on } \bar{S}_B \tag{5.49}$$

where n_j are defined with normal and position vector of hull surface

$$\begin{aligned} (n_1, n_2, n_3) &= \mathbf{n} \\ (n_4, n_5, n_6) &= \mathbf{r} \times \mathbf{n} \end{aligned} \tag{5.50}$$

and m_j are so-called m-terms, which are related with forward speed, and following Ogilvie and Tuck (1969),

$$\begin{aligned} (m_1, m_2, m_3) &= \mathbf{m} = -(\mathbf{n} \cdot \nabla)\mathbf{W} \\ (m_4, m_5, m_6) &= \mathbf{W} \times \mathbf{n} + \mathbf{r} \times \mathbf{m} = -(\mathbf{n} \cdot \nabla)(\mathbf{r} \times \mathbf{W}) \end{aligned} \tag{5.51}$$

The body boundary condition given in equation (5.49) is associated with steady velocity vector and if the steady perturbation potential $\bar{\phi}$ is assumed to be small, the m-terms can be further simplified with slender body approximation as follow

$$\begin{aligned} m_1 &= m_2 = m_3 = m_4 = 0 \\ m_5 &= n_3 \\ m_6 &= -n_2 \end{aligned} \tag{5.52}$$

The body boundary condition given in equation (5.49) associated with m-terms in equation (5.52) can be directly compared with equation (5.43) since the simplified forms of m-terms act like aforementioned angle of attack.

5.5 Boundary Integral Method

5.5.1 Formulation of boundary integral method

To solve the boundary value problem the concept of velocity potential has been introduced with relevant boundary conditions in the previous section. Although the corresponding boundary conditions were linearised for practical applications, analytic solution for the boundary value problem is still available only for some simple bodies under restricted conditions. Therefore several methods have been studied by many researchers to find the solution for more general bodies.

To explain fully the rapid changes of hull shape and corresponding properties of flow field near stern region, three-dimensional approach has much more advantages than two-dimensional strip method. As discussed in the literature review in Chapter 3, there are mainly two three-dimensional methods in the frequency domain to solve the boundary value problem: Green function method and Rankine source method. Advantages and disadvantages of each method are compared in Table 5.1.

Table 5.1 Comparisons of Green function and Rankine source methods

	Green function	Rankine source
Calculation of function	difficult	easy
Distribution of singularity	body surface	body and free surface
Size of system of equations (number of panels)	small	large
Computational cost	high	low
Radiation condition	automatically satisfied	difficult to satisfy
Application to non-linear problem	partly based on perturbation expansion	fully for non-linear free surface condition
Occurrence of irregular frequency	often	rarely

In this study, three-dimensional Green function method, which is also called as boundary integral method, is used for the solution of a linearised boundary value problem for unsteady flow induced by forward and oscillatory motions of a ship. The formulation of the boundary integral method is based on Green's second identity to calculate a velocity potential using a Green function on the boundary of the fluid domain. This results in a surface integral equation with a complex kernel function, which represents the Green function. The Green function satisfies Laplace's equation and all the boundary conditions except the body boundary condition on the body surface. The boundary integral method has the advantage that the governing equation in a given domain is recast into the solution of an integral equation which applies only to the boundary of the domain and incorporates the boundary conditions directly.

In order to satisfy the linearised free surface condition of the boundary value problem, the Green function may be defined by a source submerged below the free surface. This source is represented by a translating source for a steady motion and a translating pulsating source for an unsteady motion of the ship. For a stationary but oscillating body, the Green function is simply represented by a pulsating source.

Let us consider a Green function $G(p,q)$, which is defined by

$$G(p,q) = \frac{1}{r} + H(p,q) \tag{5.53}$$

where p and q denote field and source points respectively in the fluid domain. $1/r$ is a source singularity and $H(p,q)$ is a wave function. The Green function given in equation (5.53) is the modified singularity, which satisfies the free surface condition, sea bottom boundary condition and radiation condition at infinity. A variety of the Green functions for the linear boundary value problem is well described systematically by Wehausen and Laiton (1960).

In order to solve the given boundary value problem, two types of boundary integral equations can be introduced. The first can be derived by applying Green's theorem to

the unknown velocity potential and source potential. Then the unknown velocity potential can be represented by distribution of source and dipole over the body surface. Alternatively the velocity potential can be expressed by a source distribution over the body surface. The former is often referred to as 'direct method' since the velocity potential can be obtained directly from the integral equation, while the latter as 'indirect method', where unknown source strength is first solved and then used to obtain velocity potential. Both of these formulations lead to Fredholm integral equations with Neumann boundary condition prescribing the normal velocity of the fluid on the body surface.

One of the major disadvantages of these methods is the existence of irregular frequency where the solutions of integral equations either do not exist or are not unique. The linear systems for the unknown potential or source strength on the body surface become ill-conditioned and the discrete approximation of the given integral equations leads to unacceptable solutions. These difficulties are consequences of the fact that Green function satisfies the free surface boundary condition both inside and outside of the body and the irregular frequency coincides with the eigen-frequency of the non-physical wave motion inside of the body.

The width of affected frequency band may be reduced by increasing the number of panels although in practice it is not acceptable because of a substantial increase in the computational effort. In order to remove irregular frequency phenomenon, Ohmatsu (1975) suggested the addition of a rigid lid in the interior free surface. Its presence eliminates the resonance associated with the interior Dirichlet eigen-problem and therefore removes the effects of irregular frequency. Lee et al. (1996) employed modified boundary integral equations for both source-dipole distribution and source distribution methods for the removal of irregular frequency effects. It should be noted that the irregular frequency is related to the selection of the specific boundary integral equation and does not reflect an irregularity in the solution of the original boundary value problem.

In the case of the steady and unsteady problem with forward speed, the boundary integral equations based on the source distribution technique using an appropriate Green function on the boundary of the fluid domain read as

$$4\pi\phi(p) = \iint_{\overline{S}_B} \sigma(q)G(p,q)ds + \frac{U^2}{g}\oint_{L_F} \sigma(q)G(p,q)n_1 dy \qquad (5.54)$$

where σ denotes the source strength, L_F the intersection line between the body surface and the free surface and n_1 the x-component of normal vector on the body surface.

In order to solve equation (5.54), the unknown source strength σ should be solved and therefore normal derivative of $\phi(p)$ with respect to the field point p, which is lied on the mean wetted body surface $\overline{S}_B$, will be taken as follows.

$$\begin{aligned} 4\pi\frac{\partial\phi(p)}{\partial n} &= 2\pi\sigma(p) + \iint_{\overline{S}_B} \sigma(q)\frac{\partial G(p,q)}{\partial n}ds \\ &+ \frac{U^2}{g}\oint_{L_F} \sigma(q)\frac{\partial G(p,q)}{\partial n}n_1 dy \end{aligned} \qquad (5.55)$$

It should be noted that when field point p coincides with source point q, the singular part of the normal derivative of Green function is taken by first term of right hand side of equation (5.55).

To solve the velocity potential, the representation of integral equation (5.54) and (5.55) can be used by means of the source distribution over the known body surface. With the body boundary condition and Green function the unknown source strength σ can be calculated indirectly in equation (5.55) and thus this method is often referred as indirect method. Indirect method to evaluate the velocity potential is sometimes more useful than direct method, which calculates the velocity potential directly. Once the source strength is provided, it could be used to evaluate higher-order derivatives of the velocity potential for further calculation.

5.6 Green Function

5.6.1 Formulation of Green function

To solve the integral equation formulated in the previous section, it is required to calculate Green function, which satisfies the Laplace's equation, the linearised free surface boundary condition, the sea bottom condition and radiation condition. In the linearised unsteady forward motion problem the flow disturbance can be represented by a translating pulsating source submerged below the undisturbed free surface.

For a fully three-dimensional problem of a ship moving in a seaway, the Green function is defined as a function of the variables such as the locations of field point $p(x,y,z)$ and source point $q(\xi,\eta,\zeta)$, forward speed U and encounter frequency ω. For infinite water depth, Wehausen and Laitone (1960) suggested Green function in the form

$$G(p,q)=\frac{1}{r}-\frac{1}{r_1}+\frac{2g}{\pi}\left\{\int_0^{\gamma}\int_0^{\infty}+\int_{\gamma}^{\frac{\pi}{2}}\int_{L_1}+\int_{\frac{\pi}{2}}^{\pi}\int_{L_2}\right\}f(\theta,k)\,dk\,d\theta \quad (5.56)$$

where

$$r=\sqrt{(x-\xi)^2+(y-\eta)^2+(z-\zeta)^2} \quad (5.57)$$

$$r_1=\sqrt{(x-\xi)^2+(y-\eta)^2+(z+\zeta)^2} \quad (5.58)$$

$$\gamma=\begin{cases}0 & if\ \ \tau<0.25\\ \cos^{-1}(1/4\tau) & if\ \ \tau\geq 0.25\end{cases} \quad (5.59)$$

$$\tau=\frac{\omega U}{g} \quad (5.60)$$

$$f(\theta,k)=\frac{k\exp\left[k\{(z+\zeta)-i(x-\xi)\cos\theta\}\right]\cos\{k(y-\eta)\sin\theta\}}{gk-(\omega+Uk\cos\theta)^2} \quad (5.61)$$

Since the double integrals of Green function given in equation (5.56) have many difficulties for numerical calculations, an alternative formulation of Green function is required to remove the double integrals. So, the denominator of $f(\theta,k)$ can be decomposed as

$$gk-(\omega+Uk\cos\theta)^2=-U^2\cos^2\theta(k-k_{01})(k-k_{02})$$

$$\left.\begin{matrix}k_{01}\\k_{02}\end{matrix}\right\}=\left\{\frac{1-2\tau\cos\theta\mp i\sqrt{4\tau\cos\theta-1}}{2\tau^2\cos^2\theta}\right\}\frac{\omega^2}{g}$$

$$\text{when } 0\le\theta\le\gamma \tag{5.62}$$

$$gk-(\omega+Uk\cos\theta)^2=-U^2\cos^2\theta(k-k_1)(k-k_2)$$

$$\left.\begin{matrix}k_1\\k_2\end{matrix}\right\}=\left\{\frac{1-2\tau\cos\theta\mp\sqrt{1-4\tau\cos\theta}}{2\tau^2\cos^2\theta}\right\}\frac{\omega^2}{g}$$

$$\text{when } \gamma\le\theta\le\frac{\pi}{2} \tag{5.63}$$

$$gk-(\omega+Uk\cos\theta)^2=-U^2\cos^2\theta(k-k_3)(k-k_4)$$

$$\left.\begin{matrix}k_3\\k_4\end{matrix}\right\}=\left\{\frac{1-2\tau\cos\theta\mp\sqrt{1-4\tau\cos\theta}}{2\tau^2\cos^2\theta}\right\}\frac{\omega^2}{g}$$

$$\text{when } \frac{\pi}{2}\le\theta\le\pi \tag{5.64}$$

There are two singular points in the range of $0\le\theta\le\gamma$ and they lie in the opposite quadrant in the complex plane, which means complex conjugate as shown in Figure 5.4 (a). The integration paths of the singular points in the range of $\gamma\le\theta\le\pi$ are shown in Figure 5.4 (b) and (c).

Meanwhile the integrand $f(\theta,k)$ can be further rewritten as

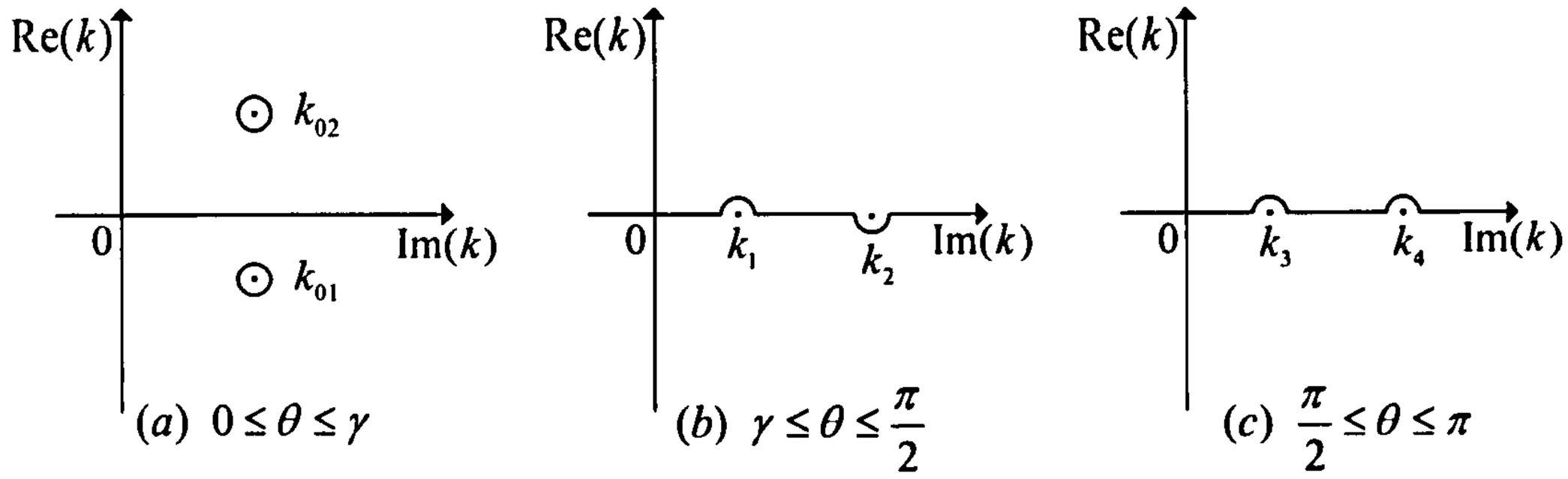

Figure 5.4 Integration paths in the complex plane

$$f(\theta,k) = \frac{1}{gi\sqrt{4\tau\cos\theta - 1}}\left(\frac{k_{01}}{k-k_{01}} - \frac{k_{02}}{k-k_{02}}\right) \times \exp\left[k\{(z+\zeta) - i(x-\xi)\cos\theta\}\right]\cos\{k(y-\eta)\sin\theta\}$$

when $0 \le \theta \le \gamma$ (5.65)

$$f(\theta,k) = \frac{1}{g\sqrt{1-4\tau\cos\theta}}\left(\frac{k_1}{k-k_1} - \frac{k_2}{k-k_2}\right) \times \exp\left[k\{(z+\zeta) - i(x-\xi)\cos\theta\}\right]\cos\{k(y-\eta)\sin\theta\}$$

when $\gamma \le \theta \le \frac{\pi}{2}$ (5.66)

$$f(\theta,k) = \frac{1}{g\sqrt{1-4\tau\cos\theta}}\left(\frac{k_3}{k-k_3} - \frac{k_4}{k-k_4}\right) \times \exp\left[k\{(z+\zeta) - i(x-\xi)\cos\theta\}\right]\cos\{k(y-\eta)\sin\theta\}$$

when $\frac{\pi}{2} \le \theta \le \pi$ (5.67)

If we change the expression of cosine terms in $f(\theta,k)$ using the relationship

$$\cos Z = \frac{1}{2}\{e^{iZ} + e^{-iZ}\} \quad (5.68)$$

Equations (5.65) to (5.67) can be rewritten as

$$f(\theta,k)=\frac{1}{2gi\sqrt{4\tau\cos\theta-1}}\left(\frac{k_{01}}{k-k_{01}}-\frac{k_{02}}{k-k_{02}}\right)$$
$$\times\exp k\left[(z+\zeta)+i\{-(x-\xi)\cos\theta+(y-\eta)\sin\theta\}\right]$$
$$+\frac{1}{2gi\sqrt{4\tau\cos\theta-1}}\left(\frac{k_{01}}{k-k_{01}}-\frac{k_{02}}{k-k_{02}}\right)$$
$$\times\exp k\left[(z+\zeta)+i\{-(x-\xi)\cos\theta-(y-\eta)\sin\theta\}\right]$$
$$\text{when } 0\le\theta\le\gamma \tag{5.69}$$

$$f(\theta,k)=\frac{1}{2g\sqrt{1-4\tau\cos\theta}}\left(\frac{k_1}{k-k_1}-\frac{k_2}{k-k_2}\right)$$
$$\times\exp k\left[(z+\zeta)+i\{-(x-\xi)\cos\theta+(y-\eta)\sin\theta\}\right]$$
$$+\frac{1}{2gi\sqrt{1-4\tau\cos\theta}}\left(\frac{k_1}{k-k_1}-\frac{k_2}{k-k_2}\right)$$
$$\times\exp k\left[(z+\zeta)+i\{-(x-\xi)\cos\theta-(y-\eta)\sin\theta\}\right]$$
$$\text{when } \gamma\le\theta\le\frac{\pi}{2} \tag{5.70}$$

$$f(\theta,k)=\frac{1}{2g\sqrt{1-4\tau\cos\theta}}\left(\frac{k_3}{k-k_3}-\frac{k_4}{k-k_4}\right)$$
$$\times\exp k\left[(z+\zeta)+i\{-(x-\xi)\cos\theta+(y-\eta)\sin\theta\}\right]$$
$$+\frac{1}{2g\sqrt{1-4\tau\cos\theta}}\left(\frac{k_3}{k-k_3}-\frac{k_4}{k-k_4}\right)$$
$$\times\exp k\left[(z+\zeta)+i\{-(x-\xi)\cos\theta-(y-\eta)\sin\theta\}\right]$$
$$\text{when } \frac{\pi}{2}\le\theta\le\pi \tag{5.71}$$

If we replace the terms in exponential function with new variables

$$\chi_1=(z+\zeta)-i[(x-\xi)\cos\theta-(y-\eta)\sin\theta]$$
$$\chi_2=(z+\zeta)-i[(x-\xi)\cos\theta+(y-\eta)\sin\theta] \tag{5.72}$$

then Green function becomes

$$
\begin{aligned}
G(p,q) = {} & \frac{1}{r} - \frac{1}{r_1} \\
& + \frac{1}{\pi}\int_0^{\gamma} d\theta \int_0^{\infty} \frac{\exp(k\chi_1)}{i\sqrt{4\tau\cos\theta - 1}} \left(\frac{k_{01}}{k-k_{01}} - \frac{k_{02}}{k-k_{02}} \right) dk \\
& + \frac{1}{\pi}\int_0^{\gamma} d\theta \int_0^{\infty} \frac{\exp(k\chi_2)}{i\sqrt{4\tau\cos\theta - 1}} \left(\frac{k_{01}}{k-k_{01}} - \frac{k_{02}}{k-k_{02}} \right) dk \\
& + \frac{1}{\pi}\int_{\gamma}^{\frac{\pi}{2}} d\theta \int_0^{\infty} \frac{\exp(k\chi_1)}{\sqrt{1-4\tau\cos\theta}} \left(\frac{k_1}{k-k_1} - \frac{k_2}{k-k_2} \right) dk \\
& + \frac{1}{\pi}\int_{\gamma}^{\frac{\pi}{2}} d\theta \int_0^{\infty} \frac{\exp(k\chi_2)}{\sqrt{1-4\tau\cos\theta}} \left(\frac{k_1}{k-k_1} - \frac{k_2}{k-k_2} \right) dk \\
& + \frac{1}{\pi}\int_{\frac{\pi}{2}}^{\pi} d\theta \int_0^{\infty} \frac{\exp(k\chi_1)}{\sqrt{1-4\tau\cos\theta}} \left(\frac{k_3}{k-k_3} - \frac{k_4}{k-k_4} \right) dk \\
& + \frac{1}{\pi}\int_{\frac{\pi}{2}}^{\pi} d\theta \int_0^{\infty} \frac{\exp(k\chi_2)}{\sqrt{1-4\tau\cos\theta}} \left(\frac{k_3}{k-k_3} - \frac{k_4}{k-k_4} \right) dk
\end{aligned}
\tag{5.73}
$$

or

$$
\begin{aligned}
G(p,q) = {} & \frac{1}{r} - \frac{1}{r_1} + (I_{01} + I_{02}) \\
& + (I_{11} + I_{12}) - (I_{21} + I_{22}) + (I_{33} + I_{34}) - (I_{43} + I_{44})
\end{aligned}
\tag{5.74}
$$

where

$$
\begin{aligned}
I_{0j} &= \frac{1}{\pi}\int_0^{\gamma} d\theta \int_0^{\infty} \frac{\exp(k\chi_j)}{i\sqrt{4\tau\cos\theta - 1}} \left(\frac{k_{01}}{k-k_{01}} - \frac{k_{02}}{k-k_{02}} \right) dk \\
I_{ij} &= \frac{1}{\pi}\int_{\gamma}^{\frac{\pi}{2}} d\theta \int_0^{\infty} \frac{\exp(k\chi_j)}{\sqrt{1-4\tau\cos\theta}} \cdot \frac{k_i}{k-k_i} dk
\end{aligned}
\tag{5.75}
$$

$$
\begin{aligned}
\chi_1 &= (z+\zeta) - i[(x-\xi)\cos\theta - (y-\eta)\sin\theta] \\
\chi_2 &= (z+\zeta) - i[(x-\xi)\cos\theta + (y-\eta)\sin\theta] \\
\chi_3 &= \chi_1 \\
\chi_4 &= \chi_2
\end{aligned}
\tag{5.76}
$$

Direct evaluations of the Green function given in equations (5.73) or (5.74) are still cumbersome and time-consuming for numerical calculation because of the infinite double integrals with singularities in the integrand. Especially the location of singularity in the integrand is a complicated function of θ, which requires more detailed integration step length. To overcome this difficulty in the numerical integration, complex exponential integral with contour integral in the complex domain can be introduced. Complex exponential integral defined as

$$E_1(Z) = \int_Z^{\infty} \frac{e^{-u}}{u} du \qquad \text{for } |\arg(Z)| < \pi \tag{5.77}$$

5.6.2 First terms in the integrals I_{01} and I_{02}

The components of Green function I_{01} and I_{02} in equations (5.74) and (5.75) have two singular points in the denominator as

$$\begin{aligned} I_{01} &= I_{01A} - I_{01B} \\ &= \frac{1}{\pi} \int_0^{\gamma} d\theta \int_0^{\infty} \frac{\exp(k\chi_1)}{i\sqrt{4\tau\cos\theta - 1}} \left(\frac{k_{01}}{k - k_{01}} - \frac{k_{02}}{k - k_{02}} \right) dk \\ I_{02} &= I_{02A} - I_{02B} \\ &\frac{1}{\pi} \int_0^{\gamma} d\theta \int_0^{\infty} \frac{\exp(k\chi_2)}{i\sqrt{4\tau\cos\theta - 1}} \left(\frac{k_{01}}{k - k_{01}} - \frac{k_{02}}{k - k_{02}} \right) dk \end{aligned} \tag{5.78}$$

To avoid these singularities and express the integrals in equation (5.78) in terms of exponential integral, change of variables can be introduced in the complex plane as

$$u = -\chi_1(k - k_{01}) \tag{5.79}$$

Then corresponding integration intervals can be changed as

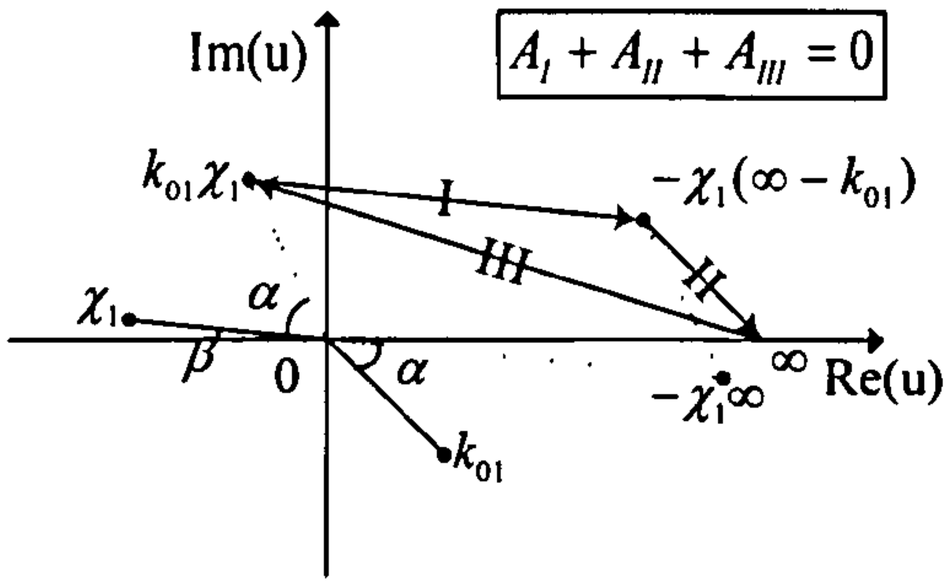

(*a*) $\mathrm{Im}(\chi_1) \geq 0, \quad 0 \leq \alpha + \beta < \frac{\pi}{2}$

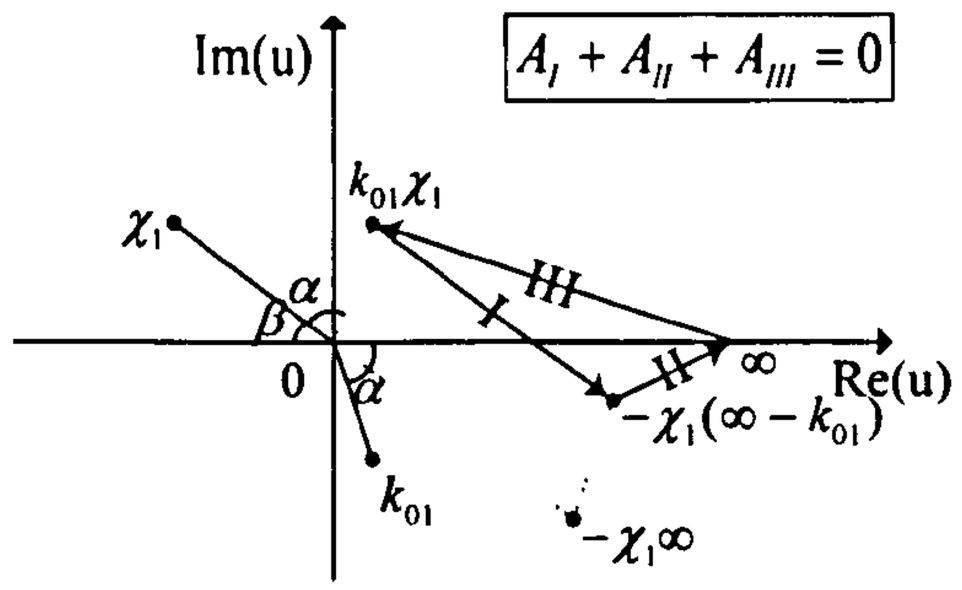

(*b*) $\mathrm{Im}(\chi_1) \geq 0, \quad \frac{\pi}{2} \leq \alpha + \beta < \pi$

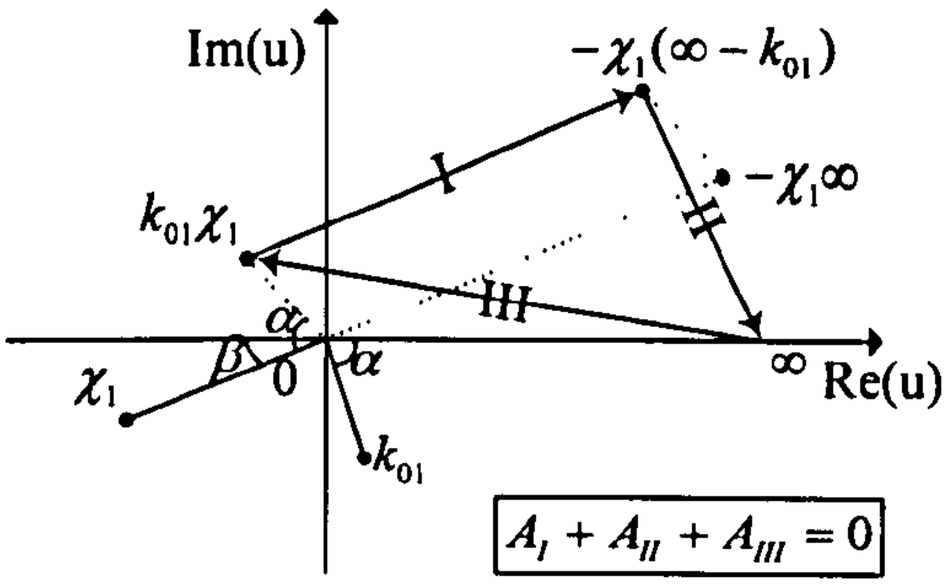

(*c*) $\mathrm{Im}(\chi_1) < 0, \quad \alpha \geq \beta$

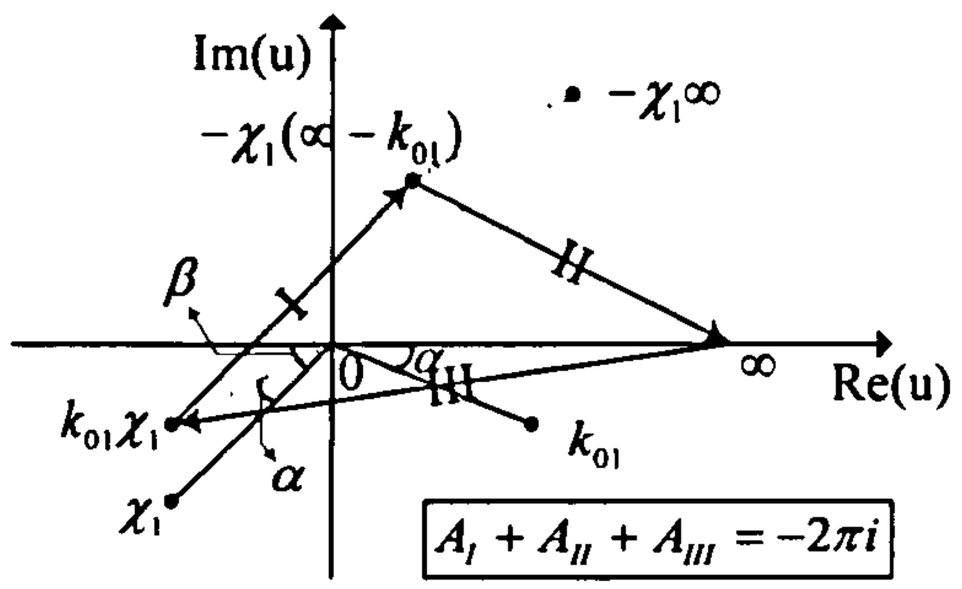

(*d*) $\mathrm{Im}(\chi_1) < 0, \quad \alpha < \beta$

Figure 5.5 Integration path of the first term I_{01A} in the integral I_{01}

$$\begin{aligned} k = 0 \quad &\rightarrow \quad u = k_{01}\chi_1 \\ k = \infty \quad &\rightarrow \quad u = -\chi_1(\infty - k_{01}) \end{aligned} \tag{5.80}$$

If the new variable in equation (5.79) is applied to the first term I_{01A} of I_{01}, the integrand is changed as

$$\begin{aligned} I_{01A} &= \frac{1}{\pi}\int_0^{\pi} d\theta \int_0^{\infty} \frac{\exp(k\chi_1)}{i\sqrt{4\tau\cos\theta - 1}} \cdot \frac{k_{01}}{k - k_{01}} dk \\ &= \frac{1}{\pi}\int_0^{\pi} \frac{k_{01}\exp(k_{01}\chi_1)}{i\sqrt{4\tau\cos\theta - 1}} d\theta \int_{k_{01}\chi_1}^{-\chi_1(\infty - k_{01})} \frac{e^{-u}}{u} du \end{aligned} \tag{5.81}$$

The integration path should be chosen carefully considering the locations of integral ranges in the complex plane, which is described in Figure 5.5. If we take the contour integral of $A_I + A_{II} + A_{III}$, integrals A_{II} and A_{III} will become zero and exponential

integral function respectively. By applying Cauchy's integral theorem, integration value depends on whether or not the singular point is inside of the contour because singular point lies at $u = 0$.

$$\begin{aligned} A_I + A_{II} + A_{III} &= \int_{k_{01}\chi_1}^{\chi_1(\infty - k_{01})} \frac{e^{-u}}{u} du + \int_{\chi_1(\infty - k_{01})}^{\infty} \frac{e^{-u}}{u} du + \int_{\infty}^{k_{01}\chi_1} \frac{e^{-u}}{u} du \\ &= \int_{k_{01}\chi_1}^{\chi_1(\infty - k_{01})} \frac{e^{-u}}{u} du - E_1(k_{01}\chi_1) \end{aligned} \tag{5.82}$$

To describe the locations of variables in the complex plane, we need to introduce modified argument of k_{01} and χ_1 as

$$\begin{aligned} \alpha &= \arctan\left\{\left|\mathrm{Im}(k_{01}) / \mathrm{Re}(k_{01})\right|\right\}, \qquad 0 \le \alpha < \frac{\pi}{2} \\ \beta &= \arctan\left\{\left|\mathrm{Im}(\chi_1) / \mathrm{Re}(\chi_1)\right|\right\}, \qquad 0 \le \beta < \frac{\pi}{2} \end{aligned} \tag{5.83}$$

When $\mathrm{Im}(\chi_1) \ge 0$ and $0 \le \alpha + \beta < \frac{\pi}{2}$, the integration path will follow Figure 5.5 (a) and the contour integration becomes $A_I + A_{II} + A_{III} = 0$ because this path does not contain any singular point. Similarly when $\mathrm{Im}(\chi_1) \ge 0$ and $\frac{\pi}{2} \le \alpha + \beta < \pi$ described in Figure 5.5 (b), the contour integration also becomes $A_I + A_{II} + A_{III} = 0$. Therefore, when $\mathrm{Im}(\chi_1) \ge 0$, the integral A_I can be expressed as

$$\int_{k_{01}\chi_1}^{\chi_1(\infty - k_{01})} \frac{e^{-u}}{u} du = E_1(k_{01}\chi_1) \qquad \text{when } \mathrm{Im}(\chi_1) \ge 0 \tag{5.84}$$

When $\mathrm{Im}(\chi_1) < 0$ and $\alpha \ge \beta$ described in Figure 5.5 (c), the contour integration becomes $A_I + A_{II} + A_{III} = 0$. Thus integration A_I can be expressed as

$$\int_{k_{01}\chi_1}^{\chi_1(\infty - k_{01})} \frac{e^{-u}}{u} du = E_1(k_{01}\chi_1) \qquad \text{when } \mathrm{Im}(\chi_1) < 0,\ \alpha \ge \beta \tag{5.85}$$

When $\mathrm{Im}(\chi_1) < 0$ and $\alpha < \beta$ described in Figure 5.5 (d), since the integration path contains singular point, the contour integration becomes $A_I + A_{II} + A_{III} = -2\pi i$. Thus integration A_I can be expressed as

$$\int_{k_{01}\chi_1}^{\chi_1(\infty - k_{01})} \frac{e^{-u}}{u} du = E_1(k_{01}\chi_1) - 2\pi i \qquad \text{when } \mathrm{Im}(\chi_1) < 0,\ \alpha < \beta \qquad (5.86)$$

Similar method can be applied to the integral I_{02A} and finally following results for the first terms I_{01A} and I_{01B} are obtained.

$$I_{01A} = \frac{1}{\pi} \int_0^{\gamma} \frac{k_{01} \exp(k_{01}\chi_1) E_p(k_{01}\chi_1)}{i\sqrt{4\tau\cos\theta - 1}} d\theta$$
$$I_{02A} = \frac{1}{\pi} \int_0^{\gamma} \frac{k_{01} \exp(k_{01}\chi_2) E_p(k_{01}\chi_2)}{i\sqrt{4\tau\cos\theta - 1}} d\theta \qquad (5.87)$$

where

$$E_p(k_{01}\chi_j) = \begin{cases} E_1(k_{01}\chi_j) - 2\pi i & \text{when } \mathrm{Im}(\chi_j) < 0, \alpha < \beta \\ E_1(k_{01}\chi_j) & \text{otherwise} \end{cases} \qquad (5.88)$$

Although the results in equation (5.88) are obtained only for $\mathrm{Re}(k_{01}) > 0$, equation (5.88) is still valid regardless the sign of $\mathrm{Re}(k_{01})$ because the contour integral does not include any singular point for $\mathrm{Re}(k_{01}) \le 0$.

5.6.3 Second terms in the integrals I_{01} and I_{02}

The process to express second terms in I_{01} and I_{02} in terms of exponential integral is similar to the first term cases. Again to avoid the singularities and to express the second terms in equation (5.78) in terms of exponential integral, changes of variable and corresponding integration intervals are needed in the complex plane as follow

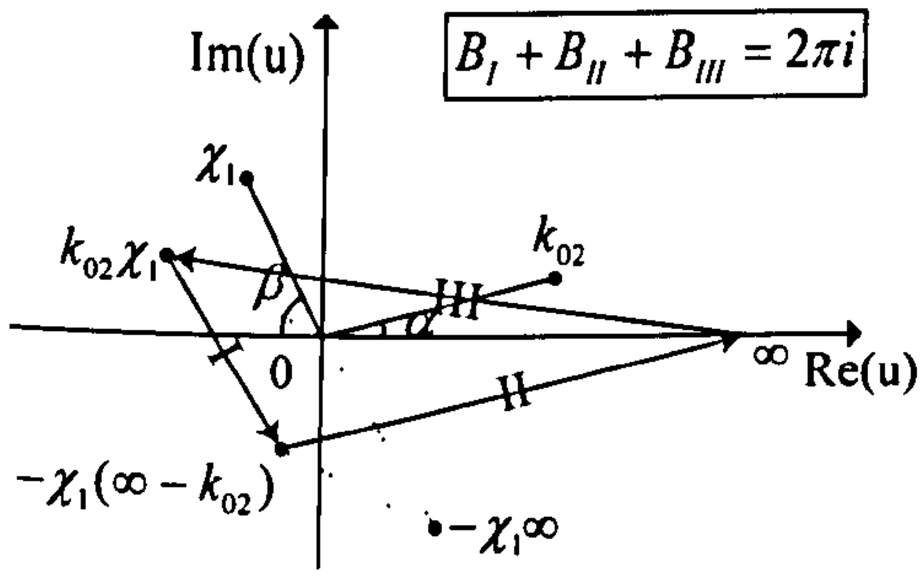

(*a*) $\mathrm{Im}(\chi_1) > 0, \quad \alpha < \beta$

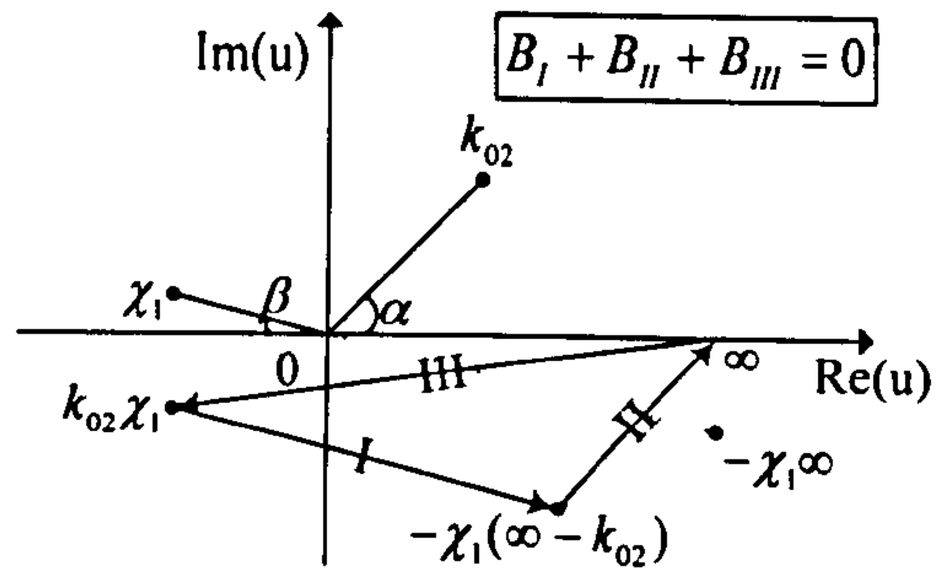

(*b*) $\mathrm{Im}(\chi_1) > 0, \quad \alpha \geq \beta$

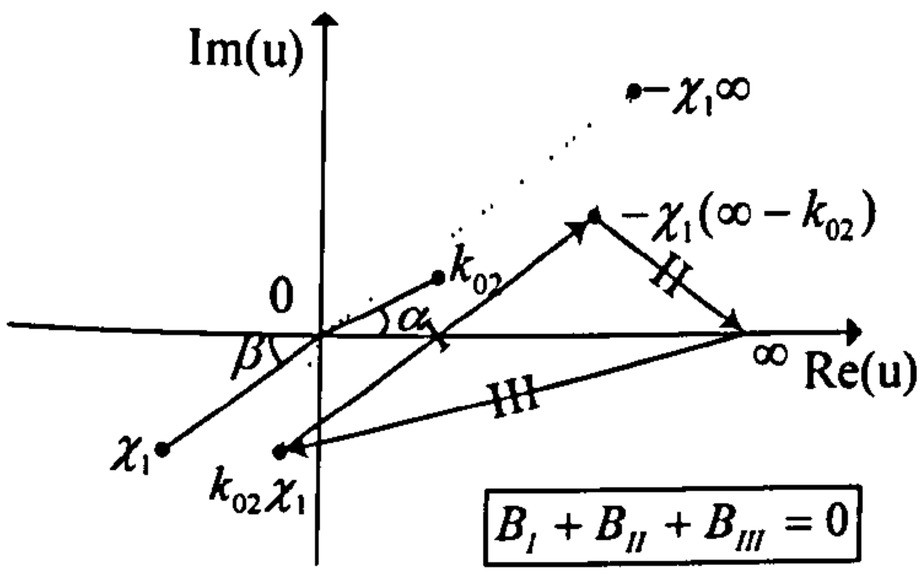

(*c*) $\mathrm{Im}(\chi_1) \leq 0, \quad 0 \leq \alpha + \beta < \frac{\pi}{2} d$

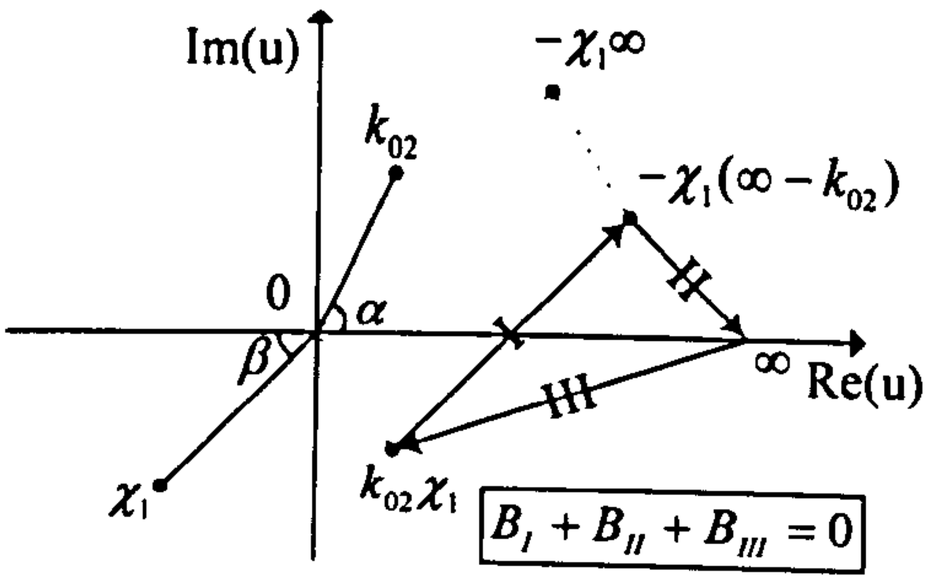

(*d*) $\mathrm{Im}(\chi_1) \leq 0, \quad \frac{\pi}{2} \leq \alpha + \beta < \pi$

Figure 5.6 Integration path of the second term I_{01B} in the integral I_{01}

$$u = -\chi_1(k - k_{02}) \tag{5.89}$$

$$\begin{aligned} k = 0 \quad &\rightarrow \quad u = k_{02}\chi_1 \\ k = \infty \quad &\rightarrow \quad u = -\chi_1(\infty - k_{02}) \end{aligned} \tag{5.90}$$

The second integral I_{01B} can be changed as

$$\begin{aligned} I_{01B} &= \frac{1}{\pi}\int_0^{\pi} d\theta \int_0^{\infty} \frac{\exp(k\chi_1)}{i\sqrt{4\tau\cos\theta - 1}} \cdot \frac{k_{02}}{k - k_{02}} dk \\ &= \frac{1}{\pi}\int_0^{\pi} \frac{k_{02}\exp(k_{02}\chi_1)}{i\sqrt{4\tau\cos\theta - 1}} d\theta \int_{k_{02}\chi_1}^{-\chi_1(\infty - k_{02})} \frac{e^{-u}}{u} du \end{aligned} \tag{5.91}$$

When $\mathrm{Im}(\chi_1) > 0$ and $\alpha < \beta$, the integration path will follow Figure 5.6 (a). The contour integration becomes $B_I + B_{II} + B_{III} = 2\pi i$ because the path contains singular point.

$$\int_{k_{02}\chi_1}^{\chi_1(\infty-k_{02})}\frac{e^{-u}}{u}du = E_1(k_{02}\chi_1)+2\pi i \qquad \text{when } \mathrm{Im}(\chi_1)>0,\ \alpha<\beta \qquad (5.92)$$

When $\mathrm{Im}(\chi_1)>0$ and $\alpha \geq \beta$, the integration path will be Figure 5.6 (b) and the contour integration becomes $B_I + B_{II} + B_{III} = 0$.

$$\int_{k_{02}\chi_1}^{\chi_1(\infty-k_{02})}\frac{e^{-u}}{u}du = E_1(k_{02}\chi_1) \qquad \text{when } \mathrm{Im}(\chi_1)>0,\ \alpha\geq\beta \qquad (5.93)$$

When $\mathrm{Im}(\chi_1)\leq 0$ described in Figure 5.6 (c) and (d), both of the contour integrations become $B_I + B_{II} + B_{III} = 0$.

$$\int_{k_{02}\chi_1}^{\chi_1(\infty-k_{02})}\frac{e^{-u}}{u}du = E_1(k_{02}\chi_1) \qquad \text{when } \mathrm{Im}(\chi_1)\leq 0 \qquad (5.94)$$

Similar method can be applied to the formulation of I_{02B}, and following results for the second terms I_{01B} and I_{02B} are obtained

$$I_{01B} = \frac{1}{\pi}\int_0^{\pi}\frac{k_{02}\exp(k_{02}\chi_1)E_q(k_{02}\chi_1)}{i\sqrt{4\tau\cos\theta-1}}d\theta$$
$$I_{02B} = \frac{1}{\pi}\int_0^{\pi}\frac{k_{02}\exp(k_{02}\chi_2)E_q(k_{02}\chi_2)}{i\sqrt{4\tau\cos\theta-1}}d\theta \qquad (5.95)$$

where

$$E_q(k_{02}\chi_j) = \begin{cases} E_1(k_{02}\chi_j)+2\pi i & \text{when } \mathrm{Im}(\chi_j)>0,\ \alpha<\beta \\ E_1(k_{02}\chi_j) & \text{otherwise} \end{cases} \qquad (5.96)$$

5.6.4 Final expression for Green function

Substituting equations (5.87) and (5.95) into (5.78) gives final expressions for I_{0j} terms, which are formulated with single integrals.

$$\begin{aligned} I_{01} &= \frac{1}{\pi}\int_0^{\pi} \frac{k_{01}\exp(k_{01}\chi_1)}{i\sqrt{4\tau\cos\theta-1}} E_p(k_{01}\chi_1)d\theta \\ &\quad -\frac{1}{\pi}\int_0^{\pi} \frac{k_{02}\exp(k_{02}\chi_1)}{i\sqrt{4\tau\cos\theta-1}} E_q(k_{02}\chi_1)d\theta \end{aligned} \tag{5.97}$$

$$\begin{aligned} I_{02} &= \frac{1}{\pi}\int_0^{\pi} \frac{k_{01}\exp(k_{01}\chi_2)}{i\sqrt{4\tau\cos\theta-1}} E_p(k_{01}\chi_2)d\theta \\ &\quad -\frac{1}{\pi}\int_0^{\pi} \frac{k_{02}\exp(k_{02}\chi_2)}{i\sqrt{4\tau\cos\theta-1}} E_q(k_{02}\chi_2)d\theta \end{aligned} \tag{5.98}$$

Corresponding exponential integrals are expressed as

$$E_p(k_{01}\chi_j) = \begin{cases} E_1(k_{01}\chi_j) - 2\pi i & \text{when } \mathrm{Im}(\chi_j) < 0, \alpha < \beta \\ E_1(k_{01}\chi_j) & \text{otherwise} \end{cases} \tag{5.99}$$

$$E_q(k_{02}\chi_j) = \begin{cases} E_1(k_{02}\chi_j) + 2\pi i & \text{when } \mathrm{Im}(\chi_j) > 0, \alpha < \beta \\ E_1(k_{02}\chi_j) & \text{otherwise} \end{cases} \tag{5.100}$$

where α and β denote modified arguments of k_{0i} and χ_j respectively as follow

$$\begin{aligned} \alpha &= \arctan\left\{\left|\mathrm{Im}(k_{0i})/\mathrm{Re}(k_{0i})\right|\right\}, \qquad 0 \le \alpha < \frac{\pi}{2} \\ \beta &= \arctan\left\{\left|\mathrm{Im}(\chi_j)/\mathrm{Re}(\chi_j)\right|\right\}, \qquad 0 \le \beta < \frac{\pi}{2} \end{aligned} \tag{5.101}$$

In order to remove the singularities in the integrands of Green function, similar but much simpler method, which is applied for I_{0j} terms, can be applied for I_{ij} terms in

equation (5.76). Further details of the method are described in Appendix A. Consequently the expressions for I_{ij} terms can be written as

$$I_{11} = \frac{1}{\pi}\int_{\gamma}^{\frac{\pi}{2}} \frac{k_1 \exp(k_1\chi_1)}{\sqrt{1-4\tau\cos\theta}} E_{r1}(k_1\chi_1)d\theta \tag{5.102}$$

$$I_{12} = \frac{1}{\pi}\int_{\gamma}^{\frac{\pi}{2}} \frac{k_1 \exp(k_1\chi_2)}{\sqrt{1-4\tau\cos\theta}} E_{r1}(k_1\chi_2)d\theta \tag{5.103}$$

$$I_{21} = \frac{1}{\pi}\int_{\gamma}^{\frac{\pi}{2}} \frac{k_2 \exp(k_2\chi_1)}{\sqrt{1-4\tau\cos\theta}} E_{r2}(k_2\chi_1)d\theta \tag{5.104}$$

$$I_{22} = \frac{1}{\pi}\int_{\gamma}^{\frac{\pi}{2}} \frac{k_2 \exp(k_2\chi_2)}{\sqrt{1-4\tau\cos\theta}} E_{r2}(k_2\chi_2)d\theta \tag{5.105}$$

$$I_{33} = \frac{1}{\pi}\int_{\frac{\pi}{2}}^{\pi} \frac{k_3 \exp(k_3\chi_3)}{\sqrt{1-4\tau\cos\theta}} E_{r3}(k_3\chi_3)d\theta \tag{5.106}$$

$$I_{34} = \frac{1}{\pi}\int_{\frac{\pi}{2}}^{\pi} \frac{k_3 \exp(k_3\chi_4)}{\sqrt{1-4\tau\cos\theta}} E_{r3}(k_3\chi_4)d\theta \tag{5.107}$$

$$I_{43} = \frac{1}{\pi}\int_{\frac{\pi}{2}}^{\pi} \frac{k_4 \exp(k_4\chi_3)}{\sqrt{1-4\tau\cos\theta}} E_{r4}(k_4\chi_3)d\theta \tag{5.108}$$

$$I_{44} = \frac{1}{\pi}\int_{\frac{\pi}{2}}^{\pi} \frac{k_4 \exp(k_4\chi_4)}{\sqrt{1-4\tau\cos\theta}} E_{r4}(k_4\chi_4)d\theta \tag{5.109}$$

Corresponding exponential integrals are defined as

$$E_{rm}(k_i\chi_j) = \begin{cases} E_1(k_i\chi_j) & \text{when } \mathrm{Im}(\chi_j) \geq 0 \\ E_1(k_i\chi_j) - 2\pi i & \text{when } \mathrm{Im}(\chi_j) < 0 \end{cases}$$

$$\text{for } m = 1,3,4 \tag{5.110}$$

$$E_{rm}(k_i\chi_j) = \begin{cases} E_1(k_i\chi_j) + 2\pi i & \text{when } \mathrm{Im}(\chi_j) \geq 0 \\ E_1(k_i\chi_j) & \text{when } \mathrm{Im}(\chi_j) < 0 \end{cases}$$

$$\text{for } m = 2 \tag{5.111}$$

The integration intervals in the integrals I_{33} through I_{44} can be changed from $[\pi/2,\pi]$ to $[0,\pi/2]$ using the transformation $\theta' = \pi - \theta$, and then these integrals can be rewritten as (θ' is exchanged to θ again)

$$I_{33} = \frac{1}{\pi}\int_0^{\frac{\pi}{2}} \frac{k_3 \exp(k_3\chi_3)}{\sqrt{1+4\tau\cos\theta}} E_{r3}(k_3\chi_3)d\theta \tag{5.112}$$

$$I_{34} = \frac{1}{\pi}\int_0^{\frac{\pi}{2}} \frac{k_3 \exp(k_3\chi_4)}{\sqrt{1+4\tau\cos\theta}} E_{r3}(k_3\chi_4)d\theta \tag{5.113}$$

$$I_{43} = \frac{1}{\pi}\int_0^{\frac{\pi}{2}} \frac{k_4 \exp(k_4\chi_3)}{\sqrt{1+4\tau\cos\theta}} E_{r4}(k_4\chi_3)d\theta \tag{5.114}$$

$$I_{44} = \frac{1}{\pi}\int_0^{\frac{\pi}{2}} \frac{k_4 \exp(k_4\chi_4)}{\sqrt{1+4\tau\cos\theta}} E_{r4}(k_4\chi_4)d\theta \tag{5.115}$$

where

$$\left.\begin{matrix} k_3 \\ k_4 \end{matrix}\right\} = \left\{\frac{1+2\tau\cos\theta \mp \sqrt{1+4\tau\cos\theta}}{2\tau^2\cos^2\theta}\right\}\frac{\omega^2}{g} \tag{5.116}$$

$$\begin{aligned} \chi_3 &= (z+\zeta) + i[(x-\xi)\cos\theta + (y-\eta)\sin\theta] = \overline{\chi}_2 \\ \chi_4 &= (z+\zeta) + i[(x-\xi)\cos\theta - (y-\eta)\sin\theta] = \overline{\chi}_1 \end{aligned} \tag{5.117}$$

Final forms of Green function in the current section are identical with the one presented in Wu and Eatock Taylor (1989). Further details of the Green function used in the present study such as, derivatives of Green function and integration technique for the singularities in the integration intervals are described in Appendix A. Special formulations of Green functions at zero speed and zero frequency are also presented in Appendix A.

5.6.5 Numerical calculation

The Green function given in equation (5.74) which is associated with the expressions of I_{0j} and I_{ij} is a function of the positions of field and source points, forward speed, forward speed and oscillating frequency. Especially, the characteristics of Green function are dependent upon the interactions between steady and unsteady motions of the translating pulsating source. The steady motion is generated by the constant forward speed of the translating source (Kelvin source) while unsteady motion is mainly due to the oscillation of the pulsating source.

In order to illustrate the effects of the forward speed and oscillating frequency, the Green function due to a translating pulsating source with unit strength has been calculated with various combinations of forward speed and oscillating frequency. The unit strength source is located at the position (0, 0, -1) and travelling in the positive x-axis with a constant speed. Field points are located on the free surface discretised with grid points, which is equally spaced in the x-y plane. The calculation results are illustrated with a three-dimensional view of real and imaginary parts of the potential calculated. The calculation values on the grid points in positive y direction are only displayed since the potential value is symmetric with respect to the x-z plane. The numerical calculation starts with two special cases of steady translating source with zero frequency and pulsating source with zero speed, and then extends to general case of translating pulsating source.

The potential values on the free surface due to the unit strength source translating at zero frequency are demonstrated in Figure 5.7 and Figure 5.8. Since the imaginary part of the potential has very small value, only real part has been presented. When forward speed is smaller than 2.0 [m/s], local disturbances are dominant and wave-like pattern starts to appear at U = 2.0 [m/s] as shown in Figure 5.7. For larger forward speed, it is clearly seen that these pattern are developed according to the forward speed as illustrated in Figure 5.8.

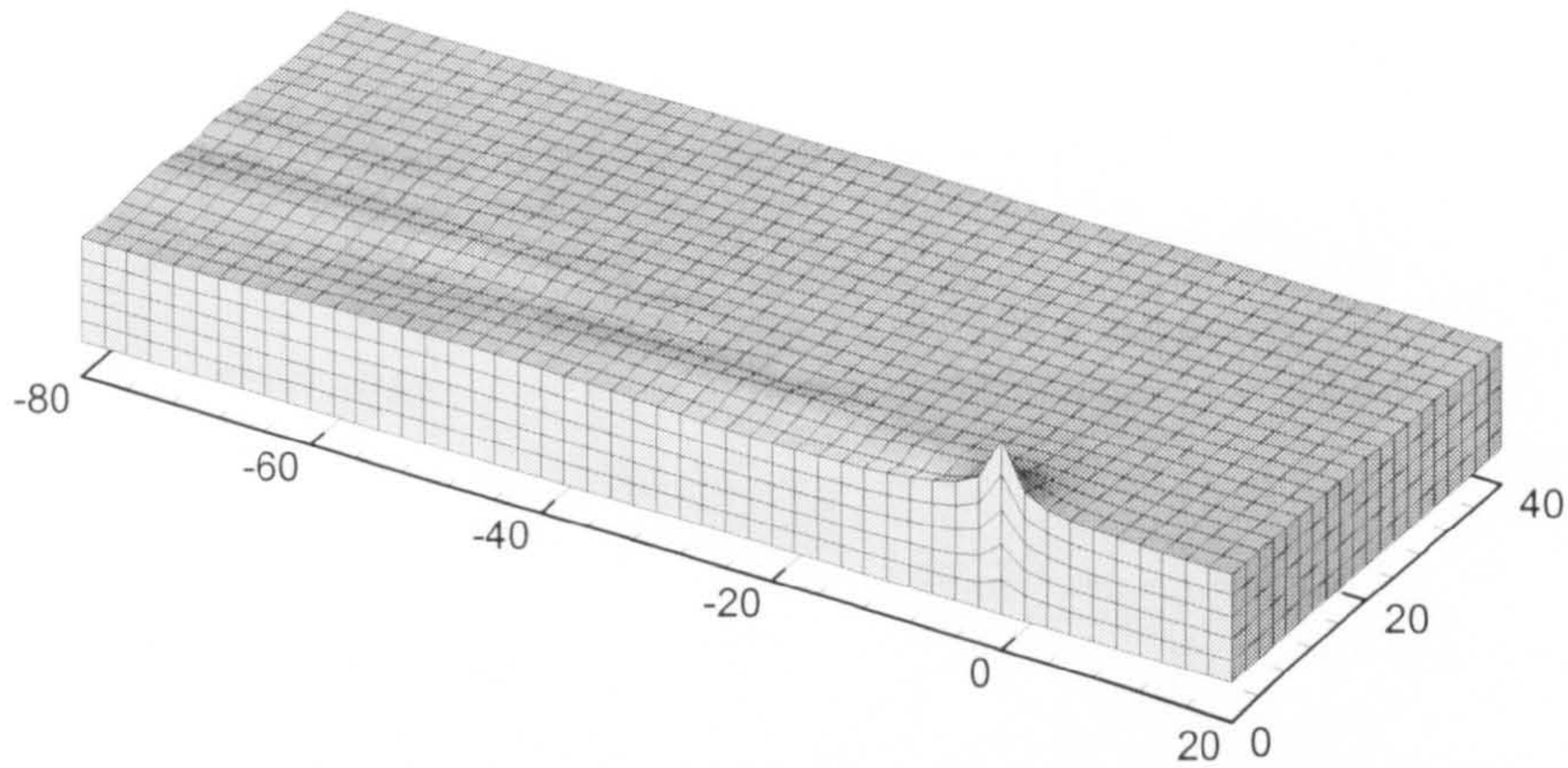

(a) U = 1.8 [m/s] and ω = 0.0 [Hz]

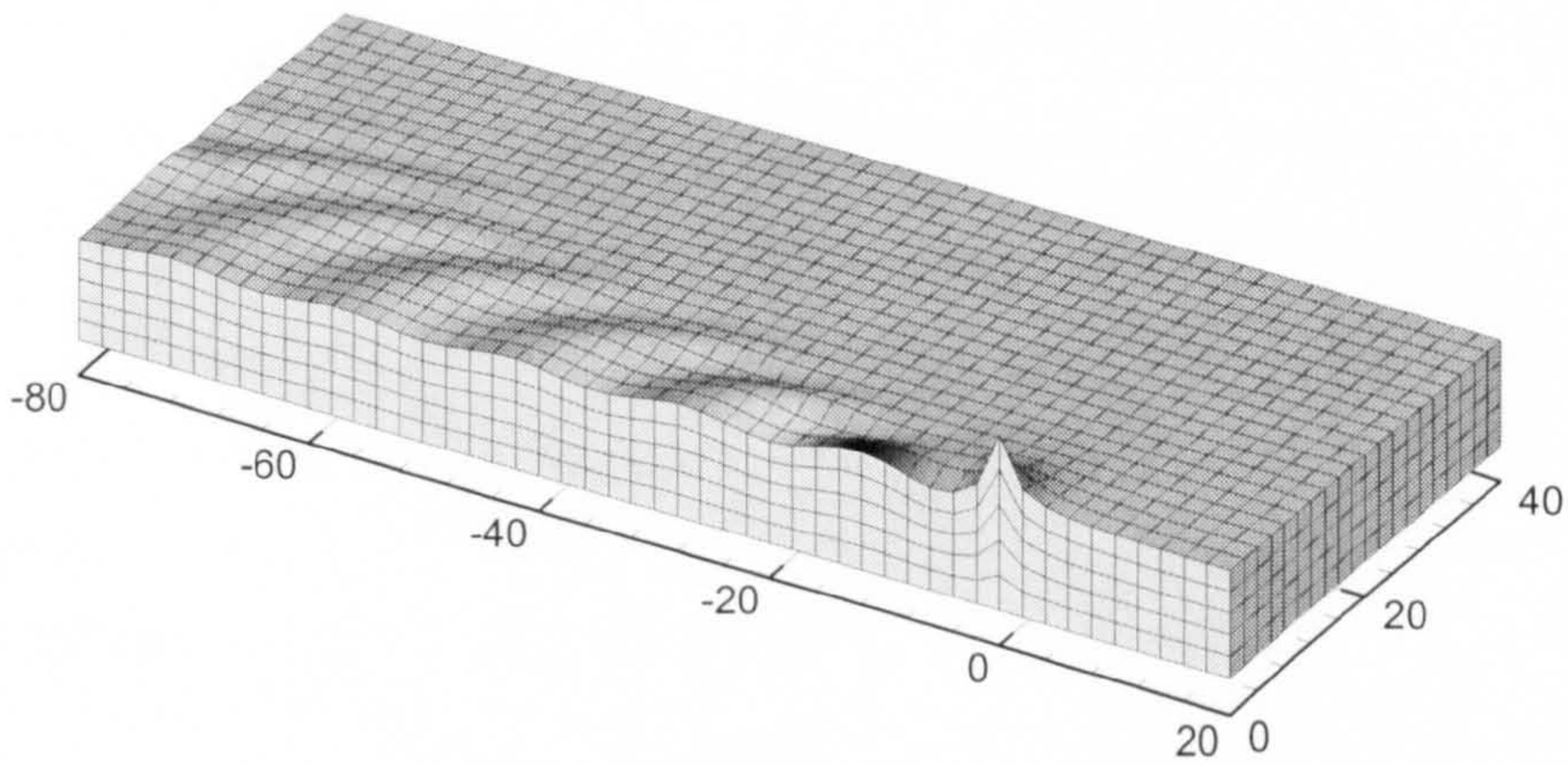

(b) U = 1.9 [m/s] and ω = 0.0 [Hz]

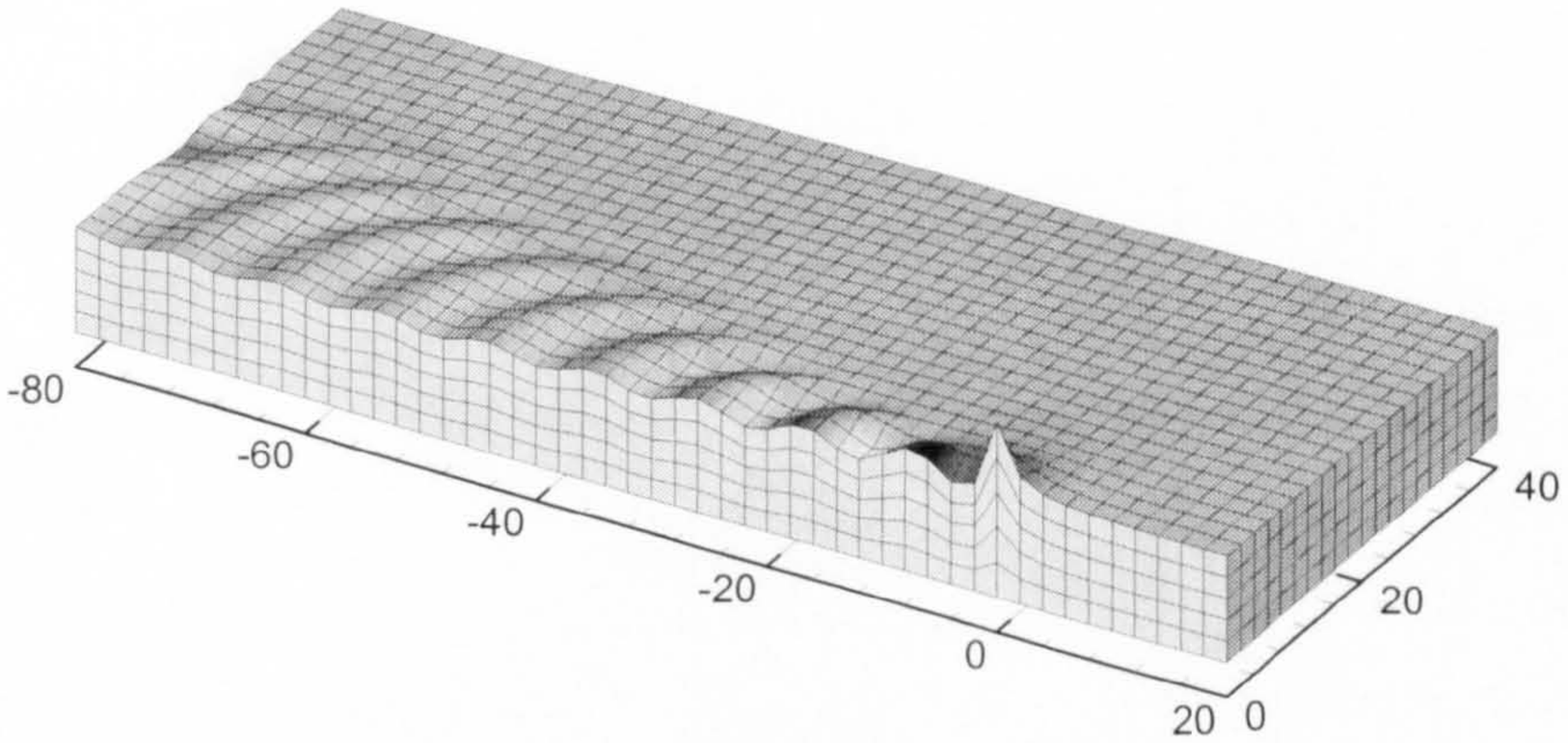

(c) U = 2.0 [m/s] and ω = 0.0 [Hz]

Figure 5.7 Real part of a translating source potential travelling at forward speed U = 1.8, 1.9 and 2.0 [m/s]

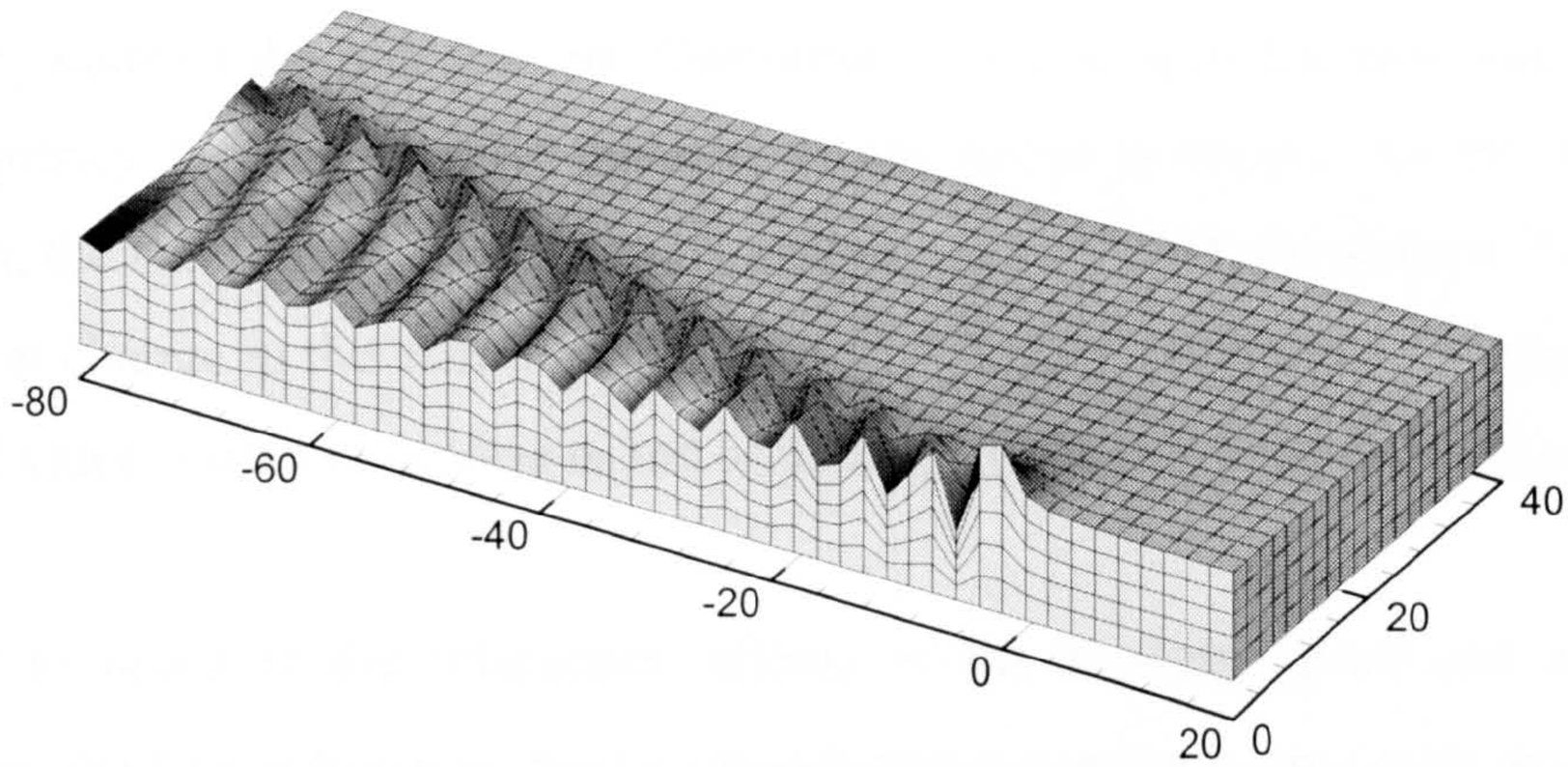

(a) U = 3.0 [m/s] and ω = 0.0 [Hz]

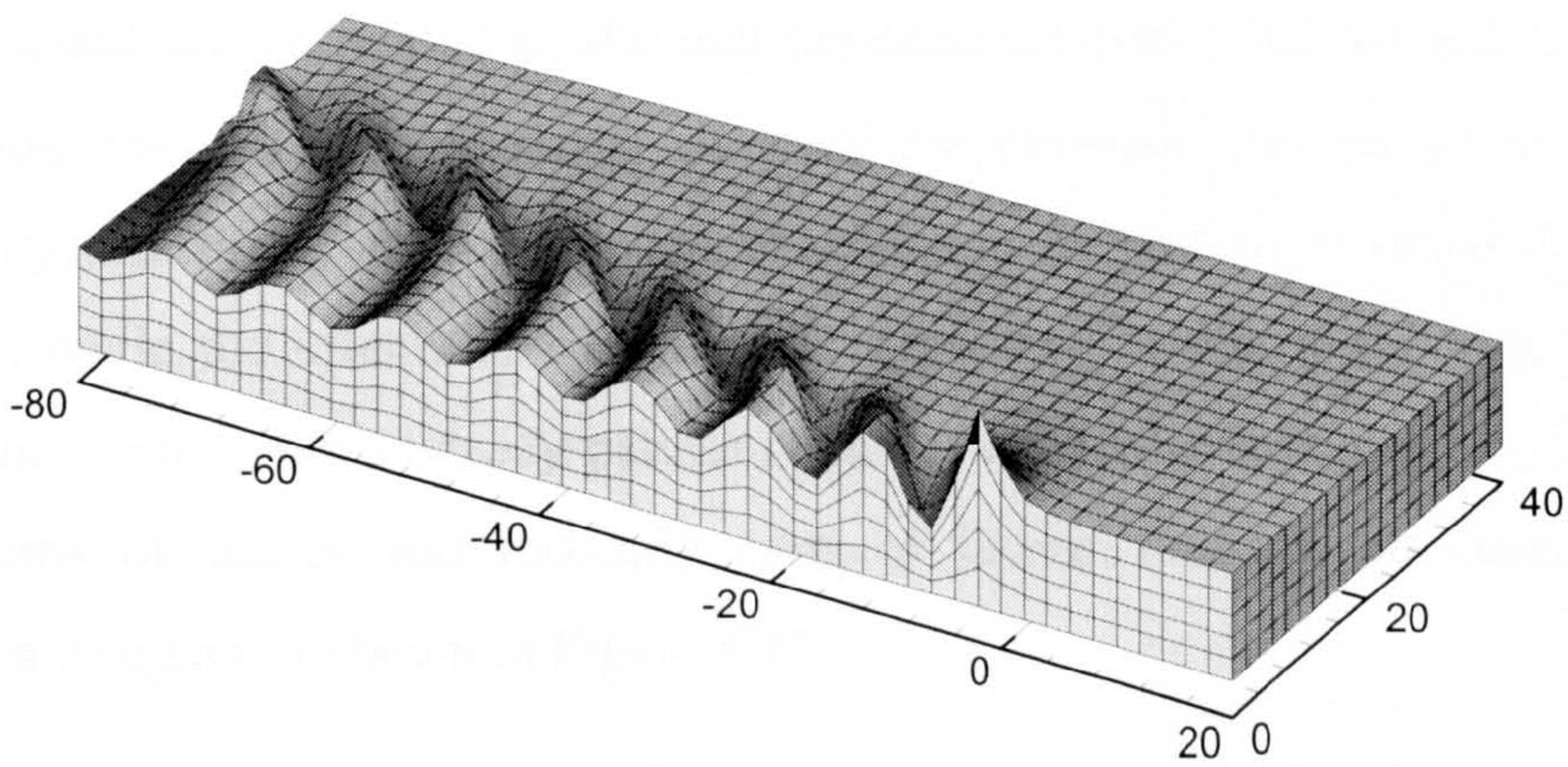

(b) U = 4.0 [m/s] and ω = 0.0 [Hz]

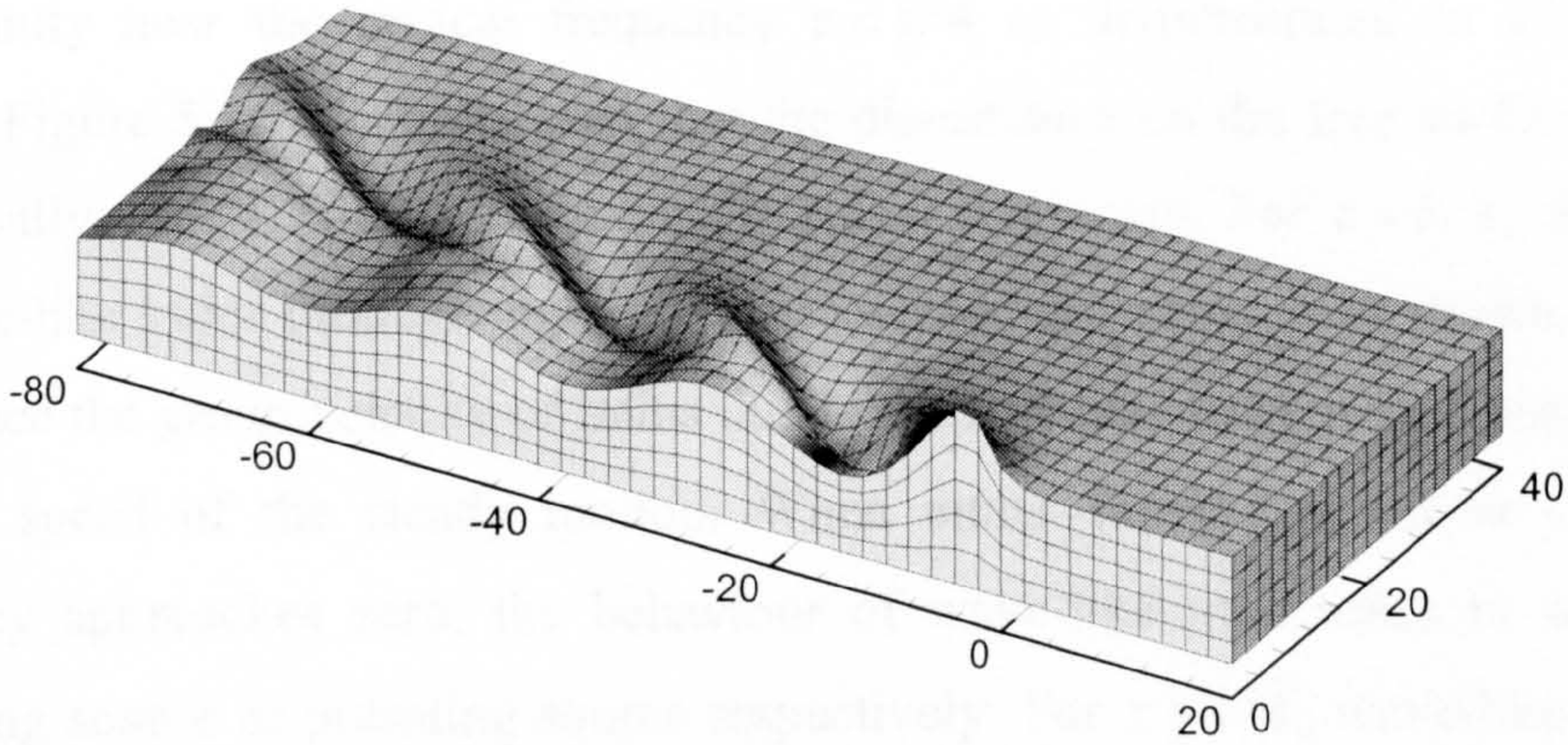

(c) U = 6.0 [m/s] and ω = 0.0 [Hz]

Figure 5.8 Real part of a translating source potential travelling at forward speed U = 3.0, 4.0 and 6.0 [m/s]

The patterns of potential values due to the unit strength source oscillating at zero forward speed are demonstrated in Figure 5.9 and Figure 5.10, where both real and imaginary parts of the potential are illustrated. It can be seen that potential values at any frequency have symmetric patterns in the radial direction. As the frequency increases, the sinusoidal patterns start to spread outward from the source. There is no significant change in the overall patterns on free surface except that the amplitude of potential value starts to decrease as the oscillating frequency becomes higher.

In order to illustrate the interaction effects of the forward speed and oscillating frequency, the Green function due to a translating pulsating source with unit strength has been illustrated in Figure 5.11 through Figure 5.14. The oscillating frequency and forward speed are correlated in the non-dimensional parameter $\tau = \omega U / g$. Figure 5.11 shows the real and imaginary parts of the potential for $\tau = 0.2$ and various forward speeds. For a smaller forward speed unsteady pattern in radial direction is dominant while the effects of steady pattern become dominant for larger forward speed. For $\tau = 0.4$, the unsteady pattern does not appear in the upstream region and the patterns of steady and unsteady parts of Green function are mixed in the downstream region as shown in Figure 5.12.

The interaction effects between oscillating frequency and forward speed changes significantly near the critical frequency $\tau = 1/4$ as demonstrated in Figure 5.13 through Figure 5.14. It can be seen that the disturbance on the free surface changes dramatically with a small adjustment of critical frequency. For $\tau < 1/4$, there exist the wave-like trains propagating both upstream and downstream as shown in Figure 5.13, since the group velocity of trains due to the unsteady motion is greater than the forward speed of the steady motion. When either forward speed or oscillating frequency approaches zero, the behaviour of wave-like train tends to be that of translating source or pulsating source respectively. For $\tau > 1/4$, wave-like train can neither travel nor be fully developed upstream, all wave-like trains propagate downstream only. As the forward speed is further increased, the effects of forward speed become more dominant than that of oscillating frequency as shown in Figure 5.14.

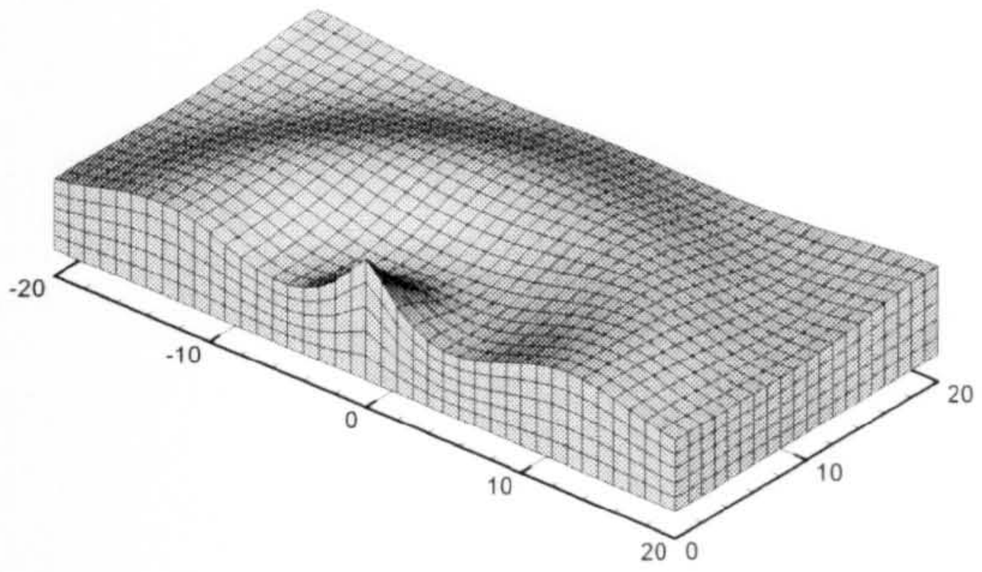

[Real part]

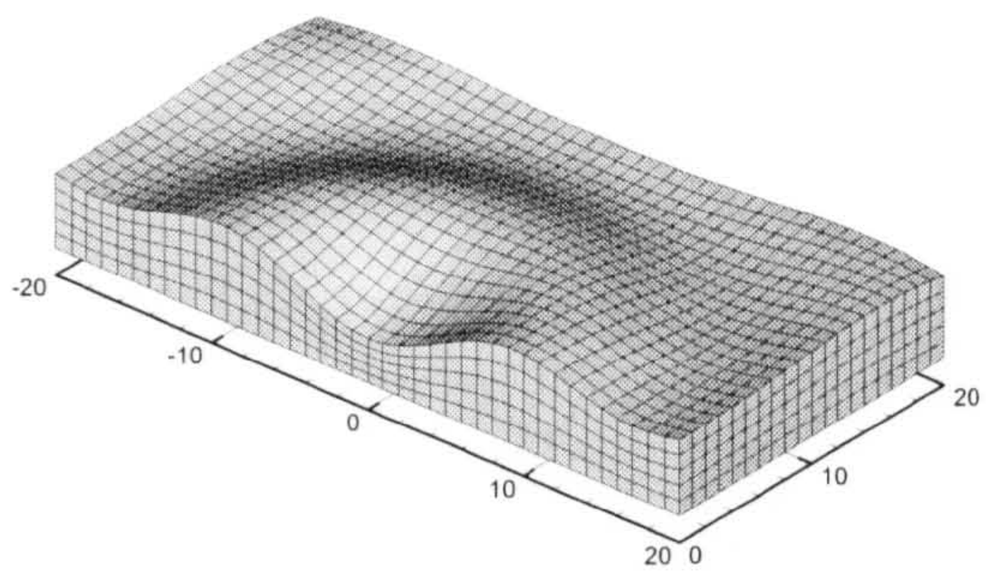

[Imaginary part]

(a) $\omega = 2.0$ [Hz] and $U = 0.0$ [m/s]

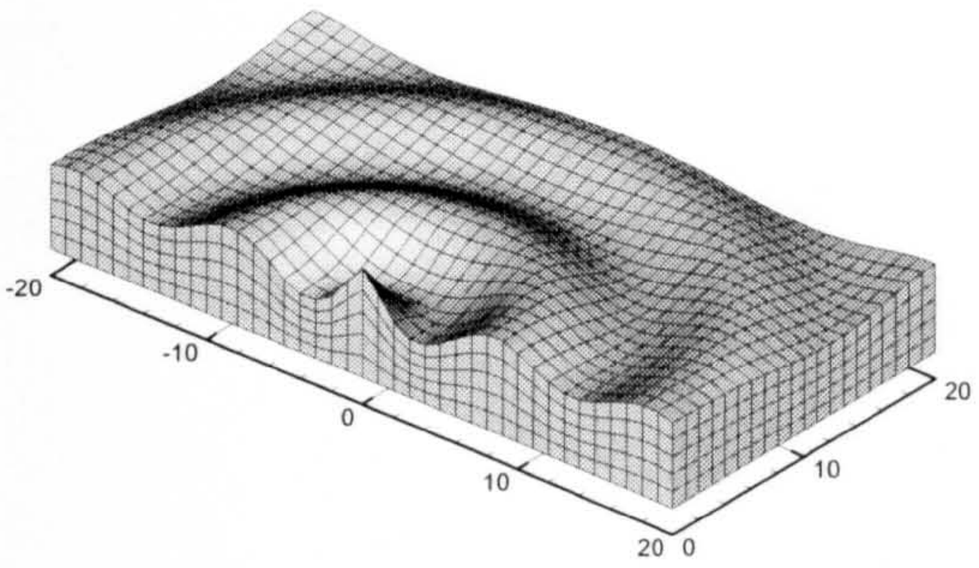

[Real part]

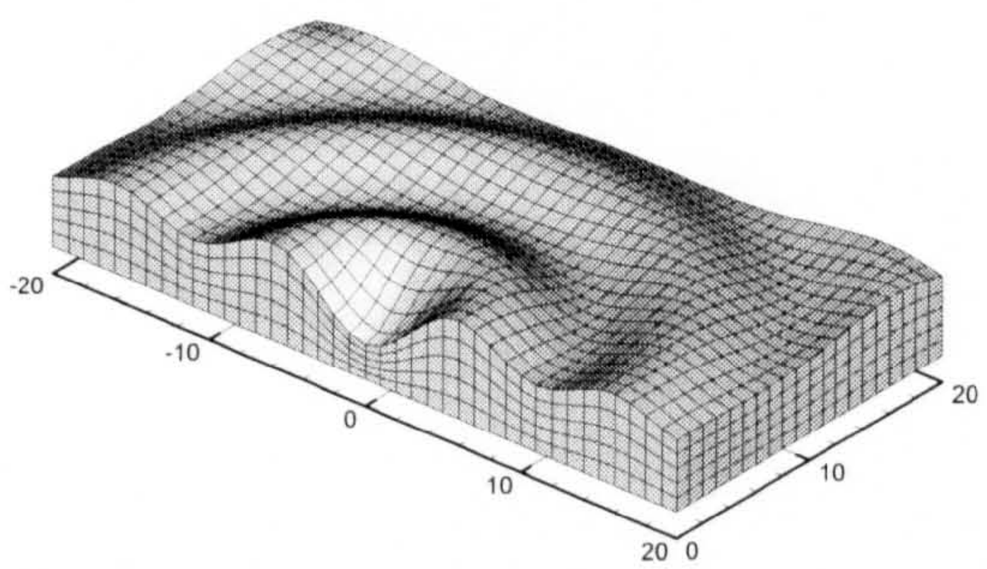

[Imaginary part]

(b) $\omega = 2.5$ [Hz] and $U = 0.0$ [m/s]

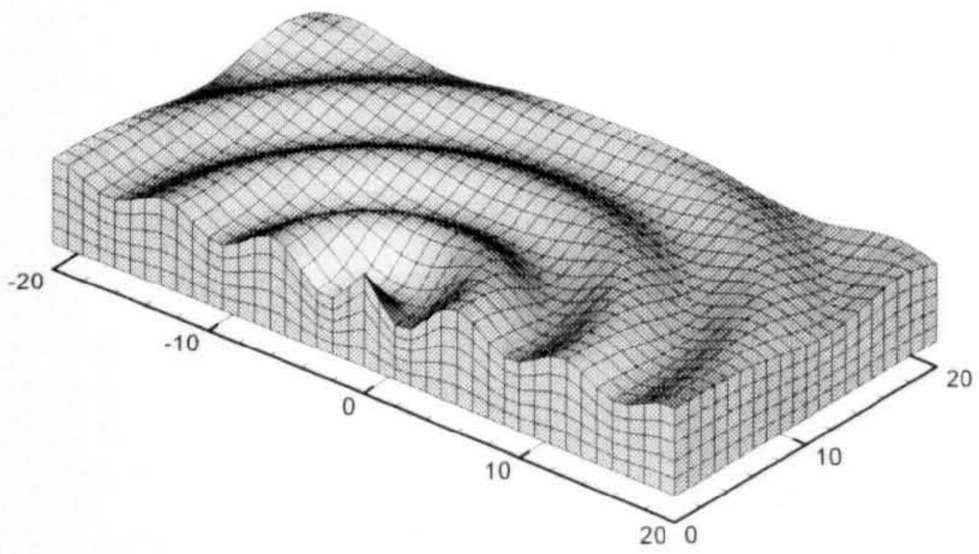

[Real part]

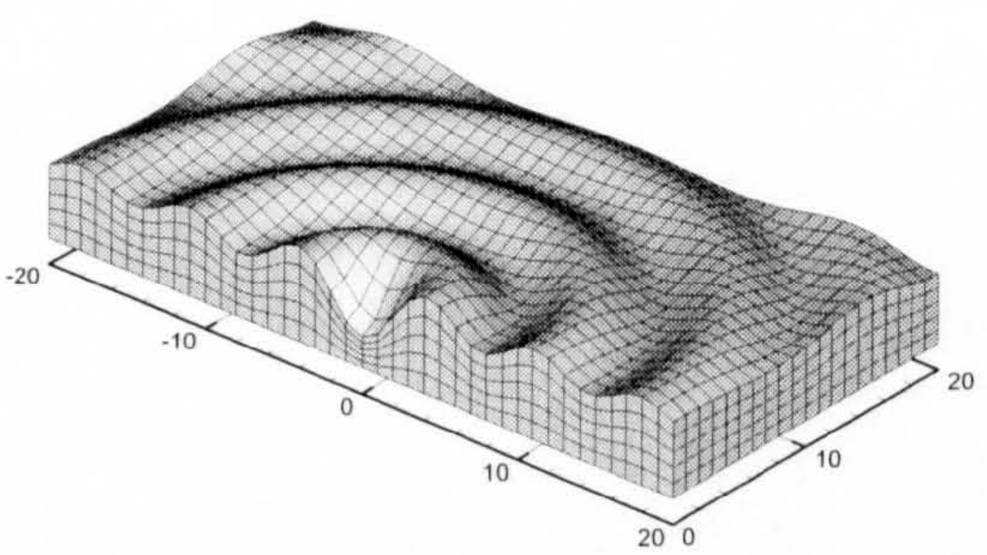

[Imaginary part]

(c) $\omega = 3.0$ [Hz] and $U = 0.0$ [m/s]

Figure 5.9 Real and imaginary parts of a pulsating source potential oscillating at frequency $\omega = 2.0$, 2.5 and 3.0 [Hz]

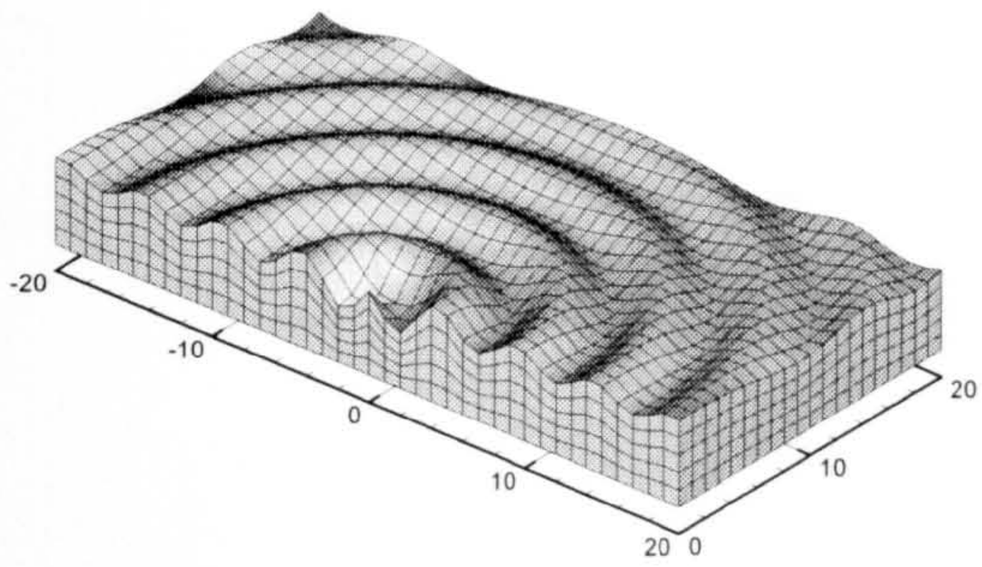

[Real part]

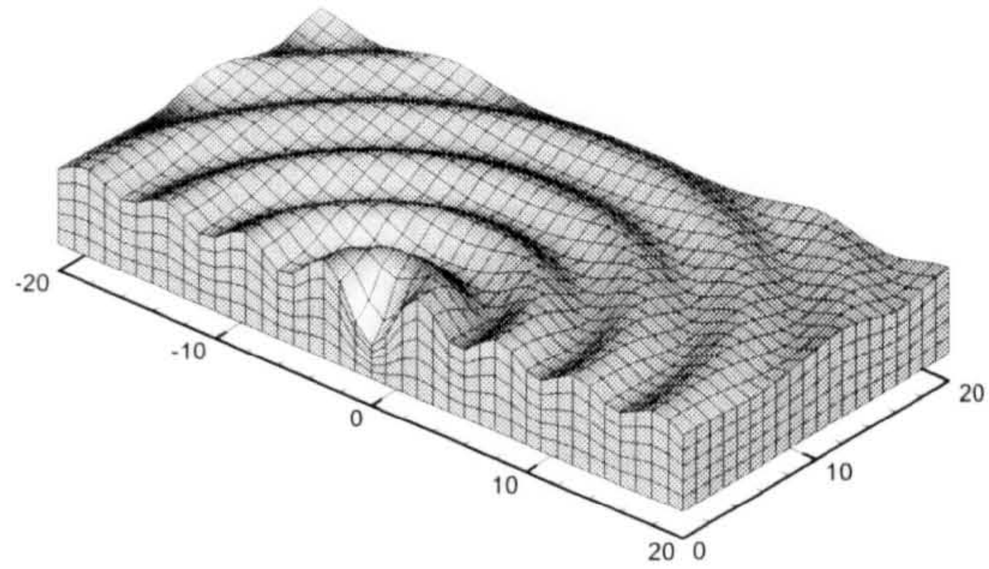

[Imaginary part]

(a) $\omega = 3.5$ [Hz] and $U = 0.0$ [m/s]

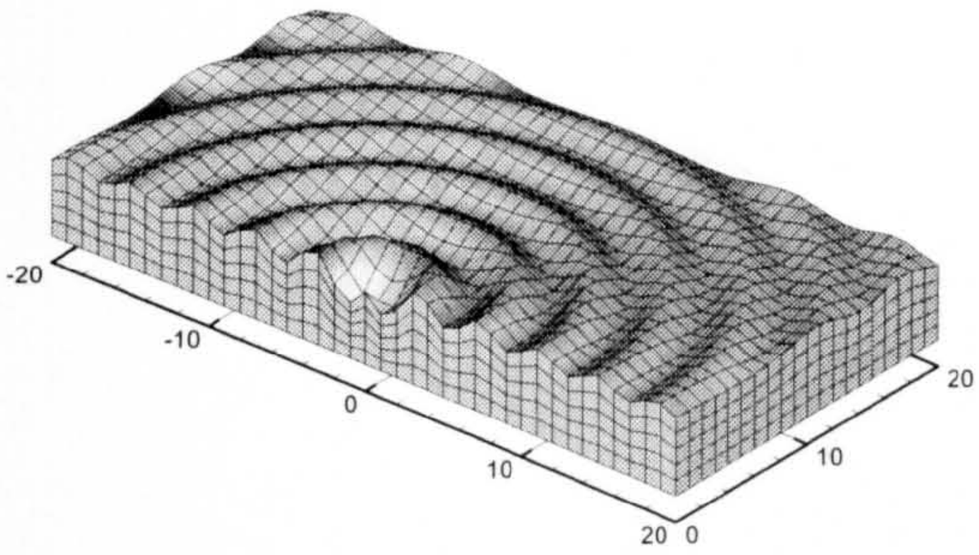

[Real part]

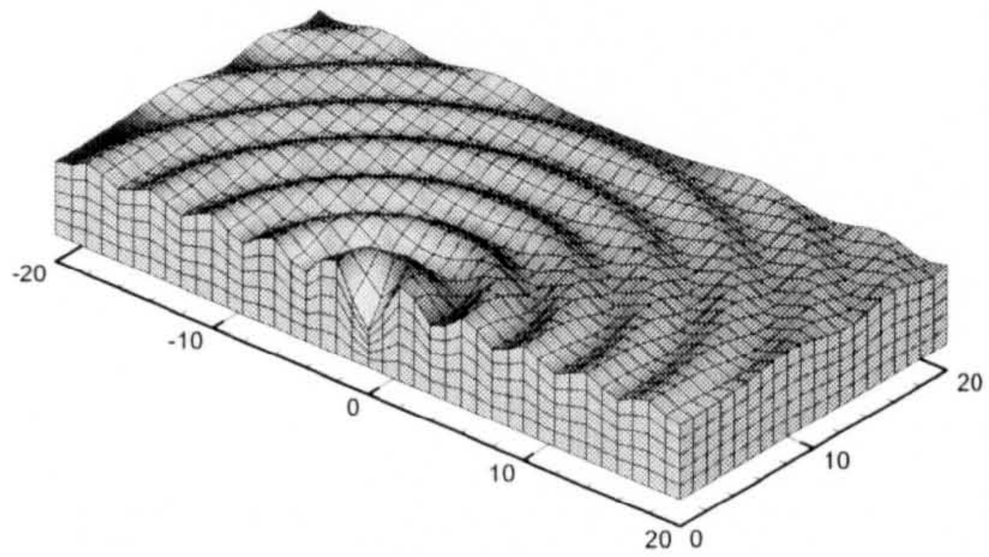

[Imaginary part]

(b) $\omega = 4.0$ [Hz] and $U = 0.0$ [m/s]

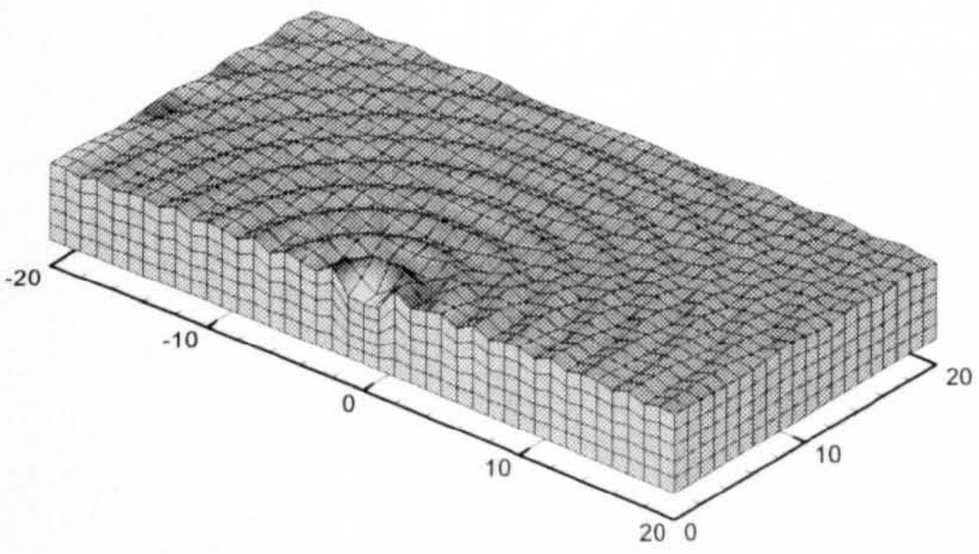

[Real part]

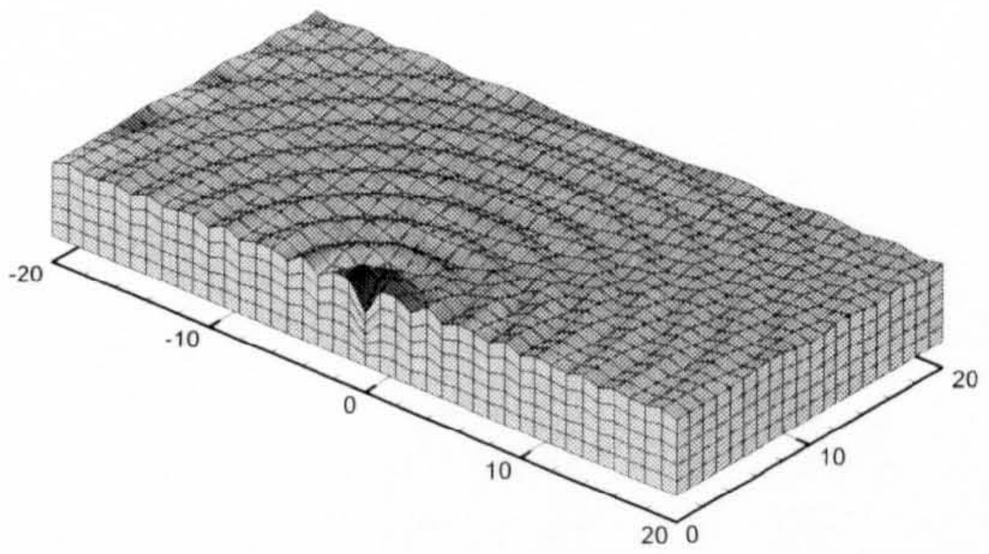

[Imaginary part]

(c) $\omega = 5.0$ [Hz] and $U = 0.0$ [m/s]

Figure 5.10 Real and imaginary parts of a pulsating source potential oscillating at frequency $\omega = 3.5$, 4.0 and 5.0 [Hz]

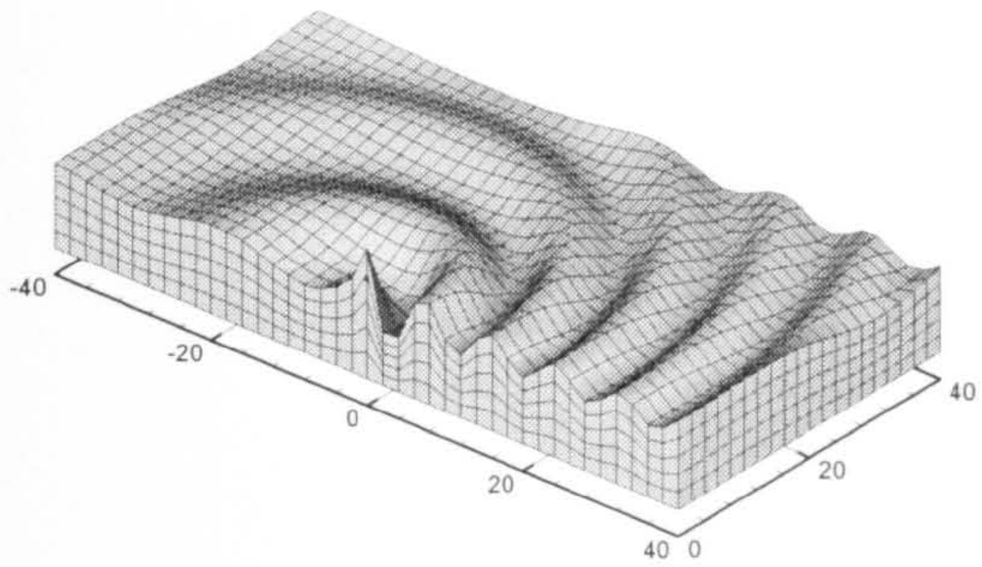

[Real part]

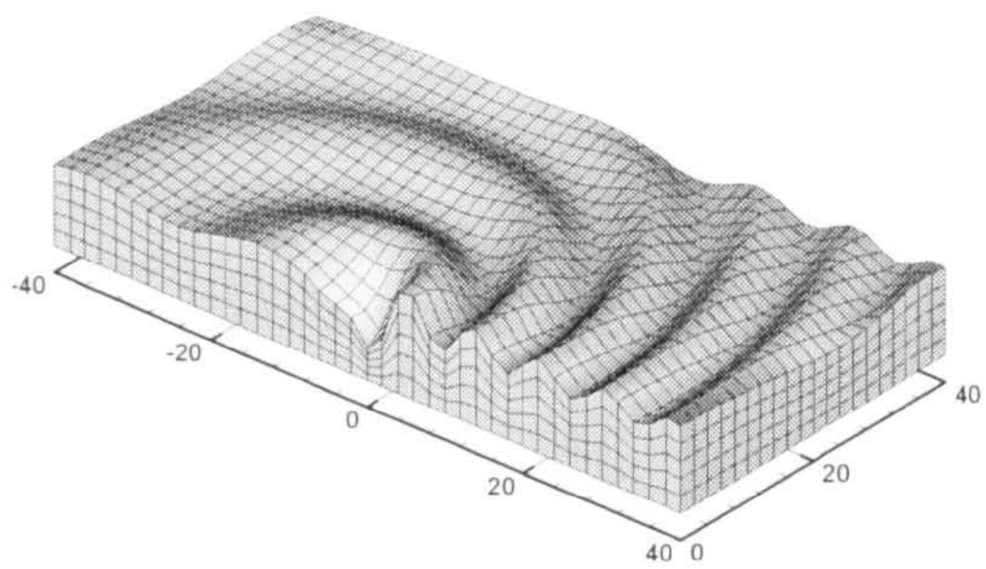

[Imaginary part]

(a) $\tau = 0.2$: $\omega = 1.962$ [Hz] and U = 1.0 [m/s]

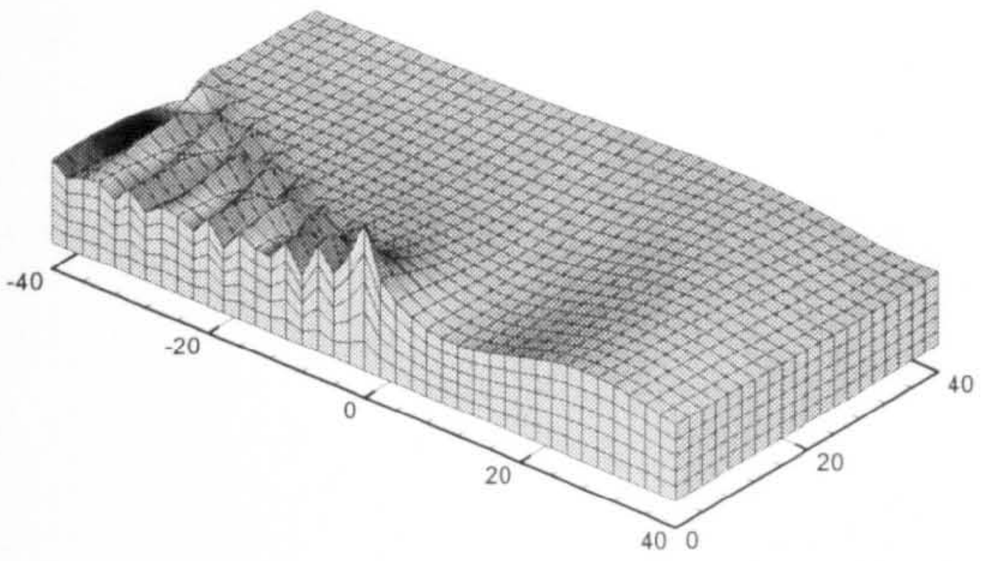

[Real part]

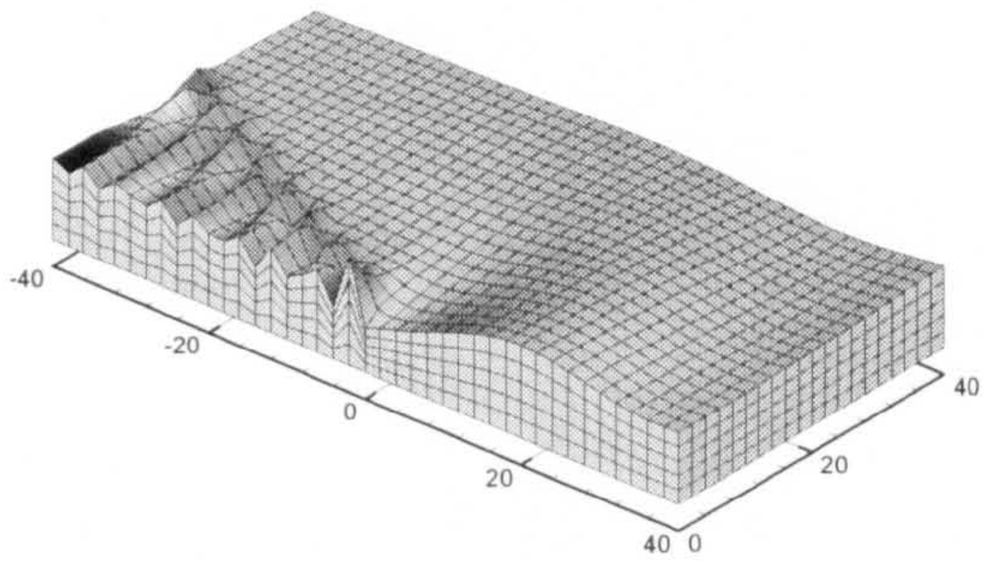

[Imaginary part]

(b) $\tau = 0.2$: $\omega = 0.981$ [Hz] and U = 2.0 [m/s]

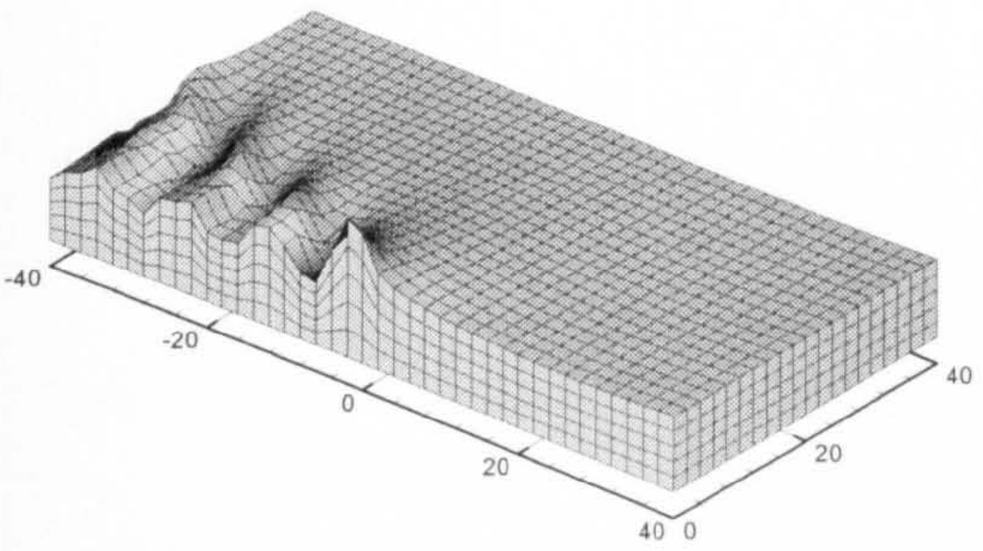

[Real part]

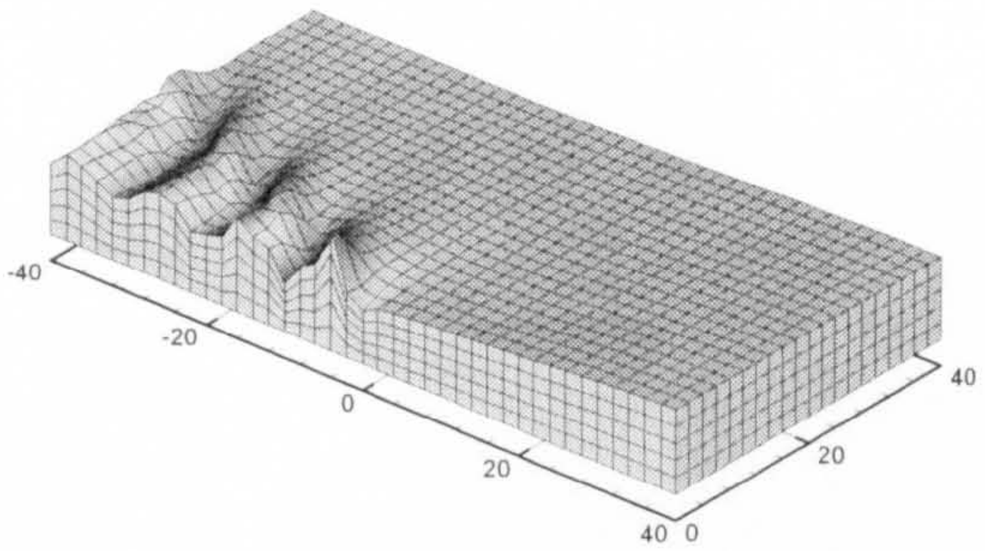

[Imaginary part]

(c) $\tau = 0.2$: $\omega = 0.654$ [Hz] and U = 3.0 [m/s]

Figure 5.11 Real and imaginary parts of a translating pulsating source potential oscillating at $\tau = 0.2$

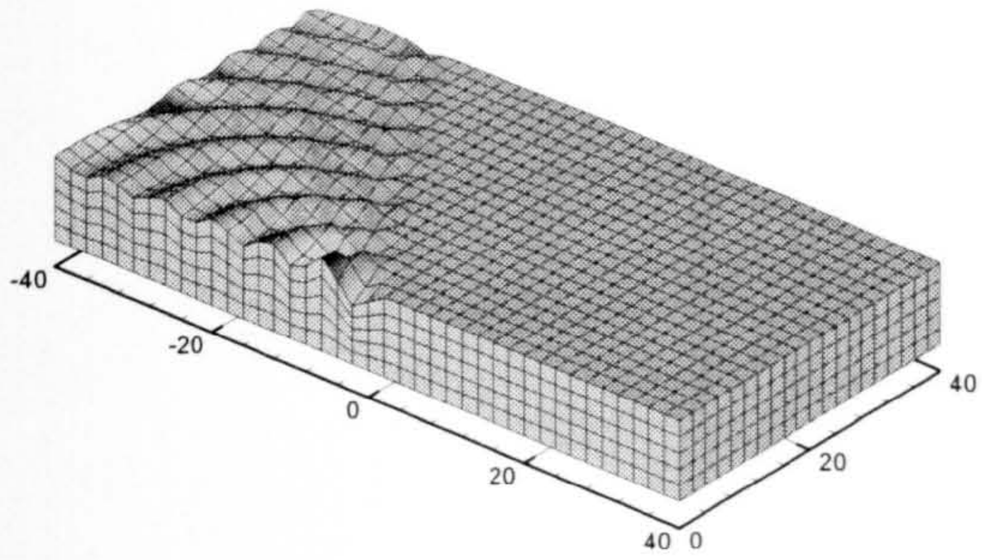

[Real part]

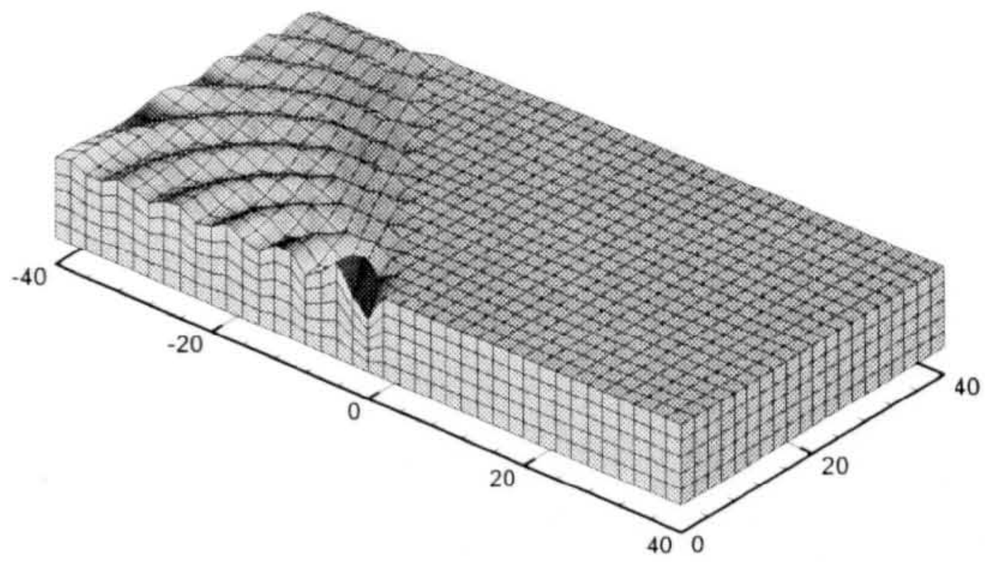

[Imaginary part]

(a) $\tau = 0.4$: $\omega = 3.924$ [Hz] and U = 1.0 [m/s]

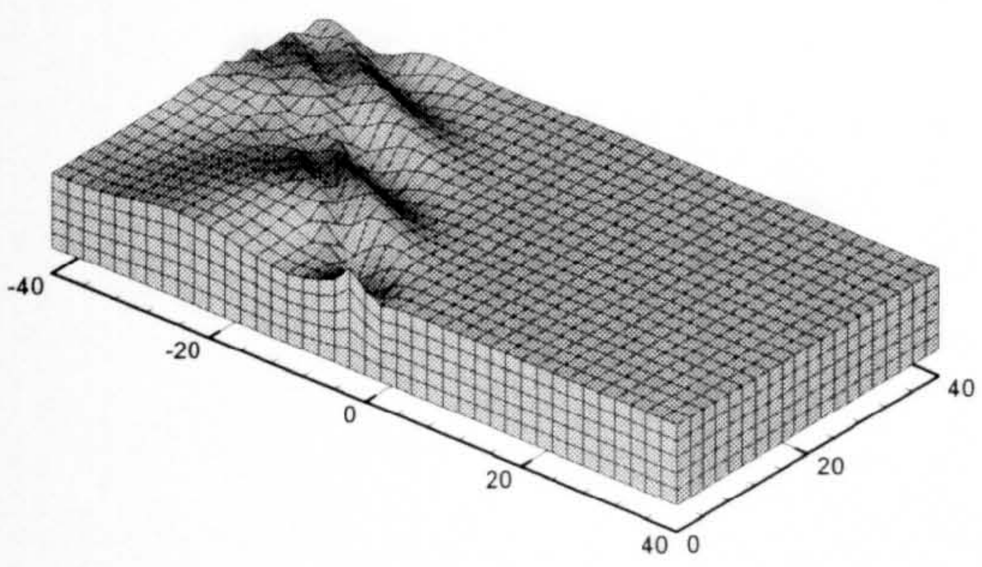

[Real part]

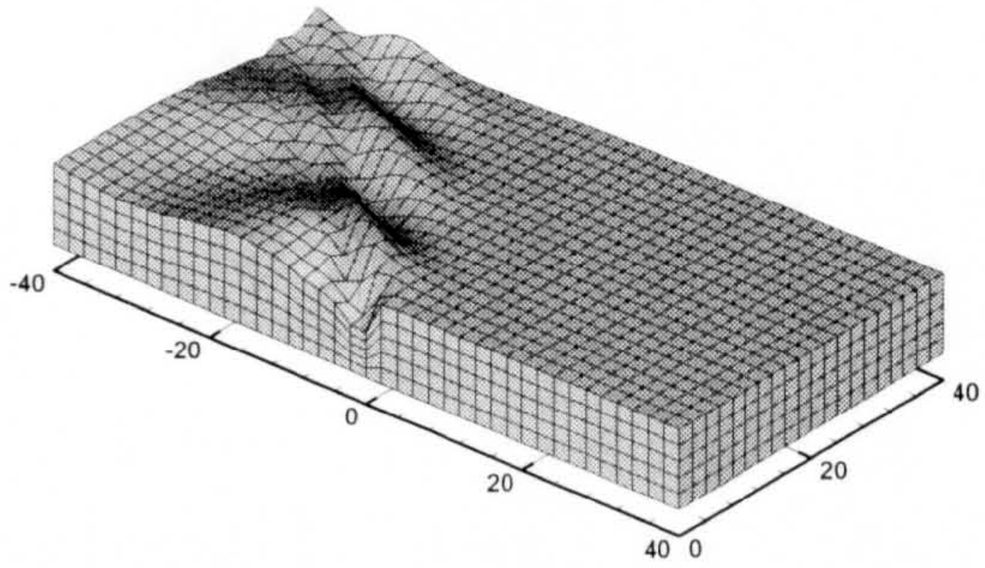

[Imaginary part]

(b) $\tau = 0.4$: $\omega = 1.962$ [Hz] and U = 2.0 [m/s]

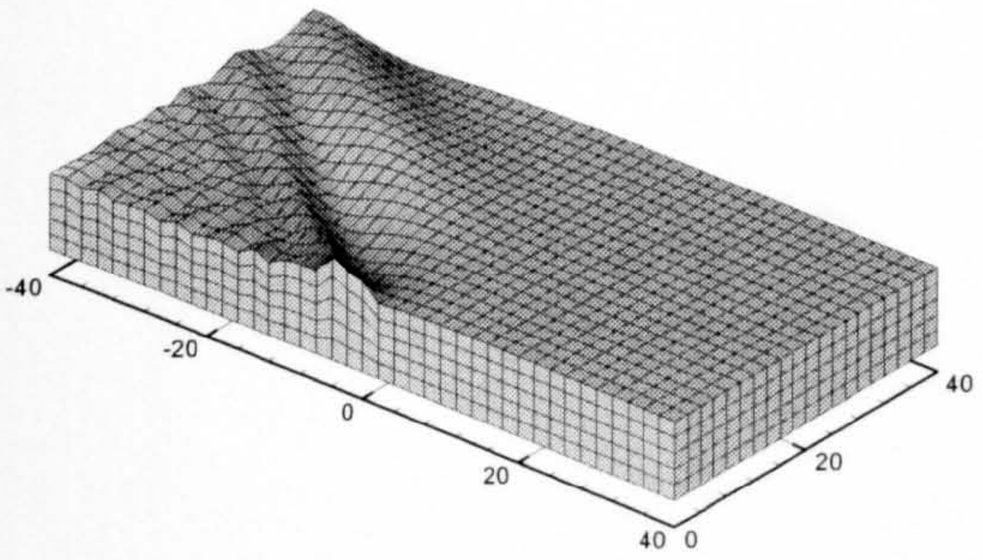

[Real part]

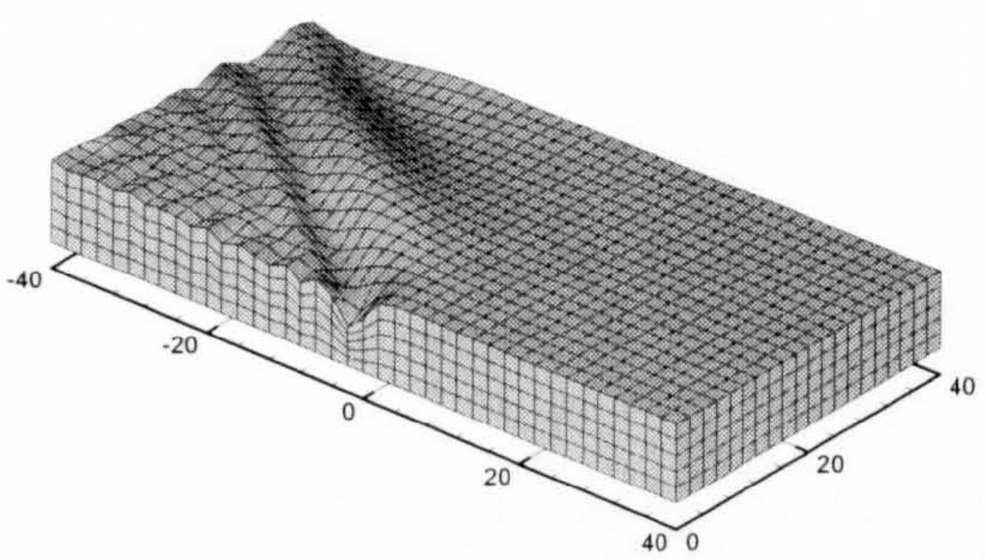

[Imaginary part]

(c) $\tau = 0.4$: $\omega = 1.308$ [Hz] and U = 3.0 [m/s]

Figure 5.12 Real and imaginary parts of a translating pulsating source potential oscillating at $\tau = 0.4$

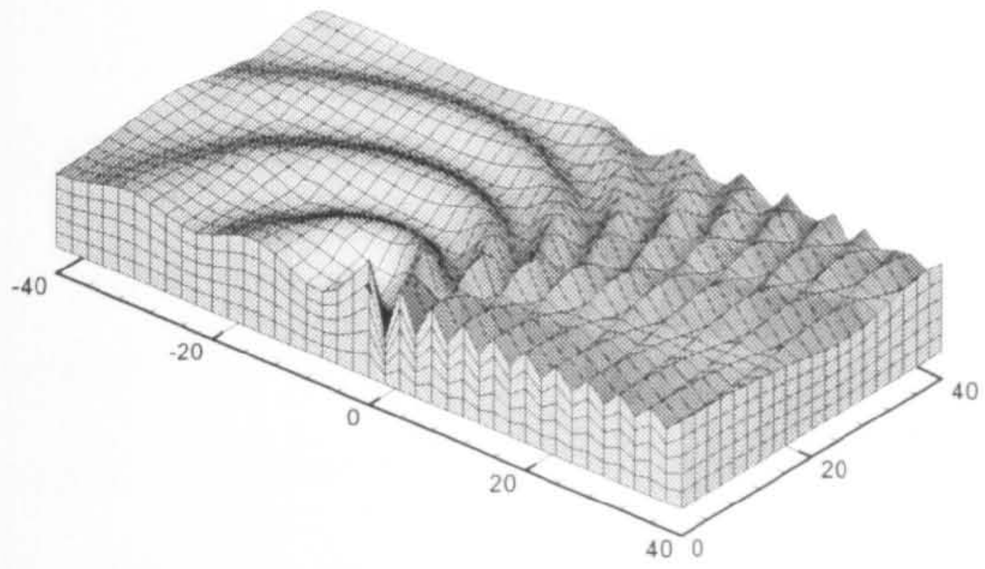

[Real part]

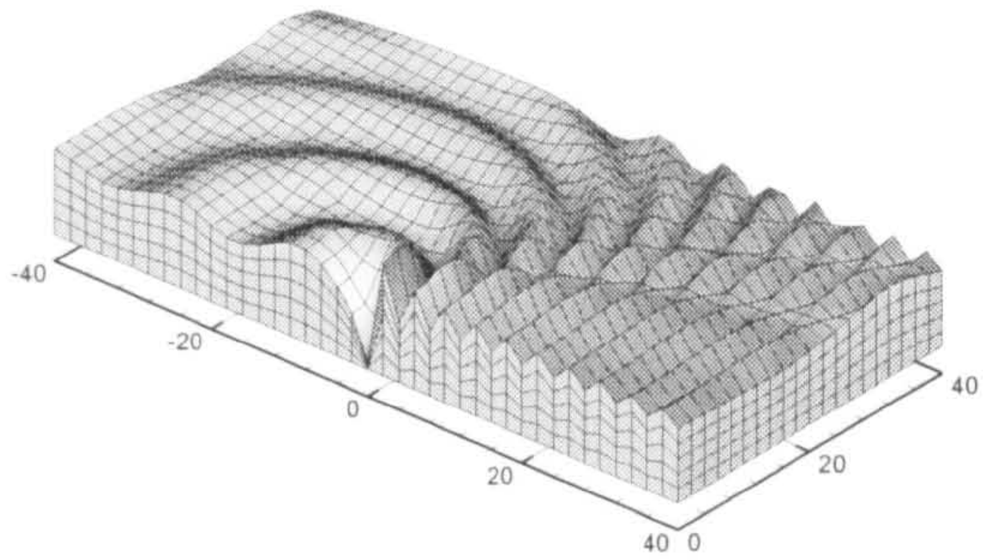

[Imaginary part]

(a) $\tau = 0.24$: $\omega = 2.354$ [Hz] and U = 1.0 [m/s]

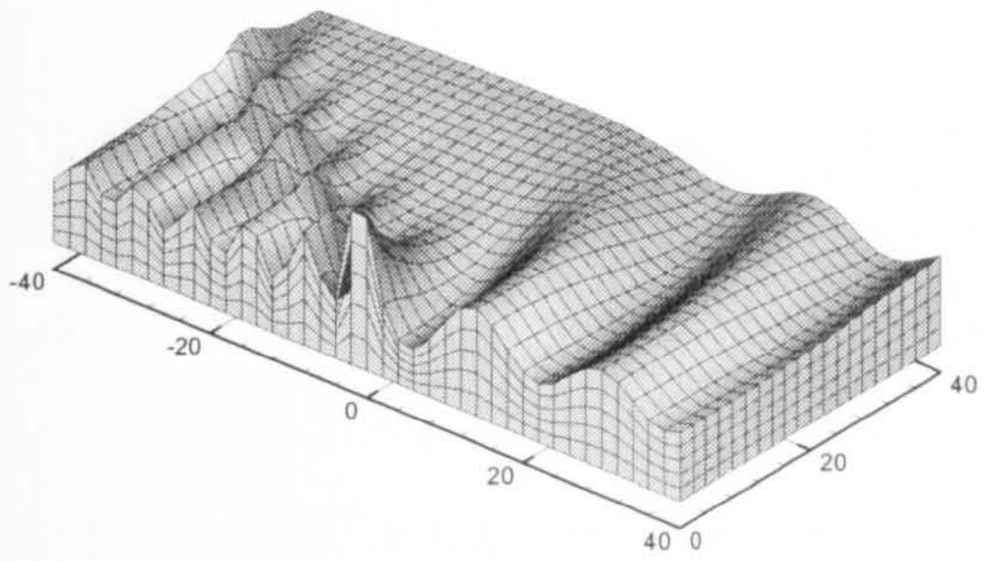

[Real part]

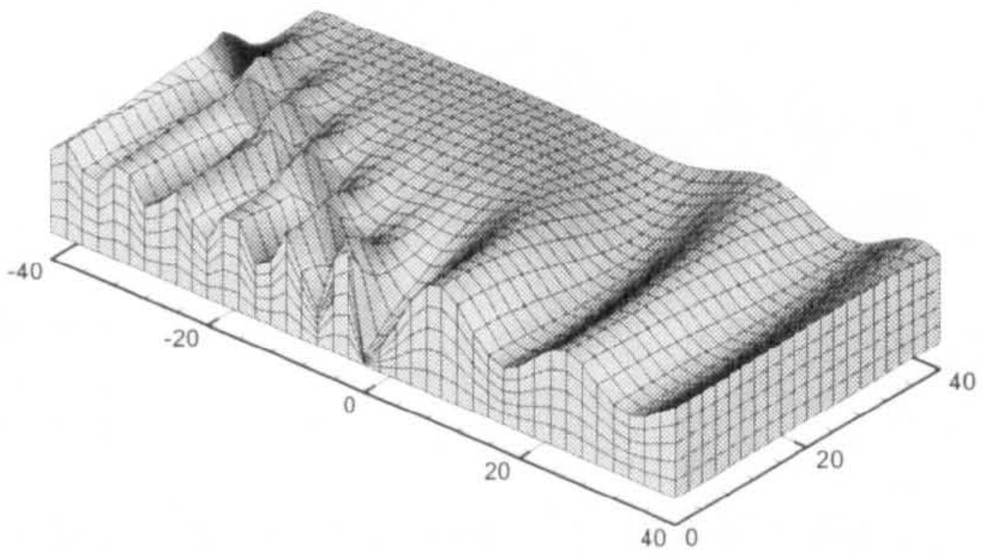

[Imaginary part]

(b) $\tau = 0.24$: $\omega = 1.177$ [Hz] and U = 2.0 [m/s]

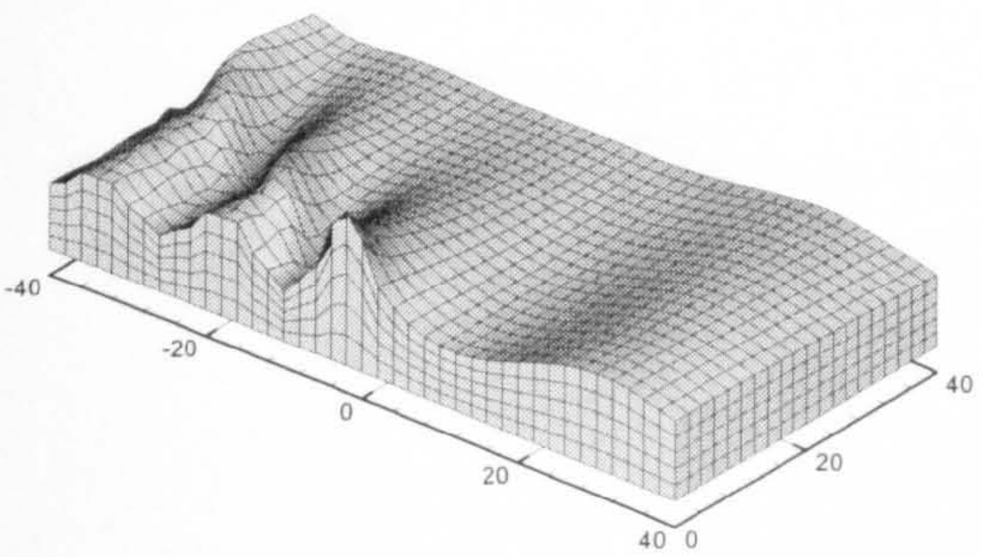

[Real part]

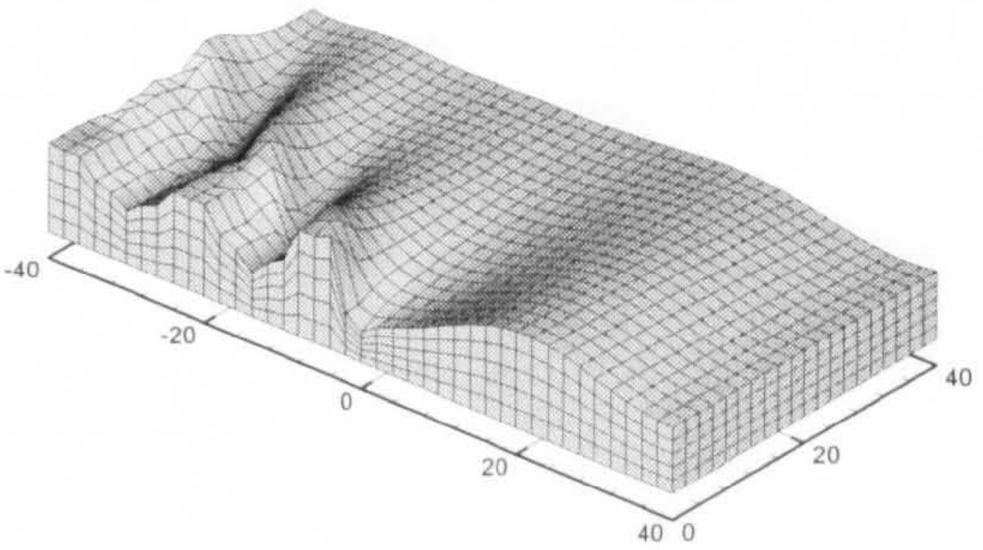

[Imaginary part]

(c) $\tau = 0.24$: $\omega = 0.785$ [Hz] and U = 3.0 [m/s]

Figure 5.13 Real and imaginary parts of a translating pulsating source potential oscillating at $\tau = 0.24$ (near critical frequency $\tau < 1/4$)

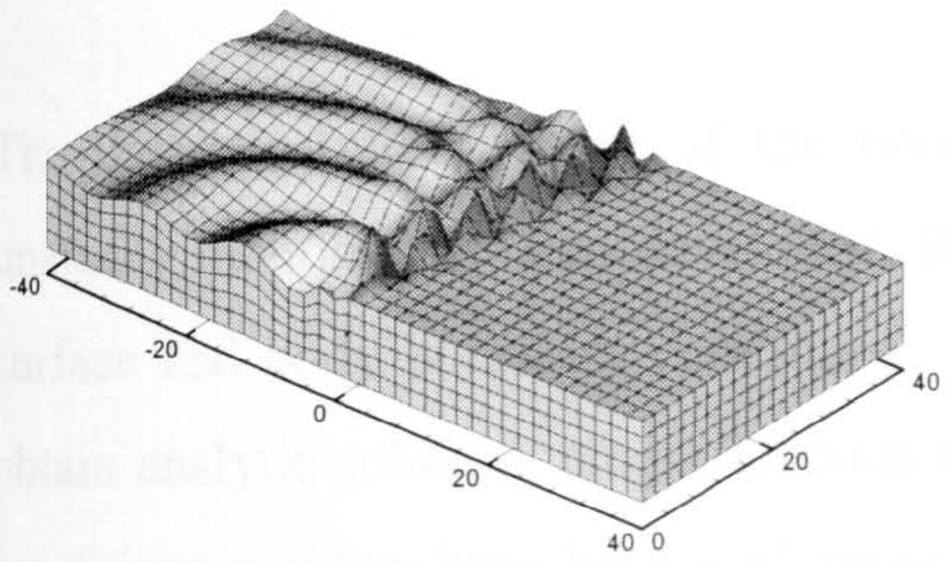

[Real part]

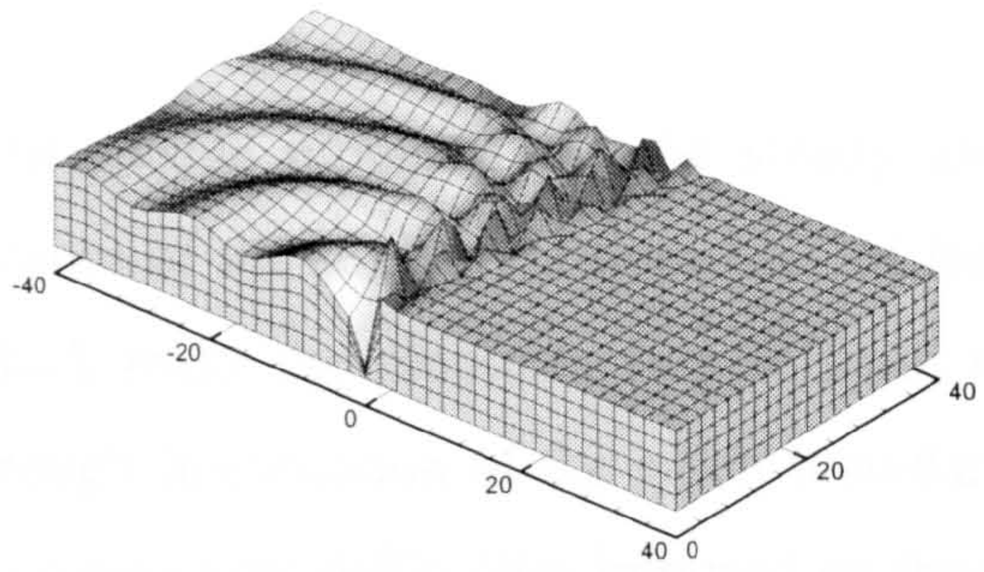

[Imaginary part]

(a) $\tau = 0.26$: $\omega = 2.551$ [Hz] and U = 1.0 [m/s]

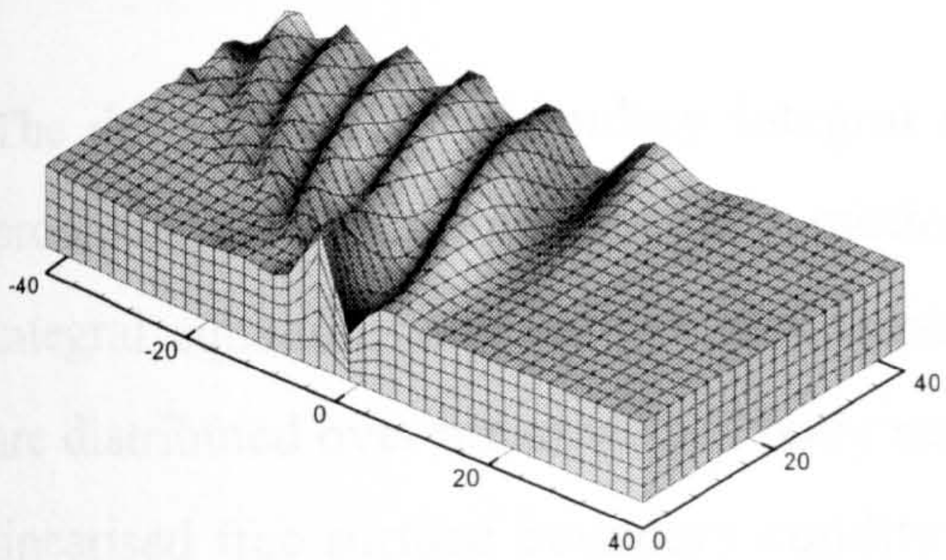

[Real part]

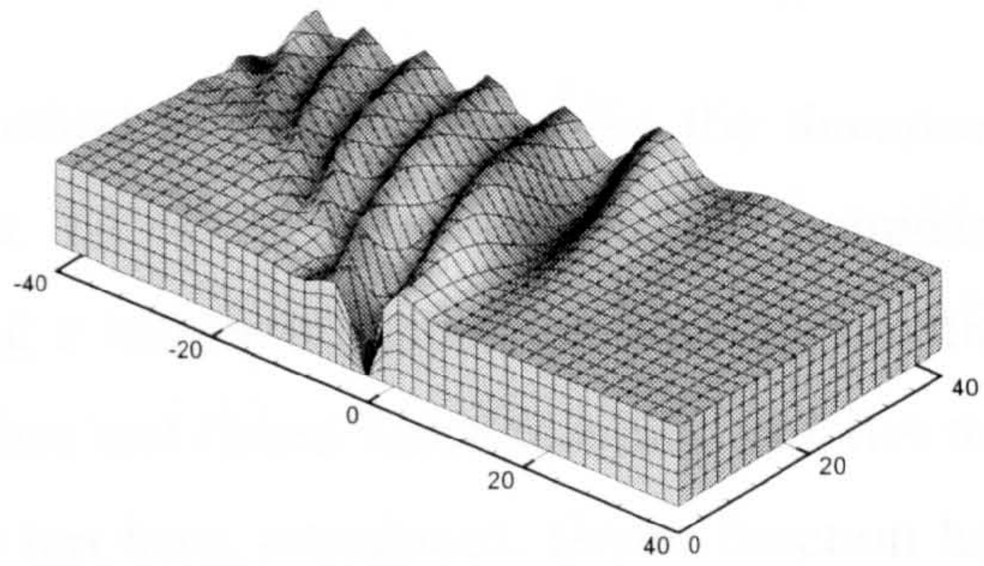

[Imaginary part]

(b) $\tau = 0.26$: $\omega = 1.275$ [Hz] and U = 2.0 [m/s]

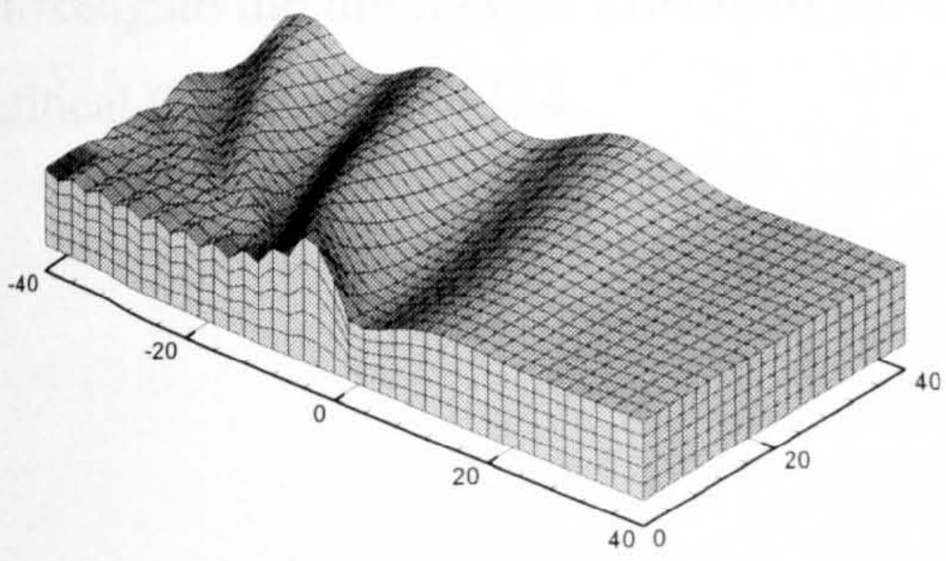

[Real part]

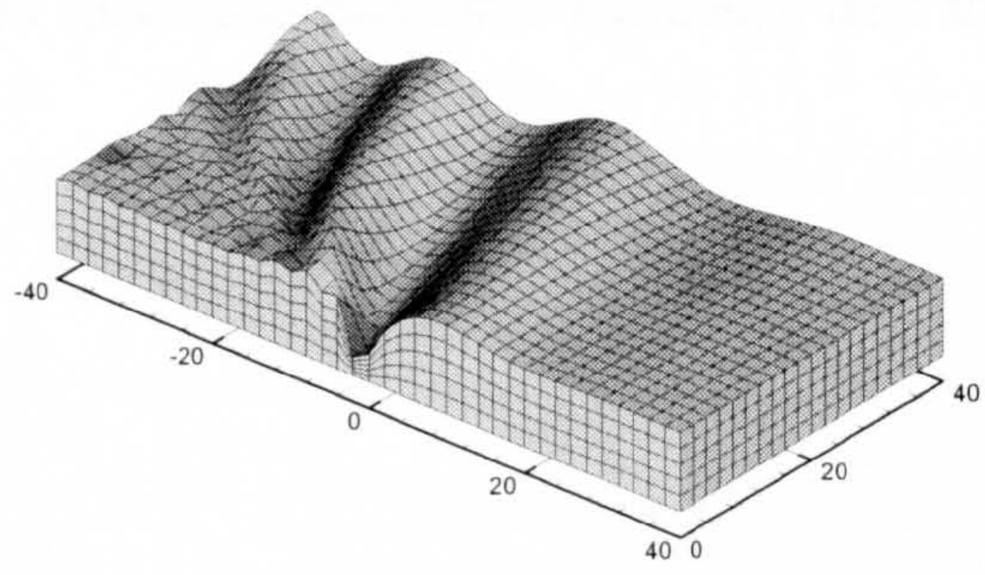

[Imaginary part]

(c) $\tau = 0.26$: $\omega = 0.850$ [Hz] and U = 3.0 [m/s]

Figure 5.14 Real and imaginary parts of a translating pulsating source potential oscillating at $\tau = 0.26$ (near critical frequency $\tau > 1/4$)

5.7 Concluding Remarks

The theoretical formulation of the boundary value problems for the steady and unsteady motions has been developed. Because of the strong non-linearities of free surface and body boundary conditions, which make the problems very difficult to obtain analytic solution, simplifications through linearisation of the given boundary conditions problem have been performed to remove the difficulties imposed on these problems. Under the assumption of small amplitude motions, the velocity potential of unsteady flow field is further decomposed into diffraction and radiation potential problem.

The development of boundary integral method is followed to solve the linearised problems of steady and unsteady motions. To obtain to solution of the boundary integral equation, singularities representing a translating pulsating source potential are distributed over mean wetted body surface and Green function which satisfies the linearised free surface boundary condition has been introduced. Green function has been formulated with a set of single integrals, which is expressed in terms of standard complex integrals. The patterns of disturbances on the free surface generated by a single source advancing under the free surface have been analysed to investigate the interaction effects of forward speed and encounter frequency near the critical frequency $\tau = 1/4$.

Chapter 6. Numerical Implementation of Green Function Method

6.1 Preamble

To predict the hydrodynamic force and the resulting motion of a floating body in the free surface, interactions between the body and surrounding fluid can be analysed in the basis of the velocity potential of the flow field. Thus the formulation of the corresponding boundary value problem has been presented in the previous chapter for the steady and unsteady motions of a body advancing in waves. This chapter is to be devoted to an implementation of the boundary value problem to obtain a practical solution of the given problem.

As shown in Chapter 5, the boundary integral equation has been formed as a surface integral over the mean wetted body surface and a line integral along the intersection between undisturbed free surface and body surface. Since the solution of boundary integral equation can be obtained by using free surface Green function method, distributions of the singularities over mean wetted hull surface require further idealisations of the body surface. According to the types of unknown source strengths, two different methods for the discretisation of the body surface will be presented. The application of the integral equation to each of the discretisation methods leads to a system of simultaneous linear equation whose solution can be obtained by standard numerical techniques. Details on the evaluation of Green function will be described to reduce the computational time and calculation of source term in Green function is also presented.

6.2 Discretisation of Body Surface

An approach adopted to solve the integral equation consists of discretising the integral equation into a set of linear algebraic equations. This is accomplished in the discretisation of the mean wetted body surface on which the body boundary condition is satisfied. The body surface is approximated by a finite but large number of surface elements, whose characteristic dimensions are small compared with those of the body. Over each surface element, the source strength σ can be assumed to be either constant or of higher-order. This reduces the problem of determining the continuous source strength σ to that of determining a finite number of σ.

In the conventional panel method, i.e. so-called Constant Panel Method, the source strength is normally taken to be constant. Since the source strength is constant over each element in the Constant Panel Method, the source distribution is discontinuous and the source strength jumps stepwise at the boundary of two elements. In order to accurately model the variation of the source strength σ over the body surface, it is necessary to use relatively large number of elements for constant source strength σ.

The secret of a good approximation to the body surface lies in the choice of the surface elements. The simplest representation of flat is quadrilateral or triangular elements. Others are also possible using polynomial or spline functions. These types of representations are normally referred to as the higher-order boundary element method, in which the geometry of the surface element and the distribution of source strength are approximated by interpolation of the values at nodes that defined this element. The shape function for hull geometry and the interpolation function for source strength are usually taken to be polynomials in terms of the nodal coordinates. The order of the polynomial determines the order of the element. Since the shape functions are coupled with the complicated Green function, the evaluation of the influence coefficients becomes complicated.

6.2.1 Quadrilateral panels

The flat panel representation was first used by Hess and Smith (1967) for the numerical solution of the potential flow around arbitrary three-dimensional bodies where the body surface was represented by quadrilateral elements. The surface of the wetted body is defined by means of the original four grid points, which do not in general lie in a plane and are grouped to form a quadrilateral element.

Let us denote four original grid points as $\mathbf{x}_1$, $\mathbf{x}_2$, $\mathbf{x}_3$ and $\mathbf{x}_4$ in the anticlockwise sense as seen from the interior of fluid domain. The numbering order of these four points is considered to determine the direction of normal vector on the boundary surfaces. The inward normal vector $\mathbf{N}$, which is positive when pointing into the fluid domain, is found form the cross product of the two diagonal vectors in the form

$$\mathbf{N} = (\mathbf{x}_3 - \mathbf{x}_1) \times (\mathbf{x}_4 - \mathbf{x}_2) \tag{6.1}$$

and the unit normal vector $\mathbf{n}$ of the quadrilateral element can be found as

$$\mathbf{n} = \frac{\mathbf{N}}{|\mathbf{N}|} \tag{6.2}$$

The control point of the quadrilateral panel $\mathbf{x}_m$ whose coordinates are the average of the coordinates of the four grid points such that

$$\mathbf{x}_m = (\mathbf{x}_1 + \mathbf{x}_2 + \mathbf{x}_3 + \mathbf{x}_4)/4$$

In order to facilitate the mathematical manipulation on panel integration, we have to use a local coordinate system $o-\xi\eta\zeta$ whose origin is temporarily defined at the average point $\mathbf{x}_m$ as shown in Figure 6.1. The z-axis is parallel to the unit normal vector $\mathbf{n}$.

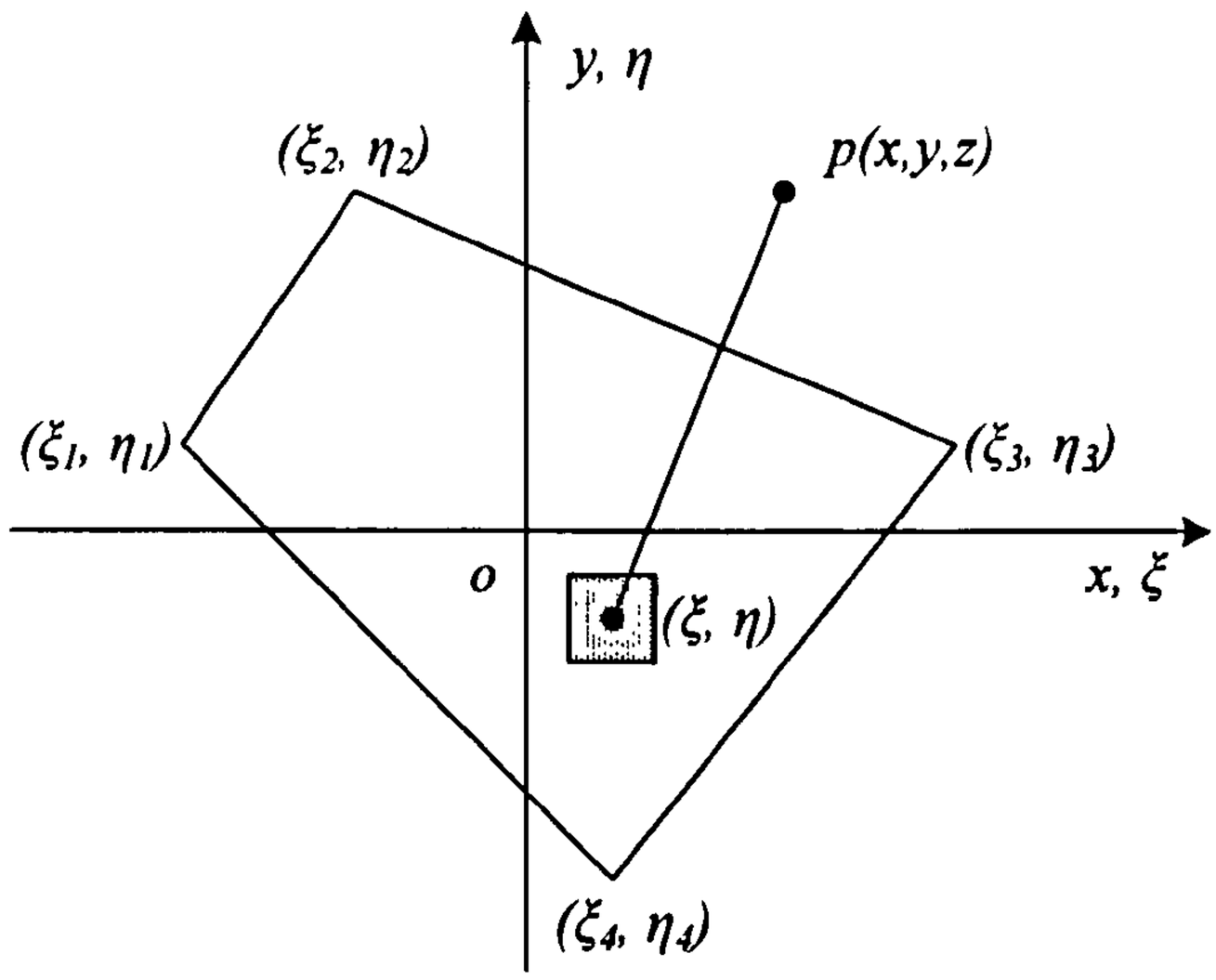

Figure 6.1 A plane quadrilateral panel lying in the local coordinate system $o-\xi\eta\zeta$

The quality of representation for the body surface depends largely on the distribution of the elements over the surface. Since the control points are taken at the element centroids and constant source strength over each element is assumed, the aspect ratio of the quadrilateral should be as close to unity as possible to ensure that the mid-point rule is valid in the evaluation of the influence coefficient. The elements should be concentrated in regions where the body geometry changes rapidly or where the flow properties, particularly the velocities, are expected to vary rapidly. It should be remarked that if several small elements are in the vicinity of a large one, the influence of the large element would swamp the effect of small neighbours. Therefore the size of the elements should change gradually between regions of concentration and the regions where the distribution is sparse. Hess and Smith (1967) suggested that the characteristic dimensions of element should be no more that 50 per cent greater that those of adjacent elements.

The accuracy of computation will increase as the number of elements increase, since smaller elements can model the curved shape better and a finer distribution of source will approximated the pressure gradient more accurately. Furthermore, the characteristic dimension of an element is also affected by the wavelength. For example, more elements are required for shorter waves than longer waves.

6.2.2 Higher-order panels

When solving the integral equation by numerical method, it is required to discretise the boundary surface into surface elements where actual calculation is carried out. Constant Panel Method adopted the assumption that the variables are always constant on each panel and geometry is represented by flat a quadrilateral panel. Because of the simplicity of Constant Panel Method, it has been widely used and given good results.

In Higher-Order Panel Method the variables and geometry are described by means of a shape function. Therefore numerical algorithm becomes relatively complicated when compared with Constant Panel Method. It is possible to realise the curved surface of general body shape with smaller number of elements. Since the changes of variables are continuous, it is easy to calculate the gradient value of variables. The general properties of Constant Panel Method and Higher-Order Panel Method are shown in Table 6.1.

Currently many researchers are using the higher-order boundary element method, which allows higher-order variations of not only the variables but also the geometry. From the accuracy point of view, the higher the order of elements becomes, the more accurate the obtained solution will be. In practice, however, compromising the order of approximation is necessary. Consequently, 'bi-quadratic elements' are taken to describe the geometry as shown in Figure 6.2.

Table 6.1 Comparisons of Constant Panel Method and Higher-Order Panel Method

	Constant Panel Method	Higher-Order Panel Method
Geometry	Flat quadrilateral	Curved surface
Change of variable	Discontinuous	Continuous
Algorithm	Simple	Complex

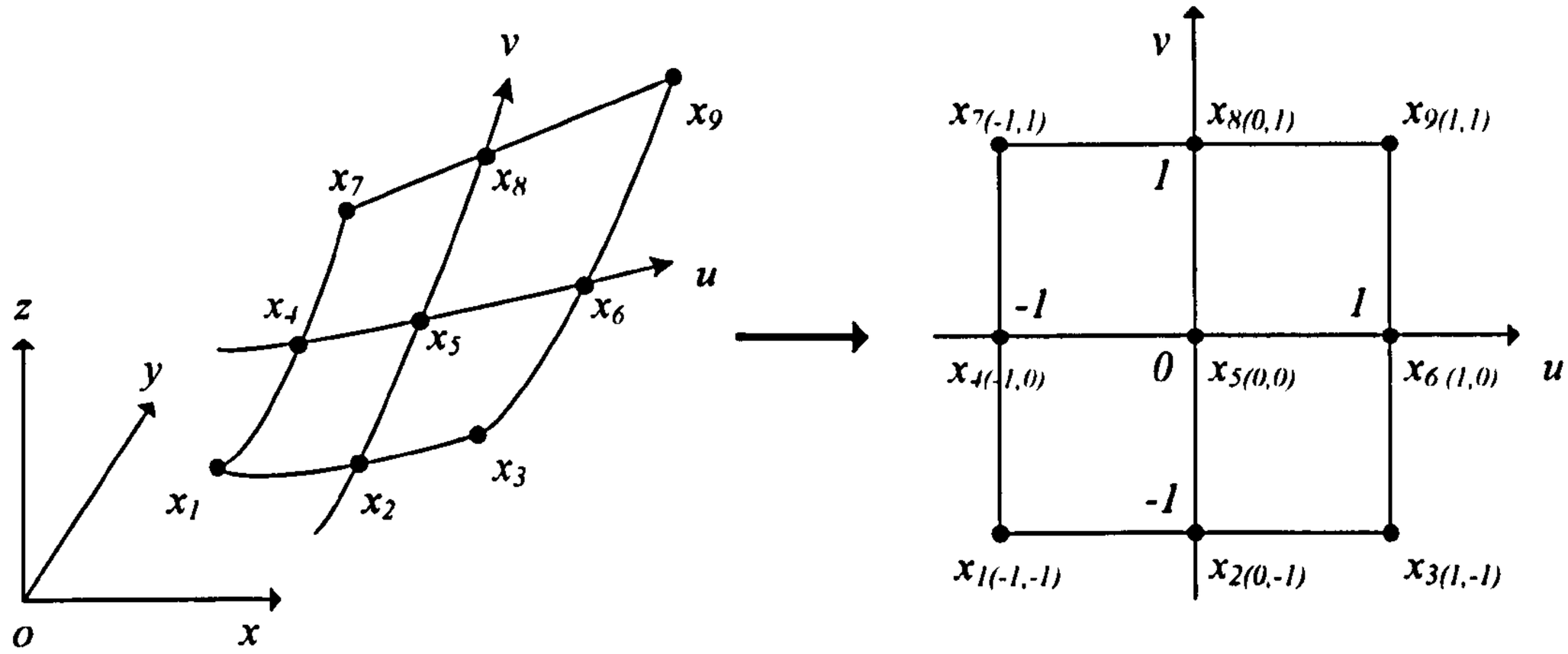

Figure 6.2 Bi-quadratic element and its parameter plane

Any point on each element can be described with a shape function N_i, which is also called as a basis function. The number of node required is either eight or nine using slightly different shape function and can be chosen by preference since there is no big difference in the result. In this research nine-point shape function has been used to describe control points on each element as follows

Using shape function N_i, the point on the element can be expressed as follows

$$x = \sum_{i=1}^{9} N_i(u,v)x_i \tag{6.3}$$

where

$$N_1 = \frac{1}{4}u(u-1)v(v-1) \qquad N_6 = -\frac{1}{2}u(u+1)(v^2-1)$$

$$N_2 = -\frac{1}{2}(u^2-1)v(v-1) \qquad N_7 = \frac{1}{4}u(u-1)v(v+1)$$

$$N_3 = \frac{1}{4}u(u+1)v(v-1) \qquad N_8 = -\frac{1}{2}(u^2-1)v(v+1) \tag{6.4}$$

$$N_4 = -\frac{1}{2}u(u-1)(v^2-1) \qquad N_9 = \frac{1}{4}u(u+1)v(v+1)$$

$$N_5 = (u^2-1)(v^2-1)$$

In equations (6.3) and (6.4) u and v are components of local coordinate system, which change between -1 and 1. Using the shape function any point in the element can be transformed to the local coordinate system as shown in Figure 6.2.

The control points of each element normally coincide with the nodes used in describing the body surface and thus nine control points are required in one element, which could be duplicated in another element. The utilisation of nodes as control points makes the discretisation of integral equation very complicated. In this research, therefore, six points weight function M_i was introduced for the distribution of source strength on each element in order to simplify the discretisation of integral equation and to reduce the number of control points, which has a direct relation with the total calculation time. For the present study six control points have been used in each element and the distribution of control points using weight function is described in Figure 6.3.

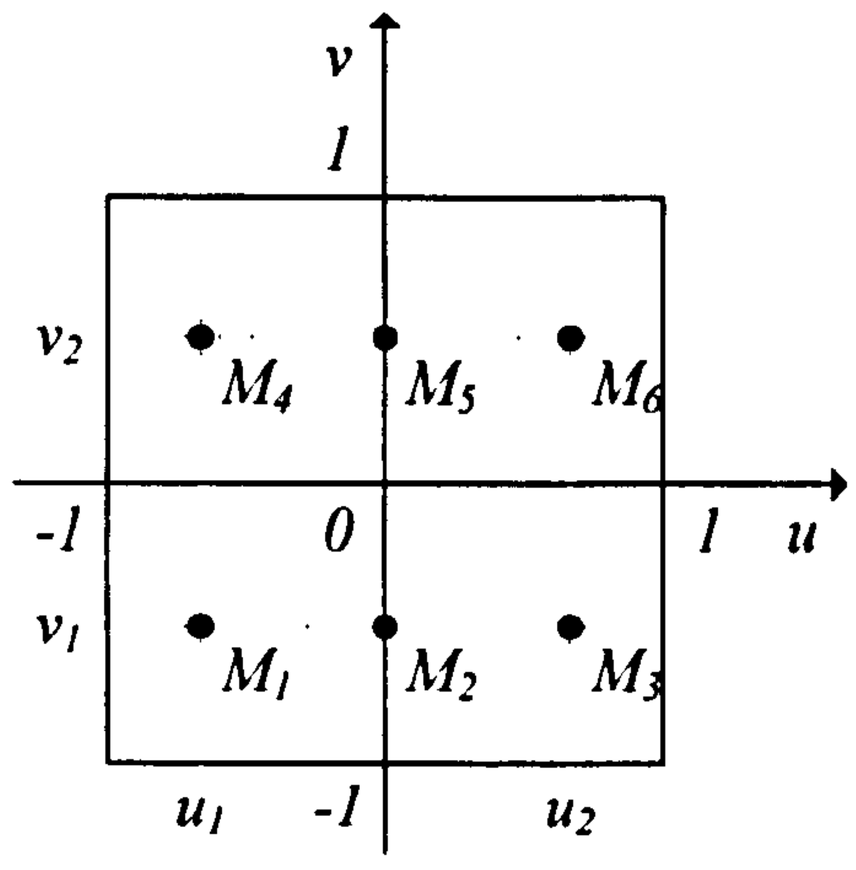

Figure 6.3 Distribution of control points using weight function

Then the source strength and velocity potential can be expressed with the weight function as follow

$$\sigma(p) = \sum_{j=1}^{6} M_j(u,v)\sigma_j \tag{6.5}$$

$$\phi(p) = \sum_{j=1}^{6} M_j(u,v)\phi_j \tag{6.6}$$

where

$$M_1 = \frac{u(u-u_2)(v-v_2)}{u_1(u_1-u_2)(v_1-v_2)} \qquad M_4 = \frac{u(u-u_2)(v-v_1)}{u_1(u_1-u_2)(v_2-v_1)}$$

$$M_2 = \frac{(u-u_1)(u-u_2)(v-v_2)}{u_1u_2(v_1-v_2)} \quad M_5 = \frac{(u-u_1)(u-u_2)(v-v_1)}{u_1u_2(v_2-v_1)} \tag{6.7}$$

$$M_3 = \frac{u(u-u_1)(v-v_2)}{u_2(u_2-u_1)(v_1-v_2)} \qquad M_6 = \frac{u(u-u_1)(v-v_1)}{u_2(u_2-u_1)(v_2-v_1)}$$

6.3 Discretisation of Boundary Integral Equation

As discussed in section 5.5, the linear boundary value problem to obtain the velocity potential can be reduced to the solution of an integral equation over the wetted surface of the body. It is, however, impossible to obtain an analytical solution of this integral equation not only because the surface is arbitrary but also the kernel function of the integral equation is very complicated. Therefore, a numerical calculation has to be adopted as an approximation of the given conditions. Due to the nature of the governing integral equation, the most obvious choice of numerical approximation includes discretisation of the wetted body surface into a finite number of surface elements. Within each of the elements, a local approximation of the unknown function, which is the source strength σ, is assumed. The application of the integral equation to each of the surface elements leads to a system of simultaneous linear algebraic equations whose solution can be easily obtained b standard matrix solvers.

In constructing the system of linear algebraic equations, various criteria can be used to approximate the variation of the source strength σ within the element. The variation could be constant, linear, piecewise linear, quadratic, cubic or higher-order polynomial. There are several ways of discretising the boundary integral equation. The conventional and most convenient is the so-called Constant Panel Method, in which the boundary is approximated by flat quadrilateral panels and the variables are

assumed to be constant on each panel. The Higher-Order Panel Method is more accurate, in which the geometry is represented by flat panels just as in the Constant Panel Method, but variables are approximated using higher-order interpolations.

$$\phi(p) = \frac{1}{4\pi}\iint_{\bar{S}_B} \sigma(q)G(p,q)ds(q) + \frac{U^2}{4\pi g}\oint_{L_F} \sigma(q)G(p,q)n_1 dy(q) \qquad (6.8)$$

$$\begin{aligned}\frac{\partial\phi(p)}{\partial n(p)} &= \alpha(p)\sigma(p) + \frac{1}{4\pi}\iint_{\bar{S}_B} \sigma(q)\frac{\partial G(p,q)}{\partial n(p)}ds(q) \\ &\quad + \frac{U^2}{4\pi g}\oint_{L_F} \sigma(q)\frac{\partial G(p,q)}{\partial n(p)}n_1 dy(q)\end{aligned} \qquad (6.9)$$

where the normal derivatives $\frac{\partial\phi(p)}{\partial n(p)}$ and $\frac{\partial G(p,q)}{\partial n(p)}$ are with respect to the point p on the body surface due to the kinematic body boundary condition. $\alpha(p)$ equals to 1/2 in the Constant Panel Method. Equation (6.9) is valid for the points on the body surface only due to the kinematic body boundary condition.

6.3.1 Constant Panel Method

In the Constant Panel Method, the change of source strength is assumed to be constant on each element of the body surface. Constant source strength approximation is utilised so that the unknown strength σ can be taken out of the integral. The continuous formulation of the solution indicates that the integral equations are to be satisfied at all points on the mean wetted body surface. In order to obtain a discretised numerical solution, it is necessary to relax this requirement and apply the body boundary condition at only N control points. On each element, a control point is selected and a normal velocity boundary condition is to be satisfied.

In selecting the control point, two cases might be considered and the difference was compared by Hess and Smith (1967). One control point is the centroid of the element and the other is the null point at which there is no self induced tangential velocity.

The difference between the null point and the centroid is not significant and it is not necessary as a more correct refinement, to use the null point instead of the centroid, which is located on the body surface. Then the discretised boundary integral equation by means of simple point collocation can be written as

$$\left(\frac{\partial \phi}{\partial n}\right)_i = \frac{1}{2}\sigma_i + \sum_{j=1}^{N} H_{ij}\sigma_j , \qquad i = 1,2,...,N \tag{6.10}$$

where

$$H_{ij} = \frac{1}{4\pi}\iint_{\Delta S_j} \frac{\partial G(p_i,q_j)}{\partial n(p_i)} ds_j + \frac{U^2}{4\pi g}\oint_{\Delta L_j} \frac{\partial G(p_i,q_j)}{\partial n(p_i)} n_1 dy_j \tag{6.11}$$

$$\left(\frac{\partial \phi}{\partial n}\right)_i = \frac{\partial \phi(p_i)}{\partial n(p_i)} \tag{6.12}$$

$$\sigma_i = \sigma(p_i) \tag{6.13}$$

In equations (6.10) and (6.11), N is the total number of elements on the wetted body surface, ΔS_j is the j-th surface element and ΔL_j is j-th line segment in the intersection line L_F. The calculation of the free surface line integral is required for those surface elements adjacent to the free surface. In the waterline integral term the source strength is assumed to be same with adjacent panel. The calculation of waterline integral might cause troublesome difficulties because of oscillating behaviour of Green function when the source point is located in the free surface. Further issues, related to the evaluation of Green function near free surface and treatment of waterline integral, are given in Appendix A. When $i = j$, that is, the field point p_i coincides with the source point q_j, the integration of the singular part of the Green function in equation (6.11) is excluded in the influence coefficient H_{ij}, which is taken over by the term 1/2.

Applying the body boundary conditions to the left hand side of equation (6.10) at each discretised element p_i leads to a system of linear algebraic equation in terms of

the unknown source strength σ_j. Since the influence coefficient H_{ij} is diagonally dominated matrix due to the self-induced panel, so the algebraic equation can be solved by standard matrix inversion solver like Gaussian elimination method. Once the distribution of source strength density over the wetted body surface is known, the velocity potential can be readily found from equation (6.8) in the following form,

$$\phi_i = \sum_{j=1}^{N} \sigma_j G_j , \qquad i = 1,2,...,N \tag{6.14}$$

where

$$G_j = \frac{1}{4\pi} \iint_{\Delta S_j} G(p_i, q_j) ds_j + \frac{U^2}{4\pi g} \oint_{\Delta L_j} G(p_i, q_j) n_1 dy_j \tag{6.15}$$

$$\phi_i = \phi(p_i) \tag{6.16}$$

6.3.2 Higher-Order Panel Method

$\alpha(p)$ is expressed as follows

$$\alpha(p) = \frac{1}{4\pi} \iint_{\bar{S}_B} \frac{\partial F(p,q)}{\partial n(q)} ds(q) \tag{6.17}$$

$$F(p,q) = \frac{1}{r} + \frac{1}{r_1} \tag{6.18}$$

Substituting equations (6.17) and (6.18) into equation (6.9) gives

$$\begin{aligned} \frac{\partial \phi(p)}{\partial n(p)} = & \frac{1}{4\pi} \iint_{\bar{S}_B} \left[\sigma(p) \frac{\partial F(p,q)}{\partial n(q)} + \sigma(q) \frac{\partial G(p,q)}{\partial n(p)} \right] ds \\ & + \frac{U^2}{4\pi g} \oint_{L_F} \sigma(q) \frac{\partial G(p,q)}{\partial n(p)} n_1 dy \end{aligned} \tag{6.19}$$

Then the discretised boundary integral equation by means of Higher-Order Panel Method can be expressed as

$$\left(\frac{\partial \phi}{\partial n}\right)_i = C_i \sigma_i + \sum_{e=1}^{NE} \sum_{j=1}^{6} H_j^e(p_i) \sigma_j^e, \qquad i = 1,2,...,ND \tag{6.20}$$

where

$$C_i = \sum_{e=1}^{NE} \frac{1}{4\pi} \iint_{\Delta S_e} \frac{\partial F(p_i, q)}{\partial n(q)} ds_e \tag{6.21}$$

$$H_j^e(p_i) = \frac{1}{4\pi} \iint_{\Delta S_e} M_j \frac{\partial G(p_i, q)}{\partial n(p_i)} ds_e + \frac{U^2}{4\pi g} \oint_{\Delta L_e} M_j \frac{\partial G(p_i, q)}{\partial n(p_i)} n_1 dy_e \tag{6.22}$$

ND is total number of control points, which represents the size of system of equation and NE is total number of elements used. $ND = 6 \times NE$ because 6 control points have been used as described in equations (6.5) and (6.6).

Once discretised boundary integral equation is obtained, remaining procedure is very similar to that of the Constant Panel Method. The solution of linear algebraic equation (6.20) gives the source strength of each control point and the unknown velocity potential can be evaluated as follows

$$\phi_i = \sum_{e=1}^{NE} \sum_{j=1}^{6} G_j^e(p_i) \sigma_j^e, \qquad i = 1,2,...,ND \tag{6.23}$$

where

$$G_j^e(p_i) = \frac{1}{4\pi} \iint_{\Delta S_e} M_j G(p_i, q) ds_e + \frac{U^2}{4\pi g} \oint_{\Delta L_e} M_j G(p_i, q) n_1 dy_e \tag{6.24}$$

6.4 Integration over Source Elements

Once mean wetted body surface has been discretised into panel elements, it is necessary to evaluate the influence matrix for each panel element. The influence of j-th panel on i-th field point can be obtained as follow

$$G(p,q) = \frac{1}{r} - \frac{1}{r_1} + H(p,q) \tag{6.25}$$

The first term is source singularity, the second term is image source, which is the image of the source singularity over the free surface, and the last term is wave function. It should be noted that the normal derivatives of the Green function in above equation are obtained by

$$\frac{\partial G}{\partial n} = n_1 \frac{\partial G}{\partial x} + n_2 \frac{\partial G}{\partial y} + n_3 \frac{\partial G}{\partial z} \tag{6.26}$$

where n_1, n_2 and n_3 are respectively the x, y and z-components of the unit normal vector at field point p.

6.4.1 Source term

To calculate source term over a given discretised quadrilateral panel, it is convenient to use method of Hess and Smith (1967). The influence of j-th panel on i-th field point can be obtained by transform all points to local coordinates system $o-\xi\eta\zeta$ using a transformation matrix as shown in Figure 6.1.

The centroid of panel (x_m, y_m, z_m) can be used as the origin of local coordinate system for convenience and the positive z-axis (upward in Figure 6.1) is in direction of the unit normal vector. The coordinate of the vertices of the quadrilateral panel

become $(\xi_k, \eta_k, 0)$ where k=1,2,3,4. Then the integration of a source term over a quadrilateral panel and its derivatives could be calculated as follows

$$\varphi = \iint_{ds} \frac{1}{r} ds \tag{6.27}$$

where $r = \sqrt{(x-\xi)^2 + (y-\eta)^2 + z^2}$

Hess and Smith (1967) have showed that the exact calculation and derivatives of the integral in equation (6.27) were obtained by analytic method as follow

$$\varphi = \sum_{k=1}^{4} (R_k Q_k + |z| J_k) - |z| \Delta\theta \tag{6.28}$$

$$\varphi_x = \sum_{k=1}^{4} S_k Q_k \tag{6.29}$$

$$\varphi_y = -\sum_{k=1}^{4} C_k Q_k \tag{6.30}$$

$$\varphi_z = \mathrm{sgn}(z)\left[\sum_{k=1}^{4} J_k - \Delta\theta\right] \tag{6.31}$$

where $R_k = (x-\xi_k)S_k - (y-\eta_k)C_k$

$$Q_k = \ln\left(\frac{r_k + r_{k+1} + d_k}{r_k + r_{k+1} - d_k}\right)$$

$$J_k = \mathrm{sgn}(R_k)\left[\tan^{-1}\left(\left|\frac{z}{R_k}\right|\frac{s_k^{(2)}}{r_{k+1}}\right) - \tan^{-1}\left(\left|\frac{z}{R_k}\right|\frac{s_k^{(1)}}{r_k}\right)\right]$$

$$C_k = \frac{\xi_{k+1} - \xi_k}{d_k}, \qquad S_k = \frac{\eta_{k+1} - \eta_k}{d_k} \tag{6.32}$$

$$d_k = \sqrt{(\xi_{k+1} - \xi_k)^2 + (\eta_{k+1} - \eta_k)^2}$$

$$r_k = \sqrt{(x-\xi_k)^2 + (y-\eta_k)^2 + z^2}$$

$$s_k^{(1)} = (\xi_k - x)C_k + (\eta_k - y)S_k$$

$$s_k^{(2)} = (\xi_{k+1} - x)C_k + (\eta_{k+1} - y)S_k$$

$$\Delta\theta = \begin{cases} 2\pi & \text{when } R_k\text{'s are all positive} \\ 0 & \text{otherwise} \end{cases}$$

It should be noted that the variables used in equations (6.28) through (6.32) with the subscript $k = 5$ are identical to those with $k = 1$. It may be verified from these equations that there is no difficulty in calculating the effects of "self-induced element", which has the control point (field point) at its own element. Q_k becomes singular if the field point is on the side of the quadrilateral. This can be avoided since field point is located at the centroid of the element. For $z = 0$, all J_k's vanish and $\varphi_z = \Delta\theta$.

Hess and Smith (1967) also gave an approximated solution by means of a multiple expansion when the field point is sufficiently far from the source element. No more approximation is, however, required due to the rapid improvement of computer technology in recent years and therefore exact solution given in equations (6.28) through (6.32) will be used in this research.

Hess and Smith (1967) suggested that exact solution or multiple expansion be used under a criteria. If a ratio $r_0/t < 4.0$, where r_0 is the distance between the field point and the centroid of the quadrilateral and t is the maximum dimension of the quadrilateral, the exact solution can be used for the integration of source term. If $r_0/t > 4$, a point-source formula can be applied as follow

$$\varphi = \frac{1}{r}\Delta s \tag{6.33}$$

$$\nabla\varphi = -\frac{\mathbf{r} - \mathbf{r}_0}{r^3}\Delta s \tag{6.34}$$

where Δs is the area of the quadrilateral. The expression given in equations (6.33) and (6.34) are valid asymptotically and very useful since there is no transformation to the local coordinate system.

The integration of image source term $1/r_1$ in equation (6.25) can be handled in the same way as those if the source term $1/r$. The potential and its derivates are calculated on the image panels above the undisturbed free surface and no difficulty is encountered during the calculations. It should be noted that the source and image source term on the free surface cancel each other when the field point or source point are located in the undisturbed free surface. There is, therefore, no contribution to the Green function in the free surface line integral in equations (6.8) and (6.9).

6.5 Concluding Remarks

The solution of the boundary value problem presented in Chapter 5 can be obtained by solving the boundary integral equation, which is known as Green function method. For the implementation of the Green function method, the discretisation of the boundary integral equation and has been introduced to obtain numerical solution of the unsteady motion problem. Corresponding body surface is also required to be discretised in the so-called panel method and two discretisation methods have been presented: Constant Panel Method and Higher-Order Panel Method; in the former, the unknown source strength is assumed to be constant in the flat quadrilateral panel. In the latter higher-order polynomials are used in the descriptions of the surface elements and source strengths in each element are no longer to be assumed as constant. Then the integral equations in each method have been approximated by a set of linear algebraic equations with unknown variables of the source strengths and numerical applications for the mathematical and realistic hull shapes will be demonstrated in the following Chapter.

Chapter 7. Hydrodynamic Forces and Ship Motions

7.1 Preamble

In order to solve ship motion in waves, the problem of dynamic equilibrium of forces and moments in an elastic ship body should be solved in the first place. Since the main focus of the present study is not structural or vibrational problems of a ship in waves, the ship body is assumed to be rigid all the time. The rigid body assumption is then used to predict the resulting motions of the body in waves.

The external forces and moments acting on the body surface can be formulated from the potential theory with the assumption of inviscid, incompressible and irrotational fluid flow as discussed in the Chapter 5. The forces and moments are further obtained from the integration of the pressure field, which can be calculated from Bernoulli's equation in terms of the velocity potential and its derivatives.

The motion of a ship is solved by the equations of motion formulated with the external forces and moments through the potential theory. In spite of the assumptions used to formulate the potential theory such as inviscid flow field, the problem should be reduced by the linearisation to obtain practical solution. In the process of linearisation perturbation expansion was adopted to allow linear superposition principles, where the complex ship responses in irregular waves can be considered as a sum of those in a regular wave. Consequently the motion problem is reduced to the study of linear harmonic oscillation in a regular sinusoidal wave. Since the steady flow has an effect on the unsteady flow field, the assumption of small amplitude is also included as discussed in the Chapter 5.

The hydrodynamic forces and moments can be separated into two components, i.e. oscillatory and non-oscillatory. The oscillatory component is proportional to the wave amplitude and first-order of the hydrodynamic forces and moments. The first-order hydrodynamic forces and moments produce the first-order motion of a ship. The non-oscillatory component is of second-order with respect to the wave amplitude and is expressed by non-zero time average value while first-order component exhibits zero mean value over a period.

By separating the hydrodynamic forces and moments up to second-order terms, the first-order and second-order hydrodynamic forces and moment acting on a ship with or without forward speed will be formulated in this chapter. On the basis of foregoing principles, numerical calculation is then carried out to predict the hydrodynamic forces and moments acting on a barge, Wigley and Todd Series 60 ship. Calculation results of each model are presented either with or without forward speed and the effects of heading and forward speed on the first- and second-order hydrodynamic forces and moments are investigated through the comparisons with experimental data.

7.2 First-Order Wave Forces

The forces and moments acting on a ship in a seaway can be evaluated with the pressure field of the fluid. The fluid pressure p acting on the instantaneous wetted body surface S_B is given by Bernoulli's equation as follows

$$p = -\rho\left(\Phi_t + \frac{1}{2}\nabla\Phi\cdot\nabla\Phi - \frac{1}{2}U^2 + gz\right) \qquad \text{on } S_B \tag{7.1}$$

Since the exact body surface S_B is displaced and rotated with respect to the mean wetted body surface $\bar{S}_B$, the fluid pressure p on $\bar{S}_B$ can be expanded by means of Taylor series as follow

$$p\big|_{S_B} = p + \boldsymbol{\alpha}\cdot\nabla p + O(\varepsilon^2)\big|_{\bar{S}_B} \qquad \text{on } S_B,\ \bar{S}_B \tag{7.2}$$

The total velocity potential Φ can be separated as steady and unsteady terms, i.e. $\Phi = \bar{\Phi} + \tilde{\Phi}$, as discussed in the Chapter 5. Substituting equation (7.1) into (7.2) and neglecting second-order terms gives

$$p = -\frac{1}{2}\rho(\mathbf{W}\cdot\mathbf{W} - U^2) - \rho(gz + g\boldsymbol{\alpha}\cdot\mathbf{k}) - \rho(\tilde{\Phi}_t + \mathbf{W}\cdot\nabla\tilde{\Phi})$$

$$\text{on } S_B, \bar{S}_B \tag{7.3}$$

The first term on the right hand side of equation (7.3) is the steady pressure on the body due to the steady flow and the second term is hydrostatic pressure. The last term comes from the action of incident wave and becomes the first-order hydrodynamic pressure acting on the oscillating body. It is evident that the interaction between steady and unsteady flow appears in the first-order hydrodynamic pressure.

The hydrodynamic forces and moments are obtained by integrating the pressure given in equation (7.3) over a mean wetted body surface $\bar{S}_B$ as follow

$$\begin{aligned} F_j &= -\iint_{\bar{S}_B} p n_j ds \\ &= \frac{1}{2}\rho \iint_{\bar{S}_B} (\mathbf{W}\cdot\mathbf{W} - U^2) n_j ds + \rho g \iint_{\bar{S}_B} z n_j ds \\ &+ \rho \iint_{\bar{S}_B} (g\boldsymbol{\alpha}\cdot\mathbf{k}) n_j ds + \rho \iint_{\bar{S}_B} (\tilde{\Phi}_t + \mathbf{W}\cdot\nabla\tilde{\Phi}) n_j ds \end{aligned} \tag{7.4}$$

The first term on the right hand side of equation (7.4) is associated with wave-making drag and dynamic lift. The second term is the buoyancy, which is cancelled by the weight of the body. The remaining terms are first-order hydrostatic restoring and hydrodynamic force respectively. First two terms are time independent and thus will be neglected in the calculation of unsteady force. Therefore the first-order hydrodynamic force can be expressed as follows

$$F_j^{(1)} = \rho \iint_{\bar{S}_B} (g\boldsymbol{\alpha}\cdot\mathbf{k}) n_j ds + \rho \iint_{\bar{S}_B} (\tilde{\Phi}_t + \mathbf{W}\cdot\nabla\tilde{\Phi}) n_j ds \tag{7.5}$$

The fist order hydrodynamic force can be divided linearly in the similar way that the unsteady velocity potential was decomposed into incident wave, diffraction and radiation potential as

$$F_j^{(1)} = F_j^{HS} + F_j^{EX} + F_j^{R} \tag{7.6}$$

where $$F_j^{HS} = \rho \iint_{\bar{S}_B} (g\boldsymbol{\alpha}\cdot\mathbf{k}) n_j ds \tag{7.7}$$

$$F_j^{EX} = \rho \iint_{\bar{S}_B} (i\omega_e + \mathbf{W}\cdot\nabla)(\phi_0 + \phi_7) e^{i\omega_e t} n_j ds \tag{7.8}$$

$$F_j^{R} = \rho \sum_{k=1}^{6} \bar{\xi}_k \iint_{\bar{S}_B} (i\omega_e + \mathbf{W}\cdot\nabla)\phi_k e^{i\omega_e t} n_j ds \tag{7.9}$$

Equations (7.7), (7.8) and (7.9) are the expressions for the hydrostatic restoring force, wave exciting force and radiation force in the j-th direction respectively.

The second term in equation (7.9), which is proportional to the steady velocity field $\mathbf{W}$, can be transformed by means of a Stoke's theorem (Ogilvie and Tuck, 1969) as follows

$$\iint_{\bar{S}_B} (\mathbf{W}\cdot\nabla)\phi_k n_j ds = -U\iint_{\bar{S}_B} \phi_k m_j ds \tag{7.10}$$

which is more amenable to evaluate since the steady and unsteady terms are uncoupled by adopting small amplitude assumption.

7.2.1 Hydrostatic forces

The hydrostatic forces are defined as the fluid forces to restore the body to its static equilibrium state when the body is displaced freely form the rest position. According to Newman (1977) the surface integral in equation (7.7) can be transformed to the volume integral by using Gauss's theorem and finally expressed as follows

$$\begin{aligned}
F_1^{HS} &= 0\\
F_2^{HS} &= 0\\
F_3^{HS} &= (\rho g\cancel{\forall} - mg) - \rho g S_{00}\xi_3 - \rho g S_{01}\xi_4 + \rho g S_{10}\xi_5\\
F_4^{HS} &= (\rho g\cancel{\forall} y_B - mgy_G) - \rho g S_{01}\xi_3\\
&\quad -[\rho g\cancel{\forall}(S_{02}/\cancel{\forall} + z_B) - mgz_G]\xi_4\\
&\quad +\rho g S_{11}\xi_5 + (\rho g\cancel{\forall} x_B - mgx_G)\xi_6\\
F_5^{HS} &= -(\rho g\cancel{\forall} x_B - mgx_G) + \rho g S_{10}\xi_3 + \rho g S_{11}\xi_4\\
&\quad -[\rho g\cancel{\forall}(S_{20}/\cancel{\forall} + z_B) - mgz_G]\xi_5 + (\rho g\cancel{\forall} y_B + mgy_G)\xi_6\\
F_6^{HS} &= 0
\end{aligned} \tag{7.11}$$

where (x_G, y_G, z_G) and (x_B, y_B, z_B) denote the centre of buoyancy and gravity respectively. S_{ij} is defined as

$$S_{ij} = \iint x^i y^j dxdy\Big|_{z=0} \tag{7.12}$$

where the integral is over the plane $z = 0$, interior to the ship hull. When $i = j = 0$, the integral becomes the area of waterplane.

Because the hydrostatic forces are always related with gravitational forces, these two components are combined as a net hydrostatic forces in equation (7.11). The horizontal components of the hydrostatic force and the vertical component of the moment are identically zero. Equation (7.11) consists of terms of zero and first-order hydrostatic forces and moments with the body motion ξ_k.

If the body is in equilibrium state the zero order term should vanish. For the equilibrium of the vertical force, the mass of the body must equal to the displacement, i.e. $m = \rho\nabla$. With this equality, equilibrium of the zero order moments in equation (7.11) requires that centre of gravity and centre of buoyancy must lie in the same vertical line such that $x_G = x_B$ and $y_G = y_B$.

Furthermore, when a floating body is subject to horizontal moment, the centre of floatation $(x_F, y_F, 0)$ can be related to the properties in equation (7.12), where S_{10} and S_{01} are first moments of the waterplane area about y and x axis respectively. Most ship has a longitudinal plane of symmetry of both hull shape and thus integrals S_{01} and S_{11} simply become zero.

$$\begin{aligned}(x_F, y_F, 0) &= (S_{10}/S_{00}, S_{01}/S_{00}, 0) \\ &= (S_{10}/S_{00}, 0, 0)\end{aligned} \tag{7.13}$$

In order to simplify the notation, individual components of hydrostatic force in equation (7.11) can be written in a more general matrix notation as

$$F_j^{HS} = -\sum_{k=1}^{6} C_{jk}\xi_k \tag{7.14}$$

where C_{jk} is the hydrostatic restoring coefficient such that

$$\begin{aligned} C_{33} &= \rho g S_{00} \\ C_{35} &= C_{53} = -\rho g S_{00} \cdot x_F \\ C_{44} &= \rho g \nabla \cdot \overline{GM}_T \\ C_{55} &= \rho g \nabla \cdot \overline{GM}_L \end{aligned} \tag{7.15}$$

The terms in C_{44} and C_{55} are the vertical distances between the metacentre and centre of gravity. These differences are well known as metacentric heights in transverse and longitudinal directions respectively.

7.2.2 Wave exciting forces

The wave exciting forces acting on the body in the unsteady problem can be obtained by the direct integration of the pressure associated with incident wave and diffraction potential as given in equation (7.8) and can be further decomposed as follows

$$F_j^{EX} = F_j^{FK} + F_j^{D} \tag{7.16}$$

where $$F_j^{FK} = \rho \iint_{\bar{S}_B} (i\omega_e + \mathbf{W} \cdot \nabla)\phi_0 e^{i\omega_e t} n_j ds \tag{7.17}$$

$$F_j^{D} = \rho \iint_{\bar{S}_B} (i\omega_e + \mathbf{W} \cdot \nabla)\phi_7 e^{i\omega_e t} n_j ds \tag{7.18}$$

F_j^{FK} is called Froude-Krylov force resulting from the presence of the vessel in an undisturbed flow. The integrand of the Froude-Krylov force involves the incident potential only, and thus it corresponds to the force experienced by the ship, which the incident waves pass through as if the hull is transparent to the waves. The accuracy

of the incident wave force increases as the wavelength relative to the ship's characteristic length becomes longer. Therefore one would anticipate that Froude-Krylov force is relatively more significant in the long wave regime or a thin body in head waves where little wave scattering occurs. It is easy to calculate equation (7.17) since the expression for incident wave potential is already given in Chapter 5 and it can be further simplified with the result $(i\omega_e + \mathbf{W}\cdot\nabla)\phi_0 = i\omega_0\phi_0$ as follows

$$F_j^{FK} = \rho i\omega_0 \iint_{\bar{S}_B} \phi_0 e^{i\omega_e t} n_j ds \tag{7.19}$$

F_j^D is called diffraction force due to the scattered wave of incident wave in the presence of the ship. Diffraction potential can be solved such that the combination with incident wave potential and it is possible to calculate diffraction force mathematically without solving diffraction potential directly. Since diffraction and radiation potentials satisfies all the boundary conditions except for body boundary conditions, by applying Green's theorem to these potentials, we have

$$\iint_{\bar{S}_B} (\phi_j \frac{\partial \phi_7}{\partial n} - \phi_7 \frac{\partial \phi_j}{\partial n}) ds = 0 \tag{7.20}$$

Together with the boundary condition given in equation (5.48), the diffraction force can be rewritten as follows

$$F_j^D = \rho \iint_{\bar{S}_B} \phi_7 \frac{\partial \phi_j}{\partial n} e^{i\omega_e t} ds = -\rho \iint_{\bar{S}_B} \phi_j \frac{\partial \phi_0}{\partial n} e^{i\omega_e t} ds \tag{7.21}$$

This process is referred as Haskind relations using Green's theorem and body boundary condition to relate diffraction potential to incident wave and radiation potential at zero forward speed. Newman (1962) has derived more generalised Haskind relations for a body with a constant forward speed, where radiation potential has to be determined within reverse flow radiation problem, taking an opposite sign into account for the constant forward speed.

7.2.3 Radiation forces

The radiation forces result from the radiation of waves away from the ship, which is forced to oscillate in calm water. Expression given in equation (7.9) can be represented as hydrodynamic force in the j-th direction due to the k-th mode of motion as follows

$$F_{jk}^{R} = \rho \bar{\xi}_k \iint_{\bar{S}_B} (i\omega_e + \mathbf{W} \cdot \nabla)\phi_k e^{i\omega_e t} n_j ds \tag{7.22}$$

The radiation force is often expressed with two coefficients which are proportional to the acceleration and velocity of the body as follow

$$\begin{aligned} F_{jk}^{R} &= A_{jk}\ddot{\bar{\xi}}_k + B_{jk}\dot{\bar{\xi}}_k \\ &= (-\omega_e^2 A_{jk} + i\omega_e B_{jk})\bar{\xi}_k e^{i\omega_e t} \end{aligned} \tag{7.23}$$

The real quantities A_{jk} and B_{jk} are referred as added mass and damping coefficients in the j-th direction due to the k-th mode of motion respectively. These names are chosen because of their physical contribution in the equations of motion. Added mass which is in phase with the acceleration acts as apparent mass, adding to the mass of the ship. Similarly damping coefficient is in phase with the velocity and obtained from imaginary part of radiation force. It should be noted that both added mass and damping coefficients are functions of forward speed and encounter frequency.

For convenience the expression for added mass and damping coefficients can be rewritten as

$$T_{jk} = \rho \iint_{\bar{S}_B} (i\omega_e + \mathbf{W} \cdot \nabla)\phi_k n_j ds \tag{7.24}$$

Substituting equation (7.10) into (7.24) gives

$$T_{jk} = \rho \iint_{\bar{S}_B} (i\omega_e n_j - U m_j)\phi_k ds \tag{7.25}$$

where m-terms are defined in equations (5.51) and (5.52).

Then added mass and damping coefficients can be evaluated from

$$T_{jk} = \omega_e^2 A_{jk} - i\omega_e B_{jk} \tag{7.26}$$

$$A_{jk} = \frac{\mathrm{Re}(T_{jk})}{\omega_e^2} \qquad \text{and} \qquad B_{jk} = -\frac{\mathrm{Im}(T_{jk})}{\omega_e} \tag{7.27}$$

For a body with one longitudinal plane of symmetry, these two coefficients have a properties such that

$$\begin{aligned} A_{jk} = B_{jk} &= 0 \qquad \text{for } j = 1,3,5 \text{ and } k = 2,4,6 \\ A_{jk} = B_{jk} &= 0 \qquad \text{for } j = 2,4,6 \text{ and } k = 1,3,5 \end{aligned} \tag{7.28}$$

For zero speed case, m-terms m_j vanish with forward speed and the coefficients satisfies the symmetry relationship as

$$A_{jk} = A_{kj} \qquad \text{and} \qquad B_{jk} = B_{kj} \qquad \text{for } U = 0 \tag{7.29}$$

7.3 Equations of Motion

If the ship has an axis of symmetric in xz-plane, y component of centre of gravity is equal to zero. Then the general form of the basic linearised equations of motion in six-degree-of-freedom is,

$$\sum_{k=1}^{6} M_{jk}\ddot{\xi}_k = F_j \qquad j = 1,2,...,6 \tag{7.30}$$

In the left hand side of equation (7.30), ξ_k are six components of ship motion ($\xi_k = \bar{\xi}_k e^{i\omega_e t}$) and M_{jk} are the body inertia coefficients for the j-th force induced by k-th mode of motion, which can be expressed following matrix form.

$$M_{jk} = \begin{bmatrix} m & 0 & 0 & 0 & mz_G & -my_G \\ 0 & m & 0 & -mz_G & 0 & mx_G \\ 0 & 0 & m & my_G & -mx_G & 0 \\ 0 & -mz_G & my_G & I_{xx} & -I_{xy} & -I_{xz} \\ mz_G & 0 & -mx_G & -I_{yx} & I_{yy} & -I_{yz} \\ -my_G & mx_G & 0 & -I_{zx} & -I_{zy} & I_{zz} \end{bmatrix} \tag{7.31}$$

where m is mass of the ship. I_{xx}, I_{yy} and I_{zz} are moment of inertia about x, y and z axes respectively and remaining terms are products of inertia. When the ship has one longitudinal plane of symmetry, $y_G = 0$ and $I_{xy} = I_{yx} = I_{yz} = I_{zy} = 0$.

F_j is total fluid force acting on the body in the j-th direction given in equation (7.6) and consists of hydrostatic and hydrodynamic components described in the foregoing section. Substituting equations (7.14), (7.16) and (7.23) into (7.30) and taking up to the first-order of the force give the six-degree-of-freedom equations of motion in the frequency domain in the form

$$\sum_{k=1}^{6}\left[-\omega_e^2(M_{jk}+A_{jk})+i\omega_e B_{jk}+C_{jk}\right]\bar{\xi}_k = F_j^{EX} \qquad j=1,2,...,6 \quad (7.32)$$

The linearisation of the given problem with one longitudinal plane of symmetry separates the motions into two groups. One is the linear coupled surge-heave-pitch motion in the vertical plane and the other is sway-roll-yaw motion in the horizontal plane. The motions in one plane are coupled with each other, but are entirely independent from those in the other plane.

Once the radiation and diffraction potentials are solved, corresponding added mass and damping coefficients can be obtained and wave exciting force can be evaluated from direct integration of the fluid pressure over the hull surface using known incident wave potential. Then motion response amplitude is readily obtained by a standard matrix solver.

7.4 Mean Second-Order Wave Forces

7.4.1 Background of second-order forces

The oscillatory forces exerted on a ship floating in a regular wave are proportion to the wave amplitude and generate sinusoidal motion response of the ship as discussed in the foregoing section. These first-order forces have a zero mean value over a period while second-order components with respect to wave amplitude show non-zero average and are time-independent constant. These second-order forces are generally too small compared to the first-order forces but they cannot be ignored in certain circumstance. The second-order forces are responsible for low frequency horizontal motions in a slow or zero speed.

The mean second-order forces are often known as drift forces in the horizontal plane of motion. Longitudinal component of drift forces acting on a ship advancing in a wave can be applied to the prediction of added resistance. The lateral components of drift forces can be applied to the modelling of steering and control devices and vertical components are important to a submerged body travelling near free surface.

Since the second-order steady forces are dependent on the first-order velocity potential, theoretical method to calculate the second-order forces are involved with the solution of first-order potential theory. In the modelling process of second-order forces, two different approaches have been studied by many researches. One is far field method and the other is near field method. Both methods are developed under same assumptions and techniques adopted in the conventional potential theory.

In the far field method, the change of momentum of the fluid is considered within a control surface surrounding the body and the boundary surface is normally taken to be a cylindrical surface of a large radius extending vertically from the free surface to the sea bottom. Using the rate of change of the linear or angular momentum within the fluid domain, the forces and moments acting on the body can be related to the

fluid flow characteristics in other boundary surface. When the control surface is taken to infinity, the horizontal components of the mean second-order forces and moments can be easily evaluated from the asymptotic form of the velocity potential. The far field method is a very significant simplification in practical problems.

Although simple procedure in the far field method is available, this method is less attractive when vertical component is in question since supplementary integrals over the free surface and sea bottom should be followed. Then near field method can be adopted by using direct integration of the fluid pressure over mean wetted body surface. Because the direct integration of the fluid pressure requires detailed characteristics of the flow field on the body surface, this method provides a great deal of physical insight into the mechanism of second-order forces and moments. The advantage of the near field method is that six components of the mean second-order forces and moments can be obtained. On the other hand, this approach is more complex to programme and demands more computational time than near field method.

In the following section the calculation method for the second-order forces based on the near field method will be derived. Due to the direct integration of fluid pressure, the final expressions will be valid for all six-degree-of-freedom and zero speed case can be obtained by removing speed dependent terms

7.4.2 Expansion of second-order forces

Consider a ship travelling with constant forward speed U in a regular sinusoidal wave where general assumptions of potential theory are applicable. The fluid domain is represented by a velocity potential which can be decomposed into steady and unsteady part as follows

$$\Phi(\mathbf{x},t) = \bar{\Phi}(\mathbf{x}) + \tilde{\Phi}(\mathbf{x},t) \tag{7.33}$$

The steady potential $\bar{\Phi}$, which is caused by a steady translating motion of a ship in calm water, is further divided by a uniform stream and steady perturbation potential $\bar{\phi}$. The unsteady potential $\tilde{\Phi}$ consists of incident wave, diffraction and radiation potential and the motion response of the ship is assumed to be harmonic with a encounter frequency ω_e as discussed in Chapter 5.

The process to obtain second-order hydrodynamic forces and moments are very similar to the first-order case. Fluid pressure on the instantaneous wetted body surface S_B is given from Bernoulli equation and can be expanded to second-order in the form

$$p = -\rho[gz + \frac{1}{2}(\mathbf{W}\cdot\mathbf{W} - \bar{U}^2) + \tilde{\Phi}_t + \mathbf{W}\cdot\nabla\tilde{\Phi} + \frac{1}{2}\nabla\tilde{\Phi}\cdot\nabla\tilde{\Phi}] \quad \text{on } S_B \tag{7.34}$$

To calculate hydrodynamic forces acting on the body surface it is required to integrate the pressure directly over the instantaneous wetted body surface as

$$\mathbf{F} = -\iint_{S_B} p\mathbf{n}dS$$
$$\mathbf{M} = -\iint_{S_B} p(\mathbf{r}\times\mathbf{n})dS \tag{7.35}$$

The unit normal vector $\mathbf{n}$, position vector $\mathbf{r}$ and their product $\mathbf{r}\times\mathbf{n}$ in equation (7.35) should be evaluated instantaneously since the exact wetted surface S_B is varying with time. Therefore these vectors can be expanded from the exact wetted surface S_B to the mean wetted surface $\bar{S}_B$ by means of perturbation expansions

$$\mathbf{r} = \mathbf{r}^{(0)} + \varepsilon\mathbf{r}^{(1)} + \varepsilon^2\mathbf{r}^{(2)} + \cdots \tag{7.36}$$

$$\mathbf{n} = \mathbf{n}^{(0)} + \varepsilon\mathbf{n}^{(1)} + \varepsilon^2\mathbf{n}^{(2)} + \cdots \tag{7.37}$$

$$\mathbf{r}\times\mathbf{n} = (\mathbf{r}\times\mathbf{n})^{(0)} + \varepsilon(\mathbf{r}\times\mathbf{n})^{(1)} + \varepsilon^2(\mathbf{r}\times\mathbf{n})^{(2)} + \cdots \tag{7.38}$$

where $\mathbf{r}^{(0)} = \mathbf{r}$, $\mathbf{r}^{(1)} = \boldsymbol{\delta}^{(1)} + \boldsymbol{\Omega}^{(1)} \times \mathbf{r}$, $\mathbf{r}^{(2)} = [\mathbf{H}]\mathbf{r}$ (7.39)

$\mathbf{n}^{(0)} = \mathbf{n}$, $\mathbf{n}^{(1)} = \boldsymbol{\Omega}^{(1)} \times \mathbf{n}$, $\mathbf{n}^{(2)} = [\mathbf{H}]\mathbf{n}$ (7.40)

$(\mathbf{r} \times \mathbf{n})^{(0)} = \mathbf{r} \times \mathbf{n}$, $(\mathbf{r} \times \mathbf{n})^{(1)} = \boldsymbol{\delta}^{(1)} \times \mathbf{n} + \boldsymbol{\Omega}^{(1)} \times (\mathbf{r} \times \mathbf{n})$,

$(\mathbf{r} \times \mathbf{n})^{(2)} = (\boldsymbol{\delta}^{(1)} + \boldsymbol{\Omega}^{(1)} \times \mathbf{r}) \times (\boldsymbol{\Omega}^{(1)} \times \mathbf{n}) + \mathbf{r} \times [\mathbf{H}]\mathbf{n} + [\mathbf{H}]\mathbf{r} \times \mathbf{n}$ (7.41)

The vectors $\boldsymbol{\delta} = (\xi_1, \xi_2, \xi_3)$ and $\boldsymbol{\Omega} = (\xi_4, \xi_5, \xi_6)$ are unsteady displacement of translation and rotation vector respectively. The matrix $[\mathbf{H}]$ are defined as follows

$$[\mathbf{H}] = -\frac{1}{2}\begin{bmatrix} \xi_5^{(1)2} + \xi_6^{(1)2} & 0 & 0 \\ -2\xi_4^{(1)}\xi_5^{(1)} & \xi_4^{(1)2} + \xi_6^{(1)2} & 0 \\ -2\xi_4^{(1)}\xi_6^{(1)} & -2\xi_5^{(1)}\xi_6^{(1)} & \xi_4^{(1)2} + \xi_5^{(1)2} \end{bmatrix} \tag{7.42}$$

The fluid pressure given by equation (7.34) can be expanded from the instantaneous wetted surface S_B to the mean wetted surface $\bar{S}_B$ by means of Taylor series expansion. Then the integration on S_B can be divided into two parts: the mean wetted surface $\bar{S}_B$ of the body in its equilibrium state and the time varying part ΔS_B between $z = 0$ and $z = \varepsilon(\zeta^{(1)} - \boldsymbol{\alpha}^{(1)} \cdot \mathbf{k})$. Consequently equation (7.35) can be expanded as in the form

$$\begin{aligned} \mathbf{F} &= -\left(\iint_{\bar{S}_B} + \iint_{\Delta S_B} \right)(p + \boldsymbol{\alpha} \cdot \nabla p + \cdots)\mathbf{n} dS \\ \mathbf{M} &= -\left(\iint_{\bar{S}_B} + \iint_{\Delta S_B} \right)(p + \boldsymbol{\alpha} \cdot \nabla p + \cdots)\mathbf{r} \times \mathbf{n} dS \end{aligned} \tag{7.43}$$

The expressions for hydrodynamic forces can be obtained as follow

$$\mathbf{F} = \mathbf{F}^{(0)} + \varepsilon \mathbf{F}^{(1)} + \varepsilon^2 \mathbf{F}^{(2)} + \cdots \tag{7.44}$$

$$\mathbf{F}^{(0)} = \rho g \forall \mathbf{k} + \frac{1}{2}\rho \iint_{S_B} (\mathbf{W} \cdot \mathbf{W} - \bar{U}^2)\mathbf{n} dS \tag{7.45}$$

$$
\begin{aligned}
\mathbf{F}^{(1)} = \rho\Big[& \iint_{\bar{S}_B} (\tilde{\Phi}_t^{(1)} + \mathbf{W}\cdot\nabla\tilde{\Phi}^{(1)} + g\boldsymbol{\alpha}^{(1)}\cdot\mathbf{k})\mathbf{n}dS \\
& + \frac{1}{2}\iint_{\bar{S}_B} [\boldsymbol{\alpha}^{(1)}\cdot\nabla(\mathbf{W}\cdot\mathbf{W})]\mathbf{n}dS \\
& + \frac{1}{2}\iint_{\bar{S}_B} (\mathbf{W}\cdot\mathbf{W} - \bar{U}^2)\boldsymbol{\Omega}^{(1)}\times\mathbf{n}dS \\
& + \frac{1}{2}\oint_{L_F} (\mathbf{W}\cdot\mathbf{W} - \bar{U}^2)\zeta_r^{(1)}\mathbf{n}dl'\Big]
\end{aligned}
\tag{7.46}
$$

$$
\begin{aligned}
\mathbf{F}^{(2)} = \rho\Big[& \iint_{\bar{S}_B} [\tilde{\Phi}_t^{(2)} + \frac{1}{2}\nabla\tilde{\Phi}^{(1)}\cdot\nabla\tilde{\Phi}^{(1)} + \mathbf{W}\cdot\nabla\tilde{\Phi}^{(2)}]\mathbf{n}dS \\
& + \iint_{\bar{S}_B} [\boldsymbol{\alpha}^{(1)}\cdot\nabla\tilde{\Phi}_t^{(1)} + \boldsymbol{\alpha}^{(1)}\cdot\nabla(\mathbf{W}\cdot\nabla\tilde{\Phi}^{(1)})]\mathbf{n}dS \\
& + \iint_{\bar{S}_B} (\tilde{\Phi}_t^{(1)} + \mathbf{W}\cdot\nabla\tilde{\Phi}^{(1)} + g\boldsymbol{\alpha}^{(1)}\cdot\mathbf{k})\boldsymbol{\Omega}^{(1)}\times\mathbf{n}dS \\
& + \frac{1}{2}\iint_{\bar{S}_B} [\boldsymbol{\alpha}^{(2)}\cdot\nabla(\mathbf{W}\cdot\mathbf{W})]\mathbf{n}dS + \frac{1}{2}\iint_{\bar{S}_B} (\mathbf{W}\cdot\mathbf{W} - \bar{U}^2)[\mathbf{H}]\mathbf{n}dS \\
& + \frac{1}{2}\iint_{\bar{S}_B} [\boldsymbol{\alpha}^{(1)}\cdot\nabla(\mathbf{W}\cdot\mathbf{W})]\boldsymbol{\Omega}^{(1)}\times\mathbf{n}dS \\
& + \frac{1}{2}\oint_{L_t} \frac{\partial}{\partial z}(\mathbf{W}\cdot\mathbf{W})\zeta_r^{(1)2}\mathbf{n}dl' \\
& + \frac{1}{2}\oint_{l_t} (\mathbf{W}\cdot\mathbf{W} - \bar{U}^2)\zeta_r^{(1)}\boldsymbol{\Omega}^{(1)}\times\mathbf{n}dl' - \frac{1}{2}g\oint_{l_t} \zeta_r^{(1)2}\mathbf{n}dl' \\
& - g[\xi_3^{(2)}S_{00} + \xi_4^{(2)}S_{01} - \xi_5^{(2)}S_{10} + \xi_6^{(1)}(\xi_4^{(1)}S_{10} + \xi_5^{(1)}S_{01})]\mathbf{k}\Big]
\end{aligned}
\tag{7.47}
$$

where S_{ij} is the properties of waterplane at $z=0$ already defined in the foregoing section. The first-order relative wave elevation $\zeta_r^{(1)}$ and the steady wave elevation $\bar{\zeta}$ are defined as follows,

$$\zeta_r^{(1)} = \zeta^{(1)} - \xi_3^{(1)} - y\xi_4^{(1)} + x\xi_5^{(1)} \tag{7.48}$$

$$\bar{\zeta} = -\frac{1}{2g}(\mathbf{W}\cdot\mathbf{W} - \bar{U}^2) \tag{7.49}$$

The third term in equation (7.46) can be calculated as follows,

$$g\iint_{S_B} (\boldsymbol{\alpha}^{(1)}\cdot\mathbf{k})\mathbf{n}dS = -g(\xi_3^{(1)}S_{00} + \xi_4^{(1)}S_{01} - \xi_5^{(1)}S_{10})\mathbf{k} \tag{7.50}$$

In order to account for the slope of the wetted surface at the free surface, the line segment dl' along the free surface line integral is written as

$$dl' = dl/(n_1^2 + n_2^2)^{1/2} \tag{7.51}$$

Similarly the expressions for hydrodynamic moments can also be obtained as follow

$$\mathbf{M} = \mathbf{M}^{(0)} + \varepsilon\mathbf{M}^{(1)} + \varepsilon^2\mathbf{M}^{(2)} + \cdots \tag{7.52}$$

$$\mathbf{M}^{(0)} = \rho g \forall (y_B\mathbf{i} - x_B\mathbf{j}) + \frac{1}{2}\rho \iint_{\bar{S}_B} (\mathbf{W}\cdot\mathbf{W} - \bar{U}^2)\mathbf{r}\times\mathbf{n}dS \tag{7.53}$$

$$\begin{aligned}\mathbf{M}^{(1)} = \rho\Bigg[& \iint_{\bar{S}_B} (\tilde{\Phi}_t^{(1)} + \mathbf{W}\cdot\nabla\tilde{\Phi}^{(1)} + g\boldsymbol{\alpha}^{(1)}\cdot\mathbf{k})\mathbf{r}\times\mathbf{n}dS \\ & + \frac{1}{2}\iint_{\bar{S}_B} [\boldsymbol{\alpha}^{(1)}\cdot\nabla(\mathbf{W}\cdot\mathbf{W})]\mathbf{r}\times\mathbf{n}dS \\ & + \frac{1}{2}\iint_{\bar{S}_B} (\mathbf{W}\cdot\mathbf{W} - \bar{U}^2)\boldsymbol{\Gamma}^{(1)}dS \\ & + \frac{1}{2}\oint_{L_F} (\mathbf{W}\cdot\mathbf{W} - \bar{U}^2)\zeta_r^{(1)}\mathbf{r}\times\mathbf{n}dl'\Bigg]\end{aligned} \tag{7.54}$$

$$\begin{aligned}\mathbf{M}^{(2)} = \rho\Bigg[& \iint_{\bar{S}_B} [\tilde{\Phi}_t^{(2)} + \frac{1}{2}\nabla\tilde{\Phi}^{(1)}\cdot\nabla\tilde{\Phi}^{(1)} + \mathbf{W}\cdot\nabla\tilde{\Phi}^{(2)}]\mathbf{r}\times\mathbf{n}dS \\ & + \iint_{\bar{S}_B} [\boldsymbol{\alpha}^{(1)}\cdot\nabla\tilde{\Phi}_t^{(1)} + \boldsymbol{\alpha}^{(1)}\cdot\nabla(\mathbf{W}\cdot\nabla\tilde{\Phi}^{(1)})]\mathbf{r}\times\mathbf{n}dS \\ & + \iint_{\bar{S}_B} (\tilde{\Phi}_t^{(1)} + \mathbf{W}\cdot\nabla\tilde{\Phi}^{(1)} + g\boldsymbol{\alpha}^{(1)}\cdot\mathbf{k})\boldsymbol{\Gamma}^{(1)}dS \\ & + \frac{1}{2}\iint_{\bar{S}_B} [\boldsymbol{\alpha}^{(2)}\cdot\nabla(\mathbf{W}\cdot\mathbf{W})]\mathbf{r}\times\mathbf{n}dS \\ & + \frac{1}{2}\iint_{\bar{S}_B} (\mathbf{W}\cdot\mathbf{W} - \bar{U}^2)\boldsymbol{\Gamma}^{(2)}dS \\ & + \frac{1}{2}\iint_{\bar{S}_B} [\boldsymbol{\alpha}^{(1)}\cdot\nabla(\mathbf{W}\cdot\mathbf{W})]\boldsymbol{\Gamma}^{(1)}dS \\ & - \frac{1}{2}g\oint_{L_F} \zeta_r^{(1)2}\mathbf{r}\times\mathbf{n}dl' + \frac{1}{2}\oint_{L_F} \frac{\partial}{\partial z}(\mathbf{W}\cdot\mathbf{W})\zeta_r^{(1)2}\mathbf{r}\times\mathbf{n}dl' \\ & + \frac{1}{2}\oint_{L_F} (\mathbf{W}\cdot\mathbf{W} - \bar{U}^2)\zeta_r^{(1)}\boldsymbol{\Gamma}^{(1)}dl'\Bigg] \\ & + (\text{other second order terms with } \mathbf{i} \text{ and } \mathbf{j} \text{ components} \\ & \quad \text{due to hydrostatic variation})\end{aligned} \tag{7.55}$$

Similarly to equation (7.50), the third term in equation (7.54) becomes

$$g\iint_{\bar{S}_B}(\boldsymbol{\alpha}^{(1)}\cdot\mathbf{k})\mathbf{r}\times\mathbf{n}dS=$$
$$-g\begin{pmatrix}-\cancel{V}\xi_2^{(1)}+\xi_3^{(1)}S_{01}+\xi_4^{(1)}(S_{02}+\cancel{V}z_B)-\xi_5^{(1)}S_{11}-\cancel{V}x_B\xi_6^{(1)}\\ \cancel{V}\xi_1^{(1)}-\xi_3^{(1)}S_{10}-\xi_4^{(1)}S_{11}+\xi_5^{(1)}(S_{20}+\cancel{V}z_B)-\cancel{V}y_B\xi_6^{(1)}\\ 0\end{pmatrix} \quad (7.56)$$

If we assume the first-order waves and motions are purely sinusoidal in time, then the time average of all the first-order terms becomes zero. The second-order potential and motions are also sinusoidal, so their mean values over one period are also zero. Finally the mean-second-order force and moment can be expressed as follows,

$$\langle\mathbf{F}^{(2)}\rangle=\left\langle-\frac{1}{2}\rho g\oint_{L_F}\zeta_r^{(1)2}\mathbf{n}dl'\right\rangle_I+\left\langle\frac{1}{2}\rho\iint_{\bar{S}_B}(\nabla\tilde{\Phi}^{(1)}\cdot\nabla\tilde{\Phi}^{(1)})\mathbf{n}dS\right\rangle_{II}$$
$$+\left\langle\rho\iint_{\bar{S}_B}(\boldsymbol{\alpha}^{(1)}\cdot\nabla\tilde{\Phi}_t^{(1)})\mathbf{n}dS\right\rangle_{III}+\langle\boldsymbol{\Omega}^{(1)}\times\mathbf{F}^{(1)}\rangle_{IV}$$
$$+\left\langle-\rho g\xi_4^{(1)}\xi_6^{(1)}S_{10}\mathbf{k}\right\rangle_V+\left\langle\underline{-\rho\bar{U}\iint_{\bar{S}_B}(\boldsymbol{\alpha}^{(1)}\cdot\nabla\tilde{\Phi}_x^{(1)})\mathbf{n}dS}\right\rangle_{VI} \quad (7.57)$$

$$\langle\mathbf{M}^{(2)}\rangle=\left\langle-\frac{1}{2}\rho g\oint_{L_F}\zeta_r^{(1)2}\mathbf{r}\times\mathbf{n}dl'\right\rangle_I+\left\langle\frac{1}{2}\rho\iint_{\bar{S}_B}(\nabla\tilde{\Phi}^{(1)}\cdot\nabla\tilde{\Phi}^{(1)})\mathbf{r}\times\mathbf{n}dS\right\rangle_{II}$$
$$+\left\langle\rho\iint_{\bar{S}_B}(\boldsymbol{\alpha}^{(1)}\cdot\nabla\tilde{\Phi}_t^{(1)})\mathbf{r}\times\mathbf{n}dS\right\rangle_{III}+\langle\boldsymbol{\delta}^{(1)}\times\mathbf{F}^{(1)}+\boldsymbol{\Omega}^{(1)}\times\mathbf{M}^{(1)}\rangle_{IV}$$
$$+\left\langle-\rho g\begin{pmatrix}\xi_2^{(1)}(\xi_3^{(1)}S_{02}-\xi_5^{(1)}S_{10})+\xi_3^{(1)}\xi_6^{(1)}S_{10}+\xi_5^{(1)}\xi_6^{(1)}(S_{02}-S_{20})\\ -\xi_1^{(1)}(\xi_3^{(1)}S_{00}-\xi_5^{(1)}S_{10})+\xi_4^{(1)}\xi_6^{(1)}(S_{02}-S_{20})\\ 0\end{pmatrix}\right\rangle_V \quad (7.58)$$
$$+\left\langle-\rho\bar{U}\iint_{\bar{S}_B}(\boldsymbol{\alpha}^{(1)}\cdot\nabla\tilde{\Phi}_x^{(1)})\mathbf{r}\times\mathbf{n}dS\right\rangle_{VI}$$

where the bracket $\langle\ \rangle$ denotes time average over one period. The first-order forces and moments can be simply obtained from the expression used in equation (7.30) as

$$\begin{bmatrix} \mathbf{F}^{(1)} \\ \mathbf{M}^{(1)} \end{bmatrix} = M_{jk}\ddot{\xi}_k \tag{7.59}$$

where M_{jk} are defined in equation (7.31).

The component of mean second-order hydrodynamic forces and moments in equations (7.57) and (7.58) consist of the product of first-order quantities. These force components can be described as follows;

(I) relative wave elevation,

(II) quadratic term of velocity,

(III) product of first-order motion and gradient of first-order pressure field,

(IV) cross product of first-order motion and force,

(V) product of first-order motion,

(VI) forward speed related term.

These first-order terms are easily obtained by solving first-order velocity potential problem and related equations of motion and demonstration of first- and second-order problems will be presented in the next sections.

7.5 Numerical Calculation of First-Order Force

In order to provide a validation of the method adopted in this study, an extensive series of comparisons with published data, which include both experimental and theoretical data, should be carried out. For this purpose numerical calculation has been performed to predict hydrodynamic coefficients, wave loads and motion responses to the wave. The calculation was applied to Wigley model and Todd Series 60 and the results were compared with other numerical results as well as experimental data where available.

All calculation results and experiment data presented in this thesis including hydrodynamic coefficients, wave exciting forces and response amplitude operator are non-dimensionalised with following forms;

- Encounter frequency

$$\omega_e' = \omega_e \sqrt{L/g} \tag{7.60}$$

- Added mass coefficient

$$\begin{aligned} A_{ij}' &= A_{ij} \big/ \rho\nabla && \text{when } i=1,2,3 \text{ and } j=1,2,3 \\ A_{ij}' &= A_{ij} \big/ \rho\nabla L && \text{when } i=1,2,3 \text{ and } j=4,5,6 \\ & && \text{or } i=4,5,6 \text{ and } j=1,2,3 \\ A_{ij}' &= A_{ij} \big/ \rho\nabla L^2 && \text{when } i=1,2,3 \text{ and } j=4,5,6 \end{aligned} \tag{7.61}$$

- Damping coefficient

$$\begin{aligned} B_{ij}' &= B_{ij} \big/ \rho\nabla\sqrt{g/L} && \text{when } i=1,2,3 \text{ and } j=1,2,3 \\ B_{ij}' &= B_{ij} \big/ \rho\nabla L\sqrt{g/L} && \text{when } i=1,2,3 \text{ and } j=4,5,6 \\ & && \text{or } i=4,5,6 \text{ and } j=1,2,3 \\ B_{ij}' &= B_{ij} \big/ \rho\nabla L^2\sqrt{g/L} && \text{when } i=1,2,3 \text{ and } j=4,5,6 \end{aligned} \tag{7.62}$$

- Wave exciting force

$$\left|F_j'\right| = \left|F_j^{EX}\right| \Big/ \rho g \nabla (\zeta_0 / L) \qquad \text{when } j = 1,2,3$$

$$\left|F_j'\right| = \left|F_j^{EX}\right| \Big/ \rho g \nabla \zeta_0 \qquad \text{when } j = 4,5,6 \tag{7.63}$$

- Response amplitude operator

$$\left|\xi_j'\right| = \left|\xi_j\right| \Big/ \zeta_0 \qquad \text{when } j = 1,2,3$$

$$\left|\xi_j'\right| = \left|\xi_j\right| \Big/ k_0 \zeta_0 \qquad \text{when } j = 4,5,6 \tag{7.64}$$

where ζ_0 is incident wave amplitude.

7.5.1 Convergence test of the numerical tools

In order to secure the practical validation of the numerical tools, it is important to check the reliability through studying convergence of results obtained in terms of the description of hull geometry. Favourable agreement in the comparison between numerical predictions and experimental measurements is not significant if the numerical predictions are dependent appreciably upon the characteristics of surface elements used for representing the ship's hull. Therefore the validation with numerical method cannot be convinced unless the reliability and accuracy of the method are established independently of hull discretisation.

Since the numerical tools are developed to represent a physical problem, it would be ideal if the obtained numerical results converge to some particular value and the solution becomes independent of the discretisation of the hull surface. Unfortunately, it is not always possible to achieve the convergence of a solution as it usually requires a large number of elements with careful distribution over the hull surface, and correspondingly a large computational effort is required to obtain a solution. Generally the actual size of an element becomes small when a large number of elements are used. If some error in the solution is acceptable then, for efficiency, fewer and bigger elements may be used to obtain a solution.

Describing hull geometry using surface elements usually involves the choice of some characteristics of elements, i.e. size and distribution. Since these characteristics are dependent on each other, it is better to control them with geometrical property like aspect ratio, which is defined as the ratio of the longitudinal to girthwise side length of a panel, and the number of panels used in the discretisation. It is quite difficult to define general rule to governing these factors because of the varying hull form and dependence between the characteristics of elements.

Using a point source at the centre of each element in the constant panel method might cause more inaccuracy as the panel aspect ratio increases. The longitudinal length of a panel must also remain much smaller than the rate of flow change along the ship length especially in the bow and stern area where the flow changes rapidly. The size of a panel is also influenced by the wavelength since elaborate distribution of elements is required for the short waves or high frequency region. The best representation of hull surface could be a compromise between accurate modelling of hull geometry and the computational effort required.

Based on the aforementioned characteristics of elements extensive numerical calculations especially for the unsteady hydrodynamic problems have been performed for a given hull form. Wigley hull form has been selected with respect to various numbers of panels in a different aspect ratio for the hull discretisation. The main reason to use Wigley hull form to validate numerical results is that its hull form is defined mathematically and therefore the geometrical errors in the discretisation can be decreased. The representation of the hull surface can be performed with any desired numbers of panels and easily applicable for numerical work. The definition of Wigley hull form used in convergence tests is given in equation (7.65).

$$\frac{y}{B/2}=\left[1-\left(\frac{z}{T}\right)^2\right]\left[1-\left(\frac{2x}{L}\right)^2\right]\left[1+0.2\left(\frac{2x}{L}\right)^2\right] + \left(\frac{z}{T}\right)^2\left[1-\left(\frac{z}{T}\right)^8\right]\left[1-\left(\frac{2x}{L}\right)^2\right]^4 \tag{7.65}$$

The hull surface is discretised equally in the longitudinal direction and then each section is divided into the same number of equal-length segments. The total number of panels was controlled by changing the number of panels in longitudinal and transverse directions. Seven Wigley hull models discretised with different numbers of panels and aspect ratios are chosen and presented in Table 7.1 and Figure 7.1. Nx and Ny are number of element in the longitudinal direction and half-section respectively. The aspect ratio is calculated in the midship section only and resultant value changes between 1.0 and 3.1.

The hydrodynamic coefficients were calculated by Constant Panel Method with three-dimensional Green function for a Wigley hull form travelling at a Froude number 0.2. The calculation was carried out in a wide range of frequencies in a head sea and calculation time for 24 wave frequencies in head sea each is given in Table 7.1. The specifications of computer used in the comparisons are Intel® Core™ 2 Duo T7250 2.0GHz CPU and 4.0GB DDR2 Memory. It is noted that the calculation time is proportional to the square of panel number since most of computational efforts are spent for the evaluation of Green function in the influence matrix given in equation (6.11).

Table 7.1 Comparison of discretised models of Wigley ship

Model	Nx	Ny	Total	Aspect ratio	CPM time[min]
Model A	20	4	160	2.0	3
Model B	20	6	240	3.1	6
Model C	40	4	320	1.0	13
Model D	40	6	480	1.5	27
Model E	40	8	640	2.0	47
Model F	60	6	720	1.0	63
Model G	60	8	960	1.4	97

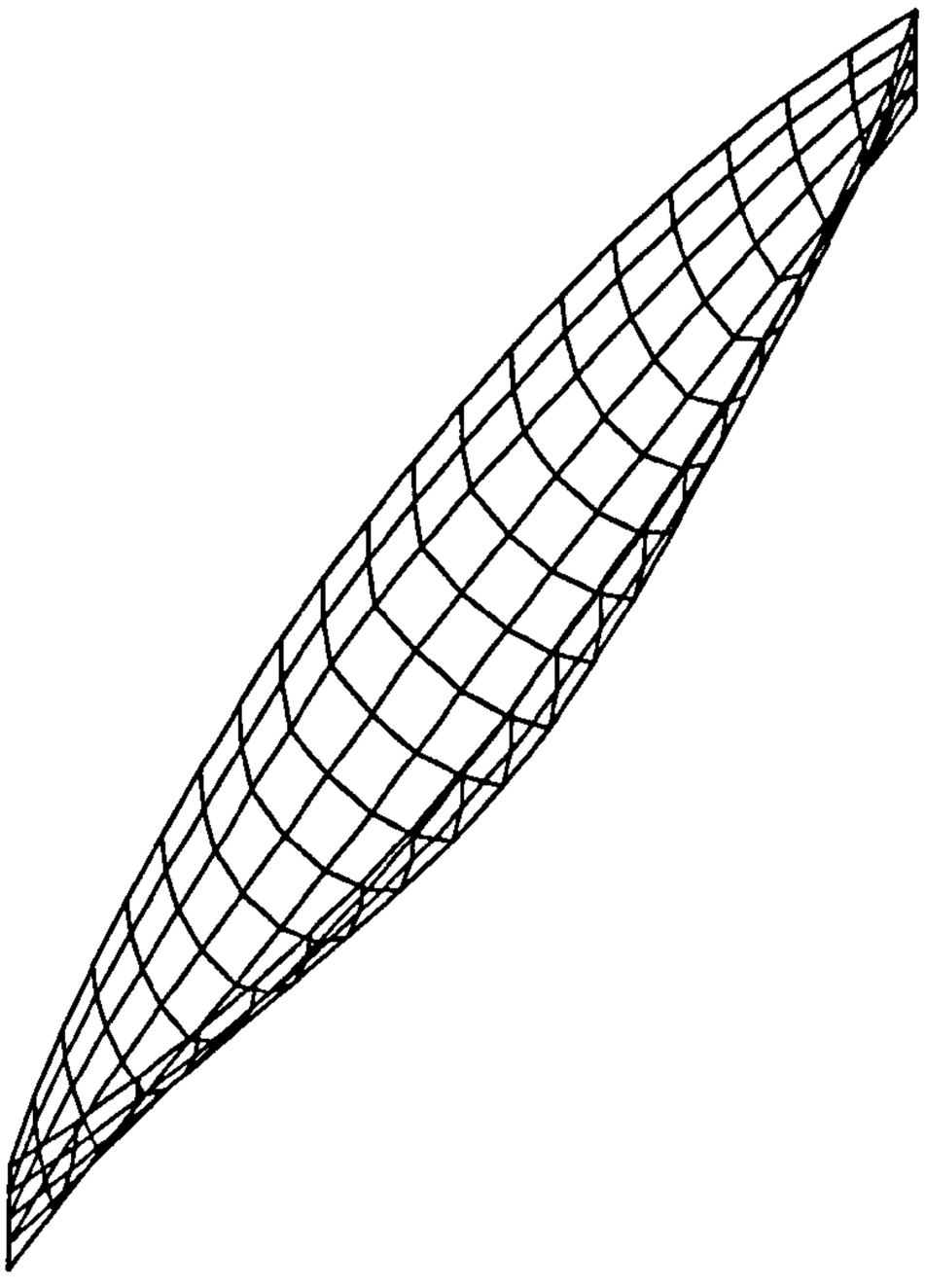

(a) Model A : 160 panels

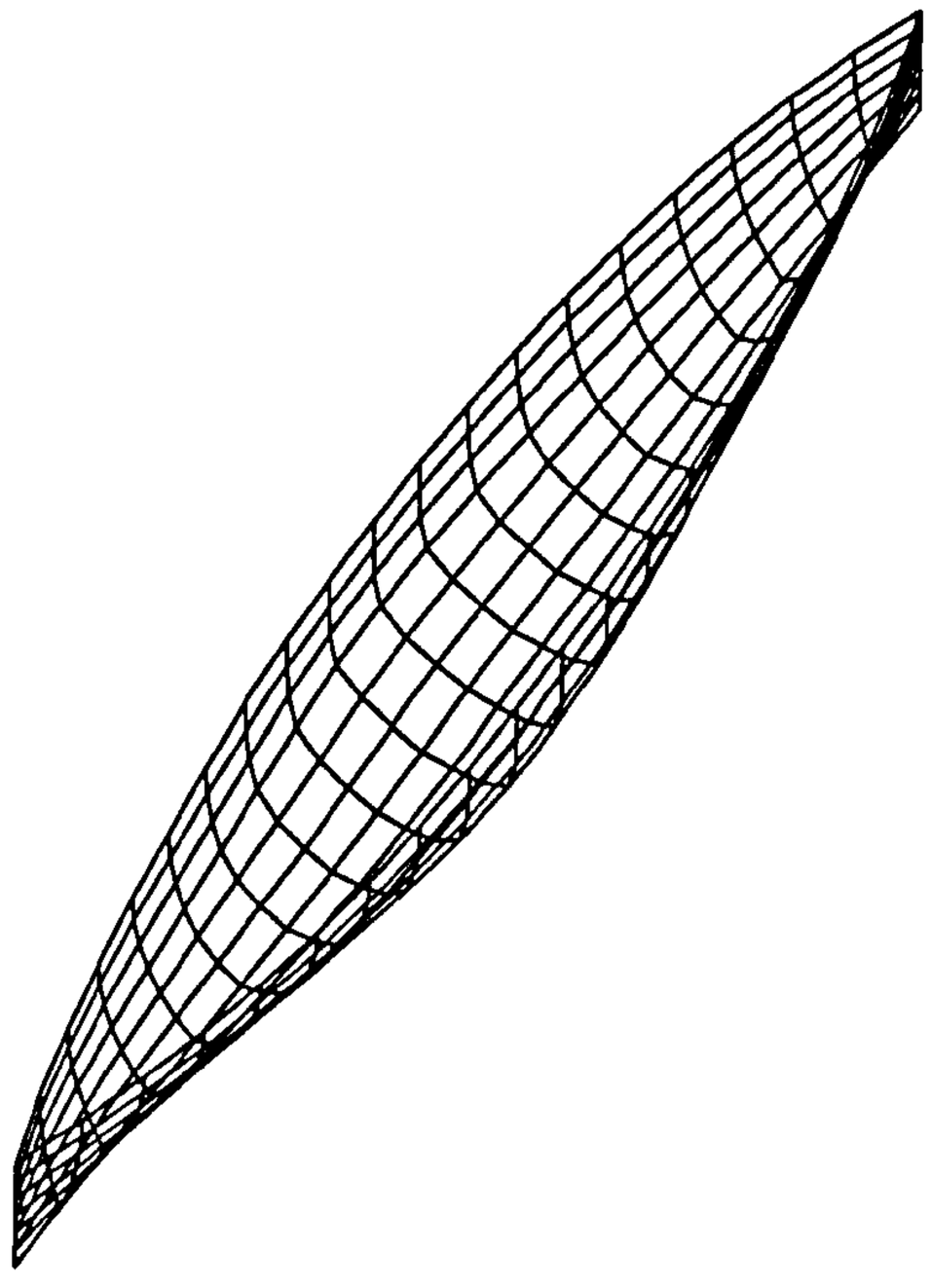

(b) Model B : 240 panels

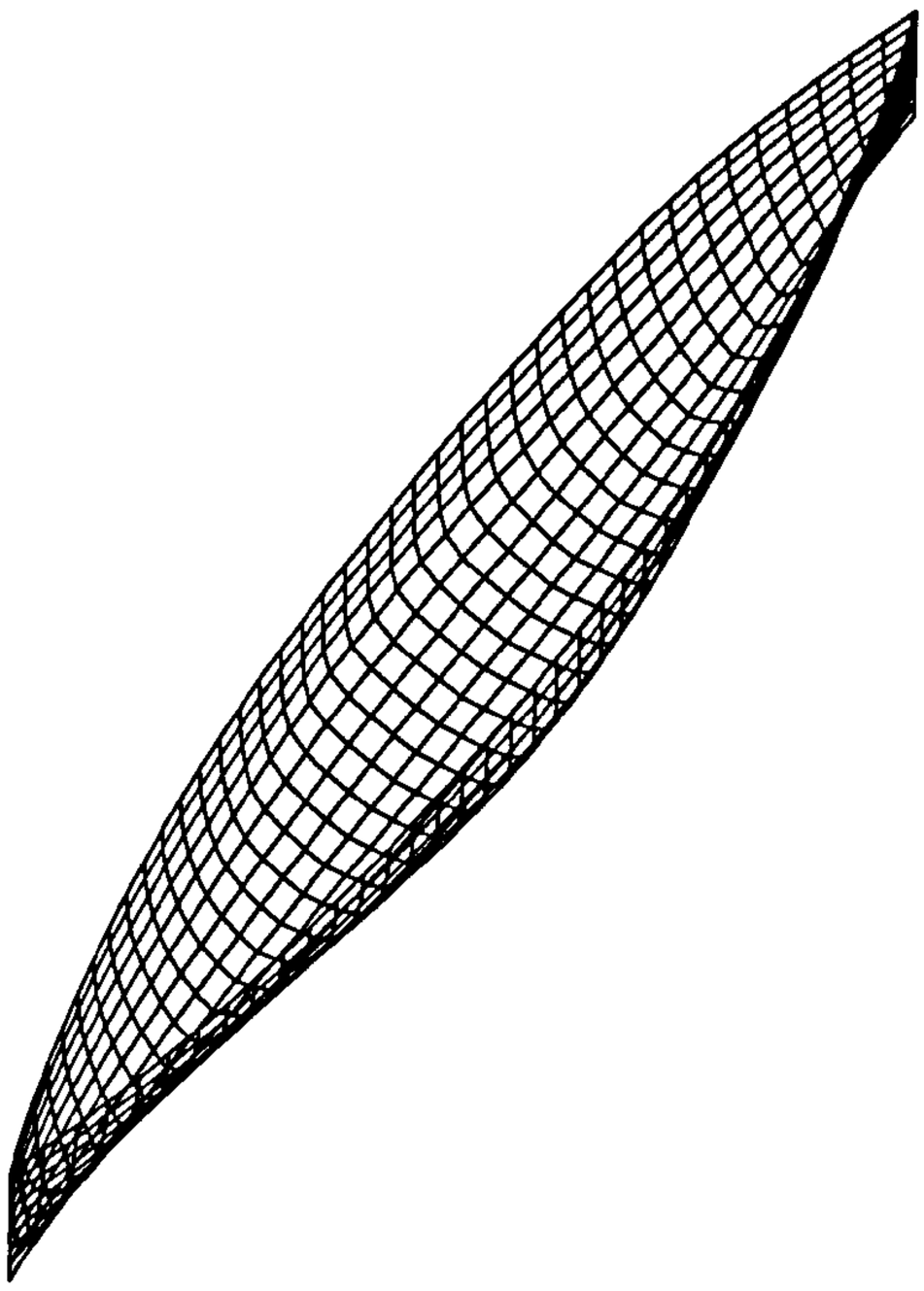

(c) Model E : 640 panels

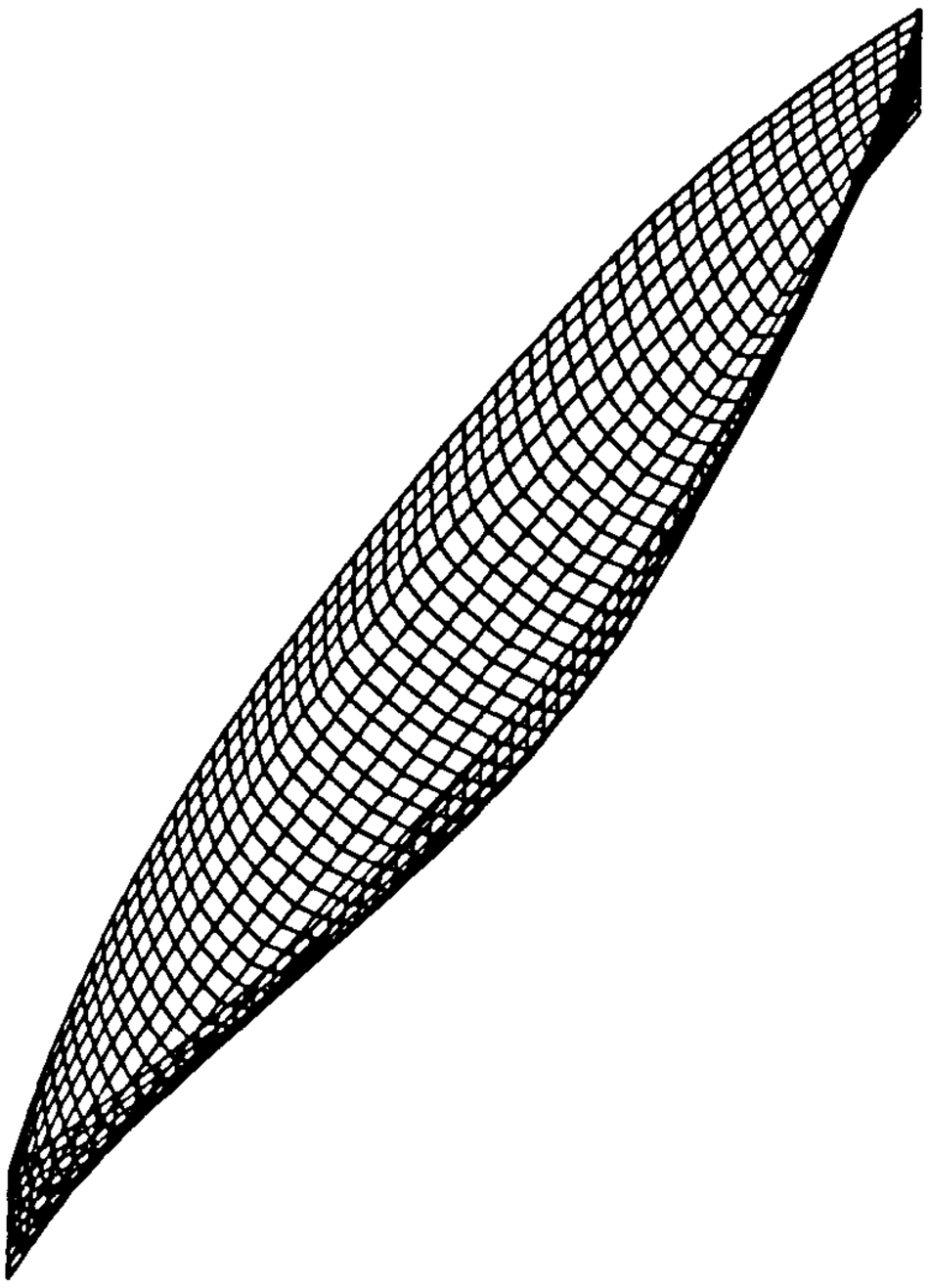

(d) Model G : 960 panels

Figure 7.1 Comparisons of panel representations of Wigley hull form

Several important hydrodynamic coefficients are focused on this investigation like heave and pitch in the vertical modes, which are presented in Figure 7.2 and Figure 7.3 and sway, yaw and roll in the horizontal modes presented in Figure 7.4 through Figure 7.6. The hydrodynamic coefficients and encounter frequency was non-dimensionalised by equations (7.60) to (7.62). For the majority of hydrodynamic coefficients in vertical mode, the influence of total number of panels on the predicted value is small. Especially convergence of added mass coefficients was achieved at any frequency regions, while that of damping coefficients show a little discrepancy in the moderate frequency region (ω_e' 4.4 to 7.6).

Predictions of hydrodynamic coefficients in horizontal mode appear to be more dependent on the hull discretisation than those in vertical mode. Again there is almost no influence of number of panels on the added mass coefficients A_{22}' and A_{66}' although small discrepancy is shown on the cross coupling term A_{26}' and A_{62}' in the low and high frequency regions. Variations in values of damping coefficients B_{22}' and B_{66}' are shown in the high frequency regions and those of cross coupling terms B_{62}' and B_{26}' become clear for frequencies greater than 3.0. The results of roll-dependent coefficients A_{44}' and B_{44}' exhibit similar tendency to other coefficients and can be grouped according to the sectional number of panels.

The result of Model B shows difference from other results and oscillation in value due to relatively small number of panels and large aspect ratio. Model A, which used fewer panels and smaller aspect ratio, shows better result than Model B. This suggests that the aspect ratio is very important characteristics in the discretisation strategy. When the increase of total number of panels is considered, better predictions might be achieved by decreasing the aspect ratio not simply increasing sectional number of panels.

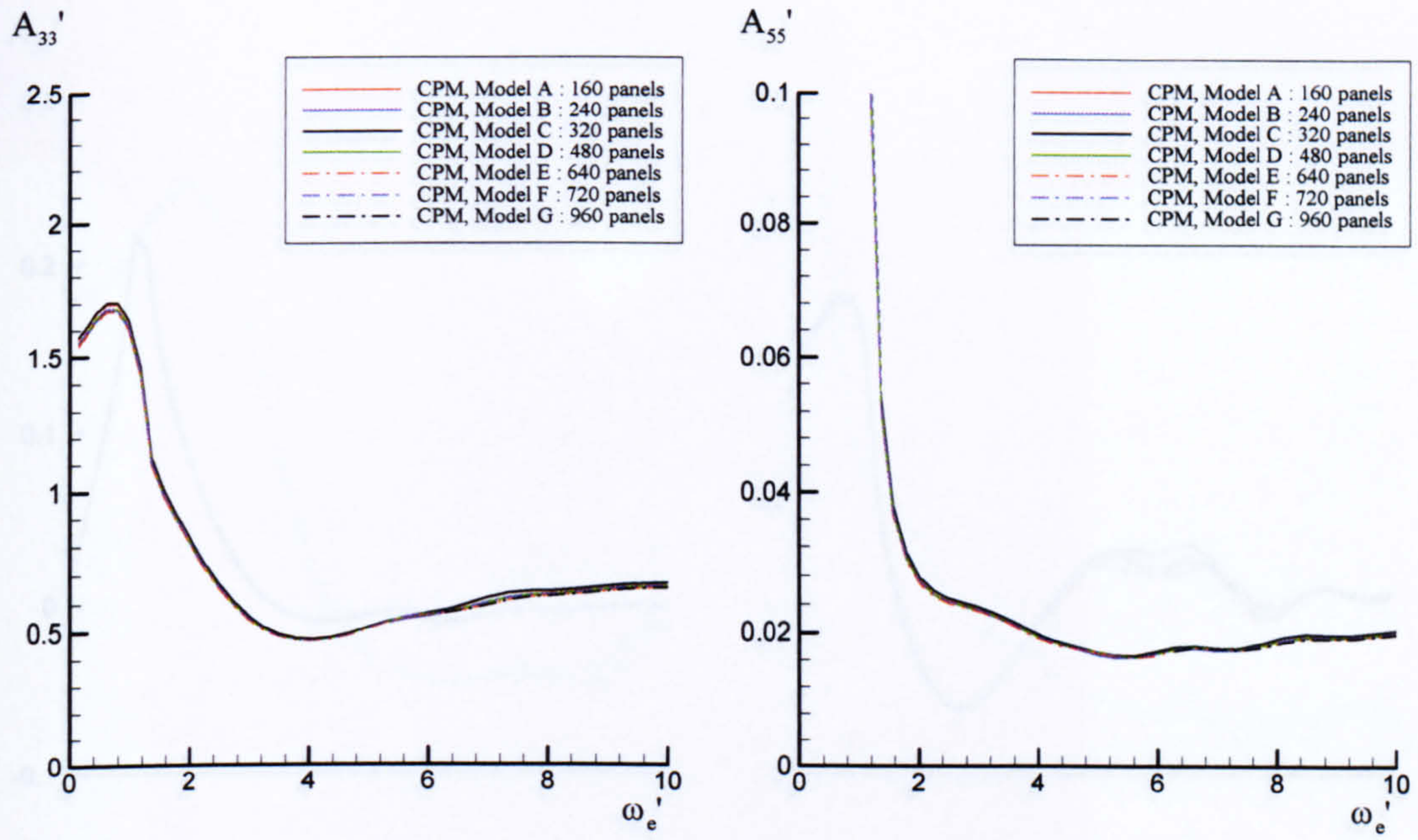

(a) Added mass

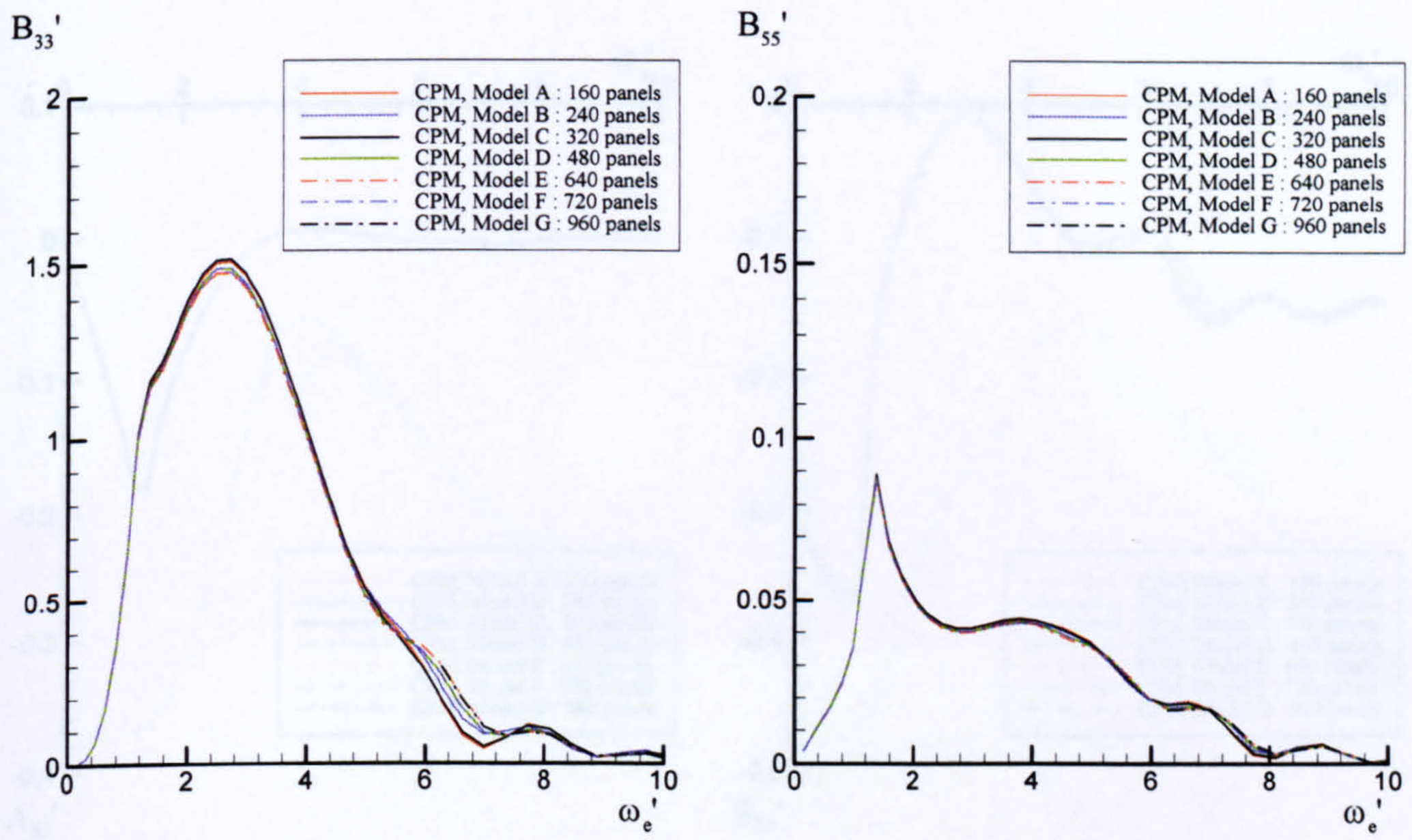

(b) Damping coefficients

Figure 7.2 Non-dimensional added mass and damping coefficients in heave and pitch modes for various discretisation models of Wigley hull form travelling at Froude number 0.2

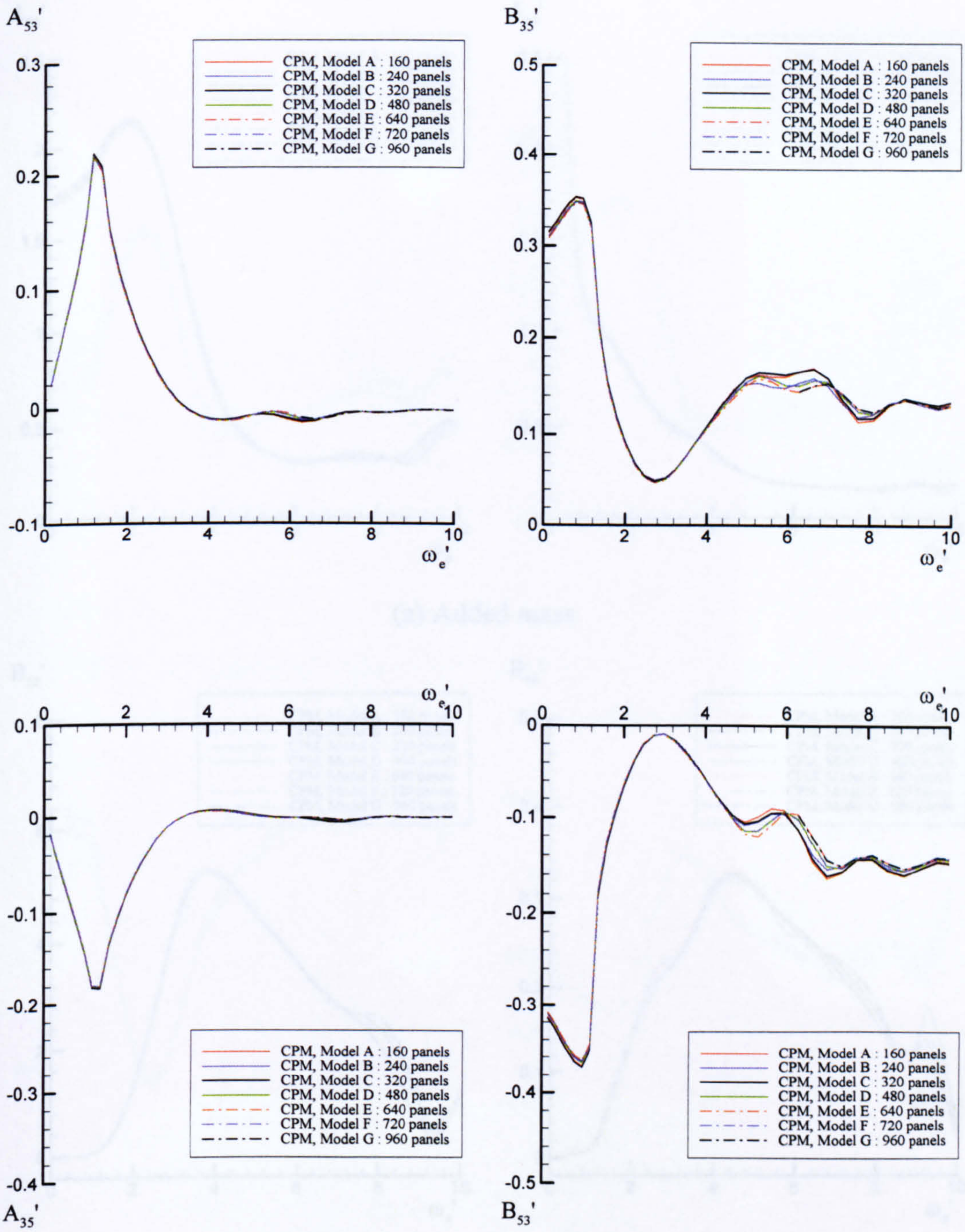

(a) Added mass (b) Damping coefficients

Figure 7.3 Non-dimensional coupled added mass and damping coefficients in heave and pitch modes for various discretisation models of Wigley hull form travelling at Froude number 0.2

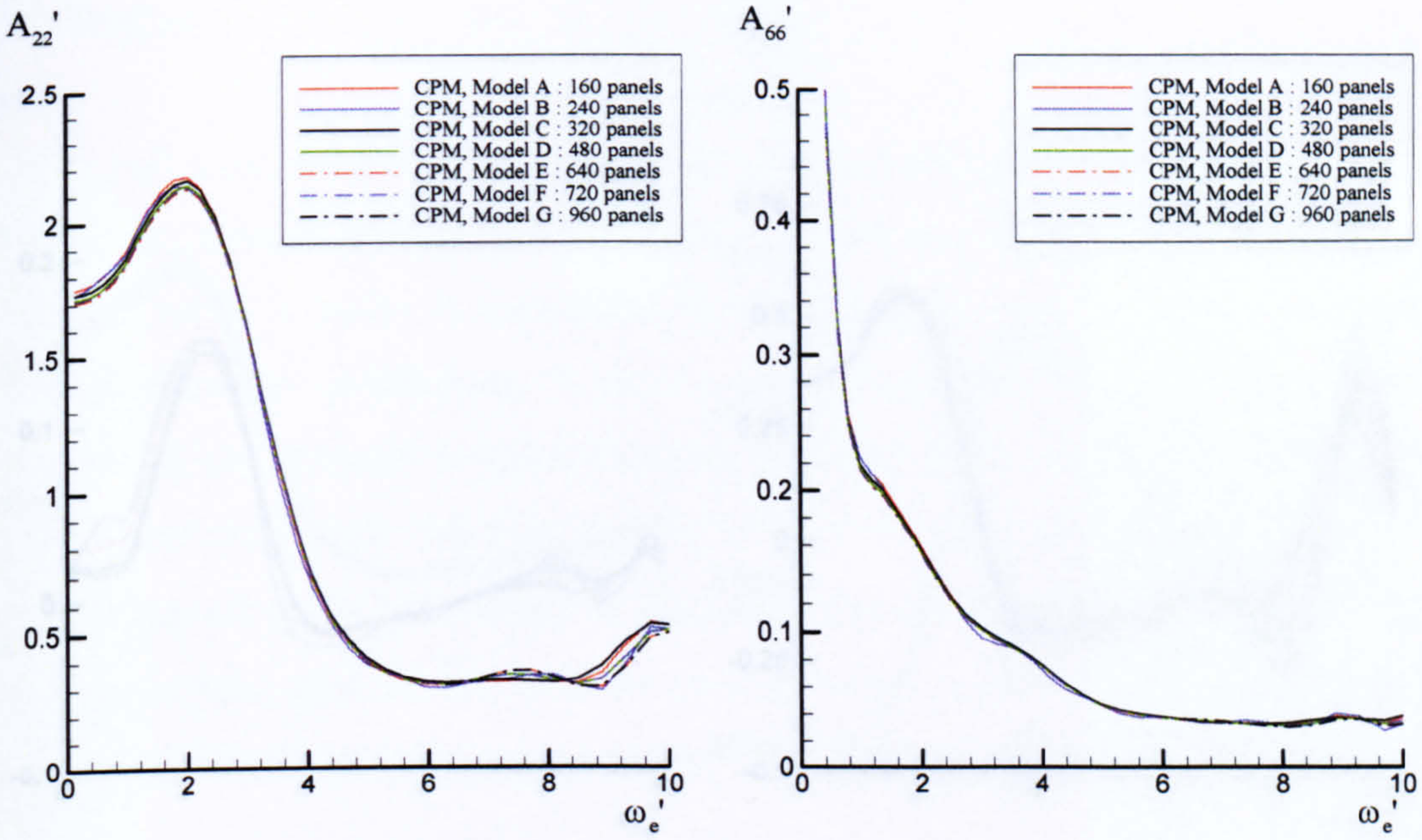

(a) Added mass

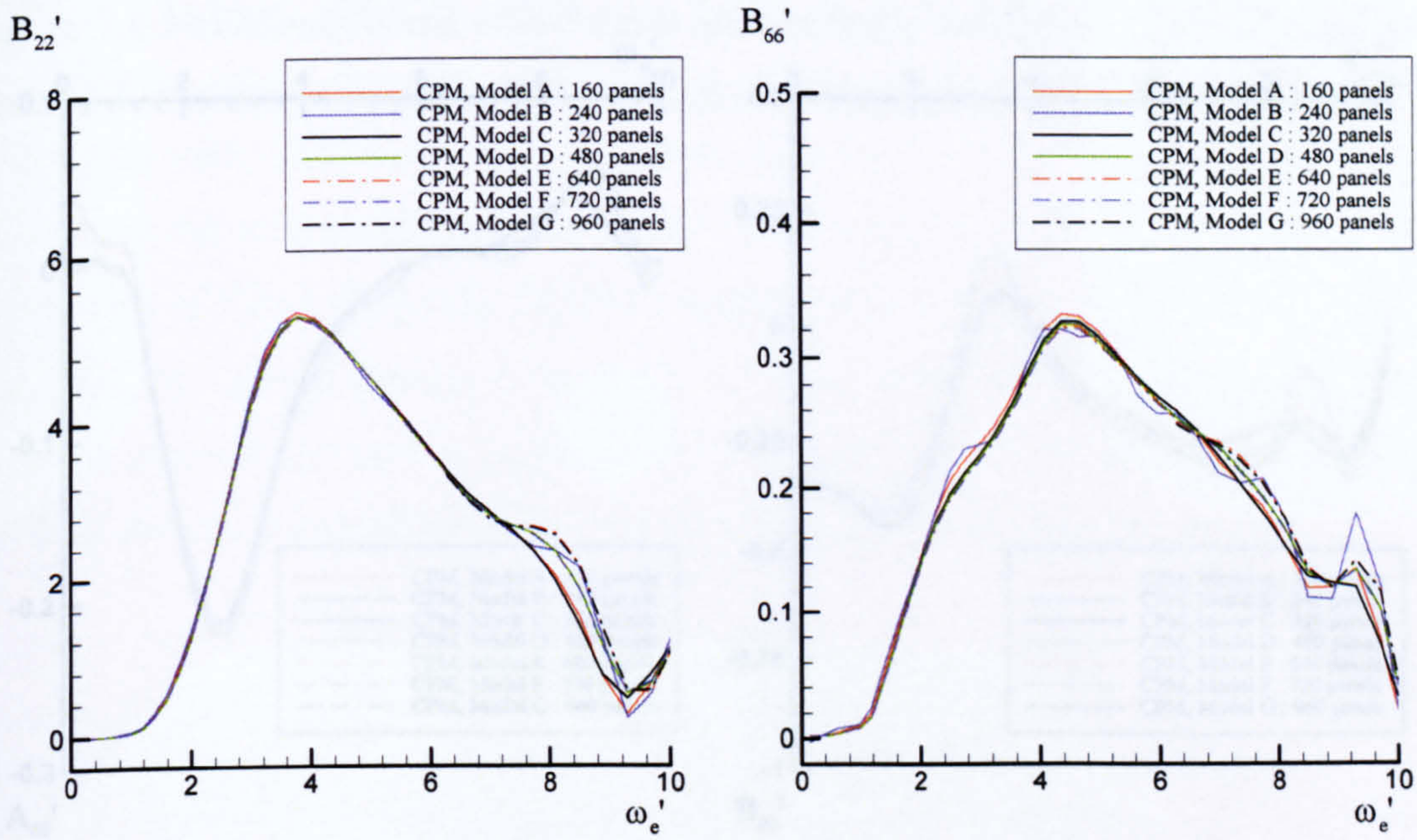

(b) Damping coefficients

Figure 7.4 Non-dimensional added mass and damping coefficients in sway and yaw modes for various discretisation models of Wigley hull form travelling at Froude number 0.2

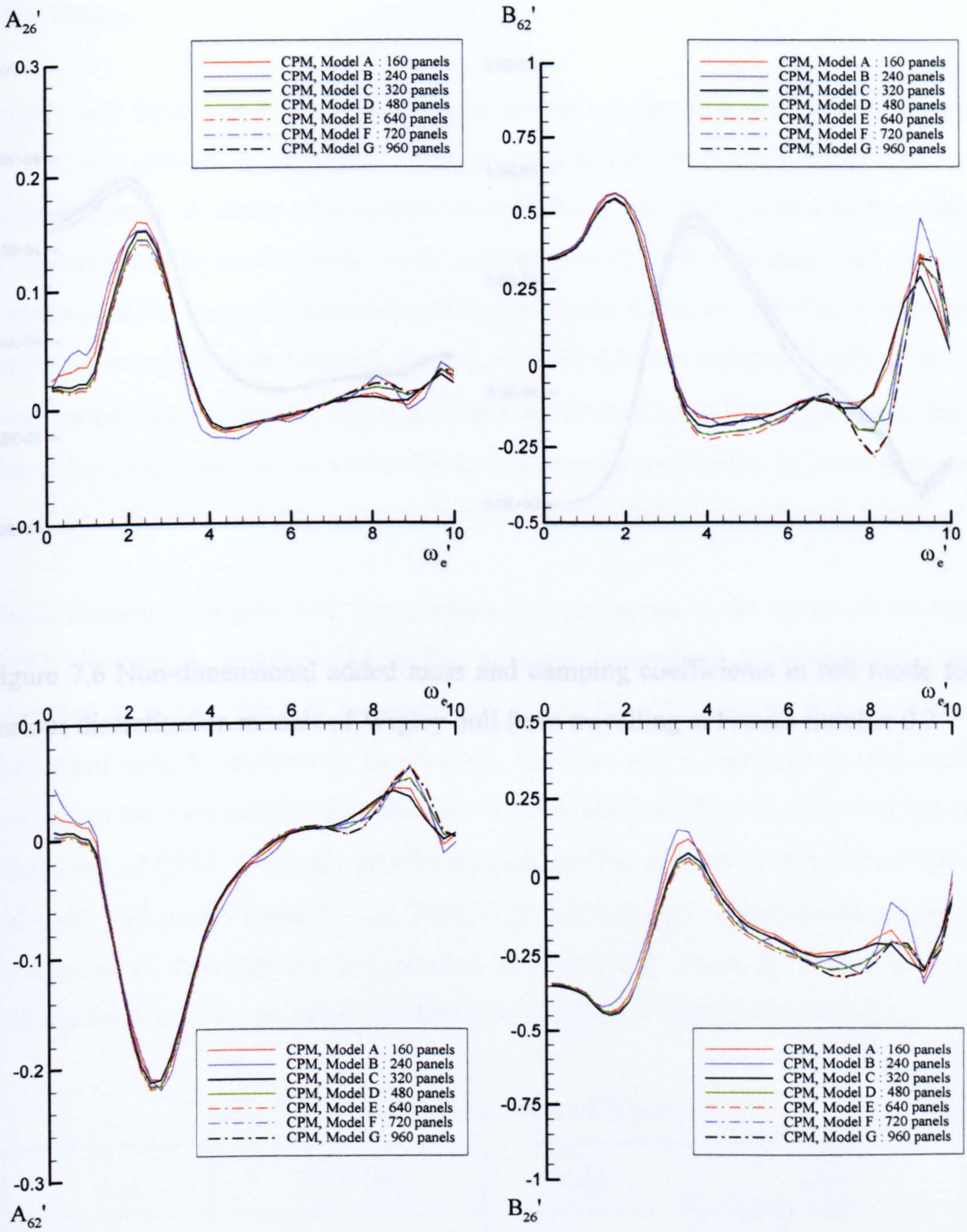

(a) Added mass (b) Damping coefficients

Figure 7.5 Non-dimensional coupled added mass and damping coefficients in sway and yaw modes for various discretisation models of Wigley hull form travelling at Froude number 0.2

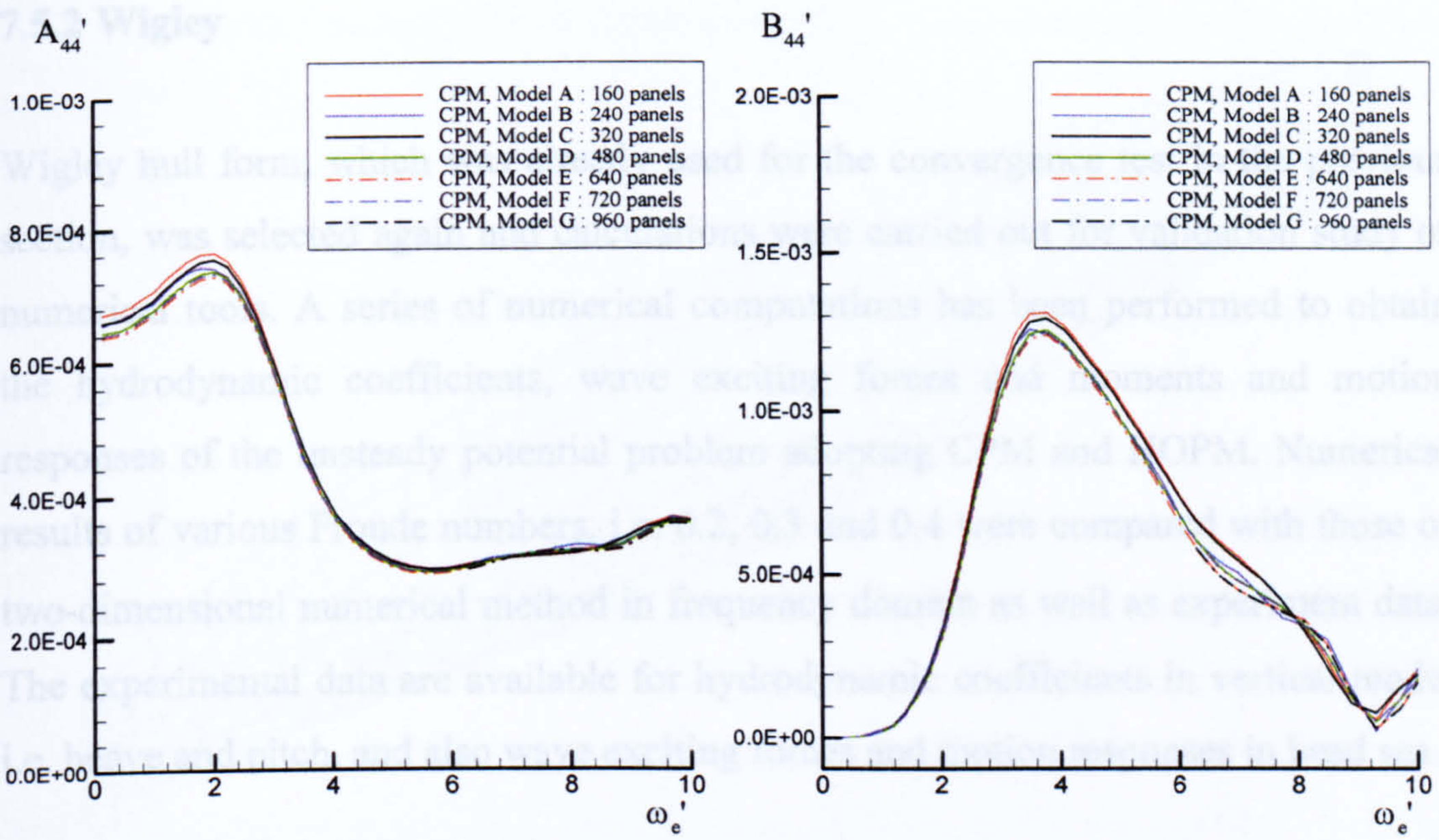

Figure 7.6 Non-dimensional added mass and damping coefficients in roll mode for various discretisation models of Wigley hull form travelling at Froude number 0.2

7.5.2 Wigley

Wigley hull form, which was already used for the convergence test in the previous section, was selected again and calculations were carried out for validation study of numerical tools. A series of numerical computations has been performed to obtain the hydrodynamic coefficients, wave exciting forces and moments and motion responses of the unsteady potential problem adopting CPM and HOPM. Numerical results of various Froude numbers, i.e. 0.2, 0.3 and 0.4 were compared with those of two-dimensional numerical method in frequency domain as well as experiment data. The experimental data are available for hydrodynamic coefficients in vertical mode, i.e. heave and pitch, and also wave exciting forces and motion responses in head sea.

The definition of Wigley hull form, which was presented in the report of Journee (1992), is given in equation (7.65). The principal dimensions of Wigley hull were expanded to actual ship size as shown in Table 7.2. The Wigley hull form was discretised with 40 sections in longitudinal direction and 6 segments in each half-section, so the total number of panels is 480 (Model D in Table 7.1) for numerical calculation of CPM. Generally HOPM requires smaller number of panels than CPM and total 160 panels (Model C in Table 7.1) was selected. The three-dimensional view of panel discretisation is presented in Figure 7.7, where the aspect ratio of midship section is maintained as 1.5 for CPM and 1.0 for HOPM respectively.

Table 7.2 Principal dimensions of Wigley model

L	120.0 [m]	L/B	10.0
B	12.0 [m]	B/T	1.6
T	7.5 [m]	k_{yy}	30.0 [m]
∇	6055.9 [m^3]	$\overline{GM}_T$	1.0 [m]
C_B	0.5607	$\overline{GM}_L$	123.52 [m]

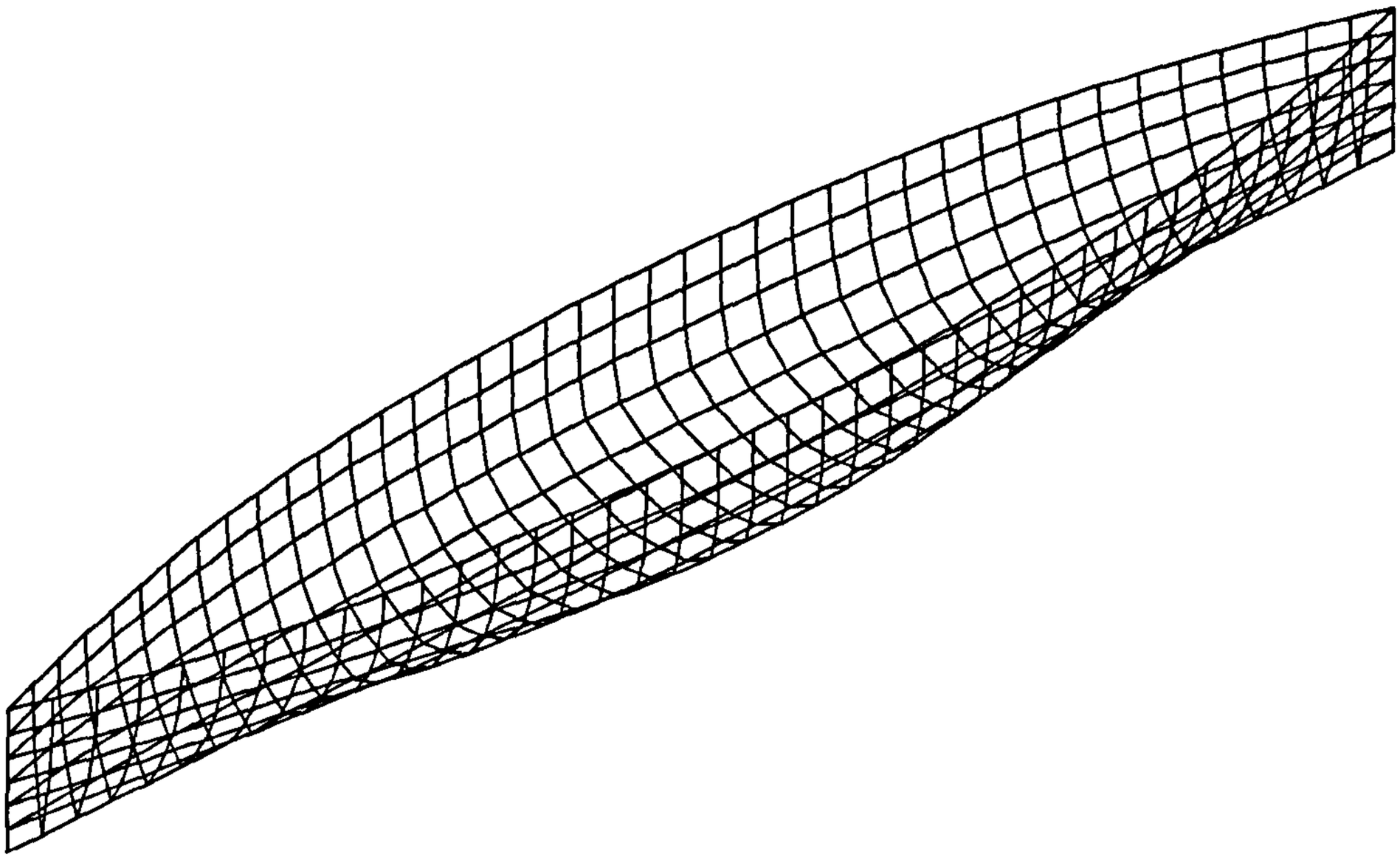

(a) Model D : 480 panels for CPM

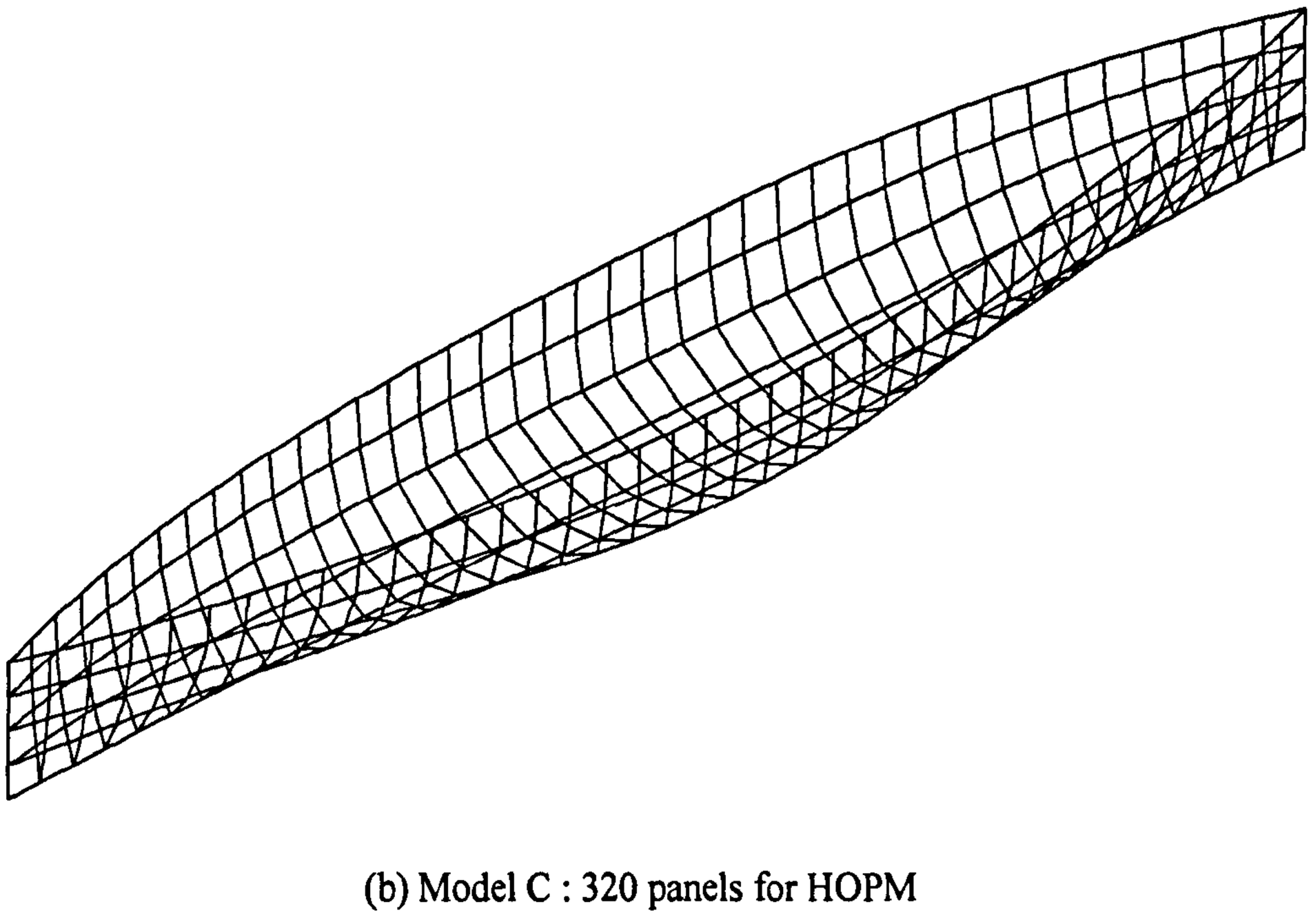

(b) Model C : 320 panels for HOPM

Figure 7.7 Panel representation of hull surface of Wigley hull form

The calculations of linear unsteady problem for Wigley hull form are carried out by each of three-dimensional Green function methods adopted in this study, i.e. CPM and HOPM. The results of computations were compared with those of two-dimensional strip method based on Rankine source distribution method (Jasionowski, 2001). For experimental data, Journee (1992) has published extensive test data on hydrodynamic coefficients for heave and pitch, wave loads and vertical motions of four different Wigley hull forms with a forward speed of Froude number 0.2, 0.3 and 0.4. The calculation results and comparisons are demonstrated for the Froude number 0.2 in head sea and further results of Froude number 0.3 and 0.4 are presented in Appendix B.

- Hydrodynamic coefficient

The hydrodynamic added mass and damping coefficients for Wigley hull travelling with the forward speed of Froude number 0.2 are presented in Figure 7.8 through Figure 7.9. Heave added mass coefficients of three-dimensional methods presented in Figure 7.8 show good agreement with measured data while there is discrepancy with strip method in low frequency region. Pitch added mass coefficients of present study are in fairly good accordance with other results. Pitch added mass approaches infinity at zero encounter frequency because $A_{jk} = \mathrm{Re}(T_{jk})/\omega_e^2$ in equations (7.25) and (7.27) together with forward speed effects, i.e. $Um_5 \neq 0$. For heave damping coefficients, similar trend to the case of heave added mass is observed. Coupled added mass coefficients of three-dimensional methods presented in Figure 7.9 (a) are in good agreement with experimental data and the change of formulation of Green function at critical value of $\tau = 1/4$ is well reflected in low frequency region, where the encounter frequency is below $\omega_e' = 1/(4 \cdot F_N) = 1.25$. Pitch damping coefficients in strip theory becomes infinity near zero frequency because it is modified with forward speed correction as follows $b_{55} = \int_L b_{33}(x)x^2 dx + U^2/\omega_e^2 \cdot b_{33}$. Coupled heave and pitch damping coefficients predicted in three-dimensional theory are fairly in good accordance with measured data as shown in Figure 7.9 (b). Generally the agreement between three-dimensional methods is very good for vertical mode of motion.

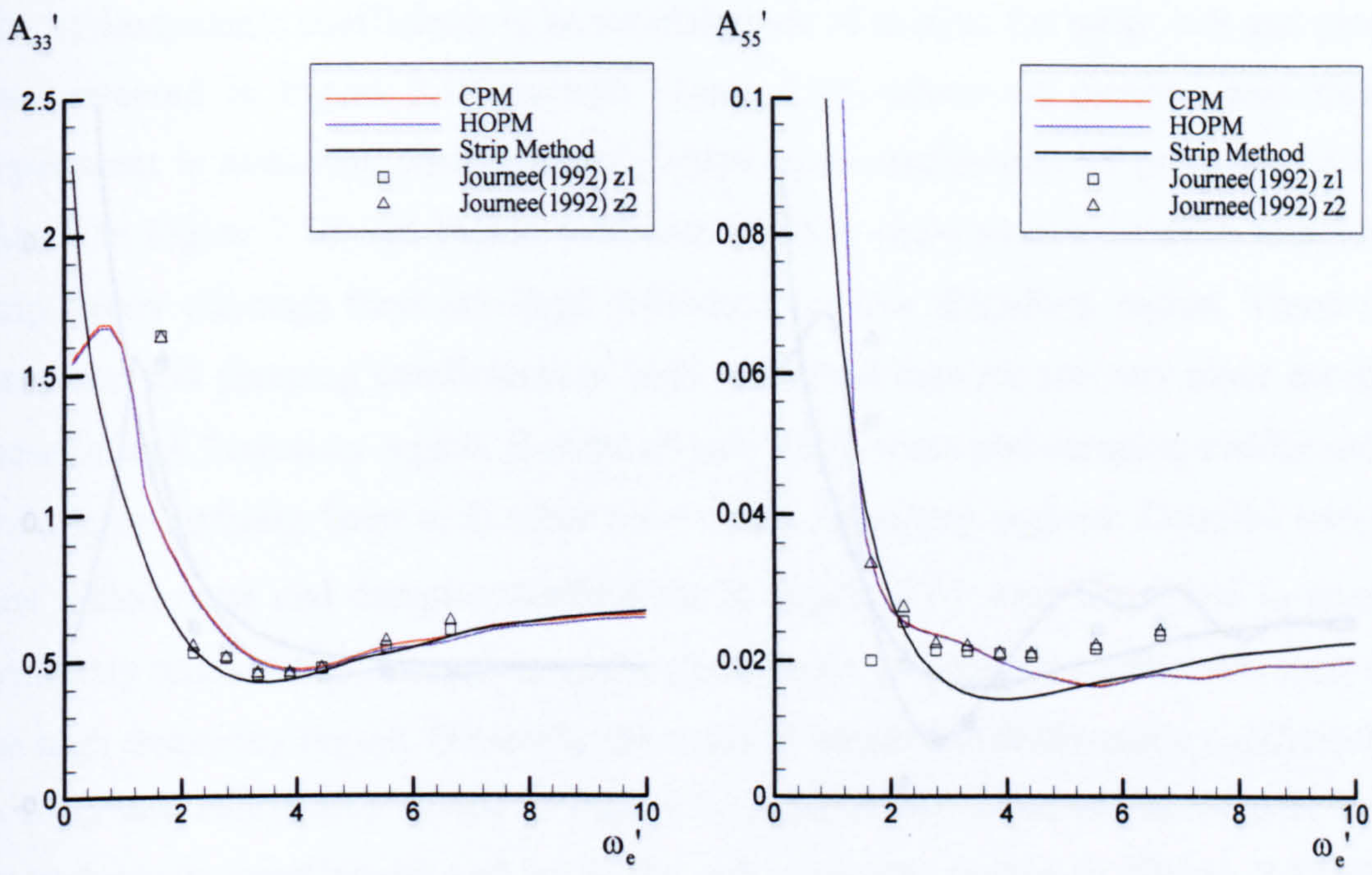

(a) Added mass

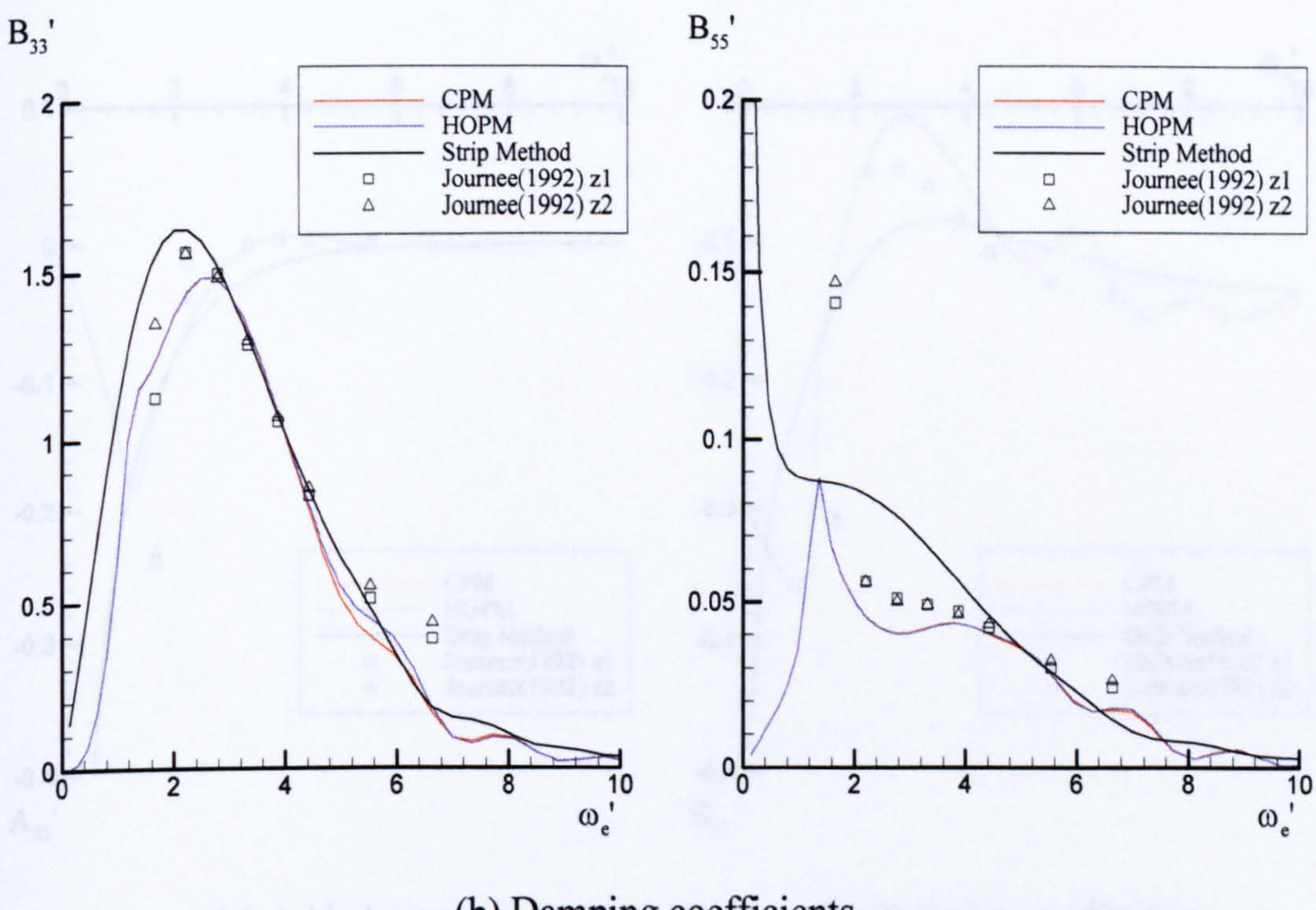

(b) Damping coefficients

Figure 7.8 Non-dimensional added mass and damping coefficients in heave and pitch modes for Wigley hull travelling at Froude number 0.2

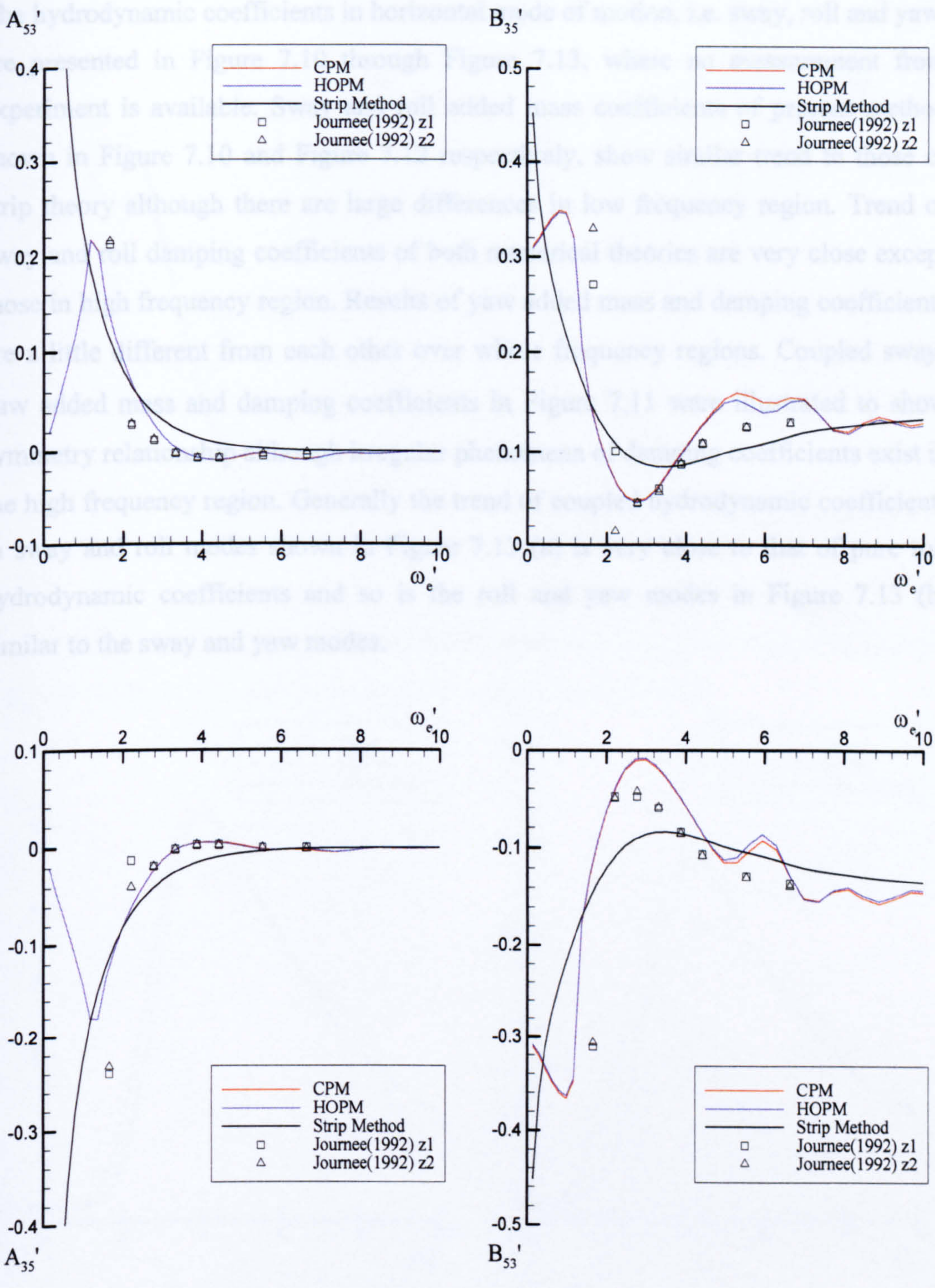

(a) Added mass (b) Damping coefficients

Figure 7.9 Non-dimensional coupled added mass and damping coefficients in heave and pitch modes for Wigley hull travelling at Froude number 0.2

The hydrodynamic coefficients in horizontal mode of motion, i.e. sway, roll and yaw, are presented in Figure 7.10 through Figure 7.13, where no measurement from experiment is available. Sway and roll added mass coefficients of present method shown in Figure 7.10 and Figure 7.12 respectively, show similar trend to those of strip theory although there are large differences in low frequency region. Trend of sway and roll damping coefficients of both numerical theories are very close except those in high frequency region. Results of yaw added mass and damping coefficients are a little different from each other over whole frequency regions. Coupled sway-yaw added mass and damping coefficients in Figure 7.11 were illustrated to show symmetry relationship although irregular phenomena of damping coefficients exist in the high frequency region. Generally the trend of coupled hydrodynamic coefficients in sway and roll modes shown in Figure 7.13 (a) is very close to that of pure roll hydrodynamic coefficients and so is the roll and yaw modes in Figure 7.13 (b) similar to the sway and yaw modes.

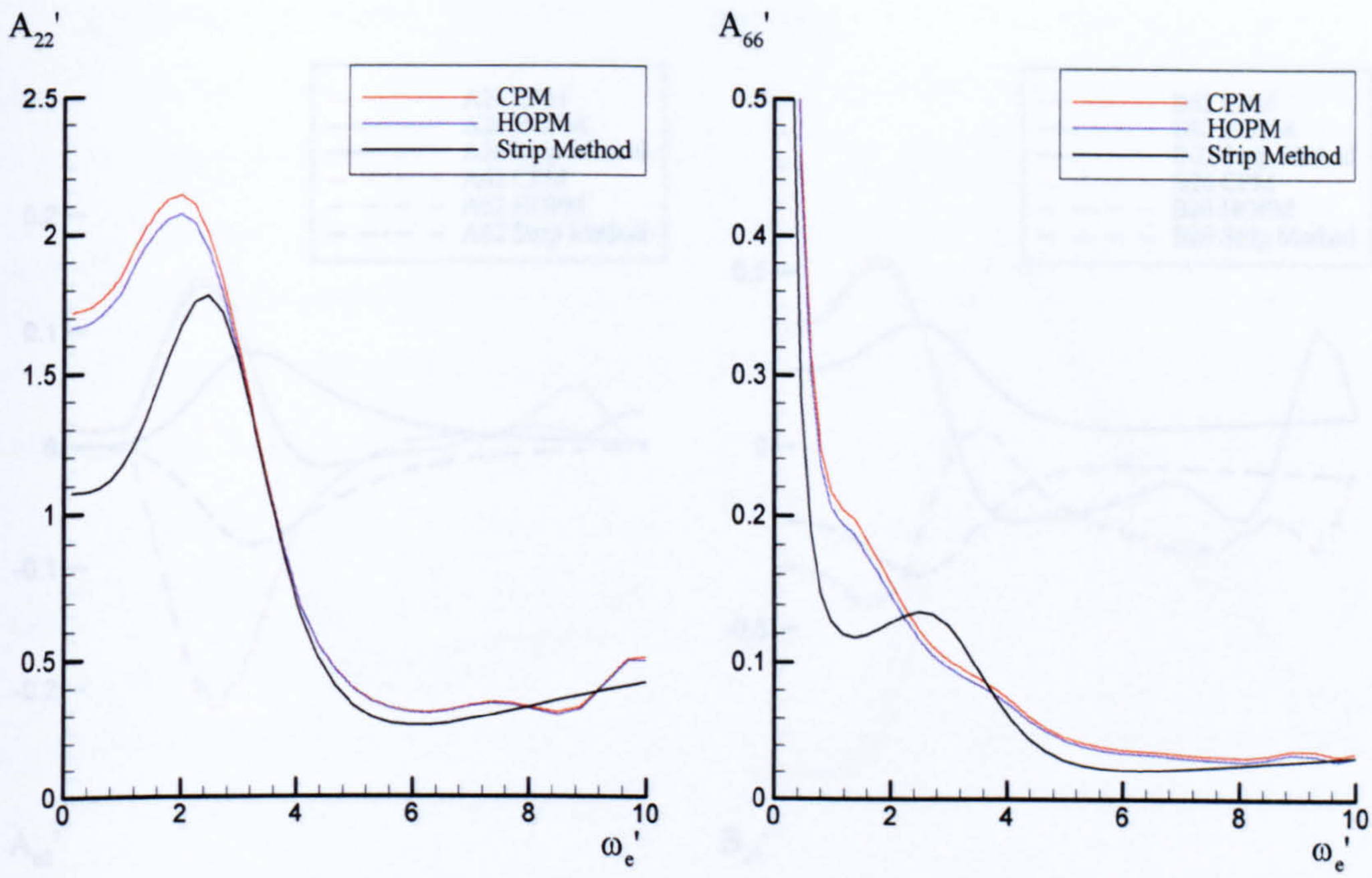

(a) Added mass

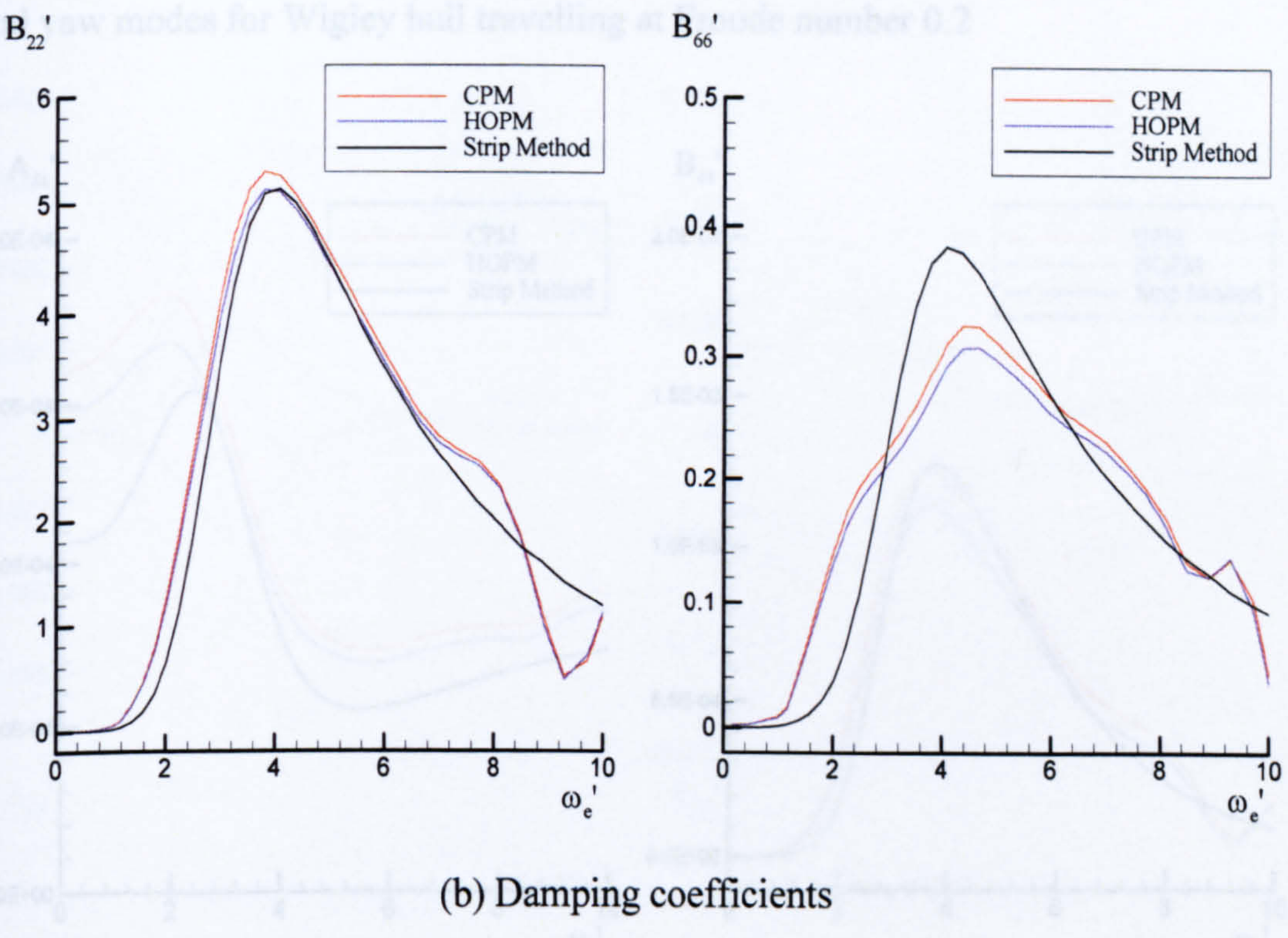

(b) Damping coefficients

Figure 7.10 Non-dimensional added mass and damping coefficients in sway and yaw modes for Wigley hull travelling at Froude number 0.2

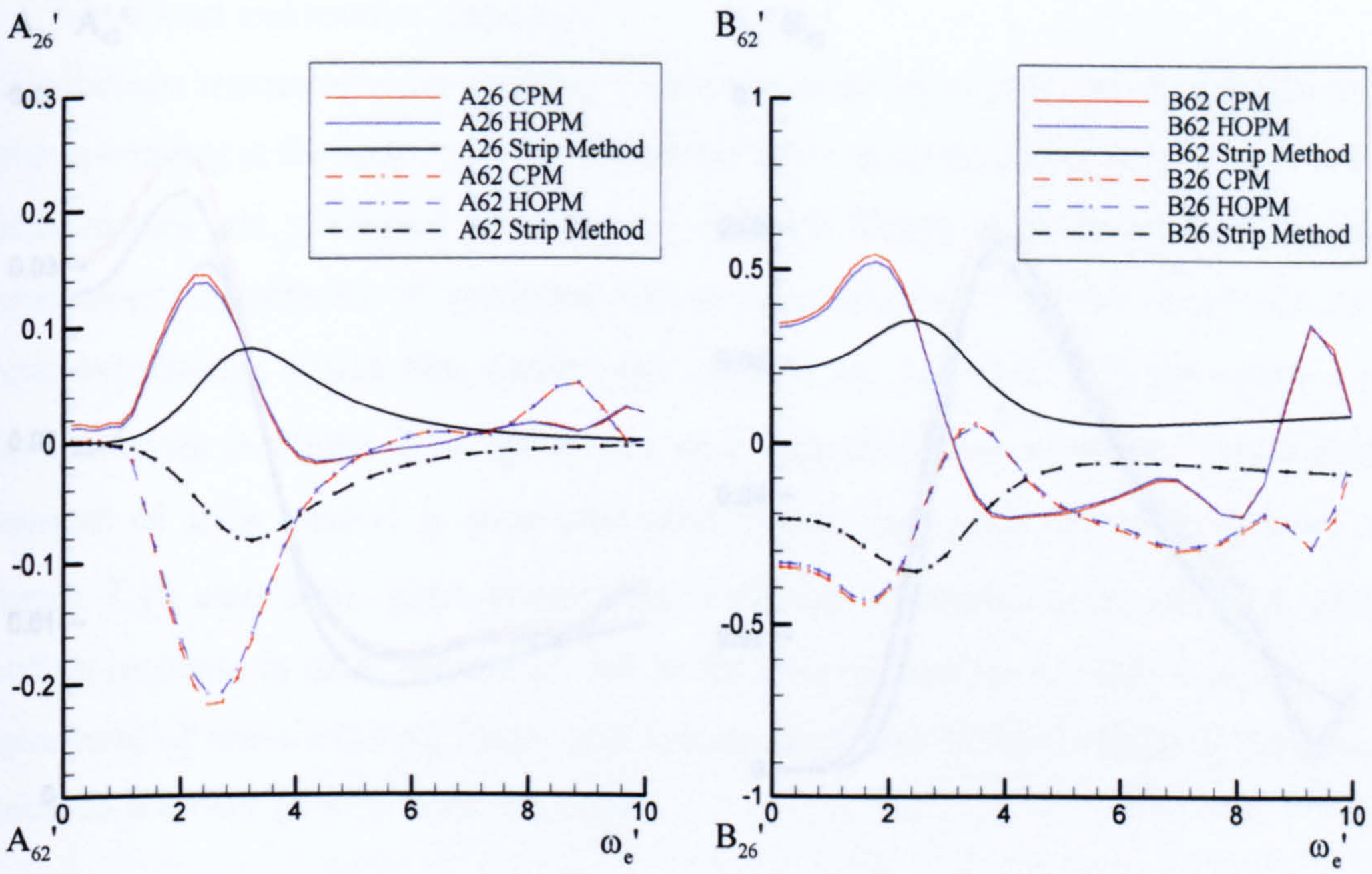

Figure 7.11 Non-dimensional coupled added mass and damping coefficients in sway and yaw modes for Wigley hull travelling at Froude number 0.2

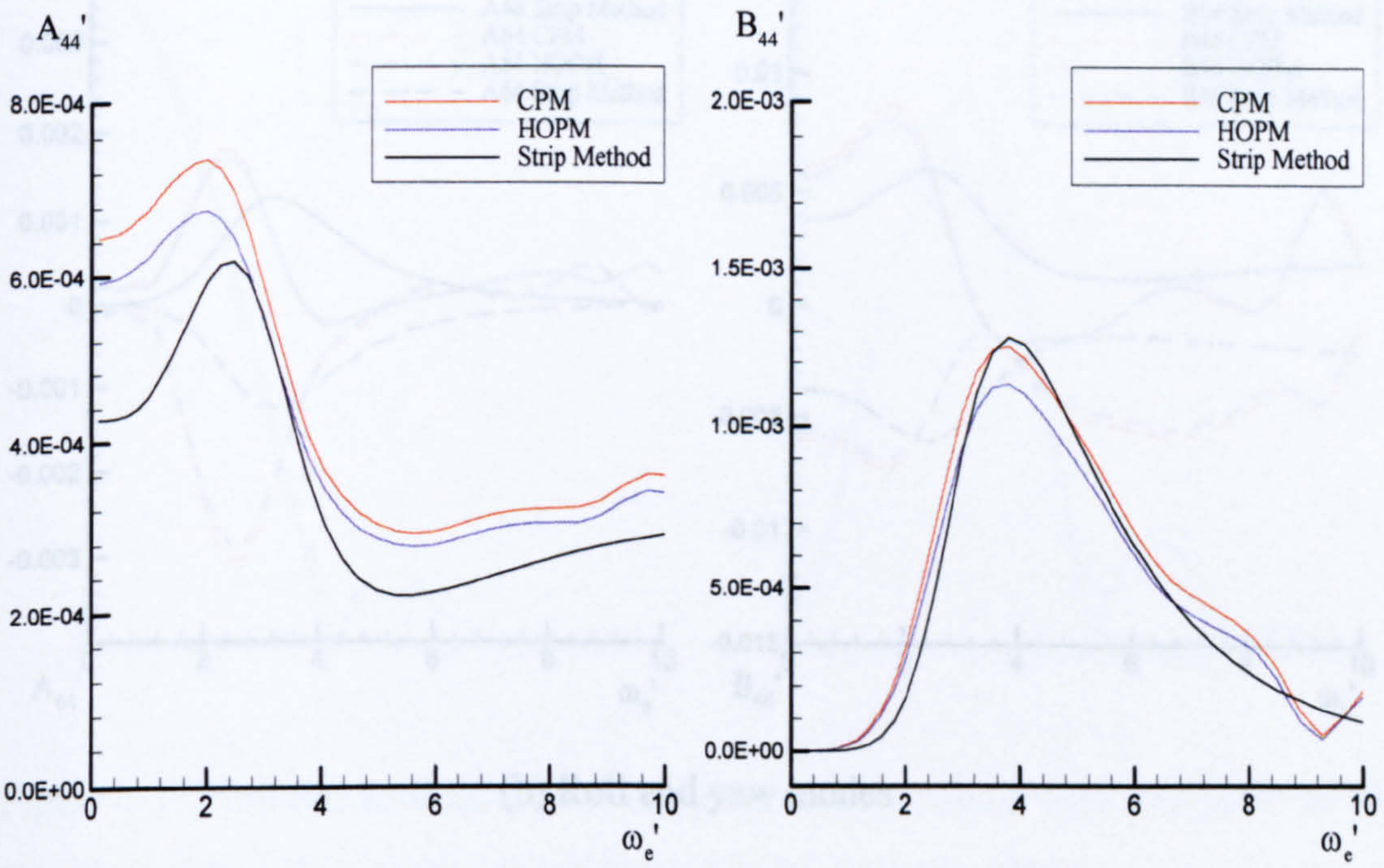

Figure 7.12 Non-dimensional added mass and damping coefficients in roll mode for Wigley hull travelling at Froude number 0.2

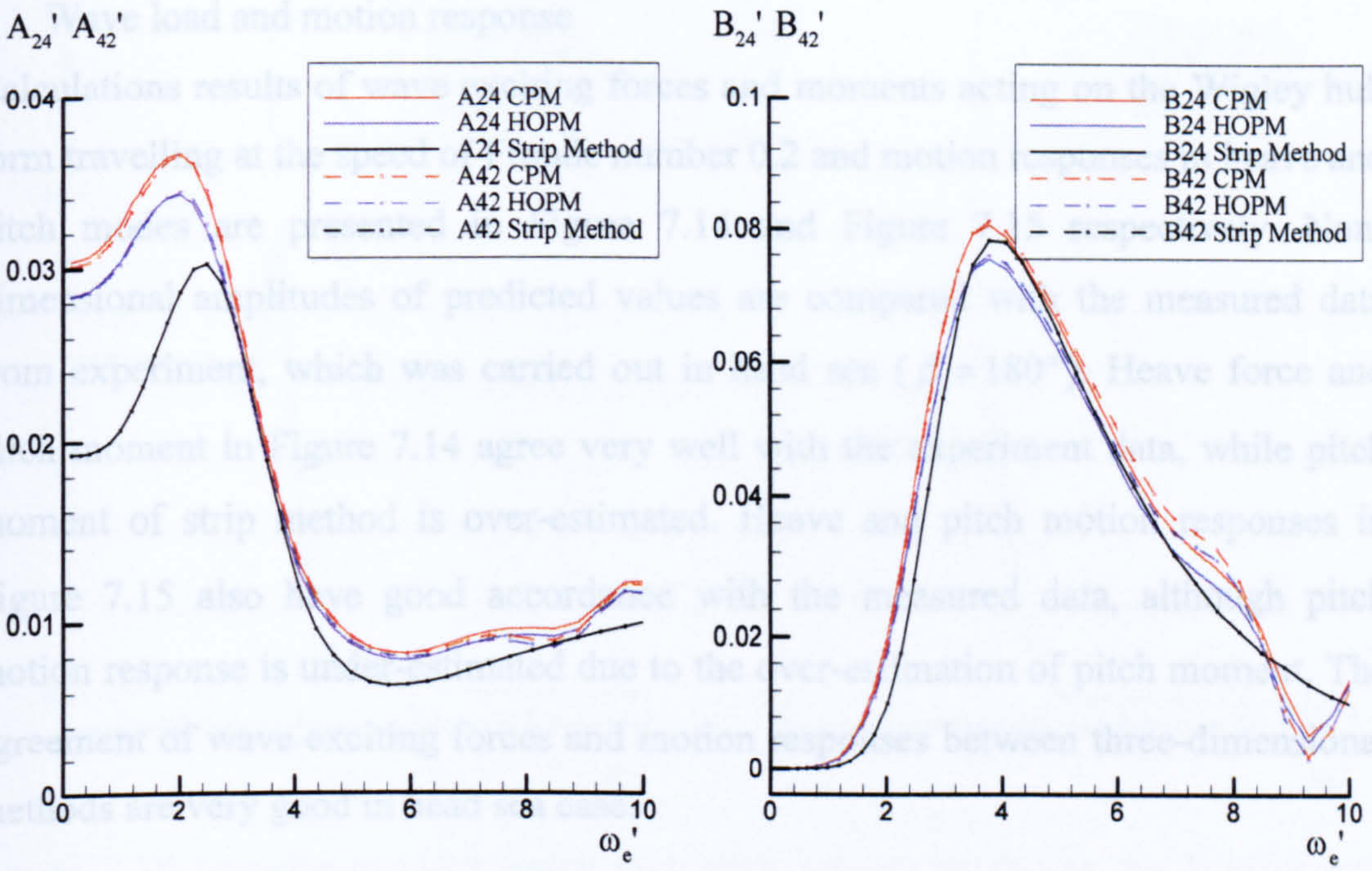

(a) Sway and roll modes

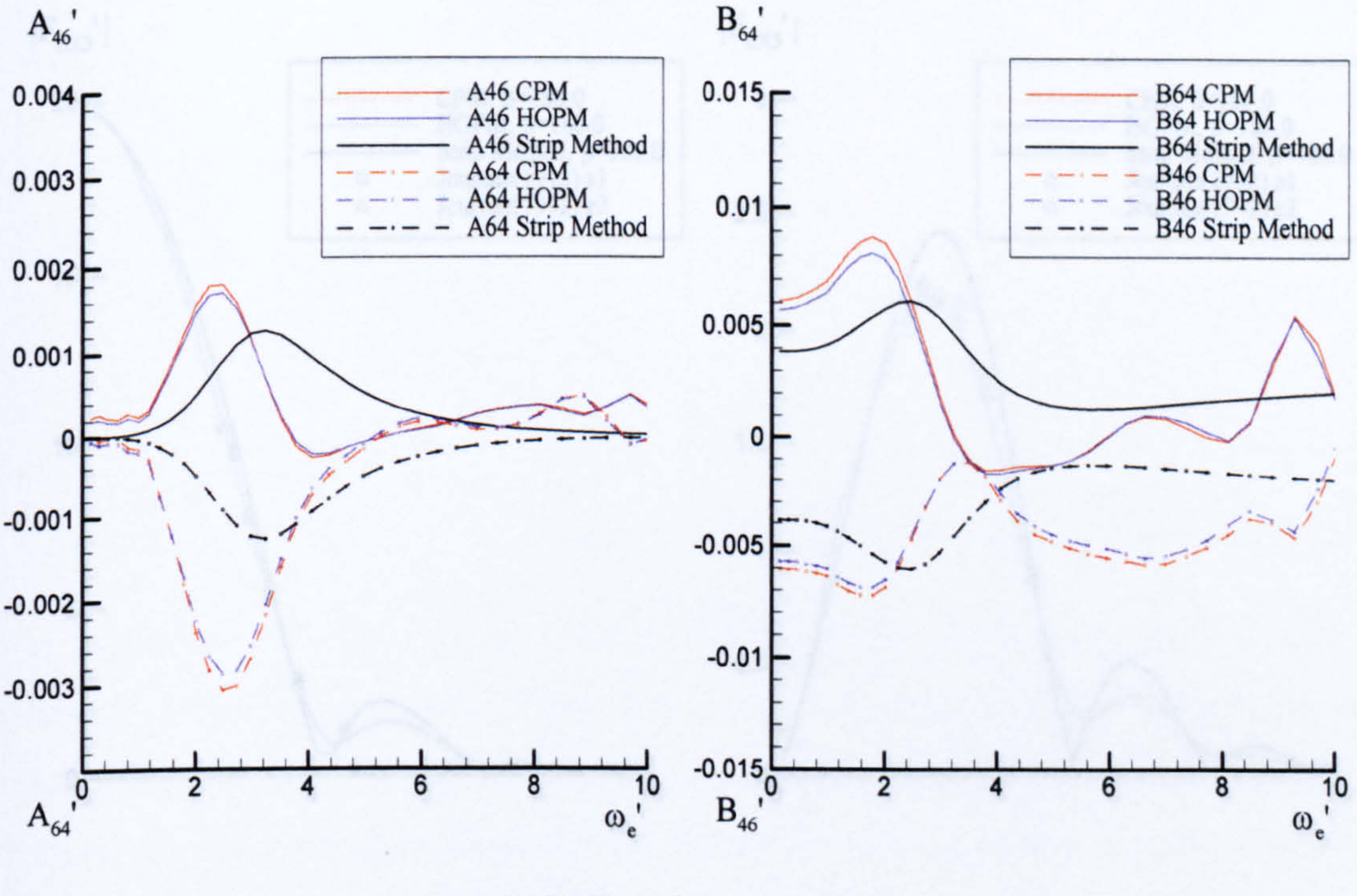

(b) Roll and yaw modes

Figure 7.13 Non-dimensional coupled added mass and damping coefficients in sway-roll and roll-yaw modes for Wigley hull travelling at Froude number 0.2

- Wave load and motion response

Calculations results of wave exciting forces and moments acting on the Wigley hull form travelling at the speed of Froude number 0.2 and motion responses in heave and pitch modes are presented in Figure 7.14 and Figure 7.15 respectively. Non-dimensional amplitudes of predicted values are compared with the measured data from experiment, which was carried out in head sea ($\beta = 180°$). Heave force and pitch moment in Figure 7.14 agree very well with the experiment data, while pitch moment of strip method is over-estimated. Heave and pitch motion responses in Figure 7.15 also have good accordance with the measured data, although pitch motion response is under-estimated due to the over-estimation of pitch moment. The agreement of wave exciting forces and motion responses between three-dimensional methods are very good in head sea case.

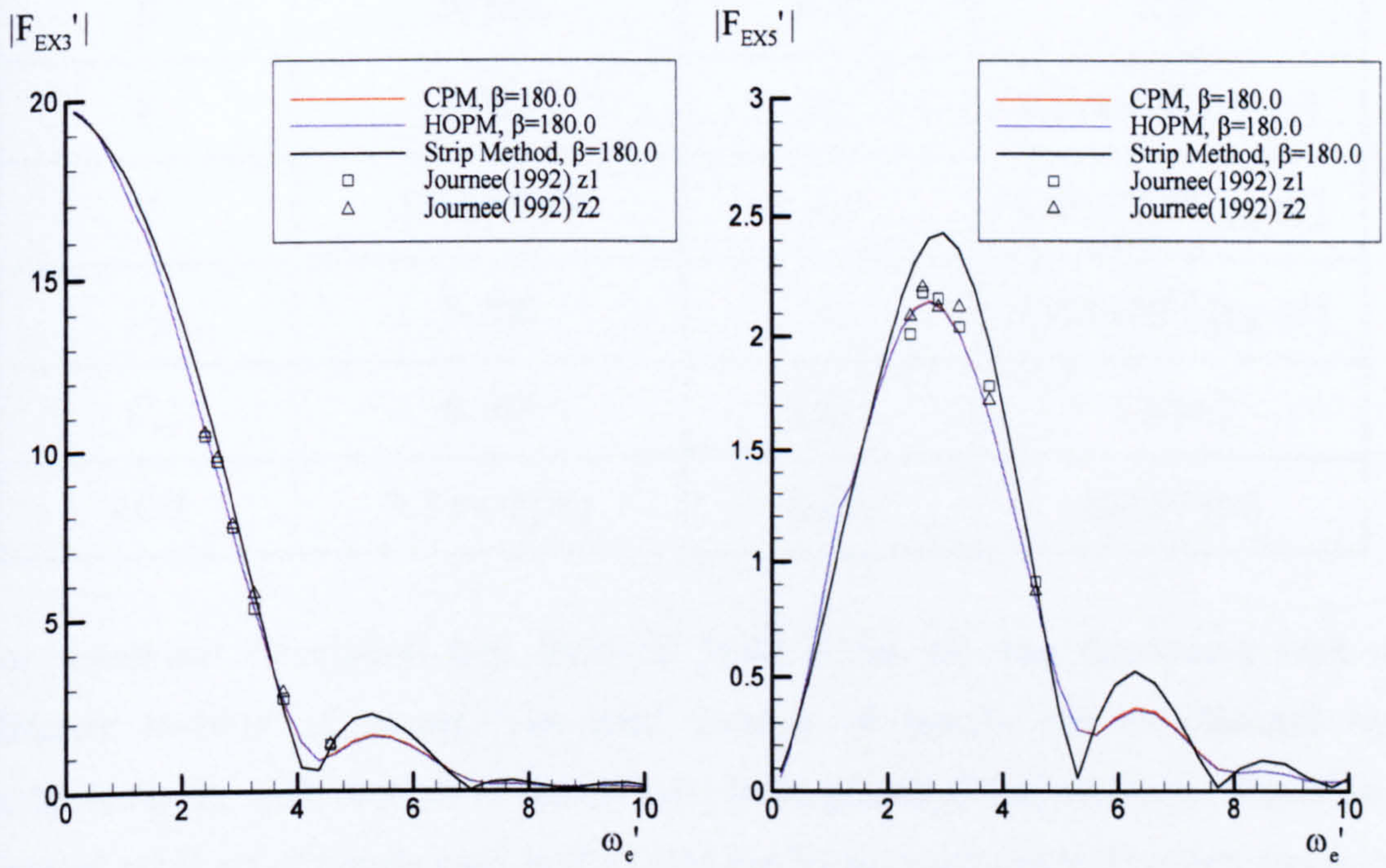

Figure 7.14 Non-dimensional heave and pitch wave exciting force and moment for Wigley hull travelling at Froude number 0.2 in head sea (β=180°)

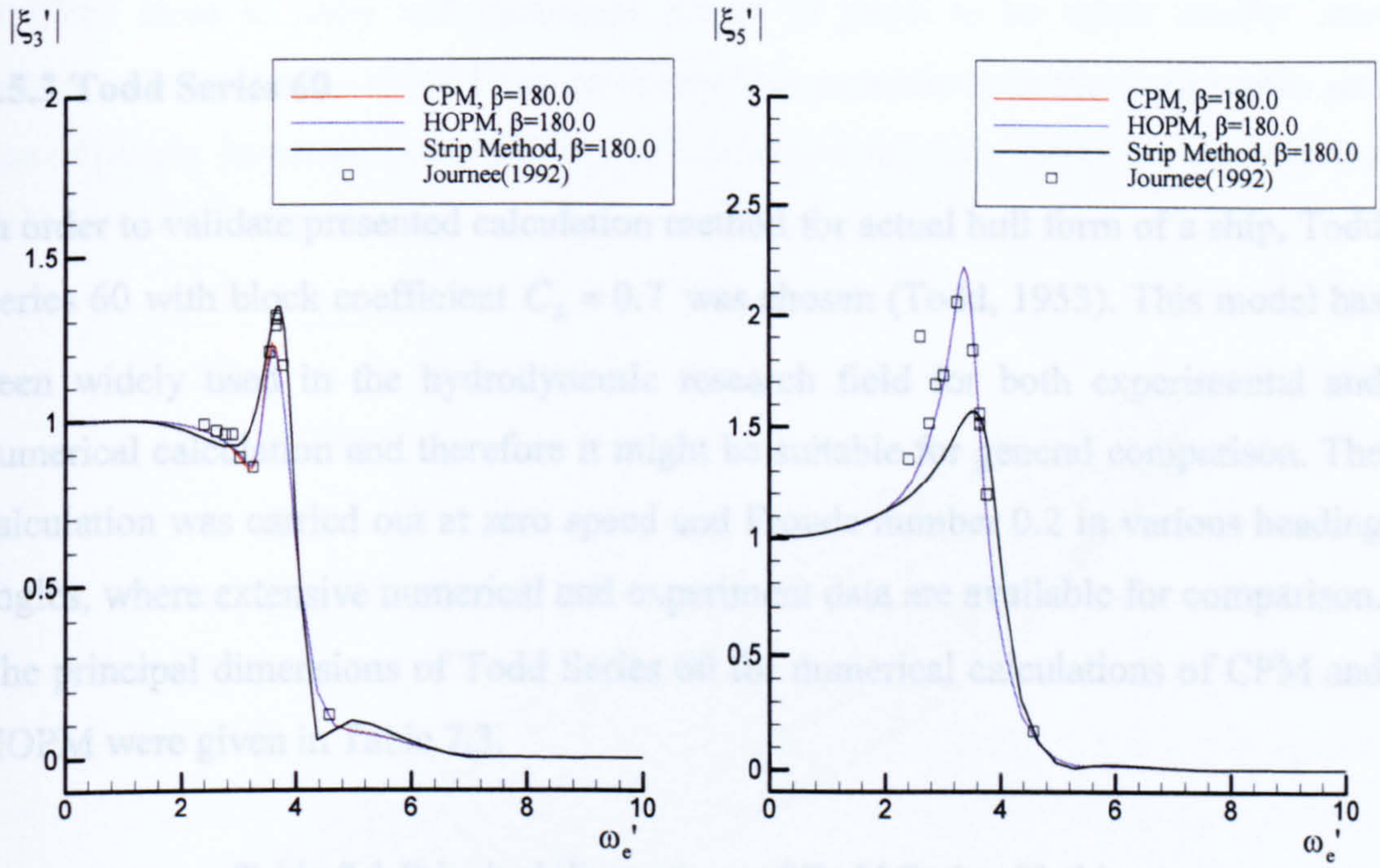

Figure 7.15 Non-dimensional heave and pitch motion responses for Wigley hull travelling at Froude number 0.2 in head sea (β=180°)

7.5.3 Todd Series 60

In order to validate presented calculation method for actual hull form of a ship, Todd Series 60 with block coefficient $C_B = 0.7$ was chosen (Todd, 1953). This model has been widely used in the hydrodynamic research field for both experimental and numerical calculation and therefore it might be suitable for general comparison. The calculation was carried out at zero speed and Froude number 0.2 in various heading angles, where extensive numerical and experiment data are available for comparison. The principal dimensions of Todd Series 60 for numerical calculations of CPM and HOPM were given in Table 7.3.

Table 7.3 Principal dimensions of Todd Series 60 ship

L	140 [m]	L/B	7.0
B	20 [m]	B/T	2.5
T	8 [m]	I_{xx}	6.178×10^{8} [kg·m²]
∇	15680 [m³]	I_{yy}	1.969×10^{10} [kg·m²]
C_B	0.700	I_{zz}	1.969×10^{10} [kg·m²]
C_w	0.785	$\overline{GM}_T$	1.0 [m]
LCB	0.7 Fwd [m]	$\overline{GM}_L$	150.27 [m]

For numerical calculation hull form of Todd Series 60 was discretised with a different number of panels. The total number of panels can be obtained by multiplying the each number of panels used in longitudinal and transverse direction. Typical numbers of panels used in the CPM are 39 in longitudinal direction and 6 in each half-section, so total 468 quadrilateral panels were used as shown in Figure 7.16. For the calculation of HOPM, 20 sections in longitudinal direction and 8 segments in each half-section and therefore total 320 panels are used as presented in Table 7.4. During the discretisation of hull surface, it is recommended to keep the aspect ratio

of CPM close to unity and maximum length of panel to be much smaller than minimum wavelength. HOPM has relatively less restrictions in the aspect ratio and size of panels, however, computational efficiency can be poor due to the complicated influence coefficient matrix.

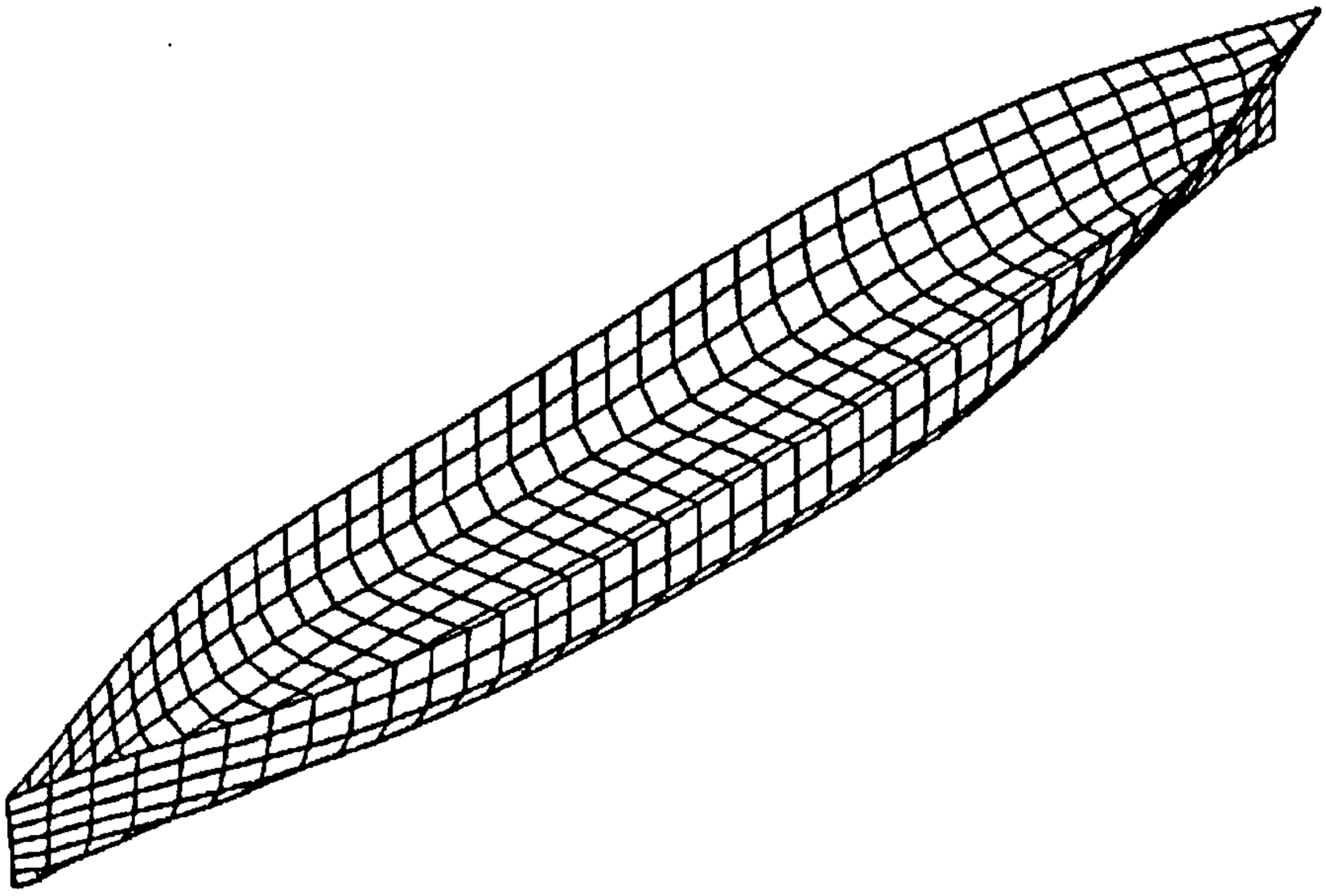

(a) Series 60 : 480 panels for CPM

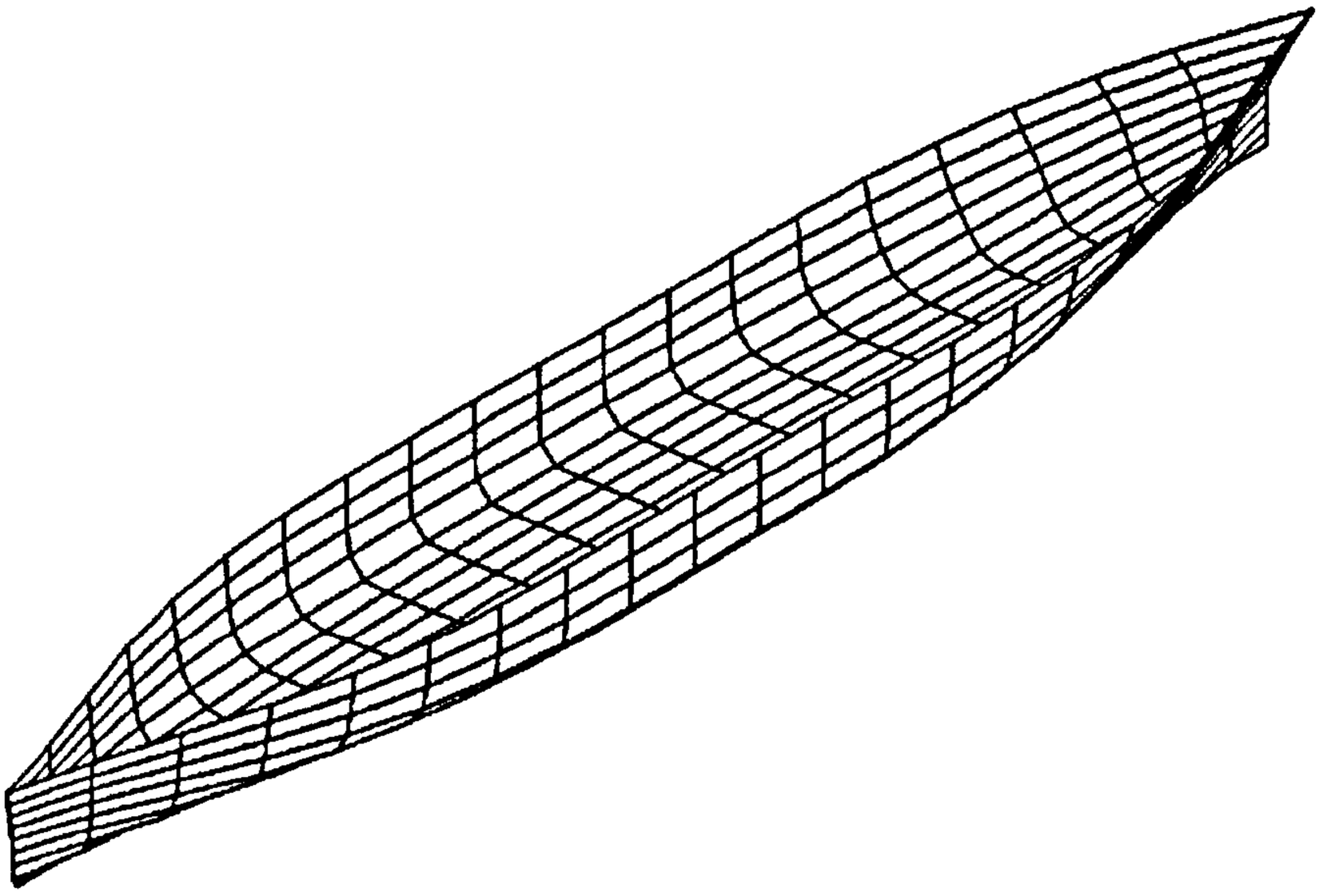

(b) Series 60 : 320 panels for HOPM

Figure 7.16 Panel representation of Todd Series 60 hull form

Table 7.4 Comparison of discretised model of Todd Series 60 ship

Method	Nx	Ny	Total	Aspect ratio
CPM	40	6	480	1.2
HOPM	20	8	320	3.3

For comparison with other theoretical results, both two-dimensional strip method and three-dimensional Green function approach were chosen. Jasionowski (2001) developed PROTEUS based on strip theory, which uses Rankine source distribution method. Inglis & Price (1982a, 1982b) carried out several theoretical calculations, which range from two-dimensional strip theory to a three-dimensional method including the influence of steady motion effects in the boundary value problem as well as simplified three-dimensional method. Every theoretical approach mentioned is based on linear potential theory in frequency domain.

Comprehensive experiment for Todd Series 60 with block coefficient $C_B = 0.7$ was performed by many researches. Gerritsma and Beukelman (1964, 1966) carried out experiment on heave and pitch hydrodynamic data and van Leeuwen (1964) performed extensive measurement on the lateral added mass and damping coefficients. Vugts (1971) performed experiment involving both vertical and horizontal motion of a model. All experimental data presented in this study are non-dimensionalised in aforementioned forms for comparison with other numerical results.

7.5.3.1 Zero speed case

- Zero speed hydrodynamic coefficient

The hydrodynamic added mass and damping coefficients for Todd Series 60 at zero speed are presented in Figure 7.17 through Figure 7.21. These hydrodynamic coefficients are calculated from various numerical method adopted in this study (i.e. CPM and HOPM) and compared with those from traditional two-dimensional strip theory and experiments.

Added mass and damping coefficients in heave and pitch modes show good agreements with the experimental data as can be seen from Figure 7.17. The predicted yaw added mass coefficient show fairly good agreement with the measured data and there is only a little discrepancy as shown in Figure 7.18. The sway damping coefficients agrees fairly well in low frequency region and shows same pattern of variation with the experimental data. The agreement between calculated and measured roll damping coefficient are worse as shown in Figure 7.19. Poor prediction of roll damping coefficient is already expected due to the non-linear effects in roll motion and negligence of viscosity when developing potential theory. For the calculation results of CPM and HOPM there are also little differences in the values over the whole frequency range except that the predicted values show little discrepancies in the high frequency region.

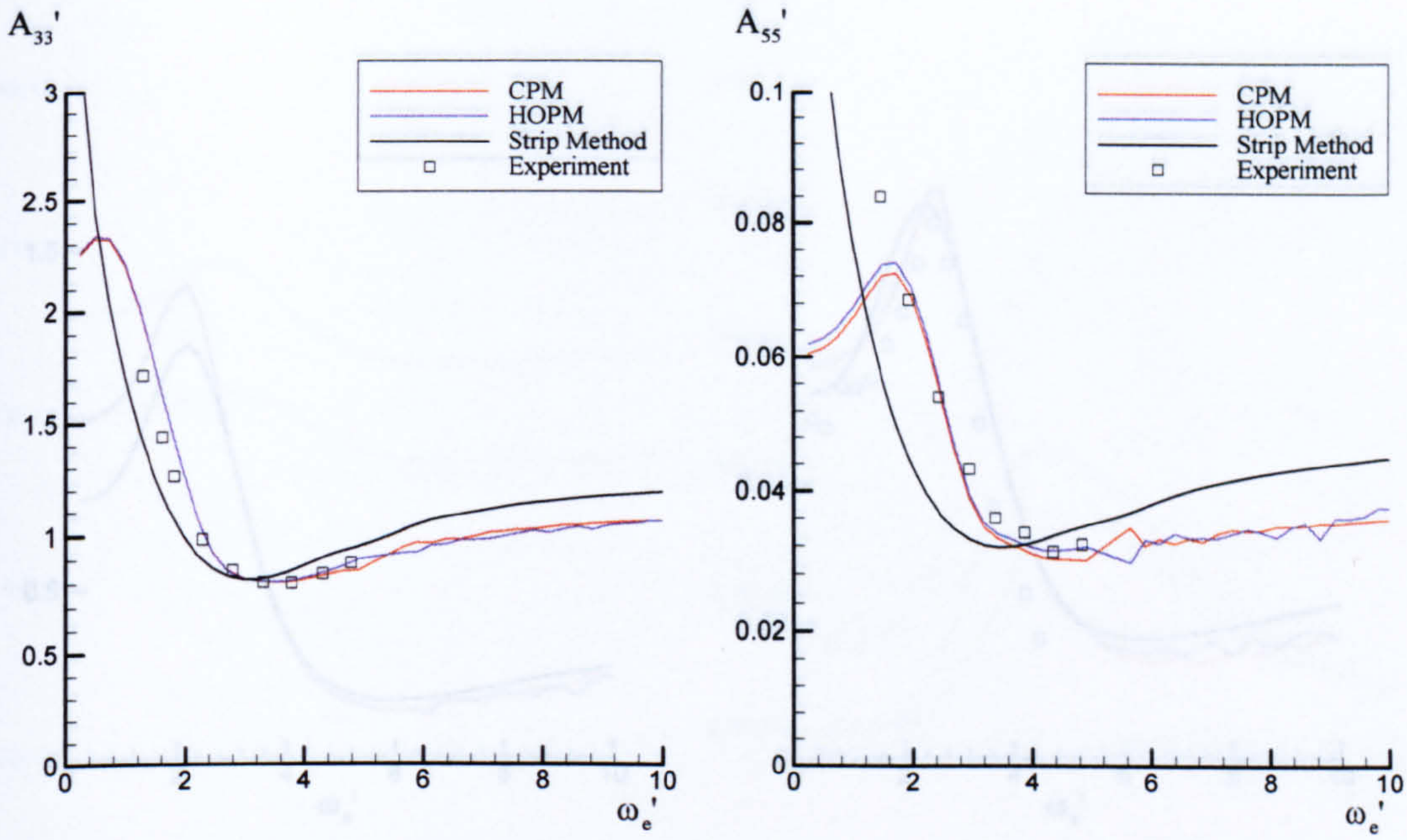

(a) Added mass

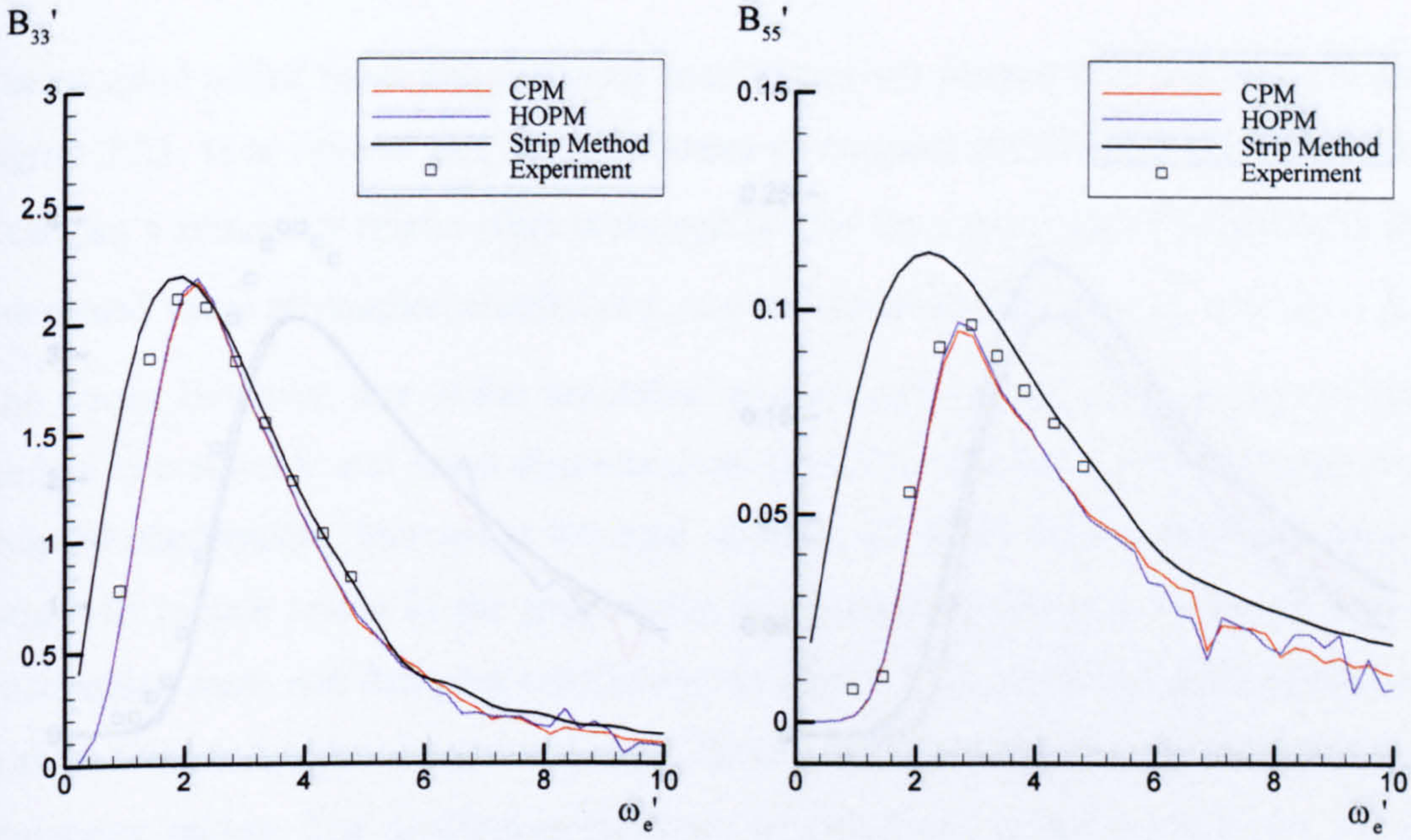

(b) Damping coefficients

Figure 7.17 Non-dimensional added mass and damping coefficients in heave and pitch modes for Todd Series 60 at zero speed

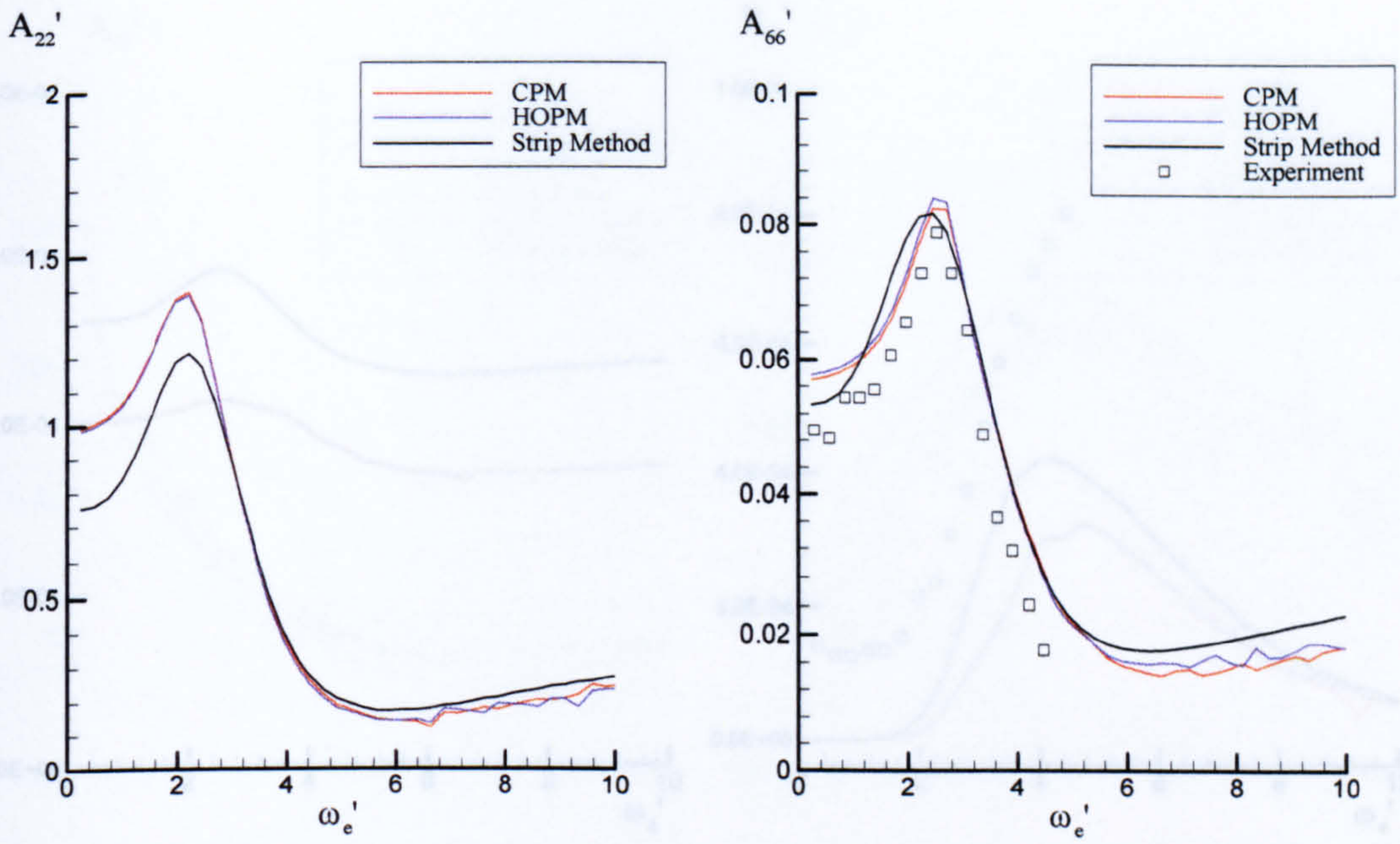

(a) Added mass

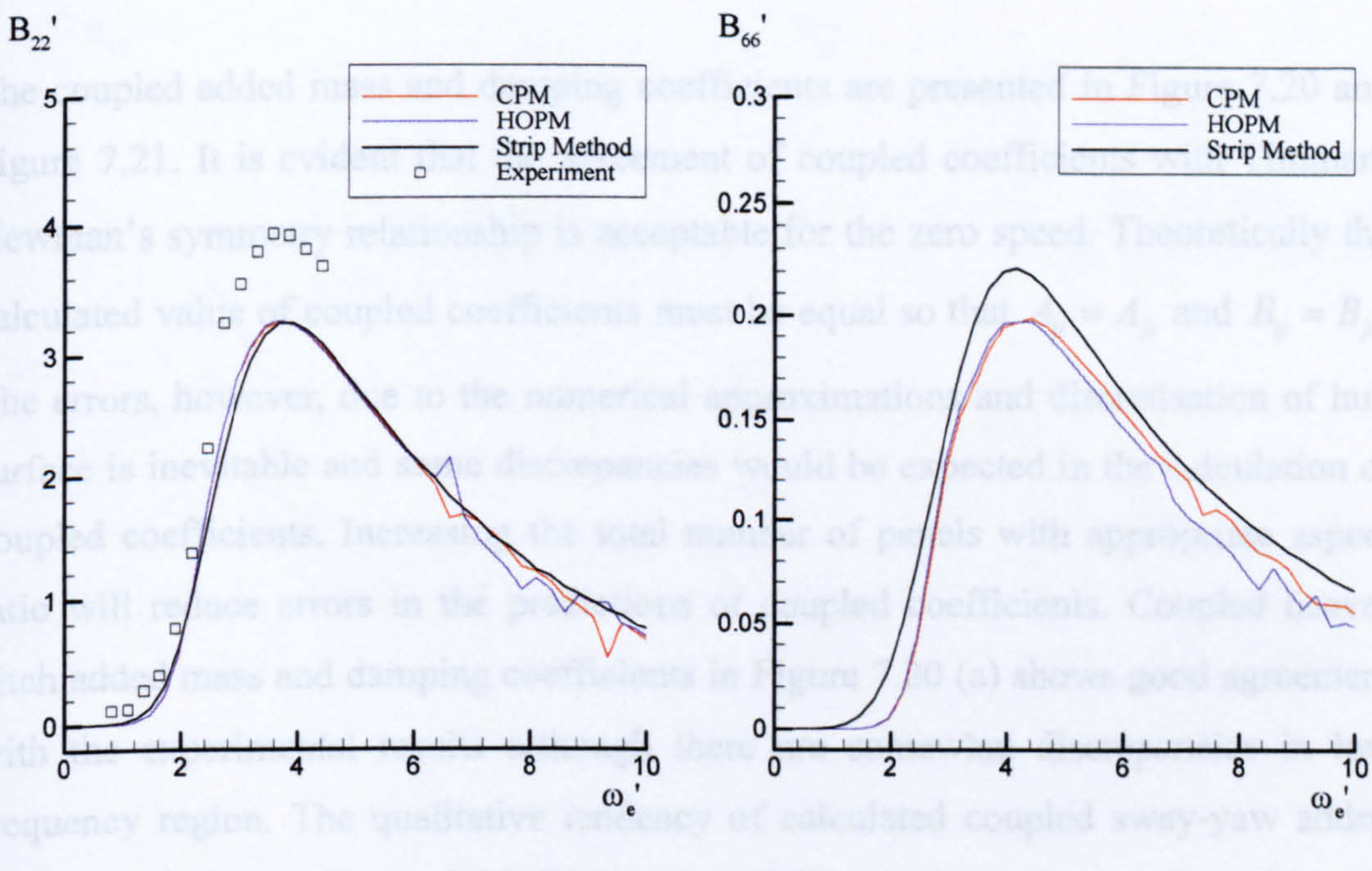

(b) Damping coefficients

Figure 7.18 Non-dimensional added mass and damping coefficients in sway and yaw modes for Todd Series 60 at zero speed

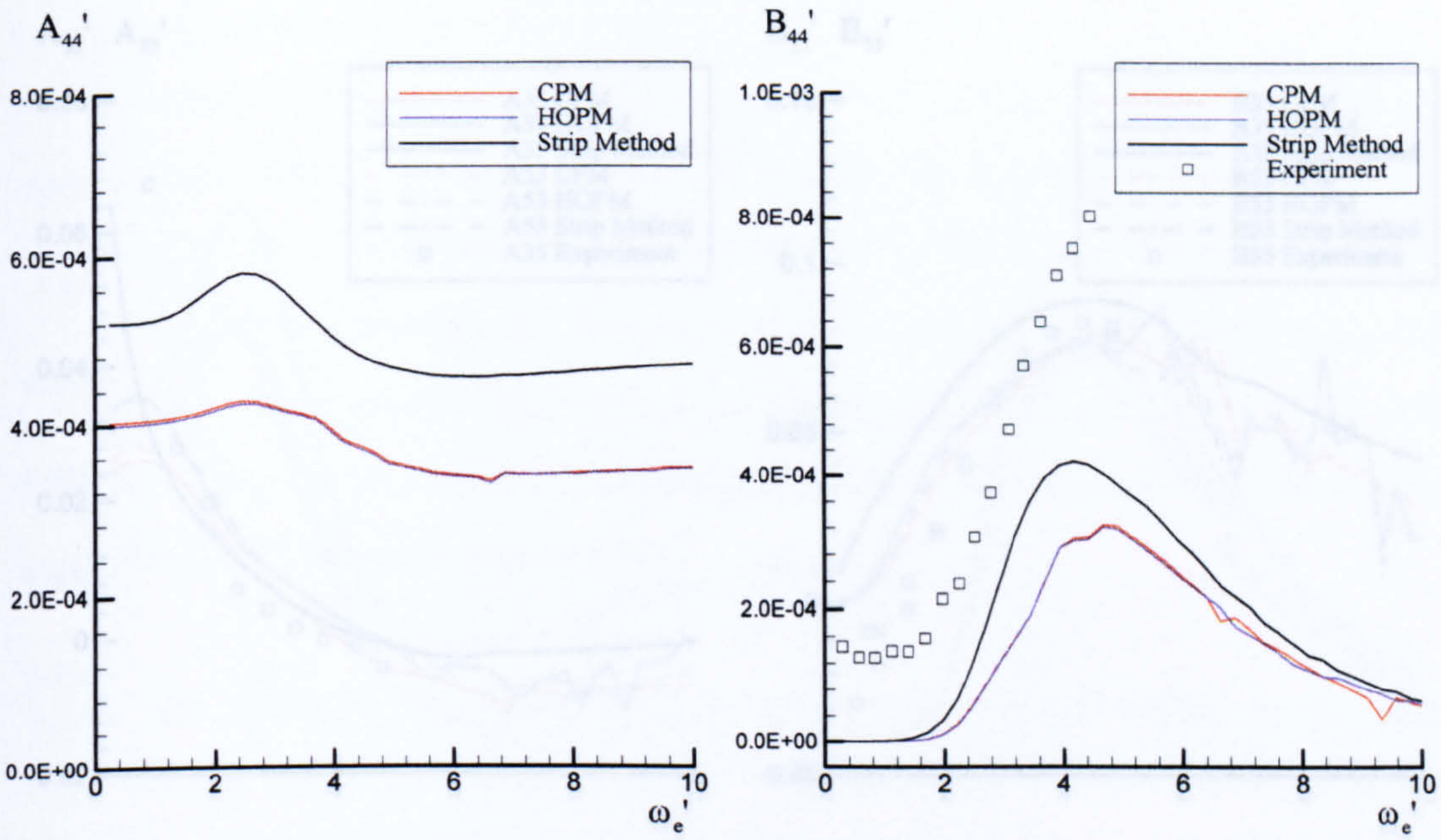

Figure 7.19 Non-dimensional added mass and damping coefficients in roll mode for Todd Series 60 at zero speed

The coupled added mass and damping coefficients are presented in Figure 7.20 and Figure 7.21. It is evident that the agreement of coupled coefficients with Timman-Newman's symmetry relationship is acceptable for the zero speed. Theoretically the calculated value of coupled coefficients must be equal so that $A_{ij} = A_{ji}$ and $B_{ij} = B_{ji}$. The errors, however, due to the numerical approximations and discretisation of hull surface is inevitable and some discrepancies would be expected in the calculation of coupled coefficients. Increasing the total number of panels with appropriate aspect ratio will reduce errors in the predictions of coupled coefficients. Coupled heave-pitch added mass and damping coefficients in Figure 7.20 (a) shows good agreement with the experimental results although there are somewhat discrepancies in low frequency region. The qualitative tendency of calculated coupled sway-yaw added mass coefficient in Figure 7.20 (b) is very similar to the measured data although differences of values are observed between CPM and HOPM. There are no experimental data available for roll-dependent hydrodynamic coefficients and general agreement between different numerical theories seems to be good as shown in Figure 7.21.

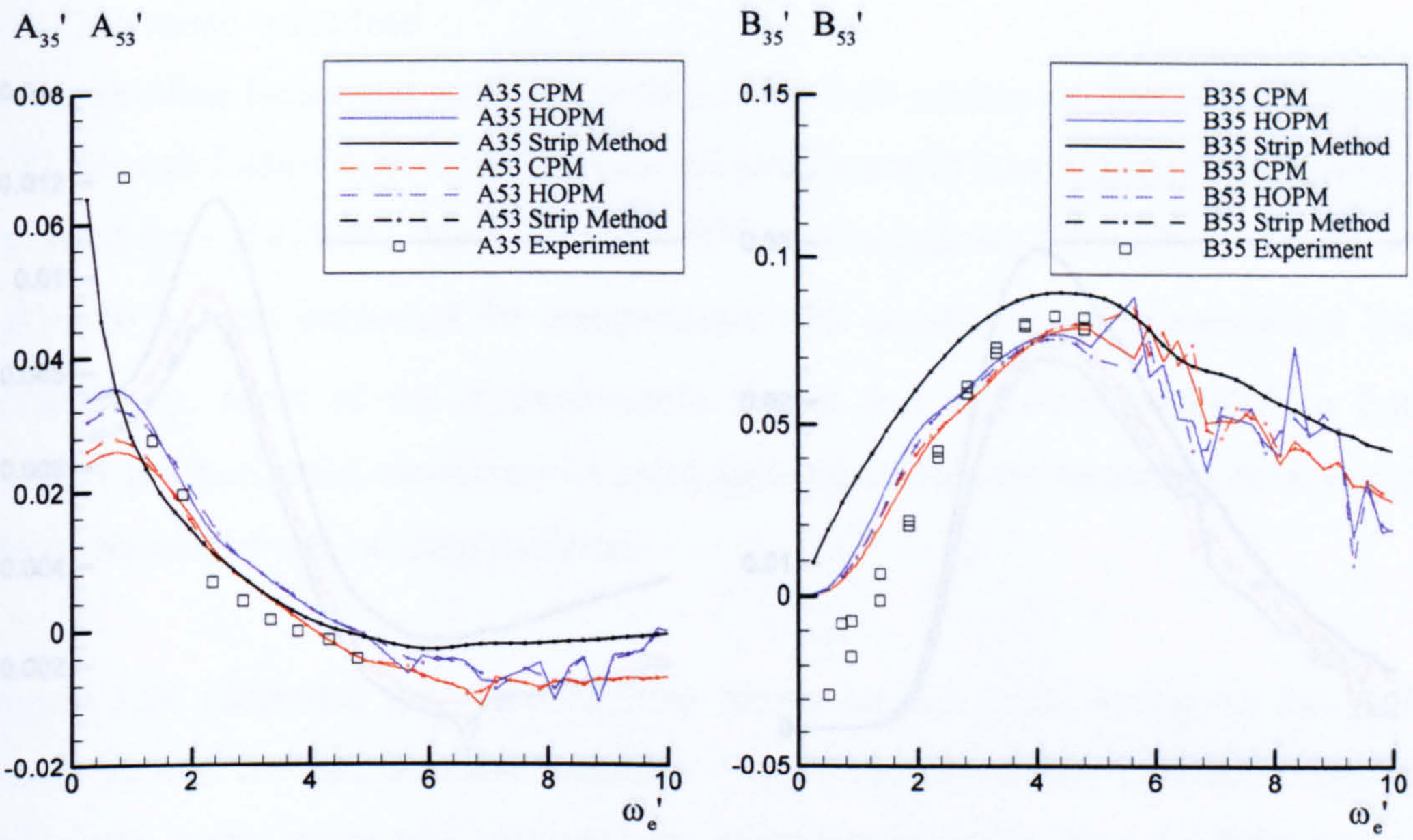

(a) Horizontal mode

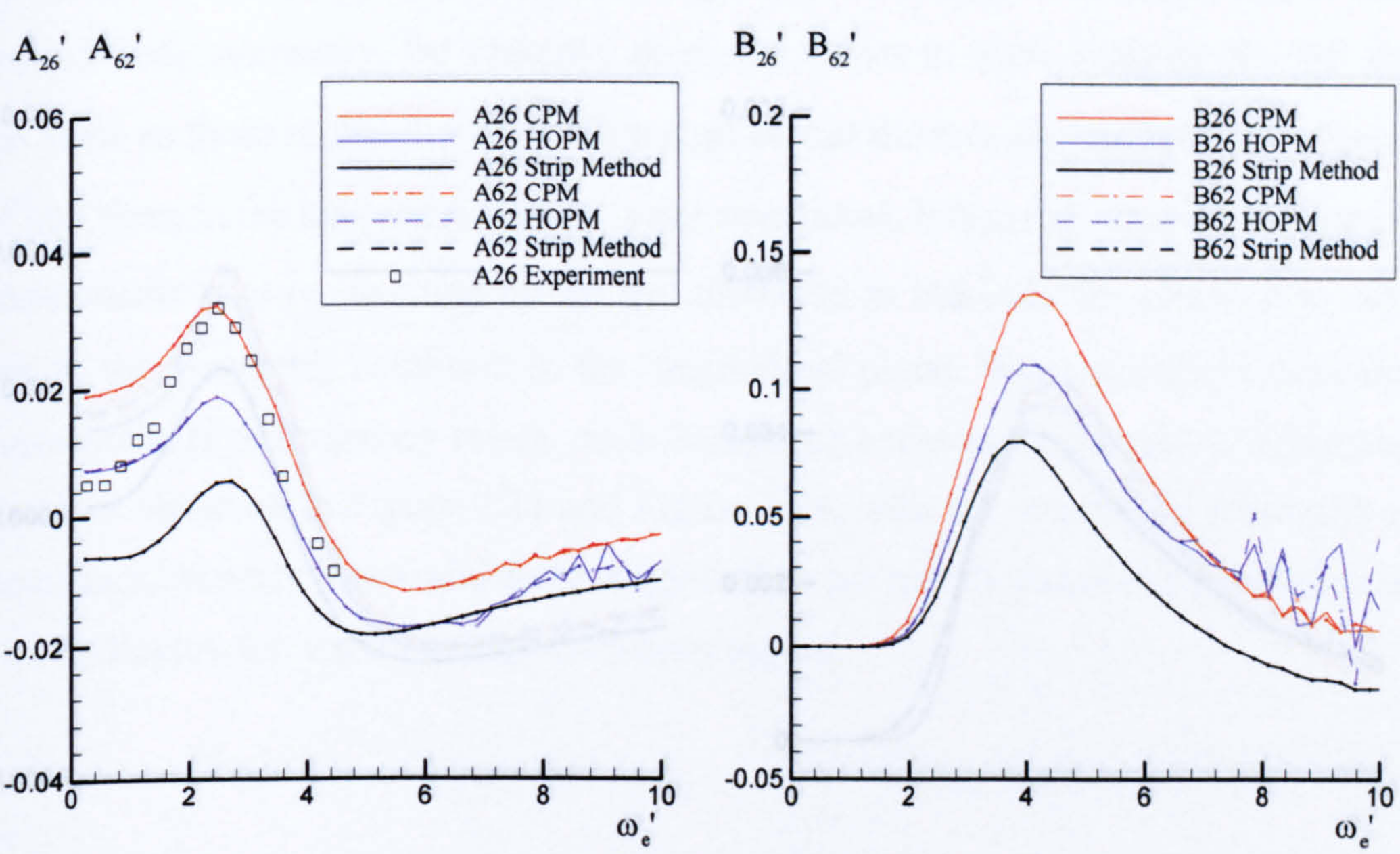

(b) Vertical mode

Figure 7.20 Non-dimensional coupled added mass and damping coefficients in heave-pitch and sway-yaw modes for Todd Series 60 at zero speed

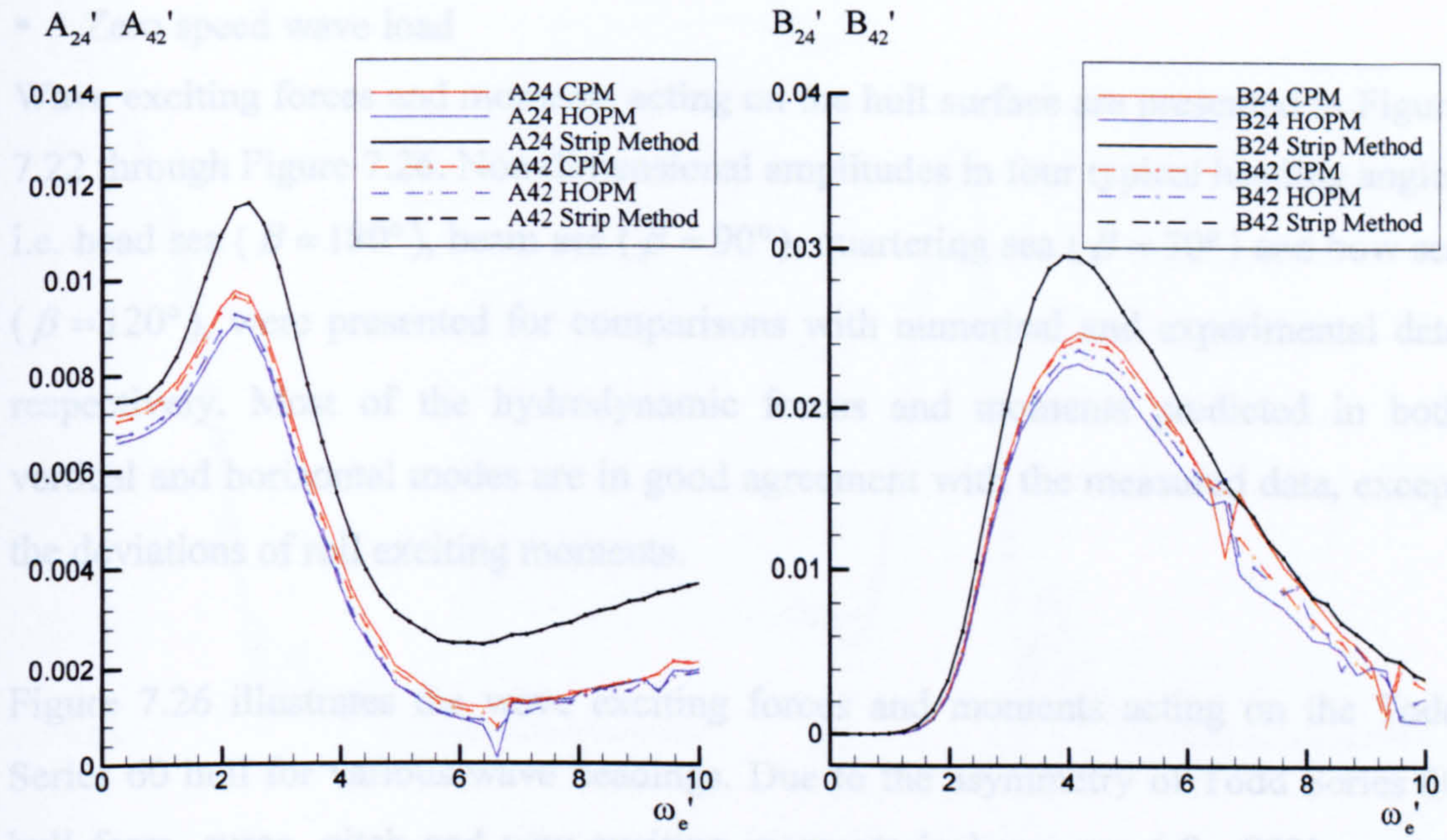

(a) Sway and roll modes

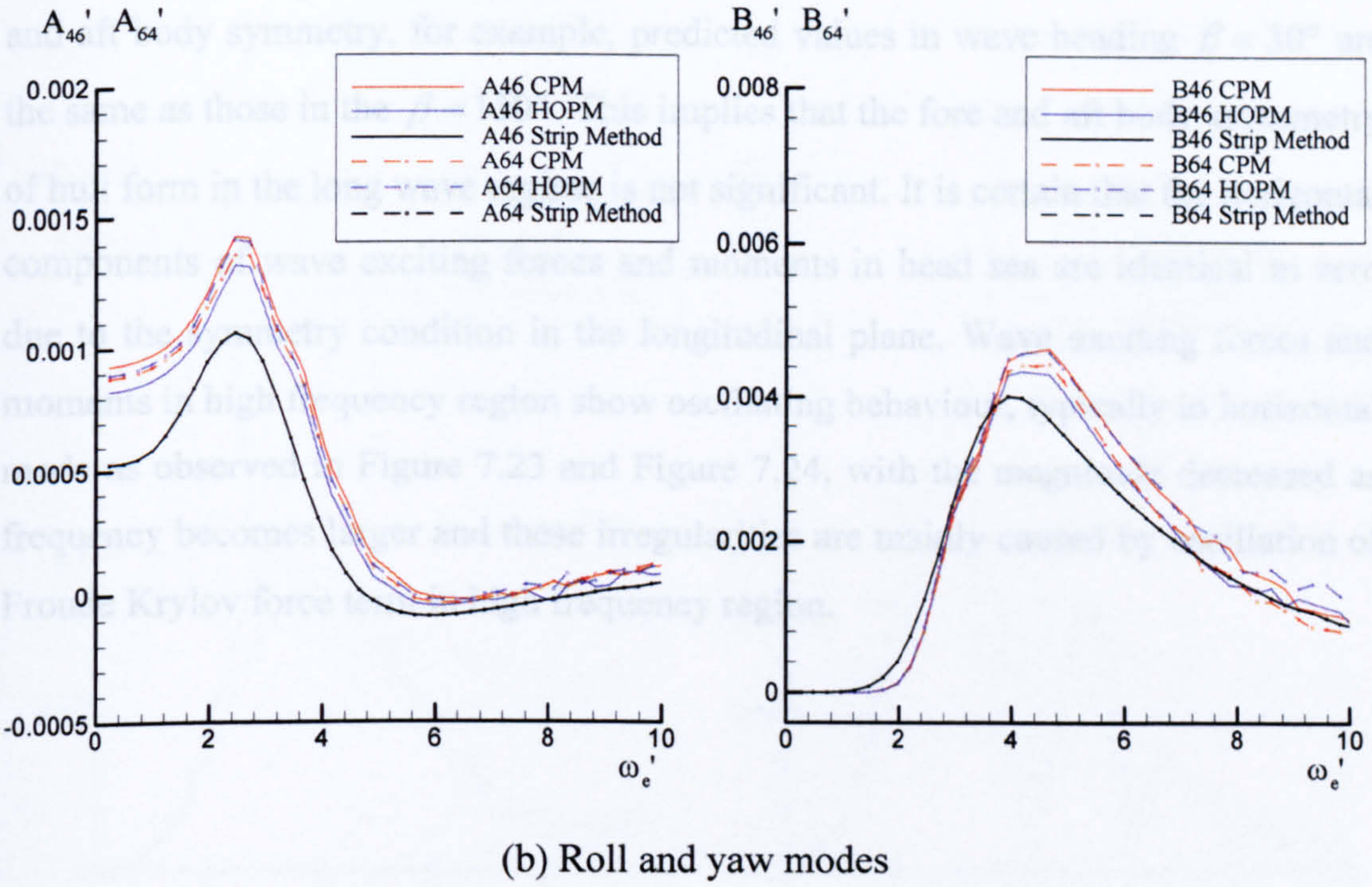

(b) Roll and yaw modes

Figure 7.21 Non-dimensional coupled added mass and damping coefficients in sway-roll and roll-yaw modes for Todd Series 60 at zero speed

- Zero speed wave load

Wave exciting forces and moments acting on the hull surface are presented in Figure 7.22 through Figure 7.26. Non-dimensional amplitudes in four typical heading angles, i.e. head sea ($\beta = 180°$), beam sea ($\beta = 90°$), quartering sea ($\beta = 30°$) and bow sea ($\beta = 120°$), were presented for comparisons with numerical and experimental data respectively. Most of the hydrodynamic forces and moments predicted in both vertical and horizontal modes are in good agreement with the measured data, except the deviations of roll exciting moments.

Figure 7.26 illustrates the wave exciting forces and moments acting on the Todd Series 60 hull for various wave headings. Due to the asymmetry of Todd Series 60 hull form, surge, pitch and yaw exciting moments in beam sea ($\beta = 90°$) are not equal to zero and smaller than other components. All the amplitudes of wave exciting forces and moments in a low frequency region, however, show the properties of fore and aft body symmetry, for example, predicted values in wave heading $\beta = 30°$ are the same as those in the $\beta = 150°$. This implies that the fore and aft body asymmetry of hull form in the long wave regime is not significant. It is certain that the horizontal components of wave exciting forces and moments in head sea are identical to zero due to the symmetry condition in the longitudinal plane. Wave exciting forces and moments in high frequency region show oscillating behaviour, typically in horizontal mode as observed in Figure 7.23 and Figure 7.24, with the magnitude decreased as frequency becomes larger and these irregularities are mainly caused by oscillation of Froude Krylov force term in high frequency region.

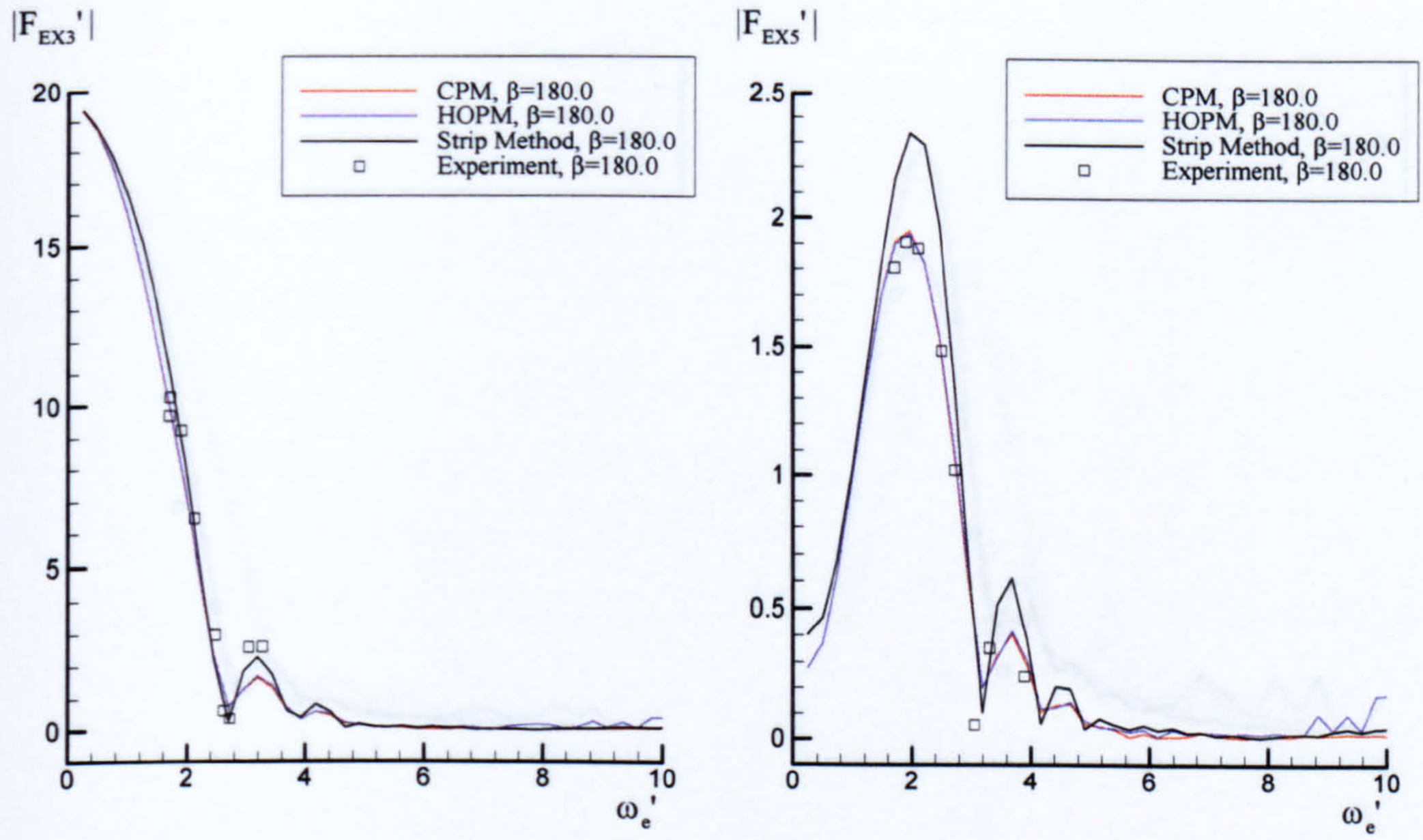

Figure 7.22 Non-dimensional heave and pitch wave exciting force and moment for Todd Series 60 at zero speed in head sea (β=180°)

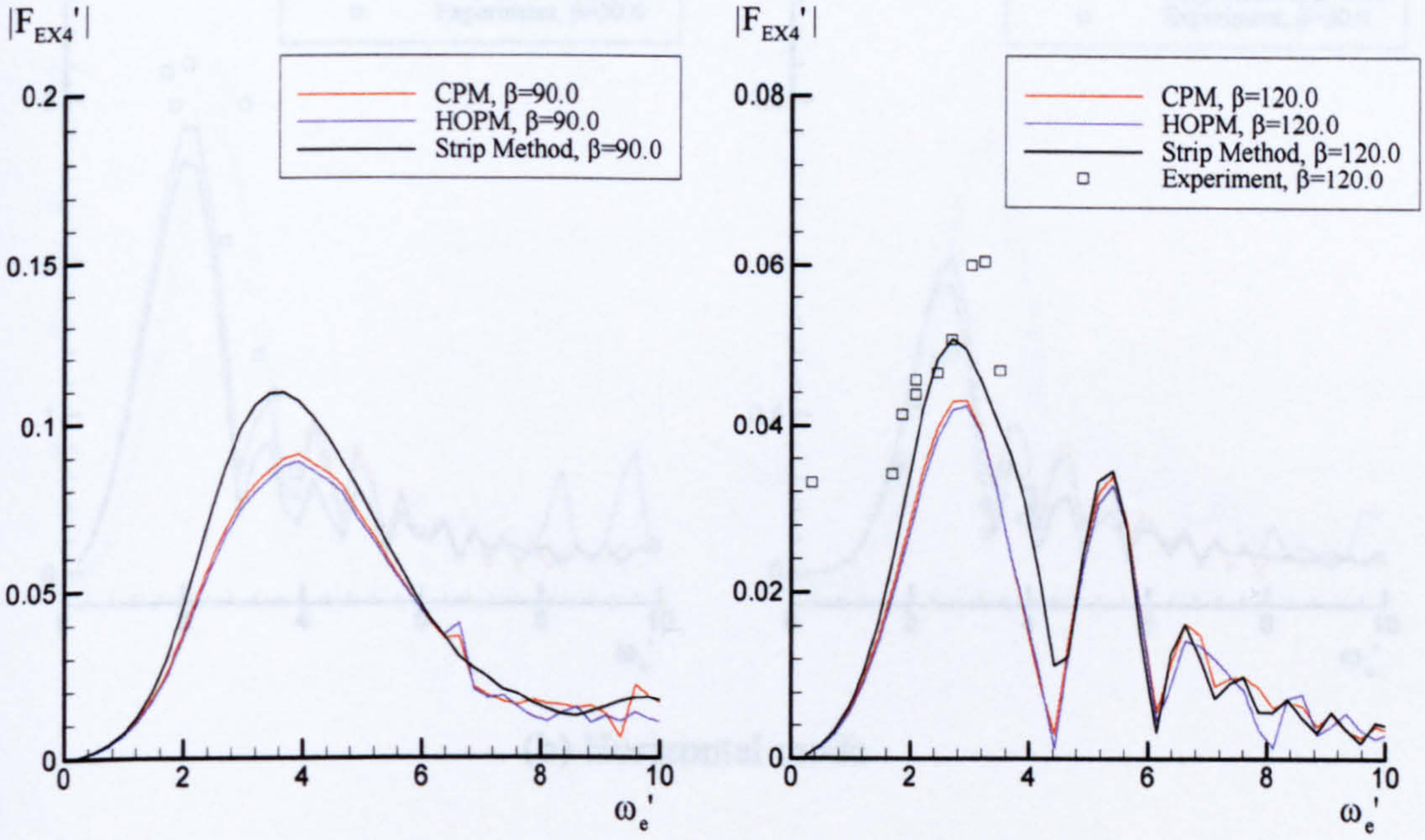

Figure 7.23 Non-dimensional roll wave exciting moment for Todd Series 60 at zero speed in beam sea (β=90°) and bow sea (β=120°)

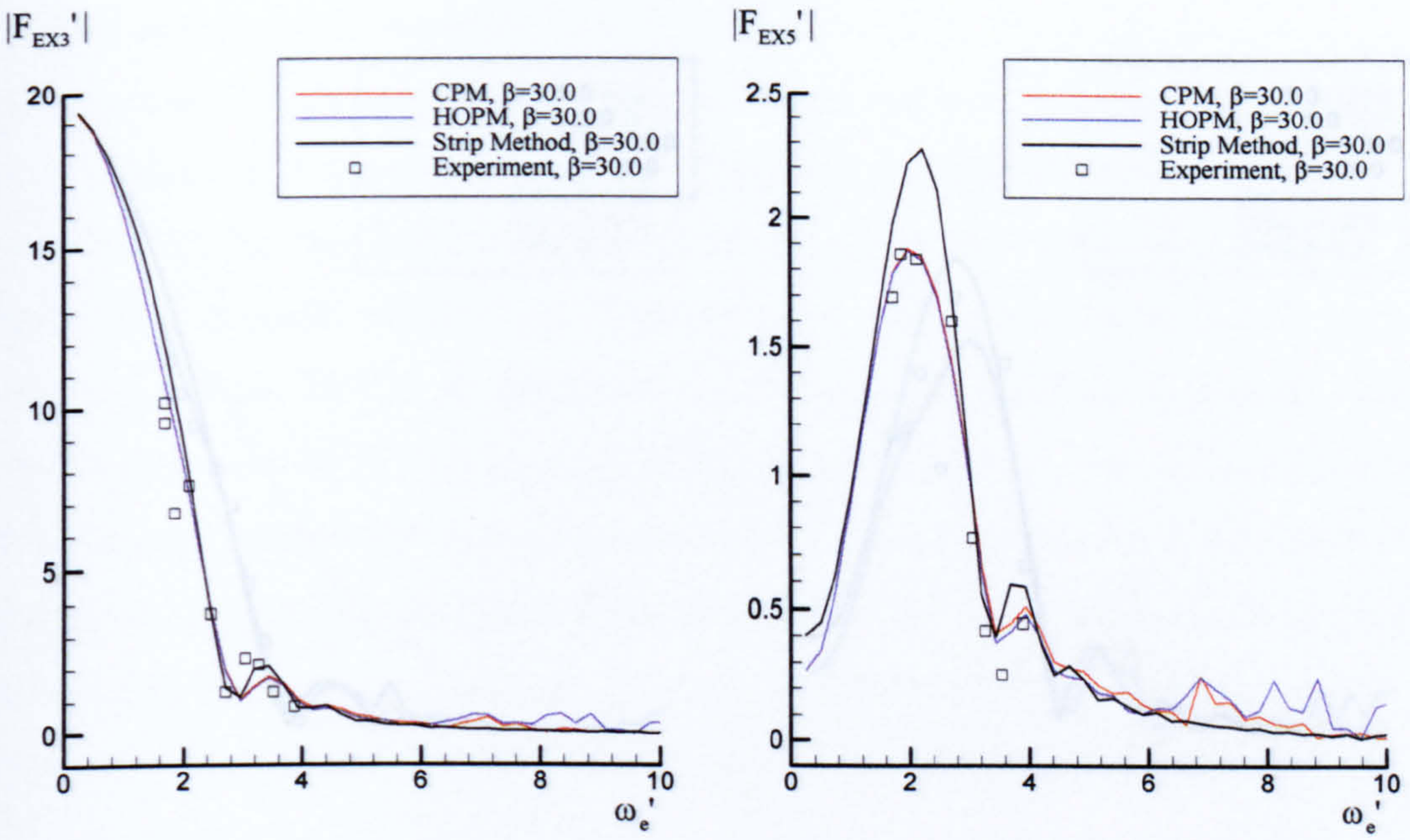

(a) Vertical mode

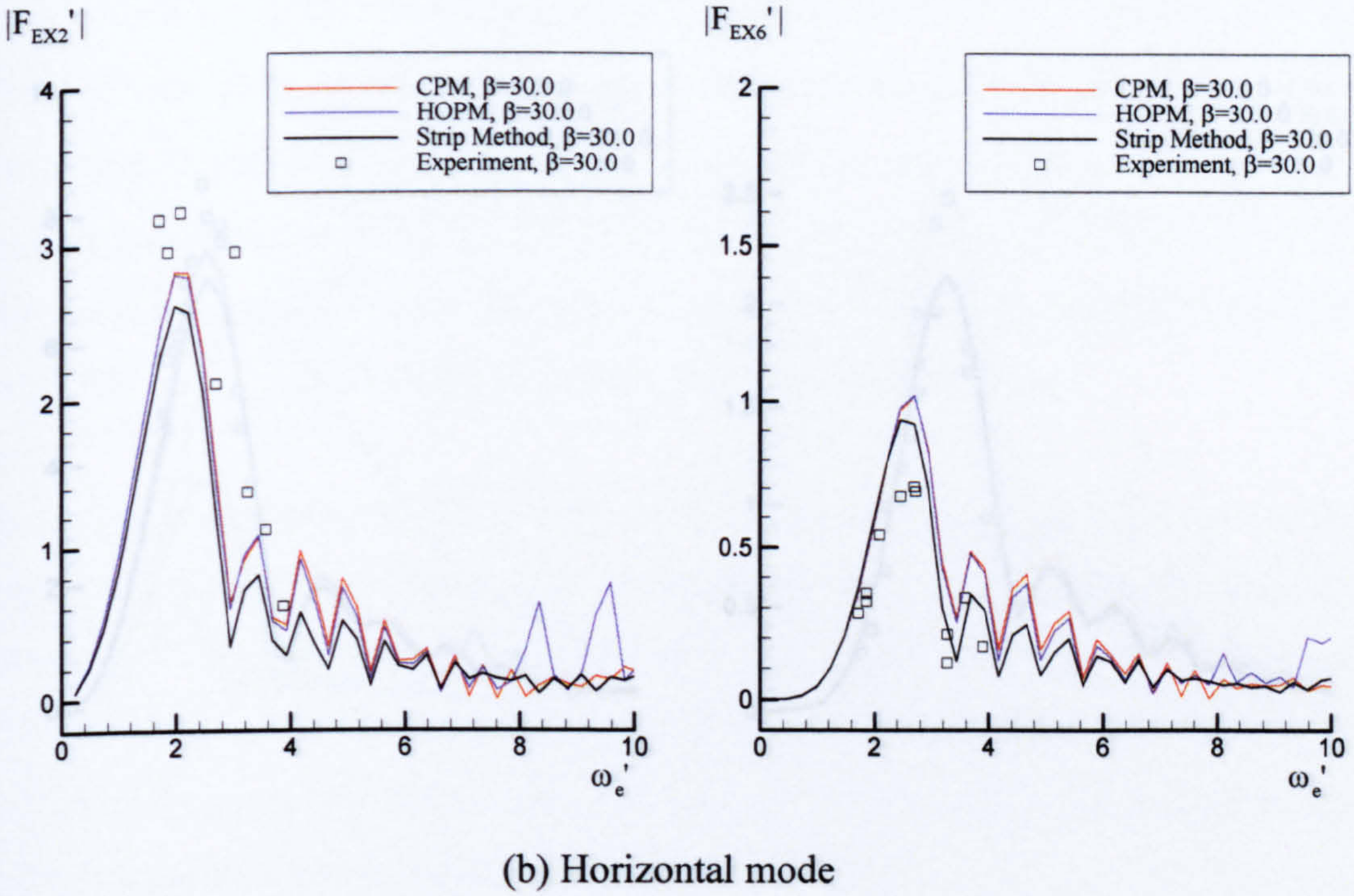

(b) Horizontal mode

Figure 7.24 Non-dimensional wave exciting forces and moments for Todd Series 60 at zero speed in quartering sea (β=30°)

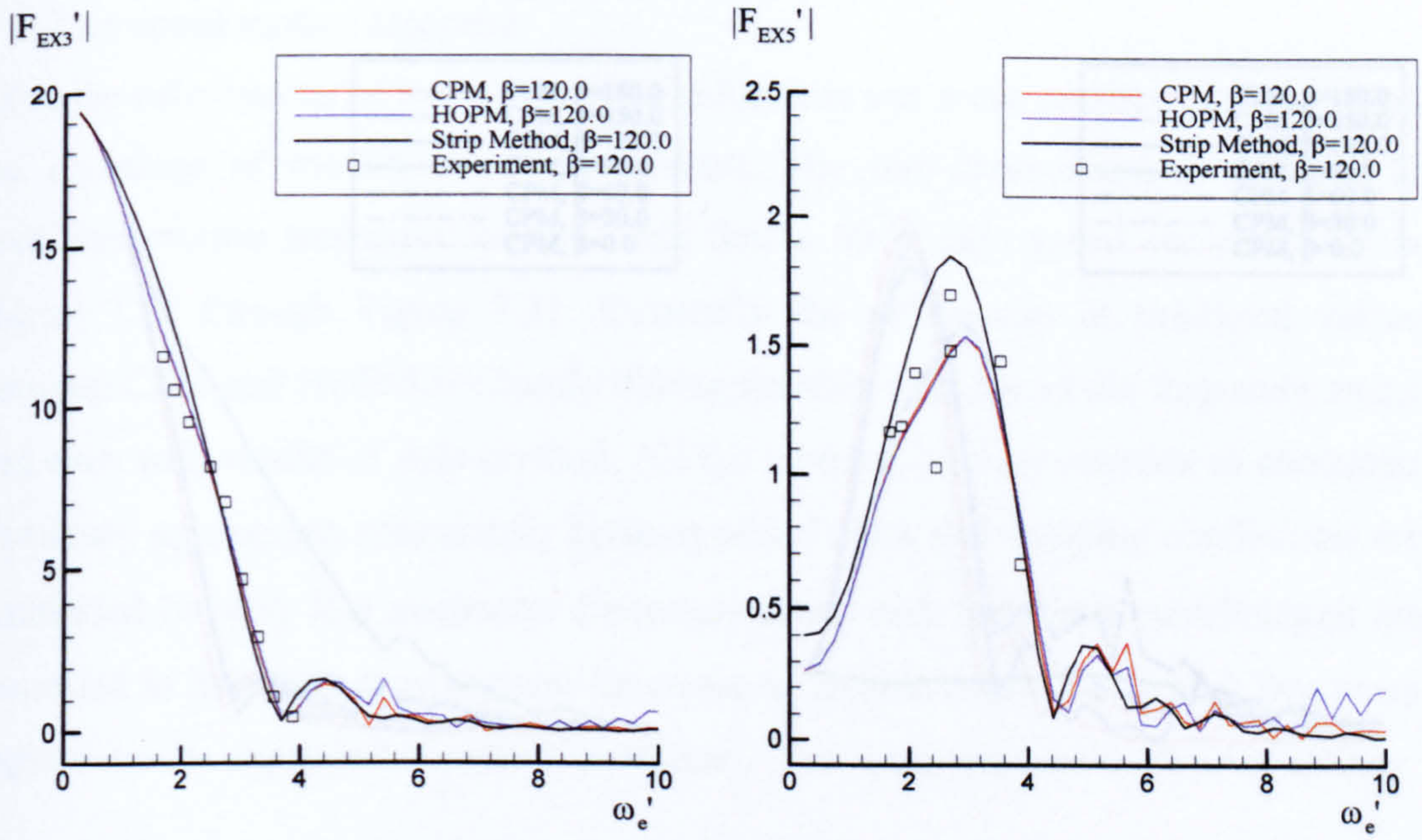

(a) Vertical mode

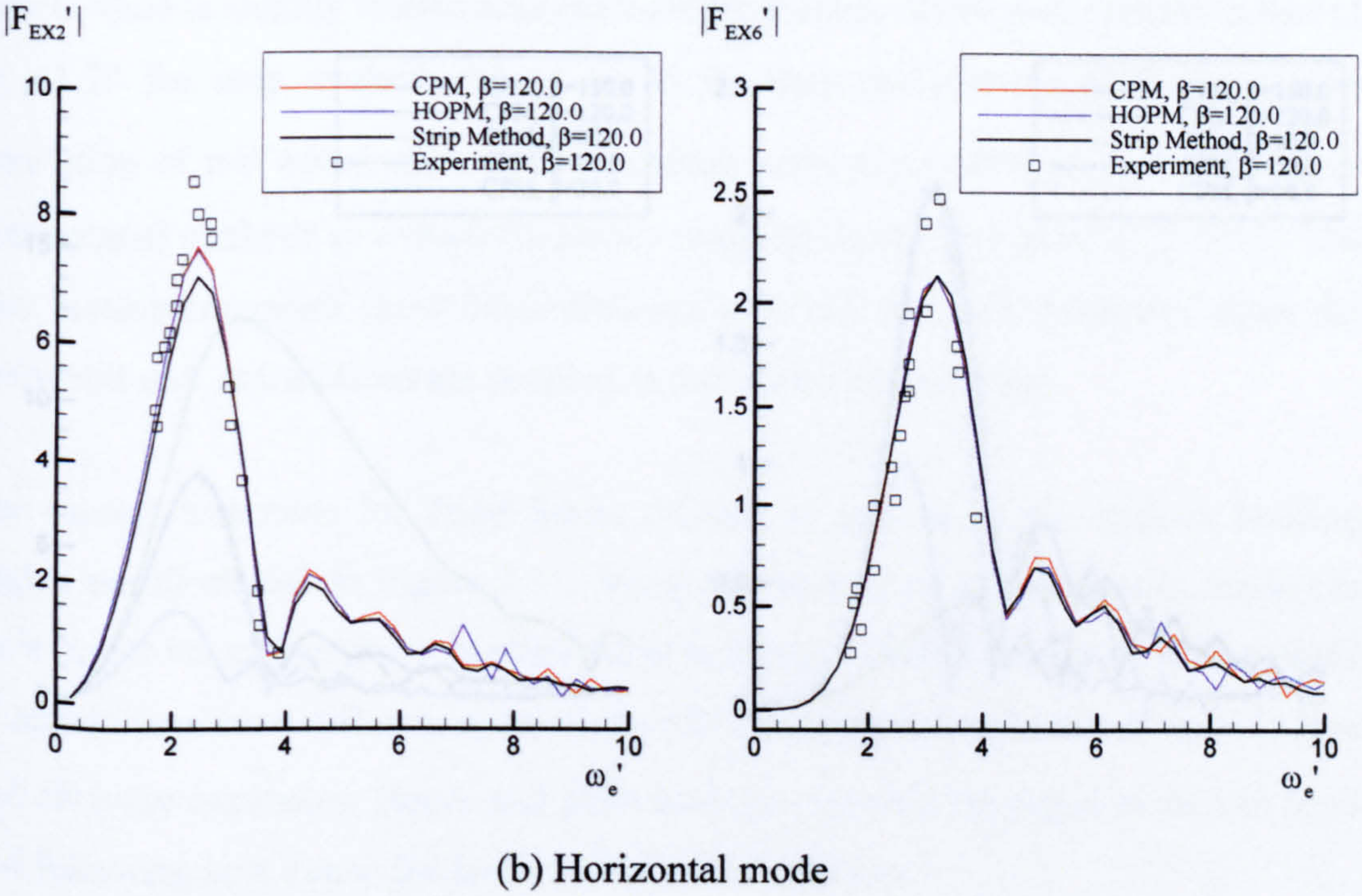

(b) Horizontal mode

Figure 7.25 Non-dimensional wave exciting forces and moments for Todd Series 60 at zero speed in bow sea (β=120°)

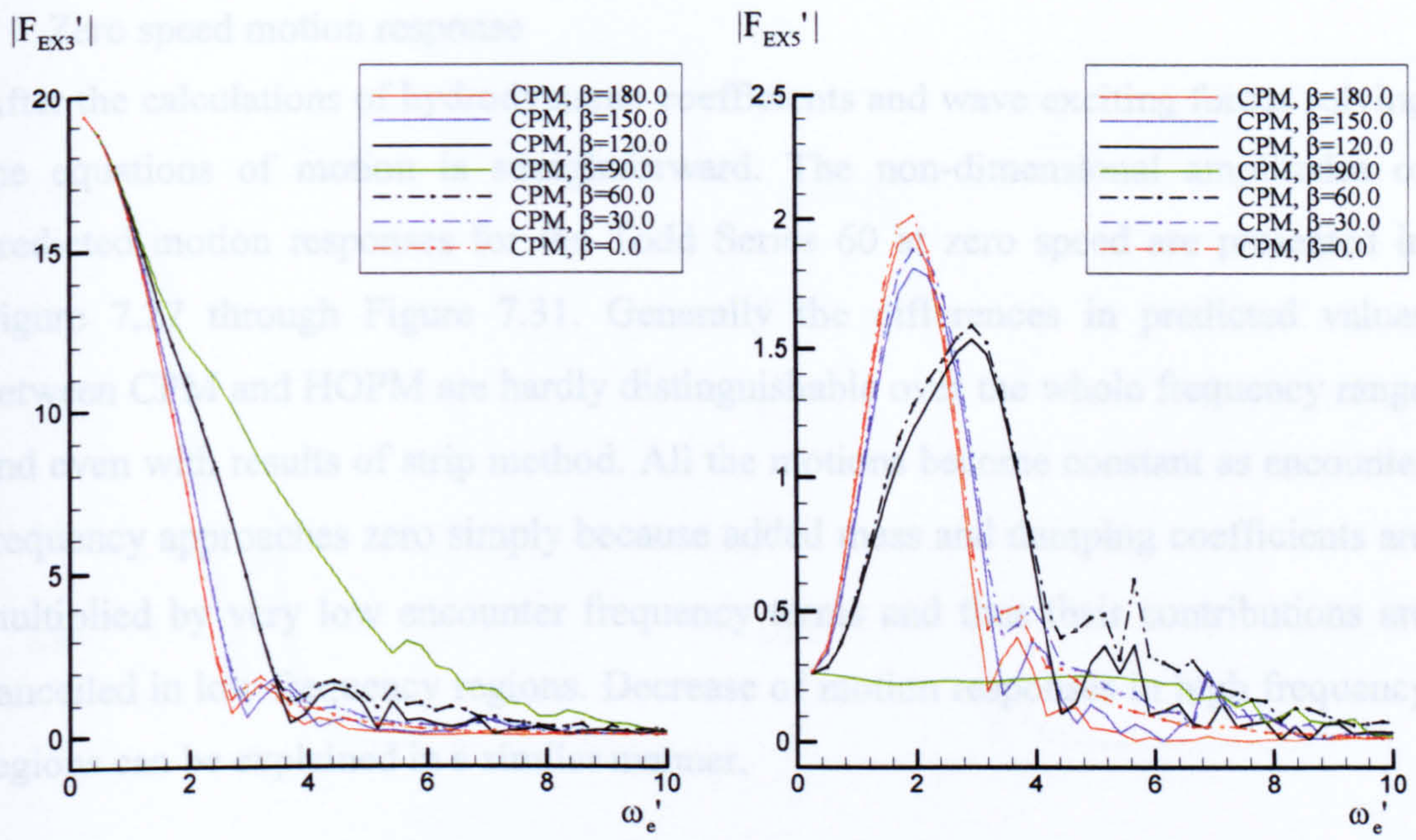

(a) Vertical mode

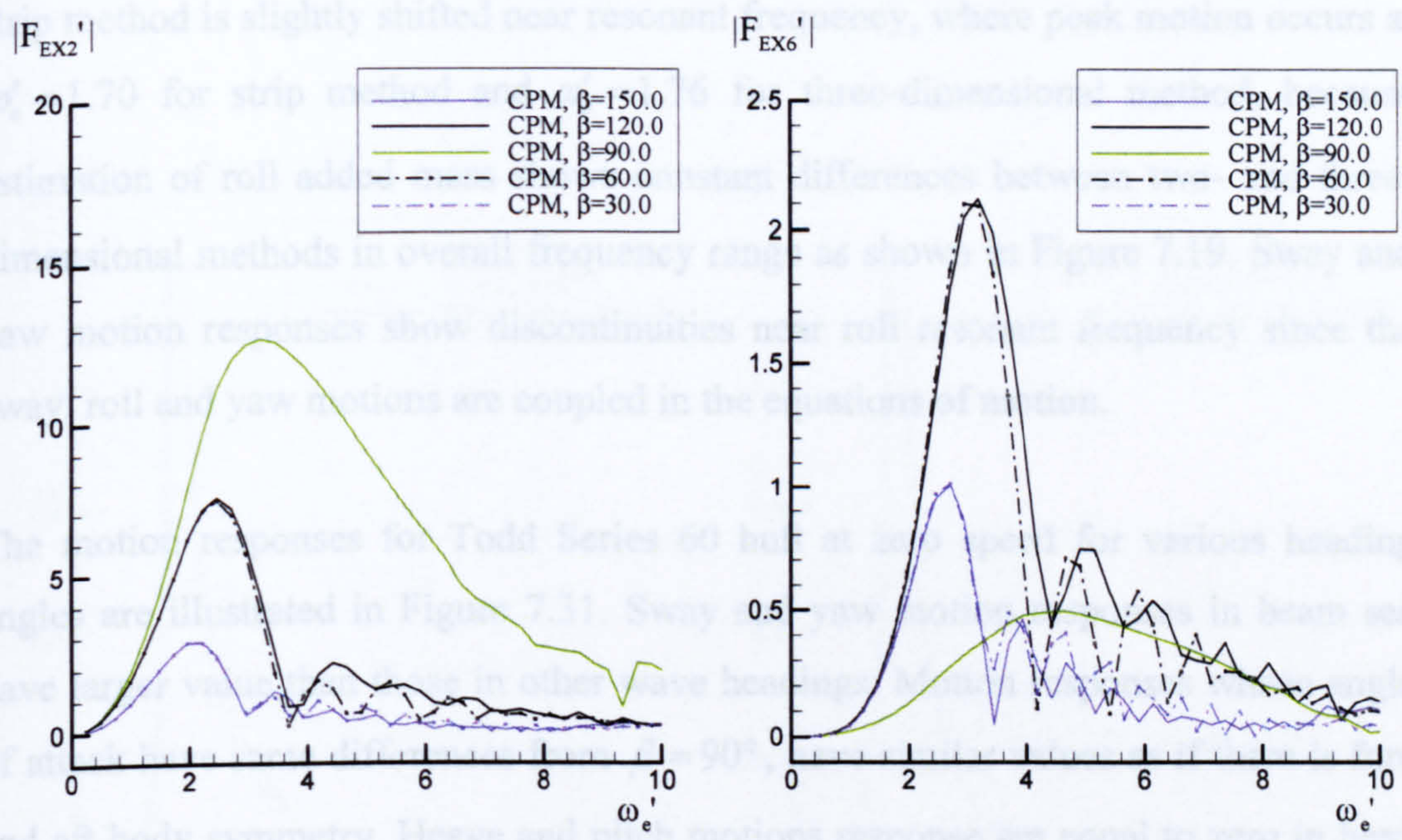

(b) Horizontal mode

Figure 7.26 Non-dimensional wave exciting forces and moments for Todd Series 60 at zero speed in various heading angles

- Zero speed motion response

After the calculations of hydrodynamic coefficients and wave exciting forces solving the equations of motion is straightforward. The non-dimensional amplitudes of predicted motion responses for the Todd Series 60 at zero speed are presented in Figure 7.27 through Figure 7.31. Generally the differences in predicted values between CPM and HOPM are hardly distinguishable over the whole frequency range and even with results of strip method. All the motions become constant as encounter frequency approaches zero simply because added mass and damping coefficients are multiplied by very low encounter frequency terms and thus their contributions are cancelled in low frequency regions. Decrease of motion responses in high frequency regions can be explained in a similar manner.

Roll motion responses shown in Figure 7.28 have resonant phenomena because of the neglect of viscous effect for roll damping. It is noted that the roll motion curve of strip method is slightly shifted near resonant frequency, where peak motion occurs at $\omega_e' = 1.70$ for strip method and $\omega_e' = 1.76$ for three-dimensional method, because estimation of roll added mass shows constant differences between two- and three-dimensional methods in overall frequency range as shown in Figure 7.19. Sway and yaw motion responses show discontinuities near roll resonant frequency since the sway, roll and yaw motions are coupled in the equations of motion.

The motion responses for Todd Series 60 hull at zero speed for various heading angles are illustrated in Figure 7.31. Sway and yaw motion responses in beam sea have larger value than those in other wave headings. Motion responses whose angle of attack have same differences from $\beta = 90°$, have similar values as if there is fore and aft body symmetry. Heave and pitch motions response are equal to zero in head and following seas due to the horizontal plane of symmetry.

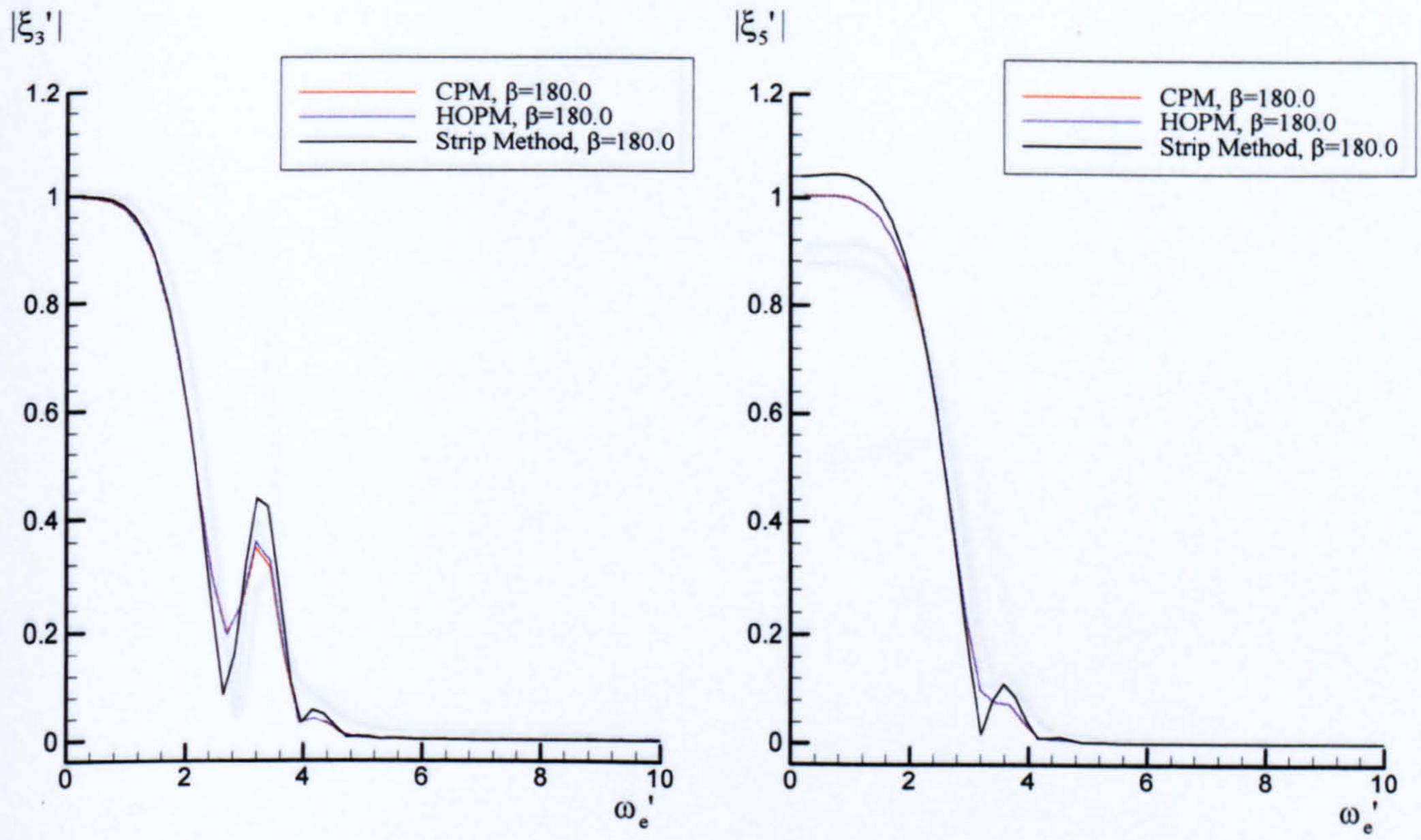

Figure 7.27 Non-dimensional heave and pitch motion responses for Todd Series 60 at zero speed in head sea (β=180°)

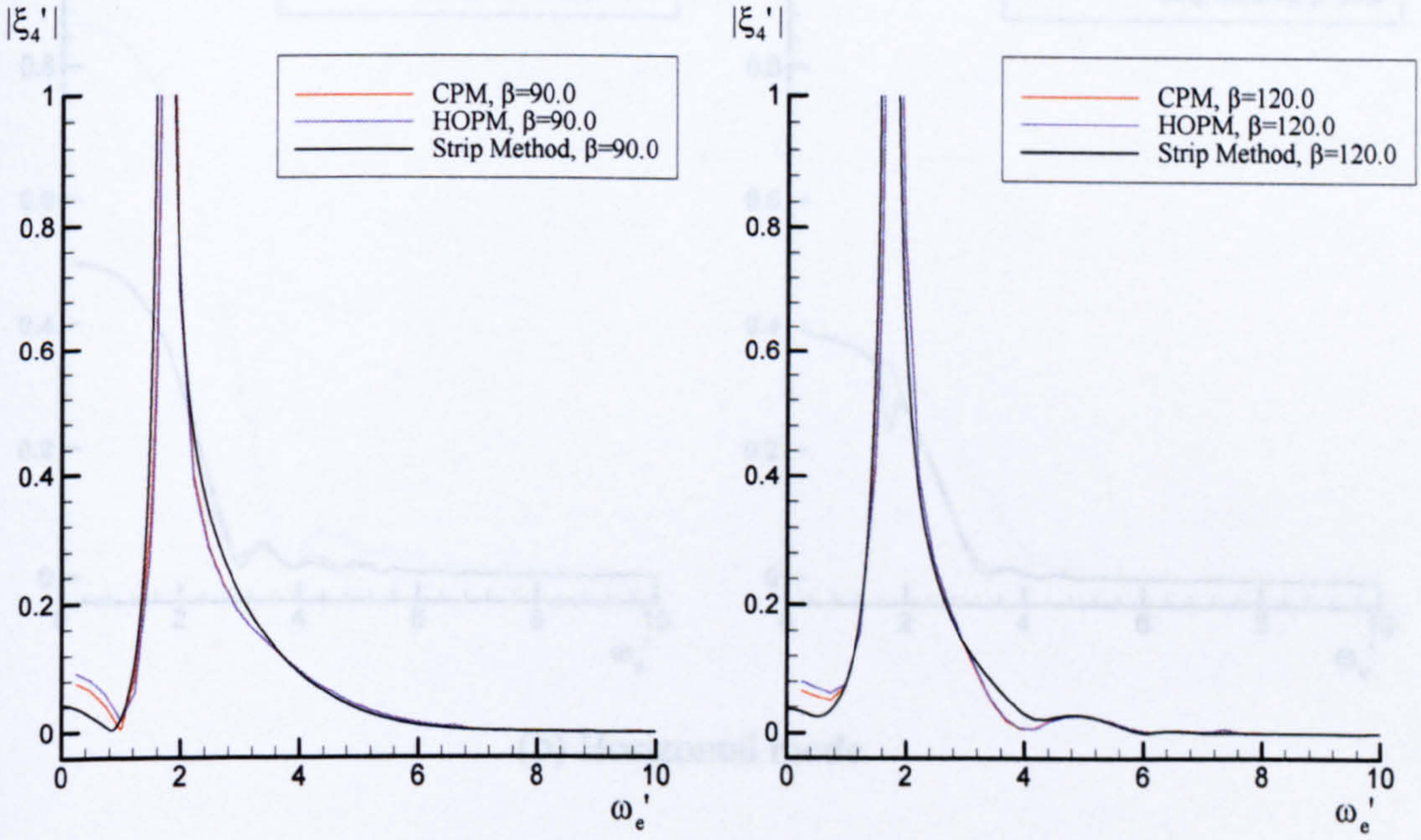

Figure 7.28 Non-dimensional roll motion response for Todd Series 60 at zero speed in beam sea (β=90°) and bow sea (β=120°)

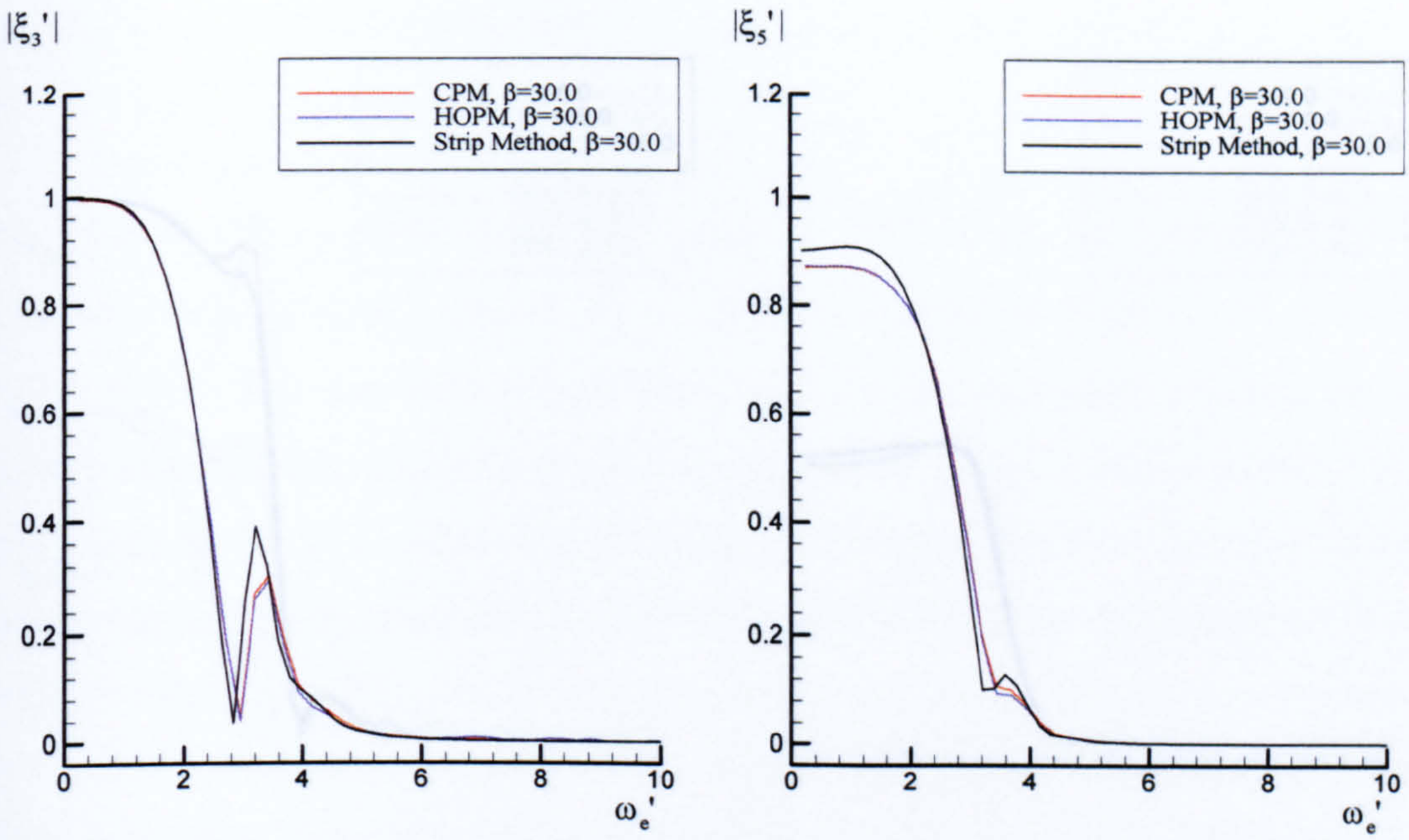

(a) Vertical mode

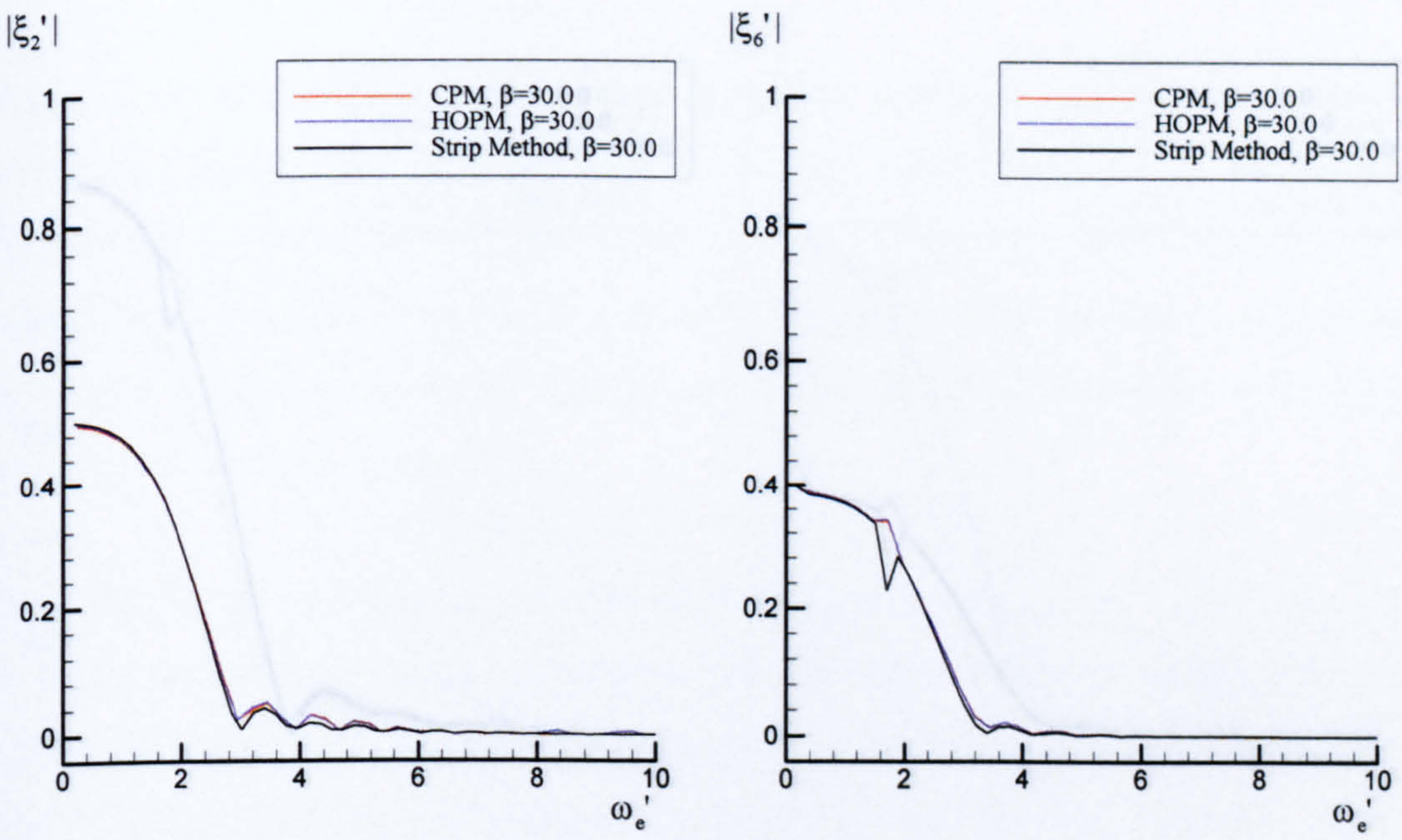

(b) Horizontal mode

Figure 7.29 Non-dimensional motion responses for Todd Series 60 at zero speed in quartering sea (β=30°)

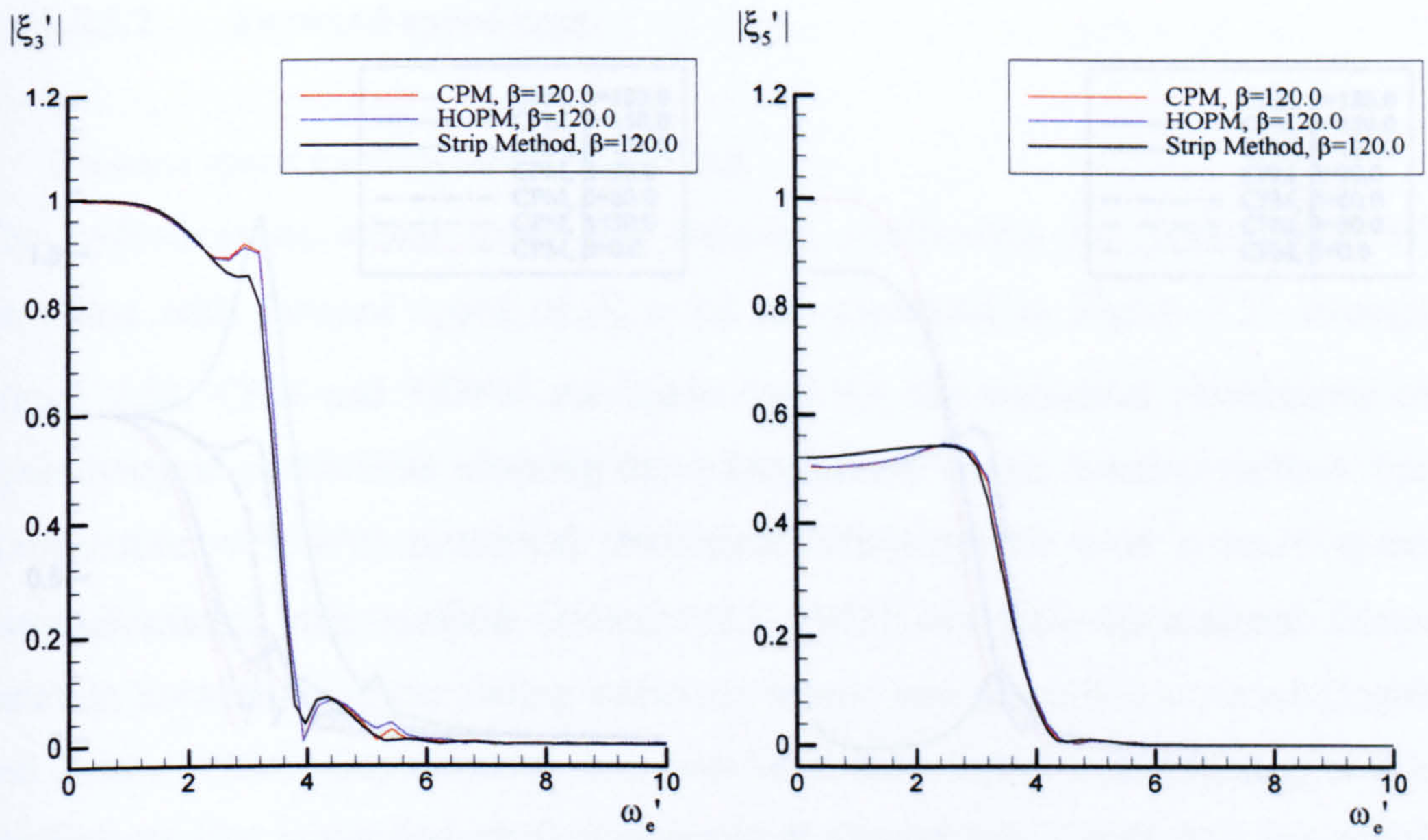

(a) Vertical mode

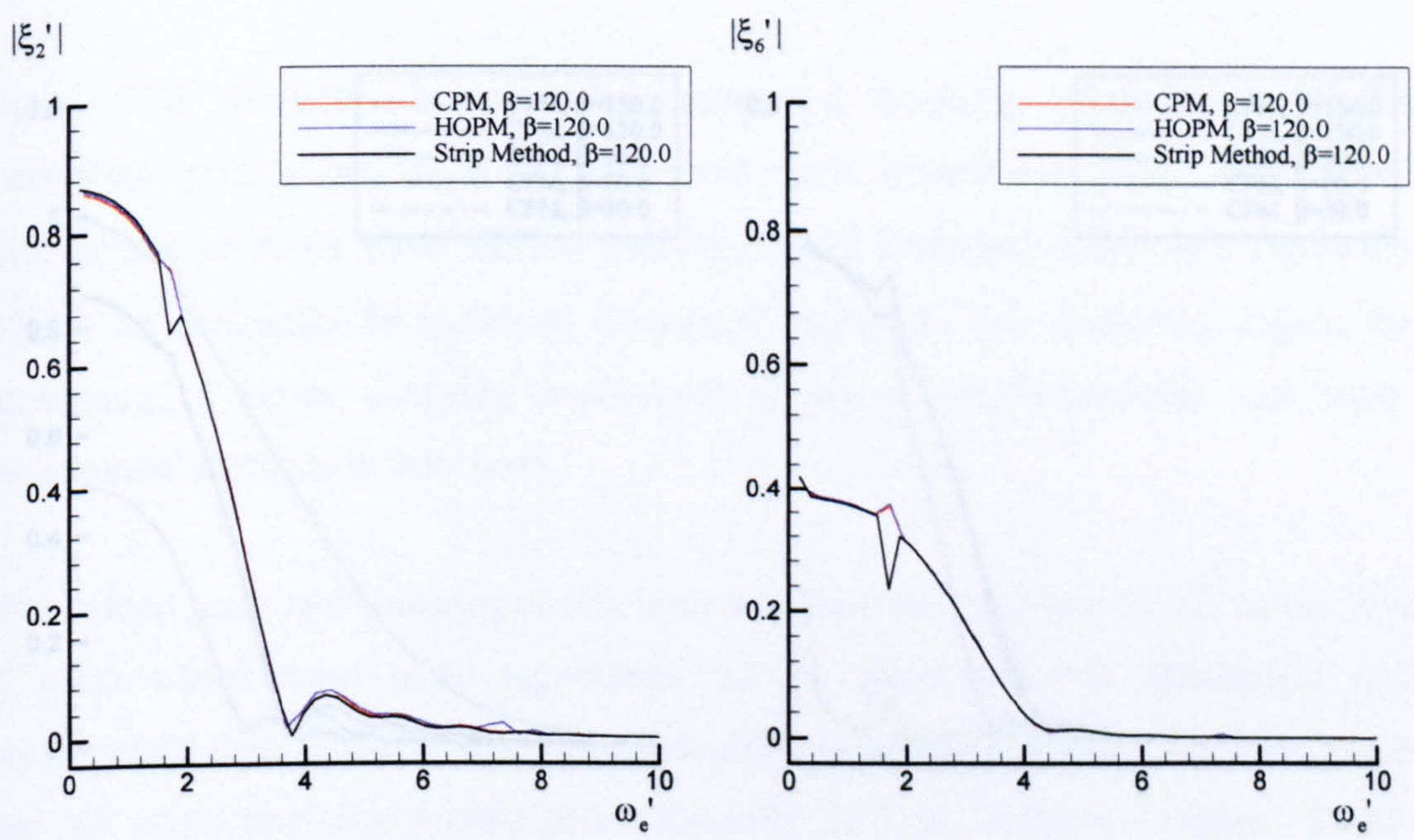

(b) Horizontal mode

Figure 7.30 Non-dimensional motion responses for Todd Series 60 at zero speed in bow sea (β=120°)

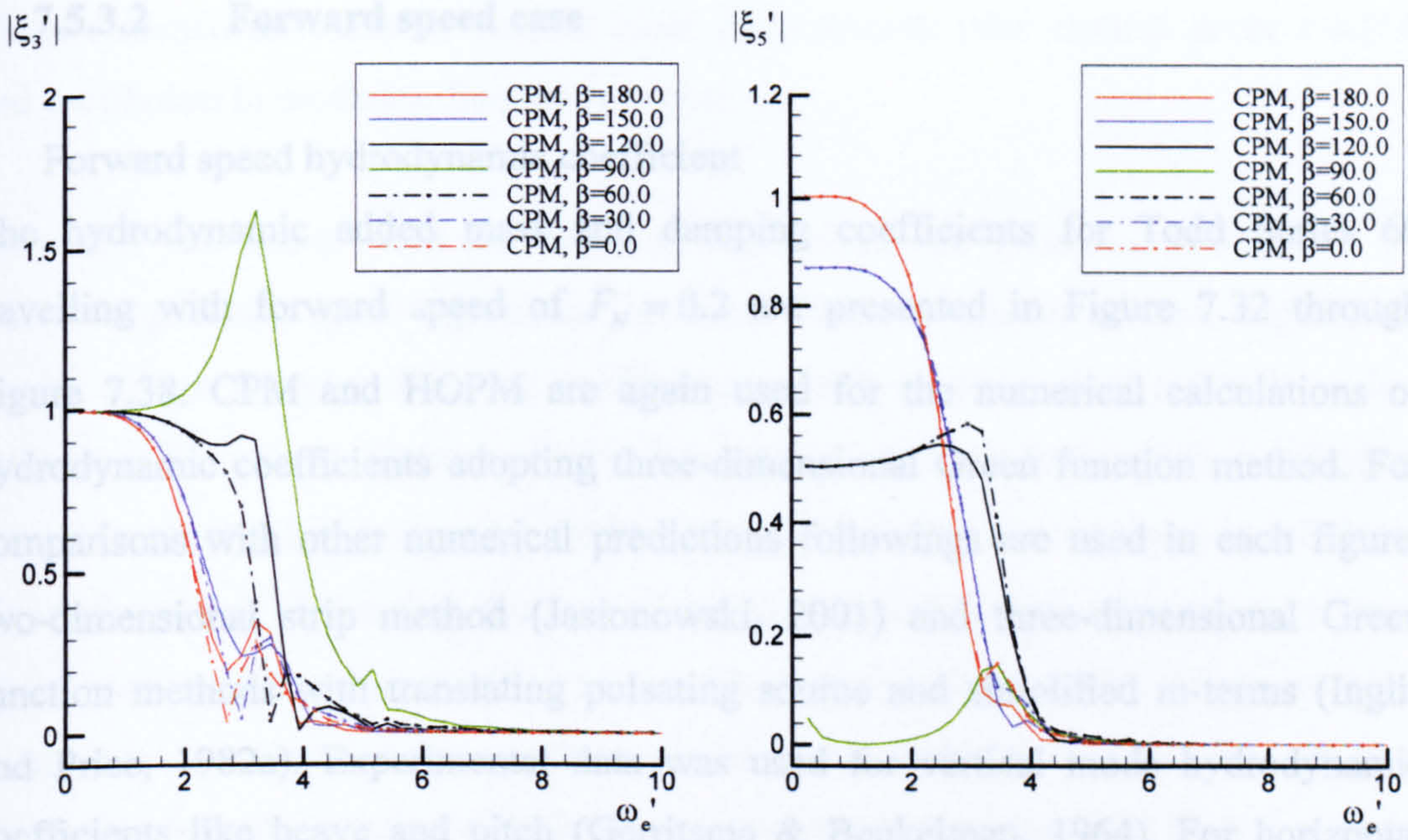

(a) Vertical mode

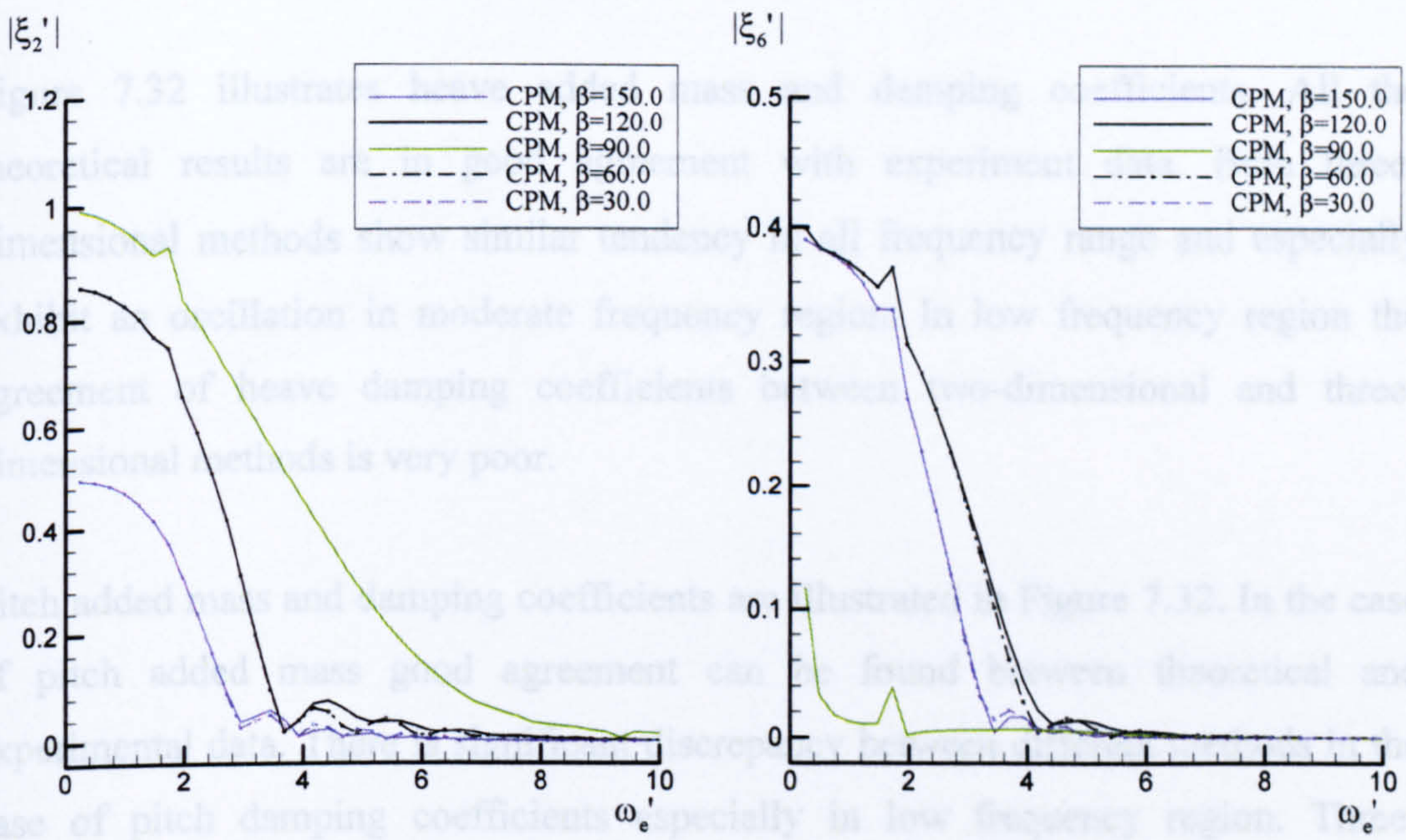

(b) Horizontal mode

Figure 7.31 Non-dimensional motion responses for Todd Series 60 at zero speed in various heading angles

7.5.3.2 Forward speed case

- Forward speed hydrodynamic coefficient

The hydrodynamic added mass and damping coefficients for Todd Series 60 travelling with forward speed of $F_N = 0.2$ are presented in Figure 7.32 through Figure 7.38. CPM and HOPM are again used for the numerical calculations of hydrodynamic coefficients adopting three-dimensional Green function method. For comparisons with other numerical predictions followings are used in each figure; two-dimensional strip method (Jasionowski, 2001) and three-dimensional Green function methods with translating pulsating source and simplified m-terms (Inglis and Price, 1982a). Experimental data was used for vertical mode hydrodynamic coefficients like heave and pitch (Gerritsma & Beukelman, 1964). For horizontal mode hydrodynamic coefficients experiment data measured for the model without a rudder and with a rudder fixed at zero angle of deflection (van Leeuwen, 1964).

Figure 7.32 illustrates heave added mass and damping coefficients. All the theoretical results are in good agreement with experiment data. Both three-dimensional methods show similar tendency in all frequency range and especially exhibit an oscillation in moderate frequency region. In low frequency region the agreement of heave damping coefficients between two-dimensional and three-dimensional methods is very poor.

Pitch added mass and damping coefficients are illustrated in Figure 7.32. In the case of pitch added mass good agreement can be found between theoretical and experimental data. There is significant discrepancy between different methods in the case of pitch damping coefficients especially in low frequency region. Three-dimensional methods show peak value near critical point $\tau = 1/4$ and it is obviously observed in the case of damping coefficients rather than added mass coefficients.

Cross-coupled heave and pitch added mass and damping coefficients are illustrated in Figure 7.33. Again results of two-dimensional method approach infinity in low

frequency region in the case of coupled heave and pitch added mass coefficients. Three-dimensional methods exhibit clear discontinuity near critical point $\tau = 1/4$ and oscillation in moderate frequency region.

Sway and yaw added mass and damping coefficients are illustrated in Figure 7.34. There is generally good agreement between different theoretical and experiment results except for yaw damping coefficients which all theoretical methods under-estimated. Smooth oscillations observed in vertical mode hydrodynamic coefficients are again observed in horizontal mode. Those phenomena are observed in relatively higher frequency region than the case of vertical mode. Cross-coupled sway and yaw added mass and damping coefficients are illustrated in Figure 7.35. There are good qualitative agreement between three-dimensional methods and experiment data although relatively rough oscillations are observed in moderate and high frequency regions.

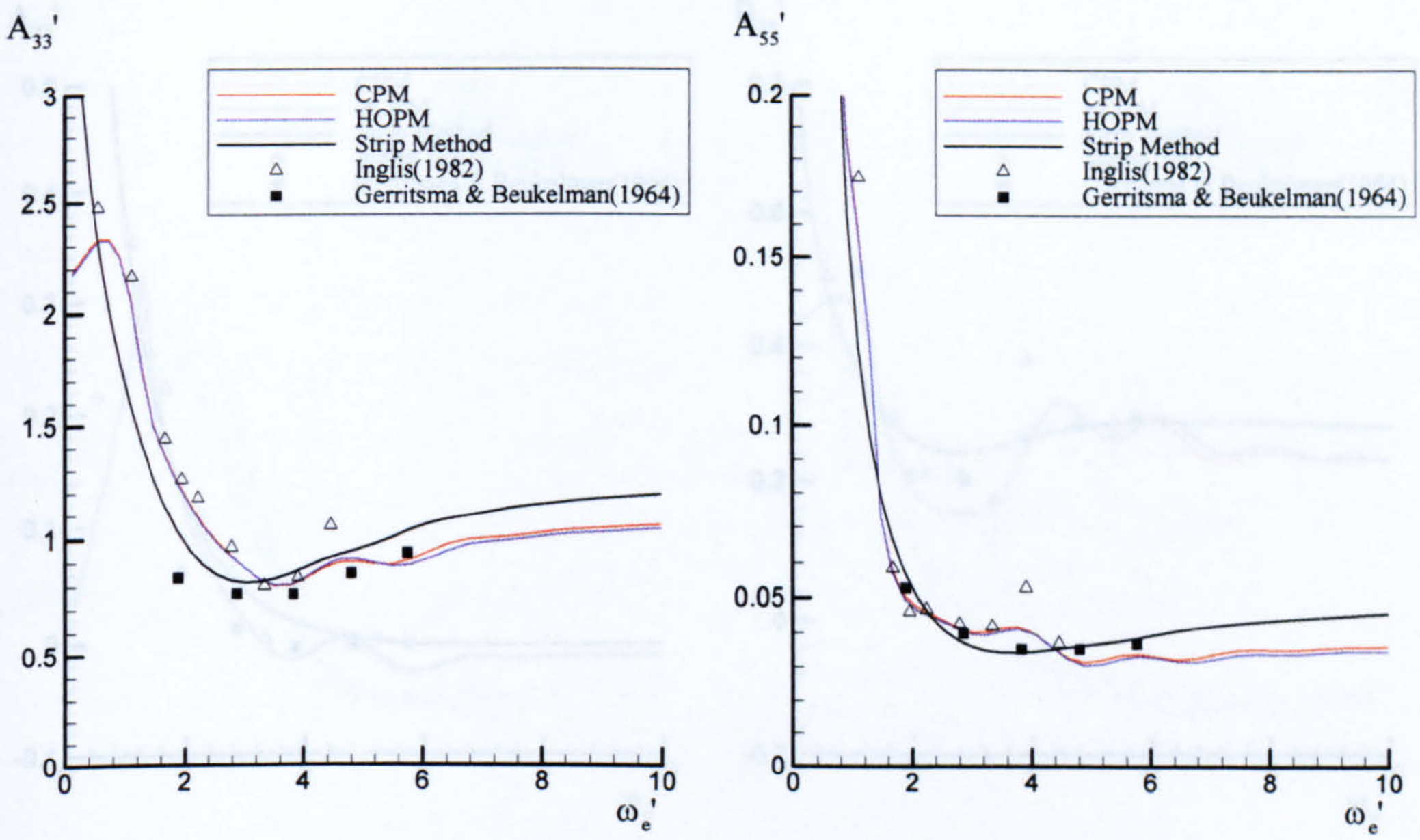

(a) Added mass

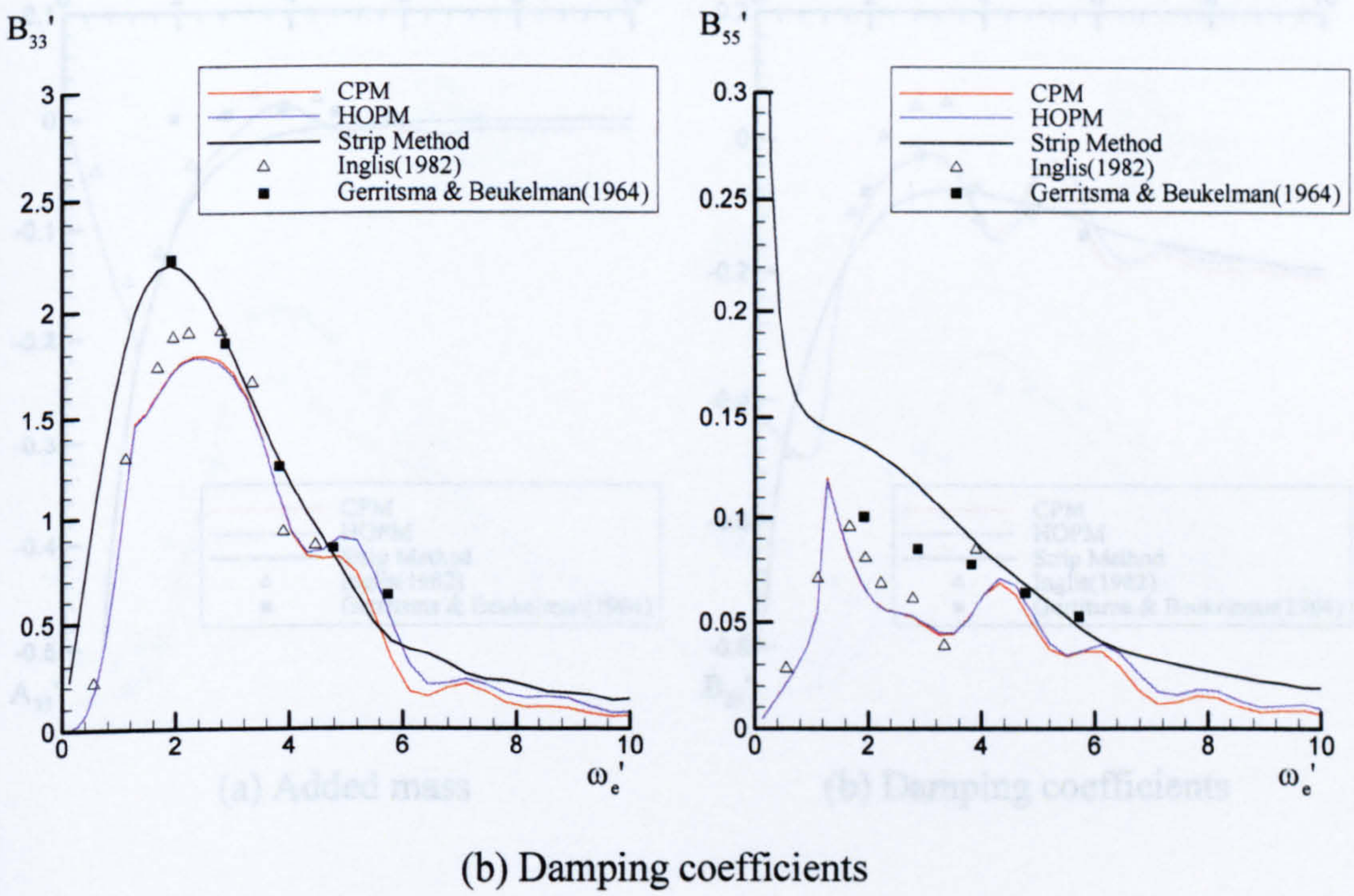

(b) Damping coefficients

Figure 7.32 Non-dimensional added mass and damping coefficients in heave and pitch modes for Todd Series 60 travelling at Froude number 0.2

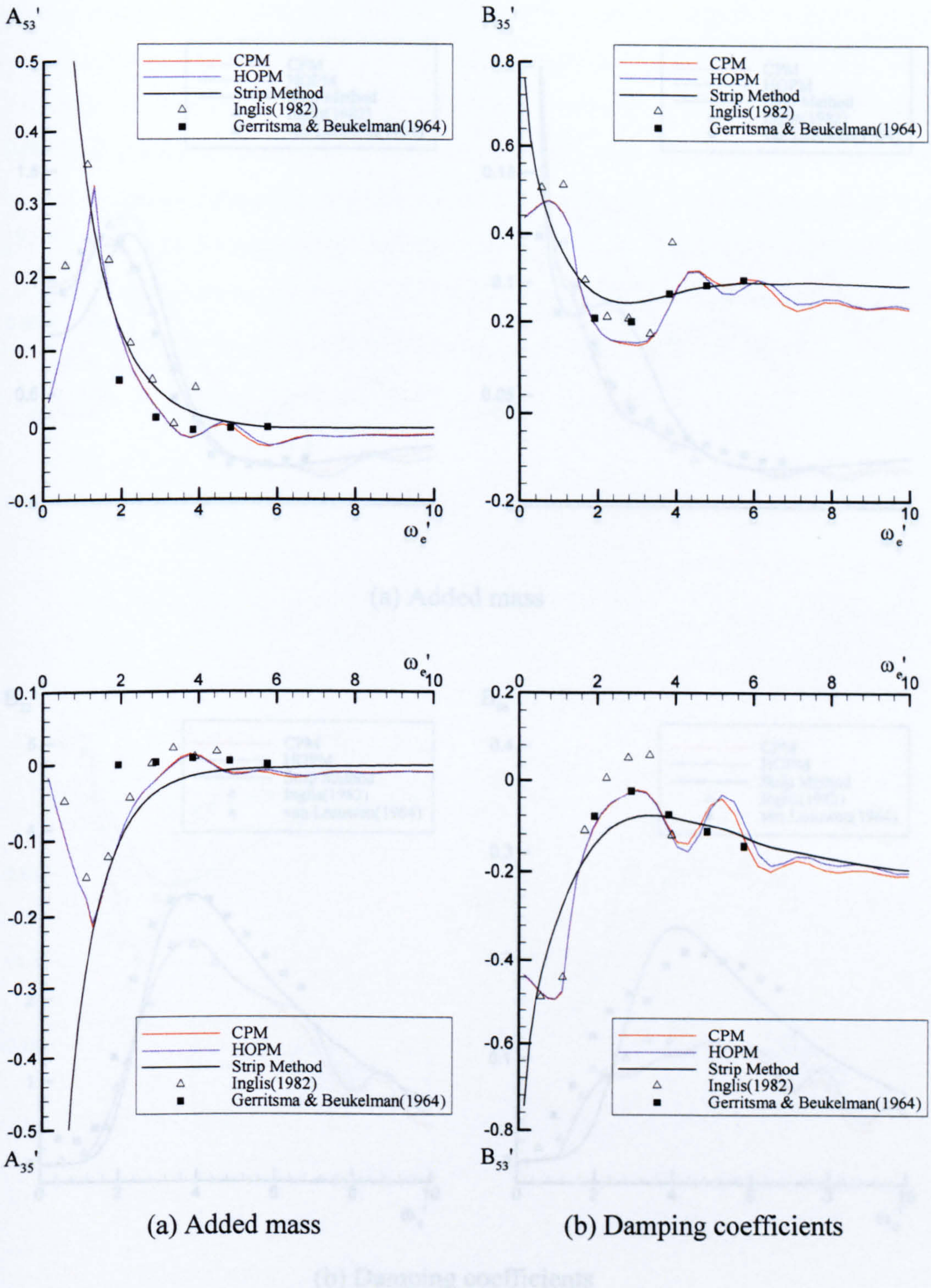

(a) Added mass (b) Damping coefficients

Figure 7.33 Non-dimensional coupled added mass and damping coefficients in heave and pitch modes for Todd Series 60 travelling at Froude number 0.2

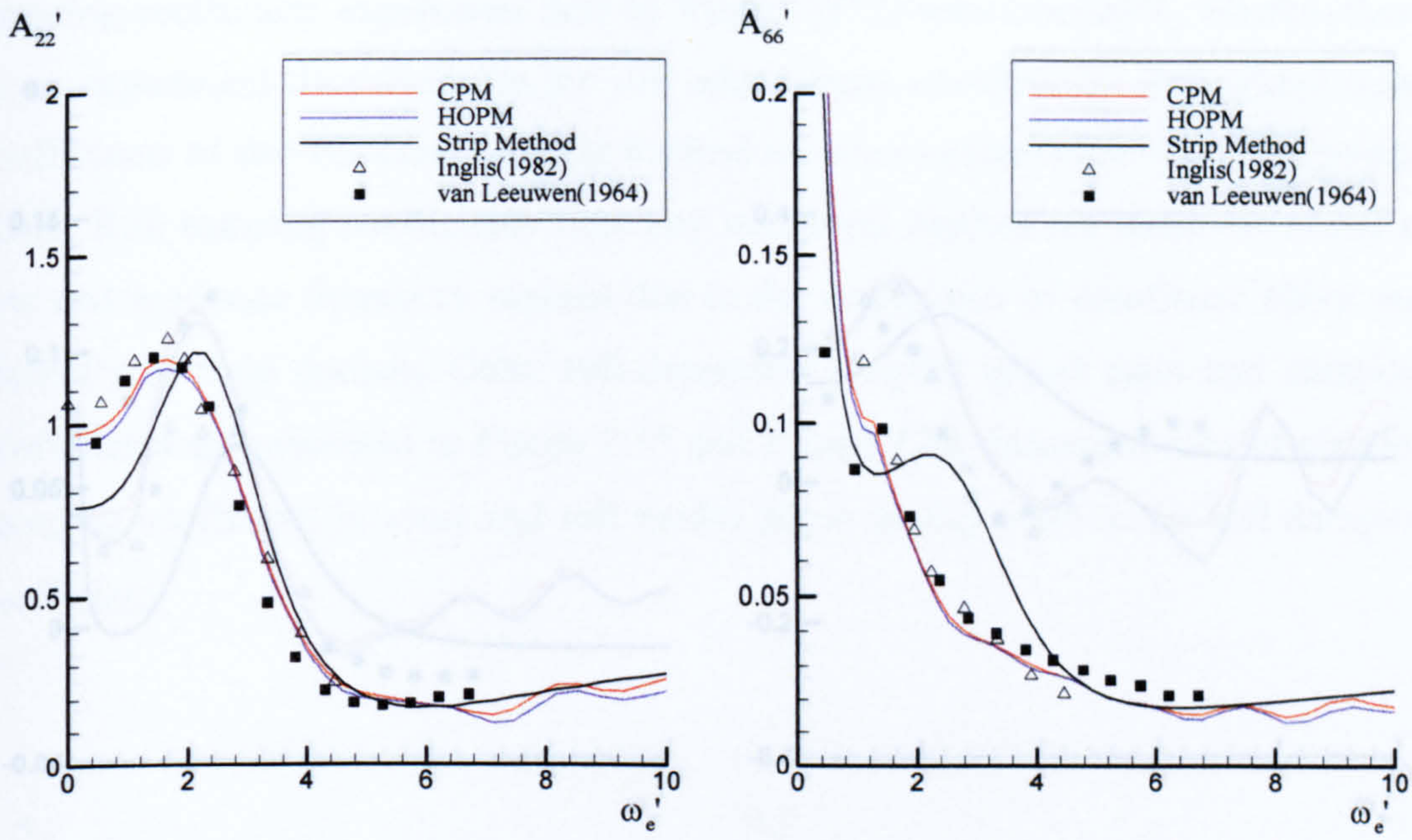

(a) Added mass

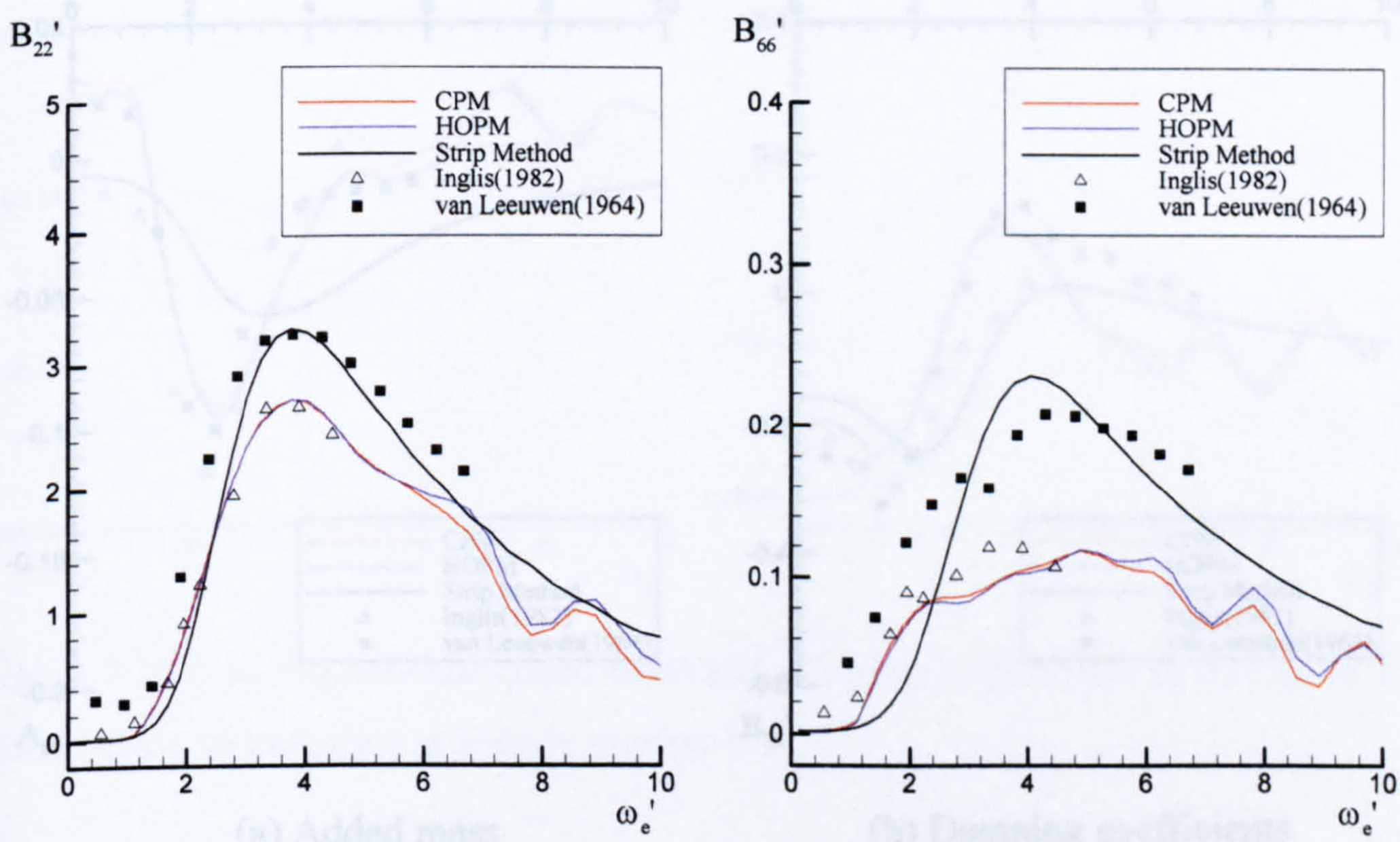

(b) Damping coefficients

Figure 7.34 Non-dimensional added mass and damping coefficients in sway and yaw modes for Todd Series 60 travelling at Froude number 0.2

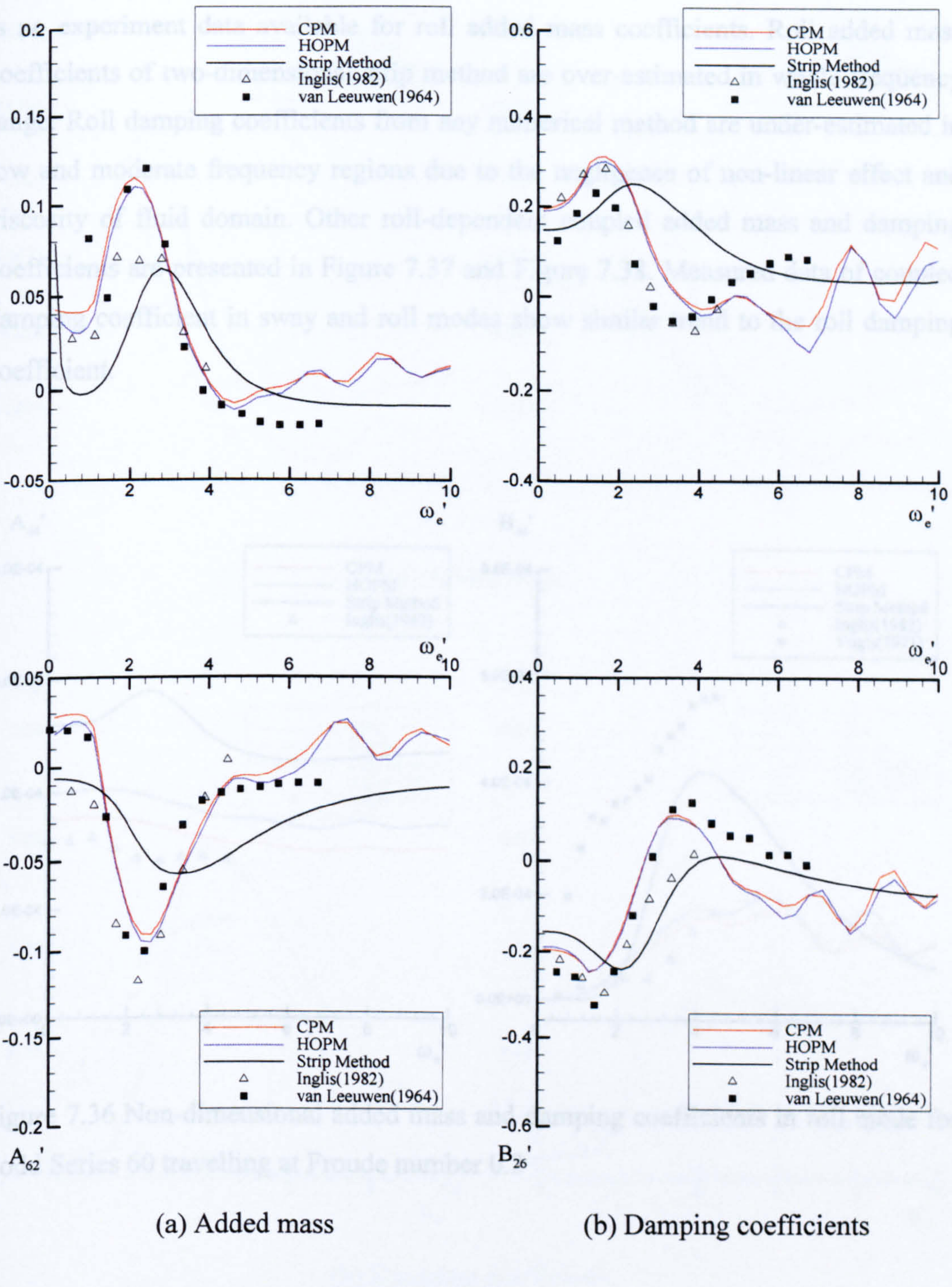

(a) Added mass (b) Damping coefficients

Figure 7.35 Non-dimensional coupled added mass and damping coefficients in sway and yaw modes for Todd Series 60 travelling at Froude number 0.2

Roll added mass and damping coefficients are shown in Figure 7.36. For roll damping coefficient, experiment data by Vugts (1971) were compared, whereas there is no experiment data available for roll added mass coefficients. Roll added mass coefficients of two-dimensional strip method are over-estimated in whole frequency range. Roll damping coefficients from any numerical method are under-estimated in low and moderate frequency regions due to the negligence of non-linear effect and viscosity of fluid domain. Other roll-dependent coupled added mass and damping coefficients are presented in Figure 7.37 and Figure 7.38. Measured data of coupled damping coefficient in sway and roll modes show similar trend to the roll damping coefficient.

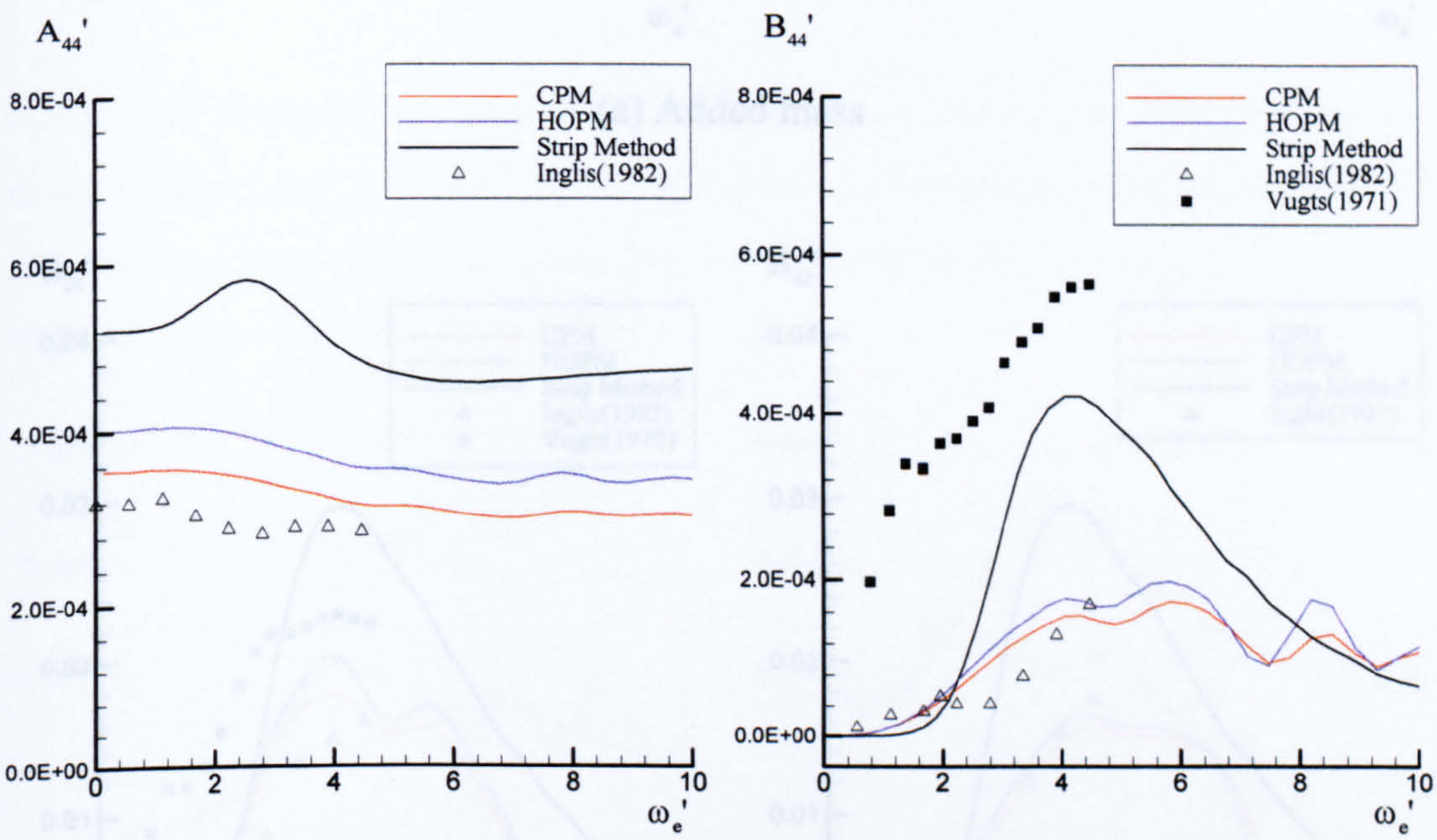

Figure 7.36 Non-dimensional added mass and damping coefficients in roll mode for Todd Series 60 travelling at Froude number 0.2

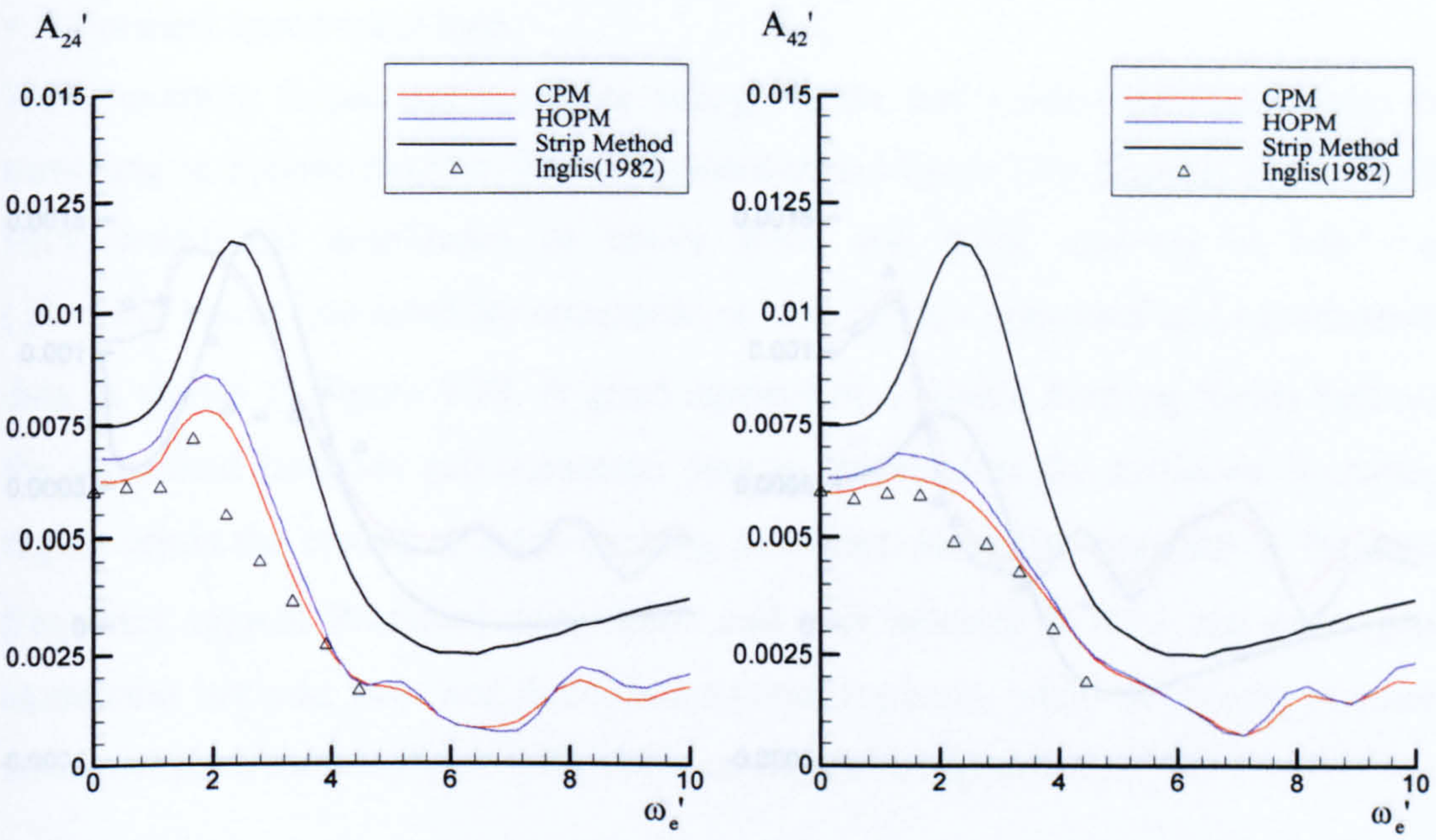

(a) Added mass

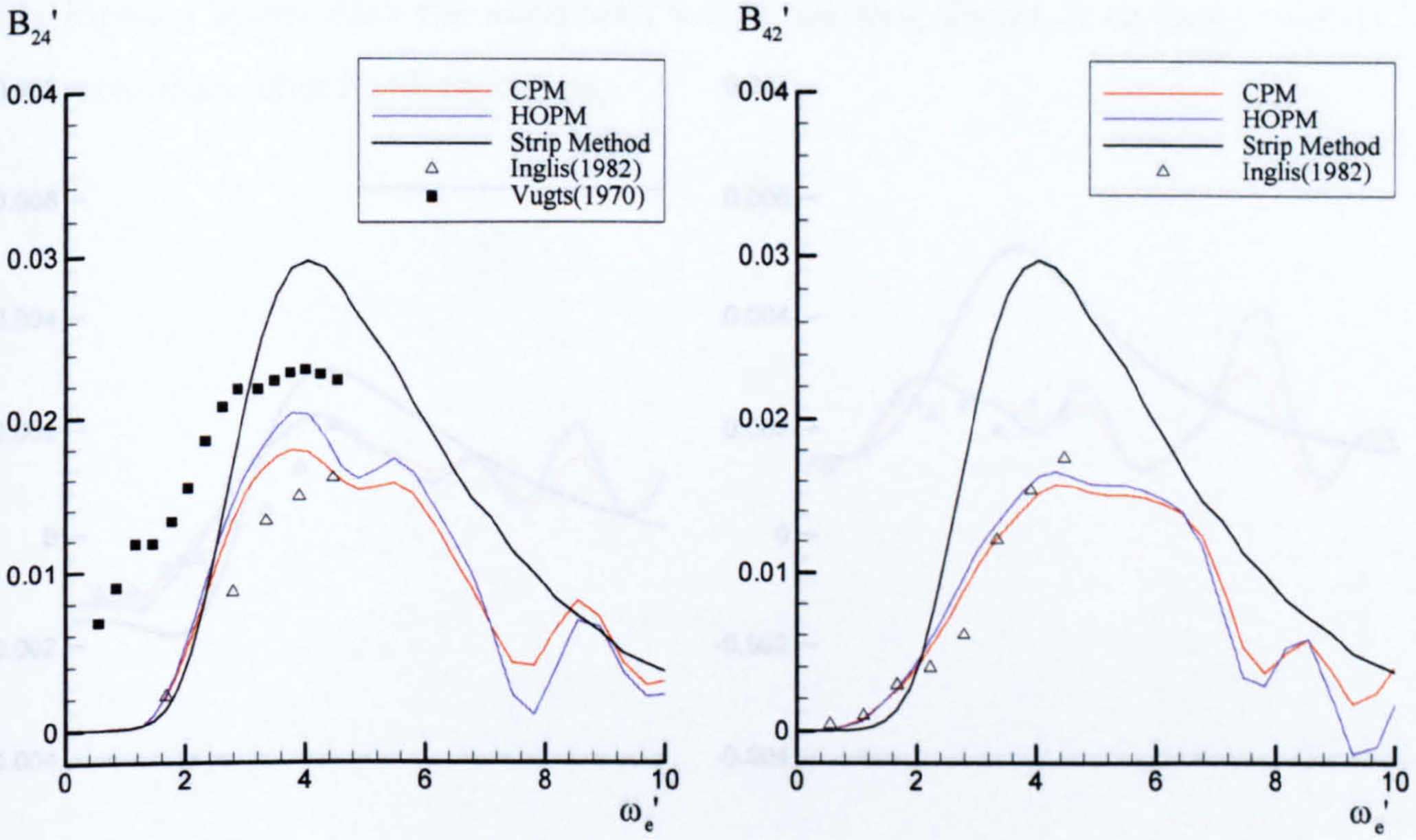

(b) Damping coefficients

Figure 7.37 Non-dimensional coupled added mass and damping coefficients in sway and roll modes for Todd Series 60 travelling at Froude number 0.2

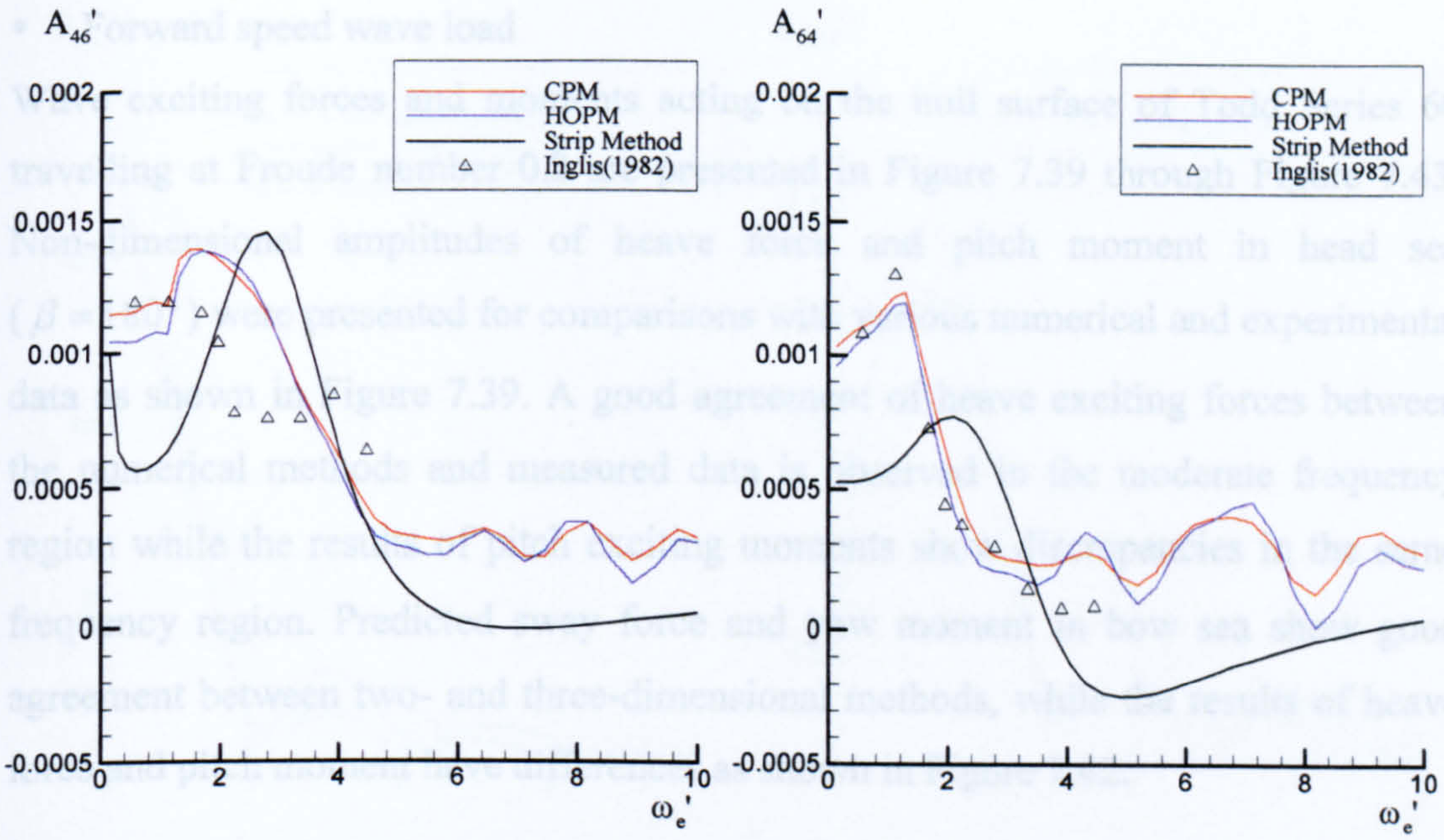

(a) Added mass

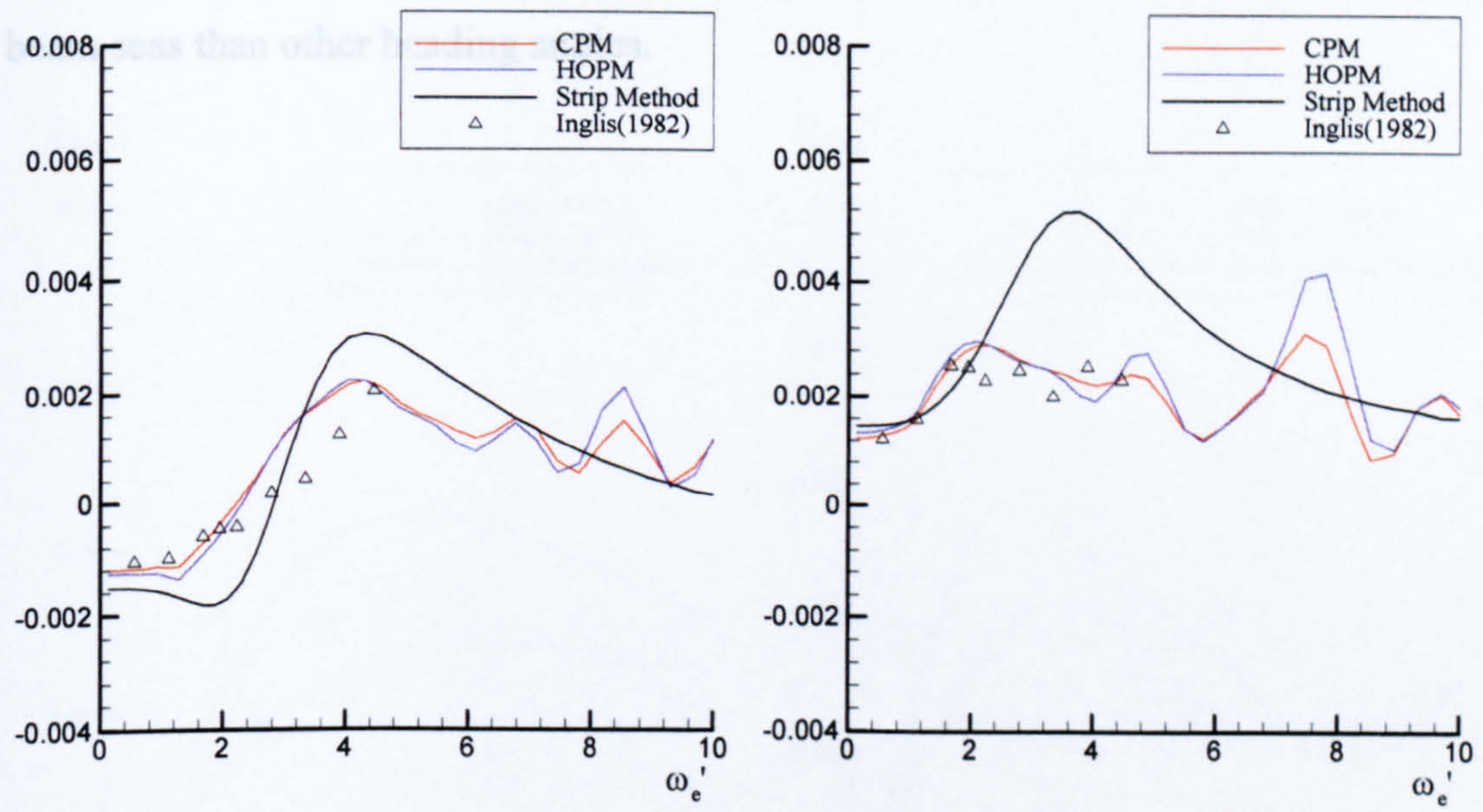

(b) Damping coefficients

Figure 7.38 Non-dimensional coupled added mass and damping coefficients in roll and yaw modes for Todd Series 60 travelling at Froude number 0.2

- Forward speed wave load

Wave exciting forces and moments acting on the hull surface of Todd Series 60 travelling at Froude number 0.2 are presented in Figure 7.39 through Figure 7.43. Non-dimensional amplitudes of heave force and pitch moment in head sea ($\beta = 180°$) were presented for comparisons with various numerical and experimental data as shown in Figure 7.39. A good agreement of heave exciting forces between the numerical methods and measured data is observed in the moderate frequency region while the results of pitch exciting moments show discrepancies in the same frequency region. Predicted sway force and yaw moment in bow sea show good agreement between two- and three-dimensional methods, while the results of heave force and pitch moment have differences as shown in Figure 7.42.

Figure 7.43 illustrates wave exciting forces and moments acting on the hull of Todd Series 60 travelling at Froude number 0.2 for various wave heading angles. As in the zero forward speed case the sway and heave exciting forces have larger values in beam seas than other heading angles.

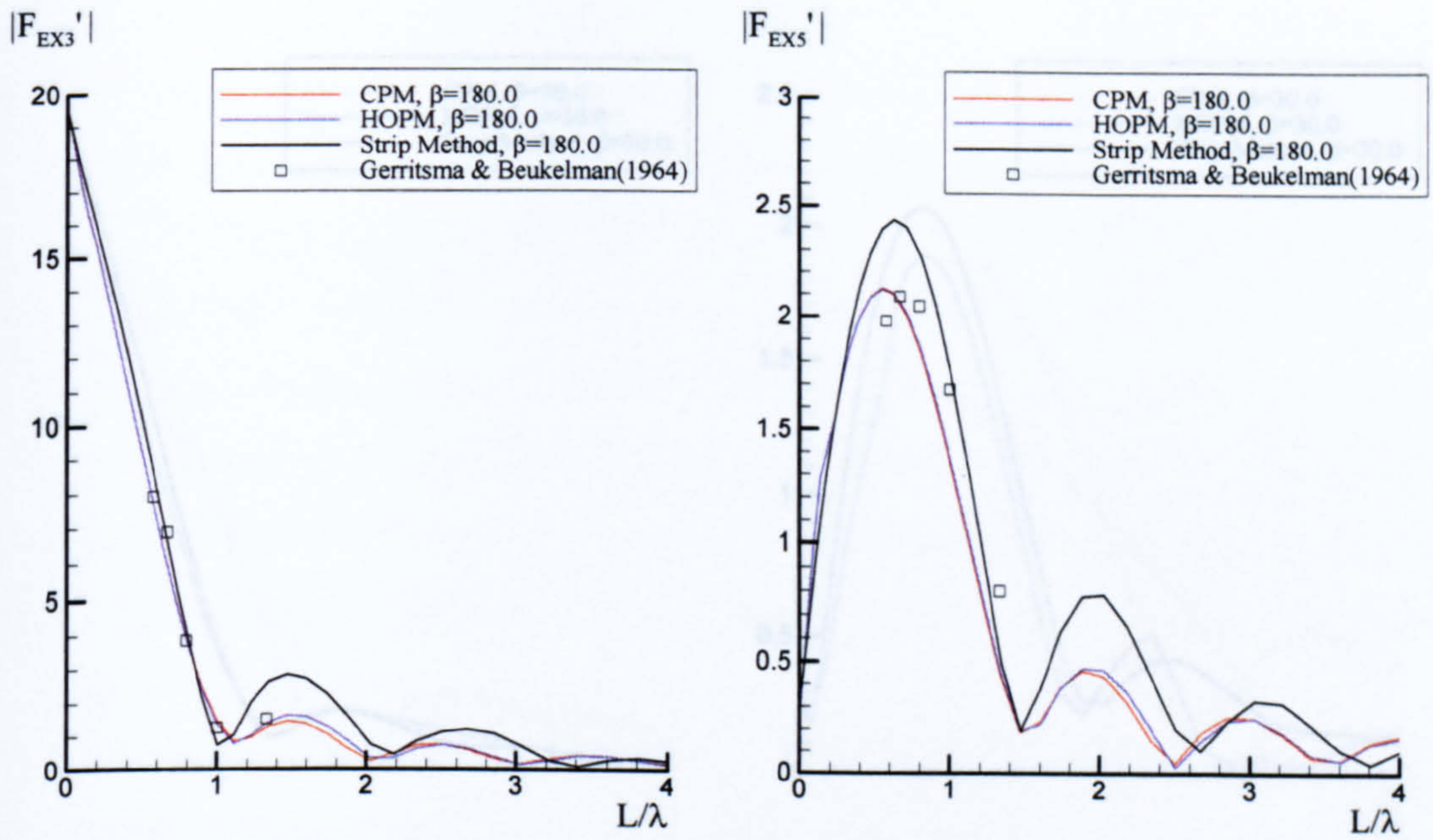

Figure 7.39 Non-dimensional heave and pitch wave exciting force and moment for Todd Series 60 travelling at Froude number 0.2 in head sea (β=180°)

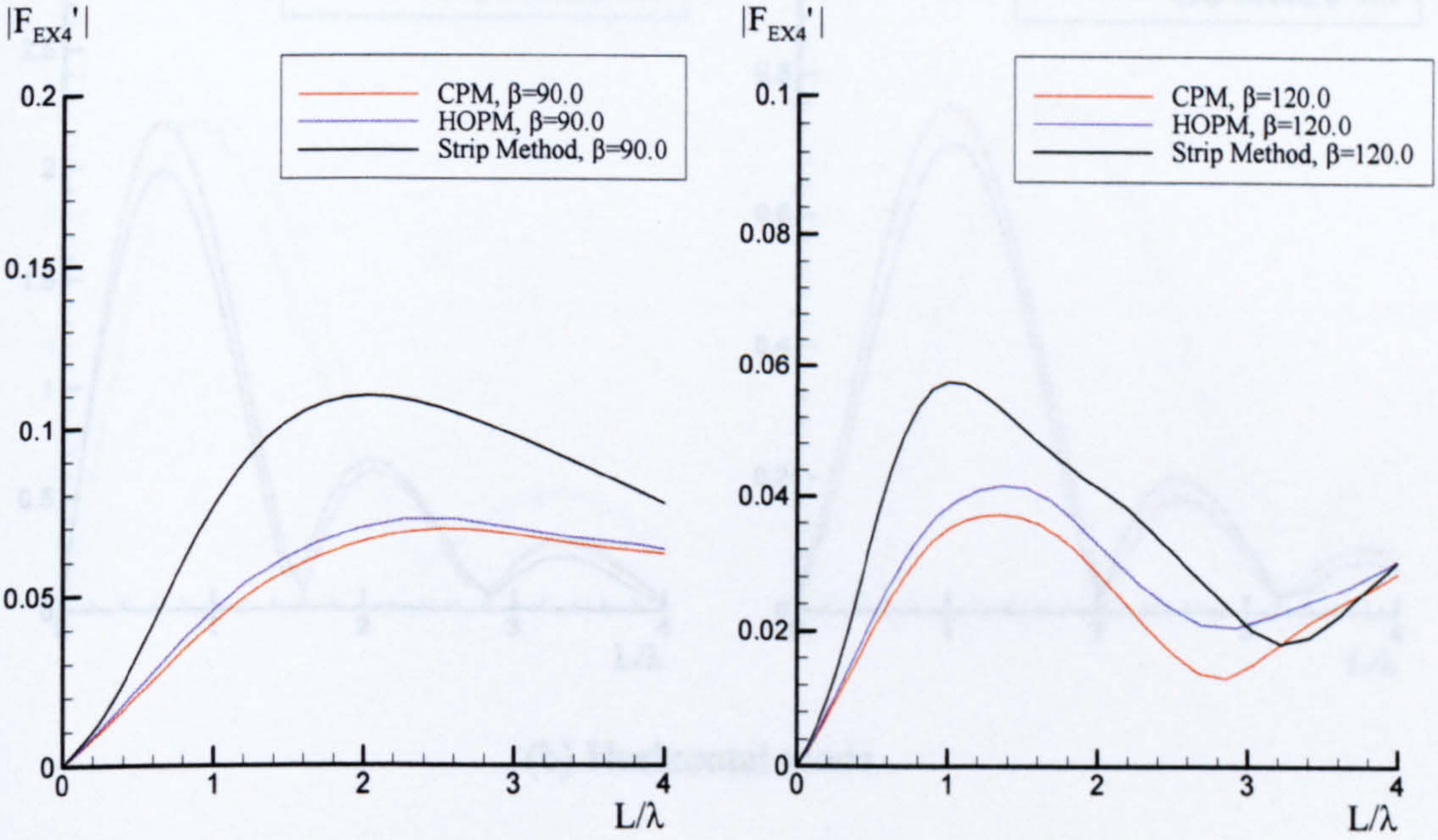

Figure 7.40 Non-dimensional roll wave exciting moment for Todd Series 60 travelling at Froude number 0.2 in beam sea (β=90°) and bow sea (β=120°)

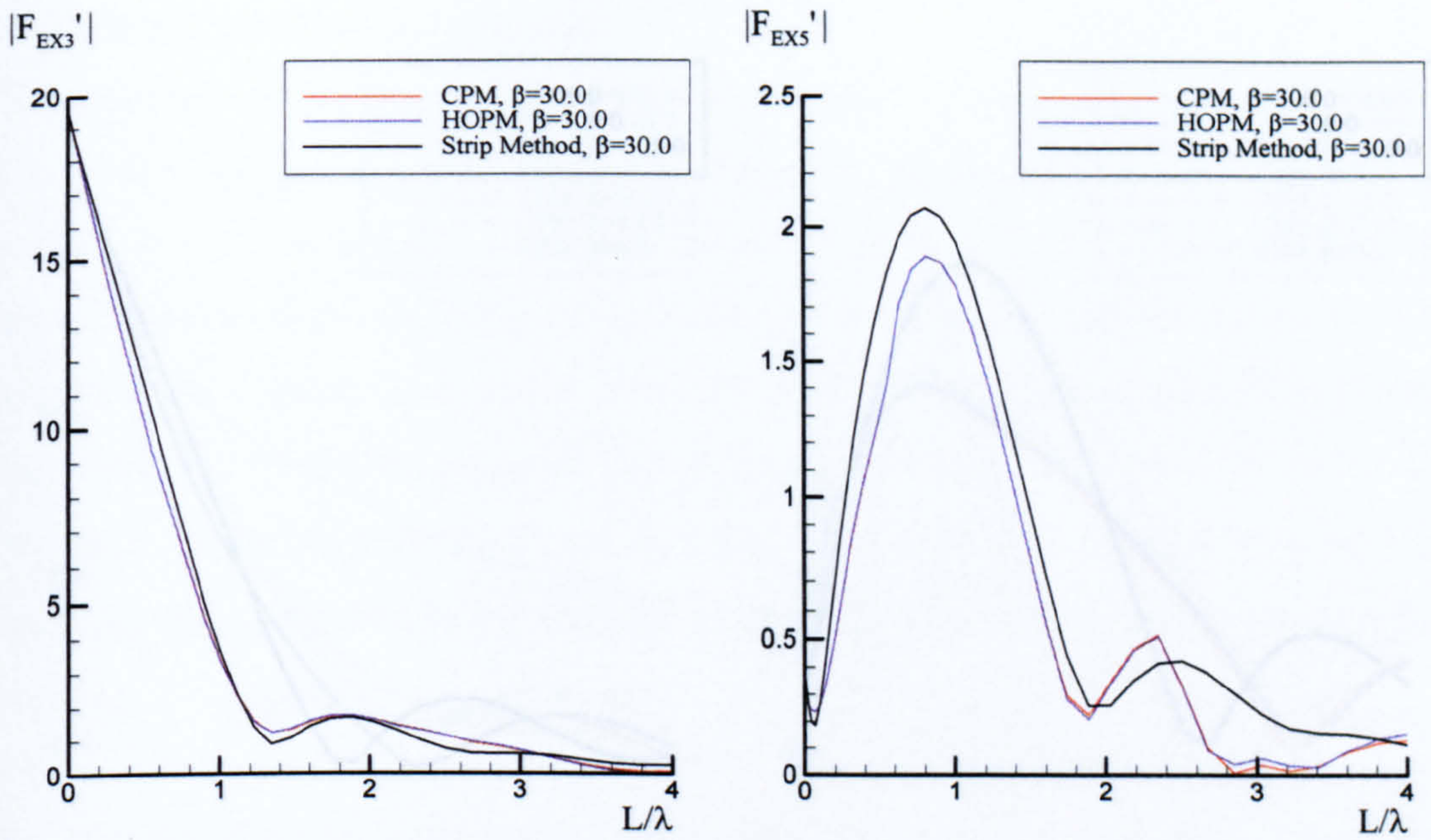

(a) Vertical mode

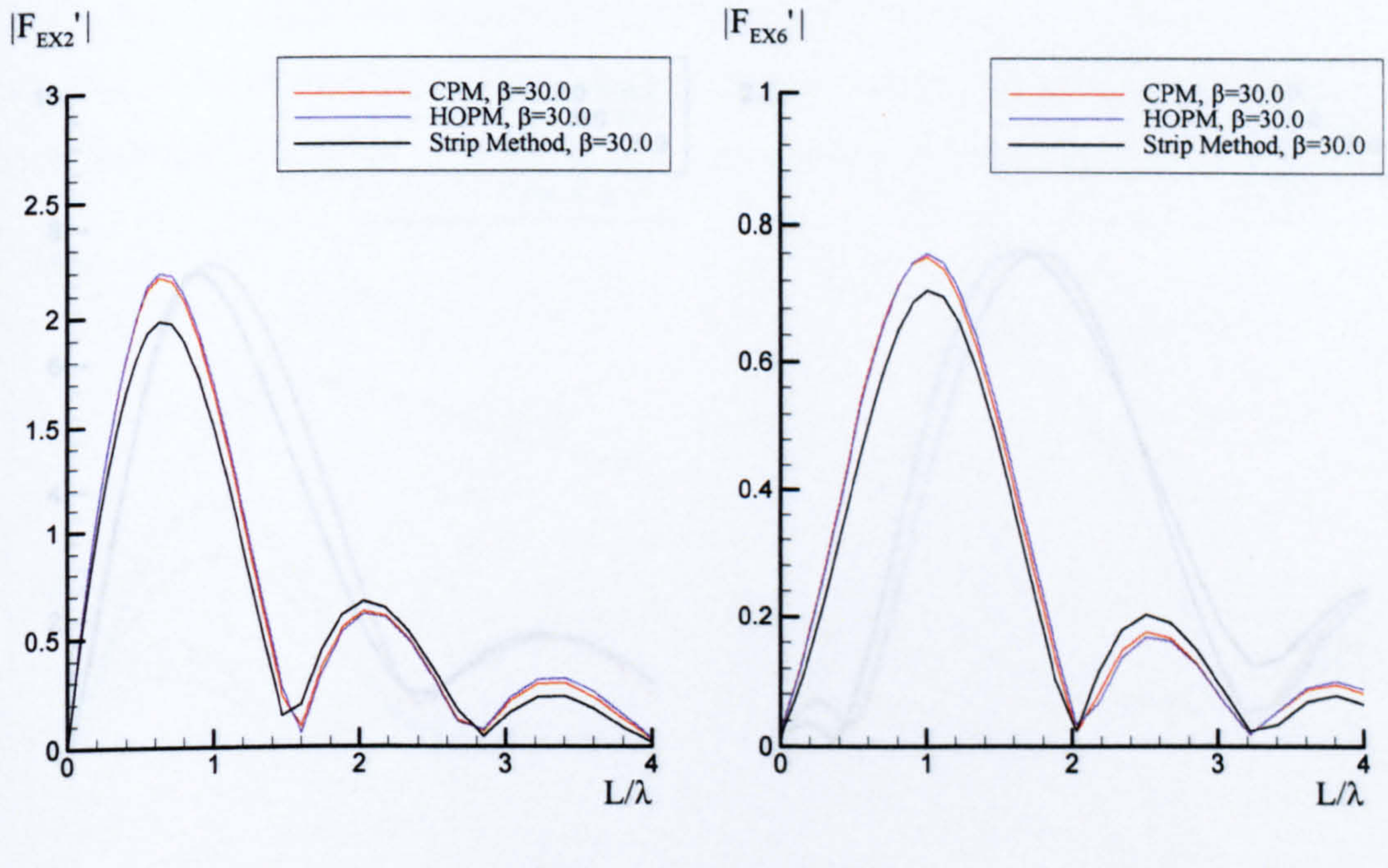

(b) Horizontal mode

Figure 7.41 Non-dimensional wave exciting forces and moments for Todd Series 60 travelling at Froude number 0.2 in quartering sea (β=30°)

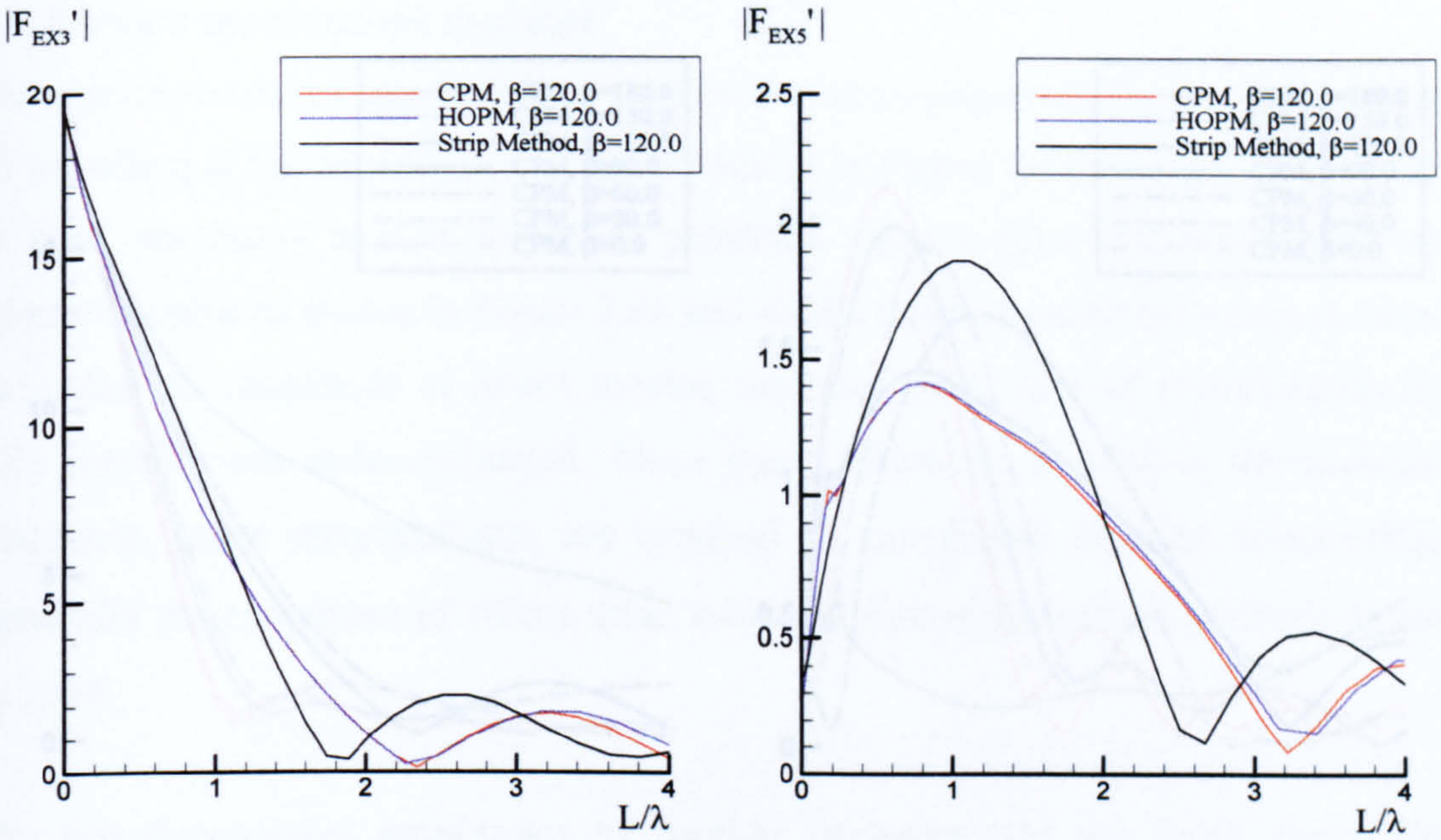

(a) Vertical mode

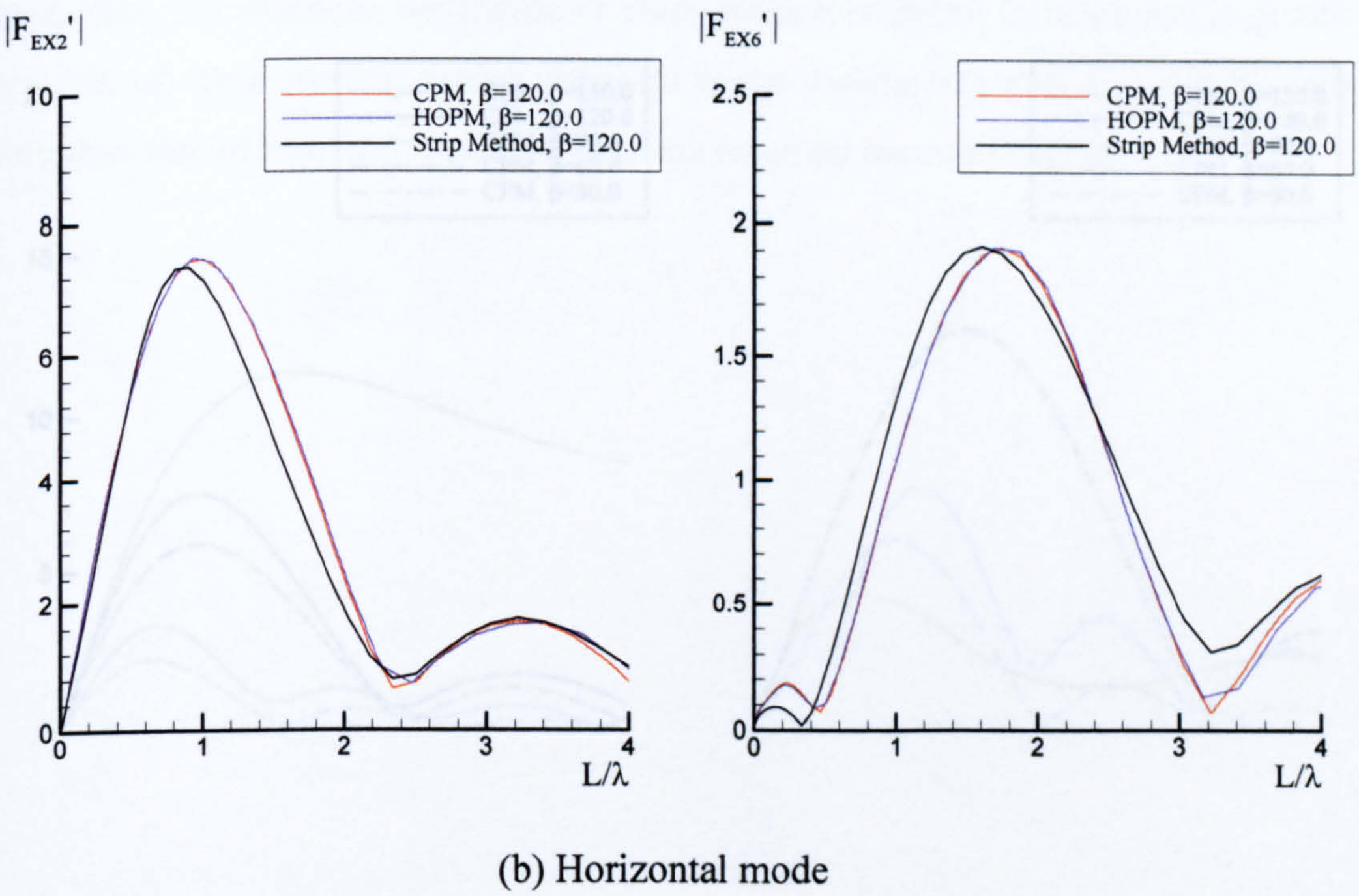

(b) Horizontal mode

Figure 7.42 Non-dimensional wave exciting forces and moments for Todd Series 60 travelling at Froude number 0.2 in bow sea (β=120°)

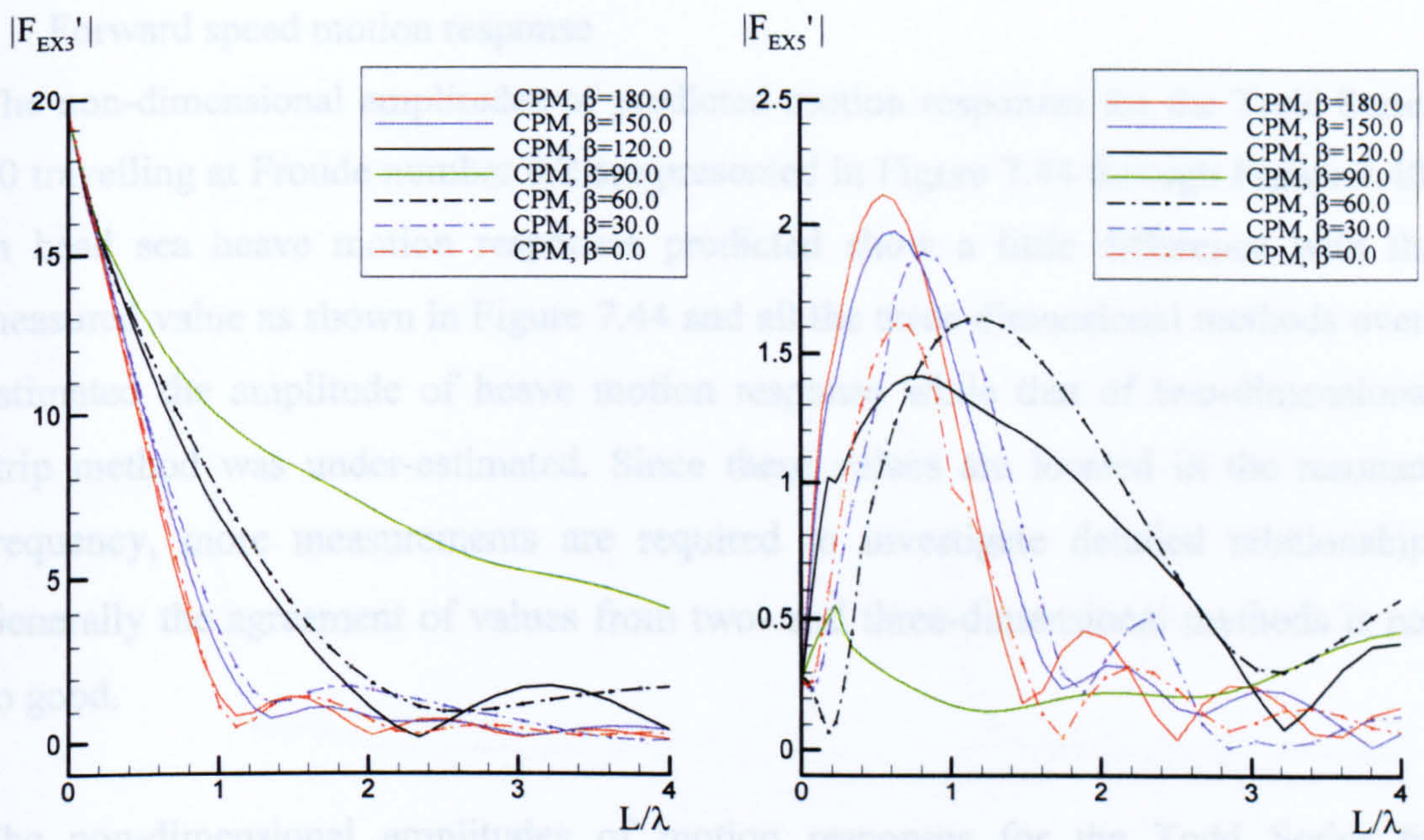

(a) Vertical mode

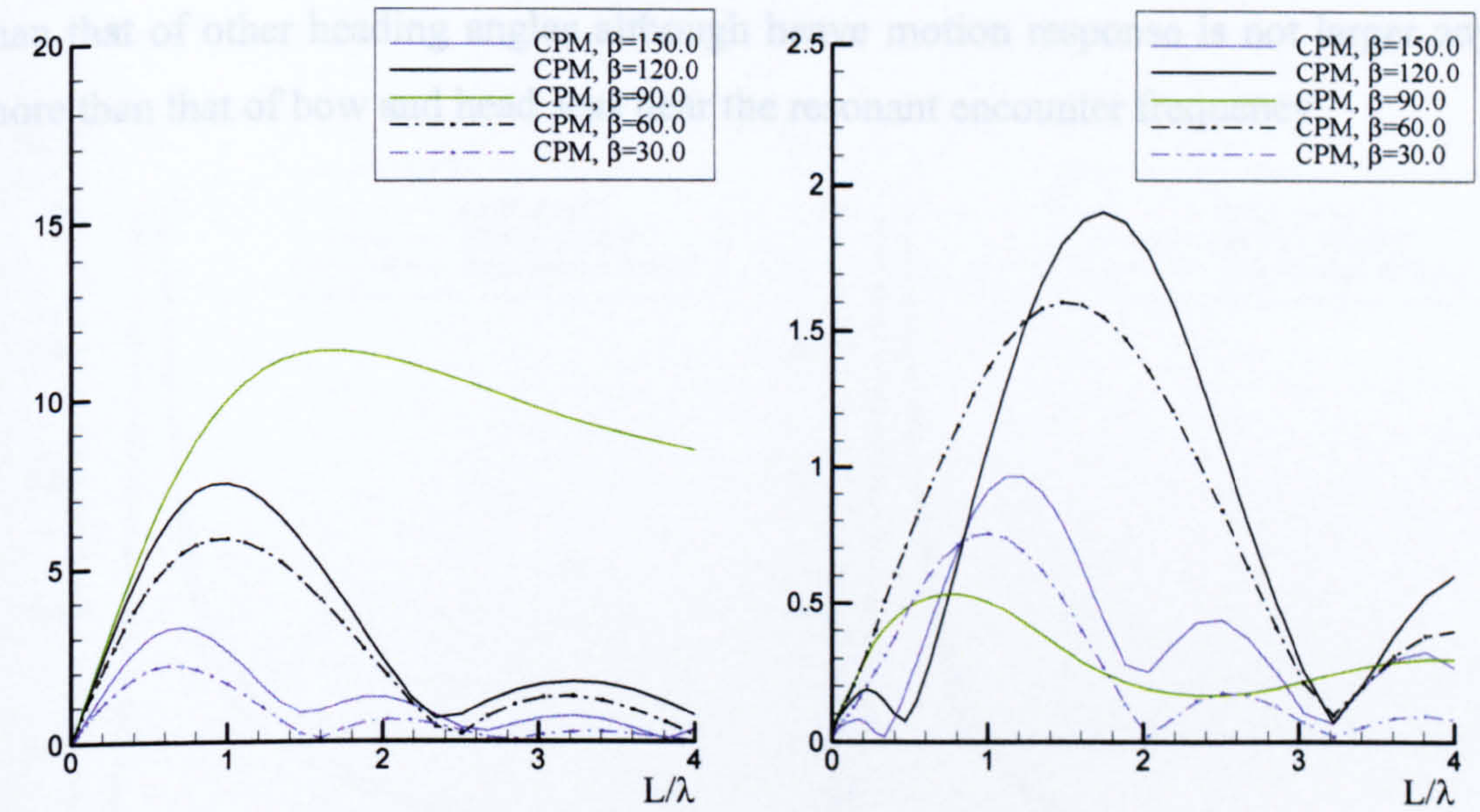

(b) Horizontal mode

Figure 7.43 Non-dimensional wave exciting forces and moments for Todd Series 60 travelling at Froude number 0.2 in various heading angles

- Forward speed motion response

The non-dimensional amplitudes of predicted motion responses for the Todd Series 60 travelling at Froude number 0.2 are presented in Figure 7.44 through Figure 7.48. In head sea heave motion responses predicted show a little difference with the measured value as shown in Figure 7.44 and all the three-dimensional methods over-estimated the amplitude of heave motion response while that of two-dimensional strip method was under-estimated. Since these values are located in the resonant frequency, more measurements are required to investigate detailed relationship. Generally the agreement of values from two- and three-dimensional methods is not so good.

The non-dimensional amplitudes of motion responses for the Todd Series 60 travelling at Froude number 0.2 in various heading angles are presented in Figure 7.48. Some trends observed in the zero speed case can be found again for the forward speed case. For example, amplitude of sway motion response in beam sea is greater than that of other heading angles although heave motion response is not larger any more than that of bow and head seas near the resonant encounter frequency.

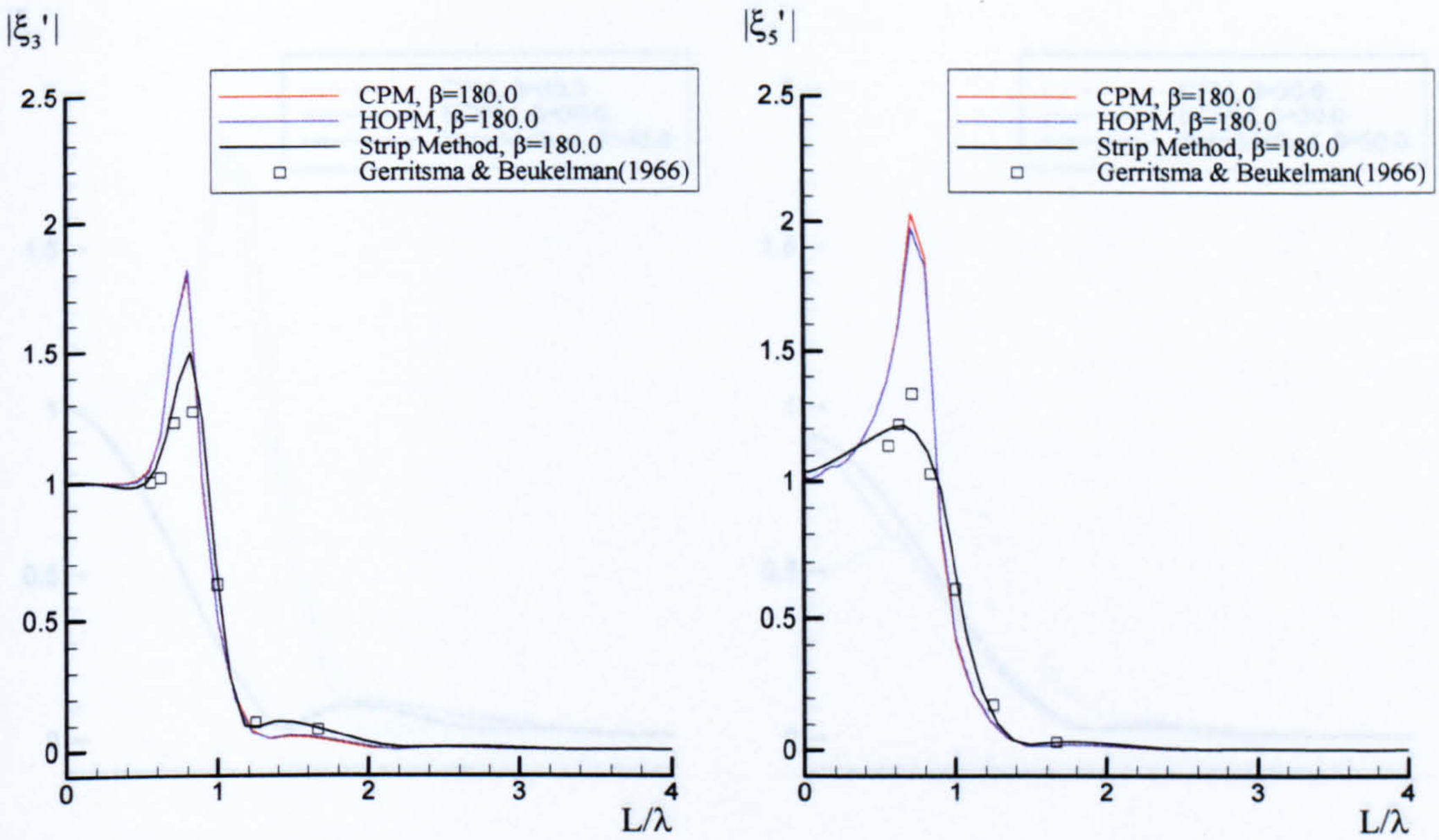

Figure 7.44 Non-dimensional heave and pitch motion responses for Todd Series 60 travelling at Froude number 0.2 in head sea (β=180°)

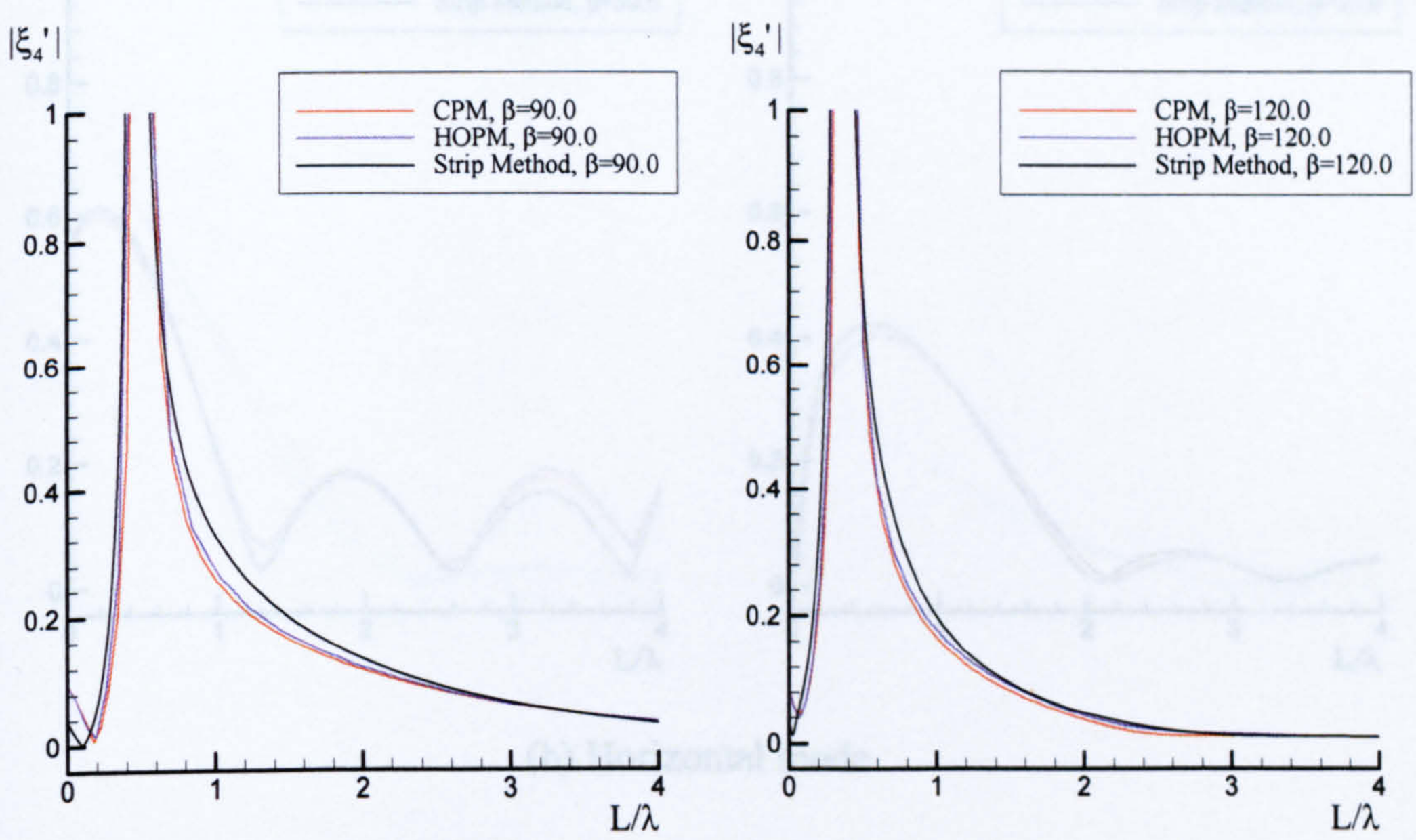

Figure 7.45 Non-dimensional roll motion response for Todd Series 60 travelling at Froude number 0.2 in beam sea (β=90°) and bow sea (β=120°)

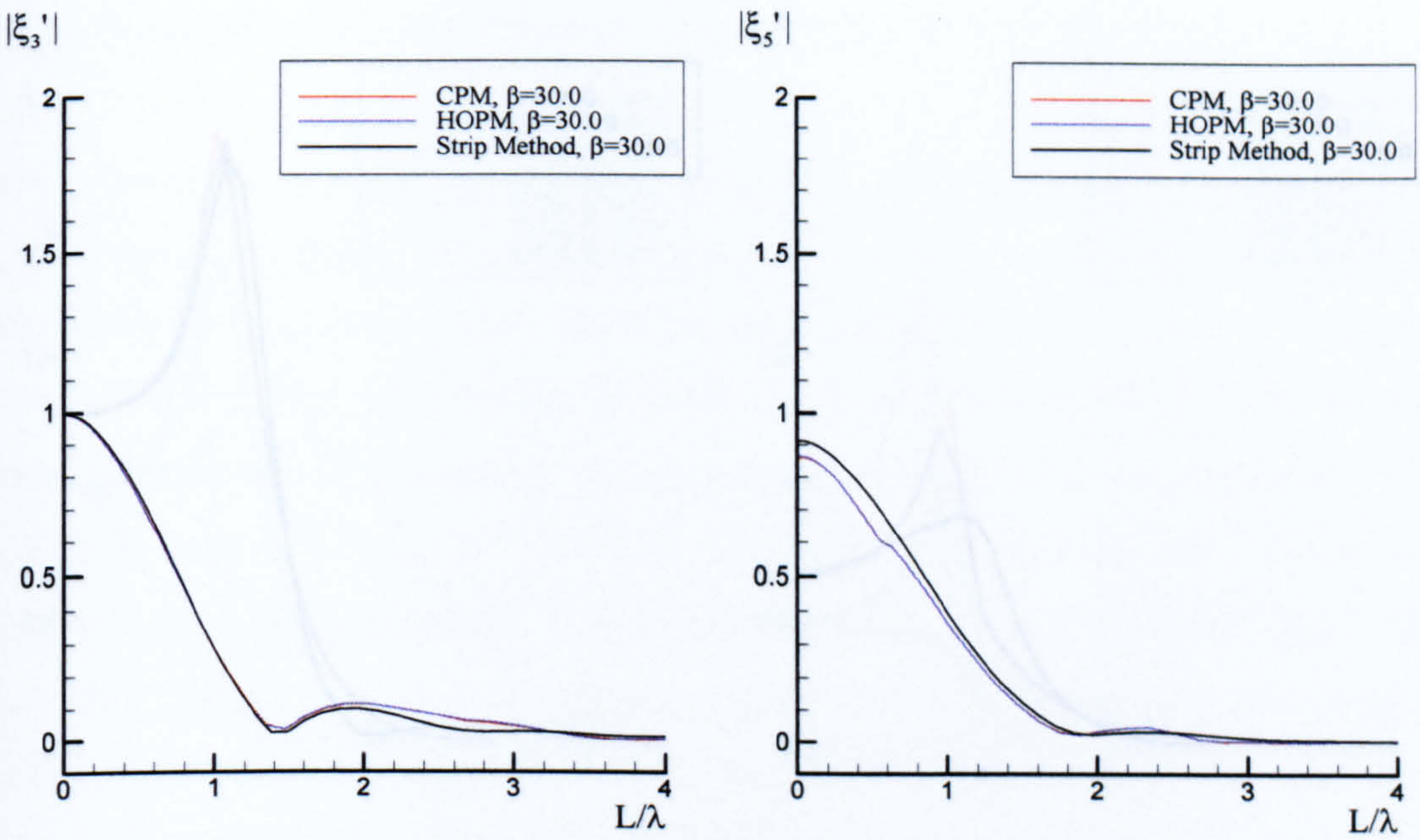

(a) Vertical mode

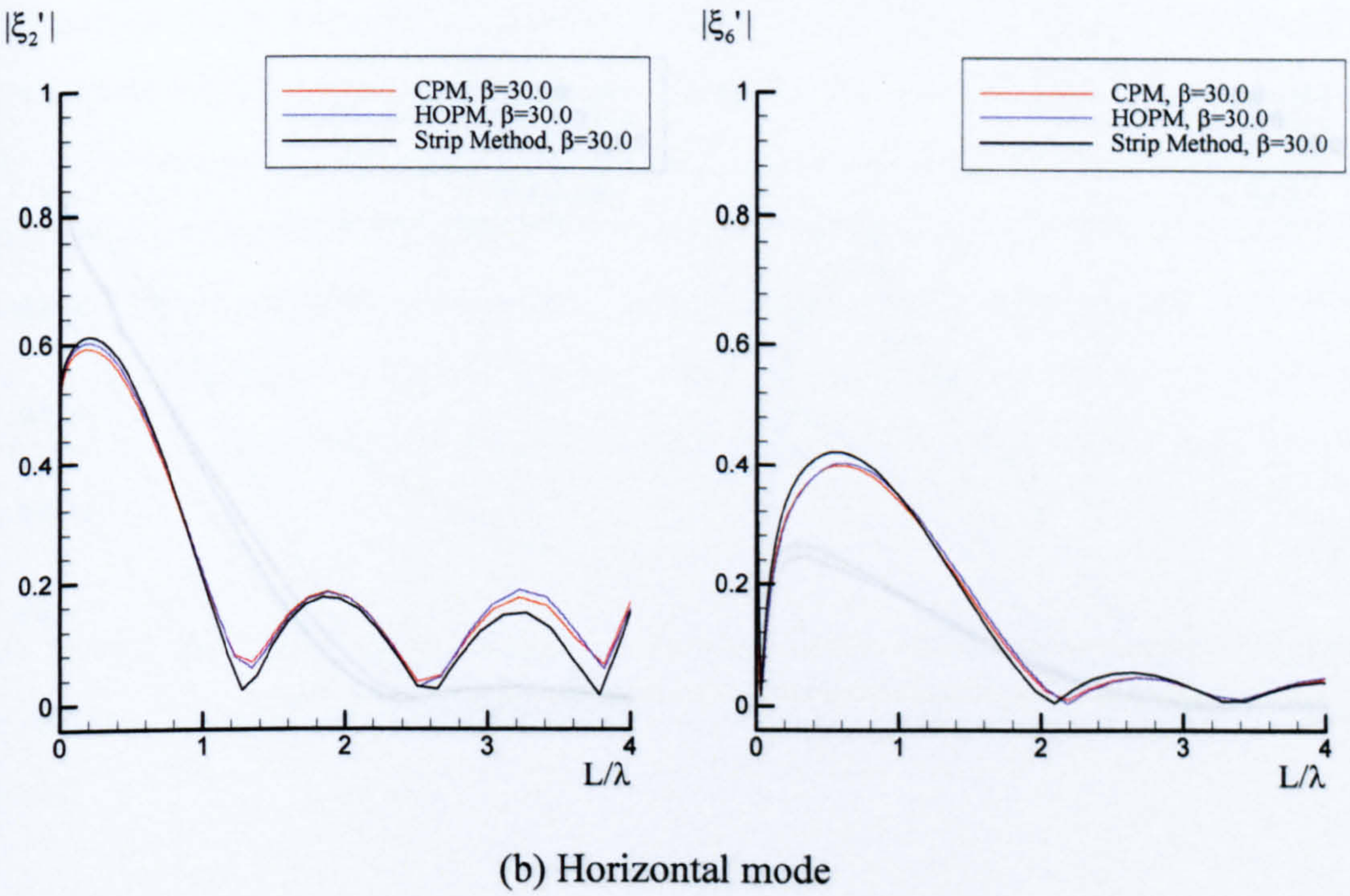

(b) Horizontal mode

Figure 7.46 Non-dimensional motion responses for Todd Series 60 travelling at Froude number 0.2 in quartering sea (β=30°)

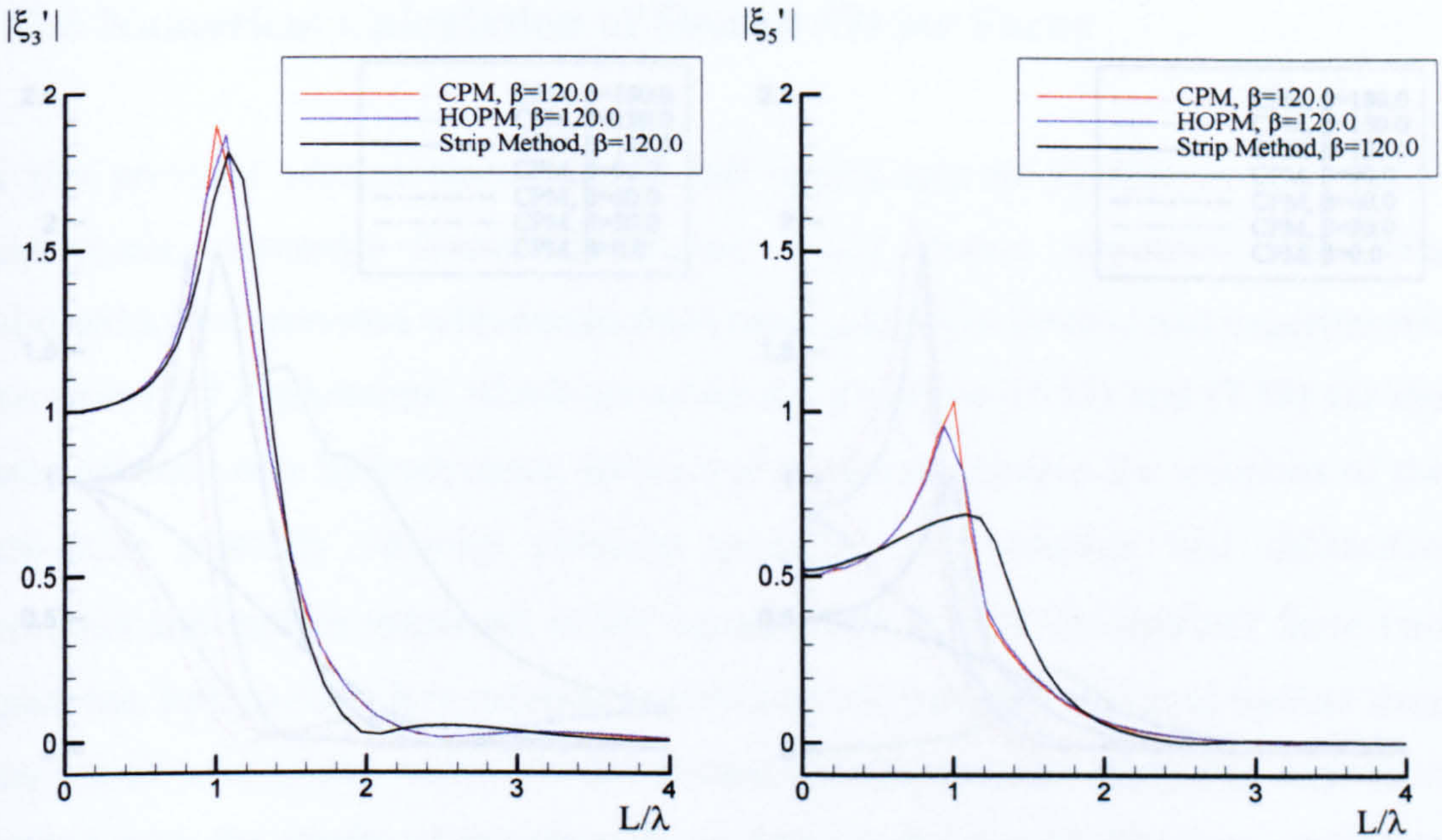

(a) Vertical mode

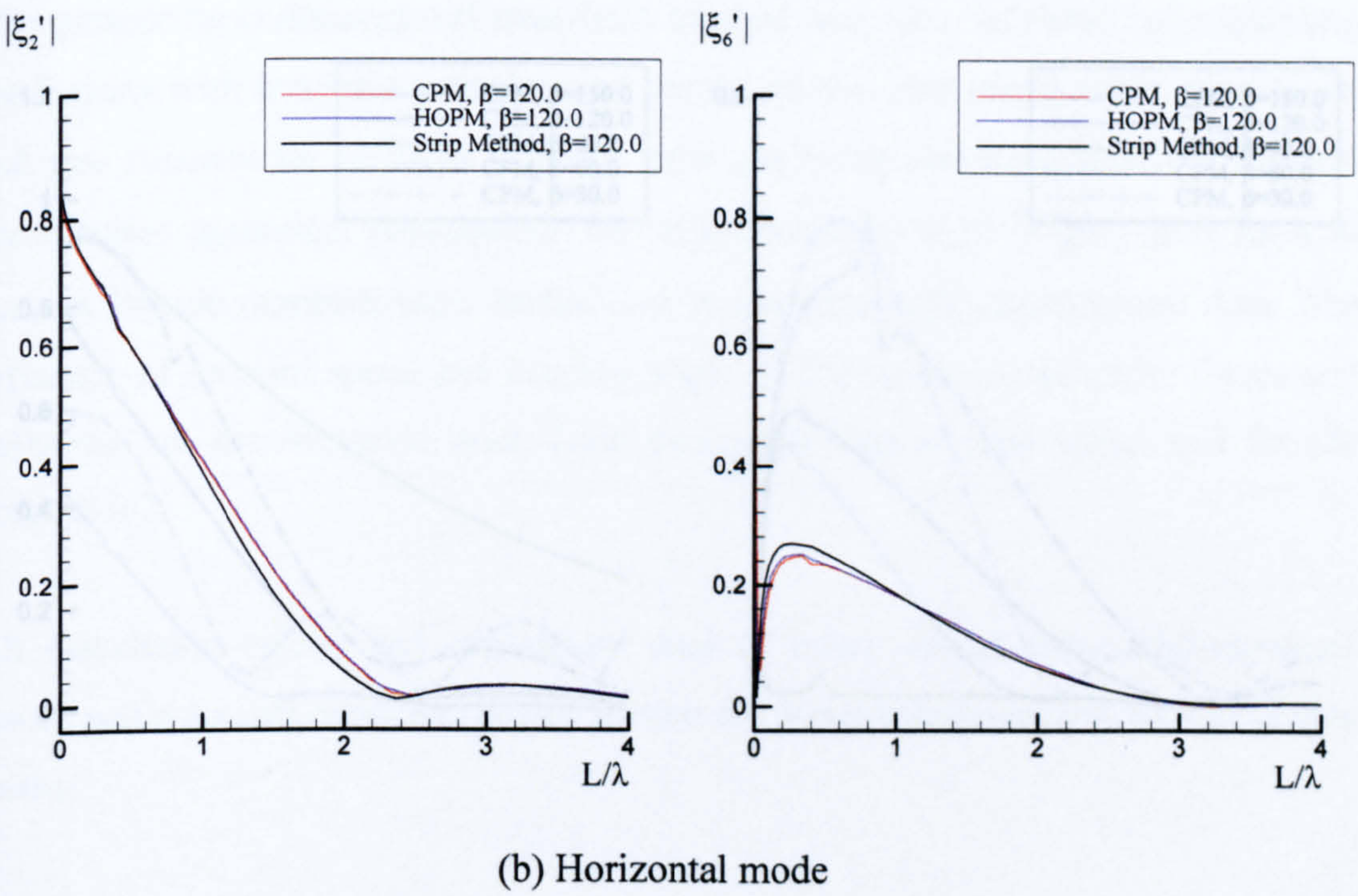

(b) Horizontal mode

Figure 7.47 Non-dimensional motion responses for Todd Series 60 travelling at Froude number 0.2 in bow sea (β=120°)

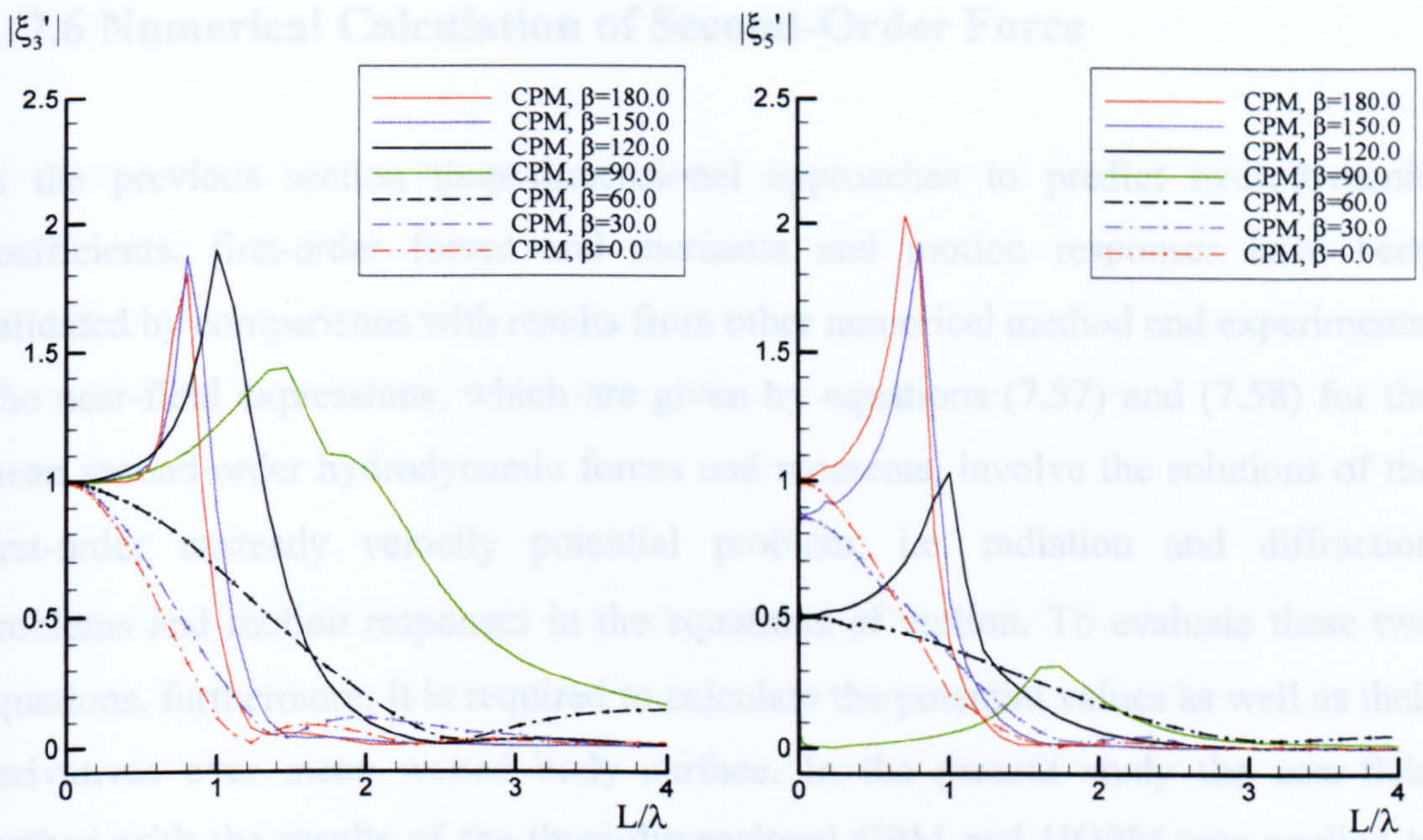

(a) Vertical mode

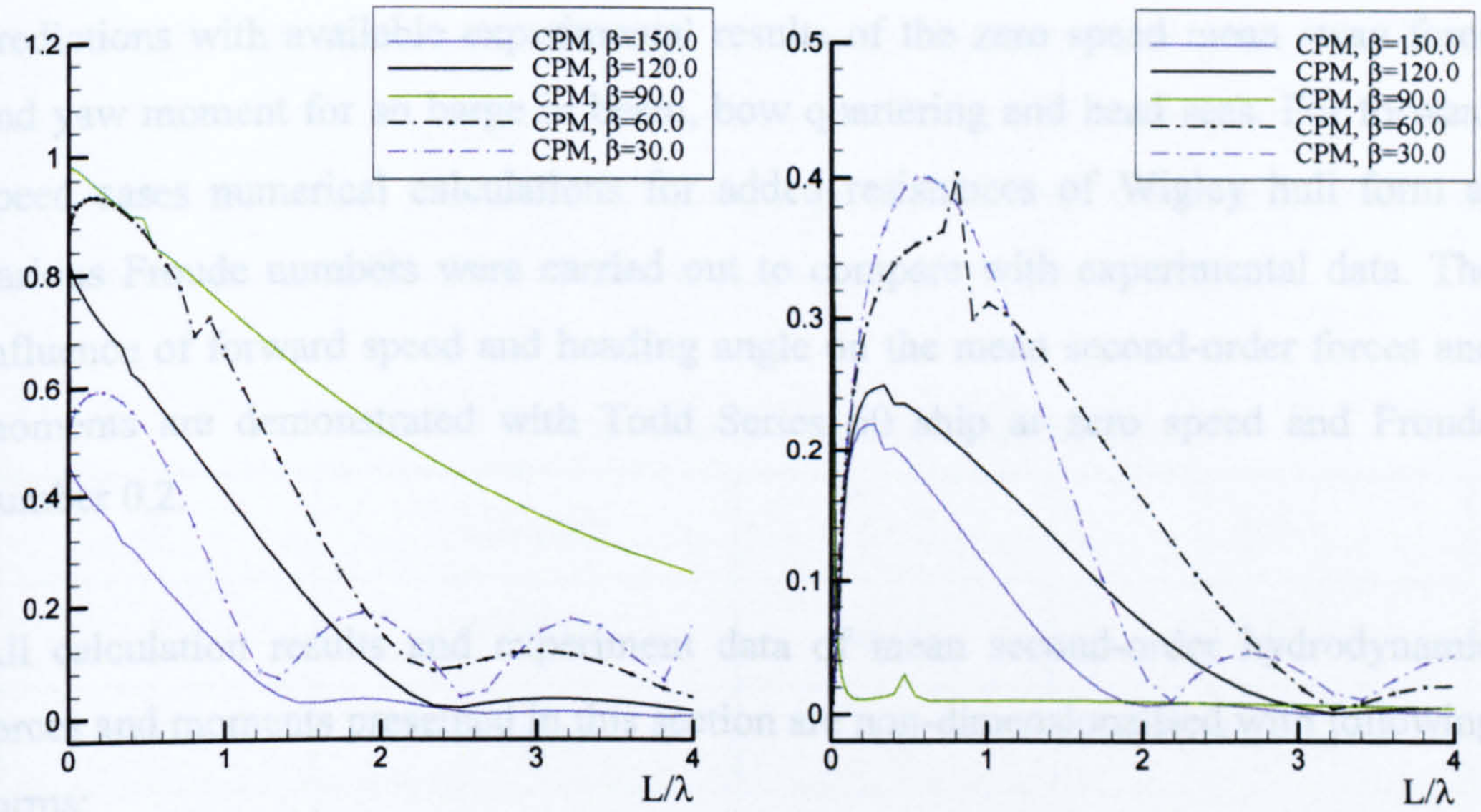

(b) Horizontal mode

Figure 7.48 Non-dimensional motion responses for Todd Series 60 travelling at Froude number 0.2in various heading angles

7.6 Numerical Calculation of Second-Order Force

In the previous section three-dimensional approaches to predict hydrodynamic coefficients, first-order forces and moments and motion responses have been validated by comparisons with results from other numerical method and experiments. The near-field expressions, which are given by equations (7.57) and (7.58) for the mean second-order hydrodynamic forces and moments, involve the solutions of the first-order unsteady velocity potential problem, i.e. radiation and diffraction problems and motion responses in the equations of motion. To evaluate these two equations, furthermore, it is required to calculate the potential values as well as their derivatives over mean wetted body surface. In the present study the near-field method with the results of the three-dimensional CPM and HOPM was applied to carry out numerical calculations.

The present three-dimensional near-field method was first validated by comparing predictions with available experimental results of the zero speed mean sway force and yaw moment for an barge in beam, bow quartering and head seas. For forward speed cases numerical calculations for added resistances of Wigley hull form at various Froude numbers were carried out to compare with experimental data. The influence of forward speed and heading angle on the mean second-order forces and moments are demonstrated with Todd Series 60 ship at zero speed and Froude number 0.2.

All calculation results and experiment data of mean second-order hydrodynamic forces and moments presented in this section are non-dimensionalised with following forms;

- Mean second-order force

$$F_j^{(2)'} = \left\langle F_j^{(2)} \right\rangle \Big/ \rho g a_0^2 B^2 / L \qquad \text{when } j = 1,2,3$$

$$F_{j+3}^{(2)'} = \left\langle M_j^{(2)} \right\rangle \Big/ \rho g a_0^2 B L \qquad \text{when } j = 1,2,3 \qquad (7.66)$$

7.6.1 Barge

The barge used in the calculation has a rectangular hull and it is possible to model exactly with flat panels. The hull form of barge is discretised with a total 672 flat quadrilateral panels whose aspect ratio in bottom plane was kept as unity as shown in Figure 7.49. The principal dimensions of barge in the calculation is illustrated in Table 7.5

Numerical calculations for the second-order hydrodynamic forces and moments acting on the stationary barge were carried out in three different heading angles, i.e. beam ($\beta = 90°$), bow ($\beta = 135°$) and head seas ($\beta = 180°$) respectively. The calculation results were compared with the numerical and experimental data performed by Pinkster and van Oortmerssen (1977).

Figure 7.50 illustrates surge drift force in head sea and sway drift force in beam sea respectively. The agreement of surge drift force between numerical result and measured data looks very good. There exists, however, discrepancy in the case of sway drift force, which is under-estimated for present method and measurement data are scattered due to difficulties of measurement in high frequency region.

Table 7.5 Principal dimensions of barge model

L	150 [m]	L/B	3.0
B	50 [m]	B/T	5.0
T	10 [m]	k_{xx}	20.0 [m]
∇	73750 [m³]	k_{yy}	39.0 [m]
C_B	0.9833	k_{zz}	39.0 [m]
C_w	1.0	$\overline{GM}_T$	16.243 [m]
LCB	0.0 [m]	$\overline{GM}_L$	185.735 [m]

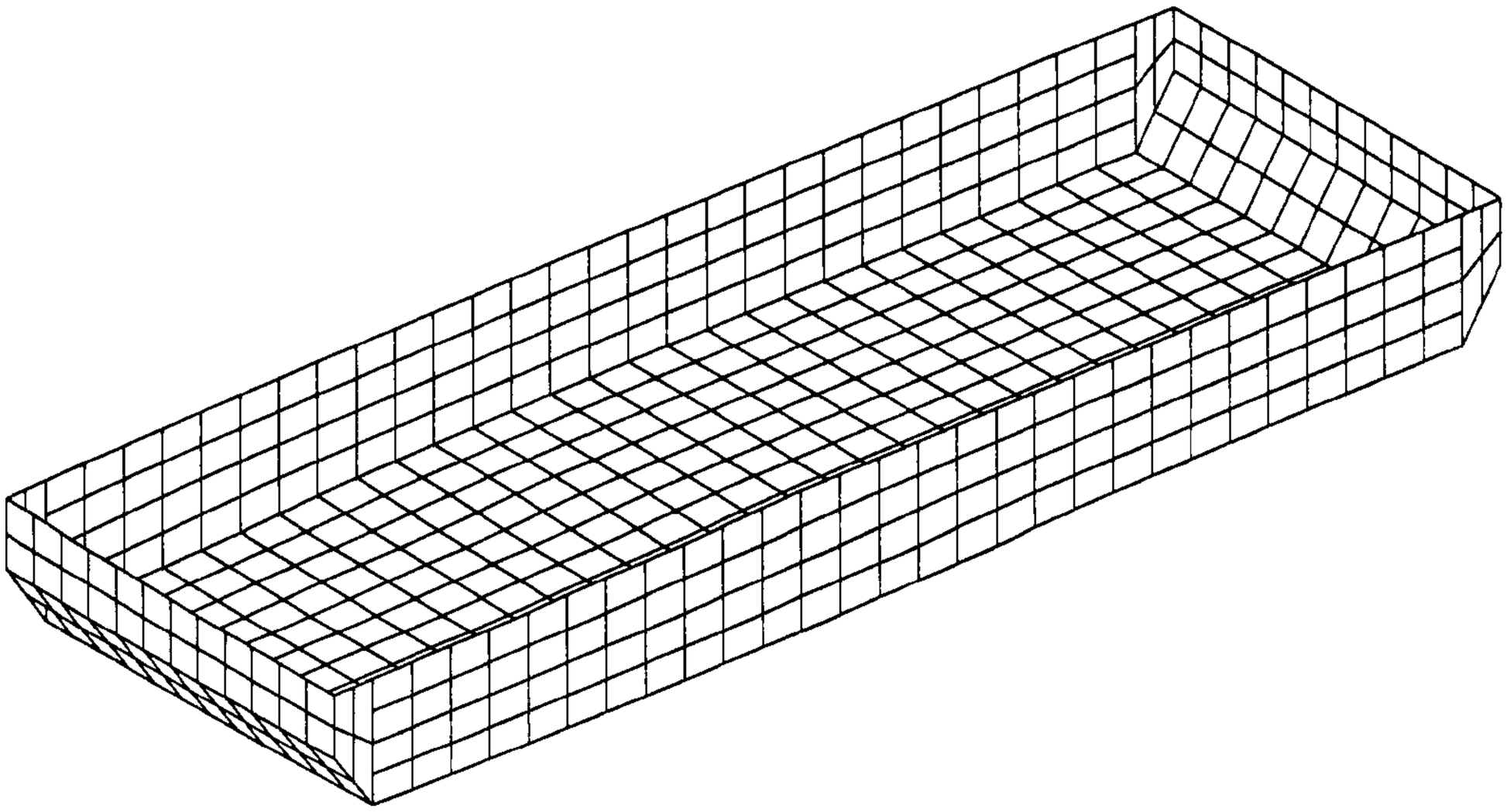

Figure 7.49 Panel representation of barge hull form

Second-order sway force and yaw moment in bow sea are presented in Figure 7.51. The agreement of sway drift force between theoretical prediction and measurement is very good. The sway force and yaw moment show peak values near the non-dimensional frequency, $\omega_e' = 2.0$, which coincides with frequency of roll resonance. As mentioned in the beginning of this section, the second-order forces and moments are strongly coupled with first-order motion responses. It is, therefore, thought that the discrepancy in yaw moment is caused by the neglect of viscous effect in the prediction of first-order roll motion.

The components of second-order hydrodynamic forces on the stationary barge are illustrated in Figure 7.52 and Figure 7.53. Full description of each force component is provided in section 7.4.2. Component I represents the force due to relative wave elevation and is seen as a dominant component in the total force. The sign of component I is generally coincides with the direction of wave propagation and this implies that the force on the facing side of incoming wave is larger than that on the shadow side of the hull. It is also noticed that the value of component I is reduced by

remaining components I in the whole frequency range. The component II represents the pressure field due to the product of first-order velocity on the mean wetted body surface. The component II tends to act on the opposite direction to the incoming wave because the first-order velocity field is larger again on the facing side than that on the shadow side.

The component III and IV correct the first-order pressure field and the first-order forces respectively on the mean wetted body surface to those on the instantaneous wetted body surface due to oscillatory motions. The contributions of components III and IV become largest when there is considerable amount of oscillation since they depend strongly on oscillatory motions of the rigid body, and therefore they can be neglected in the high frequency region. Their overall contributions on total second-order forces are small when compared to the components I and II. The component V becomes zeros for surge, sway and yaw directions and so is component VI for zero speed. Most components of sway and yaw directions shows slight irregularities due to resonance of roll motion and the existence of irregular frequency phenomenon in higher frequency regions.

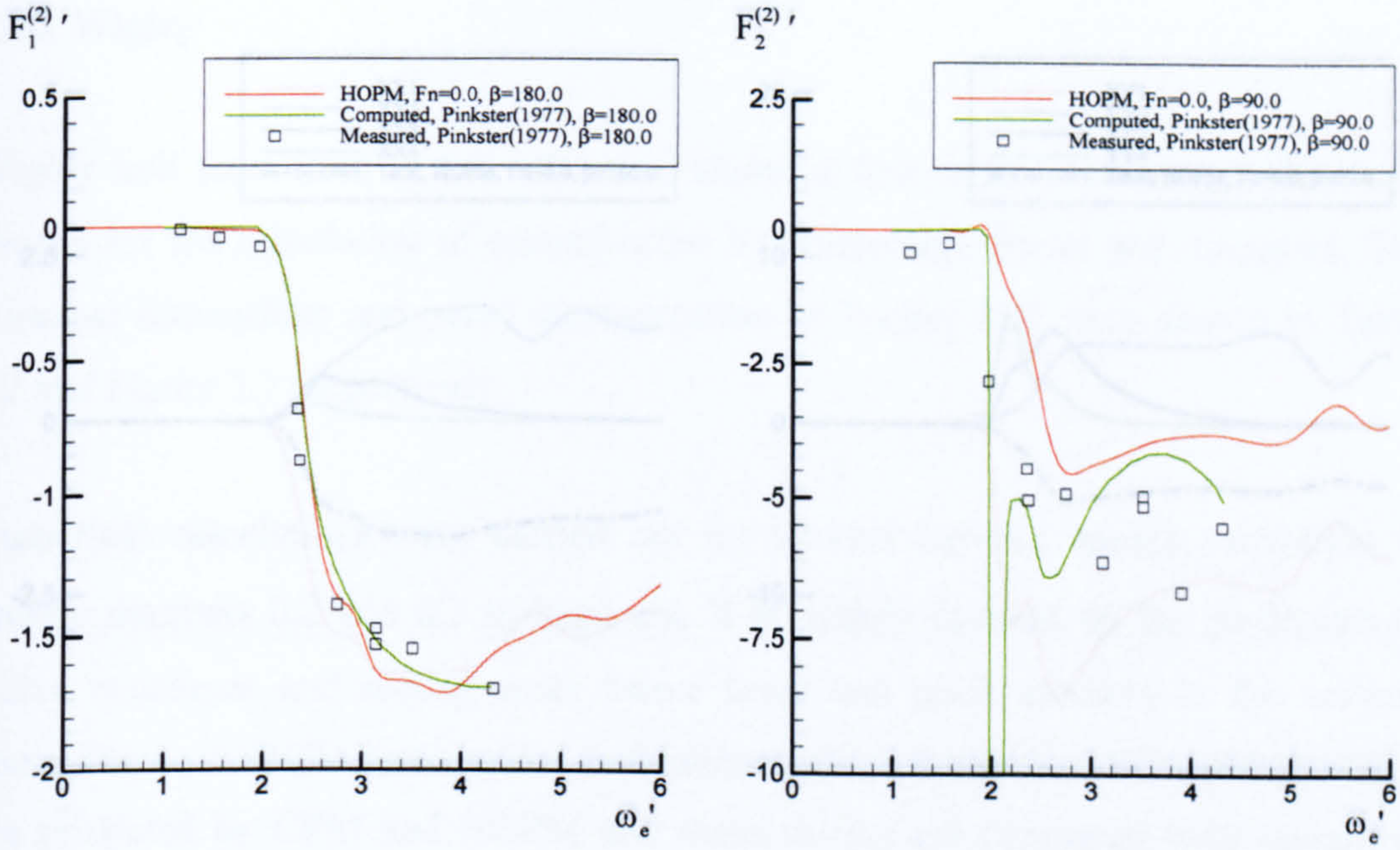

Figure 7.50 Non-dimensional second-order surge and sway forces for barge at zero speed in head sea (β=180°) and beam sea (β=90°)

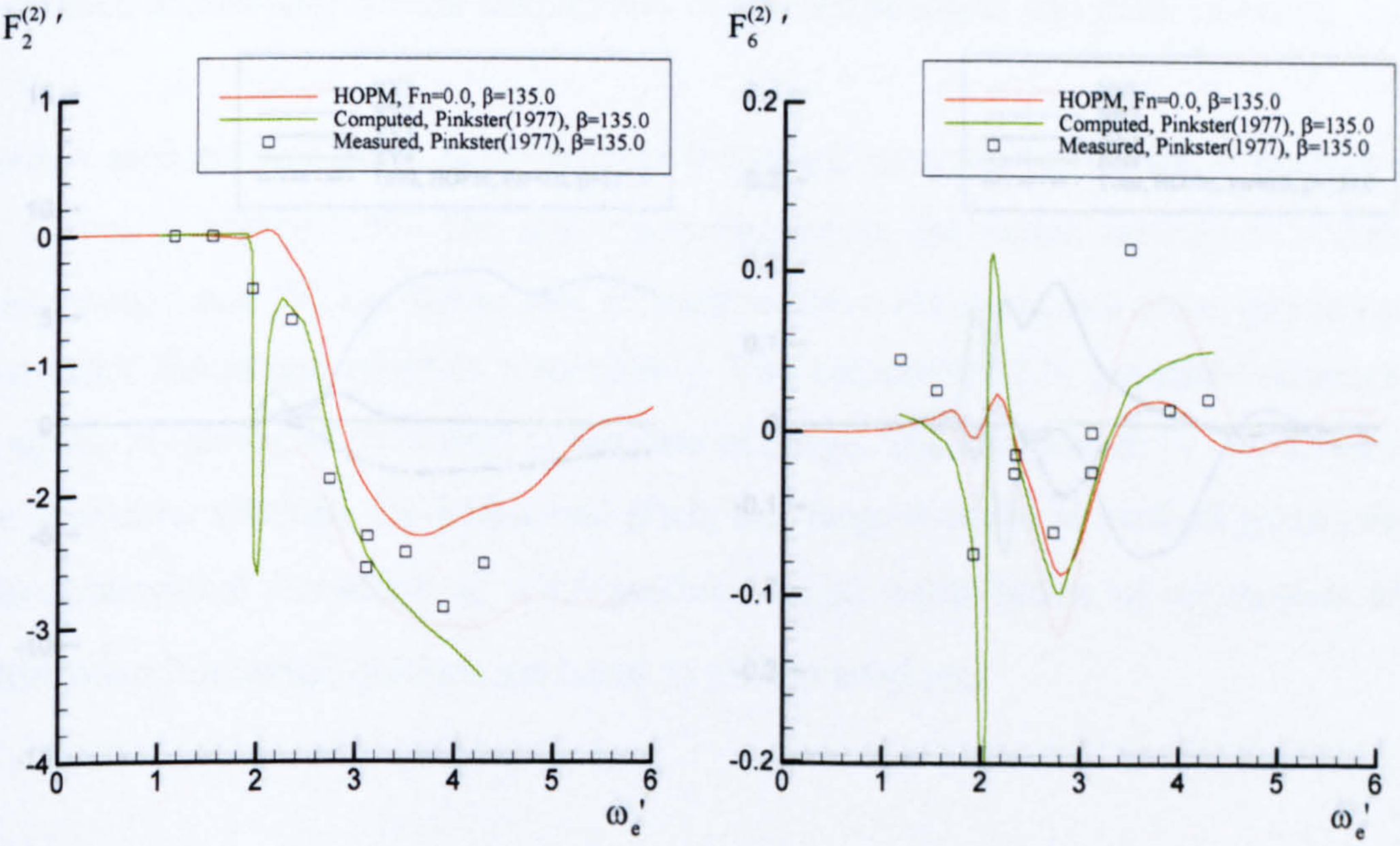

Figure 7.51 Non-dimensional second-order sway force and yaw moment for barge at zero speed in bow sea (β=135°)

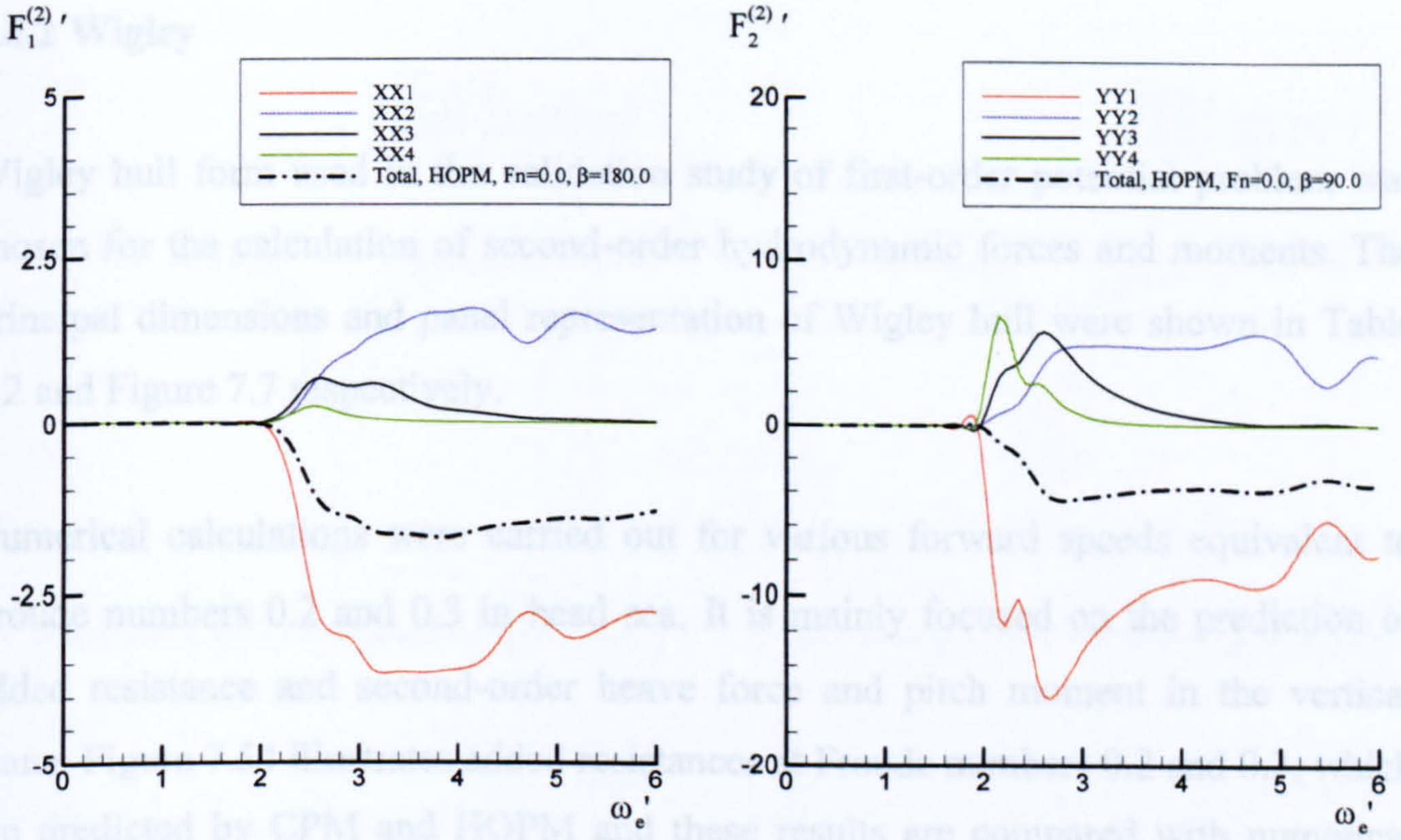

Figure 7.52 Non-dimensional components of second-order surge and sway forces for barge at zero speed in head sea (β=180°) and beam sea (β=90°)

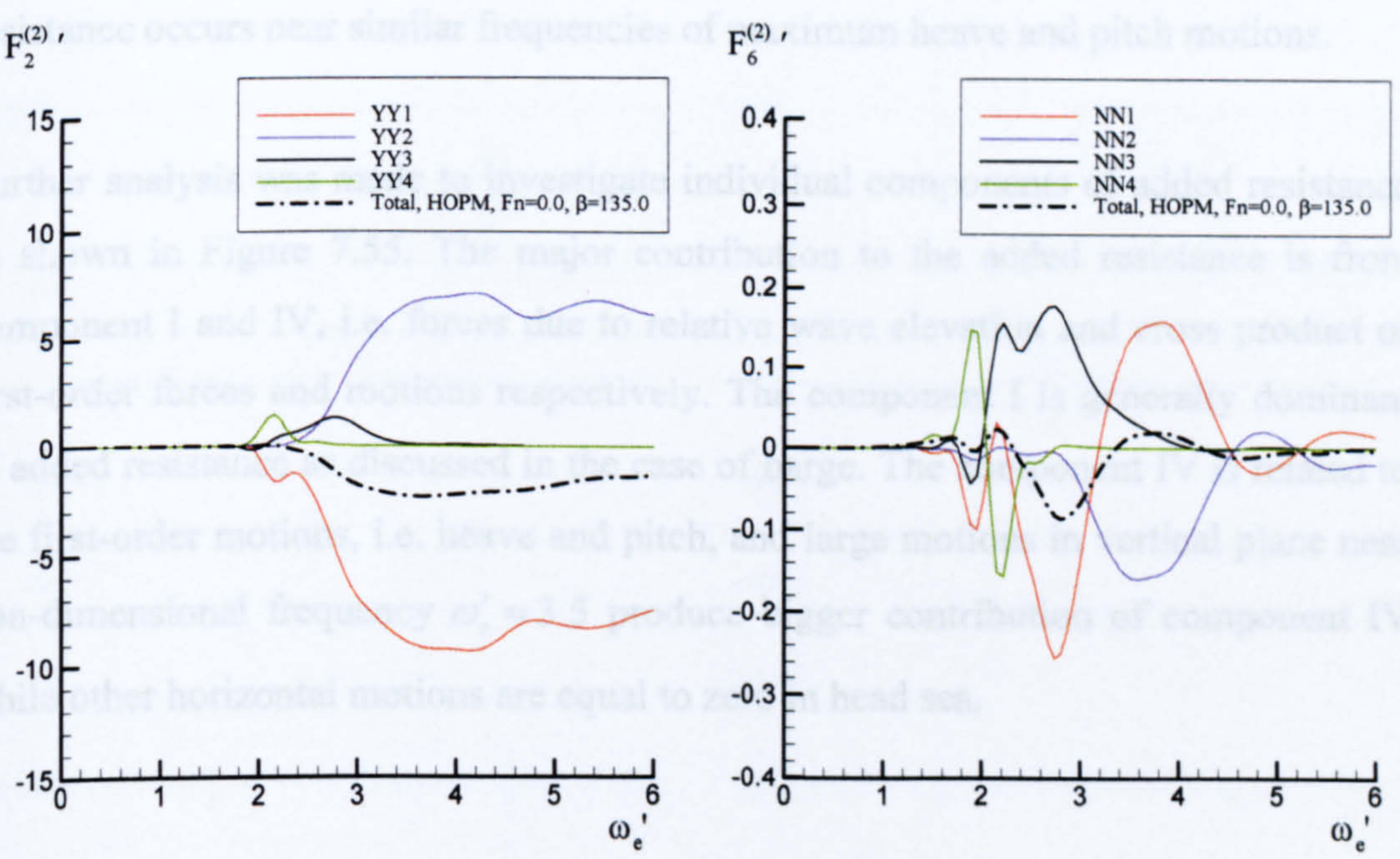

Figure 7.53 Non-dimensional components of second-order sway force and yaw moment for barge at zero speed in bow sea (β=135°)

7.6.2 Wigley

Wigley hull form used in the validation study of first-order potential problem was chosen for the calculation of second-order hydrodynamic forces and moments. The principal dimensions and panel representation of Wigley hull were shown in Table 7.2 and Figure 7.7 respectively.

Numerical calculations were carried out for various forward speeds equivalent to Froude numbers 0.2 and 0.3 in head sea. It is mainly focused on the prediction of added resistance and second-order heave force and pitch moment in the vertical plane. Figure 7.54 illustrates added resistances at Froude numbers 0.2 and 0.3, which are predicted by CPM and HOPM and these results are compared with numerical results of strip theory and experiment data by Journee (1992). The discrepancy at Froude number 0.2 shows that the peak value of prediction is under-estimated compared to that of measurement and result of Froude number 0.3 shows very little difference with experiment data. It is noted that the frequency of maximum added resistance occurs near similar frequencies of maximum heave and pitch motions.

Further analysis was made to investigate individual components of added resistance as shown in Figure 7.55. The major contribution to the added resistance is from component I and IV, i.e. forces due to relative wave elevation and cross product of first-order forces and motions respectively. The component I is generally dominant in added resistance as discussed in the case of barge. The component IV is related to the first-order motions, i.e. heave and pitch, and large motions in vertical plane near non-dimensional frequency $\omega_e' = 3.5$ produce bigger contribution of component IV while other horizontal motions are equal to zero in head sea.

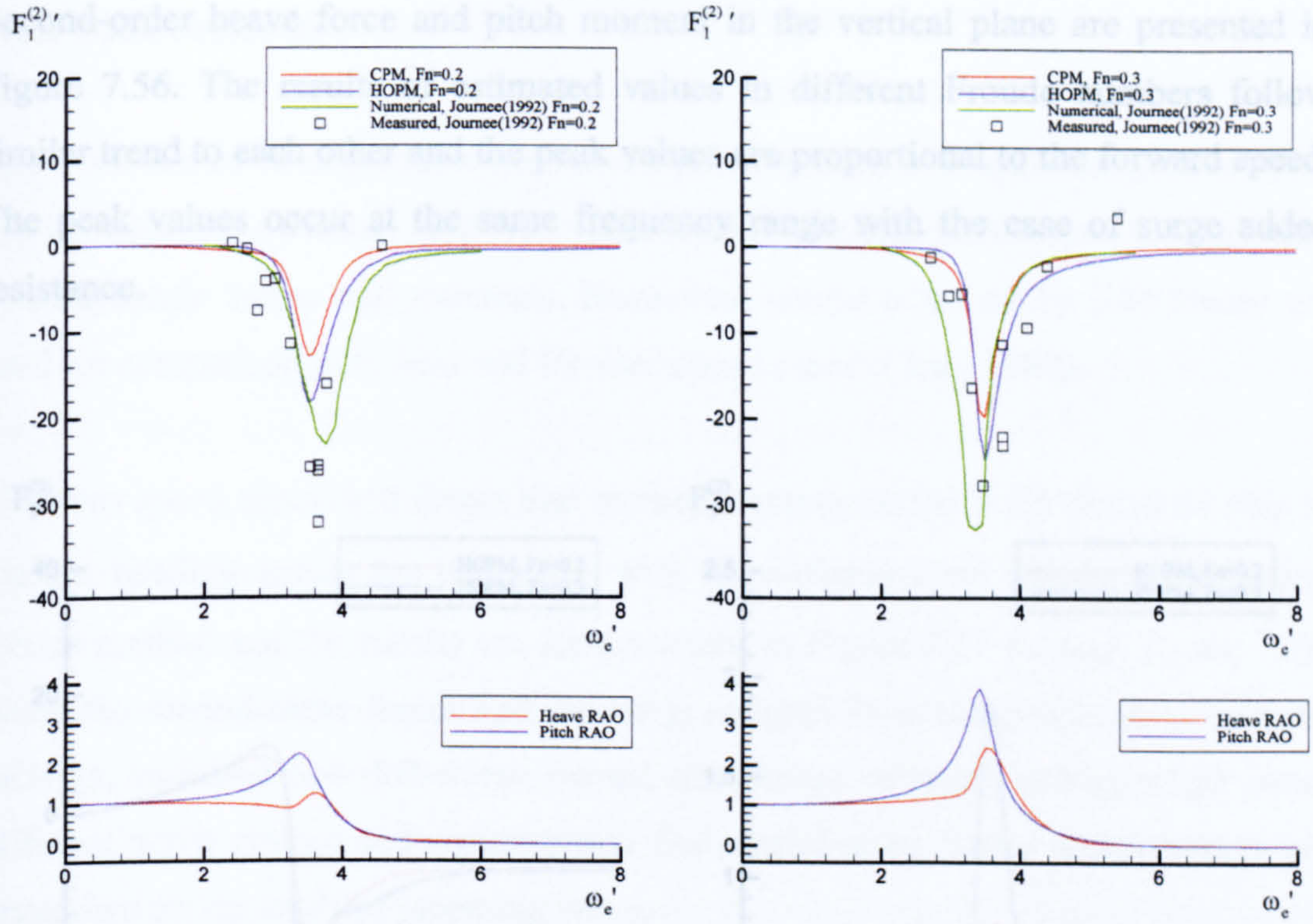

Figure 7.54 Non-dimensional second-order surge force for Wigley hull travelling at Froude number 0.2 and 0.3 in head sea

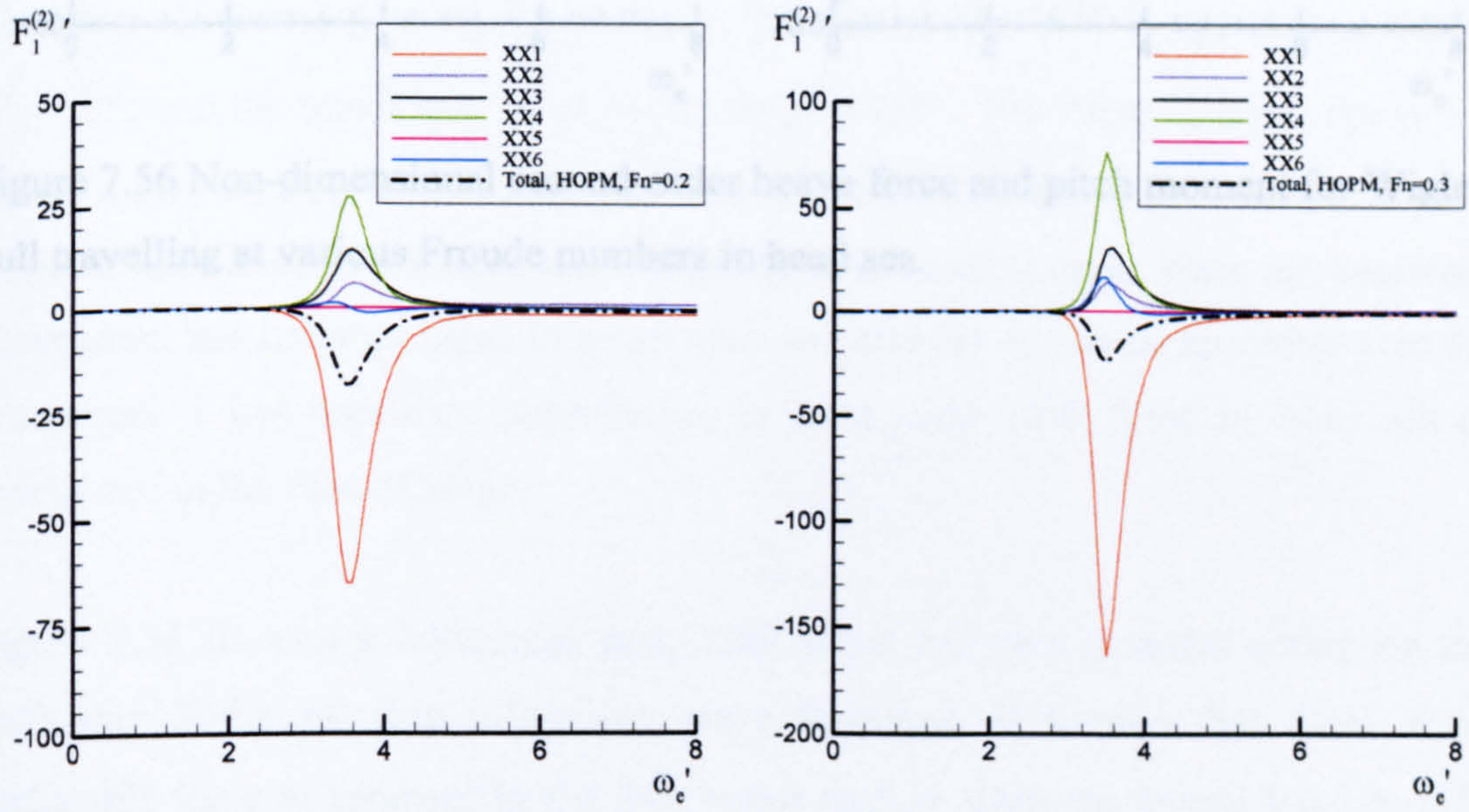

Figure 7.55 Non-dimensional components of second-order surge force for Wigley hull travelling at Froude number 0.2 and 0.3 in head sea

Second-order heave force and pitch moment in the vertical plane are presented in Figure 7.56. The results of estimated values in different Froude numbers follow similar trend to each other and the peak values are proportional to the forward speed. The peak values occur at the same frequency range with the case of surge added resistance.

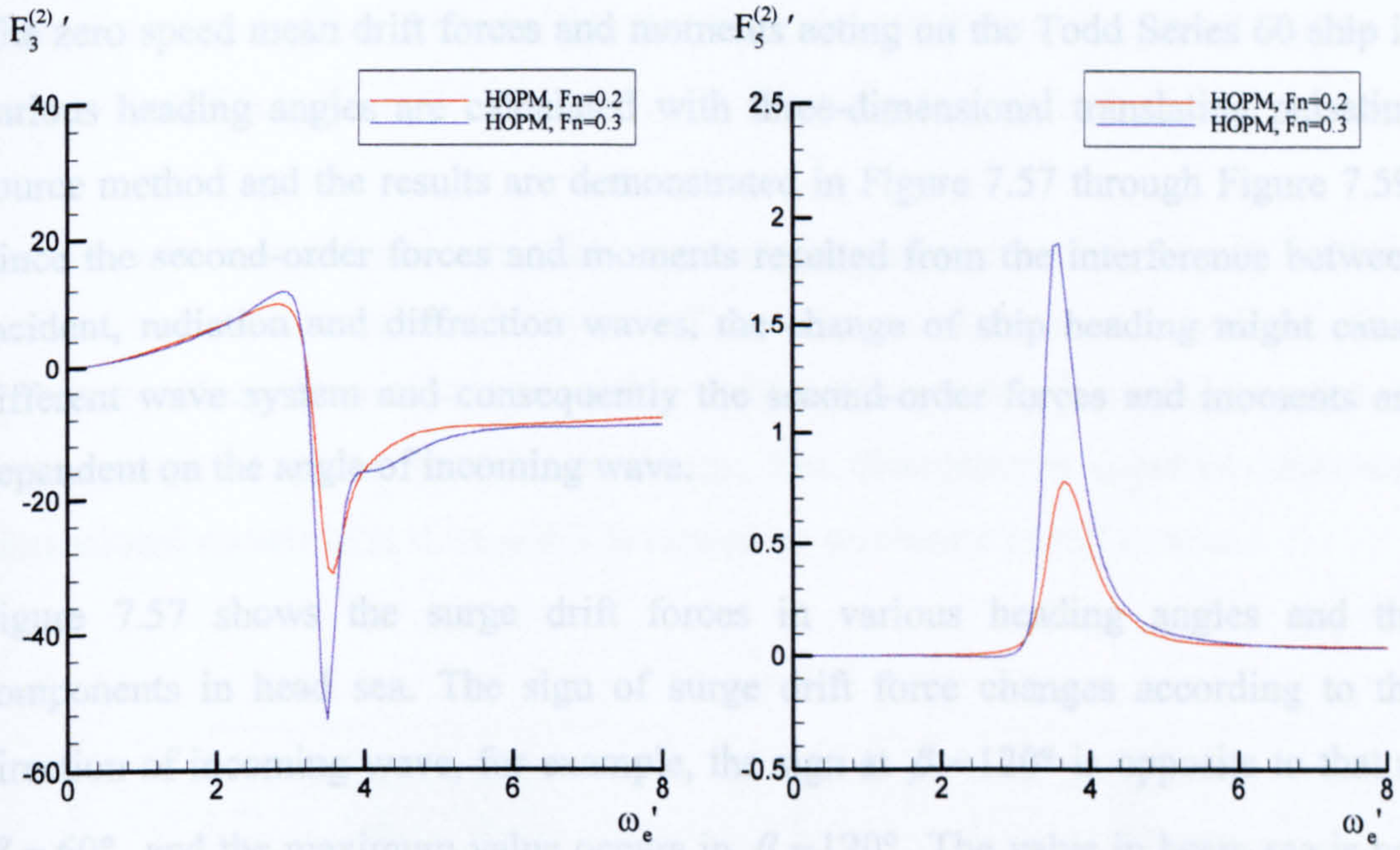

Figure 7.56 Non-dimensional second-order heave force and pitch moment for Wigley hull travelling at various Froude numbers in head sea

7.6.3 Todd Series 60

The Todd Series 60 ship model used in the previous section is again adopted to cover the applicability of actual ship hull form for the calculation of mean second-order hydrodynamic forces and moments. Numerical results obtained by 3-D theory are used for comparison with zero and forward speed cases (Chan, 1990).

The zero speed mean drift forces and moments acting on the Todd Series 60 ship in various heading angles are calculated with three-dimensional translating pulsating source method and the results are demonstrated in Figure 7.57 through Figure 7.59. Since the second-order forces and moments resulted from the interference between incident, radiation and diffraction waves, the change of ship heading might cause different wave system and consequently the second-order forces and moments are dependent on the angle of incoming wave.

Figure 7.57 shows the surge drift forces in various heading angles and the components in head sea. The sign of surge drift force changes according to the direction of incoming wave, for example, the sign at $\beta = 120°$ is opposite to that at $\beta = 60°$, and the maximum value occurs in $\beta = 120°$. The value in beam sea is not equal to zero because of asymmetry of fore- and aft-body. The ship experiences peak value of drift force at different wavelength in each heading angle since the dominant component has its large value in a different wavelength. It can be reminded that the component I has dominant contribution to total surge drift force in head sea as mentioned in the case of barge.

Figure 7.58 illustrates horizontal sway drift force and yaw moment acting on the stationary Series 60 ship in various wave headings. It is seen that there is no noticeable force or moment in the long wave regime since the lateral force is only significant for short wavelength. The lateral drift force increases dramatically as the wavelength decreases to ship length, i.e. $L/\lambda = 1.0$. The lateral drift force and yaw moment are equal to zero for head and following sea and the sway drift force

increases and approaches its maximum value as wave heading changes towards beam sea. The lateral drift forces at the same difference of angle from beam sea, for example, pairs of $\beta = 150°$ and $30°$ are slightly different in magnitude while their corresponding yaw moments have opposite signs and unequal magnitudes. This provides better prediction on the lateral drift force and yaw moment with respect to heading angle than the symmetry properties given by Newman (1967) for an arbitrary slender ship, which is freely floating in regular waves. Newman's far field method yields zero lateral drift force in beam sea because of the slender body approximation, together with the fact that the ship will follow the orbital motion of the wave itself in beam sea.

Second-order heave force and pitch moment are demonstrated in Figure 7.59 for completeness of six-degree-of-freedom. These force and moment in vertical plane are not significant because corresponding hydrostatic restoring force and moment are large enough to ignore second-order terms. The discontinuity occurred near non-dimensional wavelength, $L/\lambda = 0.5$ is caused by resonance of roll motion.

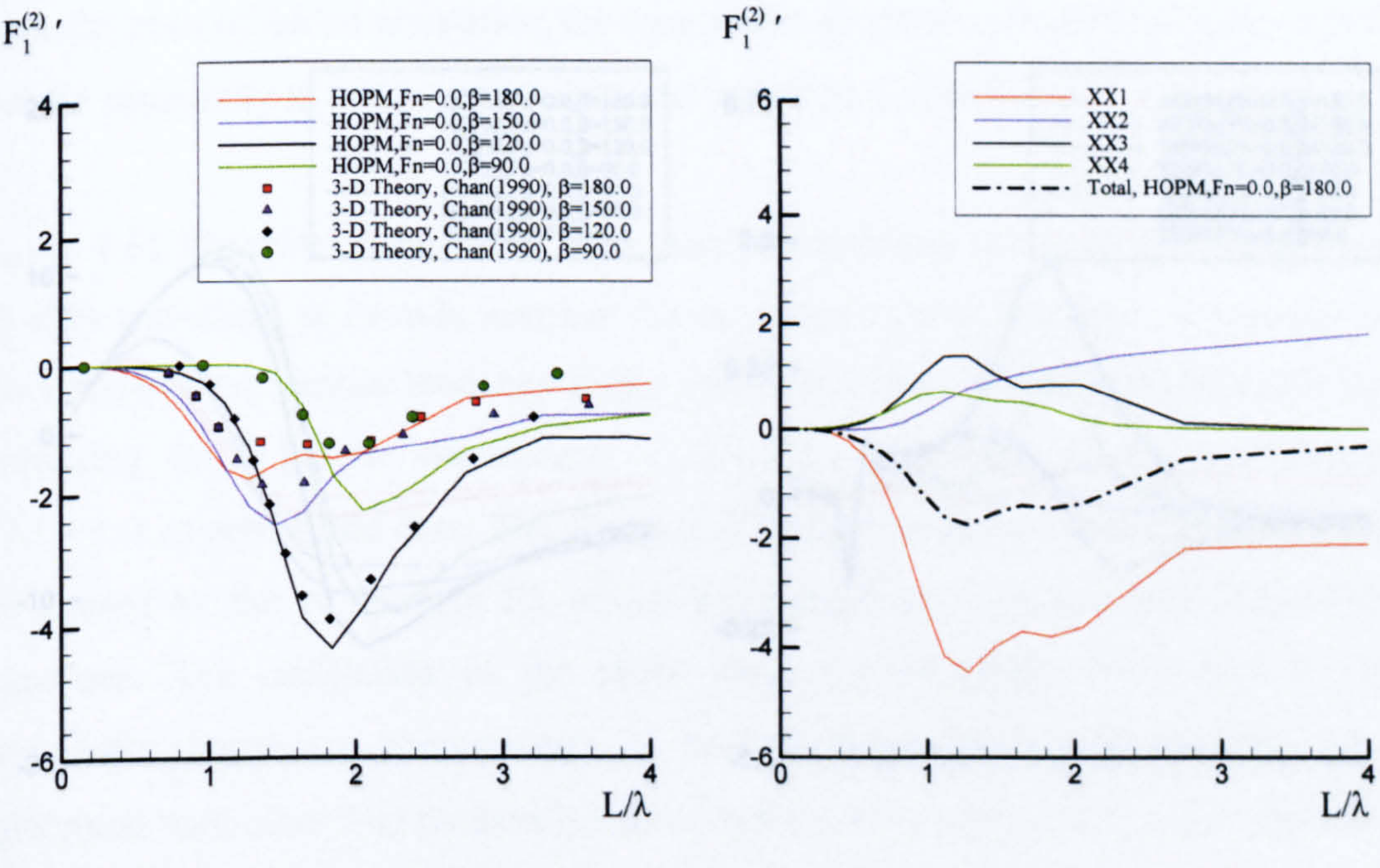

Figure 7.57 Non-dimensional second-order surge force in various heading angles and force components in head sea for Todd Series 60 at zero speed

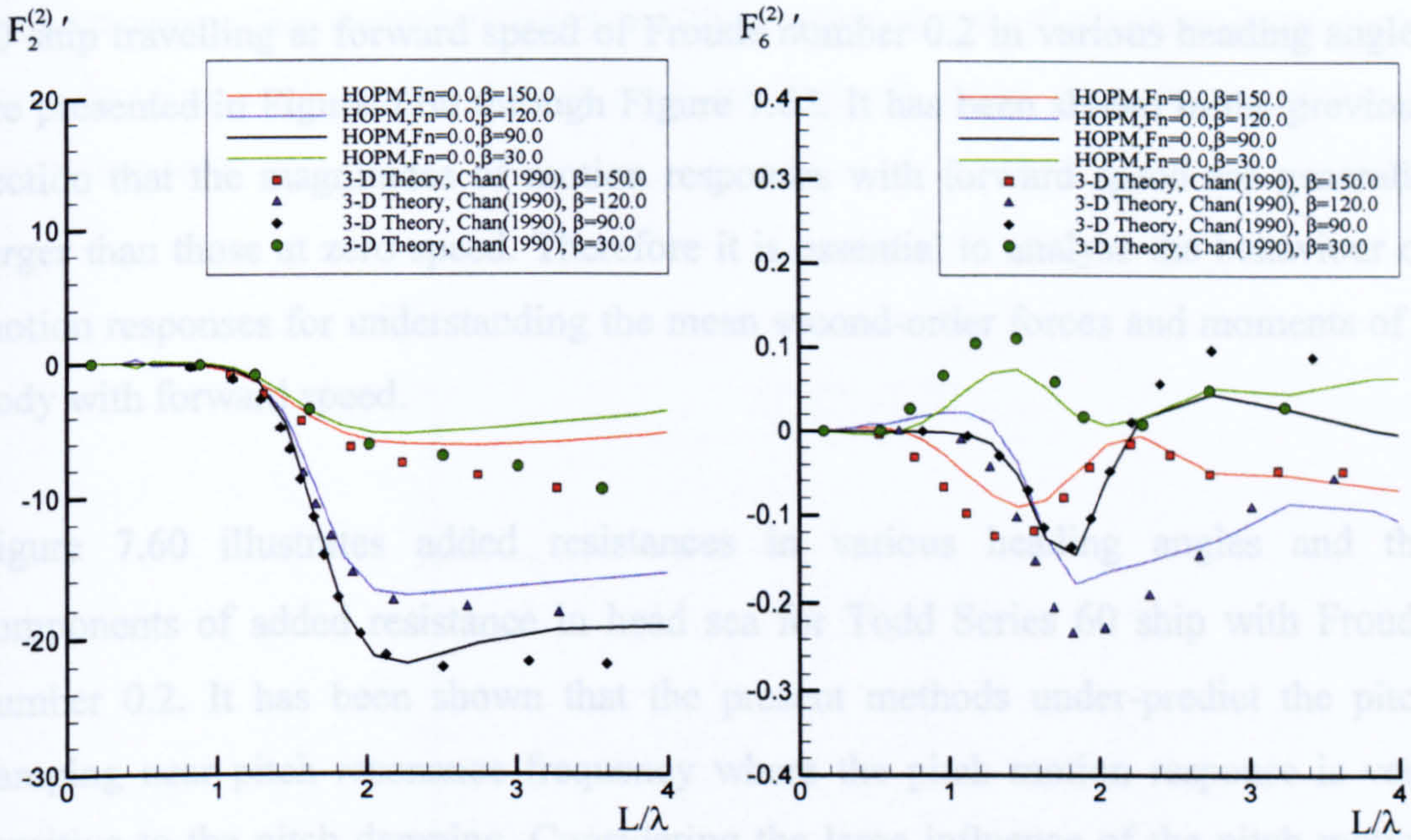

Figure 7.58 Non-dimensional second-order sway force and yaw moment for Todd Series 60 at zero speed in various heading angles

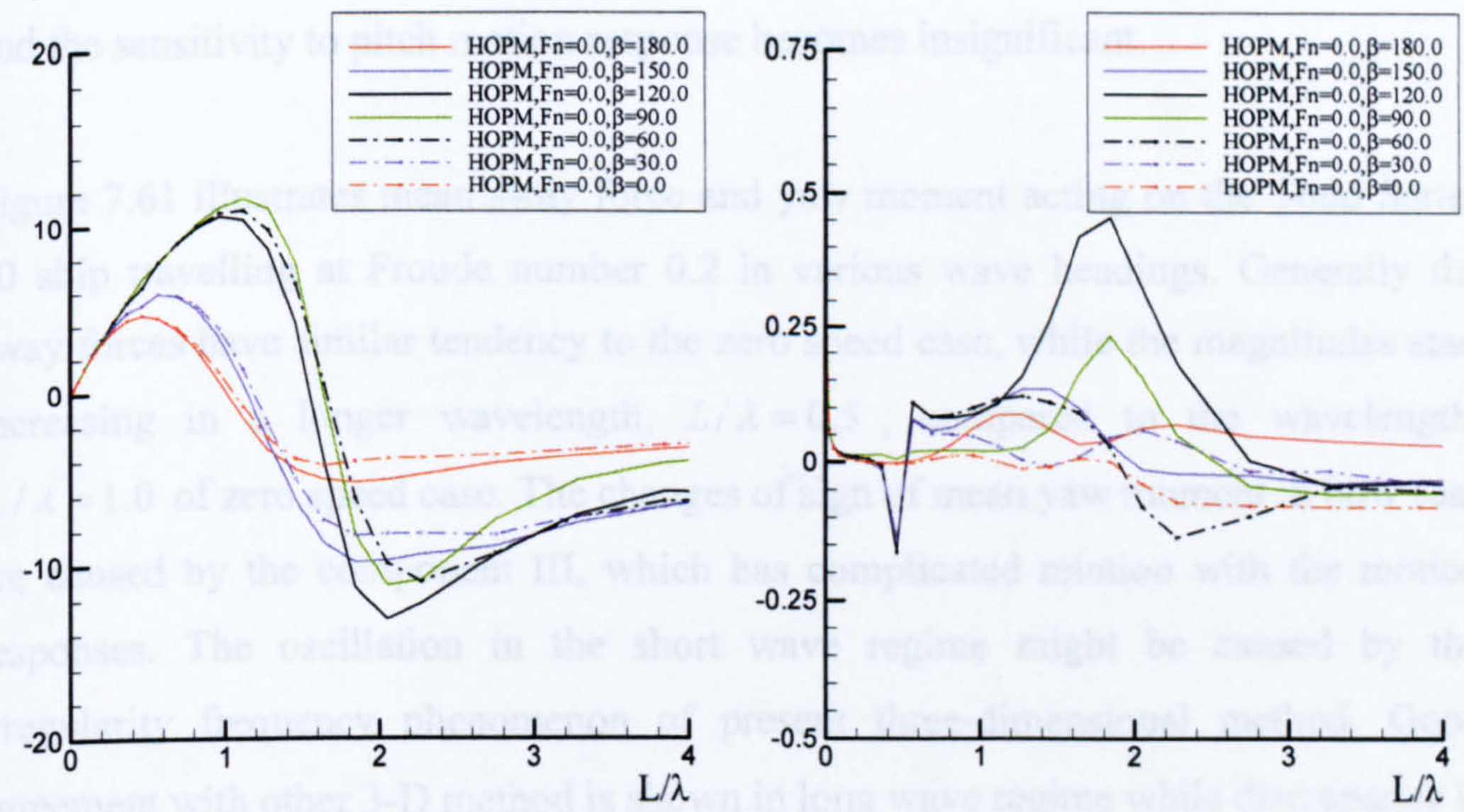

Figure 7.59 Non-dimensional second-order heave force and pitch moment for Todd Series 60 at zero speed in various heading angles

The mean second-order hydrodynamic forces and moments acting on the Todd Series 60 ship travelling at forward speed of Froude number 0.2 in various heading angles are presented in Figure 7.60 through Figure 7.62. It has been shown in the previous section that the magnitudes of motion responses with forward speed are generally larger than those at zero speed. Therefore it is essential to analyse the behaviour of motion responses for understanding the mean second-order forces and moments of a body with forward speed.

Figure 7.60 illustrates added resistances in various heading angles and the components of added resistance in head sea for Todd Series 60 ship with Froude number 0.2. It has been shown that the present methods under-predict the pitch damping near pitch resonance frequency where the pitch motion response is very sensitive to the pitch damping. Considering the large influence of the pitch motion response on the component I, which is a dominant component in added resistance, pitch motion response plays very important role in the estimation of added resistance. Comparison with experiment data for added resistance in head sea shows generally good agreement except slight shift in peak value. In the short wave regime away from the peak of added resistance, the magnitude of added resistance reduces rapidly and the sensitivity to pitch motion response becomes insignificant.

Figure 7.61 illustrates mean sway force and yaw moment acting on the Todd Series 60 ship travelling at Froude number 0.2 in various wave headings. Generally the sway forces have similar tendency to the zero speed case, while the magnitudes start increasing in a longer wavelength, $L/\lambda = 0.5$, compared to the wavelength, $L/\lambda = 1.0$ of zero speed case. The changes of sign of mean yaw moment in bow seas are caused by the component III, which has complicated relation with the motion responses. The oscillation in the short wave regime might be caused by the irregularity frequency phenomenon of present three-dimensional method. Good agreement with other 3-D method is shown in long wave regime while discrepancy is observed in short wave regime.

Mean second-order heave force and roll moment are demonstrated in Figure 7.62 for completeness of six-degree-of-freedom. The magnitude of roll moment increases as wave heading angle changes from head sea towards beam sea while vanishes in quartering seas.

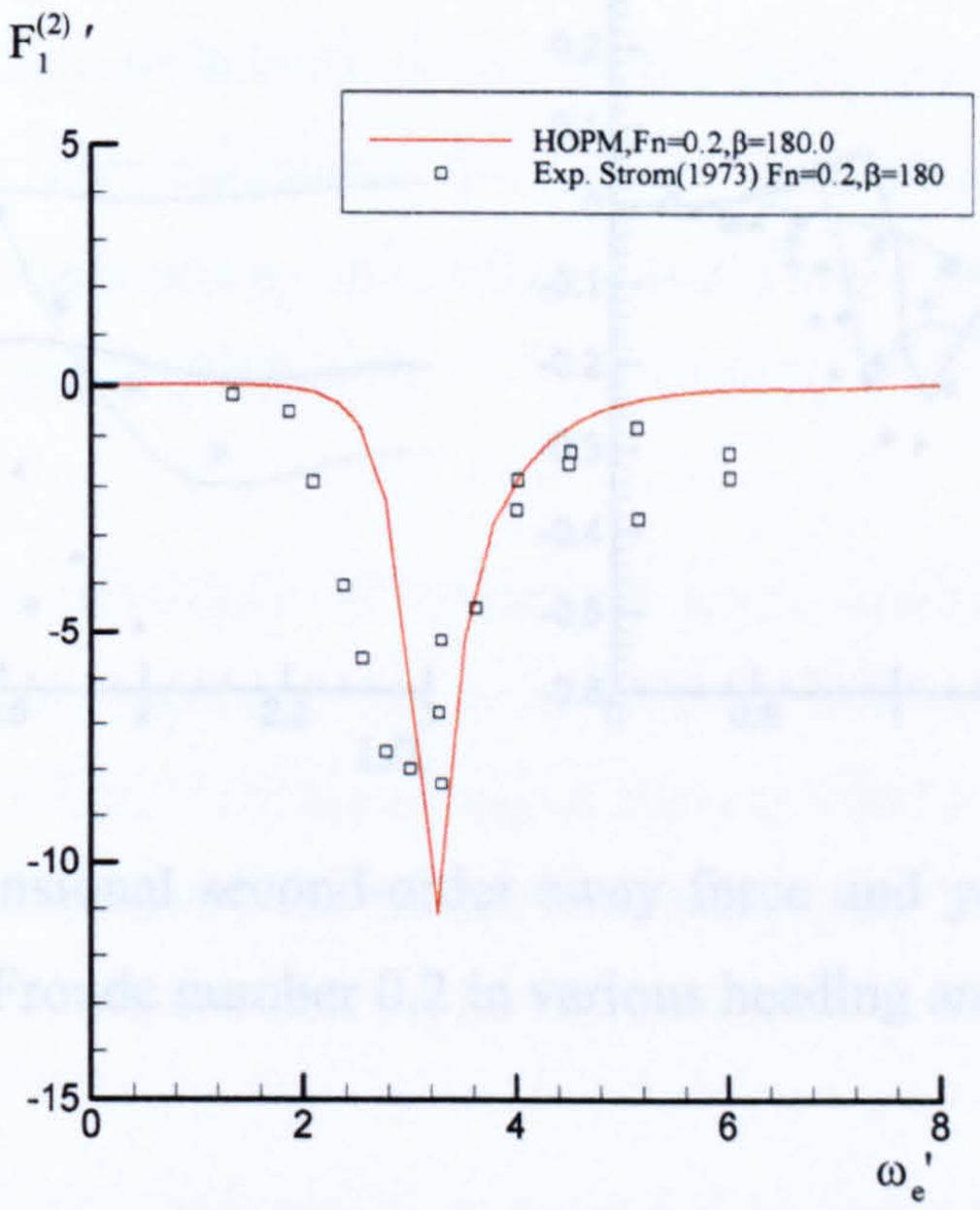

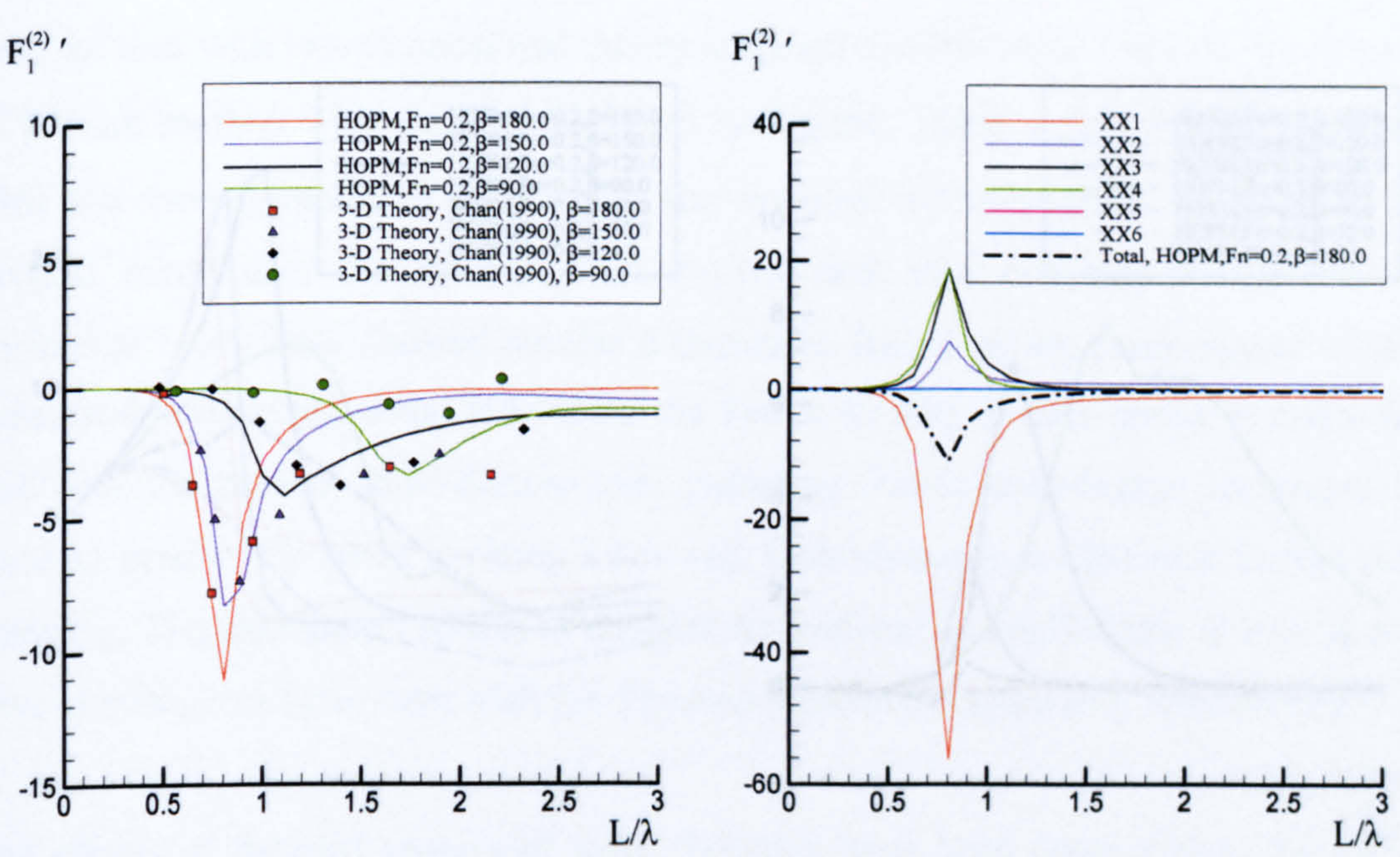

Figure 7.60 Non-dimensional second-order surge force in various heading angles and force components in head sea for Todd Series 60 travelling at Froude number 0.2

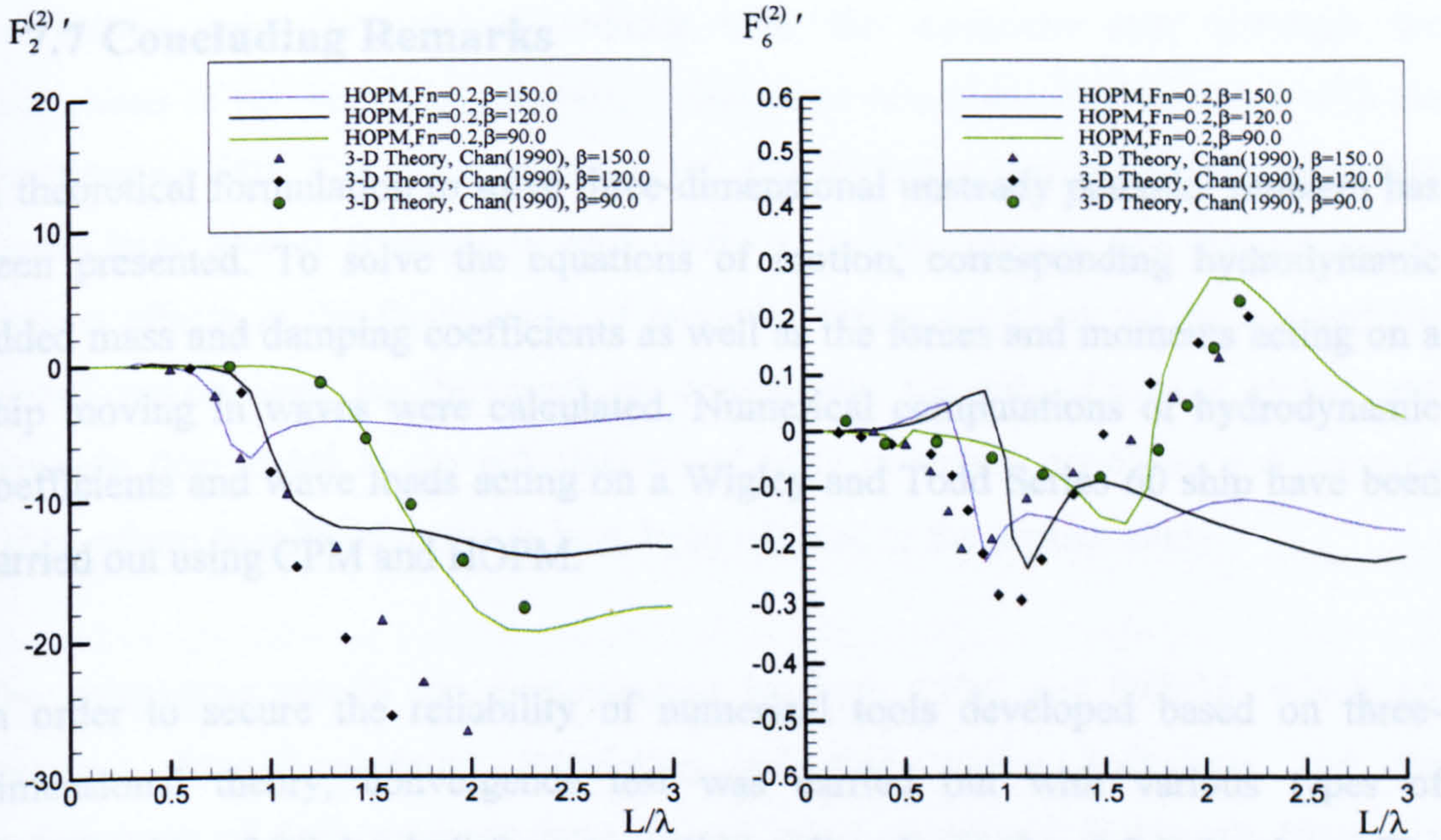

Figure 7.61 Non-dimensional second-order sway force and yaw moment for Todd Series 60 travelling at Froude number 0.2 in various heading angles

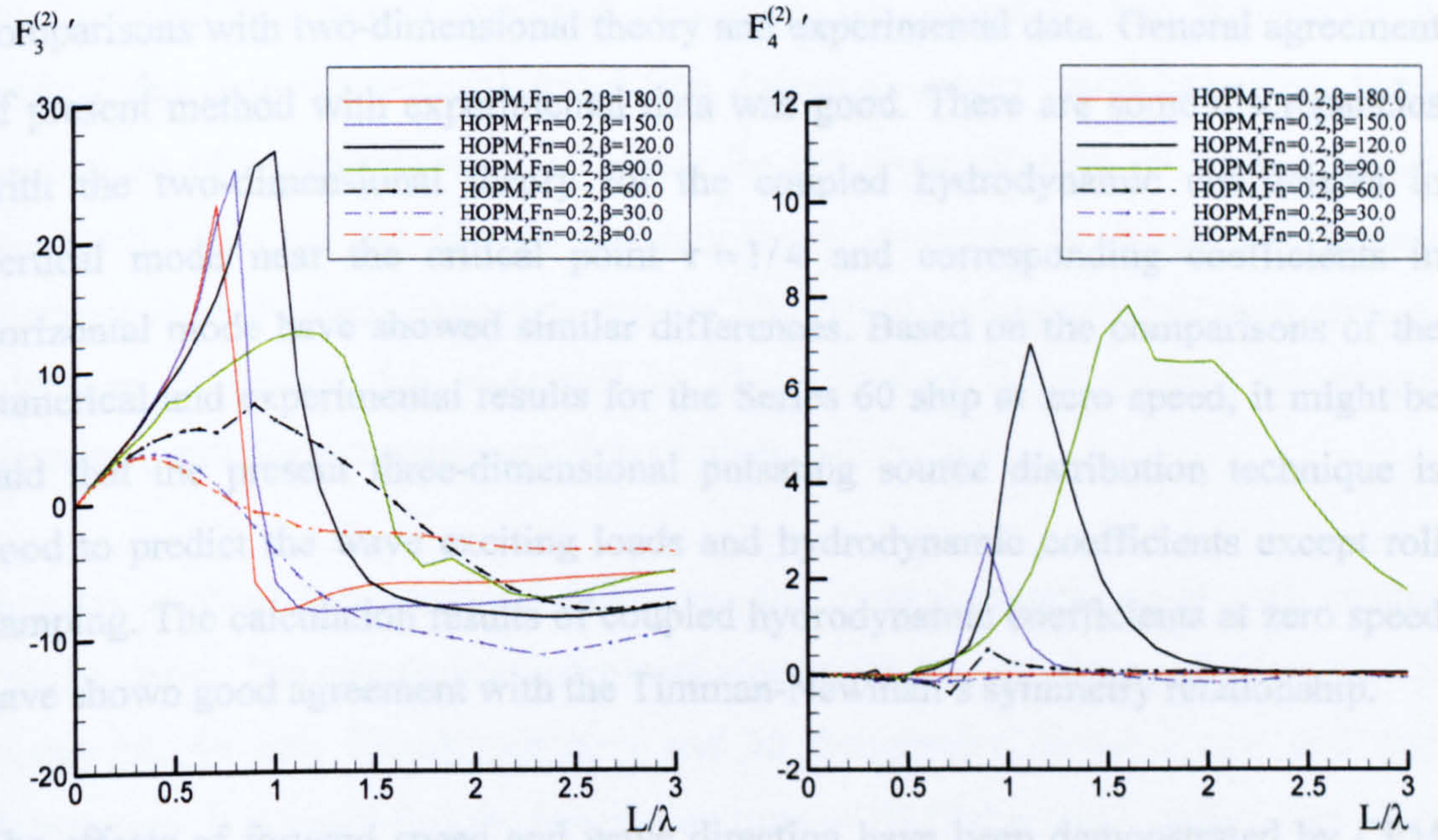

Figure 7.62 Non-dimensional second-order heave force and pitch moment for Todd Series 60 travelling at Froude number 0.2 in various heading angles

7.7 Concluding Remarks

A theoretical formulation to solve three-dimensional unsteady potential problem has been presented. To solve the equations of motion, corresponding hydrodynamic added mass and damping coefficients as well as the forces and moments acting on a ship moving in waves were calculated. Numerical computations of hydrodynamic coefficients and wave loads acting on a Wigley and Todd Series 60 ship have been carried out using CPM and HOPM.

In order to secure the reliability of numerical tools developed based on three-dimensional theory, convergence test was carried out with various types of discretisation of Wigley hull form travelling at Froude number 0.2 in head sea. The influence of total panel numbers on the hydrodynamic coefficient in vertical mode was identified to be smaller than those in horizontal mode.

Validation study for Wigley hull was then extended to various forward speeds with comparisons with two-dimensional theory and experimental data. General agreement of present method with experimental data was good. There are some discrepancies with the two-dimensional theory for the coupled hydrodynamic coefficients in vertical mode near the critical point $\tau = 1/4$ and corresponding coefficients in horizontal mode have showed similar differences. Based on the comparisons of the numerical and experimental results for the Series 60 ship at zero speed, it might be said that the present three-dimensional pulsating source distribution technique is good to predict the wave exciting loads and hydrodynamic coefficients except roll damping. The calculation results of coupled hydrodynamic coefficients at zero speed have shown good agreement with the Timman-Newman's symmetry relationship.

The effects of forward speed and wave direction have been demonstrated by CPM and HOPM adopting the three-dimensional translating pulsating source technique for the Todd Series 60 ship travelling at Froude number 0.2 with various ship headings. The influences of forward speed and ship heading play an important role in defining

general behaviour of ship motion in waves. The predicted values of hydrodynamic coefficients were in good accordance with the measured data although the estimations of roll and pitch damping values have noticeable discrepancies with the experimental data. The under-estimated roll and pitch damping coefficients have also caused large motion response in each mode of motion. For the roll case neglect of viscous effects in the formulation of potential theory could be the reason and the overall results may be improved by considering the interaction of steady and unsteady flow fields in the calculations of body boundary condition and pressure fields, where simplified methods have been adopted in the present study.

The calculation results are demonstrated by both CPM and HOPM, which are adopting three-dimensional translating pulsating source technique and the comparisons of both methods have shown good agreement in overall frequency ranges. It has been shown that the forward speed correction normally used in two-dimensional strip theory does not adequately characterise the actual speed effects observed in the low frequency regions near the critical point $\tau = 1/4$. In order to simulate the physical phenomena and obtain reasonable predictions the speed term in the linearised free surface condition adopted in the present method is essential. In general the three-dimensional translating pulsating source modelling gives better predictions of hydrodynamic coefficients for the Series 60 ship moving at Froude number 0.2 than the two-dimensional strip theory except for the irregular frequency phenomena in the high frequency region. The irregular frequency phenomenon, as addressed in section 5.5, is caused by ill-conditioned linear systems of integral equations with discrete approximation of given hull surface.

In order to check computational efficiency, the computational time of each method are compared. The calculations were performed with 320 panels over hull surface of Series 60, for two Froude numbers and 30 frequencies covering low and high frequencies. It is noted that the calculation time of HOPM is much higher than CPM since the calculations of Green function over many source points in each element cause dramatic increase of the computational efforts. In terms of calculation time and efficiency, CPM seems to be better than HOPM.

Table 7.6 Comparison of calculation time between CPM and HOPM

Method	Fn = 0.0	Fn = 0.2
CPM	6 [min]	15 [min]
HOPM	46 [min]	105 [min]

* Intel® Core™ 2 Duo T7250 2.0GHz CPU and 4.0GB DDR2 Memory

In order to consider the mean second-order forces moments acting on a ship theoretical formulation of the second-order hydrodynamic wave loads has been presented based on the first-order theory. Numerical calculations for the mean second-order forces and moments on a barge, Wigley and Todd Series 60 ship were performed by the aforementioned three-dimensional source distribution technique. The forces and moments are calculated using the near-field method, where pressure field are solved by direct integration of first-order terms without solving the second-order potential problem.

The present methods for sway and yaw drift force and moment acting on the barge at zero speed agree very well with Pinkster's experimental data. The theoretical prediction of added resistance for Wigley with various Froude numbers in head waves, calculated by CPM and HOPM, also agree well with each other although there are some differences with the measured data near the peak values of the added resistances. The effects of ship heading and forward speed on the mean second-order forces and moments for Todd Series 60 ship have been demonstrated. For zero speed the lateral drift force on the Todd Series 60 ship in beam sea has larger value than those in other wave directions. The maximum values of added resistance in head sea increase with respect to forward speed. It has been noted that the mean second-order hydrodynamic wave loads are more important in the short wave regime.

Chapter 8. A Manoeuvring Mathematical Model in Waves

8.1 Preamble

Although manoeuvring and seakeeping theory have many similarities in the point that both theories describe the motion of a ship, they have been studied in a different manner in the conventional researches. Manoeuvring theory is associated with mainly horizontal plane motion of a ship, i.e. sway and yaw, which is restricted in calm water and the motions in the vertical plane motions, i.e. heave and pitch, are often neglected. Because of this basic assumption, the hydrodynamic coefficients are found using extrapolation from the data obtained in PMM tests. Moreover manoeuvring theory is restricted to an assessment of the stability of a vessel from a prescribed reference motion, i.e. turning or zig-zag manoeuvre, without taking into account the dynamic conditions of a ship and influence of a random wave.

Seakeeping theory, however, assesses the operation of a ship at a specific speed and heading in a sinusoidal regular or irregular wave. To solve theoretically the response of a ship to the wave disturbance, it is general to use potential theory with the assumption of inviscid and irrotational fluid flow around body surface. The fluid forces are expressed in terms of added mass and damping coefficients depending on wave frequency or encounter frequency.

It has been noted that the object of this thesis is to develop an integrated mathematical model to describe general six-degree-of-freedom motion in a seaway. This integrated model should have its fundamental base on both manoeuvring and seakeeping theory and thus some skills are needed to convert values in the one theory to those in the other theory. The hydrodynamic coefficients, for example, calculated from potential theory will be converted to appropriate form for the integrated

mathematical model. Furthermore the axis systems in both theories are also different, which means adequate axis system should be chosen and axis transform between two theories should be considered. The manoeuvring equations of motion in a seaway are expressed mainly in terms of convolution integral, which was constant in the conventional theory. Each convolution integral term contains impulse response function, which is calculated by inverse Fourier Transform. External forces in the equations of motion are composed of hull force, wave excitation force and rudder force.

For the validation of integrated formulation for six-degree-of-freedom manoeuvring equations of motion, a benchmark test covering various speed ranges and initial conditions in astern wave will be carried out and the numerical results will be compared with measurement data. Furthermore, typical manoeuvring simulations like turning circle and zig-zag manoeuvre tests are to be carried out. To identify the wave effects on the manoeuvring trajectory and motion, the numerical simulation with various conditions of incoming wave are going to be performed. The predicted results will be then compared with traditional calm water calculation and the effects of individual wave condition, which are wavelength, heading angle and wave amplitude, will be investigated separately.

8.2 Mathematical Model

The aim of this section is to formulate six-degree-of-freedom equations of motion with impulse response function to describe general manoeuvring motion in a seaway. Then six-degree-of-freedom equations of motion adopting impulse response function which explains radiation forces will be formulated. For wave exciting force and other external forces traditional method used in MMG manoeuvring model will be still adopted.

8.2.1 Coordinate Systems

To describe the motion of a ship travelling in calm water or wave, it is convenient to refer the rigid body motion to both a fixed coordinate system and various types of moving coordinate systems with the body. Because the object of this study is to unify mathematical models in the conventional ship motion theory, it is required to define coordinate systems, which will be used in the unified theory and compare them with coordinate systems in the conventional theory.

The space-fixed coordinate system $O-X_0Y_0Z_0$ and body-fixed coordinate system $G-xyz$ are illustrated in Figure 8.1. The orientation of this space-fixed coordinate system is such that $O-X_0Y_0$ plane coincides with the undisturbed free surface, the OX_0 axis lies in the direction of initial ship heading and the OZ_0 axis is vertically upward. Wave is defined in this coordinate system.

The origin of body-fixed coordinate system $G-xyz$ is located in the centre of gravity with positive x-axis pointing to bow, y-axis pointing port and z-axis pointing upward. This coordinate system is similar to the one used in seakeeping theory except the location of origin, which is located in the undisturbed free surface. The

dynamics of ship in waves will be presented in this upright body-fixed coordinate system.

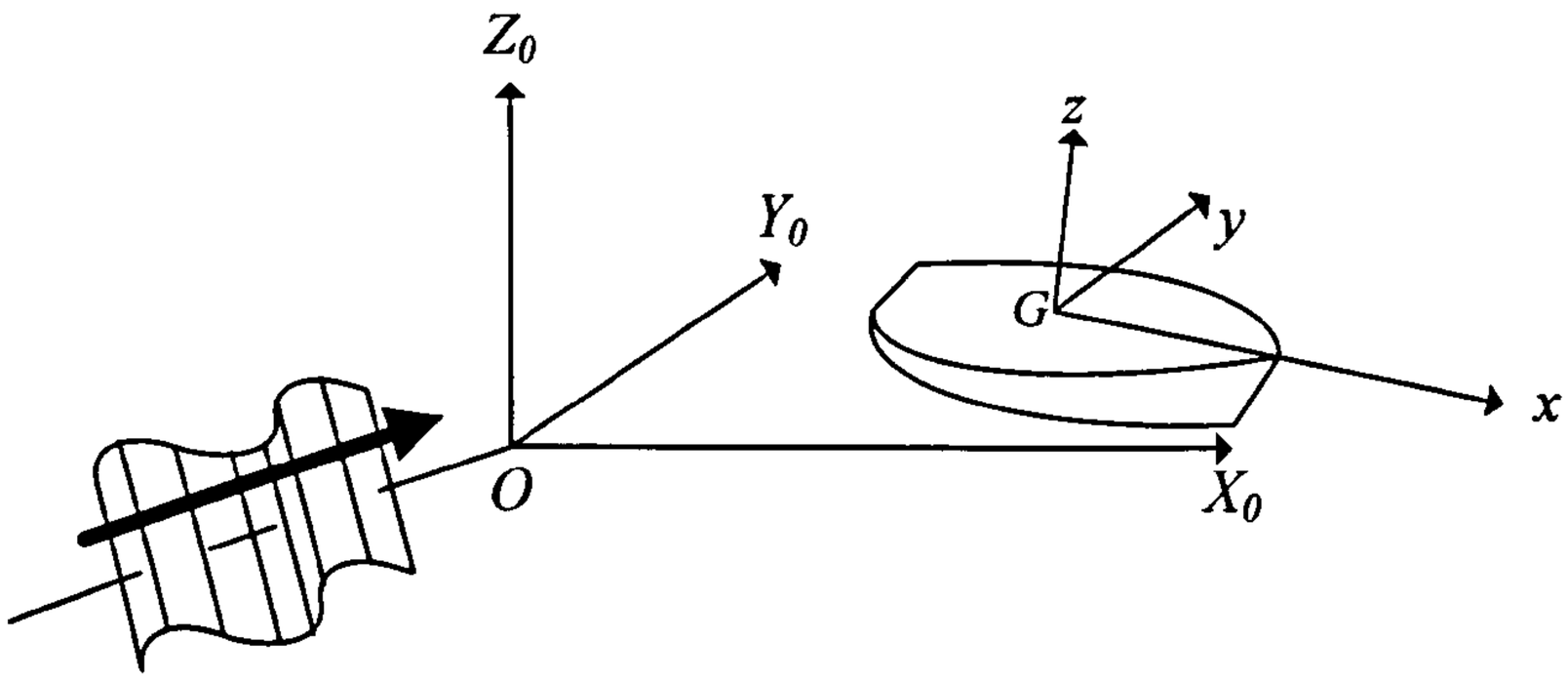

Figure 8.1 Space-fixed and body-fixed coordinate systems

8.2.2 Dynamics of a rigid body

Consider a body-fixed coordinate system $A-xyz$ rotating with an angular velocity $\omega=[\omega_x,\omega_y,\omega_z]^T$ about a space-fixed coordinate system $O-XYZ$. If the density of the body is ρ_m, the mass of the body is defined that integral of mass element as

$$m=\int_V \rho_m dV=\int_V dm \tag{8.1}$$

The mass will be assumed to be constant in time, i.e. $\frac{D}{Dt}m=0$. From the origin A of body-fixed coordinate system to the body's centre of gravity can be defined as

$$\mathbf{r}_G=\frac{1}{m}\int_V \mathbf{r}_l dm \tag{8.2}$$

The body's moment of inertia referred to $A-xyz$ can be defined as

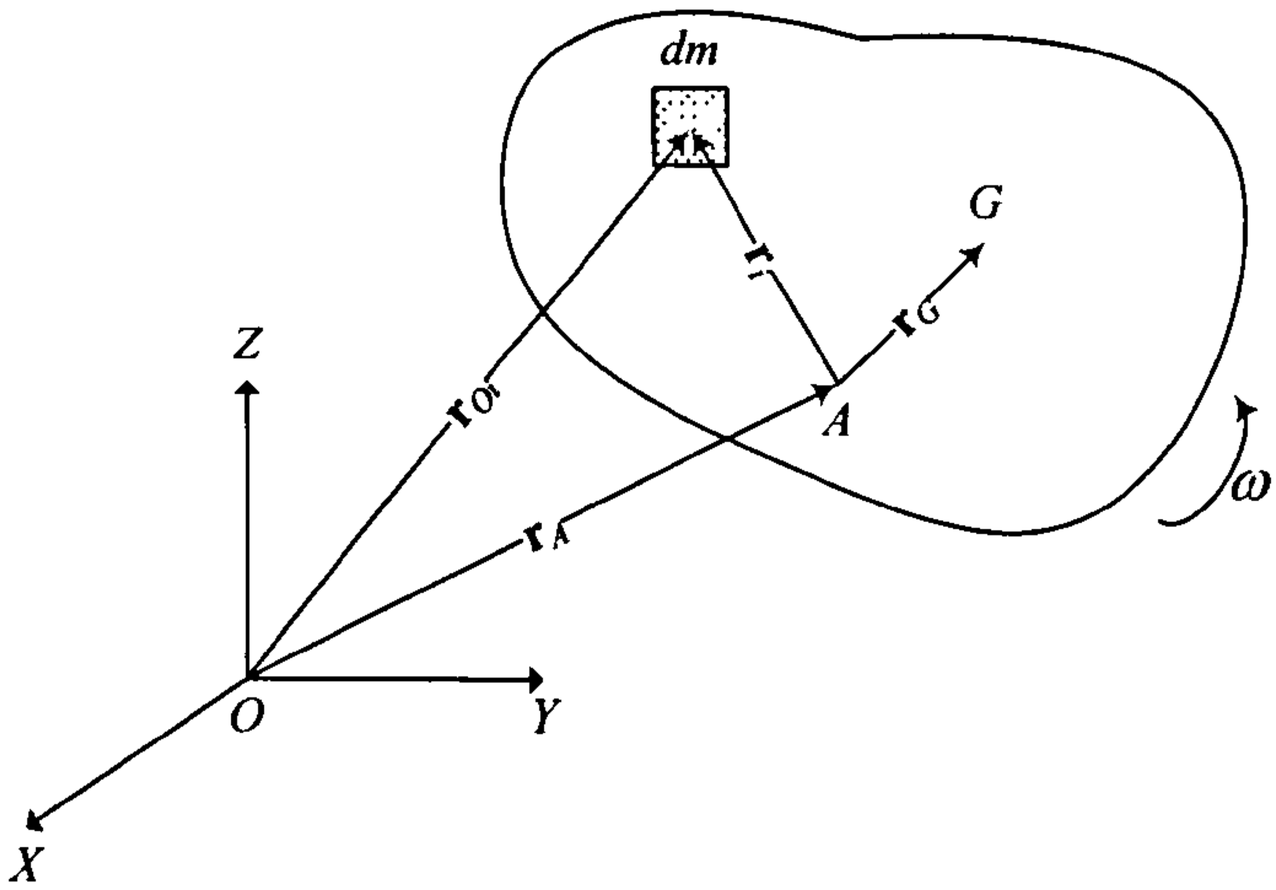

Figure 8.2 A body moving in a space-fixed coordinate system

$$\mathbf{I}_A = \begin{bmatrix} I_{xx} & -I_{xy} & -I_{xz} \\ -I_{yx} & I_{yy} & -I_{yz} \\ -I_{zx} & -I_{zy} & I_{zz} \end{bmatrix} \tag{8.3}$$

where I_{xx}, I_{yy} and I_{zz} are moment of inertia about x, y and z axes respectively and others are products of inertia defined as

$$\begin{aligned} I_{xx} &= \int_V (y^2 + z^2)dm & I_{xy} &= I_{yx} = \int_V xydm \\ I_{yy} &= \int_V (z^2 + x^2)dm & I_{yz} &= I_{zy} = \int_V yzdm \\ I_{zz} &= \int_V (x^2 + y^2)dm & I_{zx} &= I_{xz} = \int_V zxdm \end{aligned} \tag{8.4}$$

For later use vectorial expression of inertia matrix with angular velocity ω can be expressed as

$$\mathbf{I}_A\boldsymbol{\omega} = \int_V \mathbf{r}_i \times (\boldsymbol{\omega} \times \mathbf{r}_i)dm \tag{8.5}$$

When deriving the equations of motion it will be assumed that the body is rigid and the space fixed coordinate system is inertial. The first assumption eliminates the consideration of forces acting between individual elements of mass.

To calculate time derivative of an arbitrary vector **b** in both space-fixed and body-fixed coordinate system following expression is required

$$\frac{D}{Dt}\mathbf{b} = \frac{d}{dt}\mathbf{b} + \boldsymbol{\omega} \times \mathbf{b} = \dot{\mathbf{b}} + \boldsymbol{\omega} \times \mathbf{b} \tag{8.6}$$

where $\frac{D}{Dt}\mathbf{b}$ and $\frac{d}{dt}\mathbf{b}$ are time derivative of vector **b** in the space-fixed and body-fixed coordinate system respectively. It can be noticed that angular velocity is equal in both coordinate systems as

$$\frac{D}{Dt}\boldsymbol{\omega} = \frac{d}{dt}\boldsymbol{\omega} + \boldsymbol{\omega} \times \boldsymbol{\omega} = \dot{\boldsymbol{\omega}} \tag{8.7}$$

8.2.3 Conservation of momentum

In dealing with ship motion it is required to develop the fundamentals of rigid body dynamics. According to the Newton's laws of motion, the force $\mathbf{F}$ and moment $\mathbf{M}_o$ acting on a rigid body having six-degree-of-freedom motion can be expressed with conservation of linear and angular momentum respectively as follow

$$\frac{D}{Dt}\mathbf{L} = \mathbf{F} \qquad \text{and} \qquad \frac{D}{Dt}\mathbf{K}_o = \mathbf{M}_o \tag{8.8}$$

where linear momentum $\mathbf{L}$ and angular momentum $\mathbf{K}_o$ with respect to the origin of space-fixed coordinate system is defined as follow

$$\begin{aligned} \mathbf{L} &= \int_v \mathbf{v}_i dm \\ \mathbf{K}_O &= \int_v \mathbf{r}_{Oi} \times \mathbf{v}_i dm \end{aligned} \tag{8.9}$$

The translation motion of a rigid body can be explained using conservation of linear momentum as described in equations (8.8) and (8.9). Position vector of volume element can be decomposed as illustrated in the Figure 8.2.

$$\mathbf{r}_{Oi} = \mathbf{r}_A + \mathbf{r}_i \tag{8.10}$$

Then velocity vector can be expressed as

$$\mathbf{v}_i = \frac{D}{Dt}\mathbf{r}_{Oi} = \frac{D}{Dt}\mathbf{r}_A + \frac{D}{Dt}\mathbf{r}_i \tag{8.11}$$

Using relation in equation (8.6), each term in equation (8.11) can be expressed as

$$\frac{D}{Dt}\mathbf{r}_A = \mathbf{v}_A \tag{8.12}$$

$$\frac{D}{Dt}\mathbf{r}_i = \frac{d}{dt}\mathbf{r}_i + \boldsymbol{\omega} \times \mathbf{r}_i = \boldsymbol{\omega} \times \mathbf{r}_i \tag{8.13}$$

Hence

$$\mathbf{v}_i = \mathbf{v}_A + \boldsymbol{\omega} \times \mathbf{r}_i \tag{8.14}$$

Applying equation (8.14) to equations (8.8) and (8.9) yields

$$\frac{D}{Dt}\int_V (\mathbf{v}_A + \boldsymbol{\omega} \times \mathbf{r}_i)dm = \mathbf{F} \tag{8.15}$$

Once again applying the relation in equation (8.6) to (8.15) gives

$$\int_V \dot{\mathbf{v}}_A dm + \int_V \boldsymbol{\omega} \times \mathbf{v}_A dm + \int_V \dot{\boldsymbol{\omega}} \times \mathbf{r}_i dm + \int_V \boldsymbol{\omega} \times (\boldsymbol{\omega} \times \mathbf{r}_i)dm = \mathbf{F} \tag{8.16}$$

Finally substituting equations (8.1) and (8.2) into equation (8.16) gives

$$m\left[\dot{\mathbf{v}}_A + \boldsymbol{\omega} \times \mathbf{v}_A + \dot{\boldsymbol{\omega}} \times \mathbf{r}_G + \boldsymbol{\omega} \times (\boldsymbol{\omega} \times \mathbf{r}_G)\right] = \mathbf{F} \tag{8.17}$$

It should be noted that time derivative used in equation (8.17) is defined in the body-fixed coordinate system. If the origin A of the body-fixed coordinate system is chosen to coincide with the centre of gravity G, i.e. $\mathbf{r}_G = [0,0,0]^T$, equation (8.17) is simplified as

$$m\left[\dot{\mathbf{v}}_G + \boldsymbol{\omega} \times \mathbf{v}_G\right] = \mathbf{F} \tag{8.18}$$

A similar approach can be used to identify rotational motion of a rigid body. Angular momentum $\mathbf{K}_A$ with respect to the origin of the body-fixed coordinate system can be defined as

$$\begin{aligned} \mathbf{K}_A &= \int_V \mathbf{r}_i \times \mathbf{v}_i dm \\ &= \int_V (\mathbf{r}_{Oi} - \mathbf{r}_A) \times \mathbf{v}_i dm \\ &= \int_V \mathbf{r}_{Oi} \times \mathbf{v}_i dm - \int_V \mathbf{r}_A \times \mathbf{v}_i dm \\ &= \mathbf{K}_O - \mathbf{r}_A \times \mathbf{L} \end{aligned} \tag{8.19}$$

Time derivative of equation (8.19) can be expressed as

$$\begin{aligned} \frac{D}{Dt}\mathbf{K}_A &= \frac{D}{Dt}\mathbf{K}_O - \frac{D}{Dt}(\mathbf{r}_A \times \mathbf{L}) \\ &= \frac{D}{Dt}\mathbf{K}_O - \frac{D}{Dt}\mathbf{r}_A \times \mathbf{L} - \mathbf{r}_A \times \frac{D}{Dt}\mathbf{L} \end{aligned} \tag{8.20}$$

Applying equation (8.8) to equation (8.20) gives

$$\begin{aligned} \frac{D}{Dt}\mathbf{K}_A &= \mathbf{M}_O - \mathbf{v}_A \times \mathbf{L} - \mathbf{r}_A \times \mathbf{F} \\ &= \mathbf{M}_A - \mathbf{v}_A \times \mathbf{L} \end{aligned} \tag{8.21}$$

where $\mathbf{M}_A$ is moment relative to the origin of the body-fixed coordinate system and the relationship between $\mathbf{M}_A$ and $\mathbf{M}_O$ is defined as

$$\mathbf{M}_O = \mathbf{M}_A + \mathbf{r}_A \times \mathbf{F} \tag{8.22}$$

Furthermore the second term in equation (8.21) can be rewritten using equation (8.9) as follows

$$\begin{aligned} \mathbf{v}_A \times \mathbf{L} &= \mathbf{v}_A \times \int_V \mathbf{v}_i dm \\ &= \mathbf{v}_A \times \int_V (\mathbf{v}_A + \boldsymbol{\omega} \times \mathbf{r}_i) dm \\ &= \mathbf{v}_A \times \int_V \boldsymbol{\omega} \times \mathbf{r}_i dm \\ &= m\mathbf{v}_A \times (\boldsymbol{\omega} \times \mathbf{r}_G) \end{aligned} \tag{8.23}$$

Similarly left-hand side of equation (8.21) can be rewritten as

$$\begin{aligned} \mathbf{K}_A &= \int_V \mathbf{r}_i \times \mathbf{v}_i dm \\ &= \int_V \mathbf{r}_i \times (\mathbf{v}_A + \boldsymbol{\omega} \times \mathbf{r}_i) dm \\ &= \int_V \mathbf{r}_i \times \mathbf{v}_A dm + \int_V \mathbf{r}_i \times (\boldsymbol{\omega} \times \mathbf{r}_i) dm \\ &= m\mathbf{r}_G \times \mathbf{v}_A + \mathbf{I}_A \boldsymbol{\omega} \end{aligned} \tag{8.24}$$

where definition of moment of inertia in the (8.5) was used. Time derivative of equation (8.24) can be written as

$$\begin{aligned} \frac{D}{Dt}\mathbf{K}_A &= \frac{D}{Dt}(\mathbf{I}_A \boldsymbol{\omega} + m\mathbf{r}_G \times \mathbf{v}_A) \\ &= \mathbf{I}_A \dot{\boldsymbol{\omega}} + \boldsymbol{\omega} \times (\mathbf{I}_A \boldsymbol{\omega}) + m(\boldsymbol{\omega} \times \mathbf{r}_G) \times \mathbf{v}_A + m\mathbf{r}_G \times (\dot{\mathbf{v}}_A + \boldsymbol{\omega} \times \mathbf{v}_A) \end{aligned} \tag{8.25}$$

Finally substituting equations (8.23) and (8.25) into equation (8.21) and use of general vector property, $\mathbf{a} \times (\mathbf{b} \times \mathbf{c}) = -(\mathbf{b} \times \mathbf{c}) \times \mathbf{a}$, gives

$$\mathbf{I}_A\dot{\boldsymbol{\omega}} + \boldsymbol{\omega} \times (\mathbf{I}_A\boldsymbol{\omega}) + m\mathbf{r}_G \times (\dot{\mathbf{v}}_A + \boldsymbol{\omega} \times \mathbf{v}_A) = \mathbf{M}_A \tag{8.26}$$

Again if the origin of the body-fixed coordinate system is chosen to be in the centre of gravity equation (8.26) is simplified as

$$\mathbf{I}\dot{\boldsymbol{\omega}} + \boldsymbol{\omega} \times (\mathbf{I}\boldsymbol{\omega}) = \mathbf{M}_G \tag{8.27}$$

where $\mathbf{I}$ represents moment of inertia matrix defined relative to the centre of gravity. It should be noted that general hull form is symmetric about xz plane so products of inertia $I_{xy} = I_{yx} = 0$ and $I_{yz} = I_{zy} = 0$.

8.2.4 Equations of motion

In the previous section conservation of linear and angular momentum has been used to obtain equations of motion relative to arbitrary origin of body-fixed coordinate system. To simplify the equations of motion the origin of the body-fixed coordinate system will be taken at the centre of gravity. In addition the axis is assumed to be principal axis of inertia in order to simplify the momentum equation. Then the equations of motion are finally expressed as

$$\begin{aligned} m\left[\dot{\mathbf{v}} + \boldsymbol{\omega} \times \mathbf{v}\right] &= \mathbf{F} \\ \mathbf{I}\dot{\boldsymbol{\omega}} + \boldsymbol{\omega} \times (\mathbf{I}\boldsymbol{\omega}) &= \mathbf{M} \end{aligned} \tag{8.28}$$

If we consider the translation velocity $\mathbf{v} = [u, v, w]^T$, angular velocity $\boldsymbol{\omega} = [p, q, r]^T$, and external force $\mathbf{F} = [X, Y, X]^T$, and moment $\mathbf{M} = [K, M, N]^T$ in the body-fixed coordinate system and substitute corresponding components to equation (8.28), following expressions for the equations of motion with origin at the centre of gravity are acquired.

$$
\begin{aligned}
m(\dot{u} + wq - vr) &= X \\
m(\dot{v} + ur - wp) &= Y \\
m(\dot{w} + vp - uq) &= Z \\
I_{xx}\dot{p} + (I_{zz} - I_{yy})qr - (\dot{r} + pq)I_{zx} &= K \\
I_{yy}\dot{q} + (I_{xx} - I_{zz})rp + (p^2 - r^2)I_{zx} &= M \\
I_{zz}\dot{r} + (I_{yy} - I_{xx})pq + (rq - \dot{p})I_{zx} &= N
\end{aligned}
\tag{8.29}
$$

Coupled terms between horizontal and vertical planes in equation (8.29) can be neglected and finally equations of motion can be expressed as

$$
\begin{aligned}
m(\dot{u} - vr) &= X \\
m(\dot{v} + ur) &= Y \\
m(\dot{w} - uq) &= Z \\
I_{xx}\dot{p} - I_{zx}\dot{r} &= K \\
I_{yy}\dot{q} &= M \\
I_{zz}\dot{r} - I_{zx}\dot{p} &= N
\end{aligned}
\tag{8.30}
$$

The external force terms are decomposed with several components and further explained in the following section.

8.3 Comparison of Conventional Theories

8.3.1 Coordinate systems

Figure 8.3 illustrates space-fixed coordinate system $O-X_0Y_0Z_0$ and body-fixed coordinates system $A-\xi\eta\zeta$ used in seakeeping theory. The origin lies on the undisturbed free surface as well as midship of the body, which gives symmetric hull form along $A-\xi\zeta$ plane.

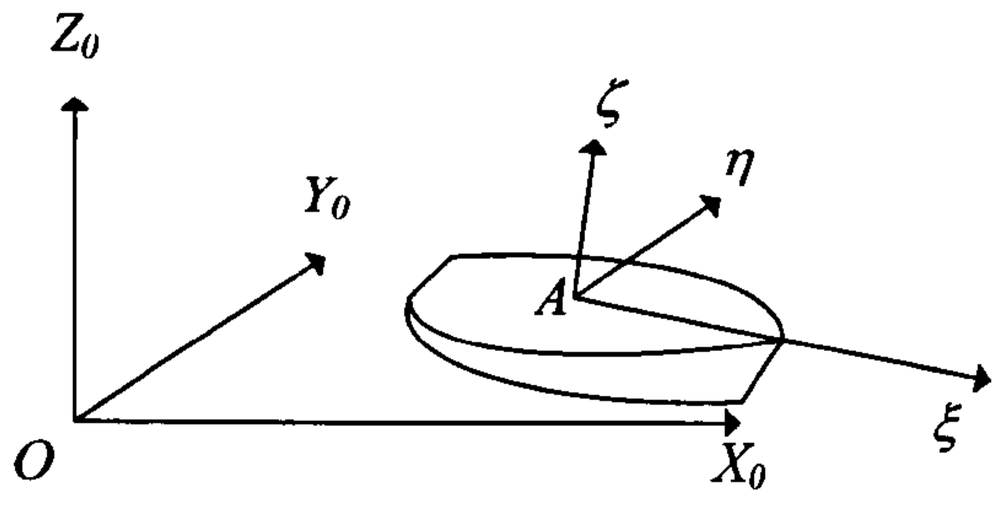

Figure 8.3 Conventional coordinate systems in seakeeping theory

Space-fixed coordinate system $O-X_0Y_0Z_0$ and body-fixed coordinate system $G-xyz$ used in the conventional manoeuvring theory are illustrated in Figure 8.4. Generally positive directions of Z_0 and z axes are set to point downward in these coordinate systems.

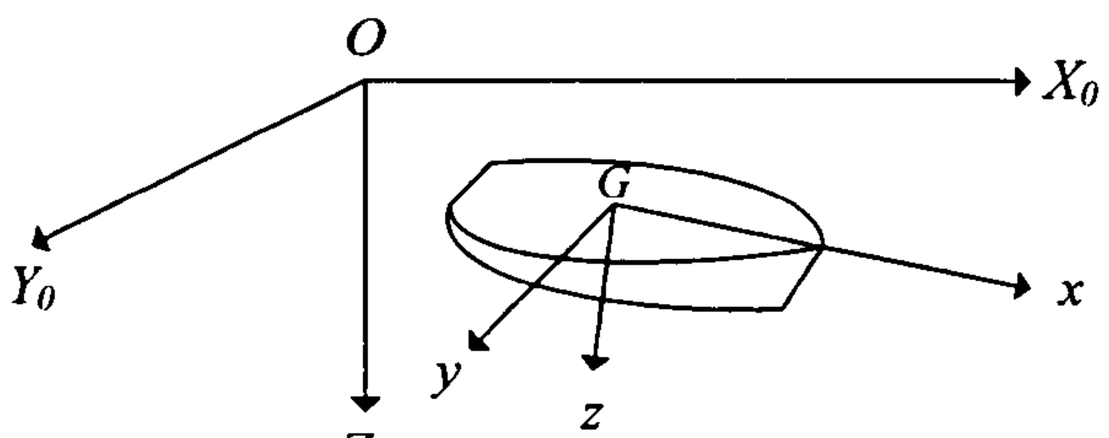

Figure 8.4 Conventional coordinate systems in manoeuvring theory

To be compared with mathematical model of seakeeping theory this conventional coordinate representations need to be converted to upright coordinate systems as

illustrated in Figure 8.1. Even if both coordinate systems are chosen so that Z_0 and z axes point upward with right-handed rule, all the mathematical formulation in the foregoing coordinate systems are still valid except the change of signs in the forces and motion variables, which are explained by Bishop and Price (1981).

8.3.2 Kinematics relationship

Kinematics conditions for velocity and angular velocity components in conventional theories can be related by identifying the relationship of motion variables between two coordinate systems. Since it is difficult to compare motion variables directly, it is required to transform motion variables defined in the body-fixed coordinate system to those in the space-fixed coordinate system. The velocity and angular velocity components in body-fixed axis systems are related with transformation matrices $\mathbf{T}_1(\boldsymbol{\eta})$ and $\mathbf{T}_2(\boldsymbol{\eta})$ as

$$\begin{aligned} \mathbf{U} &= \mathbf{T}_1(\boldsymbol{\eta})\mathbf{u} \\ \boldsymbol{\Omega} &= \mathbf{T}_1(\boldsymbol{\eta})\boldsymbol{\omega} = \mathbf{T}_1(\boldsymbol{\eta})\mathbf{T}_2(\boldsymbol{\eta})\dot{\boldsymbol{\eta}} \end{aligned} \tag{8.31}$$

where $\boldsymbol{\eta} = [\phi, \theta, \psi]^T$ is Euler angles, $\mathbf{U}$ and $\boldsymbol{\Omega}$ are velocities and angular velocity vectors referenced to space-fixed coordinate system, and $\mathbf{u}$ and $\boldsymbol{\omega}$ are in body-fixed coordinate system respectively. Transformation matrices used in equation (8.31) are defined with Euler angle as follows,

$$\mathbf{T}_1(\boldsymbol{\eta}) = \begin{bmatrix} \cos\psi\cos\theta & \begin{pmatrix} -\sin\psi\cos\phi \\ +\cos\psi\sin\theta\sin\phi \end{pmatrix} & \begin{pmatrix} \sin\psi\sin\phi \\ +\cos\psi\sin\theta\cos\phi \end{pmatrix} \\ \sin\psi\cos\theta & \begin{pmatrix} \cos\psi\cos\phi \\ +\sin\psi\sin\theta\sin\phi \end{pmatrix} & \begin{pmatrix} -\cos\psi\sin\phi \\ +\sin\psi\sin\theta\cos\phi \end{pmatrix} \\ -\sin\theta & \cos\theta\sin\phi & \cos\theta\cos\phi \end{bmatrix} \tag{8.32}$$

$$\mathbf{T}_2(\boldsymbol{\eta}) = \begin{bmatrix} 1 & 0 & -\sin\theta \\ 0 & \cos\phi & \cos\theta\sin\phi \\ 0 & -\sin\phi & \cos\theta\cos\phi \end{bmatrix}$$

If the Euler angles are assumed to be small these matrices reduce to

$$\mathbf{T}_1(\boldsymbol{\eta}) = \begin{bmatrix} 1 & -\psi & \theta \\ \psi & 1 & -\phi \\ -\theta & \phi & 1 \end{bmatrix} \text{ and } \mathbf{T}_2(\boldsymbol{\eta}) = \begin{bmatrix} 1 & 0 & -\theta \\ 0 & 1 & \phi \\ 0 & -\phi & 1 \end{bmatrix} \tag{8.33}$$

First motions defined in body-fixed coordinate system will transformed to the space-fixed reference system. If the motion variables are assumed to be small quantities about equilibrium state with steady advancing speed U, within the limit of small perturbation the products of small quantities are neglected. Two velocity vectors $\mathbf{u} = [U + u, v, w]^T$ and $\boldsymbol{\omega} = [p, q, r]^T$ can be transformed using equation (8.31) and (8.33) as follow

$$\mathbf{U} = \begin{bmatrix} U + u \\ v + U\psi \\ w - U\theta \end{bmatrix} \text{ and } \boldsymbol{\Omega} = \begin{bmatrix} p \\ q \\ r \end{bmatrix} = \begin{bmatrix} \dot{\phi} \\ \dot{\theta} \\ \dot{\psi} \end{bmatrix} \tag{8.34}$$

Velocity and angular velocity vectors of small quantity can be rewritten as

$$\mathbf{U_o} = \begin{bmatrix} u \\ v + U\psi \\ w - U\theta \end{bmatrix} \text{ and } \boldsymbol{\Omega_o} = \begin{bmatrix} p \\ q \\ r \end{bmatrix} = \begin{bmatrix} \dot{\phi} \\ \dot{\theta} \\ \dot{\psi} \end{bmatrix} \tag{8.35}$$

If yaw motion is assumed to be sinusoidal, yaw angle ψ can be expressed as $\psi = \psi_0 \sin(\omega t)$. Then yaw angle and acceleration are related using encounter frequency as follows

$$r = \dot{\psi} = \omega_e \psi_0 \cos(\omega_e t)$$
$$\dot{r} = \ddot{\psi} = -\omega_e^2 \psi_0 \sin(\omega_e t) = -\omega_e^2 \psi \tag{8.36}$$

Similarly pitch acceleration is expressed as $\dot{q} = -\omega_e^2 \theta$. Consequently velocities in equation (8.35) can be rewritten as follow

$$\mathbf{U_o} = \begin{bmatrix} u \\ v - (U/\omega_e^2)\dot{r} \\ w + (U/\omega_e^2)\dot{q} \end{bmatrix} \text{ and } \mathbf{\Omega_o} = \begin{bmatrix} p \\ q \\ r \end{bmatrix} = \begin{bmatrix} \dot{\phi} \\ \dot{\theta} \\ \dot{\psi} \end{bmatrix} \tag{8.37}$$

From equation (8.35) acceleration terms are found easily as

$$\dot{\mathbf{U}}_\mathbf{o} = \begin{bmatrix} \dot{u} \\ \dot{v} + Ur \\ \dot{w} - Uq \end{bmatrix} \text{ and } \dot{\mathbf{\Omega}}_\mathbf{o} = \begin{bmatrix} \dot{p} \\ \dot{q} \\ \dot{r} \end{bmatrix} = \begin{bmatrix} \ddot{\phi} \\ \ddot{\theta} \\ \ddot{\psi} \end{bmatrix} \tag{8.38}$$

To compare motion variables and hydrodynamic forces represented in the conventional coordinate systems, further relationship between two coordinate systems is required. As illustrated in Figure 8.5, origin A of body-fixed coordinate system used in seakeeping theory lies on the undisturbed free surface and origin G of upright body-fixed coordinate system in manoeuvring theory is located in the centre of gravity, where longitudinal and vertical distances from A to G are defined as $\overline{\xi}_G$ and $\overline{\zeta}_G$ respectively.

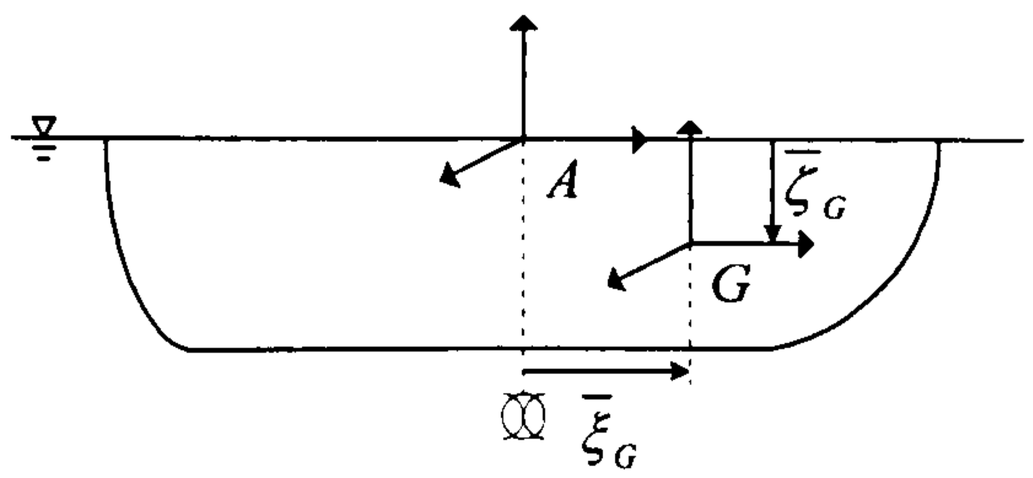

Figure 8.5 Relationship of body-fixed coordinate systems used in seakeeping theory and present mathematical model

The motion vectors $\boldsymbol{\xi}_{\mathbf{T}} = [\xi_1, \xi_2, \xi_3]^T$ and $\boldsymbol{\xi}_{\mathbf{R}} = [\xi_4, \xi_5, \xi_6]^T$ are defined as small translations and rotations referenced to $A - \xi\eta\zeta$ coordinate system. Applying equation (8.7) gives relationship of angular velocities can be expressed as follows

$$\boldsymbol{\Omega}_{\mathbf{O}} = \boldsymbol{\xi}_{\mathbf{R}} \quad \text{and} \quad \dot{\boldsymbol{\Omega}}_{\mathbf{O}} = \dot{\boldsymbol{\xi}}_{\mathbf{R}} \tag{8.39}$$

Similarly velocities in the seakeeping theory can be expressed as

$$\mathbf{U}_{\mathbf{O}} = \boldsymbol{\xi}_{\mathbf{T}} + \boldsymbol{\xi}_{\mathbf{R}} \times \mathbf{r}_{AG} \tag{8.40}$$

where $\mathbf{r}_{AG} = [\bar{\xi}_G, \bar{\eta}_G, -\bar{\zeta}_G]^T$ is position vector of centre of gravity in $A - \xi\eta\zeta$ coordinate system. When the hull form is symmetric about $\xi\zeta$ plane, y-component of $\mathbf{r}_{AG}$ is zero, i.e. $\bar{\eta}_G = 0$. When the products of small quantities are ignored again, the relations of velocities and accelerations are finally as

$$\mathbf{U}_{\mathbf{O}} = \begin{bmatrix} \dot{\xi}_1 - \bar{\zeta}_G \dot{\xi}_5 \\ \dot{\xi}_2 + \bar{\zeta}_G \dot{\xi}_4 + \bar{\xi}_G \dot{\xi}_6 \\ \dot{\xi}_3 - \bar{\xi}_G \dot{\xi}_5 \end{bmatrix} \quad \text{and} \quad \dot{\mathbf{U}}_{\mathbf{O}} = \begin{bmatrix} \ddot{\xi}_1 - \bar{\zeta}_G \ddot{\xi}_5 \\ \ddot{\xi}_2 + \bar{\zeta}_G \ddot{\xi}_4 + \bar{\xi}_G \ddot{\xi}_6 \\ \ddot{\xi}_3 - \bar{\xi}_G \ddot{\xi}_5 \end{bmatrix} \tag{8.41}$$

Using equations (8.37) to (8.41), kinematics relations between the manoeuvring and seakeeping theories adopting same upright body-fixed coordinate system for motion variables are as

$$\begin{aligned} \mathbf{U}_{\mathbf{O}} &= \begin{bmatrix} u \\ v - (U/\omega_e^2)\dot{r} \\ w + (U/\omega_e^2)\dot{q} \end{bmatrix} = \begin{bmatrix} \dot{\xi}_1 - \bar{\zeta}_G \dot{\xi}_5 \\ \dot{\xi}_2 + \bar{\zeta}_G \dot{\xi}_4 + \bar{\xi}_G \dot{\xi}_6 \\ \dot{\xi}_3 - \bar{\xi}_G \dot{\xi}_5 \end{bmatrix} \\ \dot{\mathbf{U}}_{\mathbf{O}} &= \begin{bmatrix} \dot{u} \\ \dot{v} + Ur \\ \dot{w} - Uq \end{bmatrix} = \begin{bmatrix} \ddot{\xi}_1 - \bar{\zeta}_G \ddot{\xi}_5 \\ \ddot{\xi}_2 + \bar{\zeta}_G \ddot{\xi}_4 + \bar{\xi}_G \ddot{\xi}_6 \\ \ddot{\xi}_3 - \bar{\xi}_G \ddot{\xi}_5 \end{bmatrix} \end{aligned} \tag{8.42}$$

$$\boldsymbol{\Omega}_{\mathbf{o}} = \begin{bmatrix} p \\ q \\ r \end{bmatrix} = \begin{bmatrix} \dot{\phi} \\ \dot{\theta} \\ \dot{\psi} \end{bmatrix} = \begin{bmatrix} \dot{\xi}_4 \\ \dot{\xi}_5 \\ \dot{\xi}_6 \end{bmatrix} \text{ and } \dot{\boldsymbol{\Omega}}_{\mathbf{o}} = \begin{bmatrix} \dot{p} \\ \dot{q} \\ \dot{r} \end{bmatrix} = \begin{bmatrix} \ddot{\phi} \\ \ddot{\theta} \\ \ddot{\psi} \end{bmatrix} = \begin{bmatrix} \ddot{\xi}_4 \\ \ddot{\xi}_5 \\ \ddot{\xi}_6 \end{bmatrix} \tag{8.43}$$

By rearranging equation (8.42) it can be rewritten as follows

$$\begin{bmatrix} \dot{\xi}_1 \\ \dot{\xi}_2 \\ \dot{\xi}_3 \end{bmatrix} = \begin{bmatrix} u + \bar{\zeta}_G q \\ v - (U/\omega_e^2)\dot{r} - \bar{\zeta}_G p - \bar{\xi}_G r \\ w + (U/\omega_e^2)\dot{q} + \bar{\xi}_G q \end{bmatrix}$$
$$\begin{bmatrix} \ddot{\xi}_1 \\ \ddot{\xi}_2 \\ \ddot{\xi}_3 \end{bmatrix} = \begin{bmatrix} \dot{u} + \bar{\zeta}_G \dot{q} \\ \dot{v} + Ur - \bar{\zeta}_G \dot{p} - \bar{\xi}_G \dot{r} \\ \dot{w} - Uq + \bar{\xi}_G \dot{q} \end{bmatrix} \tag{8.44}$$

The relationship of forces and moments acting on the ship in manoeuvring and seakeeping theory can be identified in a similar manner. The forces and moments acting on the ship during manoeuvring and seakeeping motions referenced to upright body-fixed coordinate systems can be related using position vector $\mathbf{r}_{GA}$, which is defined from centre of gravity G to point A located at undisturbed free surface,

$$\begin{bmatrix} X \\ Y \\ Z \end{bmatrix} = \begin{bmatrix} F_1 \\ F_2 \\ F_3 \end{bmatrix}$$
$$\begin{bmatrix} K \\ M \\ N \end{bmatrix} = \begin{bmatrix} F_4 \\ F_5 \\ F_6 \end{bmatrix} + \mathbf{r}_{GA} \times \begin{bmatrix} F_1 \\ F_2 \\ F_3 \end{bmatrix} = \begin{bmatrix} F_4 - \bar{\zeta}_G F_2 \\ F_5 + \bar{\zeta}_G F_1 + \bar{\xi}_G F_3 \\ F_6 - \bar{\xi}_G F_2 \end{bmatrix} \tag{8.45}$$

It should be noted that aforementioned comparison was made on the basis of perturbation from equilibrium state, therefore the relationship between two motion theories are only valid within linear boundary. The identified relationship will be later used to transform hydrodynamic data set obtained in seakeeping theory to integrated mathematical model.

8.4 Impulse Response Function Representation

The aim of this section is the formulation of forces and moments acting on a ship, which departs from a steady motion. It is generally assumed that the forces and moments are dependent on the small quantities of perturbation from equilibrium state at specific moment. This is the basis of formulating fluid forces acting on a ship using Taylor series expansion, which provides simple mathematical descriptions of fluid forces and moments and it allows the use of equations of motion with constant derivatives.

Although this formulation is widely used in the studies of manoeuvring theory and directional stability, the weak point might arise because the motion at any instant can be determined partly by previous motion not only by just current motion. In other words the forces and moments acting on a ship depend on the history of motion and conventional manoeuvring theory is not applicable to represent its effect. Especially to describe the general motion of a ship in a wave it is required to consider this 'memory effect' into equations of motion. In this section theoretical formulation to describe arbitrary motion which include memory effects.

The use of a convolution integral to describe fluid actions acting on the vessel allows for the incorporation of fluid memory effects. The inclusion of such memory effects is important, as the flow conditions at a particular instant cannot uniquely determine the fluid forces and moments occurring at that instant. This problem was discussed by many researchers like Cummins (1962) and by Bishop et al. (1973a and 1973b). The latter developed a rigorous mathematical model to examine manoeuvring experiment data and to express fluid force in a systematic way.

It was shown that any fluid force could be expressed in terms of Volterra convolution integral within the bounds of linear theory. In its most general form, for input $v(t)$ and output $f(t)$, the convolution integral takes the form

$$f(t) = \int_{-\infty}^{\infty} h(\tau) v(t-\tau) d\tau \tag{8.46}$$

where the impulse response function $h(t)$ is such as

$$\begin{aligned} h(\tau) &= 0 \qquad \tau < 0 \\ h(\tau) v(t-\tau) &= 0 \qquad \tau > t \end{aligned} \tag{8.47}$$

The impulse response function used to describe the fluid actions are determined using Fourier transformations of the frequency domain hydrodynamic coefficients. It has been shown that the relationship between the impulse response function and the frequency domain transfer function is given by following equation,

$$\begin{aligned} h(\tau) &= \frac{2}{\pi} \int_0^{\infty} B(\omega) \cos(\omega\tau) d\omega \\ &= -\frac{2}{\pi} \int_0^{\infty} \omega A(\omega) \sin(\omega\tau) d\omega \end{aligned} \tag{8.48}$$

This relationship enables to develop mathematical model of a ship motion using existing frequency dependent hydrodynamic coefficients data. Details to calculated equation (8.48) can be found in the Appendix C.

The hydrodynamic coefficients data used in equation (8.48) often tend to approach a non-zero constant value asymptotically as the frequency increases to infinity. As a consequence, there arise difficulties in calculating impulse response function. Bailey (1999) showed the form of impulse response function to overcome these difficulties using asymptotic value of hydrodynamic coefficients. For example, the asymptotic value of added mass and damping coefficient are denoted by $A(\infty)$ and $B(\infty)$ respectively, and the impulse response can be expressed as

$$\begin{aligned} h^*(\tau) &= \frac{2}{\pi} \int_0^{\infty} B^*(\omega) \cos(\omega\tau) d\omega \\ &= -\frac{2}{\pi} \int_0^{\infty} \omega A^*(\omega) \sin(\omega\tau) d\omega \end{aligned} \tag{8.49}$$

where

$$A^*(\omega) = A(\omega) - A(\infty)$$
$$B^*(\omega) = B(\omega) - B(\infty)$$

Now these integrals in equation (8.49) can be calculated easily because both coefficients tend to zero as frequency increase to infinity. Finally the hydrodynamic force is composed of the term with asymptotic value of hydrodynamic coefficients and convolution integral term representing memory effect. For convenience, superscript used to denote asymptotic value will be removed in the later expressions.

$$\begin{aligned} f(t) &= \int_{-\infty}^{\infty} h(\tau)v(t-\tau)d\tau \\ &= -A(\infty)\dot{v}(t) + B(\infty)v(t) + \int_{-\infty}^{\infty} h^*(\tau)v(t-\tau)d\tau \end{aligned} \tag{8.50}$$

8.5 External Forces

When a ship travels in a wave several external factors have an influence on the dynamic behaviour. Among these dynamic factors wave force, hull force, manoeuvring force, rudder and propeller force are taken into consideration in the external forces because they are most significant components for motion of a ship in a wave. The forces and moments acting on a body are divided as

$$\begin{aligned} X &= X_W + X_H + X_M + X_P + X_R \\ Y &= Y_W + Y_H + Y_M + Y_R \\ Z &= Z_W + Z_H - mg \\ K &= K_W + K_H + K(\dot{\phi}) \\ M &= M_W + M_H \\ N &= N_W + N_H + N_M + N_R \end{aligned} \tag{8.51}$$

where subscript W denotes external forces due to existence of wave, which include hydrostatic restoring force, Froude-Krylov force, diffraction force and wave drift force of a incoming wave, H hull force due to memory effect, and M manoeuvring force component. P and R are propeller and rudder force respectively and $K(\dot{\phi})$ is viscous roll damping moment.

8.5.1 Hydrostatic and Froude-Krylov forces

There exist several force components due to the existence of wave when a ship encounters a wave. Among these components, the most important parts could be divided as hydrostatic restoring force and hydrodynamic excitation (Froude-Krylov) force. In the time domain simulation of a ship in a wave, it is important to consider these two forces because the instantaneous underwater hull surface significantly differs from the mean wetted hull surface and they have an important effect on the motion of a ship.

The Froude-Krylov force is defined as the force that would result from the integration of the incident wave pressure over the wetted surface of the ship, where the pressure is imagined to be undisturbed by the presence of the ship. In seakeeping theory, this integration is carried out over the mean wetted hull surface, but in the present study, the integration is performed over the instantaneous wetted hull surface at each time step, taking into account the large motions of the ship and its exact intersection with the wave surface.

The hydrostatic force F_{HS} and Froude-Krylov force F_{FK} at the point (X_0, Y_0, Z_0) defined at the space-fixed coordinate system are expressed with static pressure p_{HS} and dynamic pressure p_{FK} as follow

$$F_{HS} + F_{FK} = \int_S (p_{HS} + p_{FK})\mathbf{n} ds \tag{8.52}$$

$$p_{HS} = -\rho g Z_0 \text{ and } p_{FK} = -\rho \frac{\partial \Phi_I}{\partial t} \tag{8.53}$$

where Φ_I is incident wave potential, which can be expressed with the sinusoidal wave elevation ζ as

$$\begin{aligned} \Phi_I &= \frac{g\zeta_0}{\omega} e^{kZ_0} \sin[k(X_0 \cos\mu + Y_0 \sin\mu) - \omega t] \\ \zeta &= \zeta_0 \cos[k(X_0 \cos\mu + Y_0 \sin\mu) - \omega t] \end{aligned} \tag{8.54}$$

The dynamic pressure is usually zero at the undisturbed water surface $Z_0 = 0$ in the linear seakeeping theory, but it should be zero at the free surface $Z_0 = \zeta$. For this reason, it is required to stretch the coordinate system with $Z_0' = Z_0 - f(Z_0)$. It can be assumed as $f(Z_0) = \zeta e^{k(Z_0 - \zeta)}$, which satisfies three conditions $f(\zeta) = \zeta$, $f(-\infty) = 0$ and $\frac{\partial f}{\partial Z_0} \propto e^{kZ_0}$. Then dynamic pressure can be expressed as

$$p_D = \rho g \zeta_0 e^{kz'} \cos[k(X_0 \cos\mu + Y_0 \sin\mu) - \omega t]$$
$$= \rho g \zeta e^{kz'} \tag{8.55}$$

The dynamic pressure in equation (8.55) becomes zero at the free surface and decreases exponentially in the deep water.

8.5.2 Diffraction force

The diffraction force results from scattering action of incident wave on the moving body in a seaway. In the potential theory, wave exciting force, which is subdivided by Froude-Krylov and diffraction terms, can be obtained by solving diffraction problem together with radiation problem in frequency domain. While Froude-Krylov force can be evaluated from direct pressure integration over instantaneous wetted hull surface in the wave, it is very time consuming to solve diffraction problem in each time step and change of heading angle during ship motion should be considered in time domain. As practical manner to consider diffraction force together with the change of incoming wave direction, diffraction force evaluated in the frequency domain will be utilised and updated in the time domain calculation as function of wavelength λ and incident wave angle μ as follows

$$F_{Diff} = \zeta_0 \cdot f(U_0, \lambda, \mu) \tag{8.56}$$

8.5.3 Added resistance

The added resistance, which is obtained from second-order wave force in seakeeping theory, could be considered in regular and irregular waves. Under regular waves, the forces are always assumed as time-independent constant values as discussed in the Chapter 7, while they could be treated as a linear superposition of regular components in irregular or random waves.

For practical purpose the second-order forces are considered in surge, sway and yaw modes only since their contribution to remaining modes of motions are not significant in magnitude. Since it is not possible to calculate exact drift force acting on the ship in each time step, some factors to decide current drift forces are considered. The second-order forces can be assumed as proportional to the square of incident wave amplitude, the total drift forces can be expressed as follows

$$F_{Add} = \zeta_0^2 \cdot f(\mu, \lambda, F_N) \tag{8.57}$$

where μ is incident wave angle and λ is wavelength.

Finally total wave force can be expressed as sum of the aforementioned forces as follows,

$$F_W = F_{HS} + F_{FK} + F_{Diff} + F_{Add} \tag{8.58}$$

8.5.4 Hull force - memory effect

Hull force component is mainly due to the frequency dependent motion of a ship in a wave. In the conventional manoeuvring theory the effect of wave is not always considered. The motion of a ship in a wave, however, depends on the encounter frequency of incident wave and its effect should be considered in the formulation of hull force. Although the formulation of hull force will starts from conventional constant form, frequency dependent terms will be introduced and functional representation will be developed.

If sway force is taken for example, sway radiation force F_2^R in the seakeeping theory can be expressed with encounter frequency of wave ω as follows

$$F_2^R = -A_{22}(\omega)\ddot{\xi}_2 - A_{24}(\omega)\ddot{\xi}_4 - A_{26}(\omega)\ddot{\xi}_6 \\ -B_{22}(\omega)\dot{\xi}_2 - B_{24}(\omega)\dot{\xi}_4 - B_{26}(\omega)\dot{\xi}_6 \tag{8.59}$$

Similar expression for sway hull force can be taken

$$Y_{Rad} = Y_{\dot{v}}(\omega)\dot{v} + Y_{\dot{p}}(\omega)\dot{p} + Y_{\dot{r}}(\omega)\dot{r} + Y_v(\omega)v + Y_p(\omega)p + Y_r(\omega)r \tag{8.60}$$

Using relationship given in equations (8.43), (8.44) and (8.45), the sway forces in equations (8.59) and (8.60) are compared directly and the relationship between frequency dependent hull force derivatives and hydrodynamic coefficients in seakeeping theory is identified as follows

$$\begin{aligned} Y_{\dot{v}}(\omega) &= -A_{22}(\omega) \\ Y_v(\omega) &= -B_{22}(\omega) \\ Y_{\dot{p}}(\omega) &= -\{A_{24}(\omega) - \bar{\zeta}_G A_{22}(\omega)\} \\ Y_p(\omega) &= -\{B_{24}(\omega) - \bar{\zeta}_G B_{22}(\omega)\} \\ Y_{\dot{r}}(\omega) &= -\{A_{26}(\omega) - \bar{\xi}_G A_{22}(\omega) - (\bar{U}/\omega^2)B_{22}(\omega)\} \\ Y_r(\omega) &= -\{B_{26}(\omega) - \xi_G B_{22}(\omega) + UA_{22}(\omega)\} \end{aligned} \tag{8.61}$$

The frequency dependent sway hull force is now identified with hydrodynamic coefficients in the seakeeping theory. Additional consideration is, however, required in the formulation of hull force since the nature of manoeuvring motion is different from that of seakeeping motion. Ship heading is often fixed during seakeeping motion since main focus of seakeeping theory is laid on the calculation of motion amplitude in a given wave direction. On the other hand ship heading in the manoeuvring motion changes with the deflection of rudder and relative wave direction to the ship might affect the hull force since encounter frequency is function of heading angle. In order to consider these effects, impulse response function representation can be adopted as discussed in the foregoing section.

Thus corresponding sway hull force, which is coupled with roll and yaw motion, can be expressed as

$$
\begin{aligned}
Y_H &= Y_{\dot{v}}(\infty)\dot{v}(t) + Y_{\dot{p}}(\infty)\dot{p}(t) + Y_{\dot{r}}(\infty)\dot{r}(t) \\
&\quad + Y_v(\infty)v(t) + Y_p(\infty)p(t) + Y_r(\infty)r(t) \\
&\quad + \int_0^t y_v(\tau)v(t-\tau)d\tau + \int_0^t y_p(\tau)p(t-\tau)d\tau \\
&\quad + \int_0^t y_r(\tau)r(t-\tau)d\tau
\end{aligned}
\tag{8.62}
$$

where ∞ denotes asymptotic value of frequency dependent hull force derivative as frequency goes to infinity.

The impulse response functions in equation (8.62) can be obtained from following expressions

$$
\begin{aligned}
y_v(\tau) &= \frac{2}{\pi}\int_0^\infty Y_v(\omega)\cos(\omega\tau)d\omega_e \\
&= -\frac{2}{\pi}\int_0^\infty \omega Y_{\dot{v}}(\omega)\sin(\omega\tau)d\omega \\
y_p(\tau) &= \frac{2}{\pi}\int_0^\infty Y_p(\omega)\cos(\omega\tau)d\omega \\
&= -\frac{2}{\pi}\int_0^\infty \omega Y_{\dot{p}}(\omega)\sin(\omega\tau)d\omega \\
y_r(\tau) &= \frac{2}{\pi}\int_0^\infty Y_r(\omega)\cos(\omega\tau)d\omega \\
&= -\frac{2}{\pi}\int_0^\infty \omega Y_{\dot{r}}(\omega)\sin(\omega\tau)d\omega
\end{aligned}
\tag{8.63}
$$

where $y_v(\tau)$, $y_p(\tau)$ and $y_r(\tau)$ denote impulse response functions corresponding to the motions defined in body-fixed coordinate system.

Finally the frequency dependent hydrodynamic forces are expressed in functional form, such that they are applicable to arbitrary motion and dependent on the history of the motion. Other forces and moments can be formulated in a similar way and these will be substituted to equations of motion as a hull force including memory effect of fluid action.

8.5.5 Manoeuvring force

In the traditional manoeuvring theory, the manoeuvring forces are expressed by higher-order Taylor series expansion and corresponding coefficients are acquired from experiment in calm water such as PMM and Rotating Arm test. Manoeuvring force component is due to mainly viscous effect of the flow and should be considered in the equations of motion because it has significant effects on horizontal plane motions and trajectories during manoeuvring motions even in calm water.

When experiment data are available, they can be used directly in estimating manoeuvring coefficients. In most cases, however, they can be estimated from empirical formulae using principal dimensions of a ship. Empirical formulae might not give accurate results, but it is very practical to use especially at the early stage of design. The manoeuvring forces are considered for surge, sway and yaw motions and linear as well as non-linear coefficients are included.

$$X_{MAN} = X_{vr}vr - X_{RES}(u)$$
$$Y_{MAN} = Y_v v + Y_r r + Y_{v|v|}v\,|v| + Y_{r|r|}r\,|r| + Y_{vvr}vvr + Y_{vrr}vrr \quad (8.64)$$
$$N_{MAN} = N_v v + N_r r + N_{v|v|}v\,|v| + N_{r|r|}r\,|r| + N_{vvr}vvr + N_{vrr}vrr$$

There are several empirical formulae available for the estimation of manoeuvring coefficients in equation (8.64) and details are found in the Appendix C.

8.5.6 Propeller force

Since the hydrodynamic force produced by propeller acts only in surge direction, the mathematical model for thrust is expressed using thrust coefficients K_T as

$$X_P = (1-t)T = (1-t)\rho n^2 D_P^4 K_T(J_P) \quad (8.65)$$

where

t : Thrust deduction factor

T : Propeller thrust

D_P : Propeller diameter

n : Propeller revolution

J_P $= U\cos\beta(1-w_P)/(nD_P)$

The effect of manoeuvring motion on thrust deduction factor t which represent interference between hull and propeller is known to be small. It can be assumed to be constant to some extent of motion, but pertinent correction should be made as the change of propeller force becomes notable.

To calculate effective wake fraction w_P, it is required to consider the change of wake due to the sway and yaw during a manoeuvring motion as well as straight forward motion of a ship. It is, however, difficult to find general expression equivalent to any motion states since the change of wake is also dependent on both the shape of hull surface and loading of propeller. Further details on the calculation of the propeller force are described in Appendix C.

8.5.7 Rudder force

The hydrodynamic action of rudder can be expressed with normal force acting on the rudder F_N in the flow field which consist of the main flow accelerated by propeller in longitudinal direction and the side flow due to yaw motion in the rudder location. The mathematical model for terms on rudder forces are assumed as

$$\begin{aligned} X_R &= -(1-t_R)F_N\sin\delta \\ Y_R &= -(1+a_H)F_N\cos\delta \\ N_R &= -(x_R+a_H x_H)F_N\cos\delta \end{aligned} \tag{8.66}$$

where

t_R : Reduction coefficient of rudder force

a_H : Ratio of additional lateral force

x_H : Distance between CG and the centre of additional lateral force

x_R : Distance between CG and the centre of lateral force

F_N : Normal force acting on rudder

δ : Rudder angle

The normal force F_N acting on rudder proposed by Kijima (1990) is explained in Appendix C. Approximate formulae for each coefficient given by Hasegawa (1980) can be expressed as follow

$$\begin{aligned} 1-t_R &= 0.28C_B + 0.55 \\ a_H &= 0.679 - 1.51C_B + 1.44C_B^2 \\ x_H &= -(0.4 + 0.1C_B)L_{PP} \end{aligned} \tag{8.67}$$

The main role of rudder action is to change or maintain the heading of ship and a good performance of rudder control can be secured from adequate design and use of automatic control system to perform rudder steering in any sea environments. So-called autopilot control for course-keeping is normally based on the measurements of heading angle and rate of heading change from equipments on board such as gyrocompass. It is common practice to use proportional, derivative and integral terms in the control law and standard proportional-differential (PD) type is employed in the present study as follows

$$K_P(\psi - \psi_d) + K_R\dot{\psi} = \delta + t_r\dot{\delta} \tag{8.68}$$

where ψ_d is the desired heading angle, K_P is proportional gain constant, K_R is differential gain constant and t_r is the time constant in rudder activation. Further effects of autopilot can be found in Fossen (1994).

8.5.8 Roll damping component

In order to describe roll motion in various wave conditions, exact estimation of roll damping term is very important. Since the roll damping term considered in frequency dependent hull force has been estimated by potential theory, viscous effect of roll damping should be included in the numerical model.

For the detailed expression of roll damping components, many different models can be used. When model test data is not available, simple linear damping term is often estimated from empirical method proposed by Himeno (1981) as follows,

$$K(\dot{\phi}) = (B_F + B_E + B_W + B_L + B_{BK})\dot{\phi} \tag{8.69}$$

Each damping component in equation (8.69) represents following contributions: B_F = skin friction, B_E = eddy making, B_W = wave making, B_L = lift, and B_{BK} = bilge keel.

In order to represent highly non-linear behaviour of large amplitude roll motion exceeding linear boundary, non-linear expressions can be chosen as follow

$$K(\dot{\phi}) = b_1\dot{\phi} + b_2\dot{\phi}\left|\dot{\phi}\right| \quad : \text{linear plus quadratic} \tag{8.70}$$

$$K(\dot{\phi}) = b_1\dot{\phi} + b_3\dot{\phi}^3 \quad : \text{linear plus cubic}$$

A quadratic term in equation (8.70) is physically based on the frictional contribution of the roll damping, but the expression of the absolute value of roll velocity may lead difficulty when roll motion is solved in an analytic manner. Generally speaking it is not possible to decide which non-linear model is better to obtain the solution of roll motion equation.

8.6 Validation of Numerical Model

In order to validate the theories and numerical techniques developed in the previous sections, a comparative study will be performed to compare numerical calculations with experimental measurements. The experiment data to be used in the validation process was obtained from ITTC benchmark test, which was co-ordinated by the ITTC Specialist Committee on Prediction of Extreme Ship Motions and Capsizing (ITTC 2002), is originally conducted with an aim of benchmark testing of existing software tools and mathematical models on the intact and damage stability of two standard ships, and thus establishment of the state-of-the-art of numerical method and computer simulation program for assessing the dynamic stability in intact and damage conditions under various environmental and operating conditions.

8.6.1 Specification of model: ITTC Ship A-1

Among two model ships used for in the benchmark tests, the first model ship, a 15,000 gross tonnes container ship (Ship A-1), has been selected for the comparison with the subsequent free running experiment with 1/60 scaled model. The panel discretisation of hull form including deck is illustrated in Figure 8.7.

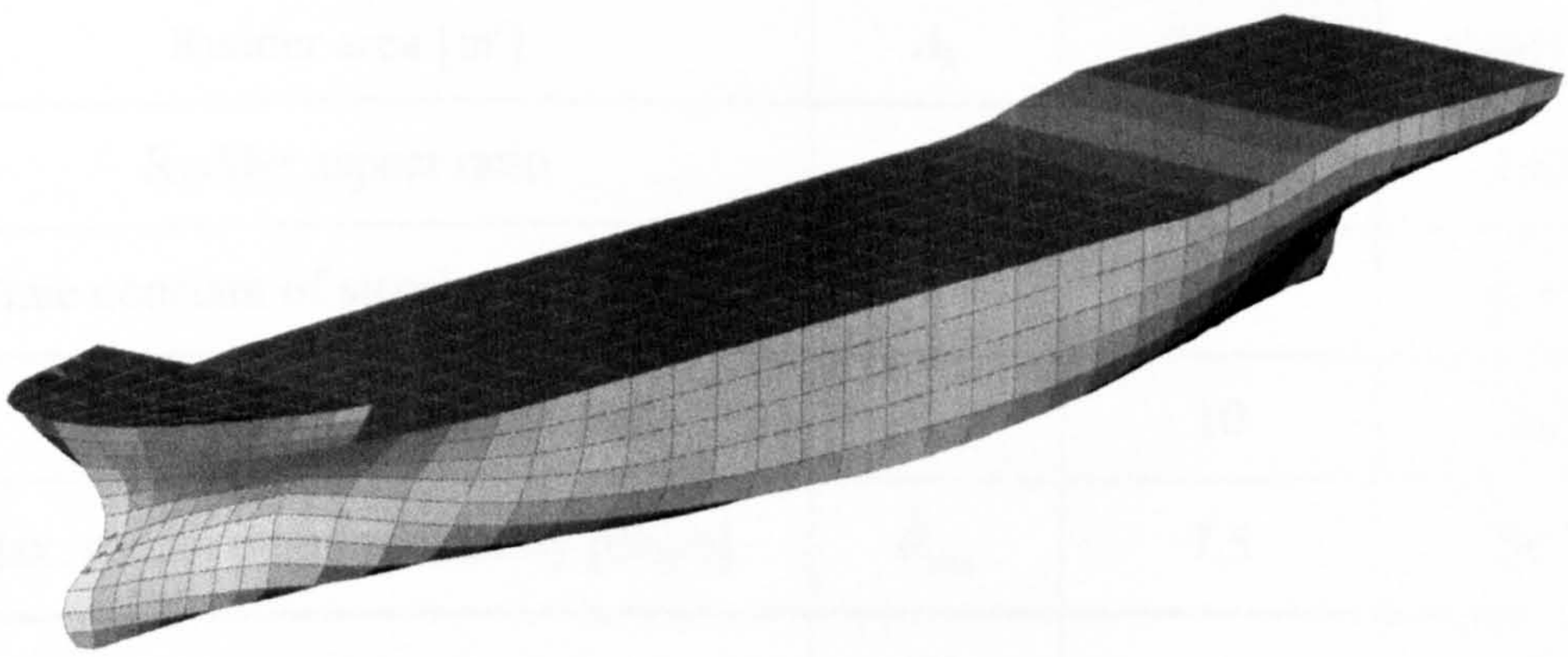

Figure 8.6 Panel representation of ITTC Ship A-1 hull form

The principal dimensions of full and 1/60 scaled model ships are given in the Table 8.1 together with practical data of propeller and rudder.

Table 8.1 Principal dimensions of ITTC Ship A-1 in full scale and 1/60 model scale

Item		Full scale	Model scale
Length [m]	L	150.0	2.5
Breadth [m]	B	27.2	0.453
Depth [m]	D	13.5	0.225
Draught [m]	T	8.5	0.142
Block coefficient	C_B	0.667	0.667
Wetted surface area [m²]	S_w	5065	1.407
Pitch radius of gyration	k_{yy}/L	0.244	0.244
Yaw radius of gyration	k_{zz}/L	0.244	0.244
Longitudinal position of centre of gravity from midship [m]	x_{CG}	-1.01	-0.0168
Vertical position of centre of gravity from keel [m]	KG	11.48	0.1913
Metacentric height [m]	$\overline{GM}_T$	0.15	0.0025
Natural roll period [sec]	T_ϕ	43.3	5.59
Rudder area [m²]	A_R	28.11	0.00781
Rudder aspect ratio	Λ	1.69	1.69
Time constant of steering gear [sec]	t_r	1.24	0.16
Maximum rudder angle [deg]	$\delta_{\max}$	10	10
Max. rudder angular velocity [deg/s]	$\dot{\delta}_{\max}$	7.5	58.1
Propeller diameter [m]	D_P	5.04	0.084
Propeller pitch ratio	P/D_P	0.7049	0.7049

8.6.2 Specifications of test conditions

The overview of the benchmark test is presented focusing on the specifications of the environmental data and benchmark model runs. The specifications of environmental data in the guidelines of benchmark test include a variety of regular waves; wavelength to ship length ratio from 0.25 to 3.00 in step of 0.25 and wave height to wavelength ratio 1/25 (constant). The specifications of benchmark tests include initial motion studies;

- calm water studies : 10°/10° zig-zag test and 35° turning circle manoeuvre at Fn=0.25.
- zero and non-zero forward speed seakeeping cases: 6-DOF response amplitude operators (frequency domain techniques) for varying wavelengths and wave headings.

In the validation study, the simulation will be focused on the intact stability studies of non-zero forward speed case with regular wave excitations, namely capsize simulation of intact Ship A-1 for the following environmental and ship conditions;

- wave length to ship length ratio, $\lambda/L = 1.5$,
- wave height to length ratio $H/\lambda = 1/25$,
- GM = 0.15m (constant),
- Case A: wave heading 0° (following seas), Fn = 0.2 (capsize)
- Case B: wave heading 45° (stern quartering seas), Fn = 0.2 (non-capsize)
- Case C: wave heading 30° (stern quartering seas), Fn = 0.3 (non-capsize)
- Case B: wave heading 30° (stern quartering seas), Fn = 0.4 (capsize)

The experiments were performed with self-propelled ship model and instead of open water test results, following formula was provided for propeller thrust coefficients;

$$K_T = \frac{T}{\rho n^2 D_P^4} = -0.0844 J_P^2 - 0.4882 J_P + 0.4539 \qquad (8.71)$$

The selected test conditions, summarised in Table 8.2, along with control parameters cover relatively low speed to very high speed for the vessel in order to increase the chance of occurrence of different type of dangerous situations.

Table 8.2 Test conditions of ITTC Ship A-1 model

Item / Case		A	B	C	D
Wave steepness	H/λ	1/25	1/25	1/25	1/25
Wave length	λ / L	1.5	1.5	1.5	1.5
Froude number, nominal	F_n	0.2	0.2	0.3	0.4
Autopilot course [deg]	ψ_d	0	-45	-30	-30
Proportional gain	K_P	1.2	1.2	0.8	0.5
Differential gain [sec]	K_R	6.84	6.84	4.56	2.85

8.6.3 Comparisons of numerical calculations with experiments

The experiments were conducted with free running and unrestrained ship model, which was steered on a specified course by auto-pilot in regular following and quartering seas. The angular velocities and angles were measured using an optical gyroscope, and were recorded on an onboard computer. Since the co-ordinate systems in the experiments are different from present study, appropriate conversions of measured data were performed.

During the experiments with test conditions specified in Table 8.2, capsizing due to sub-harmonic roll, sub-harmonic roll without capsizing, harmonic roll and capsizing due to harmonic roll were observed respectively. Comparisons between experiment and numerical calculation are displayed for roll, pitch, yaw and rudder angles in Figure 8.7 through Figure 8.10.

The first run was performed in Froude number 0.2 and autopilot course 0 degree and the results are displayed in Figure 8.9. In the experiment the model experiences significantly large roll angle when wave crest passes amidships and eventually capsizes because restoring buoyancy is not enough to keep the model upright. The numerical model simulates satisfactorily pitch angle, which is important in calculating the instantaneous wetted body surface in the wave. The numerical model also reaches the capsizing limit after displaying parametric built-up of roll angle as shown in the test. The heading angle of numerical model has been kept relatively well by autopilot and then shows a sudden increase just before capsizing. The rudder angle of numerical model shows little fluctuation at the beginning of simulation since initial heading angle is set same with direction of wave.

The results of second test are displayed in Figure 8.9, which was performed in Froude number 0.2 and autopilot course -45 degree. This time the model experiences same situation as first test that roll angle is built up significantly as heading angle approaches following sea, but the model does not capsize since enough restoring moment is recovered as heading angle returns to autopilot course by the action of rudder. Although the roll angle of experiment shows sub-harmonic oscillation with large roll amplitude, the numerical model shows sub-harmonic roll oscillation only with decreasing heading angle and also roll amplitude seems to be under-estimated. The yaw angle as well as rudder action of numerical model shows very good agreement with the experiment and so does the pitch angle.

With the increased speed of Froude number 0.3 and autopilot course -30 degree, harmonic roll oscillation has been observed in the experiment with small roll amplitude compared to previous tests, and straight heading course has been kept eventually. The numerical model exhibits very satisfactory yaw and rudder angles by approaching the autopilot course gradually. Harmonic roll oscillation has been found in the numerical model, which has very similar amplitude to experiment. Since the heading angle has been kept very straight, the estimated roll angle shows more regular oscillation compared to the experiment. The pitch angle again displays good agreements with experiment.

When the forward speed is further increased to Froude number 0.4 with autopilot course -30 degree, very rapid built-up of roll amplitude has been observed in the experiment and consequently the model reaches capsizing angle in just 10 seconds. In the numerical result the roll angle also shows harmonic oscillation with reasonable accuracy and the resonant roll oscillation ends up capsizing in a very similar way to experiment. The numerical model estimates yaw and rudder angle relatively well and shows qualitatively good agreement with experiment. The pitch angle is slightly under-estimated in the numerical model.

An overview of the benchmark tests has shown that there are good agreements in comparisons between experiments and numerical calculations. The numerical model could predict both sub-harmonic and harmonic roll oscillations in different wave conditions with reasonable accuracy except for second model test and the capsizing due to the parametric roll resonance is also quite well predicted in the numerical model. It should be noted that exact estimations of vertical motions like heave and pitch motions play important role for the calculation of instantaneous wave forces, which is directly related to the restoring moment of roll motion, and satisfactory agreements have been found in the numerical model. The horizontal motions of yaw angle, controlled by the rudder activation of autopilot in the numerical model, have showed good agreements with the experiments.

Generally speaking, the validation study of benchmark test has proved that the mathematical model developed in previous sections can be used to predict the motions of a ship in various wave conditions with reasonable accuracy. Therefore, further numerical calculations are to be made in the following sections for standard manoeuvring tests in order to investigate the effects of wave actions on ship motions.

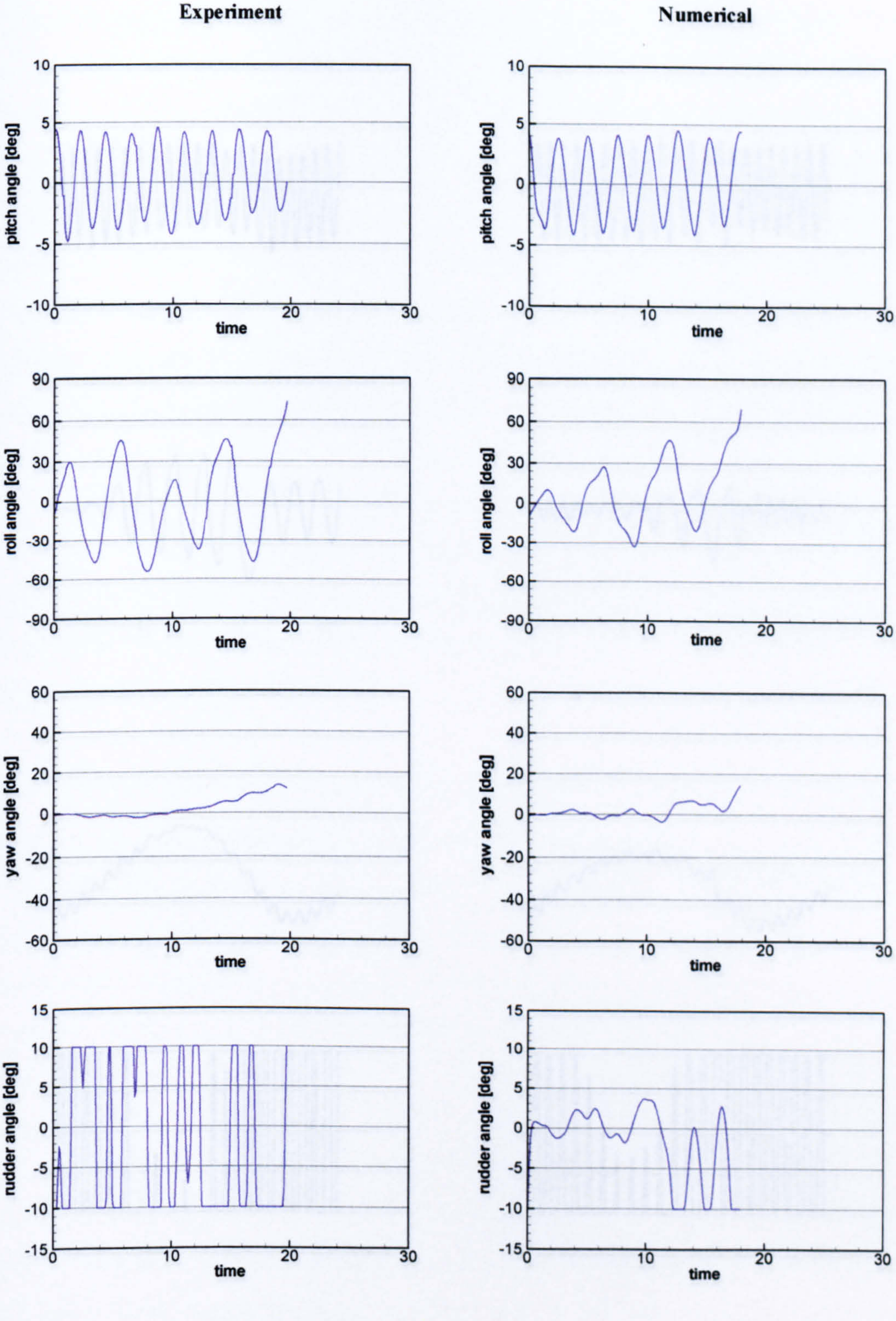

Figure 8.7 Comparison of experiment and numerical method for ITTC Ship A-1 model in H/ λ =1/25, λ /L=1.5, Fn=0.2, ψ_d=0°

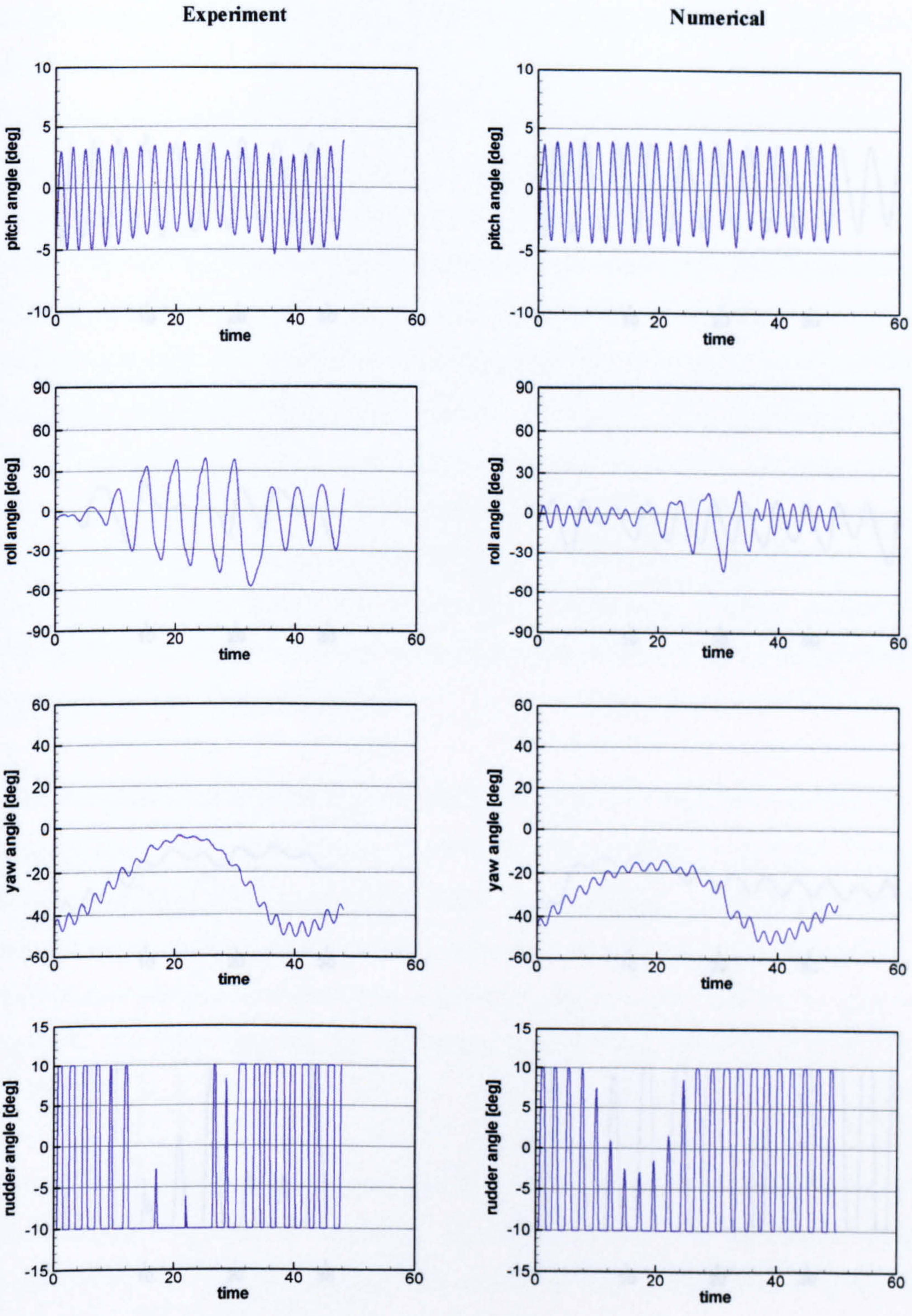

Figure 8.8 Comparison of experiment and numerical method for ITTC Ship A-1 model in H/ λ =1/25, λ /L=1.5, Fn=0.2, ψ_d=-45°

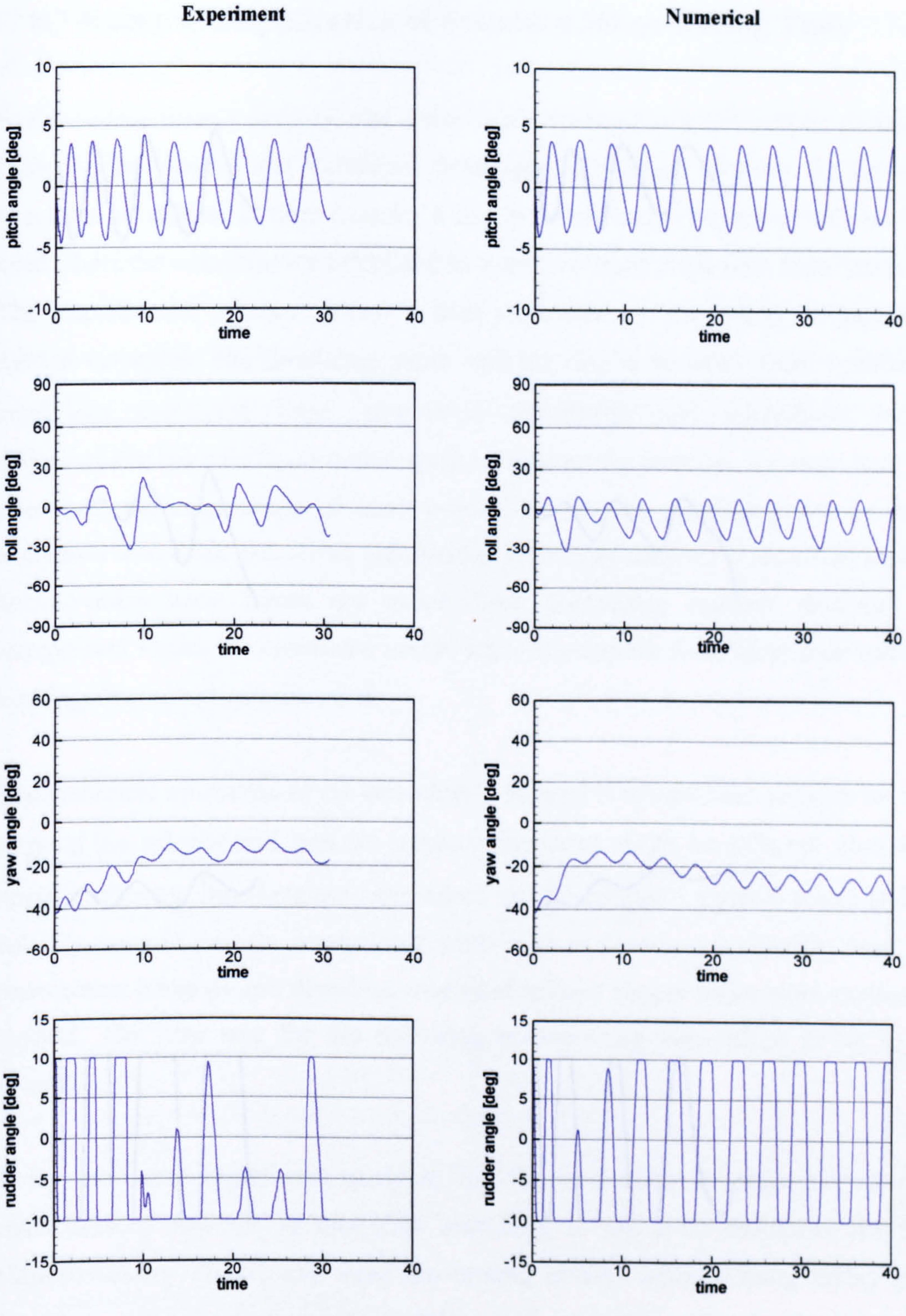

Figure 8.9 Comparison of experiment and numerical method for ITTC Ship A-1 model in H/ λ =1/25, λ /L=1.5, Fn=0.3, ψ_d=-30°

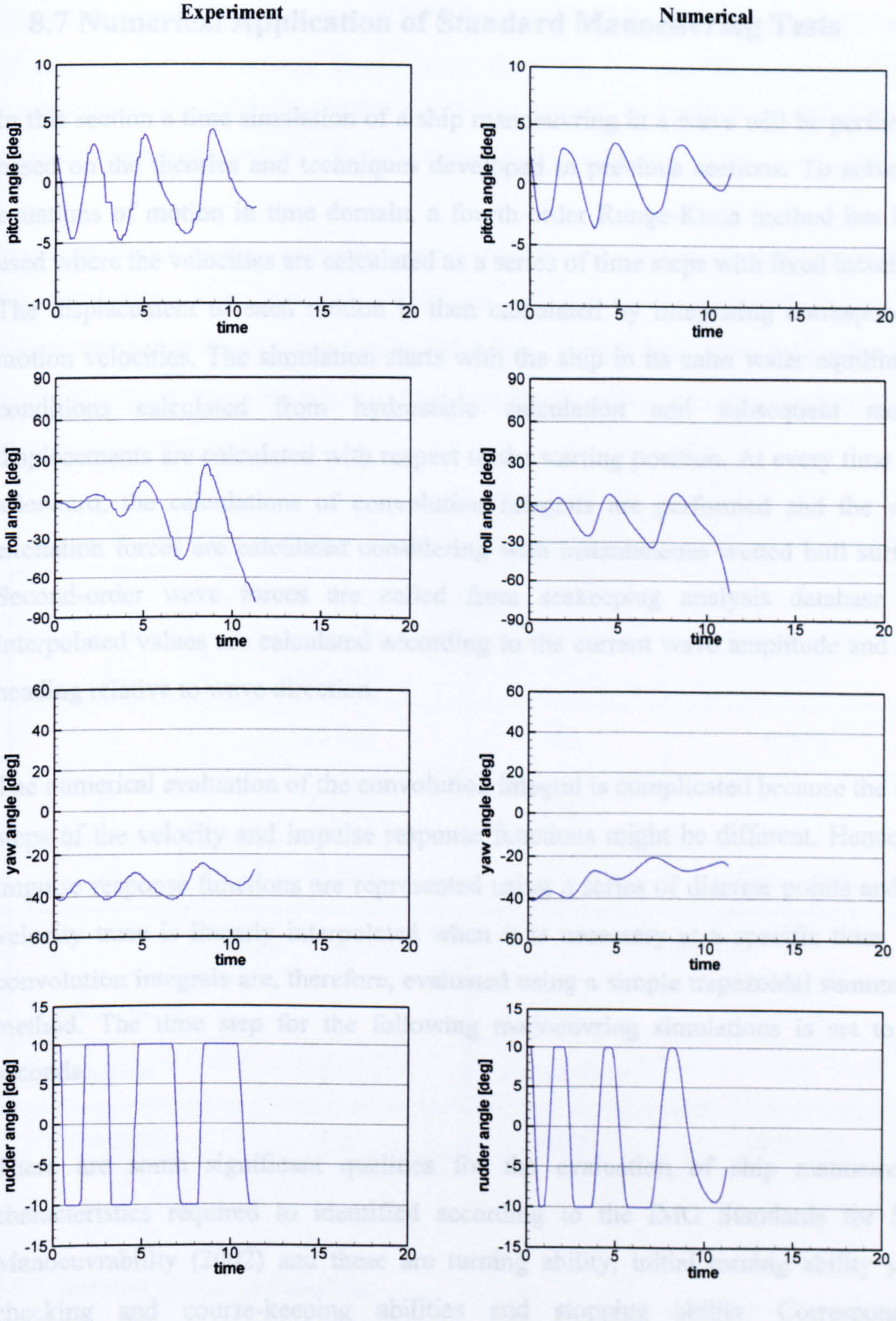

Figure 8.10 Comparison of experiment and numerical method for ITTC Ship A-1 model in H/ λ =1/25, λ /L=1.5, Fn=0.4, ψ_d=-30°

8.7 Numerical Application of Standard Manoeuvring Tests

In this section a time simulation of a ship manoeuvring in a wave will be performed based on the theories and techniques developed in previous sections. To solve the equations of motion in time domain, a fourth-order Runge-Kutta method has been used where the velocities are calculated as a series of time steps with fixed increment. The displacement of each motion is then calculated by integrating corresponding motion velocities. The simulation starts with the ship in its calm water equilibrium conditions calculated from hydrostatic calculation and subsequent motion displacements are calculated with respect to the starting position. At every time step afterward, the calculations of convolution integrals are performed and the wave excitation forces are calculated considering with instantaneous wetted hull surface. Second-order wave forces are called from seakeeping analysis database and interpolated values are calculated according to the current wave amplitude and ship heading relative to wave direction.

The numerical evaluation of the convolution integral is complicated because the time steps of the velocity and impulse response functions might be different. Hence the impulse response functions are represented using a series of discrete points and the velocity trace is linearly interpolated when it is necessary at a specific time. The convolution integrals are, therefore, evaluated using a simple trapezoidal summation method. The time step for the following manoeuvring simulations is set to 0.1 seconds.

There are some significant qualities for the evaluation of ship manoeuvring characteristics required to identified according to the IMO Standards for Ship Manoeuvrability (2002) and these are turning ability, initial turning ability yaw-checking and course-keeping abilities and stopping ability. Corresponding manoeuvring simulations suggested by the IMO Standards are turning circle and zig-zag tests, while remaining stopping test is beyond the interests raised in the present study. Definitions of standard manoeuvring procedure and associated terminology

are followed by the IMO Standards. There are several conventional test conditions to check the criteria suggested by the IMO Standards and calm water condition is one of basic conditions among them. Since there are no specific wave conditions mentioned in the IMO Standards, simulation results predicted with various wave conditions are compared with those in calm water condition.

The Todd Series 60 ship with single-screw propeller is selected as calculation model for continuity. The principal particulars of hull, propeller and rudder for manoeuvring simulation are shown in Table 8.3. The hull form representing the Todd Series 60 ship is required up to the deck line for the calculation of wave forces with various wave amplitudes.

Table 8.3 Principal particulars of hull, propeller and rudder of Todd Series 60

Hull			
L	140 [m]	C_B	0.700
B	20 [m]	C_w	0.785
T	8 [m]	$\overline{GM}_T$	0.1 [m]
D	12 [m]	$\overline{GM}_L$	150.27 [m]
Propeller		Rudder	
Blade number	4	Height	6.04 [m]
Diameter	5.6 [m]	Aspect ratio	2.1
Pitch ratio	1.1	Area	16.8 [m²]

8.7.1 Impulse response function

The impulse response functions used in the equations of motion are expressed as convolution integral with each coupled and uncoupled motion, e.g. in sway mode there are three impulse response functions like sway, sway-roll and sway-yaw. To

evaluate the impulse response functions corresponding hydrodynamic coefficients data estimated in the seakeeping methods are transformed to manoeuvring coefficients in the body-fixed coordinates system according to the relationship given in equation (8.61). Then subsequent relation given in equation (8.49) should be applied to avoid oscillation of impulse response function as $\tau \to \infty$.

The impulse response functions in horizontal and vertical modes are illustrated in Figure 8.11 through Figure 8.13. All calculation results of impulse response functions are non-dimensionalised in the following forms;

- Non-dimensionalisation of impulse response functions

$$
\begin{aligned}
x'_u(\tau) &= \frac{x_u(\tau)}{\frac{1}{2}\rho U^2 L} & x'_w(\tau) &= \frac{x_w(\tau)}{\frac{1}{2}\rho U^2 L} & x'_q(\tau) &= \frac{x_q(\tau)}{\frac{1}{2}\rho U^2 L^2} \\
y'_v(\tau) &= \frac{y_v(\tau)}{\frac{1}{2}\rho U^2 L} & y'_p(\tau) &= \frac{y_p(\tau)}{\frac{1}{2}\rho U^2 L^2} & y'_r(\tau) &= \frac{y_r(\tau)}{\frac{1}{2}\rho U^2 L^2} \\
z'_u(\tau) &= \frac{z_u(\tau)}{\frac{1}{2}\rho U^2 L} & z'_w(\tau) &= \frac{z_w(\tau)}{\frac{1}{2}\rho U^2 L} & z'_q(\tau) &= \frac{z_q(\tau)}{\frac{1}{2}\rho U^2 L^2} \\
k'_v(\tau) &= \frac{k_v(\tau)}{\frac{1}{2}\rho U^2 L^2} & k'_p(\tau) &= \frac{k_p(\tau)}{\frac{1}{2}\rho U^2 L^3} & k'_r(\tau) &= \frac{k_r(\tau)}{\frac{1}{2}\rho U^2 L^3} \\
m'_u(\tau) &= \frac{m_u(\tau)}{\frac{1}{2}\rho U^2 L^2} & m'_w(\tau) &= \frac{m_w(\tau)}{\frac{1}{2}\rho U^2 L^2} & m'_q(\tau) &= \frac{m_q(\tau)}{\frac{1}{2}\rho U^2 L^3} \\
n'_v(\tau) &= \frac{n_v(\tau)}{\frac{1}{2}\rho U^2 L^2} & n'_p(\tau) &= \frac{n_p(\tau)}{\frac{1}{2}\rho U^2 L^3} & n'_r(\tau) &= \frac{n_r(\tau)}{\frac{1}{2}\rho U^2 L^3}
\end{aligned}
\tag{8.72}
$$

Generally the impulse response functions calculated from acceleration dependent coefficients (labelled as added mass) are in good agreements with those from velocity dependent coefficients (damping) for $\tau > 0.8$. The impulse response functions calculated from acceleration dependent coefficients approach zero at $\tau = 0$ due to the formulations given in equation (8.63), while those from velocity dependent coefficients have constant non-zero value at $\tau = 0$. These differences cannot be removed, but be reduced if the upper limit of encounter frequency in equation (8.63) becomes large. Oscillations of impulse response functions almost

disappear for $\tau > 10$ and maximum time of impulse response functions used in the present study is $\tau = 20$ seconds.

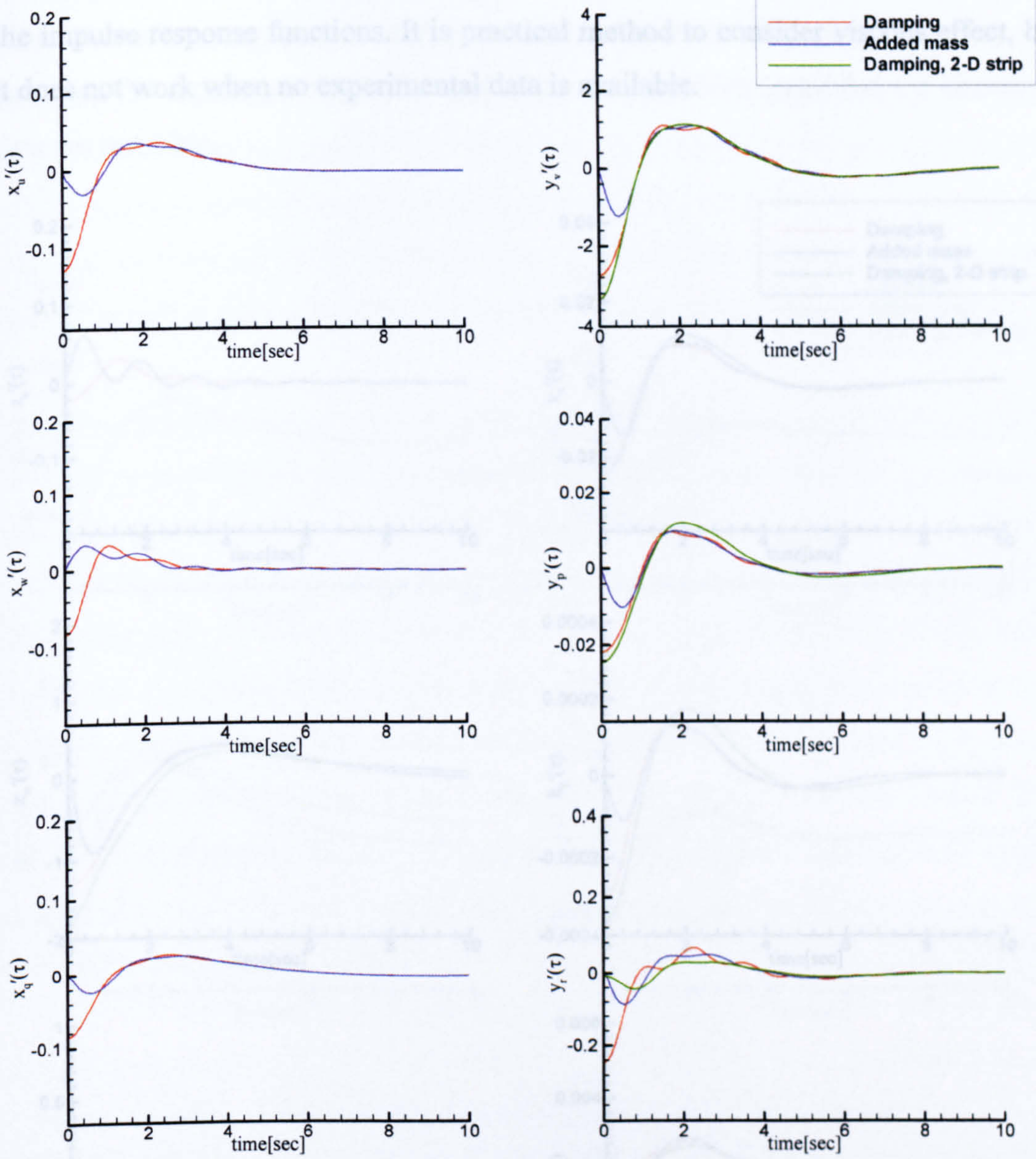

Figure 8.11 Non-dimensional impulse response functions in surge and sway modes for Todd Series 60 at Froude number 0.2

Since the frequency-dependent coefficients are estimated in the ideal fluid assumptions, corresponding impulse response functions dose not contain viscous effects, which is especially important at low frequencies. At high frequencies contribution of inertial force on the oscillating ship becomes significantly dominant

and the viscous contribution to the damping is very small (Newman, 1977). In order to consider viscous effect at low frequencies, Bailey (1999) used hybrid method by complementing low frequency experimental data with the theoretical manoeuvring coefficients data and thus all the necessary system characteristics can be contained in the impulse response functions. It is practical method to consider viscous effect, but it does not work when no experimental data is available.

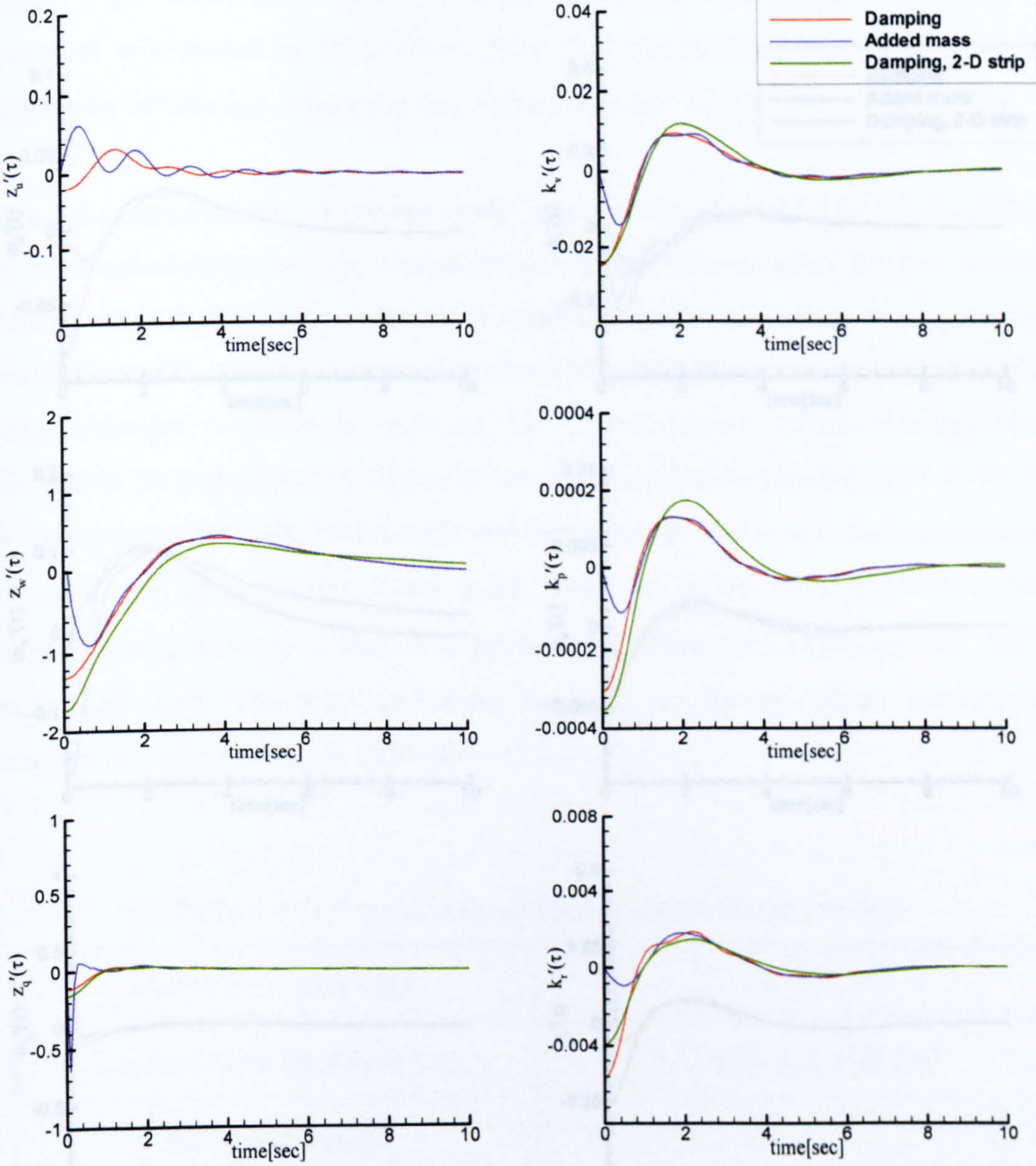

Figure 8.12 Non-dimensional impulse response functions in heave and roll modes for Todd Series 60 at Froude number 0.2

Instead of experimental data manoeuvring empirical formulas, which are widely used in the calm water manoeuvring theory, are adopted in the present study to cover viscous effects at low frequencies. The advantage of employing empirical formulas is that they can be utilised even in early design stage. The consideration on viscous effect at low frequencies is limited to the horizontal mode of motions, e.g. sway and yaw, but the arguments might be applied to the any mode provided the necessary data are available.

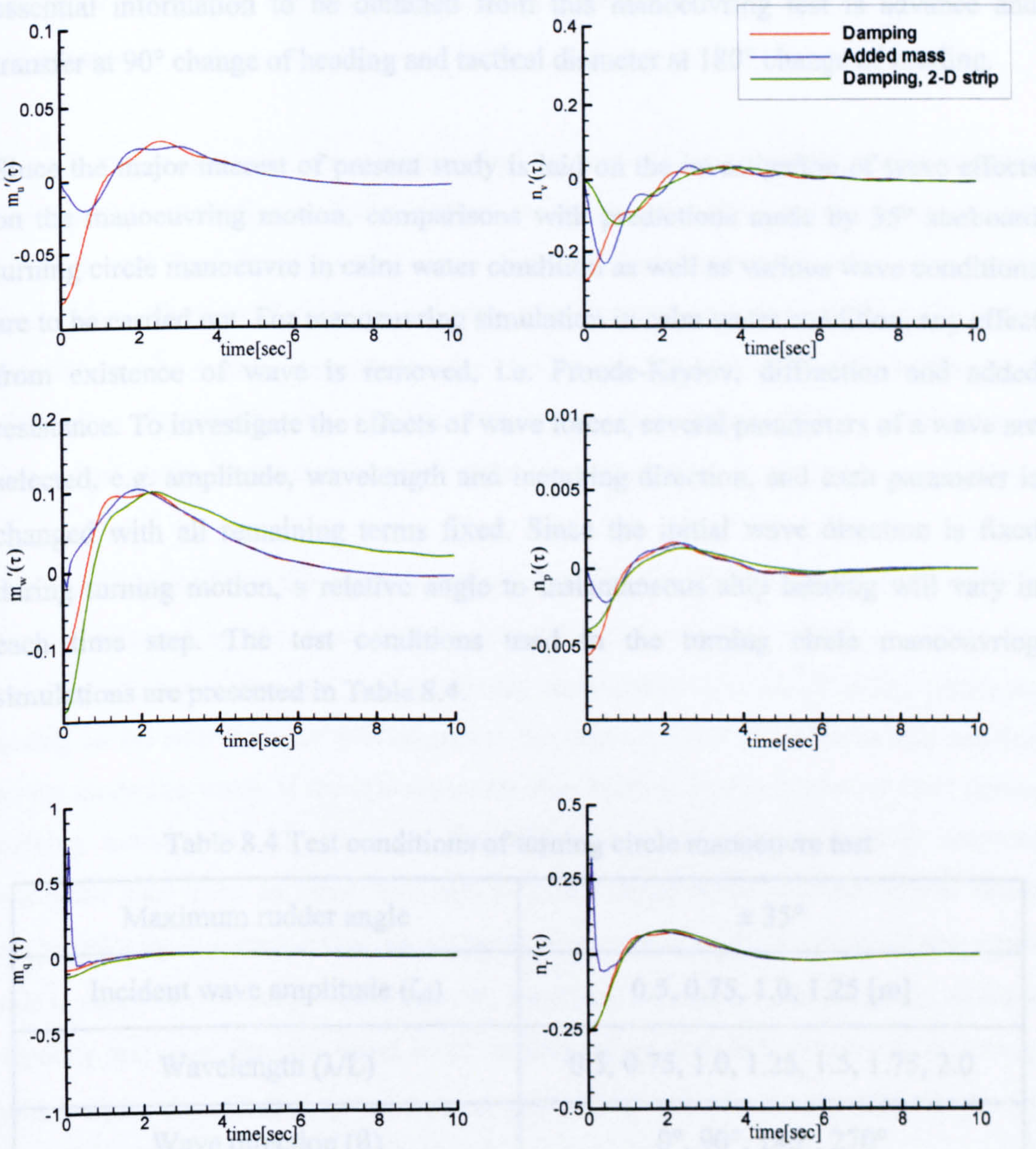

Figure 8.13 Non-dimensional impulse response functions in pitch and yaw modes for Todd Series 60 at Froude number 0.2

8.7.2 Turning circle manoeuvre

Turing ability is the measure of the capability to turn a ship using hard-over rudder and one of the significant qualities for the evaluation of ship manoeuvring characteristics addressed by the IMO Standards for ship manoeuvrability. A turning circle manoeuvring is generally performed to both starboard and port with maximum rudder angle, which is executed following a steady approach with zero yaw rate. The essential information to be obtained from this manoeuvring test is advance and transfer at 90° change of heading and tactical diameter at 180° change of heading.

Since the major interest of present study is laid on the investigation of wave effects on the manoeuvring motion, comparisons with predictions made by 35° starboard turning circle manoeuvre in calm water condition as well as various wave conditions are to be carried out. For manoeuvring simulation in calm water condition, any effect from existence of wave is removed, i.e. Froude-Krylov, diffraction and added resistance. To investigate the effects of wave forces, several parameters of a wave are selected, e.g. amplitude, wavelength and incoming direction, and each parameter is changed with all remaining terms fixed. Since the initial wave direction is fixed during turning motion, a relative angle to instantaneous ship heading will vary in each time step. The test conditions used in the turning circle manoeuvring simulations are presented in Table 8.4.

Table 8.4 Test conditions of turning circle manoeuvre test

Maximum rudder angle	± 35°
Incident wave amplitude (ζ_0)	0.5, 0.75, 1.0, 1.25 [m]
Wavelength (λ/L)	0.5, 0.75, 1.0, 1.25, 1.5, 1.75, 2.0
Wave direction (β)	0°, 90°, 180°, 270°

Figure 8.14 and Figure 8.15 illustrate the trajectories and motions in horizontal plane predicted from 35° starboard turning circle manoeuvring test with various wavelengths and fixed wave amplitude ζ_0=1.0m. The X-Y trajectories are non-dimensionalised with ship length L. It can be seen that the ship continues turning as a result of rudder input, but the shape of turning path becomes ellipse and spiral compared with that of calm water. Consequently an average shift of the ship trajectory to the direction of incoming wave is observed and it is mainly by the wave force exerted on the ship. As wavelength becomes large at high frequencies, the effects of wave force are reduced and consequently turning path approaches that of calm water.

Time histories of surge, sway, yaw velocities and roll and heading angles are also illustrated in each figure. These values are predicted with a wave of wavelength λ/L=1.0 and ζ_0=1.0m in each wave direction and compared with calm water simulation. The oscillation of velocity, which does not appear in calm water simulation, is mainly caused by the frequency dependent Froude-Krylov and diffraction forces in time domain simulation. The amplitude of oscillation is dependent on the instantaneous wave direction to the ship.

It should be noted that the deviation of velocity from calm water calculation result is further affected by the second-order wave force, i.e. added resistance. When the heading of ship is changed during turning manoeuvre, amount of added resistance acting on the ship changes with respect to the instantaneous and relative ship heading to the incoming wave. If the instantaneous ship heading becomes around 180° during turning manoeuvre, for example, the effect of added resistance term becomes strongest than those in other headings and then surge velocity is decreased. When surge velocity is decreased by the action of wave, yaw rate is also reduced since yaw rate is coupled with surge velocity in the equations of motion. The reduction of surge velocity and yaw rate can cause large turning radius and shift of turning trajectory, which make the spiral shape of turning path. Sway velocity is also affected by the change of ship heading in a similar manner.

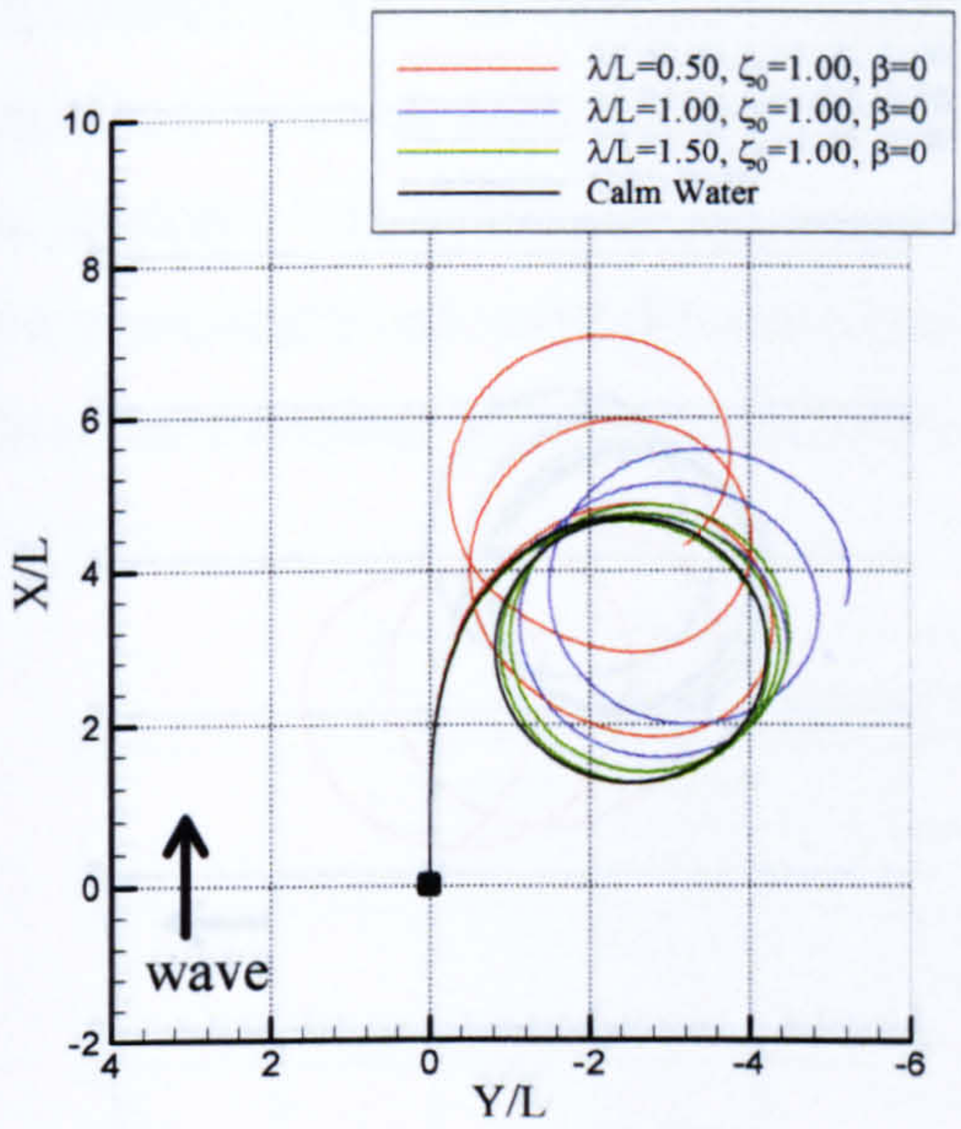

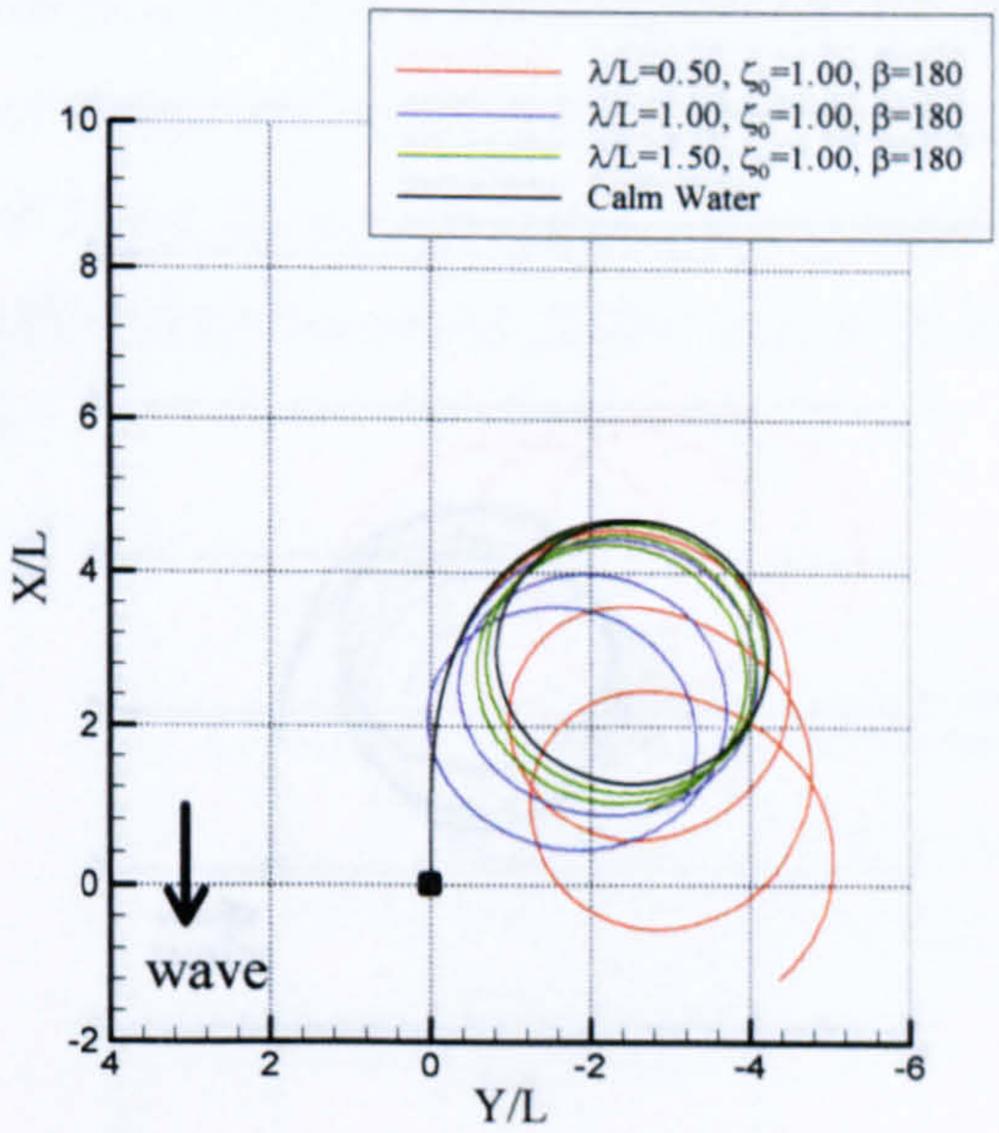

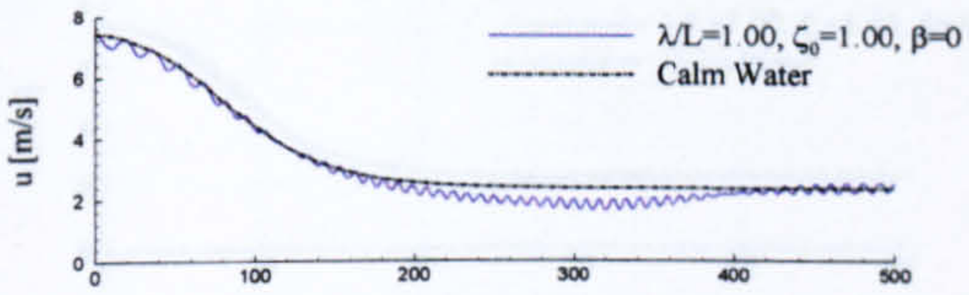

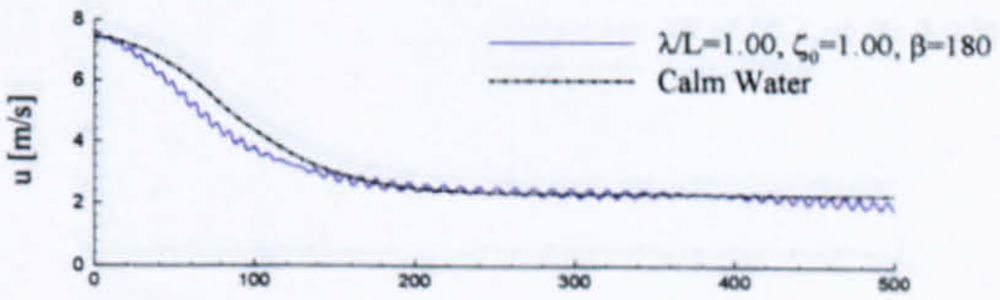

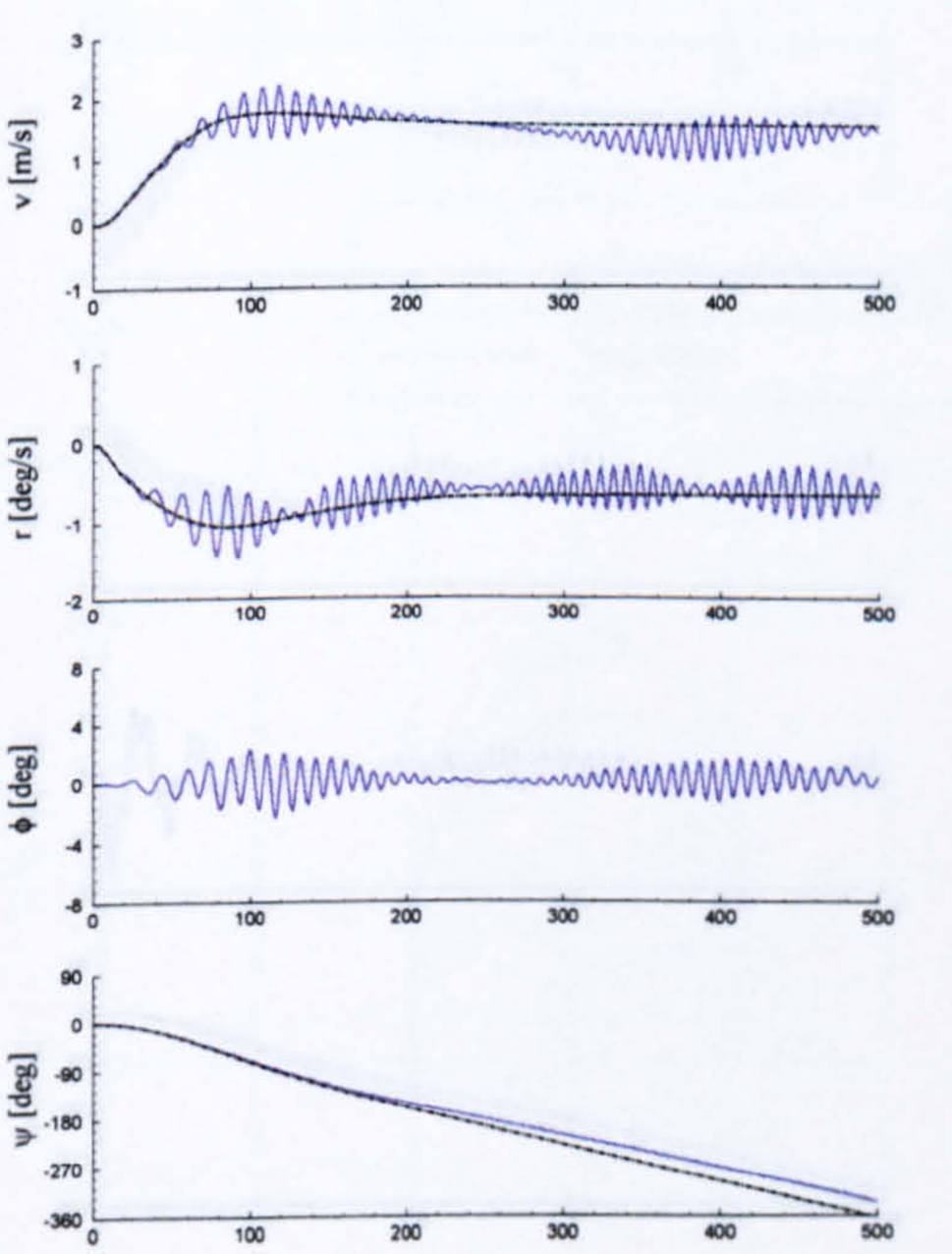

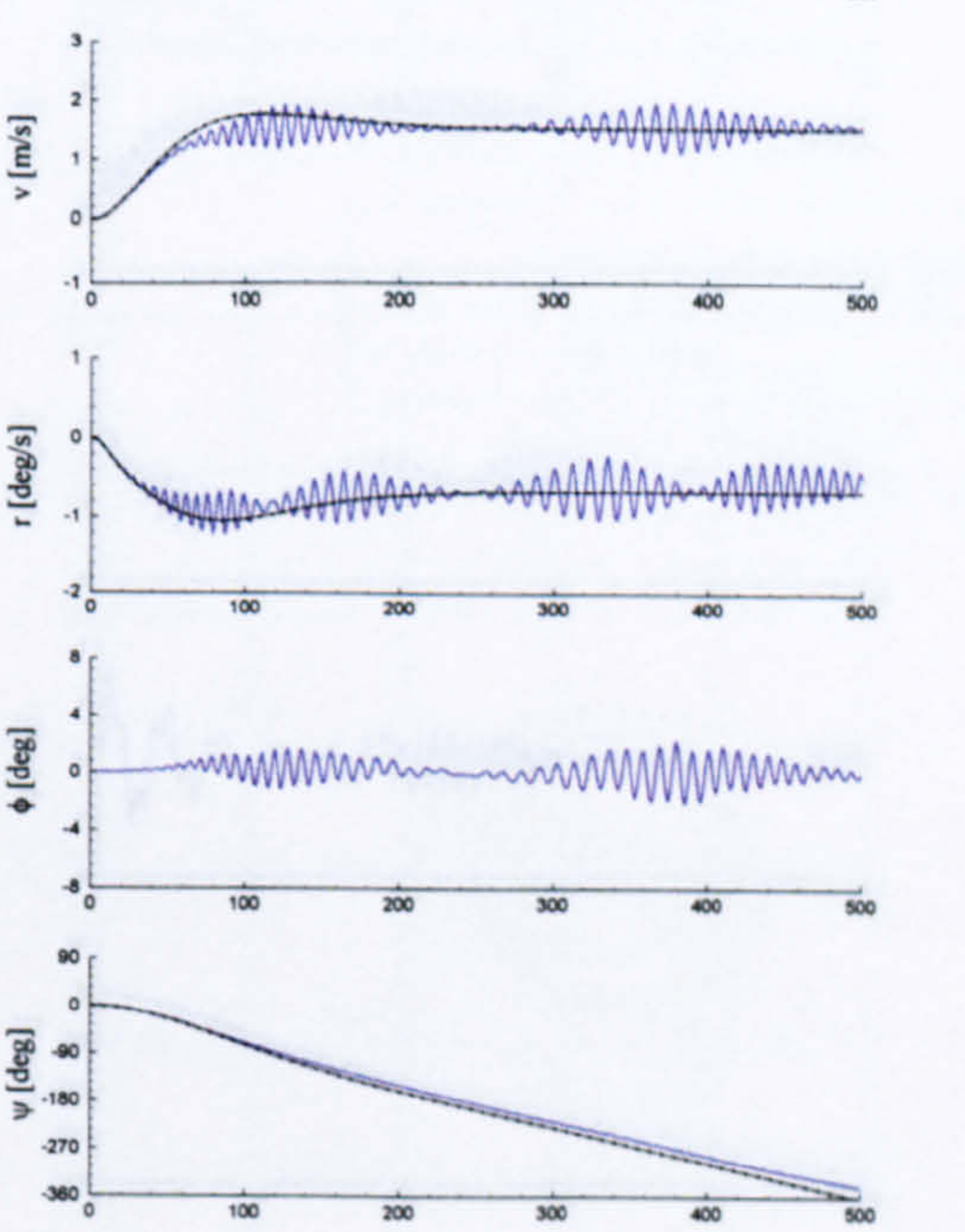

Figure 8.14 Comparisons of trajectories and motions of 35° starboard turning circle manoeuvre for various wavelengths (ζ_0=1.0m, β=0°, 180°)

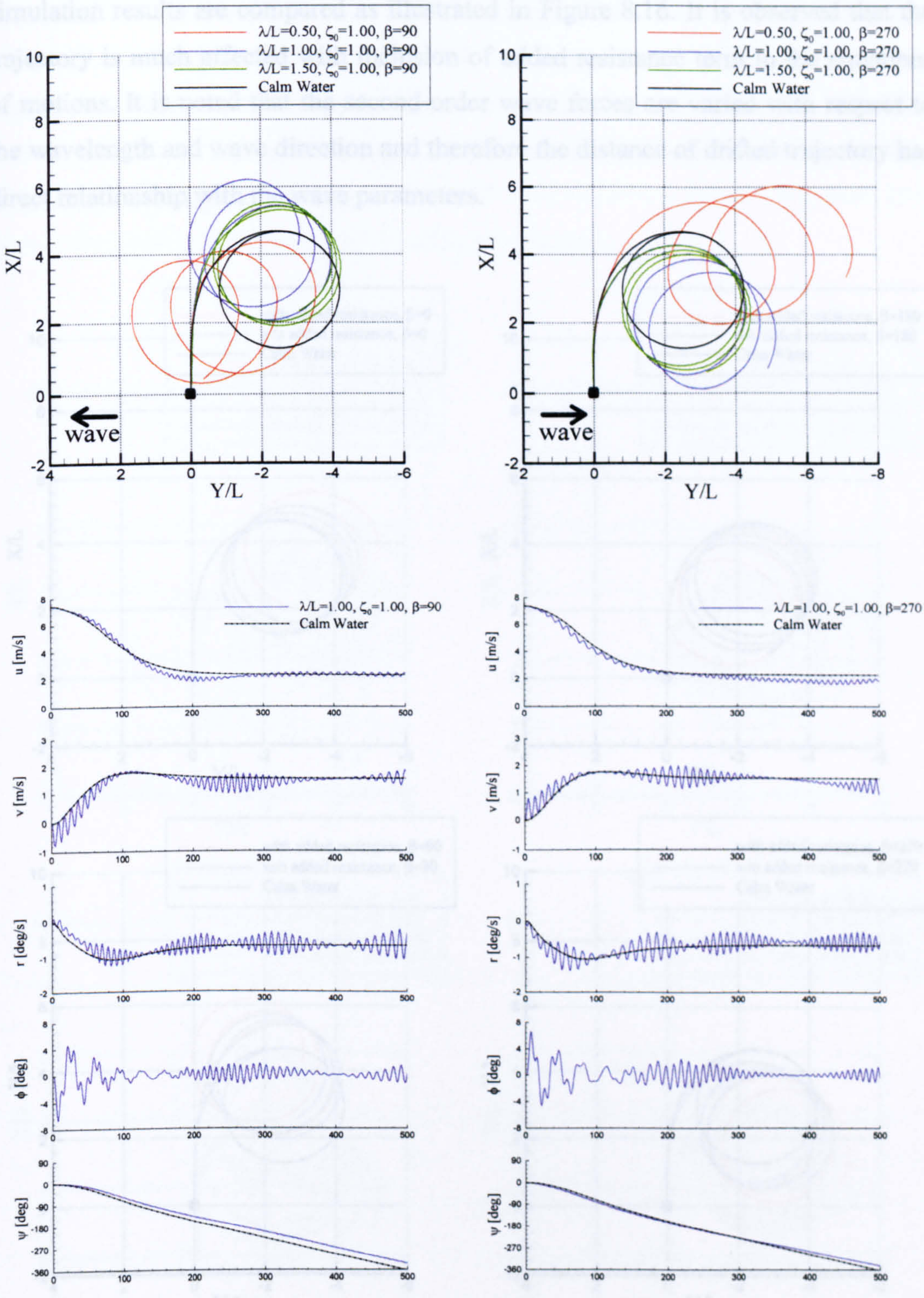

Figure 8.15 Comparisons of trajectories and motions of 35° starboard turning circle manoeuvre for various wavelengths (ζ_0=1.0m, β=90°, 270°)

In order to examine the effect of added resistance on turning manoeuvring, numerical simulation results are compared as illustrated in Figure 8.16. It is observed that the trajectory is much affected with inclusion of added resistance term in the equations of motions. It is noted that the second-order wave forces are varied with respect to the wavelength and wave direction and therefore the distance of drifted trajectory has direct relationship with the wave parameters.

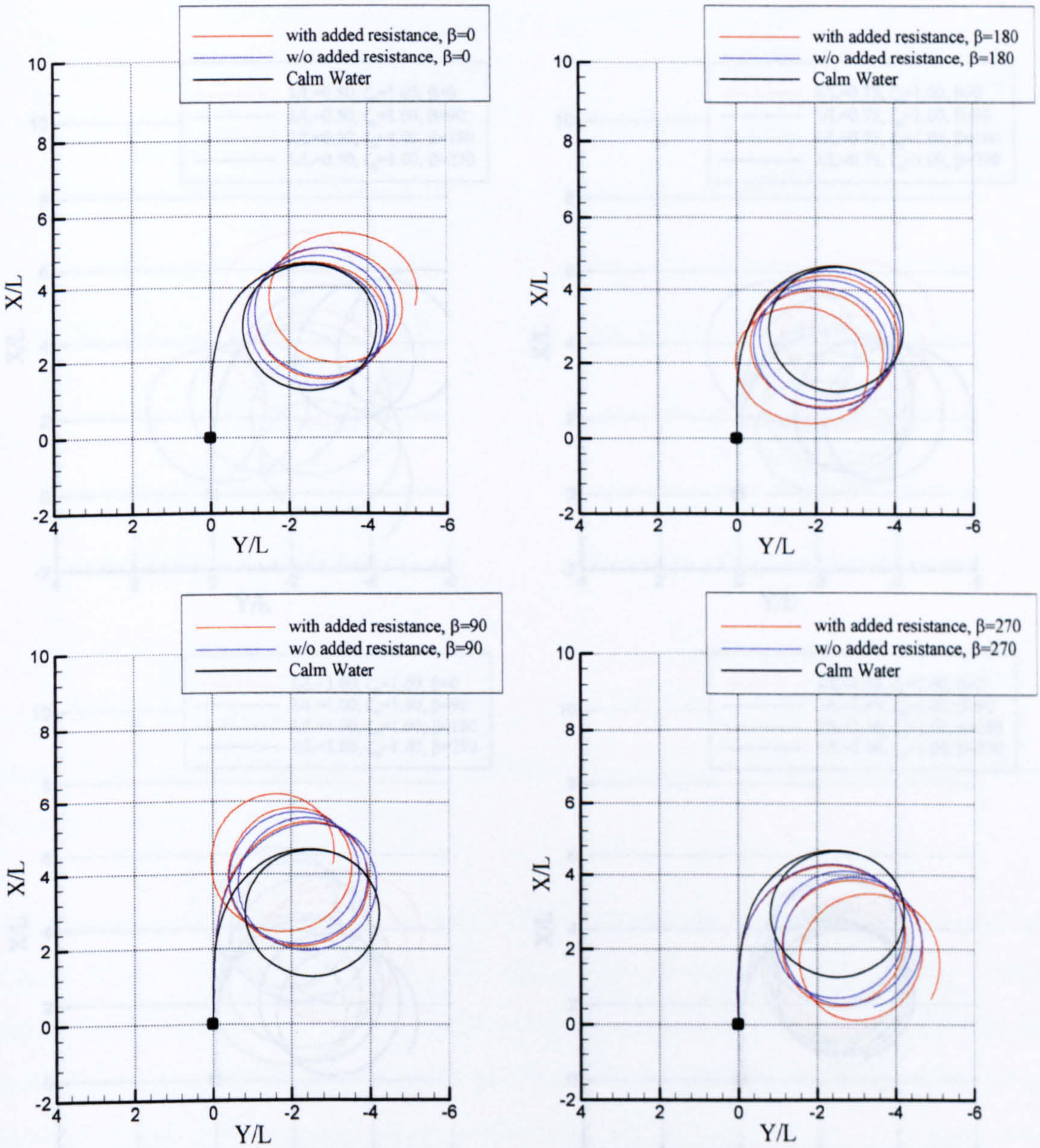

Figure 8.16 Effects of second-order force on trajectory of 35° starboard turning circle manoeuvre ($\lambda/L=1.0$, $\zeta_0=1.0m$)

The effects of wavelength and ship heading relative to the incoming wave are illustrated in Figure 8.17. In each figure wave amplitude is fixed as ζ_0=1.0m with different wavelengths λ/L=0.5, 0.75, 1.0, 1.5 respectively. Turning manoeuvre trajectories, which are drifted to the direction of incoming wave, are easily identified and the effects of varying wavelength are also clearly observed, where contribution of smaller wavelength is dominant.

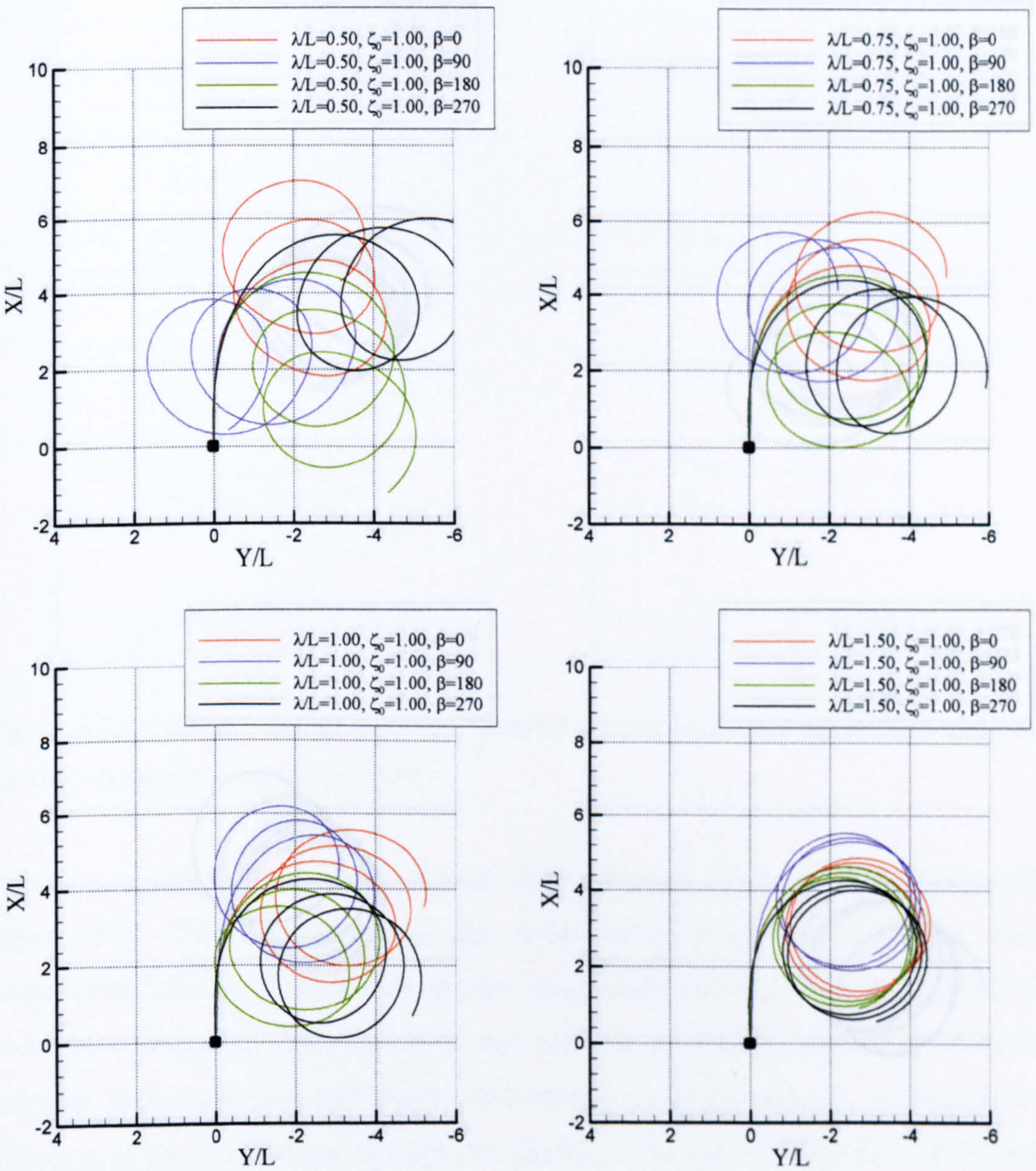

Figure 8.17 Effects of wavelength and wave direction on trajectory of 35° starboard turning circle manoeuvre (λ/L=0.5, 0.75, 1.0, 1.5, ζ_0=1.0m)

The effects of wave amplitude on the turning circle manoeuvre are presented in Figure 8.18. As mentioned above added resistance plays important role in the determining turning path and is generally known to be proportional to the square of wave amplitude. Drifted paths of turning manoeuvre vary according to different wave amplitudes since changes of surge and sway velocities and turning rates have direct relationship with the amplitude of incoming wave.

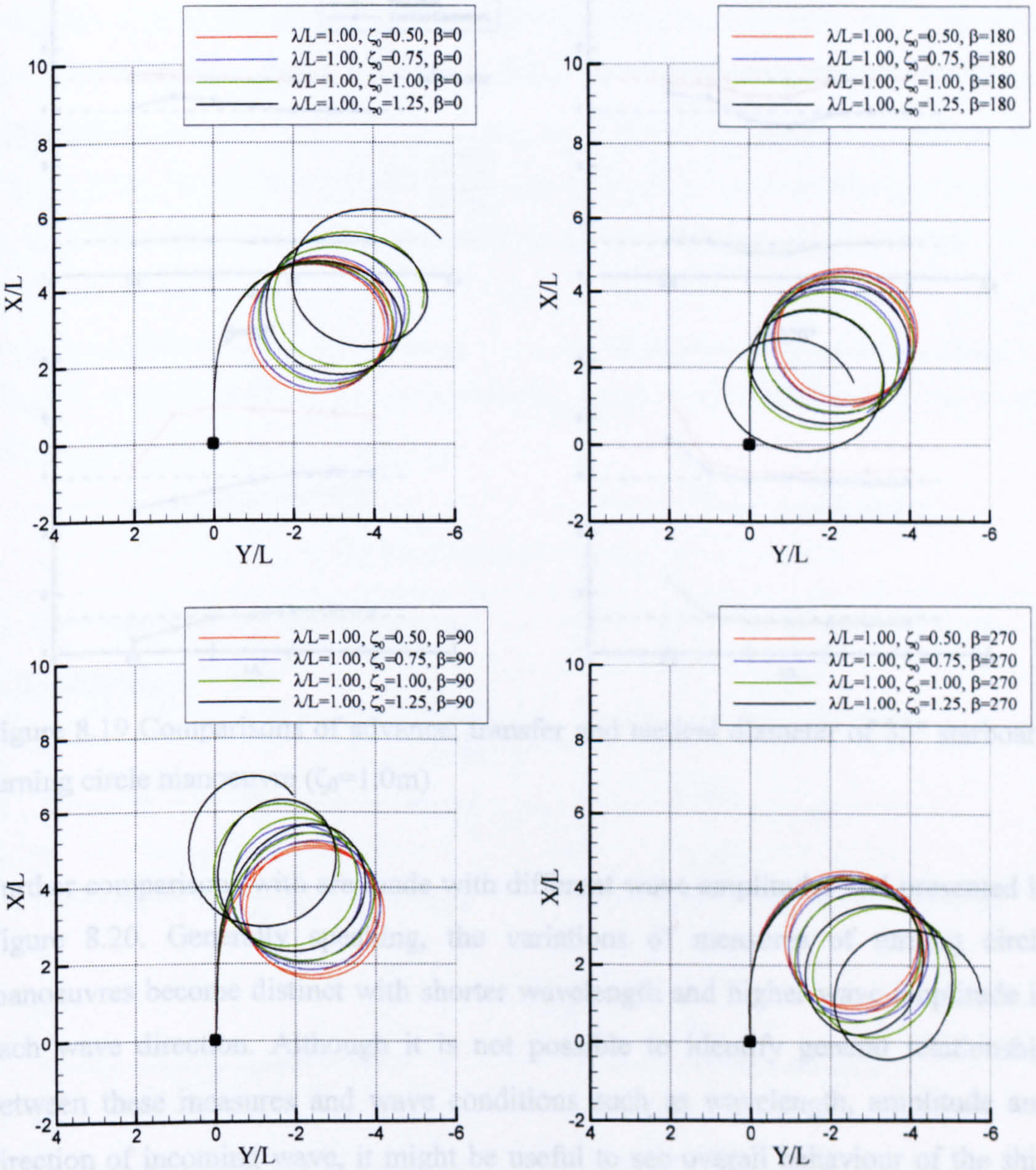

Figure 8.18 Effects of wave amplitude on trajectory of 35° starboard turning circle manoeuvre (λ/L=1.0, ζ_0=0.5, 0.75, 1.0, 1.25m)

Calculation results of important operational parameters like predicted advance, transfer and tactical diameter are illustrated in Figure 8.19 for fixed wave amplitude ζ_0=1.0m, and comparisons are made with calm water case. It is noticed that measures of advance and transfer are opposite when the initial heading is in transverse direction, i.e. β=90°, 270° and the variation becomes stronger with short wavelength as presented in the figure.

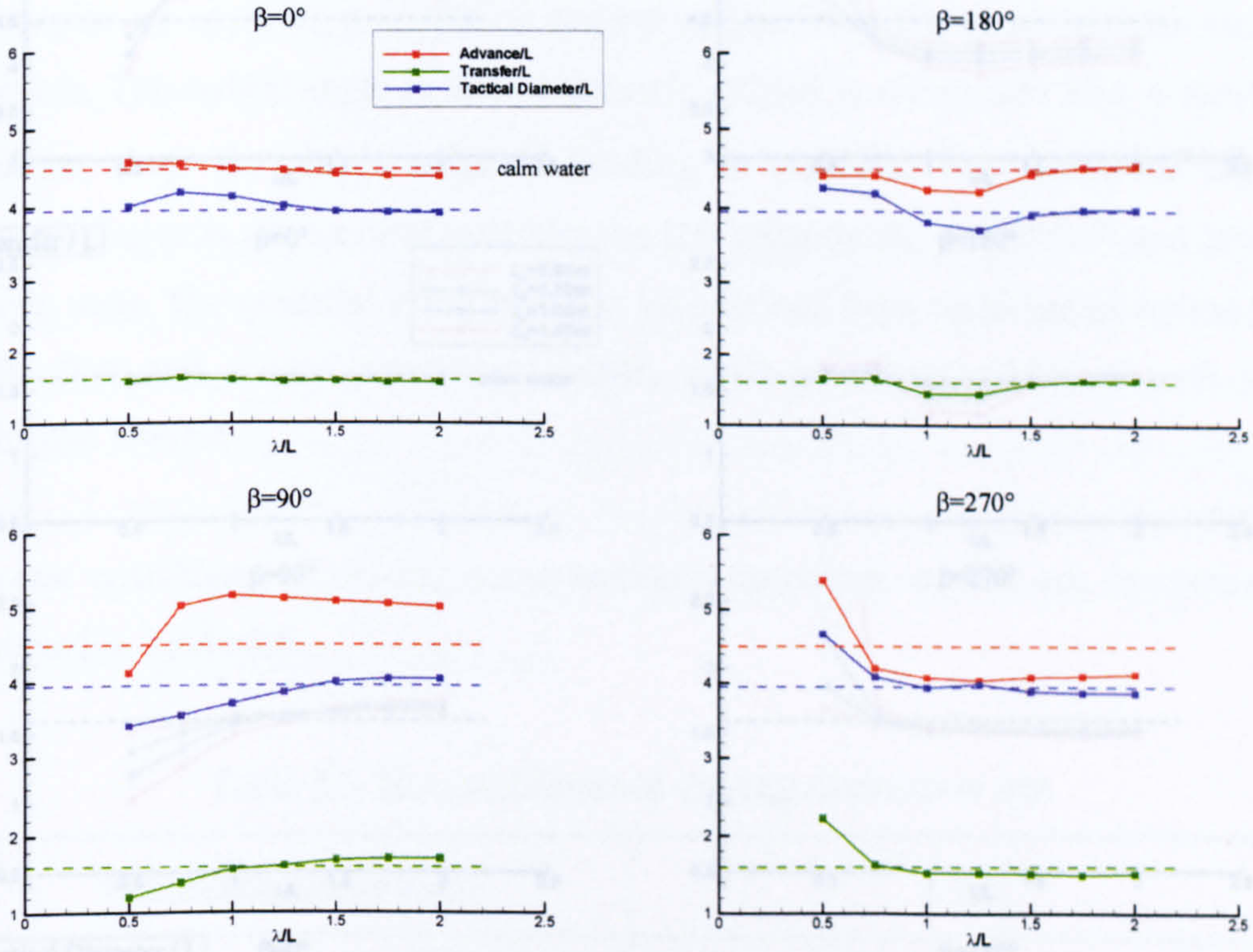

Figure 8.19 Comparisons of advance, transfer and tactical diameter of 35° starboard turning circle manoeuvre (ζ_0=1.0m)

Further comparisons with are made with different wave amplitudes and presented in Figure 8.20. Generally speaking, the variations of measures of turning circle manoeuvres become distinct with shorter wavelength and higher wave amplitude in each wave direction. Although it is not possible to identify general relationship between these measures and wave conditions such as wavelength, amplitude and direction of incoming wave, it might be useful to see overall behaviour of the ship during turning manoeuvre in a wave.

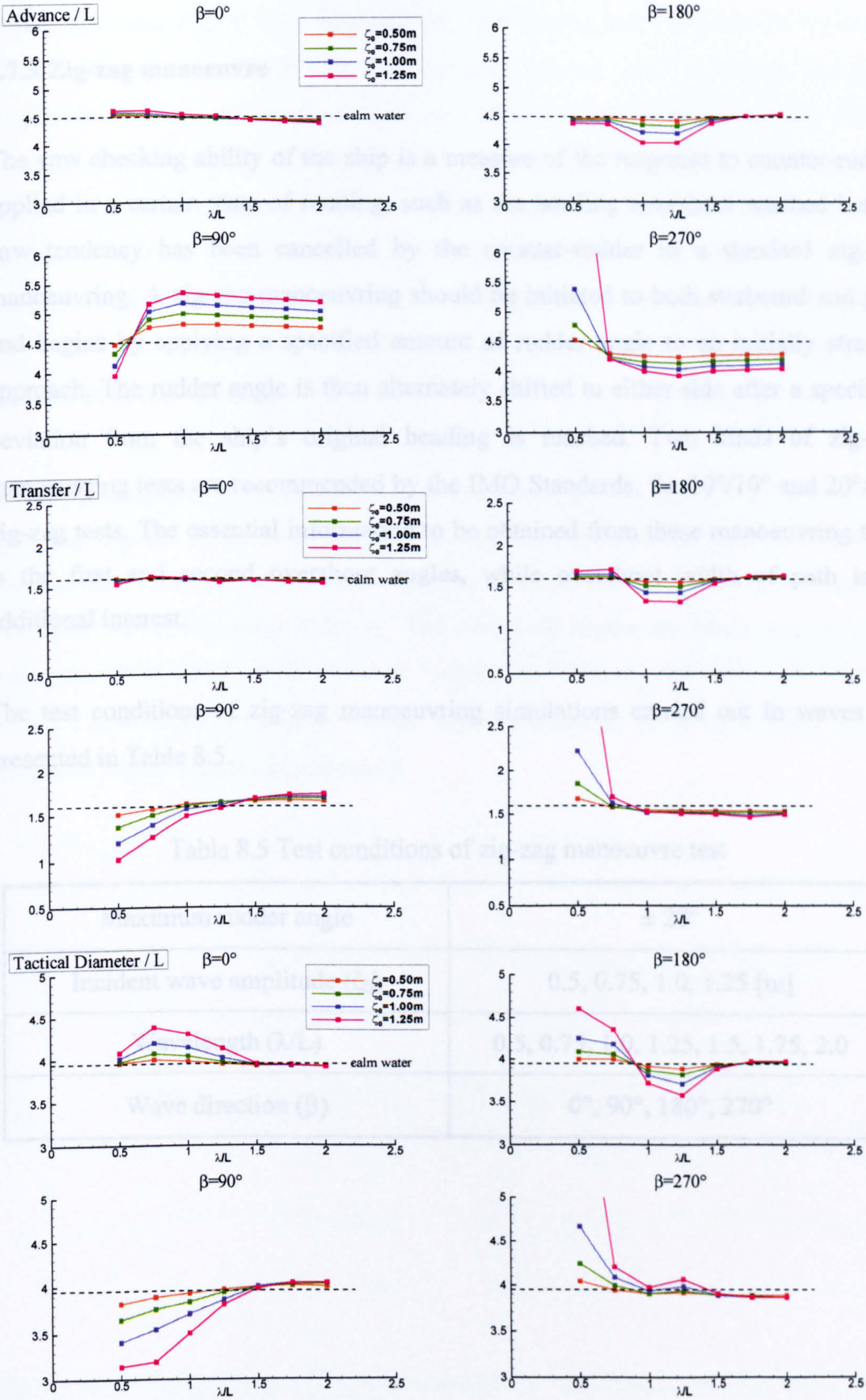

Figure 8.20 Comparisons of measurements of 35° starboard turning circle manoeuvre

8.7.3 Zig-zag manoeuvre

The yaw checking ability of the ship is a measure of the response to counter-rudder applied in a certain state of running, such as the heading overshoot reached before yaw tendency has been cancelled by the counter-rudder in a standard zig-zag manoeuvring. A zig-zag manoeuvring should be initiated to both starboard and port and begins by applying a specified amount of rudder angle to an initially straight approach. The rudder angle is then alternately shifted to either side after a specified deviation from the ship's original heading is reached. Two kinds of zig-zag manoeuvring tests are recommended by the IMO Standards, the 10°/10° and 20°/20° zig-zag tests. The essential information to be obtained from these manoeuvring tests is the first and second overshoot angles, while overshoot width of path is of additional interest.

The test conditions of zig-zag manoeuvring simulations carried out in waves are presented in Table 8.5.

Table 8.5 Test conditions of zig-zag manoeuvre test

Maximum rudder angle	± 20°
Incident wave amplitude (ζ_0)	0.5, 0.75, 1.0, 1.25 [m]
Wavelength (λ/L)	0.5, 0.75, 1.0, 1.25, 1.5, 1.75, 2.0
Wave direction (β)	0°, 90°, 180°, 270°

Figure 8.21 and Figure 8.22 illustrate the yaw angles and velocities in horizontal plane predicted from 20°/20° zig-zag test with various wave conditions and fixed amplitude ζ_0=1.0m. Although there is no differences in the time to reach second execute of rudder in the following sea β=0° and head seas β=180°, presented in Figure 8.21, clear differences are observed in the time to reach third execute of rudder. Compared with the calm water case, the time to reach third execute is increased with short wavelength in the following sea and vice versa in the head sea. One of the reasons could be the reduction of surge velocity in head sea due to the increase of added resistance.

When the direction of incoming wave is transverse, β=90° and 270°, more distinct tendency appears in the times to reach second and third execute. The differences in times to reach second and third execute is more influenced by the sway velocity and yaw rates rather than surge velocity. The overshoot angles are much more affected with transverse direction waves than longitudinal waves, especially for λ/L=0.5, β=270°, first overshoot angle is much bigger than calm water case while second overshoot angles reduces significantly.

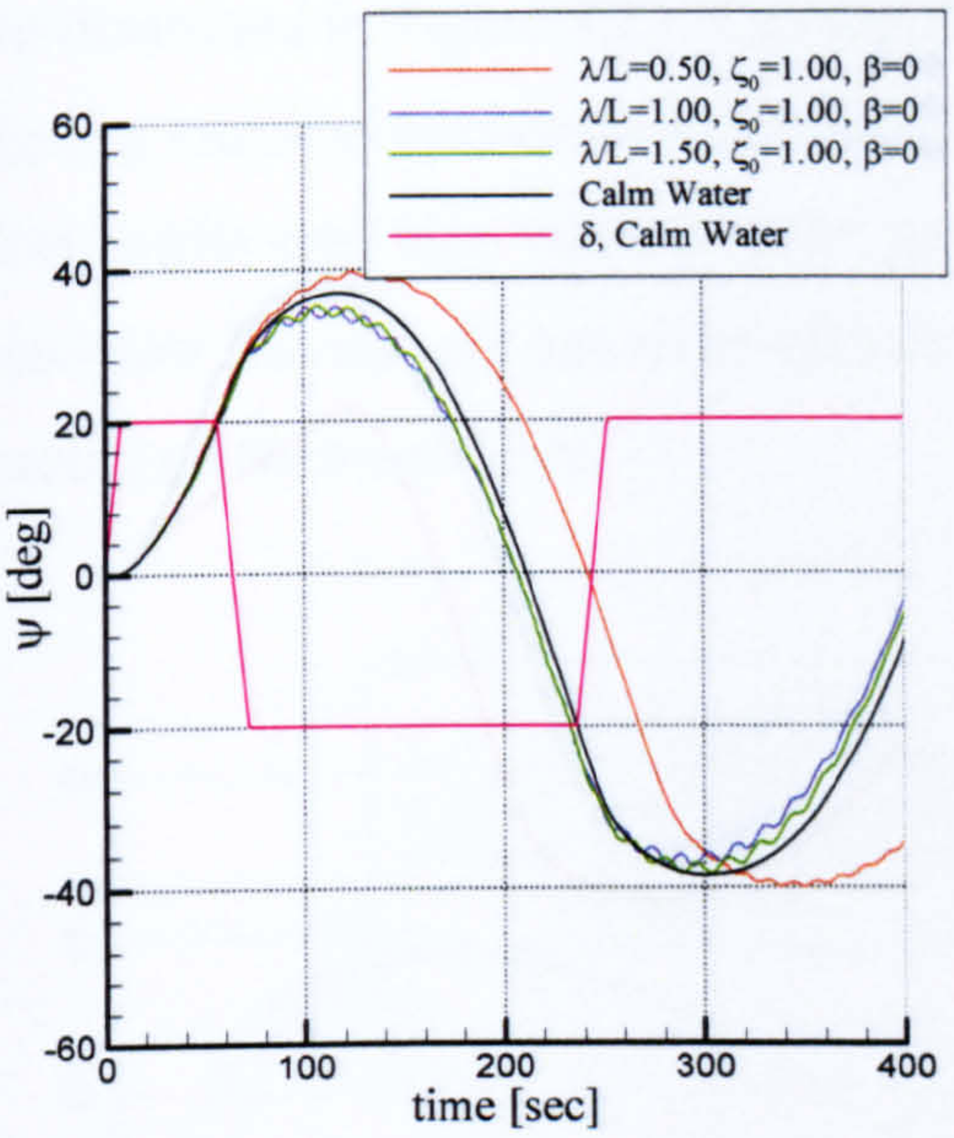

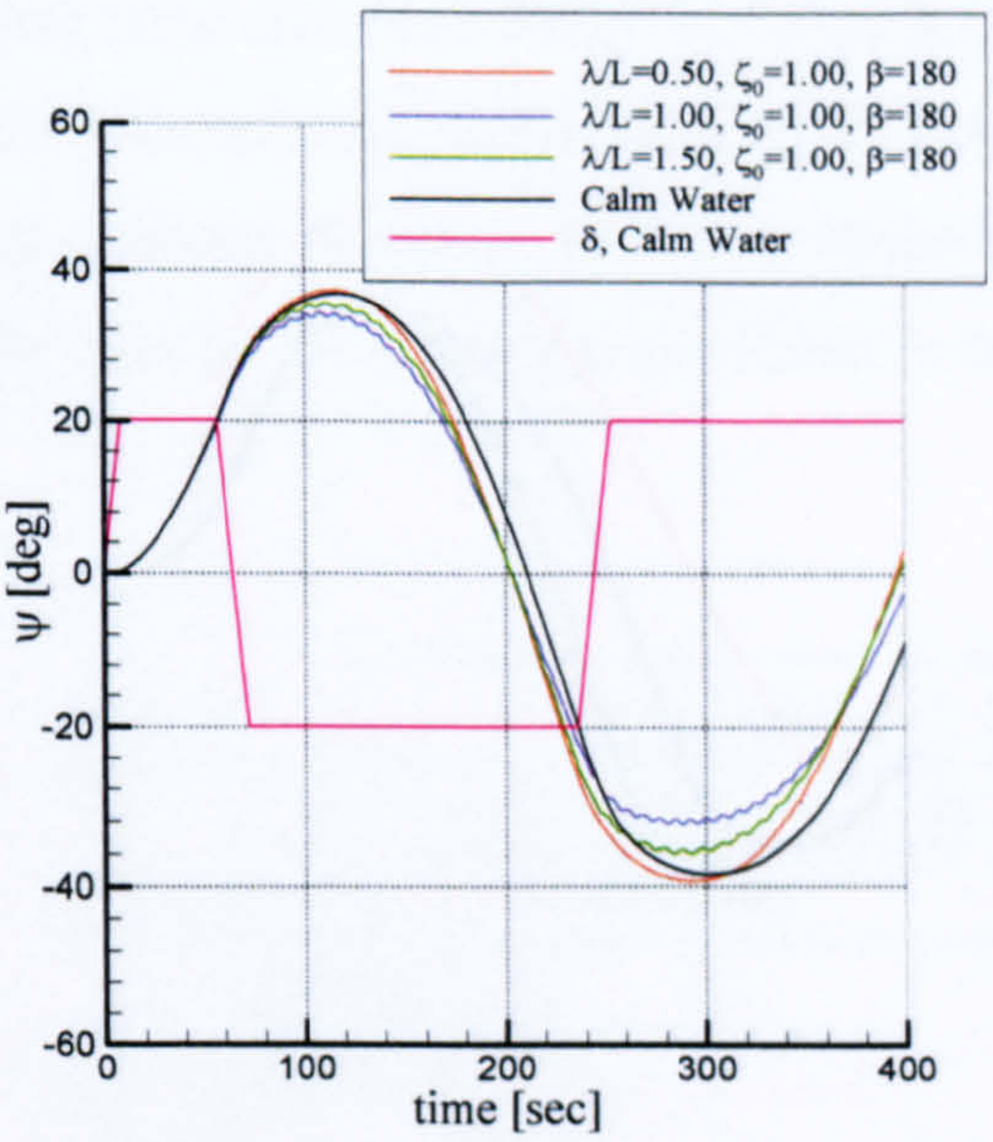

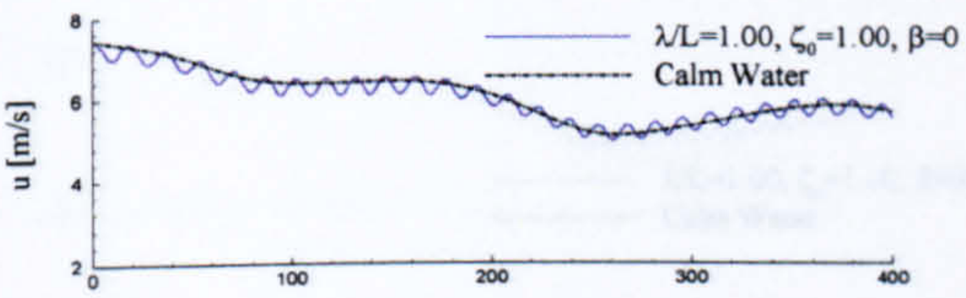

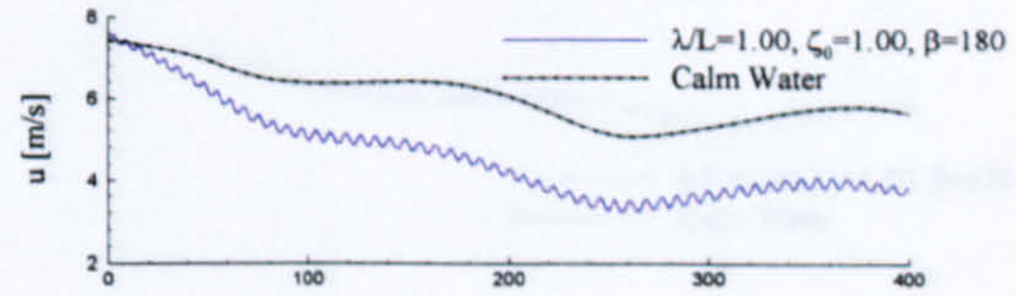

Figure 8.21 Comparisons of motions of 20°/20° zig-zag manoeuvre for various wavelengths (ζ_0=1.0m, β=0°, 180°)

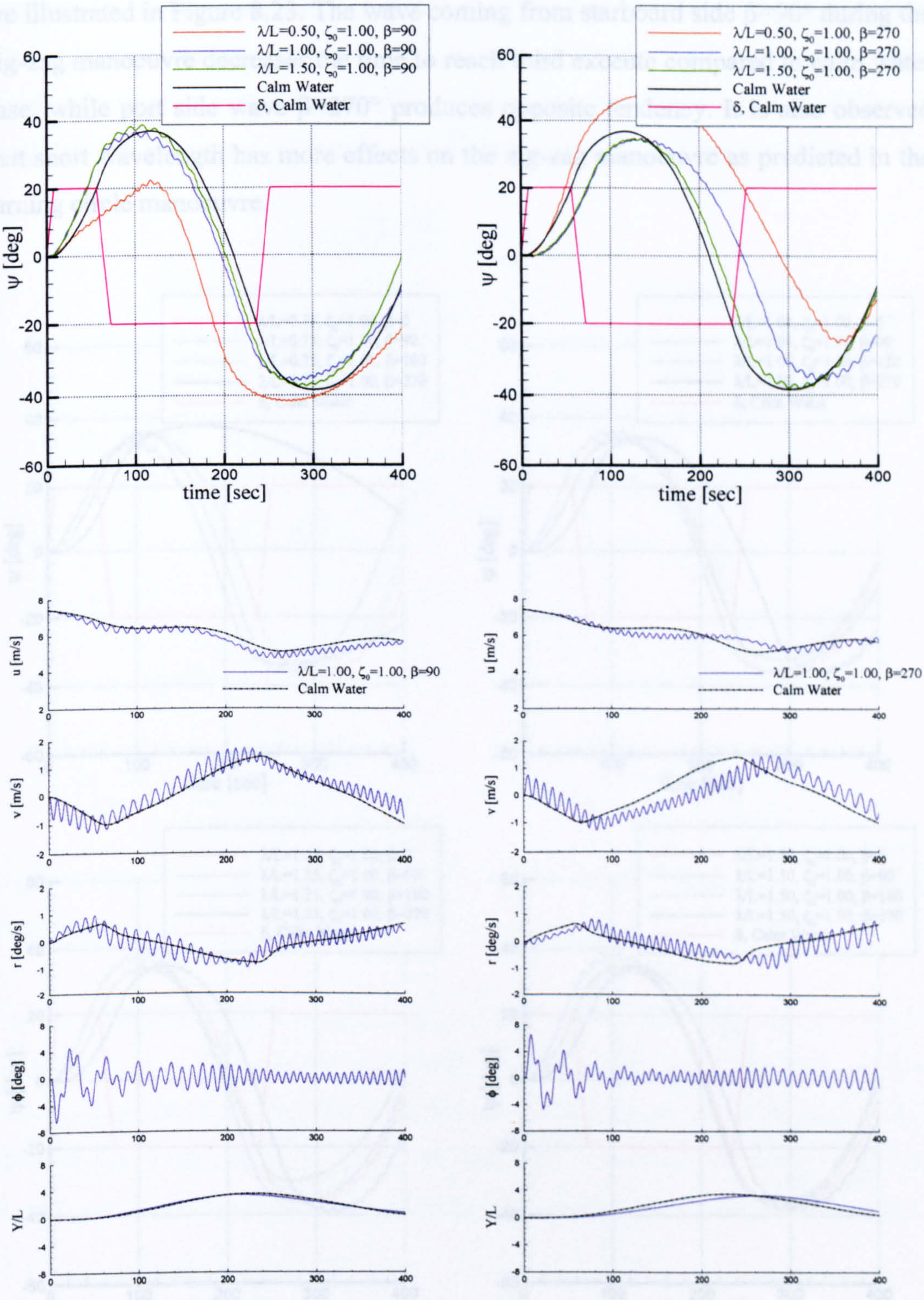

Figure 8.22 Comparisons of motions of 20°/20° zig-zag manoeuvre for various wavelengths (ζ_0=1.0m, β=90°, 270°)

More calculation results regarding the influence of wavelength and wave direction are illustrated in Figure 8.23. The wave coming from starboard side β=90° during the zig-zag manoeuvre decreases the time to reach third execute compared to calm water case, while port side wave β=270° produces opposite tendency. It is also observed that short wavelength has more effects on the zig-zag manoeuvre as predicted in the turning circle manoeuvre.

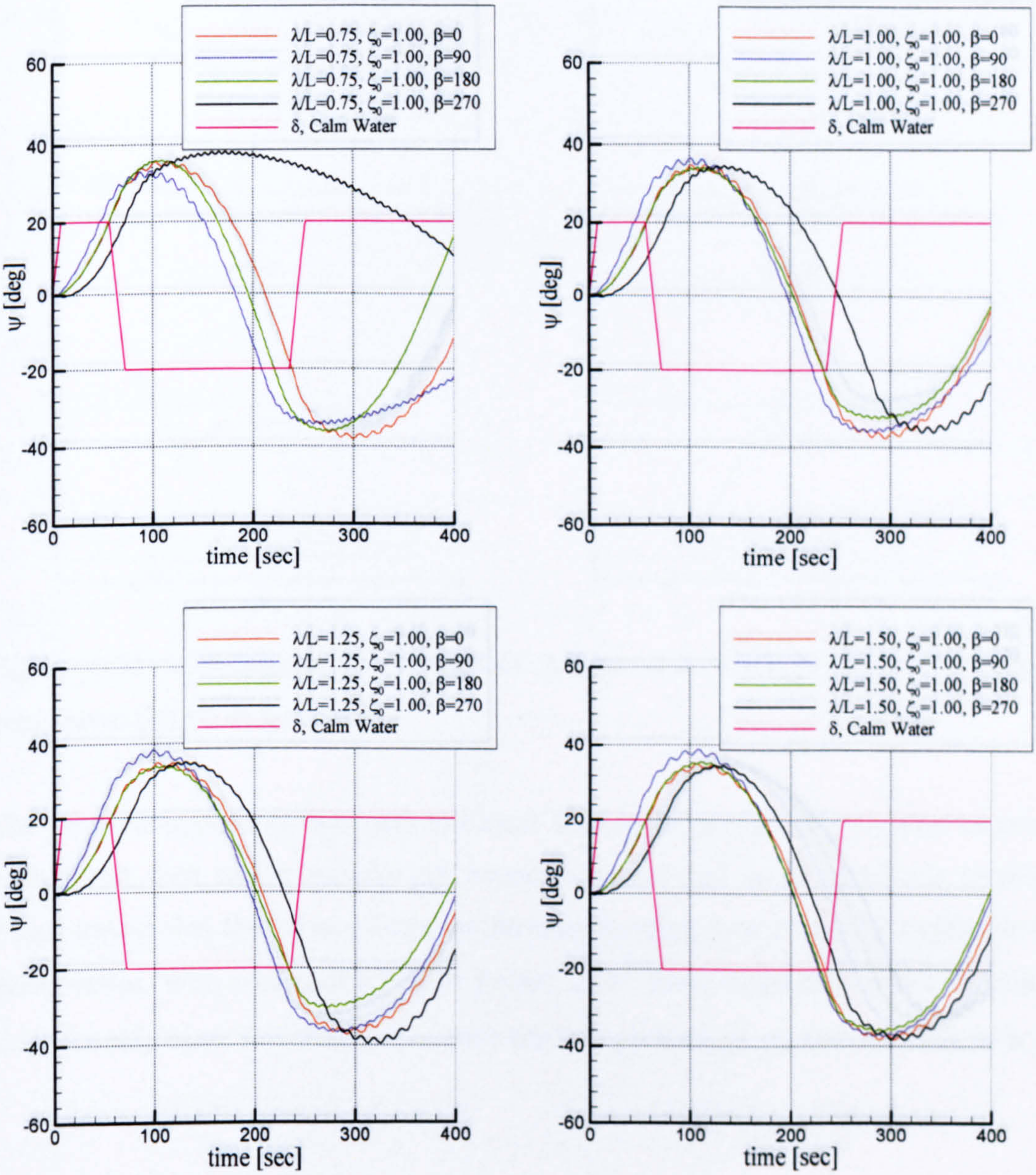

Figure 8.23 Effects of wavelength and wave direction on yaw angle of 20°/20° zig-zag manoeuvre (λ/L=0.75, 1.0, 1.25, 1.5, ζ_0=1.0m)

The effects of wave amplitude on the zig-zag manoeuvre are presented in Figure 8.24. Compared with calm water case, the effects of wave amplitude on the yaw angle of zig-zag manoeuvre are increased with higher amplitude. This tendency is more clearly observed in beam seas, β=90°, 270°, where overshoot angles and time to reach third execute are significantly varied as wave amplitude becomes higher.

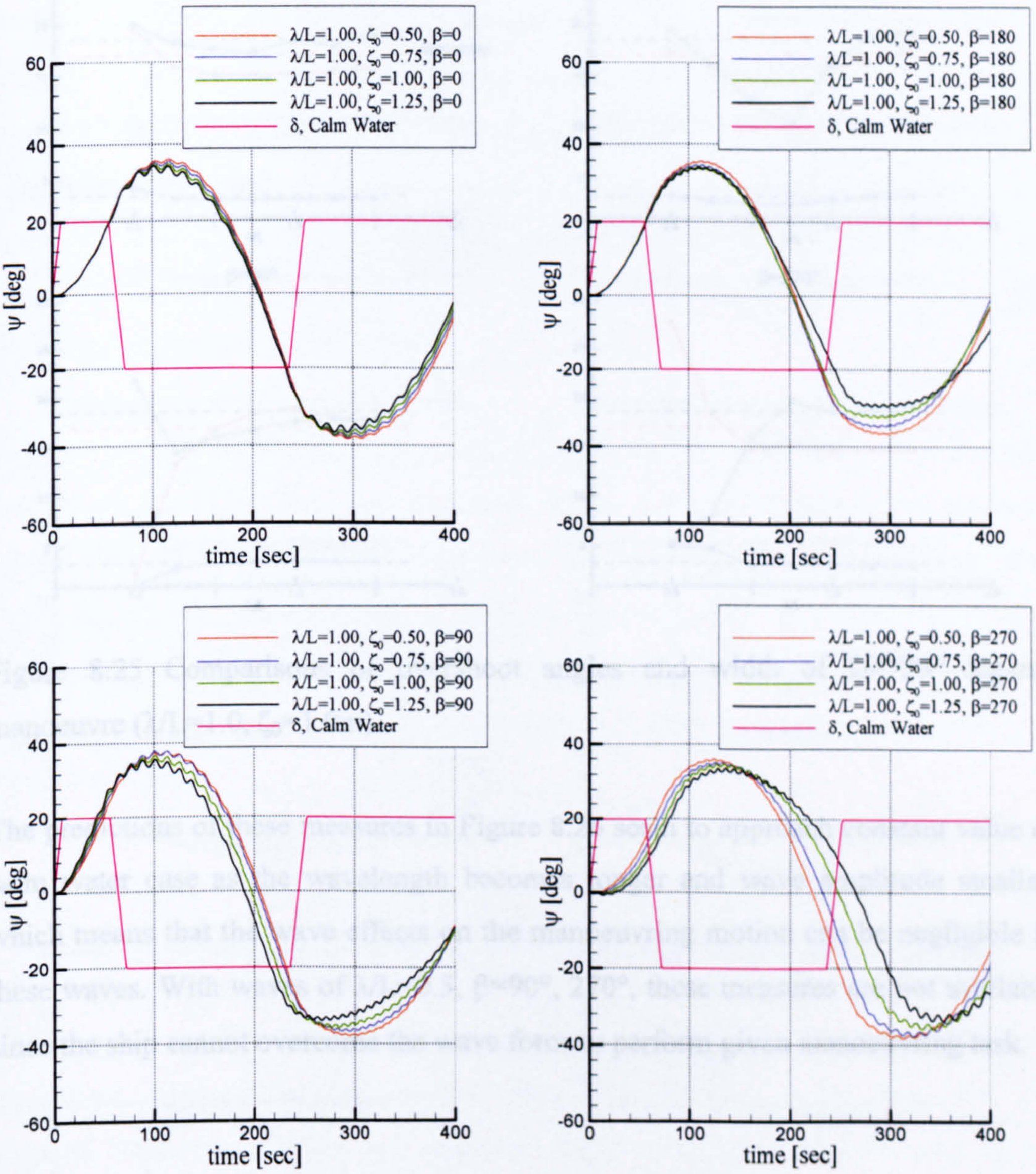

Figure 8.24 Effects of wave amplitude on yaw angle of 20°/20° zig-zag manoeuvre (λ/L=1.0, ζ_0=0.5, 0.75, 1.0, 1.25m)

Predictions of operational parameters such as first and second overshoot angles and overshoot width of path with respect to various wave conditions are illustrated in Figure 8.25. The aforementioned relationship between these operational parameters angles and wavelength, heading angles and wave amplitudes are easily found.

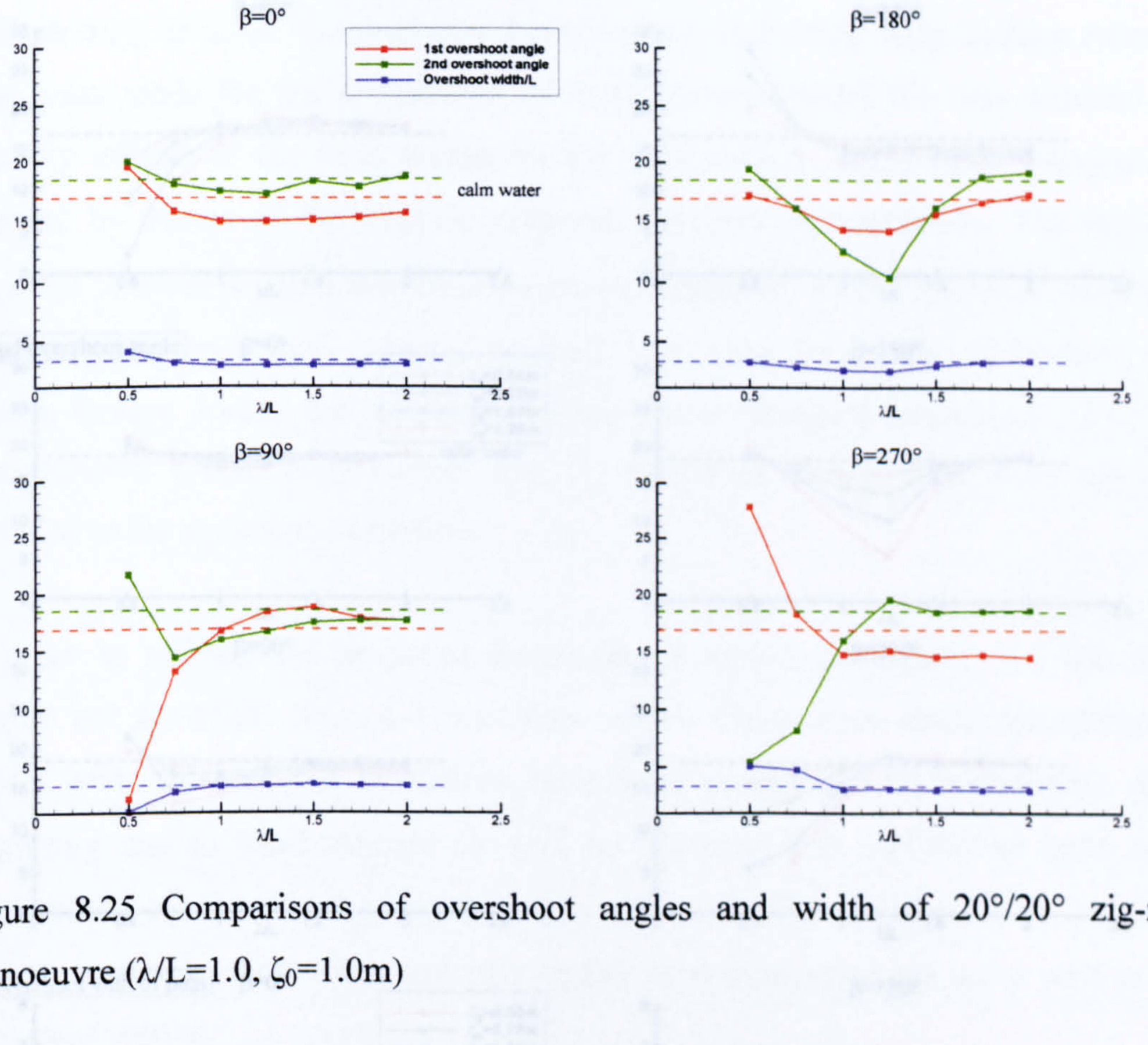

Figure 8.25 Comparisons of overshoot angles and width of 20°/20° zig-zag manoeuvre (λ/L=1.0, ζ_0=1.0m)

The predictions of these measures in Figure 8.26 seem to approach constant value of calm water case as the wavelength becomes longer and wave amplitude smaller, which means that the wave effects on the manoeuvring motion can be negligible in these waves. With waves of λ/L=0.5, β=90°, 270°, these measures are not available since the ship cannot overcome the wave force to perform given manoeuvring task.

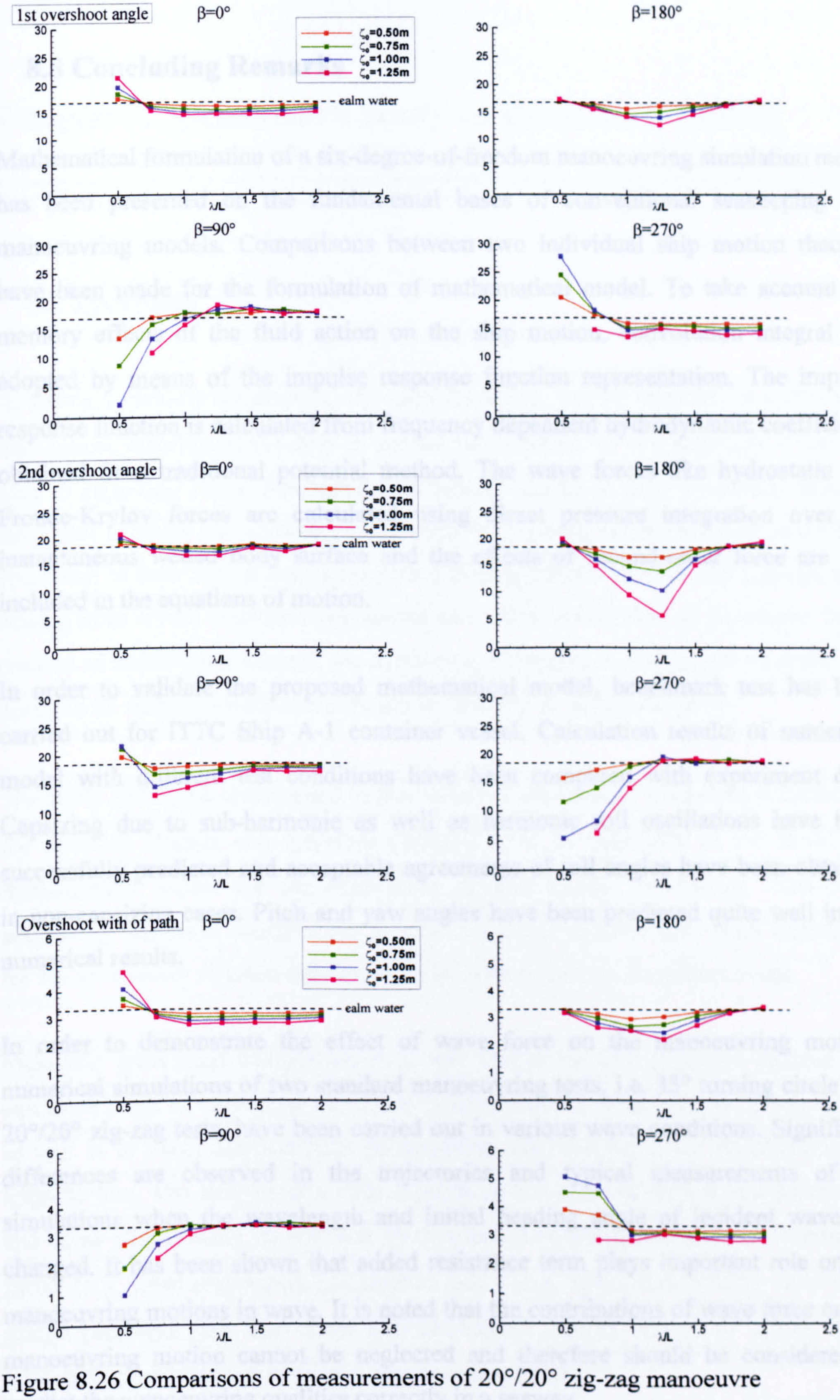

Figure 8.26 Comparisons of measurements of 20°/20° zig-zag manoeuvre

8.8 Concluding Remarks

Mathematical formulation of a six-degree-of-freedom manoeuvring simulation model has been presented on the fundamental bases of conventional seakeeping and manoeuvring models. Comparisons between two individual ship motion theories have been made for the formulation of mathematical model. To take account the memory effects of the fluid action on the ship motion, convolution integral has adopted by means of the impulse response function representation. The impulse response function is calculated from frequency dependent hydrodynamic coefficients obtained from traditional potential method. The wave forces like hydrostatic and Froude-Krylov forces are calculated using direct pressure integration over the instantaneous wetted body surface and the effects of second-order force are also included in the equations of motion.

In order to validate the proposed mathematical model, benchmark test has been carried out for ITTC Ship A-1 container vessel. Calculation results of numerical model with different test conditions have been compared with experiment data. Capsizing due to sub-harmonic as well as harmonic roll oscillations have been successfully predicted and acceptable agreements of roll angles have been obtained in non-capsizing cases. Pitch and yaw angles have been predicted quite well in the numerical results.

In order to demonstrate the effect of wave force on the manoeuvring motion, numerical simulations of two standard manoeuvring tests, i.e. 35° turning circle and 20°/20° zig-zag tests, have been carried out in various wave conditions. Significant differences are observed in the trajectories and typical measurements of the simulations when the wavelength and initial heading angle of incident wave are changed. It has been shown that added resistance term plays important role on the manoeuvring motions in wave. It is noted that the contributions of wave force on the manoeuvring motion cannot be neglected and therefore should be considered to predict the manoeuvring qualities correctly in a seaway.

Chapter 9. Benchmark Study on Parametric Rolling

9.1 Preamble

In standard stability assessment, the term instability can be regarded as a condition that creates inability of the ship to deliver the required service although it may not lead to capsizing event. Furthermore instability condition may potentially threaten the safety of ships and acceptable operation. For instant, many container ships have lost some of their cargos during operation in dangerous condition and large motions arising from severe weather environment can affect the comfort of passenger. In the context of stability assessment, the avoidance of instable condition can be given as a criterion of related hazard which should be lowered to acceptable level.

The study addressed herein aims to test different elements of modelling discussed in the previous chapter and therefore establish level of capability of the developed mathematical model for the predictions of ship motion in random seaway. In addressing this issue considerably detailed validation studies have been undertaken for the assessment of intact stability of ships with respect to hazardous event.

Especially parametric roll phenomenon was chosen for this validation purpose and extensive range of numerical simulation is carried out to investigate the phenomenon as well as to verify the feasibility of numerical tool developed for the prediction of large motion. The stability of a ship depends on a number of factors and parameters and some of following factors will be considered in the assessment: environmental factor (e.g. wave and wind), operational factor (e.g. speed and loading condition), design parameter (e.g. hull shape and anti-rolling device), control or human effect (e.g. strategy of rudder control and choice of heading).

9.2 Physics of Parametric Roll

It has been almost a half century since the phenomenon of parametric roll motion has first attracted attention of naval architects (Grim 1952, Paulling and Rosenberg 1959). Periodic changes of roll stability in waves, characterized by a decrease of stability when the ship is in the wave crest and an increase in the wave trough, are well known as the direct cause of parametric roll phenomenon. Despite the fact that the physical nature of parametric roll has been known for many years, several new elements are present in this case. In the past, the concern had been mostly for smaller ships in following seas. Now, the concern is for the vulnerability of large container carriers in head seas. The problem is particularly important given the long-standing heavy-weather maritime practice of sailing into head seas at reduced speed. It turns out that this is not necessarily the best practice for large container carriers.

Since many Post-Panamax container carriers have suffered significant cargo loss and damage, the problem of parametric roll now returned as a main subject in ship hydrodynamic research fields. In October 1998 a Post-Panamax C11 class container ship encountered extreme weather and sustained extensive loss and damage to deck stowed containers on a voyage in North Pacific (France et al., 2003). A following investigation has showed that A detailed investigation showed that a large roll motion with up to 35 degrees amplitude accompanied by significant pitch and yaw motion resulted from the periodic change of transverse stability in head seas. The large change of stability in head seas was found to be a direct result of the hull form; Geometry above waterline such as bow flare and stern overhang, typical shape in large container carrier, have a significant effect on the propensity for parametric roll in irregular seas. Also an accurate estimation of the roll damping is essential for the exact prediction of the occurrence and magnitude of parametric roll.

Bulian et al. (2004) used a 1.5-DOF non-linear mathematical model and compared the stability boundaries derived from an analytic, numerical and experimental treatment of the rolling of a ship in regular and irregular head waves. The extended

degree-of-freedom comes from treating explicitly in the roll equation, the variation in the restoring lever as a function of roll and pitch angle, heave displacement and wave position. Two techniques were considered for the derivation of the stability boundaries in irregular waves with assumptions regarding the form of the one-degree-of-freedom uncoupled roll equation. Comparison with experiment revealed that stability boundaries could be predicted satisfactorily. However, the simple solution is not sufficient to capture the magnitude of rolling once exceeded the stability zone.

Matusiak (2003) studied the influence of wave amplitude and additional roll damping created by bilge keels on the development of parametric roll of fast Ro-Pax vessel. Numerical simulation of 6-DOF motion was performed with a two-stage approach, where linear approximations and non-linear portions in the ship hydrodynamic model are decomposed, and the results of the numerical simulation were verified with a free running model test in head and following seas. It was shown that increased wave height leads to increased amplitude of parametric roll, while installation of the bilge keels decreases the amplitude and slows down development of parametric roll. Initial angle of heel speeds up development of parametric roll but has no influence on the maximum roll amplitude. Rise of yaw motion was observed along with the development of parametric roll.

Irrespective of the adopted method, either in a theoretical or experimental approach, to predict the magnitude and exceedance of roll motion, one important issue is whether parametric roll can be regarded as a stationary stochastic process. Belenky et al. (2003) described a background for assessing the risk of parametric roll of a large containership in irregular head seas. Based on numerical simulations, their study considers ergodicity and distribution of heave pitch and roll during parametric resonance. It was found that roll motion is not ergodic and does not follow a normal distribution, whereas pitch and heave are both normal and ergodic.

9.3 Benchmark Study of Numerical Model

Recently "International Benchmark Study on Numerical Simulation Methods for the Prediction of Parametric Rolling of Ships in Waves" was organized by the EU Commission funded research project SAFEDOR (Design, Operation and Regulation for Safety). This study was designed to deal with a set of well defined conditions and ship responses for which the capabilities of the benchmarked numerical methods can be tested before dealing with the more complex problem of responses in realistic and random sea conditions. (for further details, see http://www.naval.ntua.gr/~sdl/sibs/)

The performance of the numerical method for the selected loading and wave conditions was assessed in comparison to the relevant experimental data. The study comprises of the simulation of the behaviour of a containership in longitudinal waves, both head and following, and in two loading conditions. For these selected conditions the excitation of roll motion is expected as a result of parametric resonance.

9.3.1 ITTC Ship A-1

The model ship used in the benchmark test is ITTC Ship A-1 container vessel. In the experiment a bare hull without propeller and rudder was tested. The principal dimensions of full scale ship are given in Table 8.1 and the loading conditions used in the numerical calculations are given Table 9.1. The ship is considered moving in three-degree-of-freedom, those of heave-roll-pitch, in order to minimise any uncertainties related to the course-keeping effect on heading and speed.

Table 9.1 Loading conditions of ITTC Ship A-1

Item	$\overline{GM}_T$	k_{xx}	k_{yy}
Loading #1	1.38 [m]	10.33 [m]	37.5 [m]
Loading #2	1.00 [m]	10.33 [m]	38.2 [m]

9.3.2 Preliminary calculation

As an initial calculation some hydrostatic calculations are performed including GZ curve in still water and regular wave. The GZ curves in still water are compared with linear case in each loading condition as illustrated in Figure 9.1.

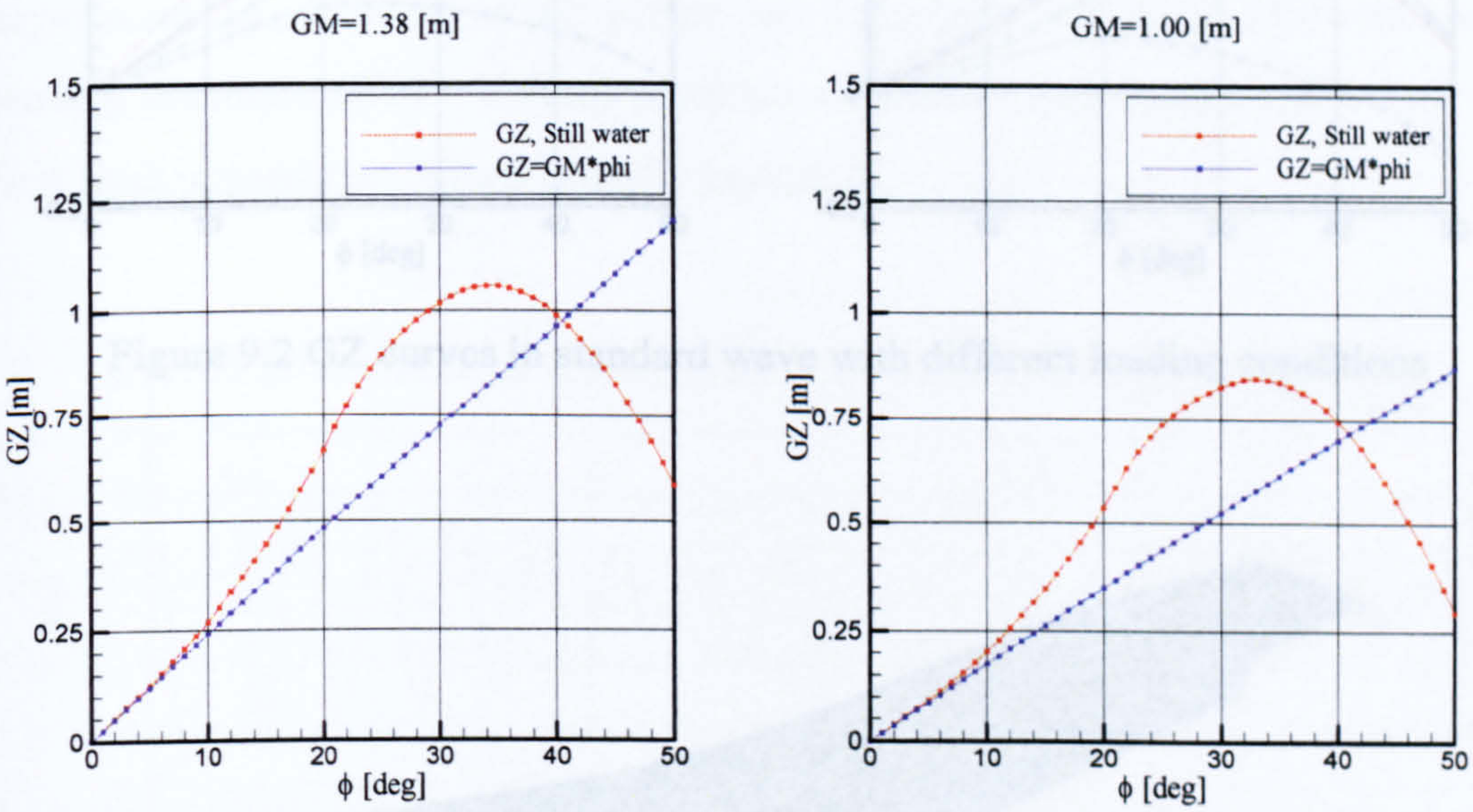

Figure 9.1 GZ curves in still water with different loading conditions

In order to investigate change of roll stability in longitudinal wave, calculation of GZ curve with different position of wave crest is performed with a standard wave. The length of standard wave is equal to the ship length ($\lambda/L=1.0$) and wave height is set as $Hw/\lambda=1/25$. The position of wave crest changes along the longitudinal direction and the results are presented in Figure 9.2.

It is observed that GZ value for the wave crest near midship is smaller than the value in calm water and GZ value for the wave trough near midship becomes larger than the value in calm water. The effect of location of a wave on GZ value can be obviously identified in Figure 9.3, when wave trough amidships produces wider and larger water plane area than wave crest amidships. Therefore GZ value in a wave should include the effect of wave crest position along the longitudinal direction.

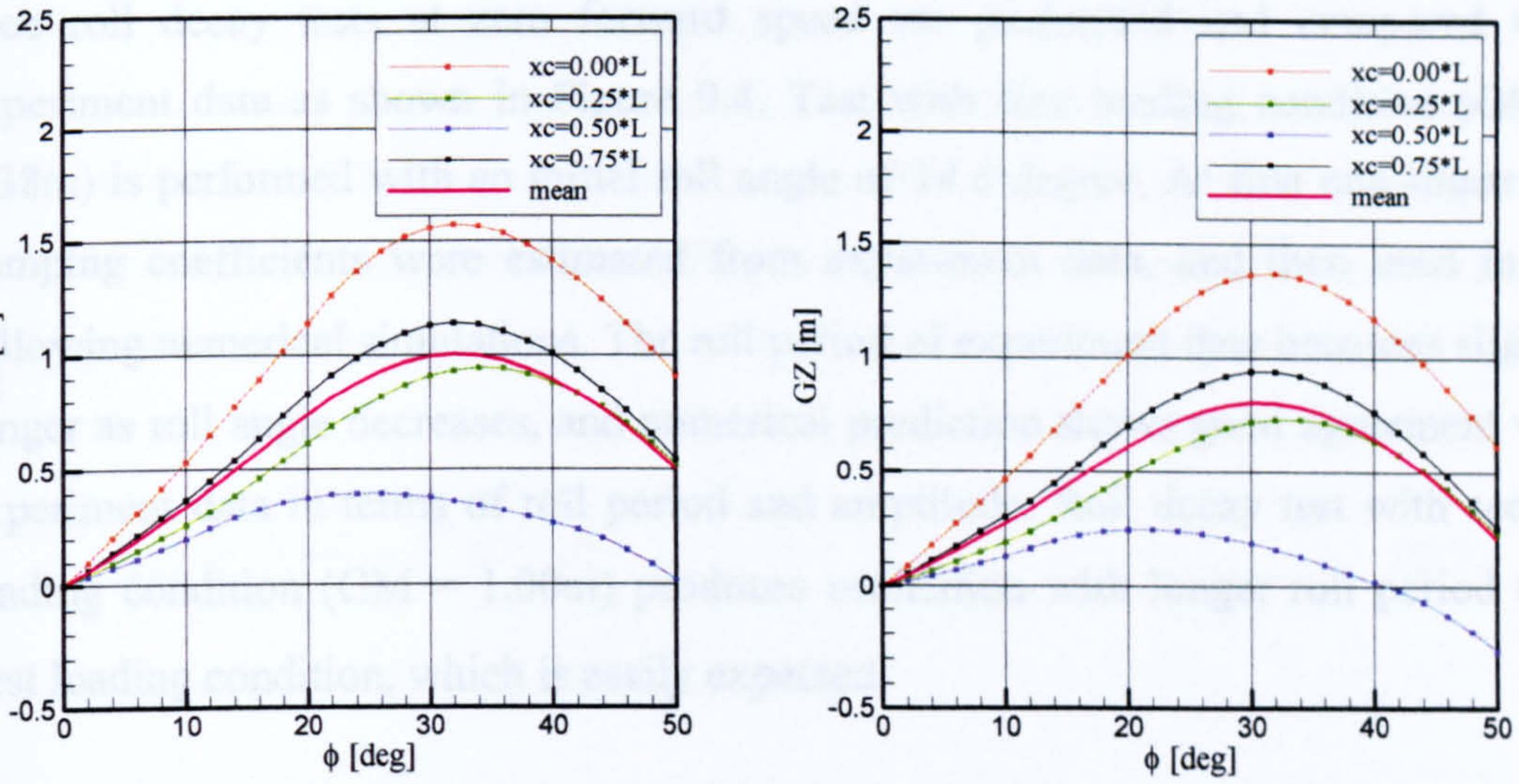

Figure 9.2 GZ curves in standard wave with different loading conditions

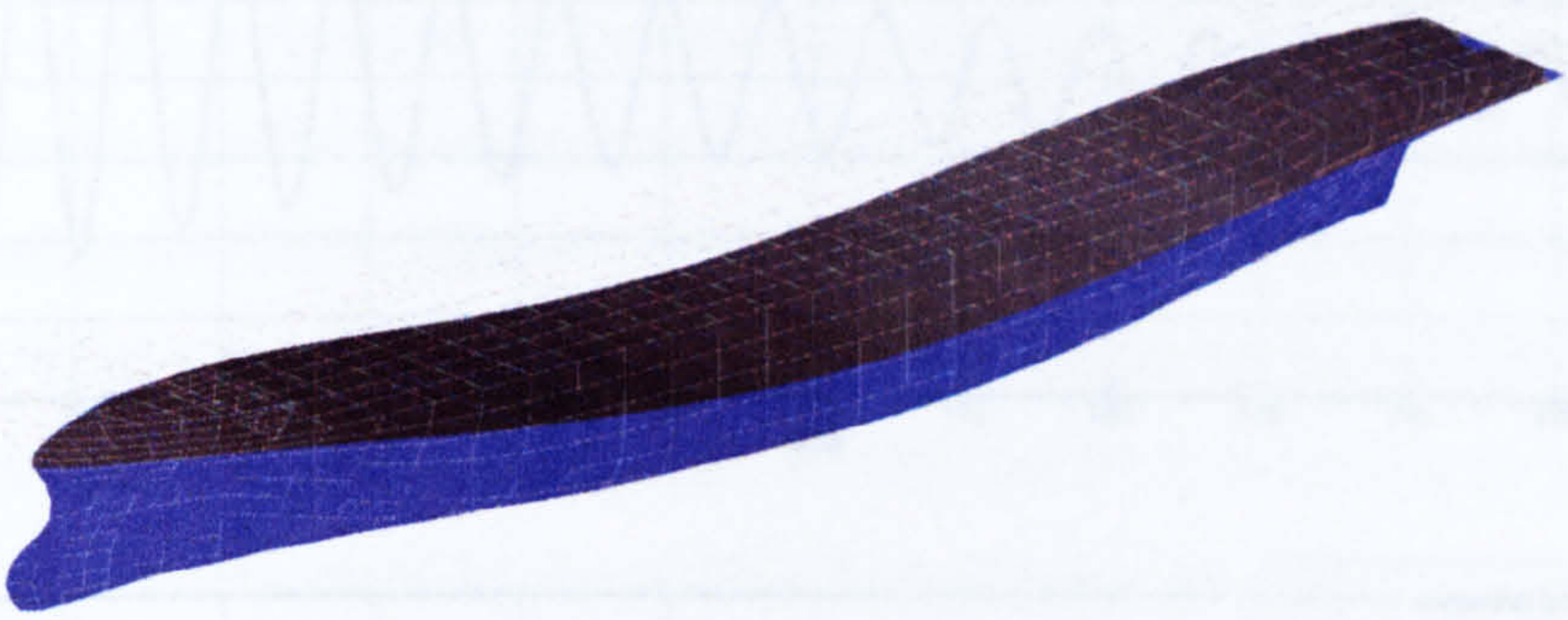

(a) wave trough amidships with large water plane area

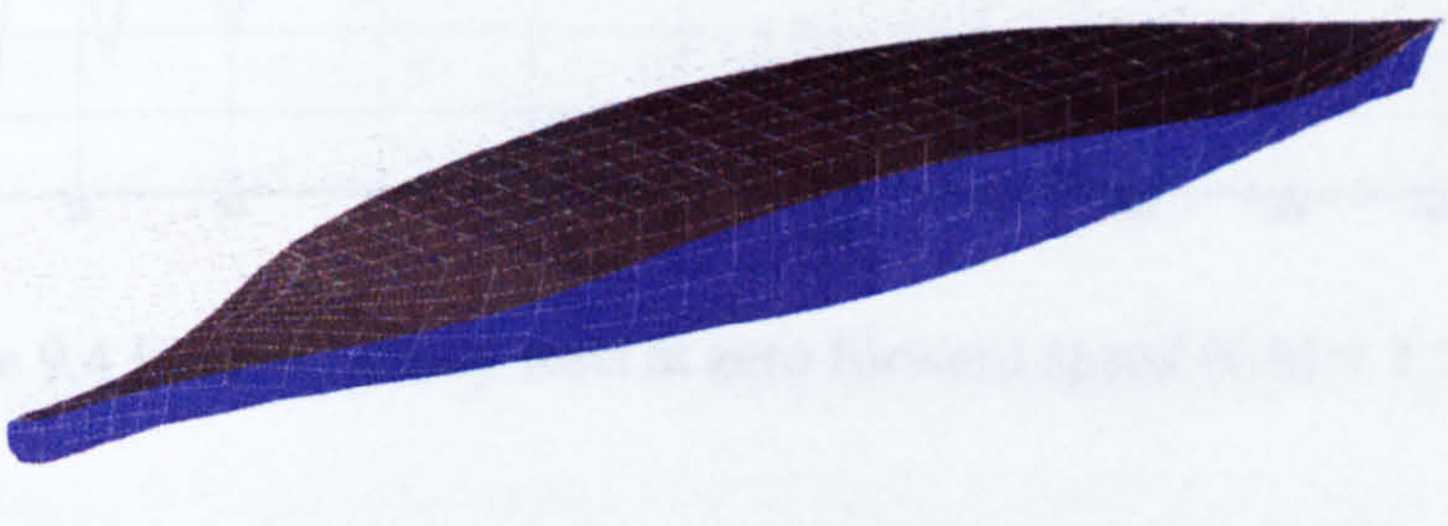

(b) wave crest amidships with small water plane area

Figure 9.3 Variation of wetted body surface between crest and trough of a standard wave ($\lambda/L=1.0$, $Hw/\lambda=1/25$)

Free roll decay tests at zero forward speed are performed and compared with experiment data as shown in Figure 9.4. Test with first loading condition (GM = 1.38m) is performed with an initial roll angle of 14.6 degree. At first non-linear roll damping coefficients were estimated from experiment data, and then used in the following numerical simulations. The roll period of experiment data becomes slightly longer as roll angle decreases, and numerical prediction shows good agreement with experiment data in terms of roll period and amplitude. Roll decay test with second loading condition (GM = 1.00m) produces oscillation with longer roll period than first loading condition, which is easily expected.

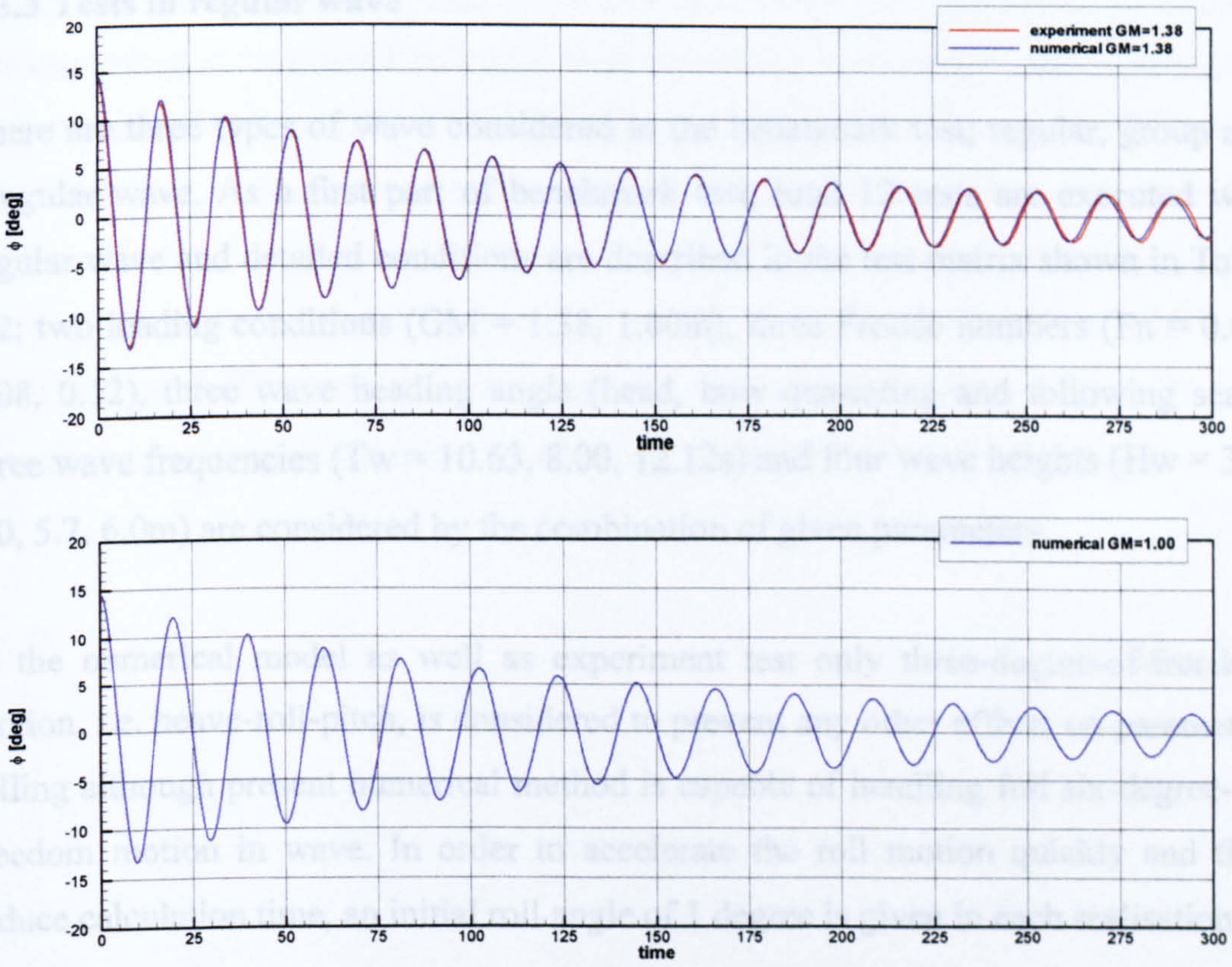

Figure 9.4 Free roll decay tests at zero forward speed (GM = 1.38, 1.00m)

In order to assess behaviour of parametric rolling, especially in a random wave, statistical approach needs to be adopted. In reality the statistical characteristics of waves in a seaway change with time. However, by introducing a hypothesis of quasi-

stationarity and hence assuming that a stationary process can be employed within a certain time period, parametric rolling can be regarded as a stationary process within the quasi-stationary period. This assumption enables statistical analysis as long as the speed, heading and loading condition are not changed during the time range. The mean roll amplitude of parametric rolling can be obtained with sufficient realisation of the process as follows

$$\phi_{mean} = \sqrt{\frac{2}{T_2 - T_1}\int_{T_1}^{T_2} \phi(t)^2 dt} \tag{9.1}$$

9.3.3 Tests in regular wave

There are three types of wave considered in the benchmark test; regular, group and irregular wave. As a first part of benchmark test, total 12 tests are executed with regular wave and detailed conditions are described in the test matrix shown in Table 9.2; two loading conditions (GM = 1.38, 1.00m), three Froude numbers (Fn = 0.04, 0.08, 0.12), three wave heading angle (head, bow quartering and following seas), three wave frequencies (Tw = 10.63, 8.00, 12.12s) and four wave heights (Hw = 3.6, 5.0, 5.7, 6.0m) are considered by the combination of given parameters.

In the numerical model as well as experiment test only three-degree-of-freedom motion, i.e. heave-roll-pitch, is considered to prevent any other effects on parametric rolling although present numerical method is capable of handling full six-degree-of-freedom motion in wave. In order to accelerate the roll motion quickly and thus reduce calculation time, an initial roll angle of 1 degree is given in each realisation.

Mean roll amplitude of each test is evaluated and compared with experiment data as shown in Figure 9.5 and time series of roll angle in each test are given in Figure 9.6 through Figure 9.11. The experiment result with regular wave can be grouped as 6 pairs of dataset and especially first 5 pairs (T02-T03, T04-T05, T09-T10, T13-T14, T15-T16) have different wave height with all other test conditions unchanged. Mean

roll amplitudes of these 5 pairs show quite different behaviour with respect to wave height; mean roll amplitudes of T02-T03 and T09-T10 decrease with larger wave height, T04-T05 and T13-T14 show little difference of roll amplitude and T15-T16 show dramatic development of parametric roll motion. It should be noted that different behaviour in the development of parametric roll is caused by highly non-linearity of ship motion and therefore realisation of these non-linear behaviour should be possible in the numerical method performed with any environment conditions.

It seems that numerical calculations corresponding to 'decrease of roll amplitude with higher wave' are able to predict this behaviour and show qualitatively agreement with experiment data (T02-T03 and T09-T10). Numerical predictions corresponding to 'consistent roll amplitude regardless wave height' show quite good agreement for head sea (T04-T05), but under-estimation for following sea (T13-T14). The behaviour of 'increase of roll amplitude with higher wave' is again quite well predicted in the numerical calculations (T15-T16). The numerical results of last pair show good prediction for T20, but poor prediction for T21. Overall capability of numerical method to predict the development of parametric rolling seem to be good though at certain cases numerical result could not match with experiment data.

Table 9.2 Benchmark test matrix for regular waves

GM [m]	Test No.	Heading [deg]	Fn	Height [m]	Period [sec]
1.38	T02	180	0.08	3.6	10.63
	T03			5.7	
	T04	180	0.12	3.6	10.63
	T05			5.7	
	T09	160	0.12	3.6	10.63
	T10			5.7	
1.00	T13	0	0.08	3.6	8.00
	T14			6.0	
	T15	0	0.04	3.6	8.00
	T16			6.0	
	T20	180	0.08	5.0	12.12
	T21		0.12	5.0	

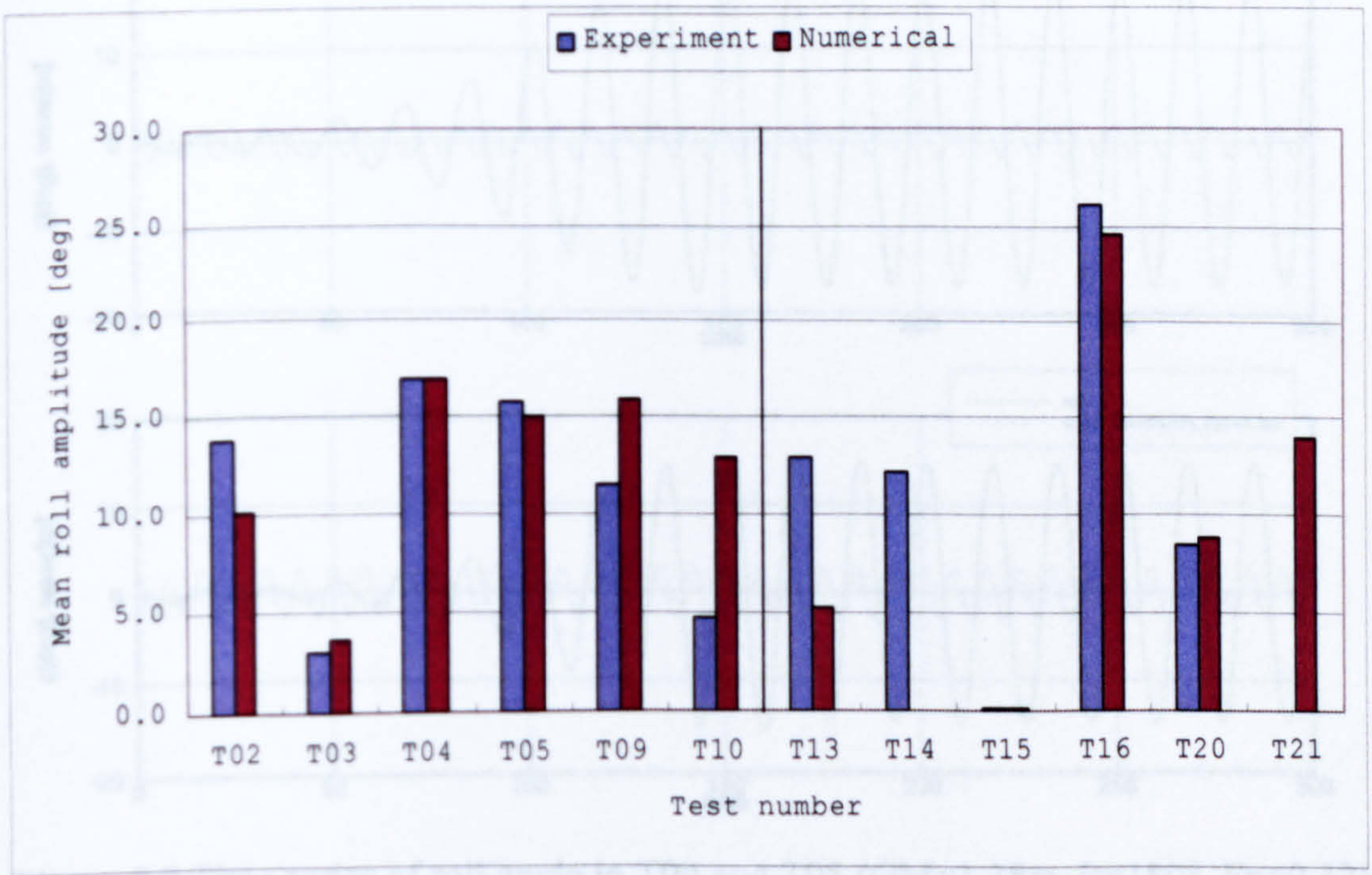

Figure 9.5 Comparison of mean roll amplitude in regular waves

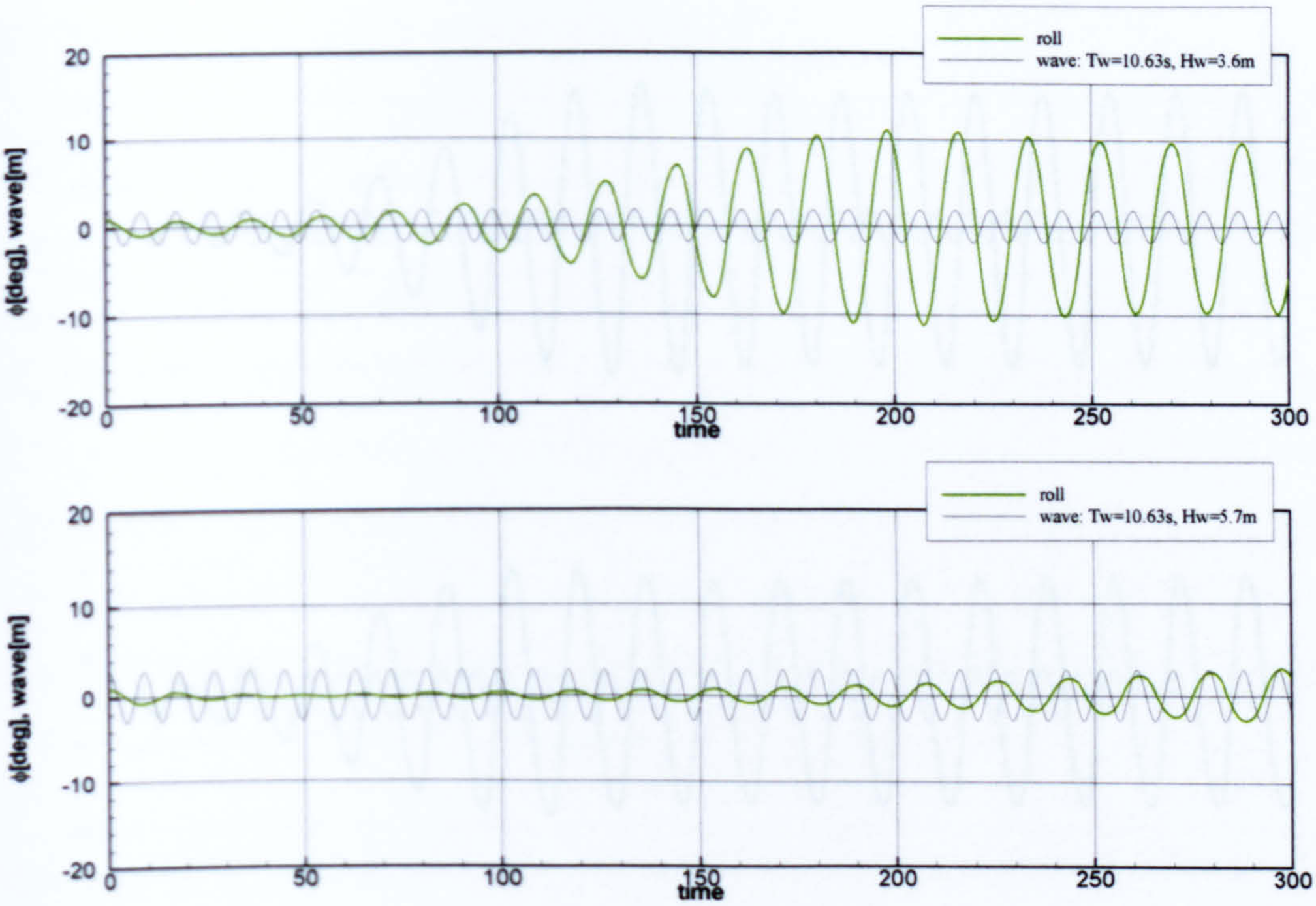

Figure 9.6 Time series of roll angle in T02 and T03 (GM=1.38m, β=180°, Fn=0.08)

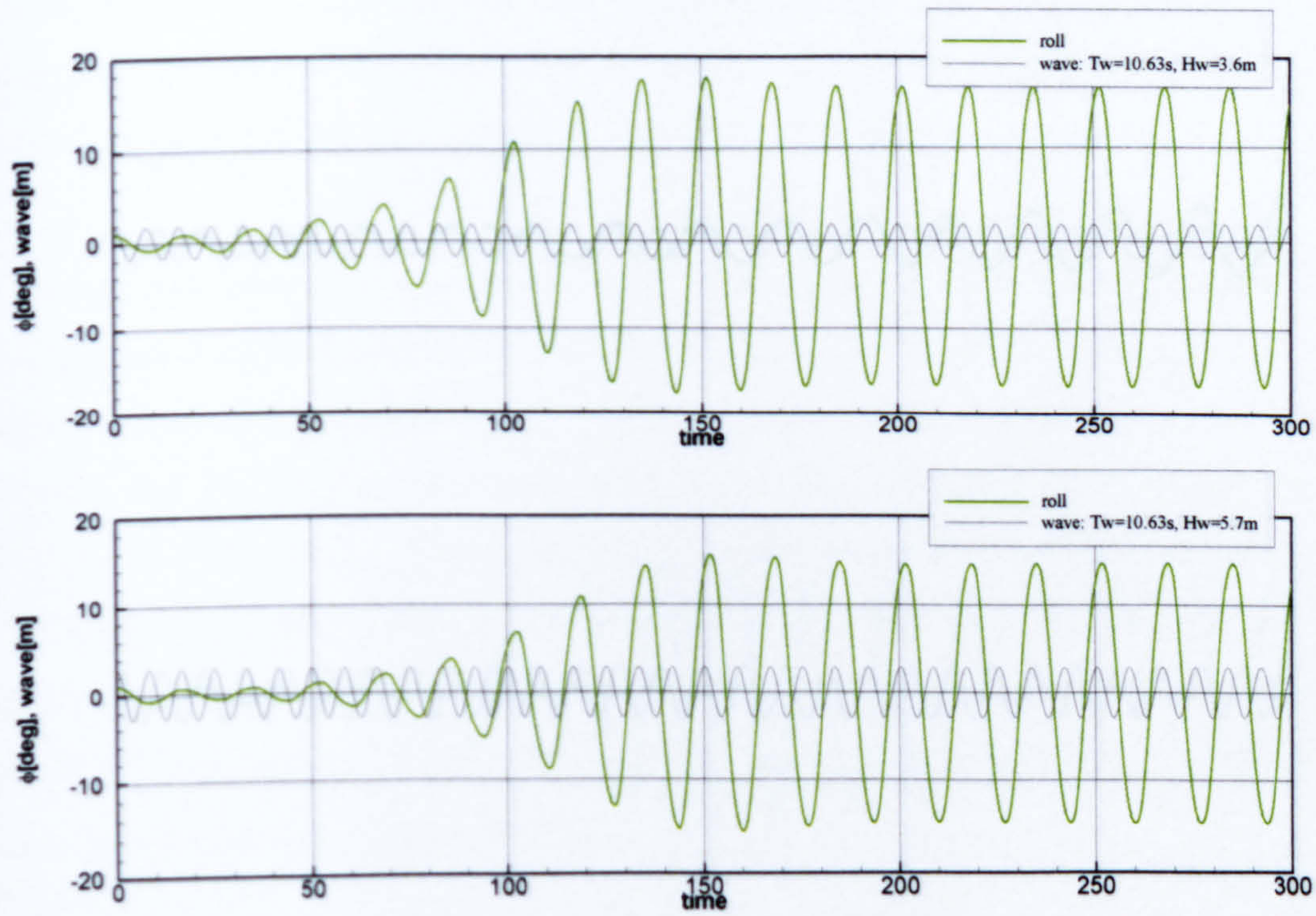

Figure 9.7 Time series of roll angle in T04 and T05 (GM=1.38m, β=180°, Fn=0.12)

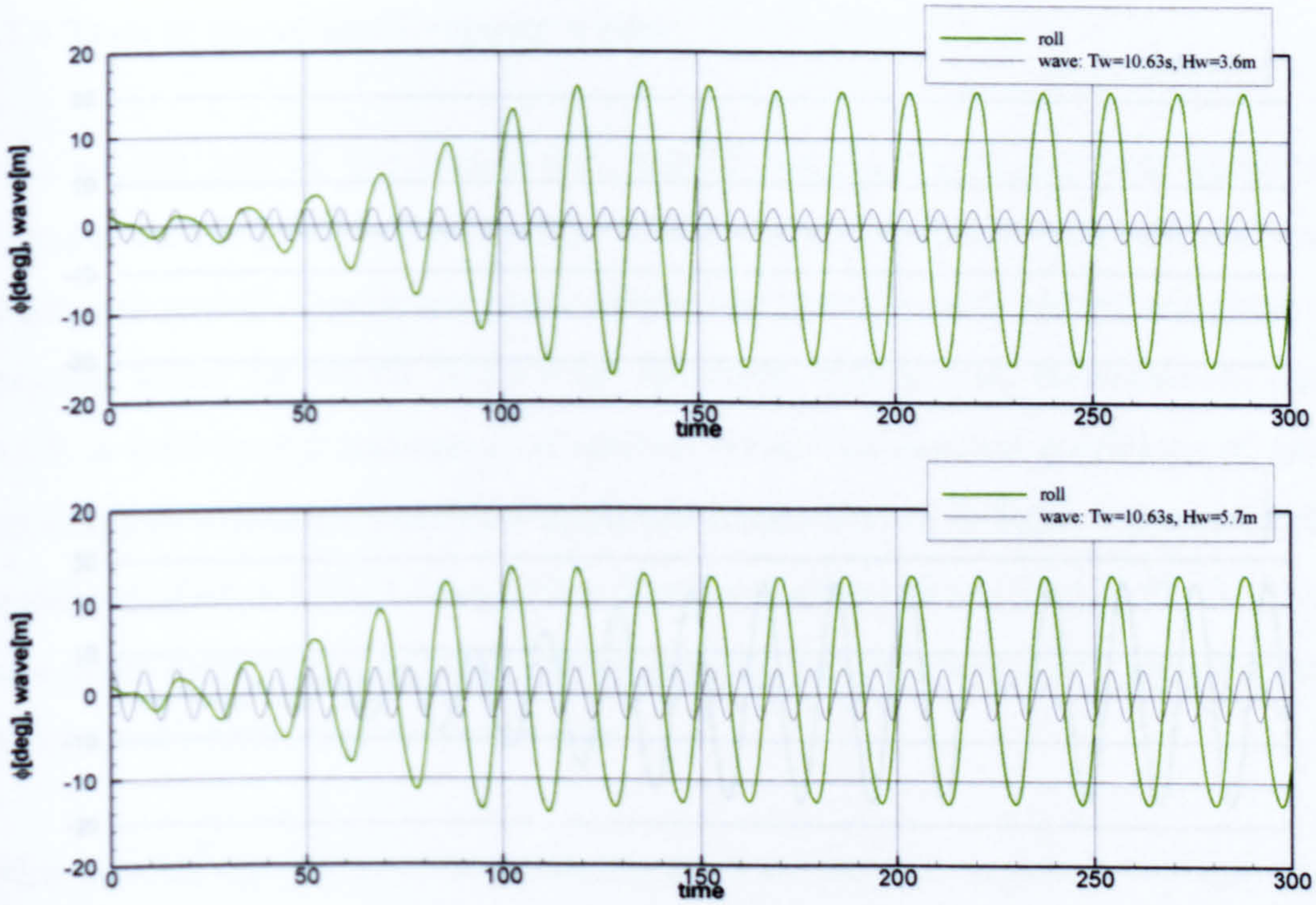

Figure 9.8 Time series of roll angle in T09 and T10 (GM=1.38m, β=160°, Fn=0.12)

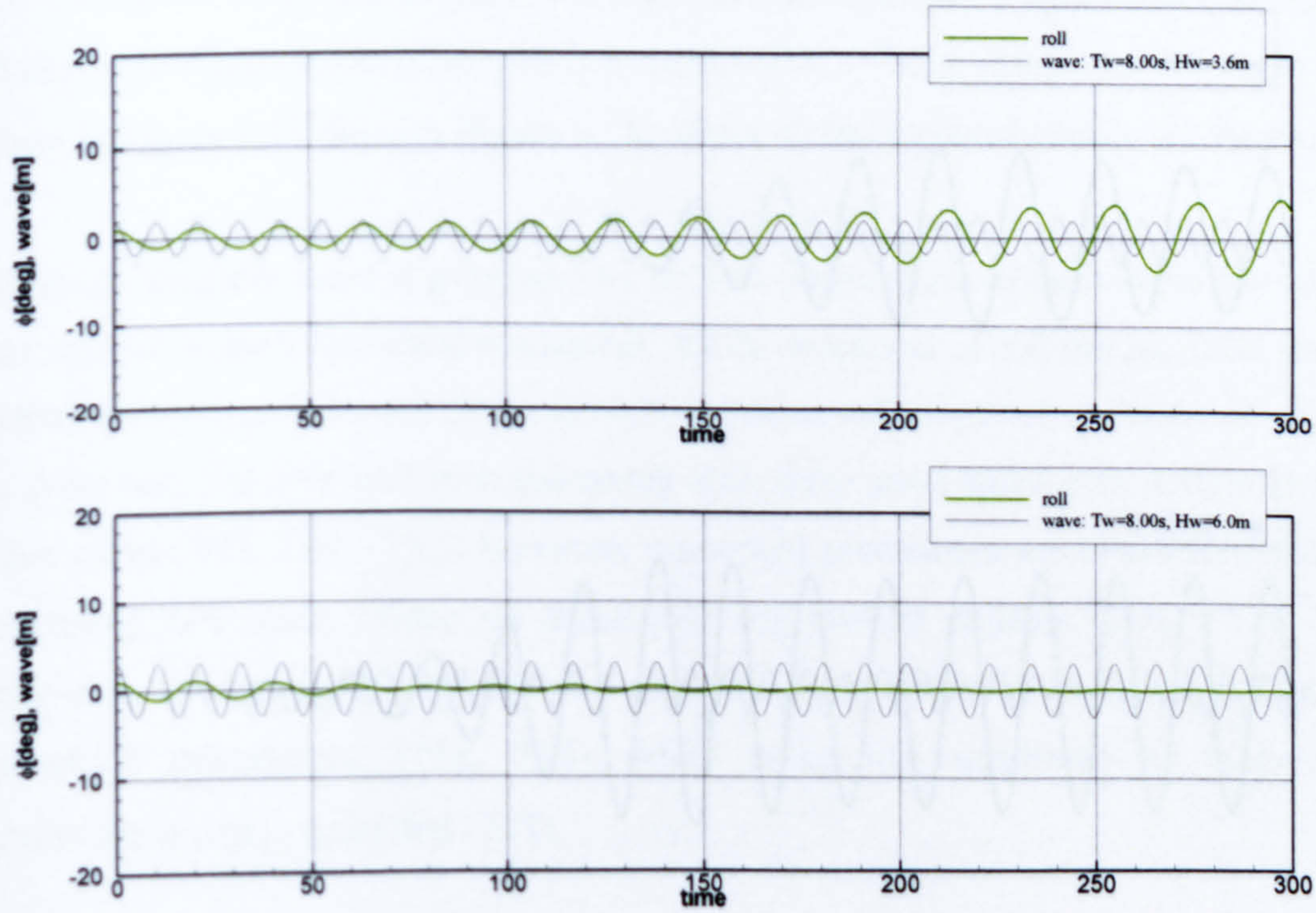

Figure 9.9 Time series of roll angle in T13 and T14 (GM=1.00m, β=0°, Fn=0.08)

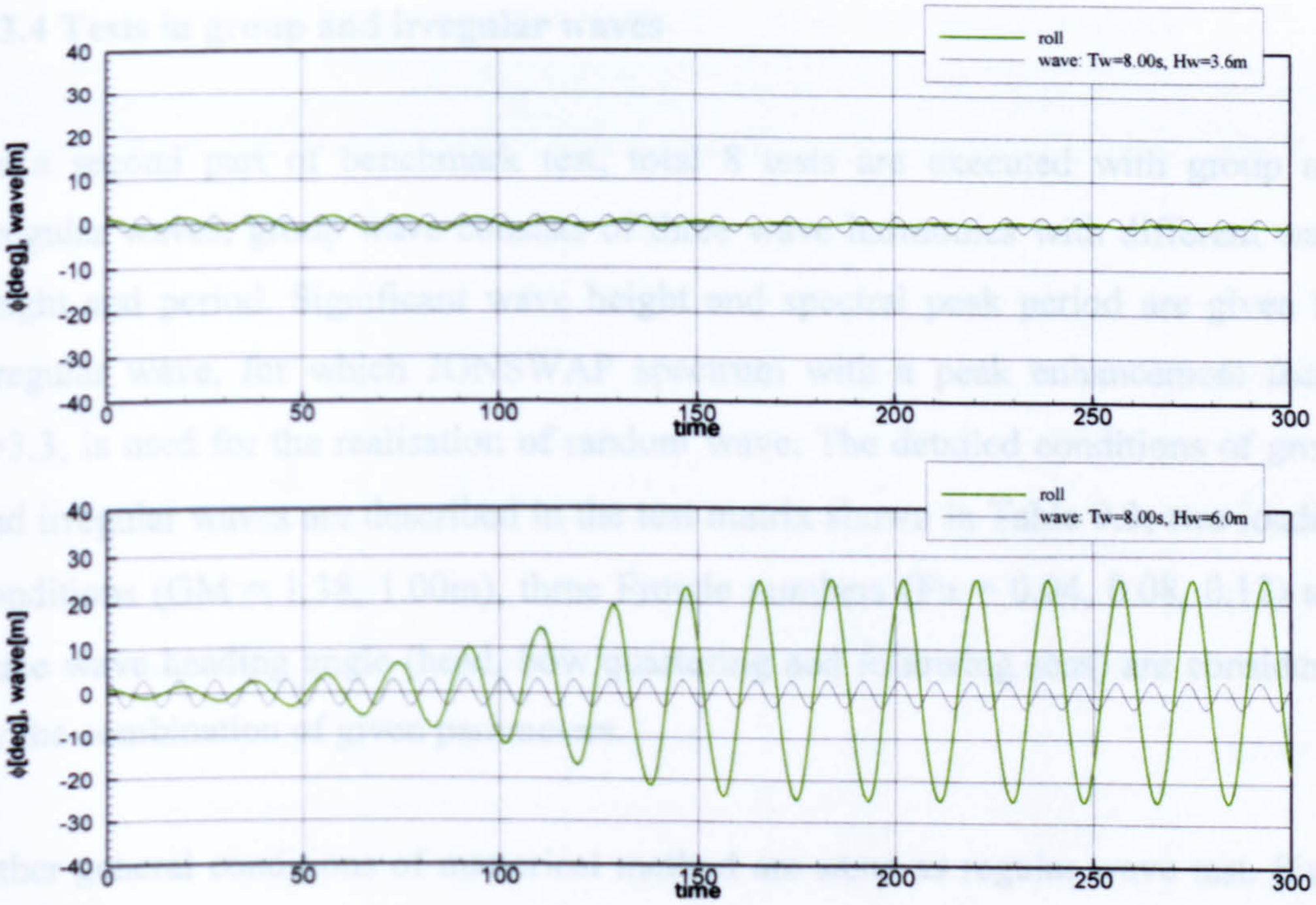

Figure 9.10 Time series of roll angle in T15 and T16 (GM=1.00m, β=0°, Fn=0.04)

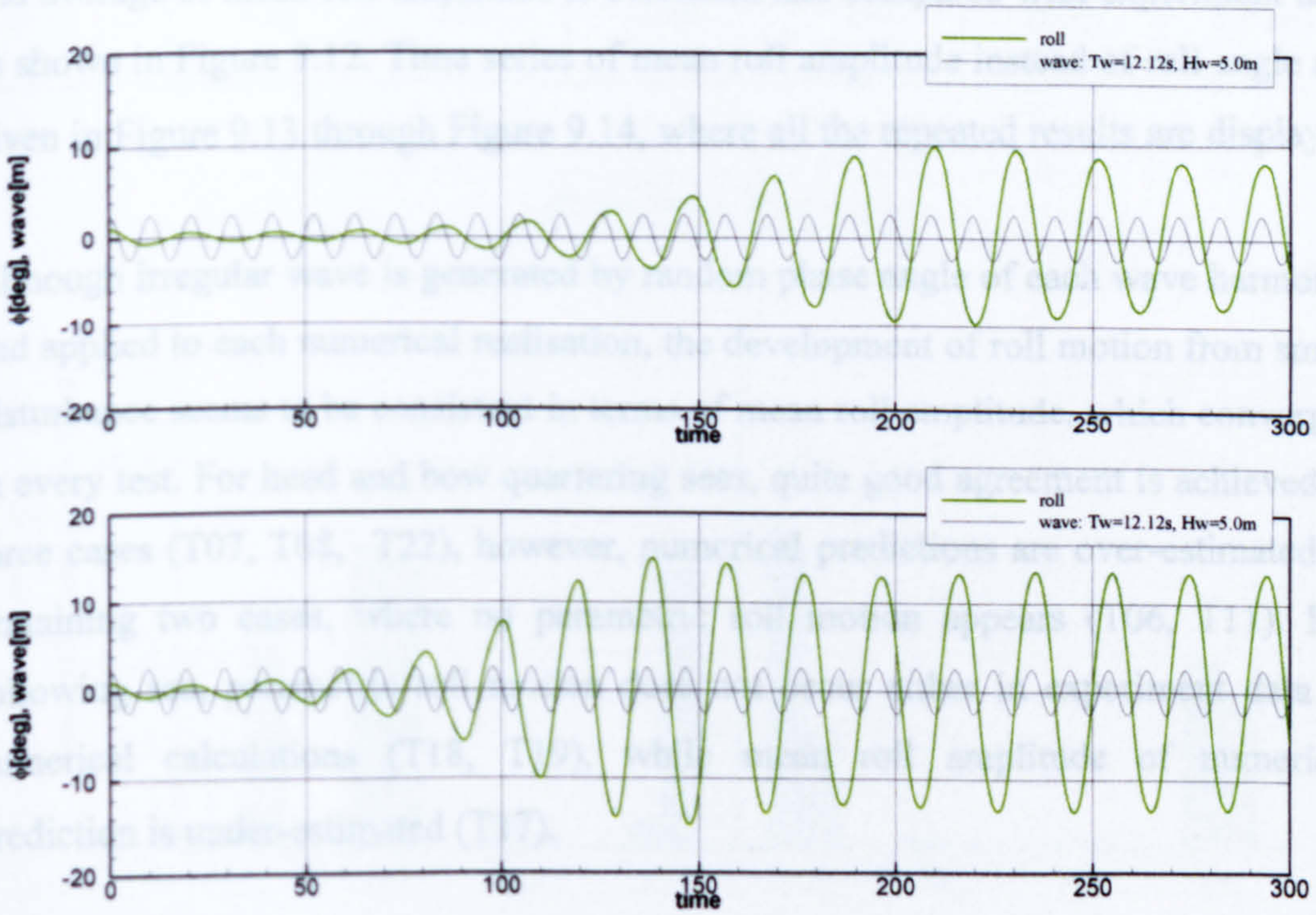

Figure 9.11 Time series of roll angle in T20 and T21 (GM=1.00m, β=180°, Fn=0.08, 0.12)

9.3.4 Tests in group and irregular waves

As a second part of benchmark test, total 8 tests are executed with group and irregular waves; group wave consists of three wave harmonics with different wave height and period. Significant wave height and spectral peak period are given for irregular wave, for which JONSWAP spectrum with a peak enhancement factor γ=3.3, is used for the realisation of random wave. The detailed conditions of group and irregular waves are described in the test matrix shown in Table 9.3; two loading conditions (GM = 1.38, 1.00m), three Froude numbers (Fn = 0.04, 0.08, 0.12) and three wave heading angle (head, bow quartering and following seas) are considered by the combination of given parameters.

Other general conditions of numerical method are same as regular wave test. Since generation of wave is performed in a random manner, a number of simulations need to be performed to obtain meaningful data. Therefore each test is carried out 50 times and average of mean roll amplitude is evaluated and compared with experiment data as shown in Figure 9.12. Time series of mean roll amplitude instead of roll angle are given in Figure 9.13 through Figure 9.14, where all the repeated results are displayed.

Although irregular wave is generated by random phase angle of each wave harmonic and applied to each numerical realisation, the development of roll motion from small disturbance seems to be consistent in terms of mean roll amplitude, which converges in every test. For head and bow quartering seas, quite good agreement is achieved in three cases (T07, T08, T22), however, numerical predictions are over-estimated in remaining two cases, where no parametric roll motion appears (T06, T11). For following sea, parametric roll motion does not occur either in experiment data or numerical calculations (T18, T19), while mean roll amplitude of numerical prediction is under-estimated (T17).

Table 9.3 Benchmark test matrix for group and irregular waves

GM [m]	Test No	Heading [deg]	Fn	Height [m]	Period [sec]	Wave type
1.38	T06	180	0.12	2.4 2.4 2.4	10.63 9.66 11.55	Group
	T07	180	0.12	4.0 1.0 1.0	10.63 9.66 11.55	Group
	T08	180	0.12	5.0	10.63	Irregular
	T11	160	0.12	4.0 1.0 1.0	10.63 9.66 11.55	Group
1.00	T17	0	0.04	2.4 2.4 2.4	8.00 7.11 8.89	Group
	T18	0	0.08	4.0 1.0 1.0	8.00 7.11 8.89	Group
	T19	0	0.08	5.0	8.00	Irregular
	T22	180	0.08	4.0 1.0 1.0	12.12 10.77 13.47	Group

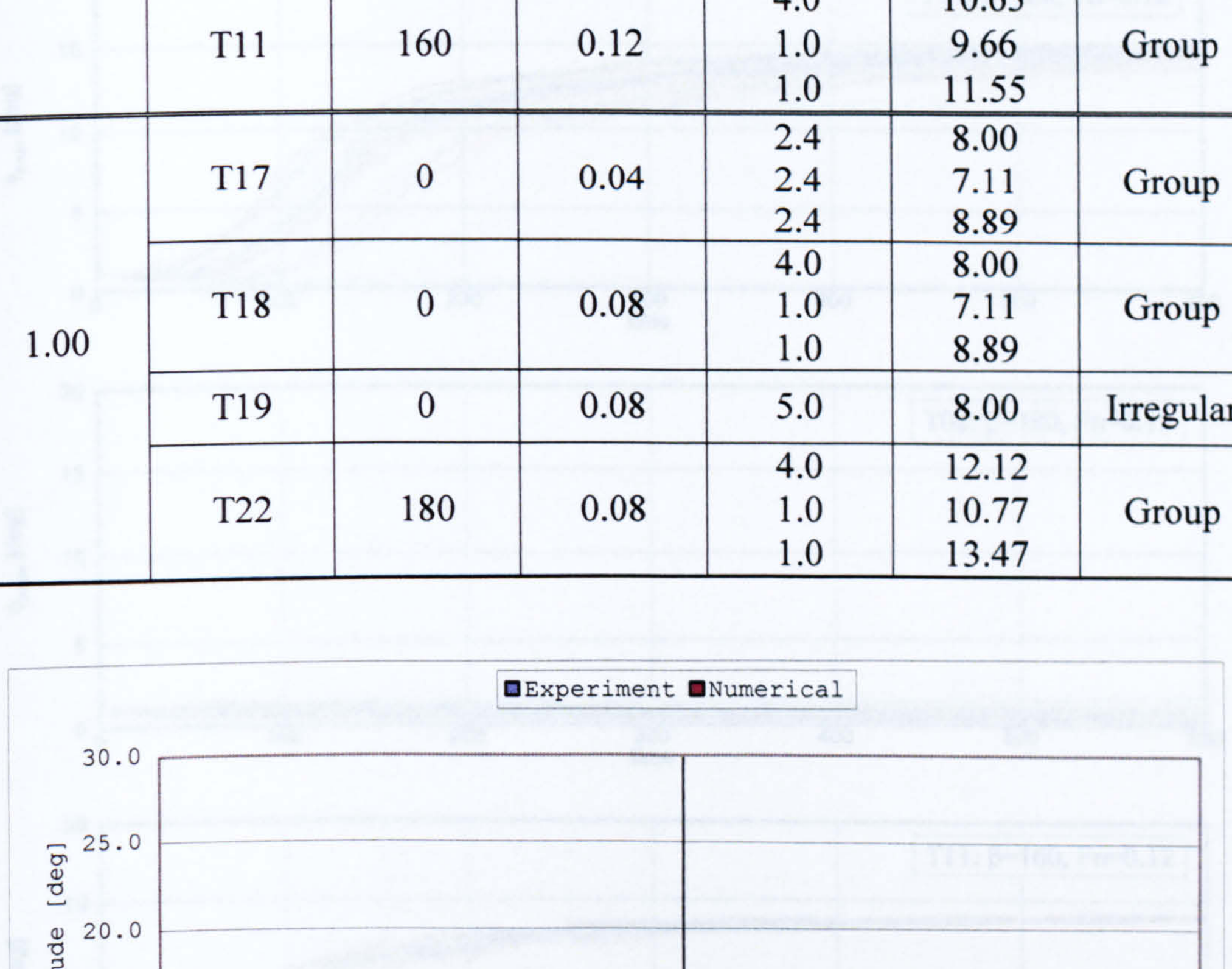

Figure 9.12 Comparison of mean roll amplitude in group and irregular waves

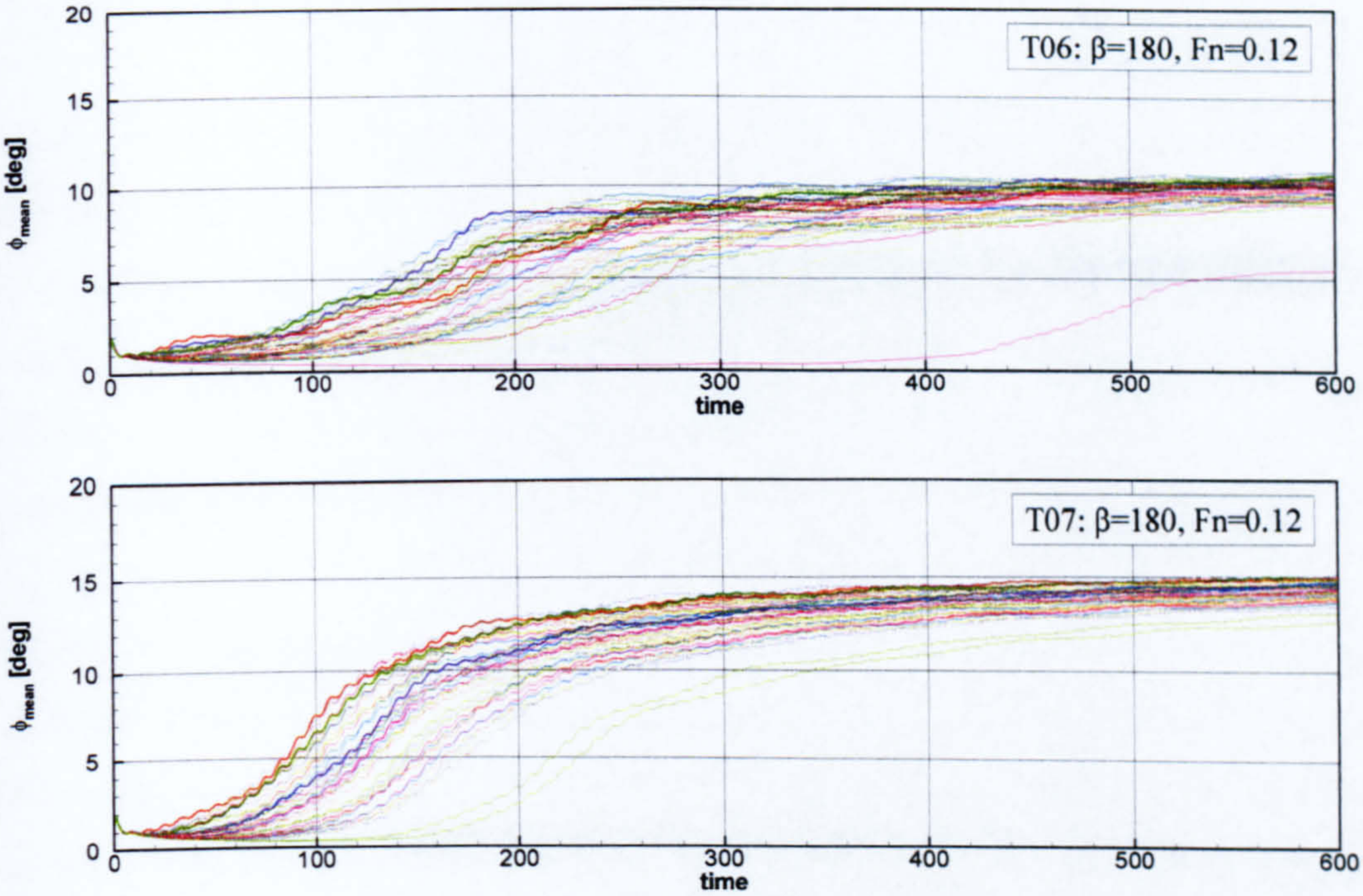

Figure 9.13 Time series of mean roll amplitude in T06, T07, T08 and T11 (GM=1.38m)

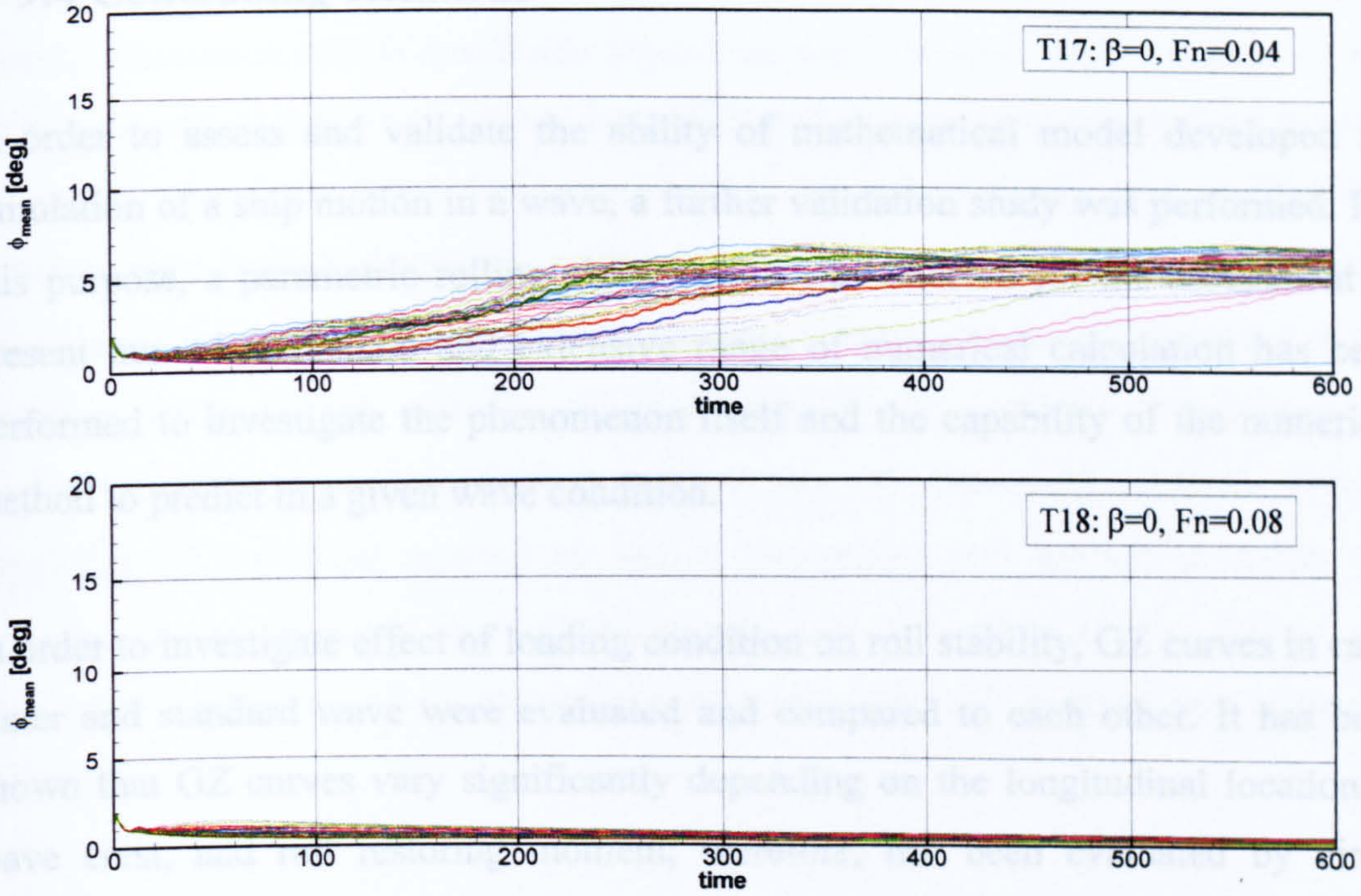

Figure 9.14 Time series of mean roll amplitude in T17, T18, T19 and T22 (GM=1.00m)

9.4 Concluding Remarks

In order to assess and validate the ability of mathematical model developed for simulation of a ship motion in a wave, a further validation study was performed. For this purpose, a parametric rolling phenomenon was selected for the assessment of present numerical method and extensive range of numerical calculation has been performed to investigate the phenomenon itself and the capability of the numerical method to predict in a given wave condition.

In order to investigate effect of loading condition on roll stability, GZ curves in calm water and standard wave were evaluated and compared to each other. It has been shown that GZ curves vary significantly depending on the longitudinal location of wave crest, and roll restoring moment, therefore, has been evaluated by direct pressure integration over instantaneous wetted hull surface as already explained in the previous chapter. Free roll decay test was carried out and comparison with experiment data shows good agreement in terms of frequency and amplitude of damped oscillation.

Roll equation of motion has been adopted to allow non-linear effect on roll damping and restoring terms during high amplitude roll motion, hence development of parametric roll motion in head and following waves could be realised in a numerical manner. In the benchmark test, numerical calculation of developed mathematical model was made in regular, group and irregular waves together with a various combination of given parameters, i.e. loading condition and forward speed of ship, and direction, height and period of incoming wave. Then comparisons between current numerical method and experiment data were made by mean roll amplitude obtained from time history of roll angle. For group and irregular waves a number of numerical simulations were performed to obtain statistically reliable value of mean roll amplitude.

Experiment data in regular waves show highly non-linear behaviour of parametric rolling and these are grouped as follow; 'decrease of roll amplitude with higher wave', 'consistent of roll amplitude regardless wave height', and 'increase of roll amplitude with higher wave'. It has been shown that numerical calculations are able to predict these non-linear behaviours either in quantitatively and qualitatively although there is slight discrepancy. Since parametric roll can be regarded as a highly non-linear phenomenon, more accurate and sophisticated model of roll damping and restoring terms in the equation of motion might be required to improve the qualitative as well as quantitative performance of numerical method. Overall capability of numerical method to predict parametric roll motion in group and irregular waves seems to be satisfactory through a number of simulations and acceptable prediction of no occurrence of parametric roll motion has been also achieved.

Chapter 10. Discussion

10.1 Preamble

Ships sailing in a wave environment experience a variety of disturbances, which make the problems to predict the motion behaviour difficult, and therefore dynamics of a ship has been of great interest in the past century. The unpredictable nature of the phenomena has attracted many studies which employed different approaches to investigate given problems. The dynamics of a ship in extreme seas might include strong non-linearities and transient effects which have not been fully explained in the conventional theories. The formulation of a mathematical model representing the true behaviour of a ship in a seaway is the most important task in developing a methodology for evaluating the qualities of ship performance and establishing a new rational criteria for safety and stability.

The field of ship dynamics is traditionally split into seakeeping and manoeuvring; in the latter field the course achievement and directional stability in calm water condition are major interests while responses to the incident waves at constant speed and heading are investigated in the former. Because of the unique treatments that employed in two distinctive fields of hydrodynamics, the research subject for general behaviour of ship motion could be considered as an integration work to combine seakeeping and manoeuvring theories which were studied separately over many years. However, based on the critical reviews on the state-of-the-art techniques to evaluate the qualities of a ship motion in waves, it seems that the only way to model highly non-linear and transient behaviour of a ship is, at present, integrated six-degree-of-freedom mathematical model in time domain, which incorporates with the frequency dependent hydrodynamic data set obtained in the traditional seakeeping theory as well as propulsion and control force formulation in manoeuvring theory.

Deriving from this theoretical background, the mathematical formulation representing ship manoeuvring motions in a seaway are presented and extended to examine parametric rolling in head and following seas in this study. Since the mathematical model incorporates with the frequency dependent hydrodynamic coefficients and wave loads, first part of present study is devoted to the development of reliable numerical tools to obtain the hydrodynamic data set from the seakeeping theory in the frequency domain. Then a novel mathematical model in time domain is formulated in the strong basis of two traditional ship motion theories to describe the motion behaviour of a ship in waves.

The achievements of the present study have been presented with the certain disadvantages or inadequacies discussed. Therefore, the aim of this study was to contribute to aforementioned efforts focusing on the some specific issues which are believed to be substantial to obtain a successful tool for the studies of ship motions in waves.

10.2 Development of Numerical Tools for Seakeeping Performance

A methodology to predict the behaviour of a ships sailing at sea has been introduced by means of potential theory for the steady and unsteady motion of surface piercing body in a seaway. The formulation of three-dimensional flow, which forms the basis for the solution of a boundary value problem, has been developed for a ship travelling with or without forward speed. In the implementation of the approach adopted, a numerical tool to solve the integral equations of unsteady motion problem with and without forward speed has been developed using two types of three-dimensional discretisation modelling. For the validation of the numerical tool, first-order hydrodynamic forces and motion responses as well as second-order wave forces have been calculated with mathematical and realistic hull forms at various wave conditions.

The theoretical formulation of the boundary value problems for the steady and unsteady motions include the non-linear free surface and body boundary conditions, which make the problems very difficult to obtain analytic or numerical solutions because of the strong non-linearities of the given boundary conditions and unknown free surface. Therefore simplifications of the problem have been introduced to reduce the difficulties imposed on these problems by means of perturbation expansion with assumption of small amplitude motion. The flow field is decomposed into steady and unsteady flows and free surface and body boundary conditions have been linearised on the mean wetted surface of a ship. The linearised free surface condition for the unsteady problem is decoupled from the steady potential on the assumption that the effect of the steady flow on the unsteady flow can be regarded to be higher order. Under the assumption of small amplitude motion, the unsteady motion problem can be decomposed into diffraction and radiation problems and consequently the linearised body boundary condition for the radiation problem contains so-called m-terms which account for steady flow due to the forward speed of a ship.

The solution of the linearised unsteady motion problem is constructed by means of integral equation method. Distributions of the singularities representing translating pulsating source potential reduce the domain of the problem to the body surface, and subsequently Green function which satisfies the linearised free surface boundary condition is introduced. A set of single integrals is introduced in the formulation of Green function, which is expressed with standard complex integral, and it has been found to be practical in the numerical calculation. Meanwhile, a distinct feature of three-dimensional flow due to the interaction of forward speed and encounter frequency of oscillation leads to the critical point of the non-dimensional frequency $\tau = \omega U / g = 1/4$ in the formulation of Green function. The wave patterns of free surface flows are strongly affected near critical frequency $\tau = 1/4$, because of the dependence on the forward speed and frequency of oscillation.

When both source and field points are located near free surface, the oscillatory behaviour of Green function makes it difficult to evaluate the integrands of wave function terms in Green function. Therefore special care has been taken in this

extreme case by using an adaptive numerical scheme to reduce the computational burden. It has been noted that the inclusion of the waterline integral term in the integral equation plays an important role in the unsteady flow field and has strong damping effect on occurrence of irregular frequency since the irregular frequency phenomenon could be more serious without waterline integral. However, difficulties in the evaluation of waterline integral can be caused by the oscillating behaviour of Green function because the source point is located in the free surface, and careful treatment is required to avoid singular behaviour of waterline integral. In the present study the source strength in the waterline integral term is matched with adjacent panel in numerical implementation.

The boundary integral equation is not still amenable to be solved analytically, thus further idealisation of the body surface is required to distribute the source singularities over mean wetted body surface. The body surface is discretised with a finite number of panels and the strength of the source potential distributed on each panel can be assumed to be either constant or higher-order polynomials. Constant Panel Method has an advantage in its easy application to the integral equation with constant source strength on each panel, whilst the derivatives of velocity potential can be easily obtained in Higher-Order Panel Method in spite of its complex implementation due to variable source strength.

It has been noted that one of the major obstacles of these methods is the existence of irregular frequency, where the solution of integral equation either does not exist or is not unique. The phenomenon is originated from non-physical flow interior of the body, so ill-conditioned systems of unknown source strength make it difficult to estimate correct hydrodynamic data set showing heavy fluctuations in high frequency range. In order to reduce irregular frequency phenomenon, the hull surface has been discretised carefully considering size as well as aspect ratio of panels, however further modification of integral equation and corresponding improvement of numerical tool are required to eliminate the phenomenon and acquire reliable hydrodynamic data set.

To secure the reliability of the hydrodynamic data set predicted, a numerical implementation and validation study have been carried out using mathematically defined Wigley hull form and realistic Todd Series 60 ship. Numerical implementations are carried out by means of CPM and HOPM and predicted results are extensively compared with the numerical results of two-dimensional strip method and the experimentally measured data available. The validation study starts with the convergence test to investigate the dependence of the numerical predictions on the characteristics of the surface elements used for representing the hull surface. Several modelling of Wigley hull form with different numbers of surface elements and aspect ratios are chosen to analyse the effect on the hydrodynamic coefficients. When the aspect ratio is closer to unity, convergence to a practical level is achieved with even less number of panels. In the discretisation strategy of the body surface, therefore, the aspect ratio is very important characteristics of the surface elements in addition to the total number of panels.

Validation study is then extended to the numerical applications for Wigley hull form at various forward speeds and calculation results are compared with two-dimensional theory and experimental data. Generally agreement of present methods with experimental data was good and predicted result of hydrodynamic data set shows strong speed dependence. Near the critical point $\tau = 1/4$, there are big discrepancies between present three-dimensional method with the strip theory for the coupled hydrodynamic coefficients because of change of physical flow pattern reflected in the formulation of Green function.

Based on the comparisons between the predicted results and measurement data for the Todd Series 60 ship at zero speed, it is believed that the present three-dimensional Green function method is good enough to predict the wave exciting forces and hydrodynamic coefficients, although roll damping coefficient cannot be predicted correctly due to the inherent assumptions of inviscid potential flow. It is confirmed that Timman-Newman's symmetry relationship for the coupled hydrodynamic coefficients at zero speed is satisfied for all frequency range.

The influences of forward speed and ship heading play an important role in predicting the behaviour of ship motion in waves and their effects on the hydrodynamic data have been demonstrated by CPM and HOPM for the Todd Series 60 ship travelling at various forward speeds and wave directions. The calculation results are demonstrated by both CPM and HOPM, which are adopting three-dimensional translating pulsating source technique and the comparisons of two discretisation methods have shown good agreement in overall frequency ranges. It has been noted that zero speed Green function together with forward speed correction used in two-dimensional strip theory does not adequately account for speed effects in the low frequency regions and therefore speed term in the linearised free surface condition adopted in the present method is essential to obtain reasonable predictions. It has also been shown that three-dimensional translating pulsating source technique adopted in the present study shows better predictions of hydrodynamic data for the forward speed case than the two-dimensional strip theory.

In order to consider higher order wave effects acting on a ship in waves, the theoretical formulation of the second-order hydrodynamic wave loads has been presented based on the first-order solution. The pressure field are expressed using the so-called near-field method, where direct integration of first-order terms are performed over mean wetted body surface without solving the second-order potential problem. To validate the formulation and corresponding computer code, numerical calculations for the mean second-order wave forces acing on the barge, Wigley hull and Todd Series 60 ship are carried out and comparisons with the experimental data are demonstrated. The mean drift forces in sway and yaw directions predicted for a barge at zero speed show a good agreement with the measurement data. Numerical computations of added resistance, that is the second-order wave force with forward speed, are performed for a Wigley hull in head sea cases and the contribution of each component to total added resistance is analysed. It has been noted that the peak value of added resistance in head sea appears near the resonance frequency of heave and pitch motions. Also the mean second-order wave forces are evaluated using first-order solution, therefore correct estimations of the first-order quantities are essential in the predictions of the second-order wave forces adopted in the present study. The

effects of ship heading and forward speed on the mean second-order forces have been demonstrated for Todd Series 60 ship at various wave conditions. It has been remarked that the effects of mean second-order hydrodynamic wave loads become more significant in the short wave regime.

10.3 Formulation of Manoeuvring Mathematical Model

In order to evaluate successfully the characteristics of ship manoeuvring motions in a seaway, a novel mathematical model is required since the conventional manoeuvring model is not capable of describing the effects of wave actions thoroughly. Therefore, a six-degree-of-freedom manoeuvring mathematical model incorporating memory effects with frequency dependent hydrodynamic coefficients in a new axis system is formulated and suitable numerical method for solving the equations of motion is proposed. This development of new model allows straightforward combination of seakeeping and manoeuvring theories whilst accounting for the instantaneous wave effects on the ship motions.

To take the so-called memory effects due to arbitrary forms of ship motions into consideration, impulse response function representation is adopted in the equations of motion such that the hydrodynamic forces are expressed in terms of convolution integral. Since the convolution integral in the time domain incorporates with frequency dependent hydrodynamic coefficients, the impulse response function used to describe the fluid force is determined using Fourier transformations of the hydrodynamic coefficients obtained in the seakeeping calculations demonstrated as a first part of present study. To account for viscous effects of damping coefficients in the low frequency regions, a hybrid method is introduced to the sway and yaw impulse response function by using the manoeuvring derivatives estimated from conventional manoeuvring theory. This hybrid method is very useful when any experimental data is available and therefore it can be directly applied to the initial stage of the design process. Since the impulse response function can be obtained

from either added mass or damping data alone, so comparisons of each numerical calculation are made.

To implement the hydrodynamic data set obtained from seakeeping calculations, a transformation of the data set from the reference frame used in the seakeeping model to the one used in the newly developed mathematical model is required. For this purpose a new body-fixed coordinate system is proposed to describe the motion of a ship in waves, since the traditional seakeeping theory employs an upright body-fixed coordinate system, while a downward coordinate system is preferred in the manoeuvring theory. Kinematics relationships of velocity and acceleration variables between the two theories are examined and corresponding relations of the data set are also derived. The comparisons of the frequency dependent hydrodynamic coefficients have provided the basis for describing the hydrodynamic forces in terms of convolution integrals.

Based on the aforementioned approaches, a set of equations of motion is finally proposed in the body-fixed coordinate system to investigate the manoeuvring motion of a ship in a seaway. The motion variables in each horizontal and vertical plane are coupled with other motions in the same plane, but the direct coupling between both planes is not included. The external forces and disturbances exerted on a ship during a manoeuvring motion in waves include wave, hull, manoeuvring, rudder and propeller forces. The wave excitation terms are very difficult to represent in a functional form, since generally the characteristics of the wave excitation change according to the heading angle with respect to the direction of incoming wave. The hydrostatic and Froude-Krylov forces are calculated using direct pressure integration over the instantaneous wetted body surface under the wave profile. In each time step the relative position and rotation of the body with respect to the exact wave profile are evaluated and it is possible to include non-linear effects of wave force and to consider correct restoring force even in large amplitude motions. It is very time consuming to calculate the wave diffraction force and added resistance exactly in each time step, so these forces are evaluated in a practical manner, where they are assumed to be function of wavelength, heading angle and forward speed.

The hull force, which is described as a motion dependent hydrodynamic force and is equivalent to the radiation force in the potential theory, is expressed in terms of convolution integrals to consider the memory effects due to the arbitrary forms of motion history. To explain the viscous effects of the flow experienced during manoeuvring motion, manoeuvring force is adopted in the equations of motion because it has significant effects on horizontal plane motions and trajectories during manoeuvring motions. The inclusion of manoeuvring force might be criticised since there is some overlapping aspects with the hull force expressed in terms of convolution integral. For the calculations of manoeuvring force together with the rudder and propeller force, empirical method, which is extensively used in the MMG model, is adopted. All of those forces are calculated using the highly efficient modular method in which each individual force is calculated and superimposed in the equations of motion.

The time domain solutions of the equations of motion are obtained using a fourth-order Runge-Kutta method. In order to obtain the impulse response functions, a numerical scheme for Fourier transform was developed and the calculation results have shown that the impulse response functions converge to zero within 20 seconds which is satisfactory for practical application. A method for calculating the hydrostatic and Froude-Krylov wave excitation has been developed in the numerical tool which is capable of integrating the pressure directly over the instantaneous wetted surface under the wave profile.

In order to validate the proposed mathematical model, numerical application for ITTC Ship A-1 container vessel has been performed with given test conditions in following seas. The numerical model could predict both sub-harmonic and harmonic roll oscillations in different wave conditions with reasonable accuracy and capsizing due to the parametric roll resonance is also quite well predicted. Additionally predictions of pitch angle, which has direct effect on the change of roll restoring moment, and yaw angle controlled by the rudder activation of autopilot show good agreement with measurement data.

In order to evaluate significant qualities of ship manoeuvring characteristics, two typical manoeuvring simulations of turning circle and zig-zag tests are performed at various conditions of wavelengths and initial heading angles. The simulation results are compared with the calm water calculation, thought further validation is not possible to be carried out because neither experimental data nor full scale trial is available. Wide range of simulation results of 35° starboard turning circle test have shown that shift of the ship trajectory to the direction of incoming wave is mainly caused by the second-order wave force, especially added resistance in surge direction, which results in large speed loss. Simulations of 20°/20° zig-zag tests with similar wave conditions to the turning circle manoeuvre have been carried out and significant differences of the times to reach third execute of rudder are observed in the cases of head and following seas.

Prediction results of the operational measurements, such as advance, transfer and tactical diameter in turning circle test and first and second overshoot angles in zig-zag test are illustrated and comparisons with the calm water case have confirmed that the wave effects on the manoeuvring simulations cannot be ignored. Since the operational parameters predicted in the standard manoeuvring simulations are very important for the criteria in Standards for Ship Manoeuvrability, full-scale trials in a real seaway should be compensated for the genuine assessment of manoeuvrability in calm water by adopting the method presented in this thesis.

10.4 Prediction of Parametric Rolling

In order to assess and validate the capability of mathematical model to predict high amplitude ship motion in a wave, additional numerical application for parametric rolling phenomenon has been performed. It has been shown that the GZ curve depends on loading condition as well as longitudinal location of wave crest thus affecting roll stability significantly in a wave. A variety of operation parameters, e.g. speed and loading condition, have been combined with regular, group and irregular

waves and applied for the numerical prediction of parametric roll motion in head and following seas. Numerical simulation continues until parametric roll is fully developed and mean value of roll amplitude is evaluated for the comparison with experiment data. For group and irregular waves simulations are repeated to obtain average value.

Highly non-linear behaviour of parametric roll has been observed in the experiment data; 'decrease of roll amplitude with higher wave', 'consistent of roll amplitude regardless wave height', and 'increase of roll amplitude with higher wave'. It has been shown that the ability of numerical method to predict these non-linear behaviours is satisfied either in quantitatively and qualitatively although there are over- and under-estimation of mean roll amplitude. Overall capability of numerical method to predict parametric roll motion seems to be satisfactory for group and irregular waves.

10.5 Contribution to the Field

The principal contribution of the research presented in the thesis is the development and implementation of a theoretical methodology for the analysis of ship motion problem in a seaway. In this respect, formulation of six-degree-of-freedom equations of motion, which is described by an integrated mathematical model in connection with the traditional seakeeping and manoeuvring theories, has been achieved and it has been further extended to the development of the corresponding numerical tools for the assessment of the ship motion performance in waves. The numerical applications showed that the integrated mathematical model could be the most robust way to simulate manoeuvring behaviour of a ship in waves as well as highly non-linear motion like parametric rolling.

In order to obtain full hydrodynamic data set required in the integrated mathematical model, a theoretical formulation and development of an efficient numerical tool for the seakeeping problem have been carried out as a first part of present study. A three-

dimensional panel method with the free surface Green function has been adopted in the frequency domain, and first-order hydrodynamic terms as well as second-order hydrodynamic wave loads have been obtained using both CPM and HOPM. It has been confirmed that the numerical tool has been successfully developed through the validation process in which comparisons are made with other numerical predictions and experimental measurements. It is believed that the numerical methods can be applied to various hull types of marine vehicles and are ready for routine design applications.

In overall, the research presented in the thesis produces an advanced ship motion simulation tool for the marine industry, suggesting the importance of wave effects on the ship manoeuvring tests required for the Standards of Ship Manoeuvrability. The development of theoretical formulation has demonstrated the potentials of the present study to derive accurate estimations of the manoeuvring qualities even in the real environmental disturbances. With the numerical applications to the simulation tests, the author would like to believe that this research constitutes a sound engineering basis for offering insights about the link between the design parameters and for attempting to lead to better design for ship safety. In this respect, the thesis has served the principal aims and objectives stated in Chapter 2.

10.6 Recommendations for Further Research

The present study has demonstrated the formulation and implementation of the numerical model adopted for the six-degree-of-freedom motion simulation of a ship in waves. To obtain more accurate results, however, further improvements could be made by considering many aspects ignored in the assumptions of development procedure. The following are some recommendations for future research and development:

- Although adaptive numerical scheme has been applied to evaluate the integrals of Green function, more fast and efficient numerical techniques regardless of the oscillating phenomena near free surface are required to reduce total calculation time, since most of the computational efforts are consumed in the evaluation of Green function.

- In order to investigate the coupling effects of the steady flow on the unsteady motion, the slender body approximation of m-terms in the body boundary condition need to be compared with exact values by solving steady potential problem.

- The hydrodynamic coefficients appear to have oscillatory trends, so-called the irregular frequency, in the high frequency regions. Although rational approaches have been utilised in the discretisation of hull surface by increasing the total number of panels together with maintaining aspect ratio to be unity, removal of the irregular frequency is little affected. Since it seems to arise from interior flow of free surface, special method to remove irregular frequency and any numerical difficulty in a translating pulsating source technique are required by employing, for example, extended boundary integral equation.

- The convolution integral accounting for the memory effect of arbitrary motion is constructed as a linear model of impulse response function. A further extension

to a non-linear formulation for the functional representation of memory effect is needed to describe large oscillatory motion in rough seas.

- Further development of the integrated mathematical model would improve the overall accuracy of its predictions. Since present mathematical model considers coupling effect between vertical and horizontal plane motions indirectly in the external forces, direct coupling of different plane motions could be taken into account in the equations of motion to predict highly non-linear motion. Theoretical and experimental studies for non-linear behaviour in the horizontal plane motions due to viscosity effects should be incorporated with the numerical tools. The effects of control surface and propulsion parameters on the manoeuvring motion are very important. Therefore, use of more sophisticated autopilot and propulsion models could be attempted.

10.7 Concluding Remarks

In this chapter the major results of the thesis were discussed. Ship motion problems, which have been separated into two research fields of conventional seakeeping and manoeuvring, have been discussed to describe more generalised behaviour of a ship motion in a seaway and formulation of an integrated mathematical model has been carried out including full developments corresponding numerical tools for the predictions of manoeuvring performance and parametric rolling in waves. The mathematical model is encompassed with the technologies available in the traditional seakeeping and manoeuvring research area, while a novel method is also adopted to include key non-linear effects arising from large amplitude motion in heavy sea states. It is hoped that this thesis has contributed positively towards this extent.

Chapter 11. Conclusions

Based on the research work presented in this thesis, it is believed that the aims of the work have been accomplished. In summary, the following concluding statements can be drawn.

- A robust numerical tool for the predictions of first-order hydrodynamic data set has been developed based on the three-dimensional panel method with the translating pulsating Green function in the frequency domain. The tool was extended to obtain the second-order wave loads accounting for drift effect and added resistance in waves. A validation process showed that both CPM and HOPM are capable of estimating and thus providing reliable data set for the following integration of mathematical model.

- A six-degree-of-freedom mathematical model has been formulated and corresponding time domain simulation technique has been developed to describe general manoeuvring behaviour of a ship in a seaway. The integrated mathematical model, allowing straightforward combination of seakeeping and manoeuvring models, incorporates the memory effect of random motion and considers wave force precisely over the instantaneous wetted hull surface. Drifted trajectory of turning circle test shows significance of wave effect, especially added resistance, on the manoeuvring motion.

- The numerical tool of integrated mathematical model is further applied for prediction of parametric roll. Highly non-linear behaviours of parametric roll have been addressed and the numerical tool has proved the capabilities to predict parametric roll with reasonable accuracy and wave effects on the variation of ship stability in a seaway.

References

Abkowitz, M.A. (1964) "Lectures on ship hydrodynamics - steering and manoeuvrability", Report No. Hy-5, Hydrodynamic Department, Hydro-og Aerodynamisk Laboratorium, Lyngby, Denmark.

Ann, S.P., Lee, H.S. and Lee, S.K. (1995) "A computation of hydrodynamic forces by using 3-dimensional higher order panel method", Sixth International Symposium on Practical Design of Ships and Mobile Units, pp. 382-393.

Artyszuk, J. (2003) "Wave effects in ship manoeuvring motion mathematical model - A review analysis", MARSIM'03, Kanazawa, Japan.

Ba, M. and Guilbaud, M. (1995) "A fast method of evaluation for the translating and pulsating Green's function", Schiffstechnik, Vol. 42, pp. 68-80.

Bailey, P.A., Price, W.G and Temarel, P. (1998) "A unified mathematical model describing the manoeuvring of a ship travelling in a seaway", Transactions of RINA, Vol. 140, pp. 131-149.

Bailey, P.A. (1999) "Manoeuvring of a ship in a seaway", Ph.D. Thesis, University of Southampton.

Bailey, P.A., Hudson, D.A., Price, W.G and Temarel, P. (2002) "Time simulation of manoeuvring and seakeeping assessments using a unified mathematical model", Transactions of RINA, Vol. 144, pp. 27-48.

Ballard, E.J., Hudson, D.A., Price, W.G. and Temarel, P. (2003) "Time domain simulation of symmetric ship motions in waves", Transactions of RINA, Vol. 145, pp. 161-180.

Beck, R.F. and Magee, A.R. (1990) "Time-domain analysis for predicting ship motions", In W.G. Price, P. Temarel and A.J. Keane (Eds.), Dynamics of marine vehicles and structures in waves (pp. 49-64), Elsevier Science Publishers B. V.

Beck, R.F. and Reed, A.M. (2001) "Modern computational methods for ships in a seaway", SNAME Transactions, Vol. 109, pp. 1-51.

Beck, R.F., Cummins, W.E., Dalzell, J.F., Mandel, P. and Webster, W.C. (1989) "Motions in waves", In Lewis E.V. (Ed.), Principles of naval architecture: Volume III, (2nd revision, pp. 1-190), Jersey City: The Society of Naval Architects and Marine Engineers.

Beck, R.F., Reed, A.M. and Rood, E.P. (1996) "Application of modern numerical methods in marine hydrodynamics" SNAME Transactions, Vol. 104, pp. 519-537.

Belenky, V. L., Weems, K. M., Lin, W. M. and Paulling, J. R. (2003) "Probabilistic analysis of roll parametric resonance in head seas", Proceedings of 8th International Conference on Stability of Ships and Ocean Vehicles, Madrid, pp. 325-340.

Bertram, V. and Yasukawa, H. (2001) "Investigation of global and local flow details by a fully three-dimensional seakeeping method", 23rd Symposium on Naval Hydrodynamics, Val de Reuil, France.

Bessho, M. (1977) "On the fundamental singularity in a theory of ship motions in a seaway", Memoirs of the Defence Academy Japan, XVII/8, pp.95-105.

Bingham, H.B., Korsmeyer, F.T., Newman, J.N. and Osborne, G.E. (1993) "The simulation of ship motions", 6th International Conference on Numerical Ship Hydrodynamics, Iowa City, Iowa, pp. 561-579.

Bishop, R.E.D., Burcher, R.K. and Price, W.G. (1973a) "The uses of functional analysis in ship dynamics", Proceedings of the Royal Society of London, Series A, Vol. 332, pp. 23-35.

Bishop, R.E.D., Burcher, R.K. and Price, W.G. (1973b) "Application of functional analysis to oscillatory ship model testing", Proceedings of the Royal Society of London, Series A, Vol. 332, pp. 37-49.

Bishop, R.E.D., Burcher, R.K. and Price, W.G. (1973c) "Directional stability analysis of a ship allowing for time history effects of the flow", Proceeding of the Royal Society of London, Series A, Vol. 335, pp. 341-354.

Bishop, R.E.D., Burcher, R.K. and Price, W.G. (1974) "A linear analysis of planar motion mechanism data", JSR, Vol. 18, No. 4, pp. 242-251.

Bishop, R.E.D. and Price, W.G. (1981) "On the use of equilibrium axes and body axes in the dynamics of a rigid Ship", Journal of Mechanical Engineering Science, Vol. 23, No. 5, pp. 243-256.

Bishop, R.E.D., Price, W.G. and Temarel, P. (1984) "A functional representation of fluid actions on ships", ISP, Vol. 31, No. 361, pp. 239-250.

Boin, J.P., Guilbaud, M. and Ba, M (2003) "On the integration of the diffraction-radiation with forward speed Green function", Schiffstechnik, Vol. 50, pp. 106-125.

Brard, R. (1972) "The representation of a given ship form by singularity distributions when the boundary condition on the free surface is linearized", JSR, Vol. 16, No.1, pp. 79-92.

Bulian, G., Francescutto, A. and Lugni, C. (2004) "On the nonlinear modeling of parametric rolling in regular and irregular waves" ISP, Vol. 51, No. 2, pp. 173-203.

Chan, H.S. (1990) "A three-dimensional technique for predicting first- and second-order hydrodynamic forces on a marine vehicle advancing in waves", Ph.D. Thesis, University of Glasgow.

Chang, M.S. (1977) "Computation of three-dimensional ship with forward speed", 2nd International Conference on Numerical Ship Hydrodynamics, Berkeley, pp. 124-135.

Chen, X.B. (1999) "An introductory treatise on ship-motion Green functions", 7th International Conference on Numerical Ship Hydrodynamics, Paris, France, pp. 1-20.

Chen, X.B. and Diebold, L. and Doutreleau, Y. (2000) "New Green-function method to predict wave-induced ship motions and loads", 23rd Symposium on Naval Hydrodynamics, Val de Reuil, France, pp. 66-81.

Chen, X.B. and Noblesse, F. (1998) "Super Green functions", 22nd Symposium on Naval Hydrodynamics, Washington, D.C., pp. 860-874.

Chen, X.B. and Wu, G.X. (2001) "On singular and highly oscillatory properties of the Green function for ship motions", Journal of Fluid Mechanics, Vol. 445, pp. 77-91.

Clarke, D., Gedling, P. and Hine, G. (1983) "The application of manoeuvring criteria in hull design using linear theory", Transactions of RINA, Vol. 125, pp. 45-68.

Cummins, W.E. (1962) "The impulse response function and ship motions", Schiffstechnik, Vol. 9, pp. 101-109.

Dawson, C.W. (1977) "A practical computer method for solving ship-wave problem", 2nd International Conference on Numerical Ship Hydrodynamics, Berkeley, pp. 30-38.

de Kat, J.O. and Paulling, J.R. (1989) "The simulation of ship motions and capsizing in severe seas", SNAME Transactions, Vol. 97, pp. 139-168.

Doctors, L.J. and Beck, R.F. (1987) "Numerical aspects of the Neumann-Kelvin problem", JSR, Vol. 31, No. 1, pp. 1-13.

Du, S.X., Hudson, D.A., Price, W.G. and Temarel, P. (2000) "A validation study on mathematical models of speed and frequency dependence in seakeeping", Proceedings of the Institution of Mechanical Engineers, Vol. 214, Part C, pp. 181-202.

Faltinsen, O.M. and Michelsen, F.C. (1974) "Motions of large structures in waves at zero Froude number", International Symposium on the Dynamics of Marine Vehicles and Structures in Waves, London, pp. 91-106.

Faltinsen, O.M., Minsaas, K.J., Liapis, N. and Skjordal, S.O. (1980) "Prediction of resistance and propulsion of a ship in a seaway", 13th Symposium on Naval hydrodynamics, Tokyo, pp. 505-529.

Fang, M.C., Luo, J.H. and Lee, M.L. (2005) "A nonlinear mathematical model for ship turning circle simulation in waves", JSR, Vol. 49, No. 2, pp. 69-79.

Fossen, T.I. (1994) "Guidance and control of ocean vehicles", John Wiley & Sons.

France, W. M, Levadou, M., Treakle, T. W., Paulling, J. R., Michel, K. and Moore, C. (2003) "An investigation of head-sea parametric rolling and its influence on container lashing systems," Marine Technology, Vol. 40, No. 1, pp. 1-19.

Frank, W. (1967) "Oscillation of cylinders in or below the free surface of deep fluids", Report No. 2375, Naval Ship Research and Development Center, Bethesda, Maryland.

Fujino, M. (1975) "The effect of frequency dependence of the stability derivatives on maneuvering motion", ISP, Vol. 22, No. 256, pp. 416-432.

Fujino, M. (1996) "Prediction of ship manoeuvrability: State of the art", MARSIM'96, Copenhagen, Denmark.

Gadd, G.E. (1976) "A method of computing the flow and surface wave pattern around Full Forms", Transactions of RINA, Vol. 118, pp. 207-219.

Garrison, C.J. (1978) "Hydrodynamic loading of large offshore structures. Three-dimensional source distribution methods", In O.C. Zienkiewicz, R.W. Lewis and K.G. Stagg (Eds.), Numerical Methods in Offshore Engineering (pp.87-140), Chichester: John Wiley & Sons.

Gerritsma, J. and Beukelman, W. (1964) "The distribution of the hydrodynamic forces on a heaving and pitching ship model in still water", 5th Symposium on Naval Hydrodynamics, pp. 219-257.

Gerritsma, J. and Beukelman, W. (1966) "Comparison of calculated and measured heaving and pitching motions of a Series 60, $C_B = 0.7$ ship model in regular longitudinal waves", Proceedings of the 11th ITTC, Tokyo, Japan, pp. 436-442.

Gerritsma, J. and Beukelman, W. (1972) "Analysis of the resistance increase in waves of a fast cargo ship", ISP, Vol. 19, No.217, pp. 285-293.

Grim, O. (1952) "Rollschwingungen, Stabilität und Sicherheit im Seegang", Schiffstechnik, Vol. 1, No. 1, pp. 10-21.

Grim, O. (1953) "Berechnung der durch schwingungen eines schiffskörpers erzeugten hydrodynamischen kräfte", Jahrbuch der Schiffsbautechnischen Gesellschaft, No. 47, pp. 277-299.

Grue, J. and Palm, E. (1985) "Wave radiation and wave diffraction from a submerged body in a uniform current", Journal of Fluid Mechanics, Vol. 151, pp. 257-278.

Guevel, P. and Bougis, J. (1982) "Ship-motions with forward speed in infinite depth", ISP, Vol. 29, No. 332, pp. 103-117.

Guo, C. (1981) "Nonlinear theory of ship maneuvering", JSR, Vol.25, No.1, pp. 21-43.

Hamamoto, M. and Kim, Y.S. (1993) "A new coordinate system and the equations describing manoeuvring motion of a ship in waves", Journal of the Society of Naval Architectures of Japan, Vol. 173, pp. 209-220.

Hasegawa, K. (1980) "On a performance criterion of auto pilot navigation", Journal of the Kansai Society of Naval Architects, Japan, No. 178, pp. 93-103.

Havelock, T.H. (1942) "The drifting force on a ship among waves", Philosophical Magazine, Vol. 33, pp. 467-475.

Hermans, A.J. and Huijsmans, R.H.M. (1987) "The effect of moderate speed on the motion of floating bodies", Schiffstechnik, Vol. 34, No. 3, pp. 132-.

Hess, J.L. and Smith, A.M.O. (1967) "Calculation of potential flow about arbitrary bodies", Progress in Aeronautical Science, Vol. 8, pp. 1-138.

Himeno, Y. (1981) "Prediction of ship roll damping - state of the art", Report No. 239. Department of Naval Architecture and Marine Engineering, University of Michigan.

Hoff, J.R. (1990) "Three-dimensional Green function of a vessel with forward speed in waves", Ph.D. Thesis, The Norwegian Institute of Technology.

IMO (1993) "Interim standards for ship manoeuvrability", Resolution A.751(18).

IMO (2002) "Standards for ship manoeuvrability", Resolution MSC.137(76).

Inglis, R.B. and Price, W.G. (1981) "Calculation of the velocity potential of a translating, pulsating source", Transactions of RINA, Vol. 123, pp. 163-175.

Inglis, R.B. and Price, W.G. (1982a) "A three dimensional ship motion theory: Comparison between theoretical predictions and experimental data of the hydrodynamic coefficients with forward speed", Transactions of RINA, Vol. 124, pp. 141-157.

Inglis, R.B. and Price, W.G. (1982b) "A three dimensional ship motion theory: Calculation of wave loading and responses with forward speed", Transactions of RINA, Vol. 124, pp. 183-192.

Inoue, S., Hirano, M. and Kijima, K. (1981) "Hydrodynamic derivatives on ship manoeuvring", ISP, Vol. 28, No.321, pp. 112-125.

ITTC (1990) "Report of the panel on validation procedures", Proceedings of the 19th ITTC, Vol. 1, Madrid, Spain, pp. 577-605.

ITTC (1999) "The loads and responses committee: Final report and recommendations to the 22nd ITTC", Proceedings of the 22nd ITTC, Seoul and Shanghai, pp. 119-172.

ITTC (2002) "The loads and responses committee: Final report and recommendations to the 23rd ITTC", Proceedings of the 23rd ITTC, Venice, Italy, Vol. 1, pp. 235-285.

ITTC (2002) "The specialist committee on prediction of extreme ship motions and capsizing: Final report and recommendations to the 23rd ITTC", Proceedings of the 23rd ITTC, Venice, Italy, Vol. 2, pp. 619-657.

ITTC (2005) "The seakeeping committee: Final report and recommendations to the 24th ITTC", Proceedings of the 24th ITTC, Edinburgh, UK, Vol. 1, pp. 199-254.

Iwashita, H. and Ohkusu, M. (1992) "The Green function method for ship motions at forward speed", Schiffstechnik, Vol. 39, pp.3-21.

Jasionowski, A. (2001) "An integrated approach to limit state performance assessment", Ph.D. Thesis, University of Strathclyde.

Journee, J.M.J. (1992) "Experiment and calculations on 4 Wigley hull forms in head waves", Report 0909, Ship Hydromechanics Laboratory, Delft University of Technology.

Kashiwagi, M. (1992) "Added resistance, wave-induced steady sway force and yaw moment on an advancing ship", Schiffstechnik, Vol. 39, No. 1, pp. 3-16.

Kashiwagi, M., Iwashita, H., Takagi, K. and Yasukawa, H. (1994) "Numerical calculation methods of the ship motion based on three-dimensional theories (in Japanese)", 11th Marine Dynamics Symposium, The Society of Naval Architects of Japan, pp. 219-292.

Kijima, K., Katsuno, T., Nakiri Y. and Furukawa, Y. (1990) "On the maneuvering performance of a ship with the parameter of loading conditions", Journal of the Society of Naval Architects of Japan, Vol. 168, pp. 141-148.

Kijima, K., Nakiri, Y. and Furukawa, Y. (2000) "On a prediction method for ship manoeuvrability", Proceeding of International Workshop on Ship Manoeuvrability, Hamburg Ship Model Basin, Hamburg, Germany.

King, B.K., Beck, R.F., and Magee, A.R. (1988) "Seakeeping calculations with forward speed using time domain analysis", 17th Symposium on Naval Hydrodynamics, Hague, Netherlands, pp. 577-596.

King, B.W. (1987) "Time-domain analysis of wave exciting forces on ships and bodies", Report No. 306, Department of Naval Architecture and Marine Engineering, University of Michigan.

Korvin-Kroukovsky, B.V. and Jacobs, W.D. (1957) "Pitching and heaving motions of a ship in regular waves", SNAME Transactions, Vol. 65, pp. 590-632.

Kose, K., Misiag, W.A. and Xiong, X. (1996) "Systematic approach for ship manoeuvrability prediction", MARSIM'96, Copenhagen, Denmark.

Kring, D.C. (1998) "Ship seakeeping through the τ=1/4 critical frequency", JSR, Vol. 42, No. 2, pp. 113-119.

Lee, C.H., Newman, J.N., and Zhu, X. (1996) "An extended boundary integral equation method for the removal of irregular frequency effects", International Journal for Numerical Methods in Fluids, Vol. 23, No. 7, pp. 637-660.

Lee, S-K. (2000) "The calculation of zig-zag maneuver in regular waves with use of the impulse response functions", Ocean Engineering, Vol. 27, pp. 87-96.

Lewis, F.M. (1929) "The inertia of water surrounding a vibrating Ship", SNAME Transactions, Vol. 37, pp. 1-20.

Liapis, S. and Beck, R.F. (1985) "Seakeeping computations using time domain analysis", 4th International Conference on Numerical Ship Hydrodynamics, Washington, D.C., pp.34-54.

Lin, W.C. and Reed, A.M. (1976) "The second order steady force and moment on a ship moving in an oblique seaway", 11th Symposium on Naval Hydrodynamics, London, pp. 333-351.

Lin, W.C. and Yue, D.K.P. (1990) "Numerical solutions for large-amplitude ship motions in the time domain" 18th Symposium on Naval Hydrodynamics, Ann Arbor, Michigan, pp.41-66.

Liu, Y. and Yue, D.K.P. (1993) "On the solution near the critical frequency for an oscillating and translating body in or near a free surface", Journal of Fluid Mechanics, Vol. 254, pp. 251-266.

Loeser, D.J. (1982) "Determination of maneuvering properties in shallow water by impulse response techniques", JSR, Vol. 26, No.1, pp. 1-15.

Martin, L.L. (1980) "Ship maneuvering and control in wind", SNAME Transactions, Vol. 88, pp. 257-281.

Maruo, H. (1960) "The drift of a body floating on waves", JSR, Vol. 4, No. 3, pp. 1-10.

Matusiak, J. (2003) "On the effects of wave amplitude, damping and initial conditions on the parametric roll resonance", Proceedings of 8th International Conference on Stability of Ships and Ocean Vehicles, Madrid, pp. 341-348.

Maury, C., Delhommeau, G., Ba, M., Boin, J.P. and Guilbaud, M., (2003) "Comparison between numerical computations and experiments for seakeeping on ship models with forward speed", JSR, Vol. 47, No. 4, pp. 347-364.

McCreight, W.R. (1986) "Ship maneuvering in waves", 16th Symposium on Naval Hydrodynamics, Berkeley, California, USA.

Mori, M. (1995) "A note on hull form design (Part24)", Journal of Ship Science, Vol. 48, pp. 40-49. (In Japanese)

Nakos, D. and Sclavounos, P. (1990) "Ship motions by a three-dimensional Rankine panel method", 18th Symposium on Naval Hydrodynamics, Ann Arbor, Michigan, pp. 21-40.

Newman, J.N. (1967) "The drift force and moment on ships in waves", JSR, Vol. 11, No. 1, pp. 51-60.

Newman, J.N. (1977) "Marine hydrodynamics", MIT Press, Cambridge, Massachusetts.

Newman, J.N. (1978) "The theory of ship motions", Advances in Applied Mechanics, Vol. 18, pp. 221-283.

Newman, J.N. and Sclavounos, P. (1980) "The unified theory of ship motions", 13th Symposium on Naval Hydrodynamics, Tokyo, pp. 373-394.

Nobless, F. and Yang, C. (2004) "A simple Green function for diffraction-radiation of time-harmonic waves with forward speed", Schiffstechnik, Vol. 51, pp. 35-52.

Norrbin, N.H. (1971) "Theory and observations on the use of a mathematical model for ship manoeuvring in deep and confined waters", SSPA, Gothenburg, Sweden, Publication No. 68.

Ogilvie, T.F. and Tuck, E.O. (1969) "A rational strip theory of ship motions: Part 1", Report No. 013, Department of Naval Architecture and Marine Engineering, University of Michigan.

Ohkusu, M. (1996) "Hydrodynamics of ships in waves", Advances in Marine Hydrodynamics, Chapter 2, Computational Mechanics Publications, Southampton, pp. 77-131.

Ohkusu, M. (1998) "Validation of theoretical methods for ship motions by means of experiment", 22nd Symposium on Naval Hydrodynamics, Washington, D.C., pp. 341-358.

Ohmatsu, S. (1975) "On the irregular frequencies in the theory of oscillating bodies in a free surface", Papers of Ship Research Institution, No. 48, pp.1-13.

Ottosson, P. and Bystrom, L. (1991) "Simulation of the dynamics of a ship maneuvering in waves", SNAME Transactions, Vol. 99, pp. 281-298.

Papanikolaou, A. and Zaraphonitis, G. (1987) "On an improved method for the evaluation of second-order motions and loads on 3D floating bodies in waves", Schiffstechnik, Vol. 34, pp. 170-211.

Papanikolaou, A. and Schellin, Th. (1992) "A three dimensional panel method for motions and loads of ships with forward speed", Schiffstechnik, Vol. 39, pp. 147-156.

Paulling, J. R. and Rosenberg, R.M. (1959) "On unstable ship motions resulting from nonlinear coupling", JSR, Vol. 3, No. 1, pp. 36-46.

Perez y Perez, L. (1974) "A time-domain solution to the motions of a steered ship in waves", JSR, Vol. 18, No.1, pp.32-45.

Pinkster, J.A. and van Oortmerssen, G. (1977) "Computation of the first and second order wave forces on oscillating bodies in regular waves", 2nd International Conference on Numerical Ship Hydrodynamics, Berkeley, pp. 136-156.

Prins, H.J. and Hermans, A.J. (1994) "Time domain calculations of the second-order drift force on a floating 3-D object in current and waves", Schiffstechnik, Vol. 41, No. 2, pp. 85-92.

Rydill, L.J. (1959) "A linear theory for the steered motion of ships in waves", Transactions of the Institution of Naval Architects, Vol. 101, pp. 81-112.

Salvesen, N., Tuck, E.O. and Faltinsen, O. (1970) "Ship motions and sea loads", SNAME Transactions, Vol. 78, pp. 250-287.

Sclavounos, P. (1996) "Computation of wave ship interactions", Advances in Marine Hydrodynamics, Chapter 4, Computational Mechanics Publications, Southampton, pp. 177-231.

Scragg, C.A. (1977) "Determination of stability derivatives by impulse-response techniques", Marine Technology, Vol. 14, No. 2, pp. 265-275.

Scragg, C.A. (1979) "Memory effects in deepwater maneuvering", JSR, Vol. 23, No. 3, pp. 175-187.

Sen, D. (2002) "Time-domain computation of large amplitude 3D ship motions with forward speed", Ocean Engineering, Vol. 29, pp. 973-1002.

St. Denis, M. and Pierson, W.J. (1953) "On the motions of ships in confused seas", SNAME Transactions, Vol. 61, pp. 280-357.

Strom-Tejsen, J., Yeh, H.Y.H. and Moran, D.D. (1973) "Added resistance in waves", SNAME Transactions, Vol. 81, pp. 109-143.

Takahashi, T. (1988) "A practical prediction of added resistance of a ship in waves and the direction of its application to hull form design", Transactions of West-Japan Society of Naval Architects, Vol. 75, pp. 75-95.

Timman, R. and Newman, J.N. (1962) "The coupled damping coefficients of a symmetric ship", JSR, Vol. 5, No. 4, pp. 1-7.

Todd, F.H. (1953) "Some further experiments on single screw merchant ship forms - Series 60", SANME Transactions, Vol. 61, pp. 516-589.

Ueno, M., Nimura, T. and Miyazaki, H (2003) "Experimental study on manoeuvring motion of a ship in waves", MARSIM'03, Kanazawa, Japan.

Ueno, M., Nimura, T. and Miyazaki, H. (2001) "Prediction of steady short wave forces and moment acting on ships in manoeuvring motion", Proceedings of Mini Symposium on Prediction of Ship Manoeuvring Performance, Tokyo, Japan, pp. 93-102.

Ursell, F. (1949) "On the heaving motions of a circular cylinder on the surface of a fluid", Quarterly Journal of Mechanics and Applied mathematics, Vol. 2, pp. 218-231.

van Leeuwen, G. (1964) "The lateral damping and added mass of a horizontally oscillating ship model", Report 65S, Netherlands Ship Research Centre TNO.

Vassalos, D., Ha, T.B. and Kara, F. (2000) "A comparative study of 3-D frequency-domain and time-domain approaches to hydrodynamic loads of HSC", KR-Report. 10104, Korean Register of Shipping, pp. 1-21.

Vugts, J.H. (1971) "The hydrodynamic forces and ship motions in oblique waves", Report 150S, Netherlands Ship Research Centre TNO.

Wagner-Smitt, L. (1970, 1971) "Steering and manoeuvring of ships - full scale and model tests", European Shipbuilding, Vol. 19, No. 6, pp.86-96, and Vol. 20, No.1, pp. 8-17.

Watanabe, Y. (1938) "Some contribution to the theory of rolling", Trans. INA, Vol. 80, pp. 408-432.

Wehausen, J.V. and Laitone, E.V. (1960) "Surface waves", Handbook der Physik (or Encyclopaedia of Physics), Vol. 9, Springer-Verlag, Berlin.

Westlake, P.C., Wilson, P.A. and Bailey, P.A. (2000) "Time domain simulation of ship motion", Transactions of RINA, Vol. 142, pp. 268-288.

Wu, G.X. and Eatock Taylor, R. (1987) "A Green's function form for ship motions at forward speed", ISP, Vol. 34, No. 389, pp. 189-196.

Wu, G.X. and Eatock Taylor, R. (1989) "The numerical solution of the motions of a ship advancing in waves", 5th International Conference on Numerical Ship Hydrodynamics, Hiroshima, Japan, pp. 529-538.

Zafer, A. and Vassalos, D. (2003) "Towards an improved mathematical model for ship manoeuvring in astern seas", MARSIM'03, Kanazawa, Japan.

Zaraphonitis, G. and Papanikolaou, A. (1993) "Second-order theory and calculations of motions and loads of arbitrarily shaped 3D bodies in waves" Marine Structures, Vol. 6, pp. 165-185.

IMO	International Maritime Organisation
ISP	International Shipbuilding Progress
ITTC	International Towing Tank Conference
JSR	Journal of Ship Research
MARSIM	International Conference on Marine Simulation and Ship Maneuverability
RINA	The Royal Institution of Naval Architects
SNAME	The Society of Naval Architects and Marine Engineers
Schiffstechnik	Ship Technology Research

Appendix A. Formulation of Green Function

A.1 Formulation of Green Function

A.1.1 Integrals I_{11} and I_{12}

The method to express integrals I_{11} and I_{12} in terms of exponential integral is very similar to that used in Chapter 5, but is much simpler.

$$I_{11} = \frac{1}{\pi}\int_{\gamma}^{\frac{\pi}{2}} d\theta \int_{0}^{\infty} \frac{\exp(k\chi_1)}{\sqrt{1-4\tau\cos\theta}} \cdot \frac{k_1}{k-k_1} dk$$
$$I_{12} = \frac{1}{\pi}\int_{\gamma}^{\frac{\pi}{2}} d\theta \int_{0}^{\infty} \frac{\exp(k\chi_2)}{\sqrt{1-4\tau\cos\theta}} \cdot \frac{k_1}{k-k_1} dk \qquad \text{(A.1)}$$

Again change of variable given in equation (A.2) will be used and integration intervals can be changed as equation (A.3) since k_1 is real.

$$u = -\chi_1(k-k_1) \qquad \text{(A.2)}$$

$$k = 0 \quad \rightarrow \quad u = k_1\chi_1$$
$$k = \infty \quad \rightarrow \quad u = -\chi_1\infty \qquad \text{(A.3)}$$

Then I_{11} can be expressed as

$$I_{11} = \frac{1}{\pi}\int_{\gamma}^{\frac{\pi}{2}} \frac{k_1\exp(k_1\chi_1)}{\sqrt{1-4\tau\cos\theta}} d\theta \int_{k_1\chi_1}^{\chi_1\infty} \frac{e^{-u}}{u} du \qquad \text{(A.4)}$$

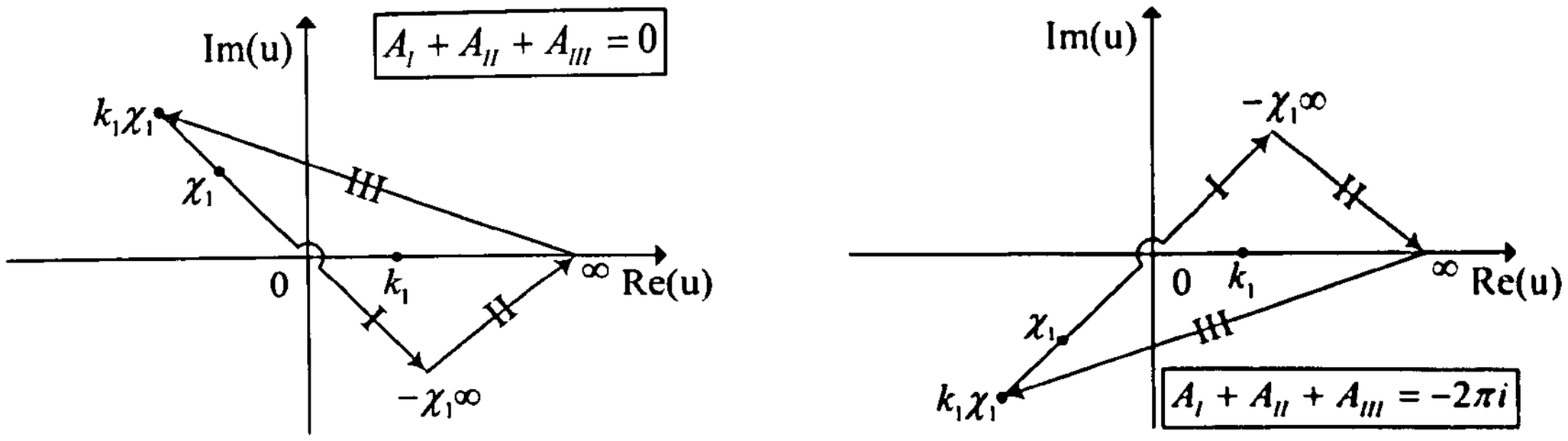

(*a*) $\mathrm{Im}(\chi_1) \geq 0$ (*b*) $\mathrm{Im}(\chi_1) < 0$

Figure A.1 Integration path of the integral I_{11}

Again we can take the contour integral of $A_I + A_{II} + A_{III}$ and by applying Cauchy's integral theorem the contour integral can be expressed as

$$\begin{aligned} A_I + A_{II} + A_{III} &= \int_{k_1\chi_1}^{\chi_1\infty} \frac{e^{-u}}{u} du + \int_{\chi_1\infty}^{\infty} \frac{e^{-u}}{u} du + \int_{\infty}^{k_1\chi_1} \frac{e^{-u}}{u} du \\ &= \int_{k_1\chi_1}^{\chi_1\infty} \frac{e^{-u}}{u} du - E_1(k_1\chi_1) \end{aligned} \tag{A.5}$$

Since $\mathrm{Im}(k_1) > 0$ and $\mathrm{Re}(\chi_1) < 0$, the imaginary part of singular point is positive

$$k = k_1 + i\varepsilon \quad \rightarrow \quad u = -i\varepsilon\chi_1 \quad \rightarrow \quad \mathrm{Im}(u) > 0 \tag{A.6}$$

When $\mathrm{Im}(\chi_1) \geq 0$, the integration path will follow Figure A.1 (a) and the contour integration becomes $A_I + A_{II} + A_{III} = 0$. Thus equation (A.5) can be rewritten in terms of exponential integral as follows

$$\int_{k_1\chi_1}^{\chi_1\infty} \frac{e^{-u}}{u} du = E_1(k_1\chi_1) \qquad \text{when } \mathrm{Im}(\chi_1) \geq 0 \tag{A.7}$$

When $\mathrm{Im}(\chi_1) < 0$, the integration path will follow Figure A.1 (b). Since this path contains singular point, the contour integration becomes $A_I + A_{II} + A_{III} = -2\pi i$ and equation (A.5) can be rewritten as

$$\int_{k_1\chi_1}^{-\chi_1\infty} \frac{e^{-u}}{u} du = E_1(k_1\chi_1) - 2\pi i \qquad \text{when } \mathrm{Im}(\chi_1) < 0 \tag{A.8}$$

Finally following results for the integrals I_{11} and I_{12} are obtained

$$\begin{aligned} I_{11} &= \frac{1}{\pi}\int_{\gamma}^{\frac{\pi}{2}} \frac{k_1 \exp(k_1\chi_1) E_{r1}(k_1\chi_1)}{\sqrt{1-4\tau\cos\theta}} d\theta \\ I_{12} &= \frac{1}{\pi}\int_{\gamma}^{\frac{\pi}{2}} \frac{k_1 \exp(k_1\chi_2) E_{r1}(k_1\chi_2)}{\sqrt{1-4\tau\cos\theta}} d\theta \end{aligned} \tag{A.9}$$

where

$$E_{r1}(k_1\chi_j) = \begin{cases} E_1(k_1\chi_j) & \text{when } \mathrm{Im}(\chi_j) \geq 0 \\ E_1(k_1\chi_j) - 2\pi i & \text{when } \mathrm{Im}(\chi_j) < 0 \end{cases} \tag{A.10}$$

Similar method can be applied for the formulations of integrals I_{33}, I_{34}, I_{43} and I_{44}, and corresponding exponential integral given in equation (A.10) can be used without any change.

A.1.2 Integrals I_{21} and I_{22}

The method to express integrals I_{21} and I_{22} in terms of exponential integral is very similar to previous section.

$$\begin{aligned} I_{21} &= \frac{1}{\pi}\int_{\gamma}^{\frac{\pi}{2}} d\theta \int_0^{\infty} \frac{\exp(k\chi_1)}{\sqrt{1-4\tau\cos\theta}} \cdot \frac{k_2}{k-k_2} dk \\ I_{22} &= \frac{1}{\pi}\int_{\gamma}^{\frac{\pi}{2}} d\theta \int_0^{\infty} \frac{\exp(k\chi_2)}{\sqrt{1-4\tau\cos\theta}} \cdot \frac{k_2}{k-k_2} dk \end{aligned} \tag{A.11}$$

Again change of variables given in equation (A.12) will be used and integration intervals can be changed as equation (A.13) since k_2 is real.

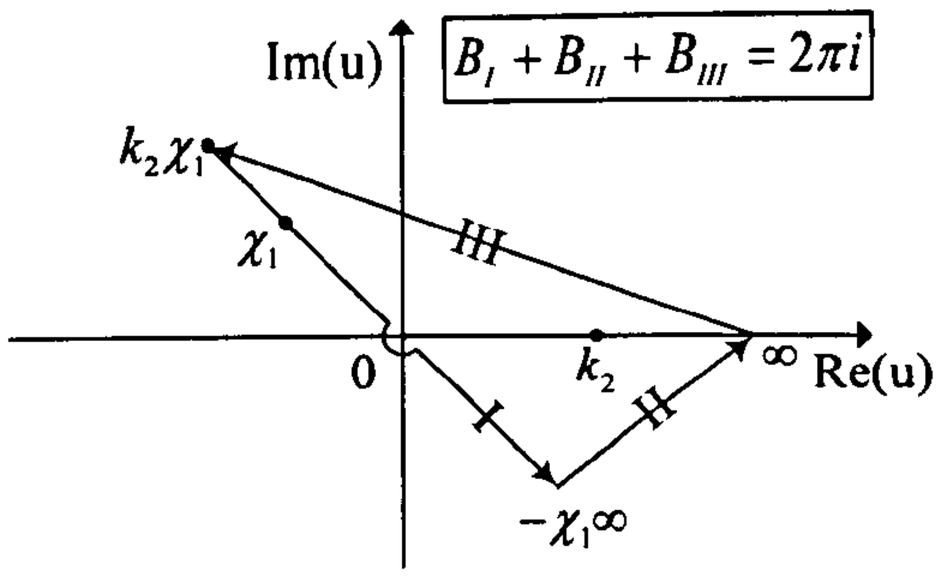

(*a*) $\mathrm{Im}(\chi_1) \geq 0$

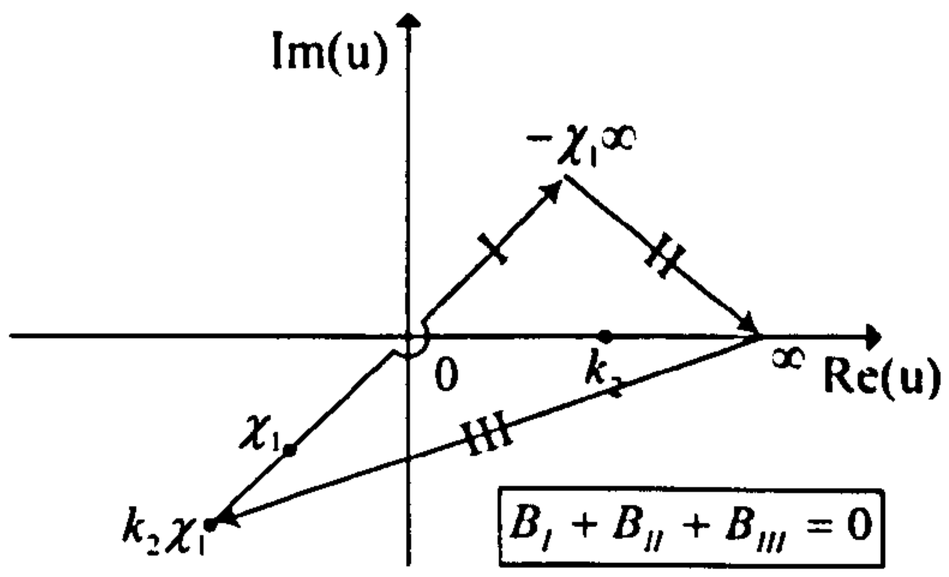

(*b*) $\mathrm{Im}(\chi_1) < 0$

Figure A.2 Integration path of the integral I_{21}

$$u = -\chi_1(k - k_2) \tag{A.12}$$

$$\begin{aligned} k = 0 \quad &\rightarrow \quad u = k_2\chi_1 \\ k = \infty \quad &\rightarrow \quad u = -\chi_1\infty \end{aligned} \tag{A.13}$$

Then I_{21} can be expressed as

$$I_{21} = \frac{1}{\pi}\int_{\gamma}^{\frac{\pi}{2}} \frac{k_2 \exp(k_2\chi_1)}{\sqrt{1 - 4\tau\cos\theta}} d\theta \int_{k_2\chi_1}^{\chi_1\infty} \frac{e^{-u}}{u} du \tag{A.14}$$

Again we can take the contour integral of $B_I + B_{II} + B_{III}$ and by applying Cauchy's integral theorem the contour integral can be expressed as

$$\begin{aligned} B_I + B_{II} + B_{III} &= \int_{k_2\chi_1}^{\chi_1\infty} \frac{e^{-u}}{u} du + \int_{\chi_1\infty}^{\infty} \frac{e^{-u}}{u} du + \int_{\infty}^{k_2\chi_1} \frac{e^{-u}}{u} du \\ &= \int_{k_2\chi_1}^{\chi_1\infty} \frac{e^{-u}}{u} du - E_1(k_2\chi_1) \end{aligned} \tag{A.15}$$

Since $\mathrm{Im}(k_2) < 0$ and $\mathrm{Re}(\chi_1) < 0$, the imaginary part of singular point is negative.

$$k = k_2 - i\varepsilon \quad \rightarrow \quad u = i\varepsilon\chi_1 \quad \rightarrow \quad \mathrm{Im}(u) < 0 \tag{A.16}$$

When $\mathrm{Im}(\chi_1) \geq 0$, the integration path will follow Figure A.2 (a). Since this path contains singular point, the contour integration becomes $B_I + B_{II} + B_{III} = 2\pi i$.

$$\int_{k_2\chi_1}^{\chi_1\infty} \frac{e^{-u}}{u} du = E_1(k_2\chi_1) + 2\pi i \qquad \text{when } \mathrm{Im}(\chi_1) \geq 0 \tag{A.17}$$

When $\mathrm{Im}(\chi_1) < 0$, the integration path will follow Figure A.2 (b) and the contour integration becomes $B_I + B_{II} + B_{III} = 0$.

$$\int_{k_2\chi_1}^{\chi_1\infty} \frac{e^{-u}}{u} du = E_1(k_2\chi_1) \qquad \text{when } \mathrm{Im}(\chi_1) < 0 \tag{A.18}$$

Finally we get following results for the integrals I_{21} and I_{22}

$$\begin{aligned} I_{21} &= \frac{1}{\pi} \int_{\gamma}^{\frac{\pi}{2}} \frac{k_2 \exp(k_2\chi_1) E_{r2}(k_2\chi_1)}{\sqrt{1 - 4\tau\cos\theta}} d\theta \\ I_{22} &= \frac{1}{\pi} \int_{\gamma}^{\frac{\pi}{2}} \frac{k_2 \exp(k_2\chi_2) E_{r2}(k_2\chi_2)}{\sqrt{1 - 4\tau\cos\theta}} d\theta \end{aligned} \tag{A.19}$$

where

$$E_{r2}(k_2\chi_j) = \begin{cases} E_1(k_2\chi_j) + 2\pi i & \text{when } \mathrm{Im}(\chi_j) \geq 0 \\ E_1(k_2\chi_j) & \text{when } \mathrm{Im}(\chi_j) < 0 \end{cases} \tag{A.20}$$

A.2 Calculation of Singularity

There exists a singularity at the point $\theta = \gamma$ and this could be avoided using the change of variables as

$$u = \sqrt{4\tau\cos\theta - 1} \tag{A.21}$$

with

$$d\theta = \frac{-udu}{2\tau\sqrt{1-\left(\frac{1+u^2}{4\tau}\right)^2}} \tag{A.22}$$

$$\begin{aligned} \theta = 0 \quad &\rightarrow \quad u = \sqrt{4\tau - 1} \\ \theta = \gamma \quad &\rightarrow \quad u = 0 \end{aligned} \tag{A.23}$$

Then the integrals I_{01} and I_{02} can be expressed as

$$\begin{aligned} I_{01} = &\frac{1}{\pi}\int_0^{\sqrt{4\tau-1}} \frac{k_{01}\exp(k_{01}\chi_1)}{2\tau i\sqrt{1-\left(\frac{1+u^2}{4\tau}\right)^2}} E_p(k_{01}\chi_1)du \\ &-\frac{1}{\pi}\int_0^{\sqrt{4\tau-1}} \frac{k_{02}\exp(k_{02}\chi_1)}{2\tau i\sqrt{1-\left(\frac{1+u^2}{4\tau}\right)^2}} E_q(k_{02}\chi_1)du \end{aligned} \tag{A.24}$$

$$\begin{aligned} I_{02} = &\frac{1}{\pi}\int_0^{\sqrt{4\tau-1}} \frac{k_{01}\exp(k_{01}\chi_2)}{2\tau i\sqrt{1-\left(\frac{1+u^2}{4\tau}\right)^2}} E_p(k_{01}\chi_2)du \\ &-\frac{1}{\pi}\int_0^{\sqrt{4\tau-1}} \frac{k_{02}\exp(k_{02}\chi_2)}{2\tau i\sqrt{1-\left(\frac{1+u^2}{4\tau}\right)^2}} E_q(k_{02}\chi_2)du \end{aligned} \tag{A.25}$$

where

$$\left.\begin{matrix} k_{01} \\ k_{02} \end{matrix}\right\} = \frac{\frac{1}{2}(1-u^2) \mp iu}{2\left(\frac{1+u^2}{4}\right)^2} \cdot \frac{\omega^2}{g} \tag{A.26}$$

$$\begin{aligned} \chi_1 &= (z+\zeta) - i[(x-\xi)\tfrac{1+u^2}{4\tau} - (y-\eta)\sqrt{1-\left(\tfrac{1+u^2}{4\tau}\right)^2}\,] \\ \chi_2 &= (z+\zeta) - i[(x-\xi)\tfrac{1+u^2}{4\tau} + (y-\eta)\sqrt{1-\left(\tfrac{1+u^2}{4\tau}\right)^2}\,] \end{aligned} \tag{A.27}$$

In a similar way the singularities in the integrals I_{11} through I_{22} can be avoided using the change of variables as

$$u = \sqrt{1 - 4\tau\cos\theta} \tag{A.28}$$

with

$$d\theta = \frac{udu}{2\tau\sqrt{1-\left(\frac{1-u^2}{4\tau}\right)^2}} \tag{A.29}$$

$$\begin{aligned} \theta = \gamma \quad &\rightarrow \quad u = 0 \\ \theta = \tfrac{\pi}{2} \quad &\rightarrow \quad u = 1 \end{aligned} \tag{A.30}$$

Then the integrals can be expressed as

$$I_{11} = \frac{1}{\pi}\int_0^1 \frac{k_1 \exp(k_1\chi_1)}{2\tau\sqrt{1-\left(\frac{1-u^2}{4\tau}\right)^2}} E_{r1}(k_1\chi_1)du \tag{A.31}$$

$$I_{12} = \frac{1}{\pi}\int_0^1 \frac{k_1 \exp(k_1\chi_2)}{2\tau\sqrt{1-\left(\frac{1-u^2}{4\tau}\right)^2}} E_{r1}(k_1\chi_2)du \tag{A.32}$$

$$I_{21} = \frac{1}{\pi}\int_0^1 \frac{k_2 \exp(k_2\chi_1)}{2\tau\sqrt{1-\left(\frac{1-u^2}{4\tau}\right)^2}} E_{r2}(k_2\chi_1)du \tag{A.33}$$

$$I_{22} = \frac{1}{\pi}\int_0^1 \frac{k_2 \exp(k_2\chi_2)}{2\tau\sqrt{1-\left(\frac{1-u^2}{4\tau}\right)^2}} E_{r2}(k_2\chi_2)du \tag{A.34}$$

where

$$\left.\begin{matrix} k_1 \\ k_2 \end{matrix}\right\} = \frac{\frac{1}{2}(1+u^2) \mp u}{2\left(\frac{1-u^2}{4\tau}\right)^2} \cdot \frac{\omega^2}{g} \tag{A.35}$$

$$\chi_1 = (z+\zeta) - i[(x-\xi)\tfrac{1-u^2}{4\tau} - (y-\eta)\sqrt{1-\left(\tfrac{1-u^2}{4\tau}\right)^2}]$$

$$\chi_2 = (z+\zeta) - i[(x-\xi)\tfrac{1-u^2}{4\tau} + (y-\eta)\sqrt{1-\left(\tfrac{1-u^2}{4\tau}\right)^2}] \tag{A.36}$$

A.3 Derivatives of Green Function

To evaluate the derivatives of Green function, differentiations of the exponential integral $E_1(Z)$ and variables χ_j are required.

$$\frac{d}{dZ}[\exp(Z)E_1(Z)] = \exp(Z)E_1(Z) - \frac{1}{Z} \tag{A.37}$$

and

$$\begin{aligned} \frac{d}{dx}\chi_1 &= -i\cos\theta & \frac{d}{dx}\chi_2 &= -i\cos\theta \\ \frac{d}{dy}\chi_1 &= i\sin\theta & \frac{d}{dy}\chi_2 &= -i\sin\theta \\ \frac{d}{dz}\chi_1 &= 1 & \frac{d}{dx}\chi_2 &= 1 \end{aligned} \tag{A.38}$$

Using equations (A.37) and (A.38), the corresponding derivatives of Green function can be easily derived.

A.3.1 The x-derivative

The x-derivative of Green function can be expressed as

$$G_x(p,q) = -\frac{(x-\xi)}{r^3} + \frac{(x-\xi)}{r_1^3} + (I_{01} + I_{02})_x + (I_{11} + I_{12})_x - (I_{21} + I_{22})_x + (I_{33} + I_{34})_x - (I_{43} + I_{44})_x \tag{A.39}$$

where

$$(I_{01})_x = -\frac{1}{\pi}\int_0^{\gamma} \frac{{k_{01}}^2 \cos\theta \exp(k_{01}\chi_1)}{\sqrt{4\tau\cos\theta - 1}} E_p(k_{01}\chi_1)d\theta + \frac{1}{\pi}\int_0^{\gamma} \frac{k_{01}\cos\theta}{\chi_1\sqrt{4\tau\cos\theta - 1}} d\theta + \frac{1}{\pi}\int_0^{\gamma} \frac{{k_{02}}^2 \cos\theta \exp(k_{02}\chi_1)}{\sqrt{4\tau\cos\theta - 1}} E_q(k_{02}\chi_1)d\theta - \frac{1}{\pi}\int_0^{\gamma} \frac{k_{02}\cos\theta}{\chi_1\sqrt{4\tau\cos\theta - 1}} d\theta \tag{A.40}$$

$$(I_{02})_x = -\frac{1}{\pi}\int_0^{\gamma} \frac{{k_{01}}^2 \cos\theta \exp(k_{01}\chi_2)}{\sqrt{4\tau\cos\theta - 1}} E_p(k_{01}\chi_2)d\theta + \frac{1}{\pi}\int_0^{\gamma} \frac{k_{01}\cos\theta}{\chi_2\sqrt{4\tau\cos\theta - 1}} d\theta + \frac{1}{\pi}\int_0^{\gamma} \frac{{k_{02}}^2 \cos\theta \exp(k_{02}\chi_2)}{\sqrt{4\tau\cos\theta - 1}} E_q(k_{02}\chi_2)d\theta - \frac{1}{\pi}\int_0^{\gamma} \frac{k_{02}\cos\theta}{\chi_2\sqrt{4\tau\cos\theta - 1}} d\theta \tag{A.41}$$

$$(I_{11})_x = -\frac{1}{\pi}\int_{\gamma}^{\frac{\pi}{2}} \frac{i{k_1}^2 \cos\theta \exp(k_1\chi_1)}{\sqrt{1 - 4\tau\cos\theta}} E_{r1}(k_1\chi_1)d\theta + \frac{1}{\pi}\int_{\gamma}^{\frac{\pi}{2}} \frac{ik_1\cos\theta}{\chi_1\sqrt{1 - 4\tau\cos\theta}} d\theta \tag{A.42}$$

$$(I_{12})_x = -\frac{1}{\pi}\int_{\gamma}^{\frac{\pi}{2}} \frac{i{k_1}^2 \cos\theta \exp(k_1\chi_2)}{\sqrt{1 - 4\tau\cos\theta}} E_{r1}(k_1\chi_2)d\theta + \frac{1}{\pi}\int_{\gamma}^{\frac{\pi}{2}} \frac{ik_1\cos\theta}{\chi_2\sqrt{1 - 4\tau\cos\theta}} d\theta \tag{A.43}$$

$$(I_{21})_x = -\frac{1}{\pi}\int_{\gamma}^{\frac{\pi}{2}} \frac{ik_2^{\,2}\cos\theta\exp(k_2\chi_1)}{\sqrt{1-4\tau\cos\theta}} E_{r2}(k_2\chi_1)d\theta + \frac{1}{\pi}\int_{\gamma}^{\frac{\pi}{2}} \frac{ik_2\cos\theta}{\chi_1\sqrt{1-4\tau\cos\theta}}d\theta \tag{A.44}$$

$$(I_{22})_x = -\frac{1}{\pi}\int_{\gamma}^{\frac{\pi}{2}} \frac{ik_2^{\,2}\cos\theta\exp(k_2\chi_2)}{\sqrt{1-4\tau\cos\theta}} E_{r2}(k_2\chi_2)d\theta + \frac{1}{\pi}\int_{\gamma}^{\frac{\pi}{2}} \frac{ik_2\cos\theta}{\chi_2\sqrt{1-4\tau\cos\theta}}d\theta \tag{A.45}$$

$$(I_{33})_x = \frac{1}{\pi}\int_{0}^{\frac{\pi}{2}} \frac{ik_3^{\,2}\cos\theta\exp(k_3\chi_3)}{\sqrt{1+4\tau\cos\theta}} E_{r3}(k_3\chi_3)d\theta - \frac{1}{\pi}\int_{0}^{\frac{\pi}{2}} \frac{ik_3\cos\theta}{\chi_3\sqrt{1+4\tau\cos\theta}}d\theta \tag{A.46}$$

$$(I_{34})_x = \frac{1}{\pi}\int_{0}^{\frac{\pi}{2}} \frac{ik_3^{\,2}\cos\theta\exp(k_3\chi_4)}{\sqrt{1+4\tau\cos\theta}} E_{r3}(k_3\chi_4)d\theta - \frac{1}{\pi}\int_{0}^{\frac{\pi}{2}} \frac{ik_3\cos\theta}{\chi_4\sqrt{1+4\tau\cos\theta}}d\theta \tag{A.47}$$

$$(I_{43})_x = \frac{1}{\pi}\int_{0}^{\frac{\pi}{2}} \frac{ik_4^{\,2}\cos\theta\exp(k_4\chi_3)}{\sqrt{1+4\tau\cos\theta}} E_{r4}(k_4\chi_3)d\theta - \frac{1}{\pi}\int_{0}^{\frac{\pi}{2}} \frac{ik_4\cos\theta}{\chi_3\sqrt{1+4\tau\cos\theta}}d\theta \tag{A.48}$$

$$(I_{44})_x = \frac{1}{\pi}\int_{0}^{\frac{\pi}{2}} \frac{ik_4^{\,2}\cos\theta\exp(k_4\chi_4)}{\sqrt{1+4\tau\cos\theta}} E_{r4}(k_4\chi_4)d\theta - \frac{1}{\pi}\int_{0}^{\frac{\pi}{2}} \frac{ik_4\cos\theta}{\chi_4\sqrt{1+4\tau\cos\theta}}d\theta \tag{A.49}$$

Definitions of the exponential integrals E_p, E_q and E_{ri}, and complex variables χ_i are given in Chapter 5.

A.3.2 The y-derivative

The y-derivative of Green function can be expressed as

$$G_y(p,q) = -\frac{(y-\eta)}{r^3} + \frac{(y-\eta)}{r_1^3} + (I_{01} + I_{02})_y + (I_{11} + I_{12})_y - (I_{21} + I_{22})_y + (I_{33} + I_{34})_y - (I_{43} + I_{44})_y \tag{A.50}$$

where

$$\begin{aligned}(I_{01})_y = &\frac{1}{\pi}\int_0^\gamma \frac{{k_{01}}^2 \sin\theta \exp(k_{01}\chi_1)}{\sqrt{4\tau\cos\theta - 1}} E_p(k_{01}\chi_1)d\theta \\ &-\frac{1}{\pi}\int_0^\gamma \frac{k_{01}\sin\theta}{\chi_1\sqrt{4\tau\cos\theta - 1}}d\theta \\ &-\frac{1}{\pi}\int_0^\gamma \frac{{k_{02}}^2 \sin\theta \exp(k_{02}\chi_1)}{\sqrt{4\tau\cos\theta - 1}} E_q(k_{02}\chi_1)d\theta \\ &+\frac{1}{\pi}\int_0^\gamma \frac{k_{02}\sin\theta}{\chi_1\sqrt{4\tau\cos\theta - 1}}d\theta\end{aligned} \tag{A.51}$$

$$\begin{aligned}(I_{02})_y = &-\frac{1}{\pi}\int_0^\gamma \frac{{k_{01}}^2 \sin\theta \exp(k_{01}\chi_2)}{\sqrt{4\tau\cos\theta - 1}} E_p(k_{01}\chi_2)d\theta \\ &+\frac{1}{\pi}\int_0^\gamma \frac{k_{01}\sin\theta}{\chi_2\sqrt{4\tau\cos\theta - 1}}d\theta \\ &+\frac{1}{\pi}\int_0^\gamma \frac{{k_{02}}^2 \sin\theta \exp(k_{02}\chi_2)}{\sqrt{4\tau\cos\theta - 1}} E_q(k_{02}\chi_2)d\theta \\ &-\frac{1}{\pi}\int_0^\gamma \frac{k_{02}\sin\theta}{\chi_2\sqrt{4\tau\cos\theta - 1}}d\theta\end{aligned} \tag{A.52}$$

$$\begin{aligned}(I_{11})_y = &\frac{1}{\pi}\int_\gamma^{\frac{\pi}{2}} \frac{i{k_1}^2 \sin\theta \exp(k_1\chi_1)}{\sqrt{1 - 4\tau\cos\theta}} E_{r1}(k_1\chi_1)d\theta \\ &-\frac{1}{\pi}\int_\gamma^{\frac{\pi}{2}} \frac{ik_1\sin\theta}{\chi_1\sqrt{1 - 4\tau\cos\theta}}d\theta\end{aligned} \tag{A.53}$$

$$\begin{aligned}(I_{12})_y = &-\frac{1}{\pi}\int_\gamma^{\frac{\pi}{2}} \frac{i{k_1}^2 \sin\theta \exp(k_1\chi_2)}{\sqrt{1 - 4\tau\cos\theta}} E_{r1}(k_1\chi_2)d\theta \\ &+\frac{1}{\pi}\int_\gamma^{\frac{\pi}{2}} \frac{ik_1\sin\theta}{\chi_2\sqrt{1 - 4\tau\cos\theta}}d\theta\end{aligned} \tag{A.54}$$

$$(I_{21})_y = \frac{1}{\pi}\int_{\gamma}^{\frac{\pi}{2}} \frac{ik_2^{\,2}\sin\theta\exp(k_2\chi_1)}{\sqrt{1-4\tau\cos\theta}} E_{r2}(k_2\chi_1)d\theta - \frac{1}{\pi}\int_{\gamma}^{\frac{\pi}{2}} \frac{ik_2\sin\theta}{\chi_1\sqrt{1-4\tau\cos\theta}}d\theta \tag{A.55}$$

$$(I_{22})_y = -\frac{1}{\pi}\int_{\gamma}^{\frac{\pi}{2}} \frac{ik_2^{\,2}\sin\theta\exp(k_2\chi_2)}{\sqrt{1-4\tau\cos\theta}} E_{r2}(k_2\chi_2)d\theta + \frac{1}{\pi}\int_{\gamma}^{\frac{\pi}{2}} \frac{ik_2\sin\theta}{\chi_2\sqrt{1-4\tau\cos\theta}}d\theta \tag{A.56}$$

$$(I_{33})_y = \frac{1}{\pi}\int_{0}^{\frac{\pi}{2}} \frac{ik_3^{\,2}\sin\theta\exp(k_3\chi_3)}{\sqrt{1+4\tau\cos\theta}} E_{r3}(k_3\chi_3)d\theta - \frac{1}{\pi}\int_{0}^{\frac{\pi}{2}} \frac{ik_3\sin\theta}{\chi_3\sqrt{1+4\tau\cos\theta}}d\theta \tag{A.57}$$

$$(I_{34})_y = -\frac{1}{\pi}\int_{0}^{\frac{\pi}{2}} \frac{ik_3^{\,2}\sin\theta\exp(k_3\chi_4)}{\sqrt{1+4\tau\cos\theta}} E_{r3}(k_3\chi_4)d\theta + \frac{1}{\pi}\int_{0}^{\frac{\pi}{2}} \frac{ik_3\sin\theta}{\chi_4\sqrt{1+4\tau\cos\theta}}d\theta \tag{A.58}$$

$$(I_{43})_y = \frac{1}{\pi}\int_{0}^{\frac{\pi}{2}} \frac{ik_4^{\,2}\sin\theta\exp(k_4\chi_3)}{\sqrt{1+4\tau\cos\theta}} E_{r4}(k_4\chi_3)d\theta - \frac{1}{\pi}\int_{0}^{\frac{\pi}{2}} \frac{ik_4\sin\theta}{\chi_3\sqrt{1+4\tau\cos\theta}}d\theta \tag{A.59}$$

$$(I_{44})_y = -\frac{1}{\pi}\int_{0}^{\frac{\pi}{2}} \frac{ik_4^{\,2}\sin\theta\exp(k_4\chi_4)}{\sqrt{1+4\tau\cos\theta}} E_{r4}(k_4\chi_4)d\theta + \frac{1}{\pi}\int_{0}^{\frac{\pi}{2}} \frac{ik_4\sin\theta}{\chi_4\sqrt{1+4\tau\cos\theta}}d\theta \tag{A.60}$$

All parameters in above equations are given in the Chapter 5.

A.3.3 The z-derivative

The z-derivative of Green function can be expressed as

$$G_z(p,q) = -\frac{(z-\zeta)}{r^3} + \frac{(z+\zeta)}{r_1^3} + (I_{01}+I_{02})_z + (I_{11}+I_{12})_z - (I_{21}+I_{22})_z + (I_{33}+I_{34})_z - (I_{43}+I_{44})_z \tag{A.61}$$

where

$$\begin{aligned}(I_{01})_z = &\frac{1}{\pi}\int_0^{\gamma} \frac{{k_{01}}^2 \exp(k_{01}\chi_1)}{i\sqrt{4\tau\cos\theta - 1}} E_p(k_{01}\chi_1)d\theta \\ &-\frac{1}{\pi}\int_0^{\gamma} \frac{k_{01}}{i\chi_1\sqrt{4\tau\cos\theta - 1}} d\theta \\ &-\frac{1}{\pi}\int_0^{\gamma} \frac{{k_{02}}^2 \exp(k_{02}\chi_1)}{i\sqrt{4\tau\cos\theta - 1}} E_q(k_{02}\chi_1)d\theta \\ &+\frac{1}{\pi}\int_0^{\gamma} \frac{k_{02}}{i\chi_1\sqrt{4\tau\cos\theta - 1}} d\theta\end{aligned} \tag{A.62}$$

$$\begin{aligned}(I_{02})_z = &\frac{1}{\pi}\int_0^{\gamma} \frac{{k_{01}}^2 \exp(k_{01}\chi_2)}{i\sqrt{4\tau\cos\theta - 1}} E_p(k_{01}\chi_2)d\theta \\ &-\frac{1}{\pi}\int_0^{\gamma} \frac{k_{01}}{i\chi_2\sqrt{4\tau\cos\theta - 1}} d\theta \\ &-\frac{1}{\pi}\int_0^{\gamma} \frac{{k_{02}}^2 \exp(k_{02}\chi_2)}{i\sqrt{4\tau\cos\theta - 1}} E_q(k_{02}\chi_2)d\theta \\ &+\frac{1}{\pi}\int_0^{\gamma} \frac{k_{02}}{i\chi_2\sqrt{4\tau\cos\theta - 1}} d\theta\end{aligned} \tag{A.63}$$

$$\begin{aligned}(I_{11})_z = &\frac{1}{\pi}\int_{\gamma}^{\frac{\pi}{2}} \frac{{k_1}^2 \exp(k_1\chi_1)}{\sqrt{1-4\tau\cos\theta}} E_{r1}(k_1\chi_1)d\theta \\ &-\frac{1}{\pi}\int_{\gamma}^{\frac{\pi}{2}} \frac{k_1}{\chi_1\sqrt{1-4\tau\cos\theta}} d\theta\end{aligned} \tag{A.64}$$

$$\begin{aligned}(I_{12})_z = &\frac{1}{\pi}\int_{\gamma}^{\frac{\pi}{2}} \frac{{k_1}^2 \exp(k_1\chi_2)}{\sqrt{1-4\tau\cos\theta}} E_{r1}(k_1\chi_2)d\theta \\ &-\frac{1}{\pi}\int_{\gamma}^{\frac{\pi}{2}} \frac{k_1}{\chi_2\sqrt{1-4\tau\cos\theta}} d\theta\end{aligned} \tag{A.65}$$

$$(I_{21})_z = \frac{1}{\pi}\int_{\gamma}^{\frac{\pi}{2}} \frac{k_2^{\,2}\exp(k_2\chi_1)}{\sqrt{1-4\tau\cos\theta}} E_{r2}(k_2\chi_1)d\theta - \frac{1}{\pi}\int_{\gamma}^{\frac{\pi}{2}} \frac{k_2}{\chi_1\sqrt{1-4\tau\cos\theta}}d\theta \tag{A.66}$$

$$(I_{22})_z = \frac{1}{\pi}\int_{\gamma}^{\frac{\pi}{2}} \frac{k_2^{\,2}\exp(k_2\chi_2)}{\sqrt{1-4\tau\cos\theta}} E_{r2}(k_2\chi_2)d\theta - \frac{1}{\pi}\int_{\gamma}^{\frac{\pi}{2}} \frac{k_2}{\chi_2\sqrt{1-4\tau\cos\theta}}d\theta \tag{A.67}$$

$$(I_{33})_z = \frac{1}{\pi}\int_{0}^{\frac{\pi}{2}} \frac{k_3^{\,2}\exp(k_3\chi_3)}{\sqrt{1+4\tau\cos\theta}} E_{r3}(k_3\chi_3)d\theta - \frac{1}{\pi}\int_{0}^{\frac{\pi}{2}} \frac{k_3}{\chi_3\sqrt{1+4\tau\cos\theta}}d\theta \tag{A.68}$$

$$(I_{34})_z = \frac{1}{\pi}\int_{0}^{\frac{\pi}{2}} \frac{k_3^{\,2}\exp(k_3\chi_4)}{\sqrt{1+4\tau\cos\theta}} E_{r3}(k_3\chi_4)d\theta - \frac{1}{\pi}\int_{0}^{\frac{\pi}{2}} \frac{k_3}{\chi_4\sqrt{1+4\tau\cos\theta}}d\theta \tag{A.69}$$

$$(I_{43})_z = \frac{1}{\pi}\int_{0}^{\frac{\pi}{2}} \frac{k_4^{\,2}\exp(k_4\chi_3)}{\sqrt{1+4\tau\cos\theta}} E_{r4}(k_4\chi_3)d\theta - \frac{1}{\pi}\int_{0}^{\frac{\pi}{2}} \frac{k_4}{\chi_3\sqrt{1+4\tau\cos\theta}}d\theta \tag{A.70}$$

$$(I_{44})_z = \frac{1}{\pi}\int_{0}^{\frac{\pi}{2}} \frac{k_4^{\,2}\exp(k_4\chi_4)}{\sqrt{1+4\tau\cos\theta}} E_{r4}(k_4\chi_4)d\theta - \frac{1}{\pi}\int_{0}^{\frac{\pi}{2}} \frac{k_4}{\chi_4\sqrt{1+4\tau\cos\theta}}d\theta \tag{A.71}$$

All parameters in above equations are given in the Chapter 5.

A.4 Green Function at Zero Forward Speed

At zero speed $U = 0$, non-dimensional parameters become zero, i.e. $\tau = 0$ and $\gamma = 0$, and the singularity of the integrand $f(\theta,k)$ in the original form of Green function is reduced to one degree.

$$f(\theta,k) = \frac{k \exp\left[k\{(z+\zeta) - i(x-\xi)\cos\theta\}\right]\cos\{k(y-\eta)\sin\theta\}}{gk - \omega^2} \tag{A.72}$$

The denominator of integrand $f(\theta,k)$ has one singular point and $f(\theta,k)$ can be rewritten as

$$f(\theta,k) = \frac{1}{g}\cdot\frac{k}{k-k_1}\exp\left[k\{(z+\zeta) - i(x-\xi)\cos\theta\}\right] \times\cos\{k(y-\eta)\sin\theta\} \tag{A.73}$$

$$k_1 = \frac{\omega^2}{g} \tag{A.74}$$

Using the relationship $\cos Z = \frac{1}{2}\{e^{iZ} + e^{-iZ}\}$, the expression for $f(\theta,k)$ can be rewritten as

$$f(\theta,k) = \frac{1}{2g}\cdot\frac{k_1}{k-k_1}\left[\exp(k\chi_1) + \exp(k\chi_2)\right] + \frac{1}{2g}\left[\exp(k\chi_1) + \exp(k\chi_2)\right] \quad \text{when } 0 \le \theta \le \pi \tag{A.75}$$

where

$$\chi_1 = (z+\zeta) - i[(x-\xi)\cos\theta - (y-\eta)\sin\theta]$$
$$\chi_2 = (z+\zeta) - i[(x-\xi)\cos\theta + (y-\eta)\sin\theta] \tag{A.76}$$

Then the expression for zero speed Green function becomes

$$G(p,q)=\frac{1}{r}-\frac{1}{r_1}+\frac{1}{\pi}\int_0^{\pi}d\theta\int_0^{\infty}\left[\frac{k_1}{k-k_1}\exp(k\chi_1)+\exp(k\chi_1)\right]dk$$
$$+\frac{1}{\pi}\int_0^{\pi}d\theta\int_0^{\infty}\left[\frac{k_1}{k-k_1}\exp(k\chi_2)+\exp(k\chi_2)\right]dk \tag{A.77}$$

or

$$G(p,q)=\frac{1}{r}-\frac{1}{r_1}+I_1+I_2 \tag{A.78}$$

$$I_1=\frac{1}{\pi}\int_0^{\pi}d\theta\int_0^{\infty}\left[\frac{k_1}{k-k_1}\exp(k\chi_1)+\exp(k\chi_1)\right]dk \tag{A.79}$$

$$I_2=\frac{1}{\pi}\int_0^{\pi}d\theta\int_0^{\infty}\left[\frac{k_1}{k-k_1}\exp(k\chi_2)+\exp(k\chi_2)\right]dk \tag{A.80}$$

First term in the integral I_j can be reformulated with similar method used in the cases of I_{11} and I_{12}, and the second term can be solved analytically.

$$\int_0^{\infty}\exp(k\chi_j)dk=-\frac{1}{\chi_j} \tag{A.81}$$

Then final expressions for the integral I_j's are obtained as follow

$$I_1=\frac{1}{\pi}\int_0^{\pi}\left[k_1\exp(k_1\chi_1)E_{r1}(k_1\chi_1)-\frac{1}{\chi_1}\right]d\theta \tag{A.82}$$

$$I_2=\frac{1}{\pi}\int_0^{\pi}\left[k_1\exp(k_1\chi_2)E_{r1}(k_1\chi_2)-\frac{1}{\chi_2}\right]d\theta \tag{A.83}$$

where corresponding exponential integral is identical to the one given in equation (A.10). The Green function given in equation (A.78), which is associated with expressions (A.79) and (A.80) represents oscillating source potential.

Derivatives of zero speed Green function can be expressed as follow

The x-derivative:

$$G_x(p,q) = -\frac{(x-\xi)}{r^3} + \frac{(x-\xi)}{r_1^3} + (I_1 + I_2)_x \tag{A.84}$$

$$(I_1)_x = -\frac{1}{\pi}\int_0^{\pi} ik_1^{\,2}\cos\theta\exp(k_1\chi_1)E_{r1}(k_1\chi_1)d\theta + \frac{1}{\pi}\int_0^{\pi} i\cos\theta\frac{k_1\chi_1 - 1}{\chi_1^{\,2}}d\theta \tag{A.85}$$

$$(I_2)_x = -\frac{1}{\pi}\int_0^{\pi} ik_1^{\,2}\cos\theta\exp(k_1\chi_2)E_{r1}(k_1\chi_2)d\theta + \frac{1}{\pi}\int_0^{\pi} i\cos\theta\frac{k_1\chi_2 - 1}{\chi_2^{\,2}}d\theta \tag{A.86}$$

The y-derivative:

$$G_y(p,q) = -\frac{(y-\eta)}{r^3} + \frac{(y-\eta)}{r_1^3} + (I_1 + I_2)_y \tag{A.87}$$

$$(I_1)_y = \frac{1}{\pi}\int_0^{\pi} ik_1^{\,2}\sin\theta\exp(k_1\chi_1)E_{r1}(k_1\chi_1)d\theta - \frac{1}{\pi}\int_0^{\pi} i\sin\theta\frac{k_1\chi_1 - 1}{\chi_1^{\,2}}d\theta \tag{A.88}$$

$$(I_2)_y = -\frac{1}{\pi}\int_0^{\pi} ik_1^{\,2}\sin\theta\exp(k_1\chi_2)E_{r1}(k_1\chi_2)d\theta + \frac{1}{\pi}\int_0^{\pi} i\sin\theta\frac{k_1\chi_2 - 1}{\chi_2^{\,2}}d\theta \tag{A.89}$$

The z-derivative:

$$G_z(p,q) = -\frac{(z-\zeta)}{r^3} + \frac{(z+\zeta)}{r_1^3} + (I_1 + I_2)_z \tag{A.90}$$

$$(I_1)_z = \frac{1}{\pi}\int_0^{\pi} k_1^{\,2}\exp(k_1\chi_1)E_{r1}(k_1\chi_1)d\theta - \frac{1}{\pi}\int_0^{\pi}\frac{k_1\chi_1 - 1}{\chi_1^{\,2}}d\theta \tag{A.91}$$

$$(I_2)_z = \frac{1}{\pi}\int_0^{\pi} k_1^{\,2}\exp(k_1\chi_2)E_{r1}(k_1\chi_2)d\theta - \frac{1}{\pi}\int_0^{\pi}\frac{k_1\chi_2 - 1}{\chi_2^{\,2}}d\theta \tag{A.92}$$

A.5 Green Function at Zero Frequency

At zero frequency $\omega = 0$, non-dimensional parameters become zero, i.e. $\tau = 0$ and $\gamma = 0$, and the singularity of the integrand $f(\theta,k)$ in the original form of Green function is reduced to one degree.

$$f(\theta,k) = \frac{\exp\left[k\{(z+\zeta) - i(x-\xi)\cos\theta\}\right]\cos\{k(y-\eta)\sin\theta\}}{g - U^2 k\cos^2\theta} \tag{A.93}$$

The denominator of integrand $f(\theta,k)$ has one singular point and $f(\theta,k)$ can be rewritten as

$$f(\theta,k) = -\frac{1}{U^2\cos^2\theta}\cdot\frac{1}{k-k_2}\exp\left[k\{(z+\zeta) - i(x-\xi)\cos\theta\}\right] \times\cos\{k(y-\eta)\sin\theta\} \tag{A.94}$$

$$k_2 = \frac{g}{U^2\cos^2\theta} \tag{A.95}$$

Using the relationship $\cos Z = \frac{1}{2}\{e^{iZ} + e^{-iZ}\}$, the expression for $f(\theta,k)$ can be rewritten as

$$f(\theta,k) = -\frac{1}{2g}\cdot\frac{k_2}{k-k_2}\left[\exp(k\chi_1) + \exp(k\chi_2)\right] \text{ when } 0 \le \theta \le \pi \tag{A.96}$$

where χ_1 and χ_2 are given in equation (A.76). Then the expression for zero speed Green function becomes

$$G(p,q) = \frac{1}{r} - \frac{1}{r_1} - \frac{1}{\pi}\int_0^{\pi} d\theta \int_0^{\infty} \frac{k_2}{k-k_2}\left[\exp(k\chi_1) + \exp(k\chi_2)\right] dk \tag{A.97}$$

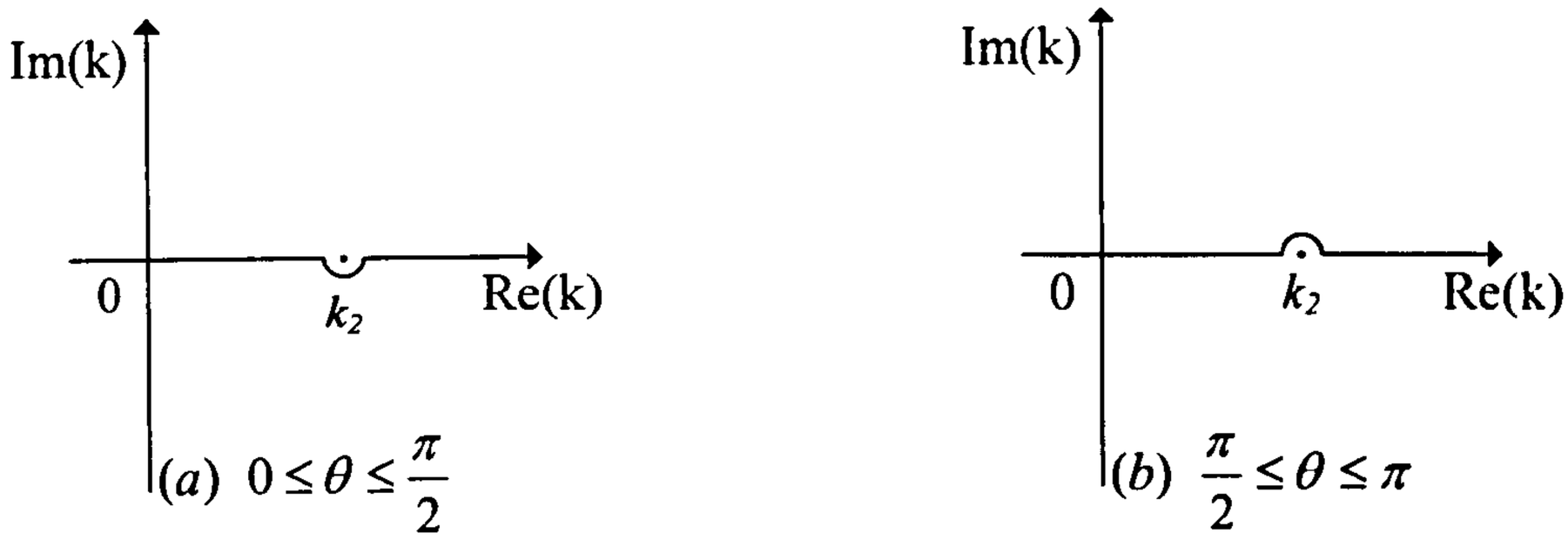

Figure A.3 Integration paths in the complex plane

Although only one singular point exists in the integrand of equation (A.97), the integration path can be divided into two regions as shown in Figure A.3. Therefore the expression given in equation (A.97) can be rewritten as

$$G(p,q) = \frac{1}{r} - \frac{1}{r_1} + I_{21} + I_{22} + I_{23} + I_{24} \tag{A.98}$$

$$I_{21} = -\frac{1}{\pi} \int_0^{\frac{\pi}{2}} d\theta \int_0^{\infty} \left[\frac{k_2}{k - k_2} \exp(k\chi_1) \right] dk \tag{A.99}$$

$$I_{22} = -\frac{1}{\pi} \int_0^{\frac{\pi}{2}} d\theta \int_0^{\infty} \left[\frac{k_2}{k - k_2} \exp(k\chi_2) \right] dk \tag{A.100}$$

$$I_{23} = -\frac{1}{\pi} \int_{\frac{\pi}{2}}^{\pi} d\theta \int_0^{\infty} \left[\frac{k_2}{k - k_2} \exp(k\chi_1) \right] dk \tag{A.101}$$

$$I_{24} = -\frac{1}{\pi} \int_{\frac{\pi}{2}}^{\pi} d\theta \int_0^{\infty} \left[\frac{k_2}{k - k_2} \exp(k\chi_2) \right] dk \tag{A.102}$$

The remaining process is straightforward as shown in the foregoing sections. The integration intervals in I_{23} and I_{24} can be changed from $\frac{\pi}{2} < \theta < \pi$ to $0 < \theta < \frac{\pi}{2}$ using change of variable demonstrated in Chapter 5. Thus final expressions for the integral I_{2j}'s are obtained as follow

$$I_{21} = -\frac{1}{\pi}\int_0^{\frac{\pi}{2}} k_2 \exp(k_2\chi_1)E_{r2}(k_2\chi_1)d\theta \tag{A.103}$$

$$I_{22} = -\frac{1}{\pi}\int_0^{\frac{\pi}{2}} k_2 \exp(k_2\chi_2)E_{r2}(k_2\chi_2)d\theta \tag{A.104}$$

$$I_{23} = -\frac{1}{\pi}\int_0^{\frac{\pi}{2}} k_2 \exp(k_2\chi_3)E_{r4}(k_2\chi_3)d\theta \tag{A.105}$$

$$I_{24} = -\frac{1}{\pi}\int_0^{\frac{\pi}{2}} k_2 \exp(k_2\chi_4)E_{r4}(k_2\chi_4)d\theta \tag{A.106}$$

where corresponding exponential integral $E_{ri}(k_2\chi_j)$ and variable χ_j's are already defined in Chapter 5. The Green function given in equation (A.98), which is associated with expressions (A.103) through (A.106), represents Kelvin source translating source potential which is travelling with steady forward speed in calm water.

Derivatives of zero frequency Green function can be expressed as follow

The x-derivative:

$$G_x(p,q) = -\frac{(x-\xi)}{r^3} + \frac{(x-\xi)}{r_1^3} + (I_{21}+I_{22})_x + (I_{23}+I_{24})_x \tag{A.107}$$

$$(I_{21})_x = \frac{1}{\pi}\int_0^{\frac{\pi}{2}} i\cos\theta\left[k_2{}^2 \exp(k_2\chi_1)E_{r2}(k_2\chi_1) - \frac{k_2}{\chi_1}\right]d\theta \tag{A.108}$$

$$(I_{22})_x = \frac{1}{\pi}\int_0^{\frac{\pi}{2}} i\cos\theta\left[k_2{}^2 \exp(k_2\chi_2)E_{r2}(k_2\chi_2) - \frac{k_2}{\chi_2}\right]d\theta \tag{A.109}$$

$$(I_{23})_x = -\frac{1}{\pi}\int_0^{\frac{\pi}{2}} i\cos\theta\left[k_2{}^2 \exp(k_2\chi_3)E_{r4}(k_2\chi_3) - \frac{k_2}{\chi_3}\right]d\theta \tag{A.110}$$

$$(I_{24})_x = -\frac{1}{\pi}\int_0^{\frac{\pi}{2}} i\cos\theta\left[k_2{}^2 \exp(k_2\chi_4)E_{r4}(k_2\chi_4) - \frac{k_2}{\chi_4}\right]d\theta \tag{A.111}$$

The y-derivative:

$$G_y(p,q) = -\frac{(y-\eta)}{r^3} + \frac{(y-\eta)}{r_1^3} + (I_{21} + I_{22})_y + (I_{23} + I_{24})_y \tag{A.112}$$

$$(I_{21})_y = -\frac{1}{\pi}\int_0^{\frac{\pi}{2}} i\sin\theta \left[k_2{}^2 \exp(k_2\chi_1) E_{r2}(k_2\chi_1) - \frac{k_2}{\chi_1} \right] d\theta \tag{A.113}$$

$$(I_{22})_y = \frac{1}{\pi}\int_0^{\frac{\pi}{2}} i\sin\theta \left[k_2{}^2 \exp(k_2\chi_2) E_{r2}(k_2\chi_2) - \frac{k_2}{\chi_2} \right] d\theta \tag{A.114}$$

$$(I_{23})_y = -\frac{1}{\pi}\int_0^{\frac{\pi}{2}} i\sin\theta \left[k_2{}^2 \exp(k_2\chi_3) E_{r4}(k_2\chi_3) - \frac{k_2}{\chi_3} \right] d\theta \tag{A.115}$$

$$(I_{24})_y = \frac{1}{\pi}\int_0^{\frac{\pi}{2}} i\sin\theta \left[k_2{}^2 \exp(k_2\chi_4) E_{r4}(k_2\chi_4) - \frac{k_2}{\chi_4} \right] d\theta \tag{A.116}$$

The z-derivative:

$$G_z(p,q) = -\frac{(z-\zeta)}{r^3} + \frac{(z+\zeta)}{r_1^3} + (I_{21} + I_{22})_z + (I_{23} + I_{24})_z \tag{A.117}$$

$$(I_{21})_z = -\frac{1}{\pi}\int_0^{\frac{\pi}{2}} \left[k_2{}^2 \exp(k_2\chi_1) E_{r2}(k_2\chi_1) - \frac{k_2}{\chi_1} \right] d\theta \tag{A.118}$$

$$(I_{22})_z = -\frac{1}{\pi}\int_0^{\frac{\pi}{2}} \left[k_2{}^2 \exp(k_2\chi_2) E_{r2}(k_2\chi_2) - \frac{k_2}{\chi_2} \right] d\theta \tag{A.119}$$

$$(I_{23})_z = -\frac{1}{\pi}\int_0^{\frac{\pi}{2}} \left[k_2{}^2 \exp(k_2\chi_3) E_{r4}(k_2\chi_3) - \frac{k_2}{\chi_3} \right] d\theta \tag{A.120}$$

$$(I_{24})_z = -\frac{1}{\pi}\int_0^{\frac{\pi}{2}} \left[k_2{}^2 \exp(k_2\chi_4) E_{r4}(k_2\chi_4) - \frac{k_2}{\chi_4} \right] d\theta \tag{A.121}$$

A.6 Calculation of Exponential Integral

To calculate the integrand of Green function efficient evaluation of the exponential integral is required. The exponential integral for complex number is given as follows

$$E_1(z) = \int_z^\infty \frac{e^{-u}}{u} du \qquad \text{for } |\arg(z)| < \pi \tag{A.122}$$

An approximate formula for the calculation of exponential integral has been proposed in Hess and Smith (1967).

$$e^z E_1(z) = \frac{M+N}{D} + \varepsilon(z),\ \varepsilon(z) \le 7\times 10^{-6} \tag{A.123}$$

M, N and D used in the rational-fraction approximation of equation (A.123) are given as

$$\begin{aligned} M &= -(1 + m_1 z + m_2 z^2 + m_3 z^3 + m_4 z^4)\ln z \\ N &= -\gamma(0.99999207 + n_1 z + n_2 z^2 + n_3 z^3 + n_4 z^4 + n_5 z^5) \\ D &= 1 + d_1 z + d_2 z^2 + d_3 z^3 + d_4 z^4 + d_5 z^5 + d_6 z^6 \end{aligned} \tag{A.124}$$

where

$$\begin{aligned} m_1 &= 0.23721365 & n_1 &= -1.49545886 & d_1 &= -0.76273617 \\ m_2 &= 0.02065430 & n_2 &= 0.041806426 & d_2 &= 0.28388363 \\ m_3 &= 0.000763297 & n_3 &= -0.03000591 & d_3 &= -0.066786033 \\ m_4 &= 9.7087007\times 10^{-6} & n_4 &= 0.0019387339 & d_4 &= 0.012982719 \\ & & n_5 &= -0.00051801555 & d_5 &= -0.0008700861 \\ & & & & d_6 &= 0.0002989204 \end{aligned}$$

and $\gamma = 0.5772156649$ is Euler constant.

A.7 Calculation of Green Function near Free Surface

When either the source or field point is close to the free surface, some integrals of Green function show very large oscillating behaviour. The real and imaginary parts of integrands in Green function are illustrated in Figure A.4 and Figure A.5 for U=3.0, ω=1.0 and τ=0.306. For both figures field points are located in (-20, 0, 0) and source points are in (0, 0, -0.01) and (0, 0, -0.01) respectively. Integrals $I_{01} + I_{02}$, $I_{11} + I_{12}$ and $I_{33} + I_{34}$ are represented as a smooth curves, while integrals of $I_{21} + I_{22}$ and $I_{43} + I_{44}$ in Figure A.5 show extreme oscillations. It should be noted that these oscillations appears when the sum of z values of source and field points becomes very small.

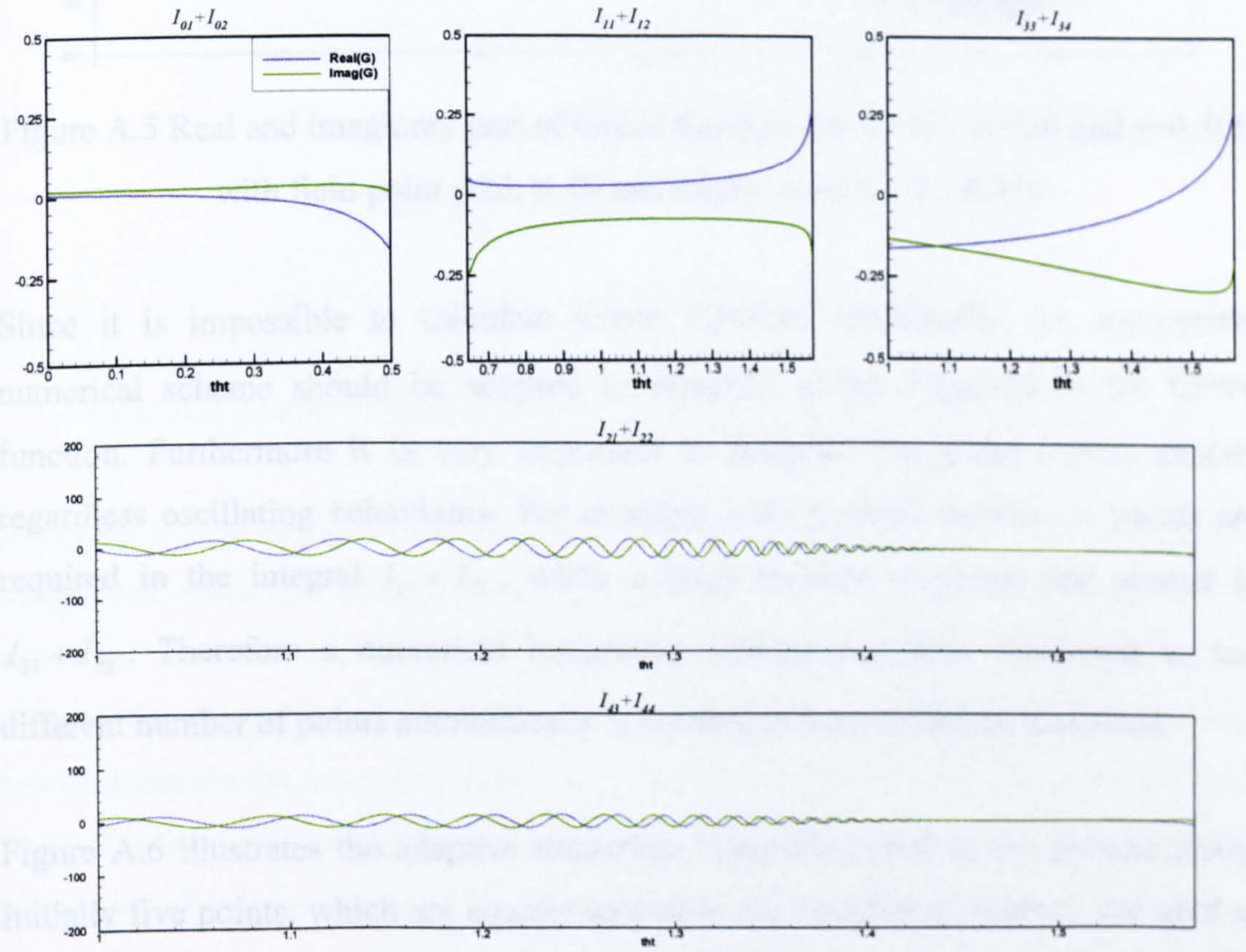

Figure A.4 Real and imaginary part of Green function for U=3.0, ω=1.0 and τ=0.306 with field point (-20, 0, 0) and source point (0, 0, -0.1)

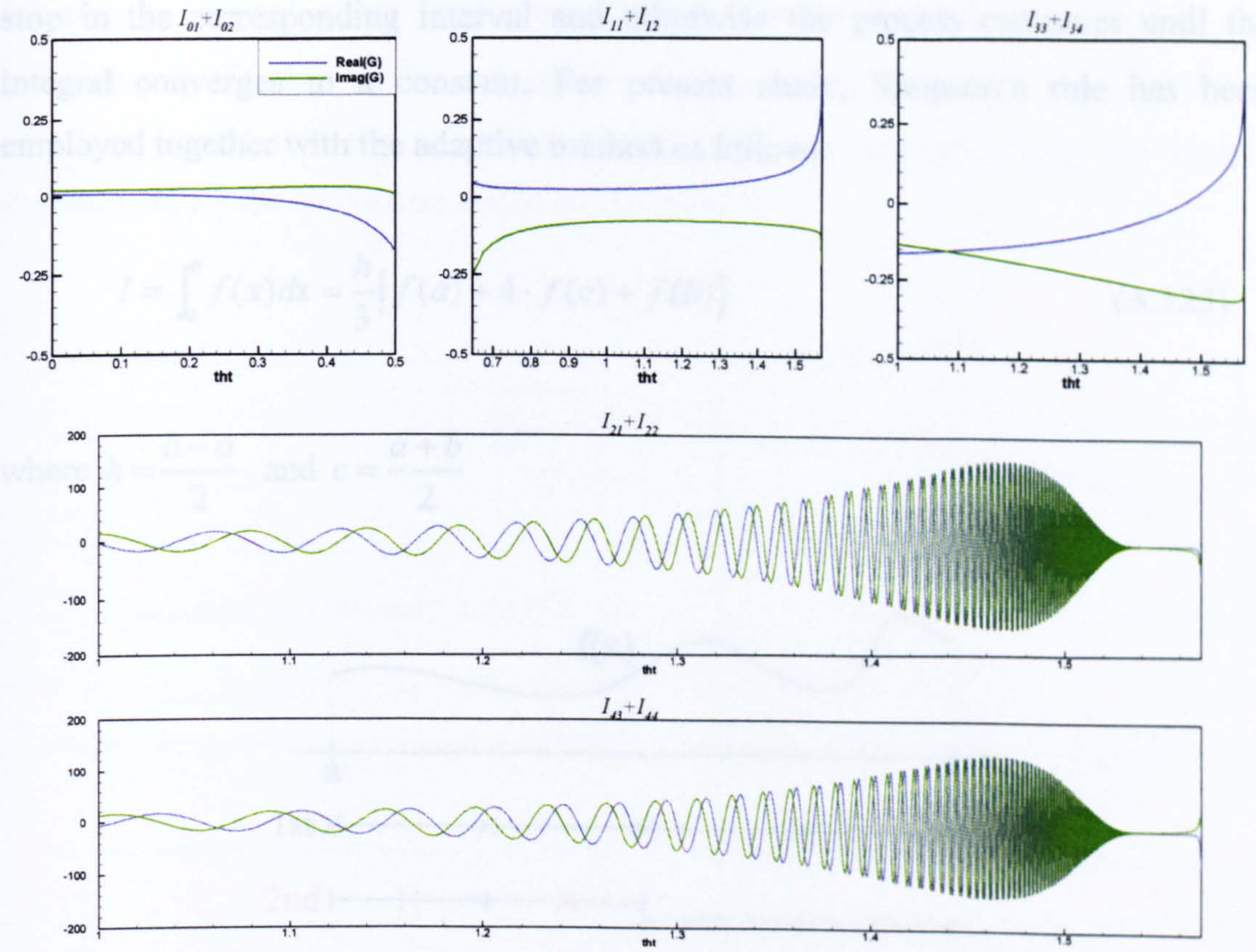

Figure A.5 Real and imaginary part of Green function for U=3.0, ω=1.0 and τ=0.306 with field point (-20, 0, 0) and source point (0, 0, -0.01)

Since it is impossible to calculate Green function analytically, an appropriate numerical scheme should be adopted to integrate given integrand in the Green function. Furthermore it is very important to integrate the given curves exactly regardless oscillating behaviours. For example, only a small number of points are required in the integral $I_{11}+I_{12}$, while a large number of points are needed in $I_{21}+I_{22}$. Therefore a numerical integration scheme has been employed to use different number of points automatically according to the oscillation behaviour.

Figure A.6 illustrates the adaptive numerical integration used in the present study. Initially five points, which are equally spaced in the integration interval, are used to calculate the integral of a given function f(x). In the next step, four additional mid-points are selected and integrals in each sub-interval are compared with previous estimate. If the integration value is within pre-determined error bound, process will

stop in the corresponding interval and otherwise the process continues until the integral converges to a constant. For present study, Simpson's rule has been employed together with the adaptive method as follows

$$I = \int_a^b f(x)dx = \frac{h}{3}[f(a) + 4 \cdot f(c) + f(b)] \tag{A.125}$$

where $h = \frac{b-a}{2}$ and $c = \frac{a+b}{2}$

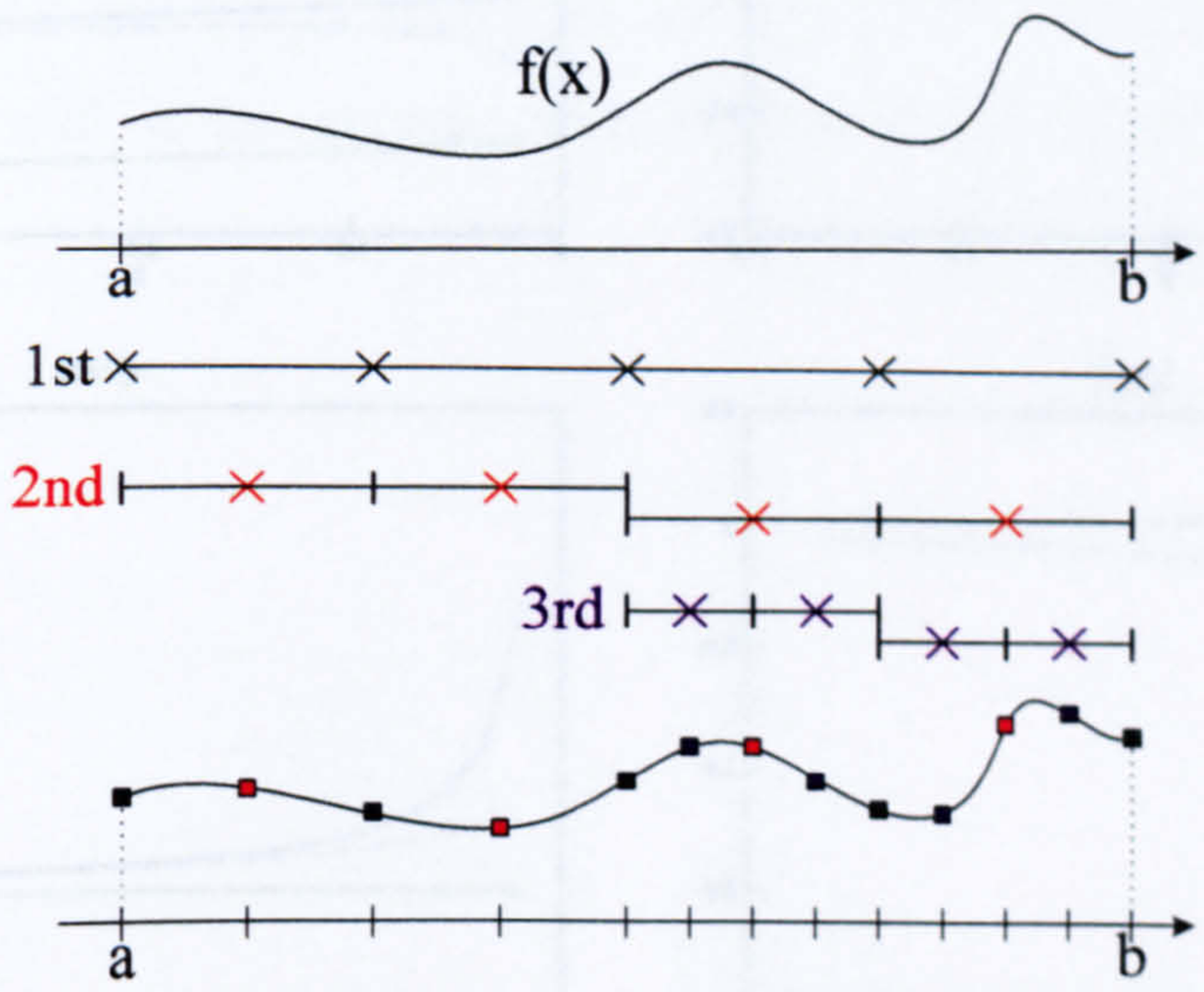

Figure A.6 Adaptive numerical scheme for the integration of Green function

Although it is possible to calculate Green function exactly with adaptive numerical integration, there are difficulties in the numerical evaluation of line integral with non-zero forward speed in the boundary integral equation. Calculations of singularities along the intersection line between body and free surface do not cause any problem for the case of vertical panels at the waterline. However, evaluations of Green function and its derivatives do not converge for non-vertical panel near free surface as shown in Figure A.7, where U=7.4, ω=1.4, field point (-63.0, 3.221, -0.366) and source point (-63.0, 3.676, 0.0). In the figure the real parts of derivatives of Green function become singular as the field point moves towards source point (z-component of field point approaches zero). In order to avoid these difficulties the

location of source point is moved slightly towards exterior free surface and consequently the singular behaviour near free surface is decreased significantly. It should be noted that the numerical treatment of line integral should be applied carefully, since the evaluation might be distorted.

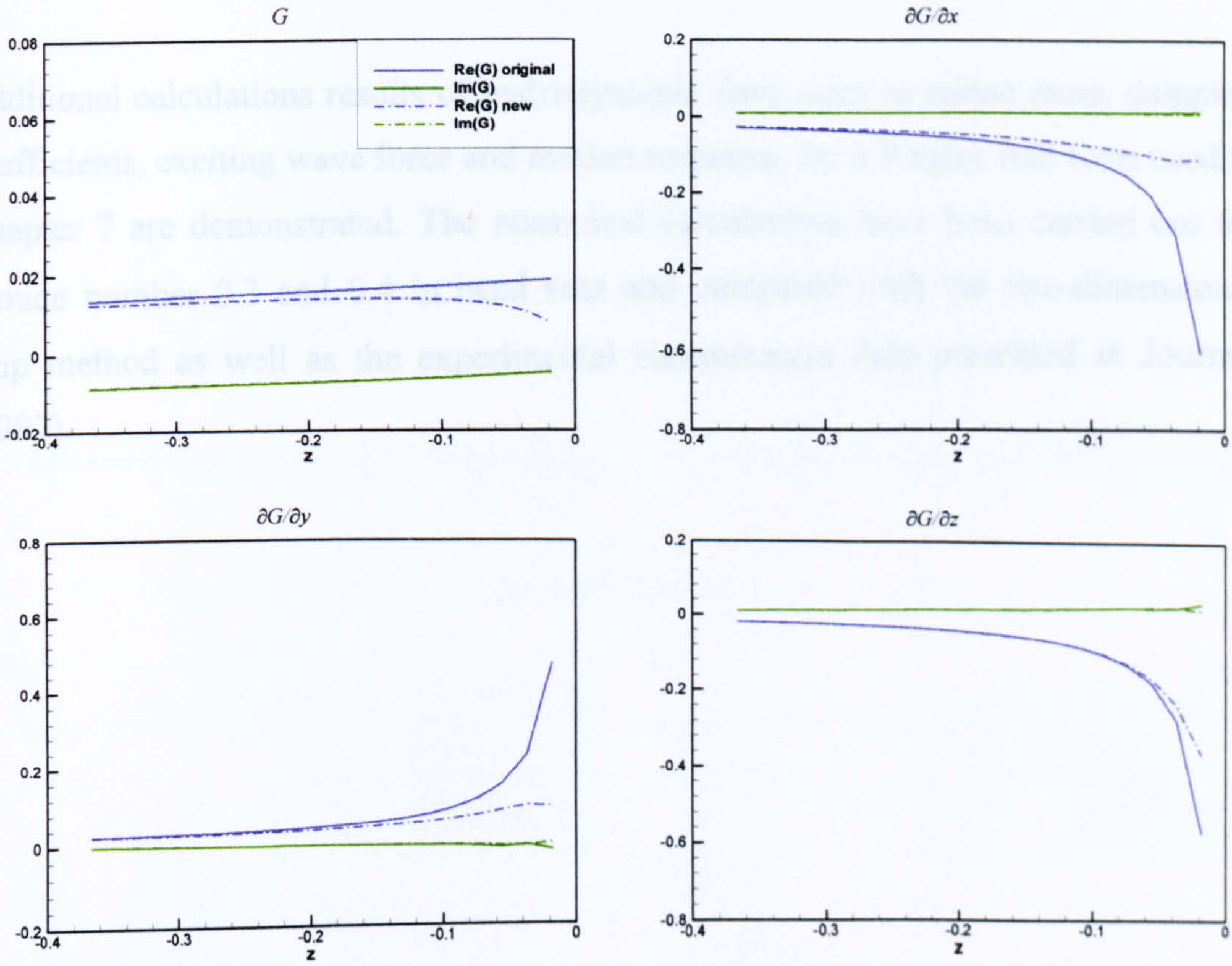

Figure A.7 Behaviour of Green function and its derivatives in the waterline integral with field point approaching free surface

Appendix B. Hydrodynamic Data for Wigley Hull

Additional calculations results of hydrodynamic data, such as added mass, damping coefficients, exciting wave force and motion response, for a Wigley hull form used in Chapter 7 are demonstrated. The numerical calculations have been carried out for Froude number 0.3 and 0.4 in head seas and compared with the two-dimensional strip method as well as the experimental measurement data presented in Journee (1992).

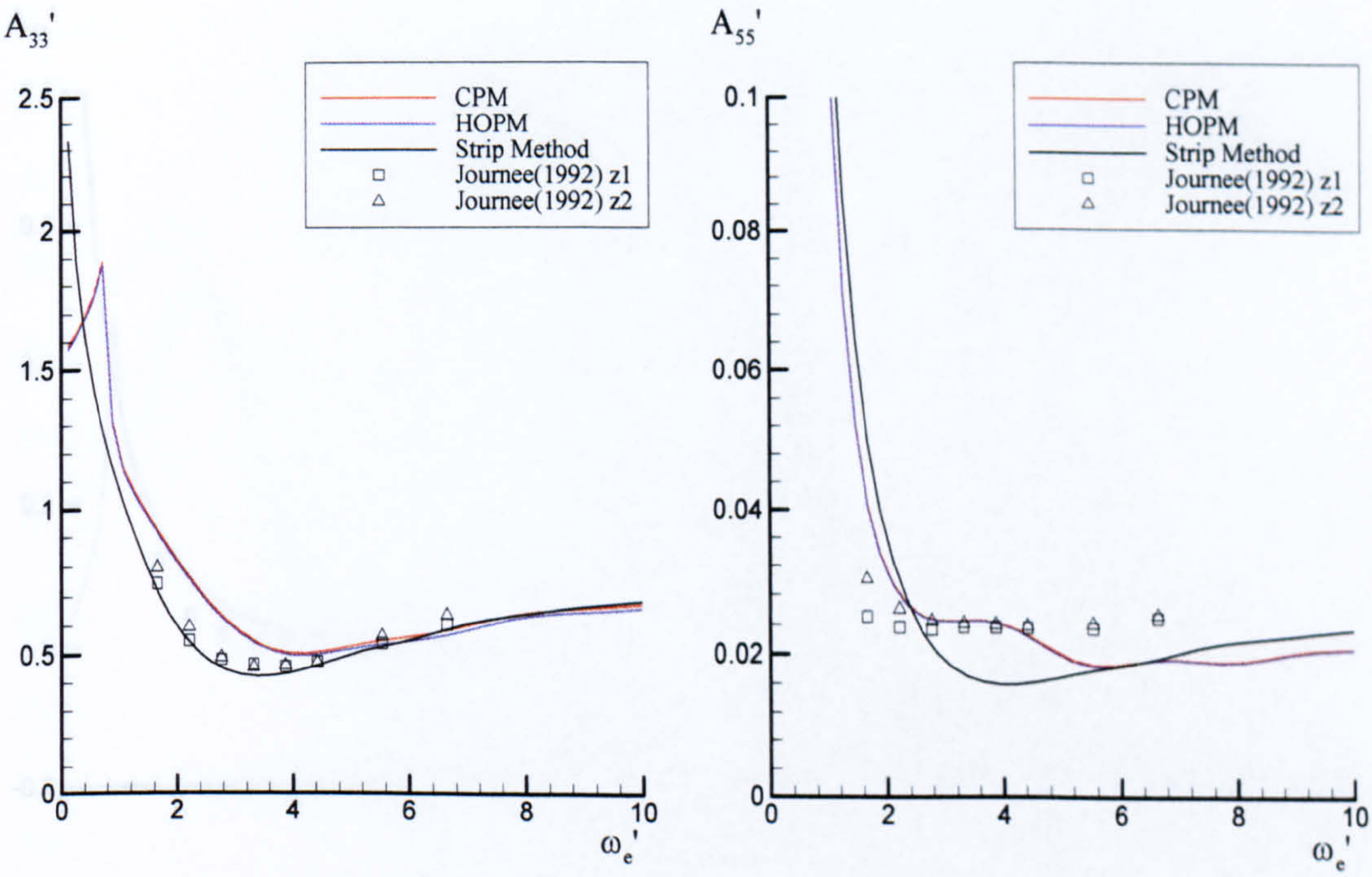

(a) Added mass

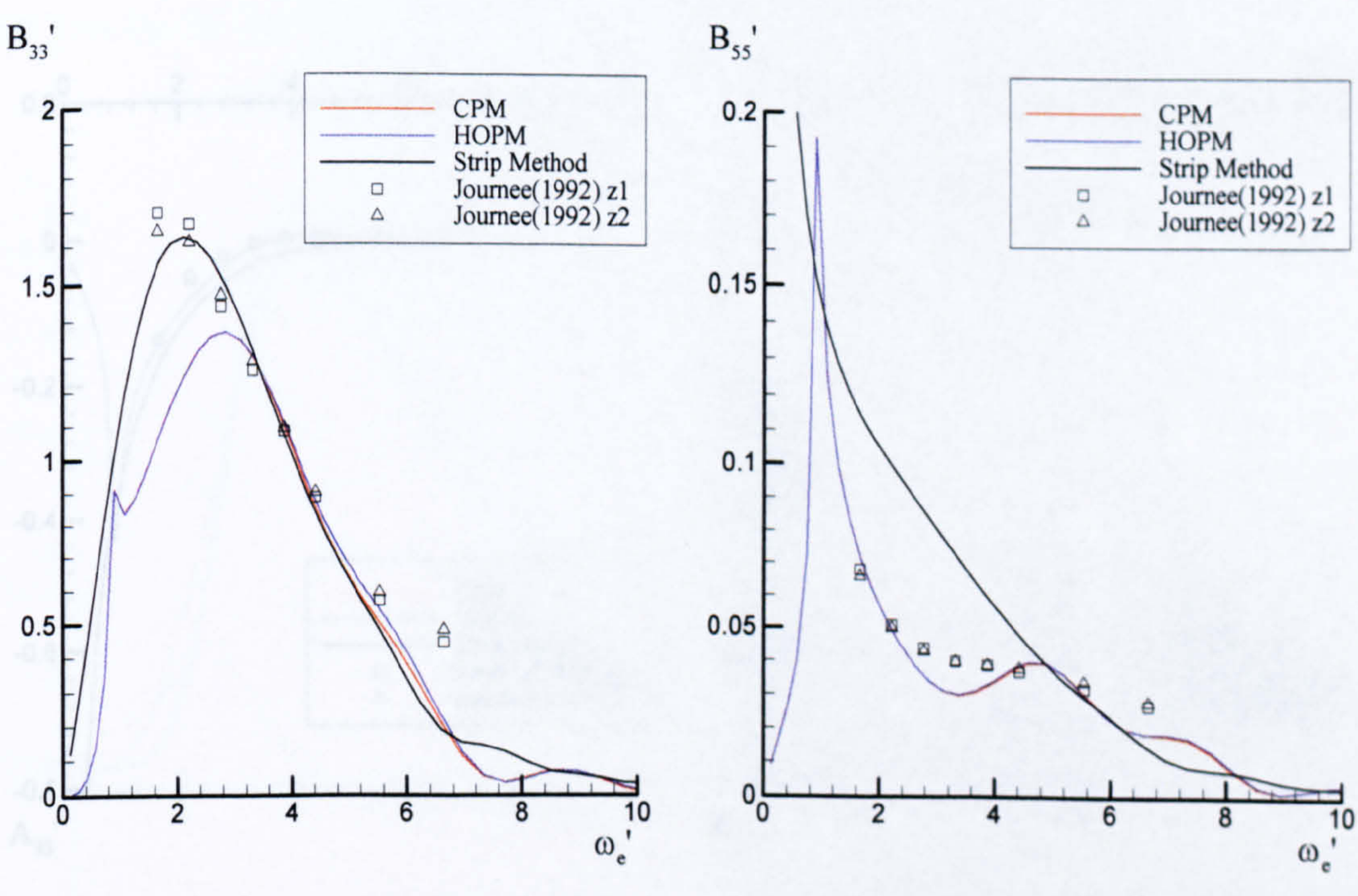

(b) Damping coefficients

Figure B.1 Non-dimensional added mass and damping coefficients in heave and pitch modes for Wigley hull travelling at Froude number 0.3

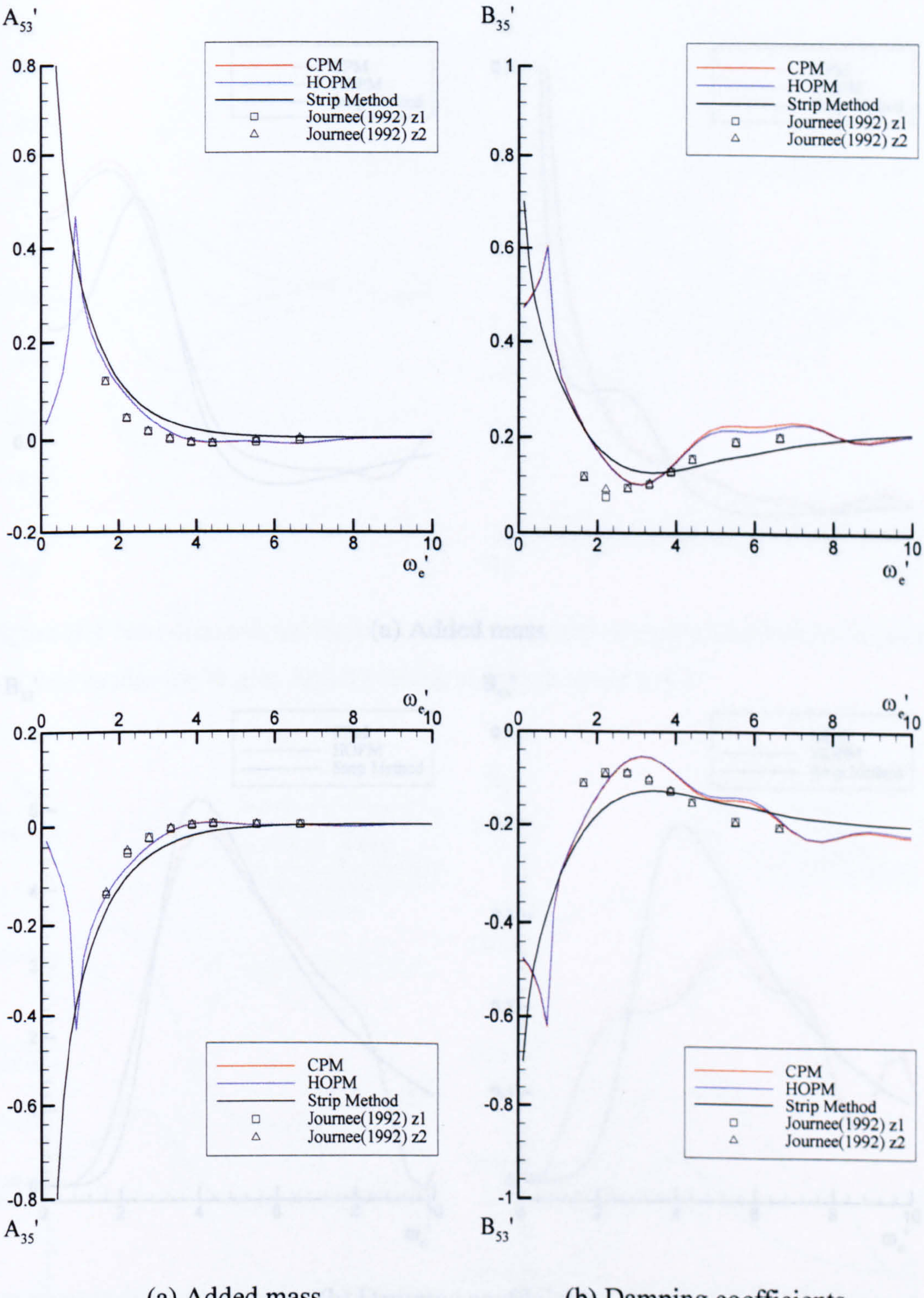

(a) Added mass (b) Damping coefficients

Figure B.2 Non-dimensional coupled added mass and damping coefficients in heave and pitch modes for Wigley hull travelling at Froude number 0.3

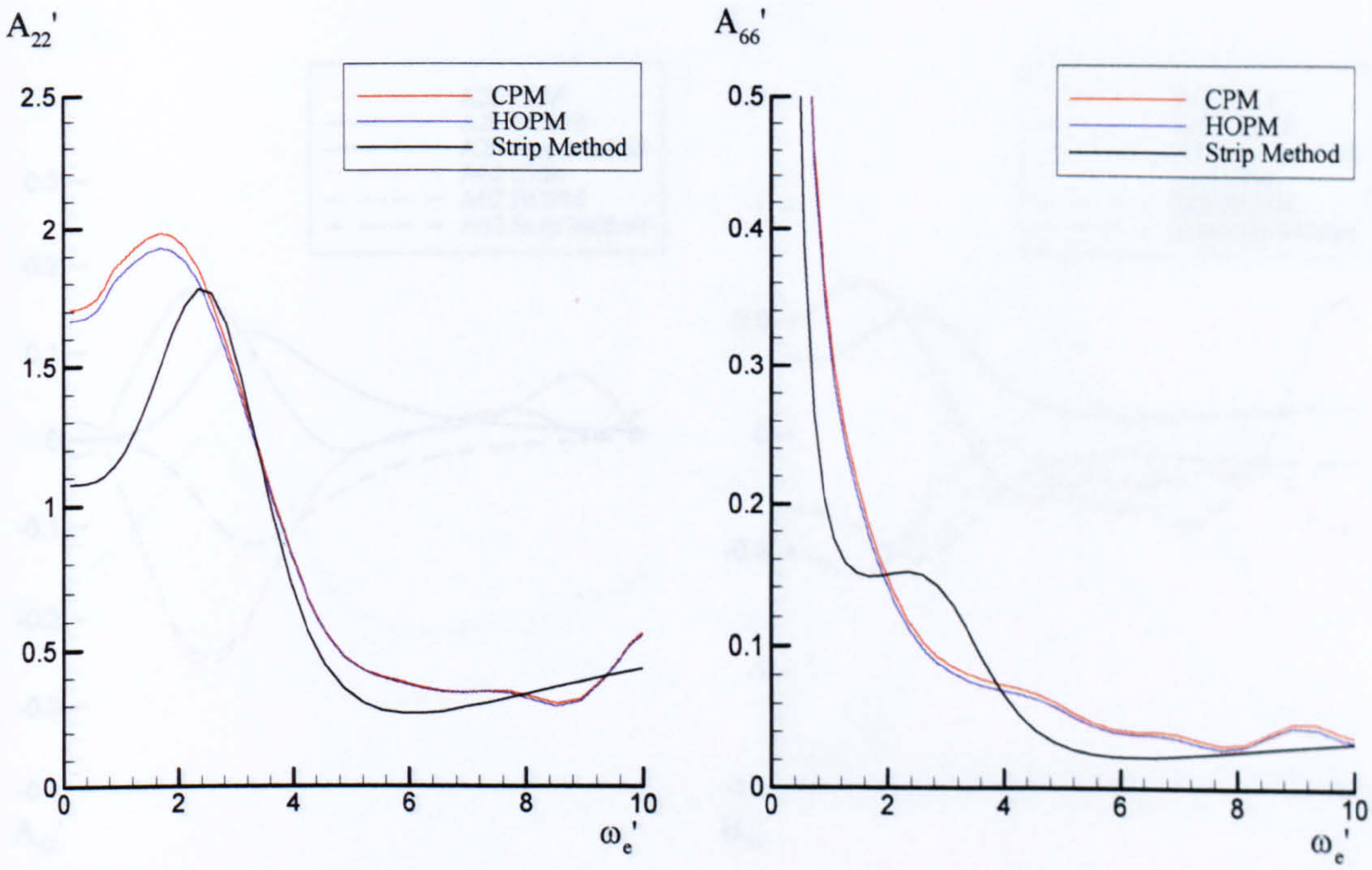

(a) Added mass

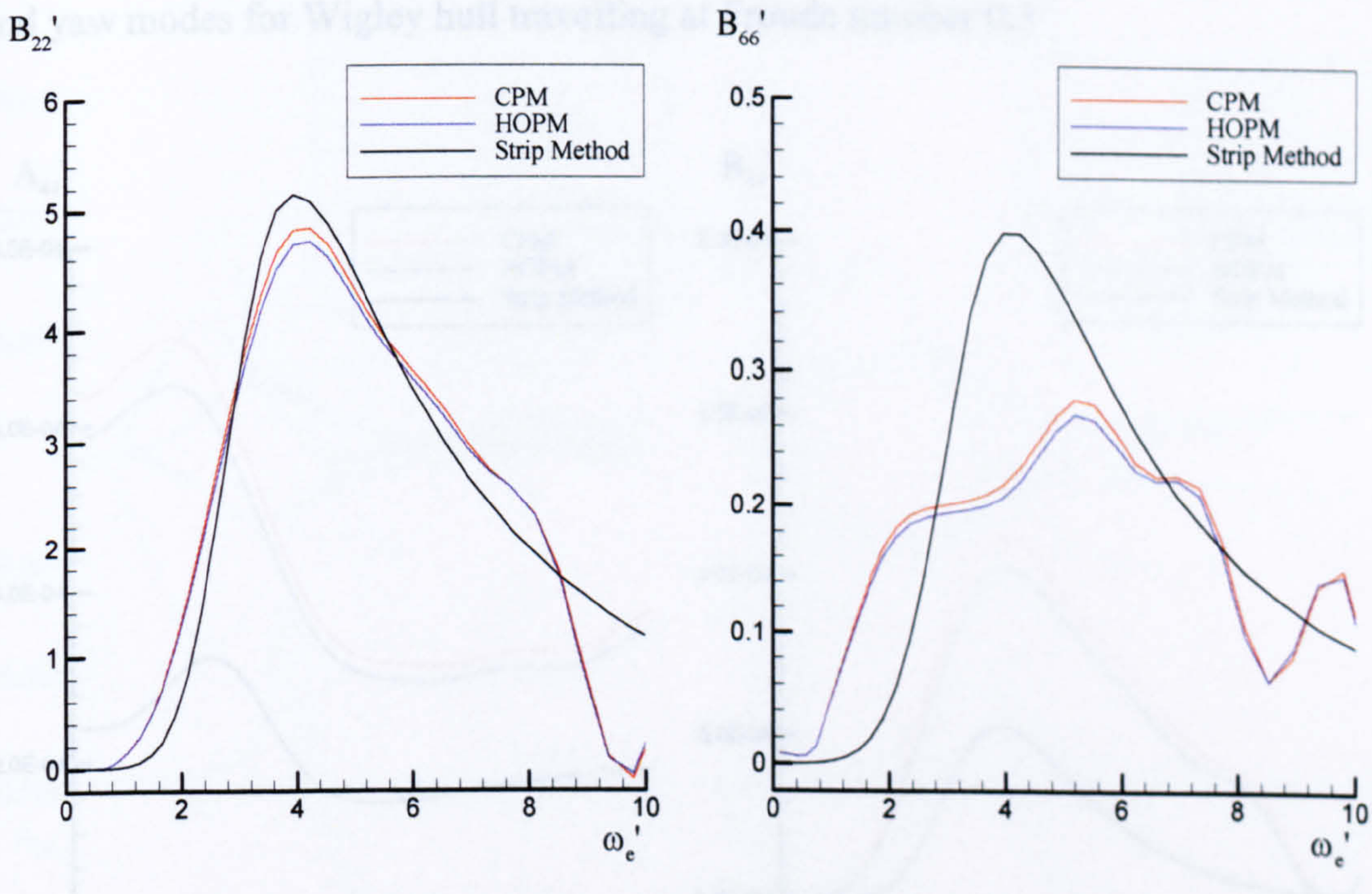

(b) Damping coefficients

Figure B.3 Non-dimensional added mass and damping coefficients in sway and yaw modes for Wigley hull travelling at Froude number 0.3

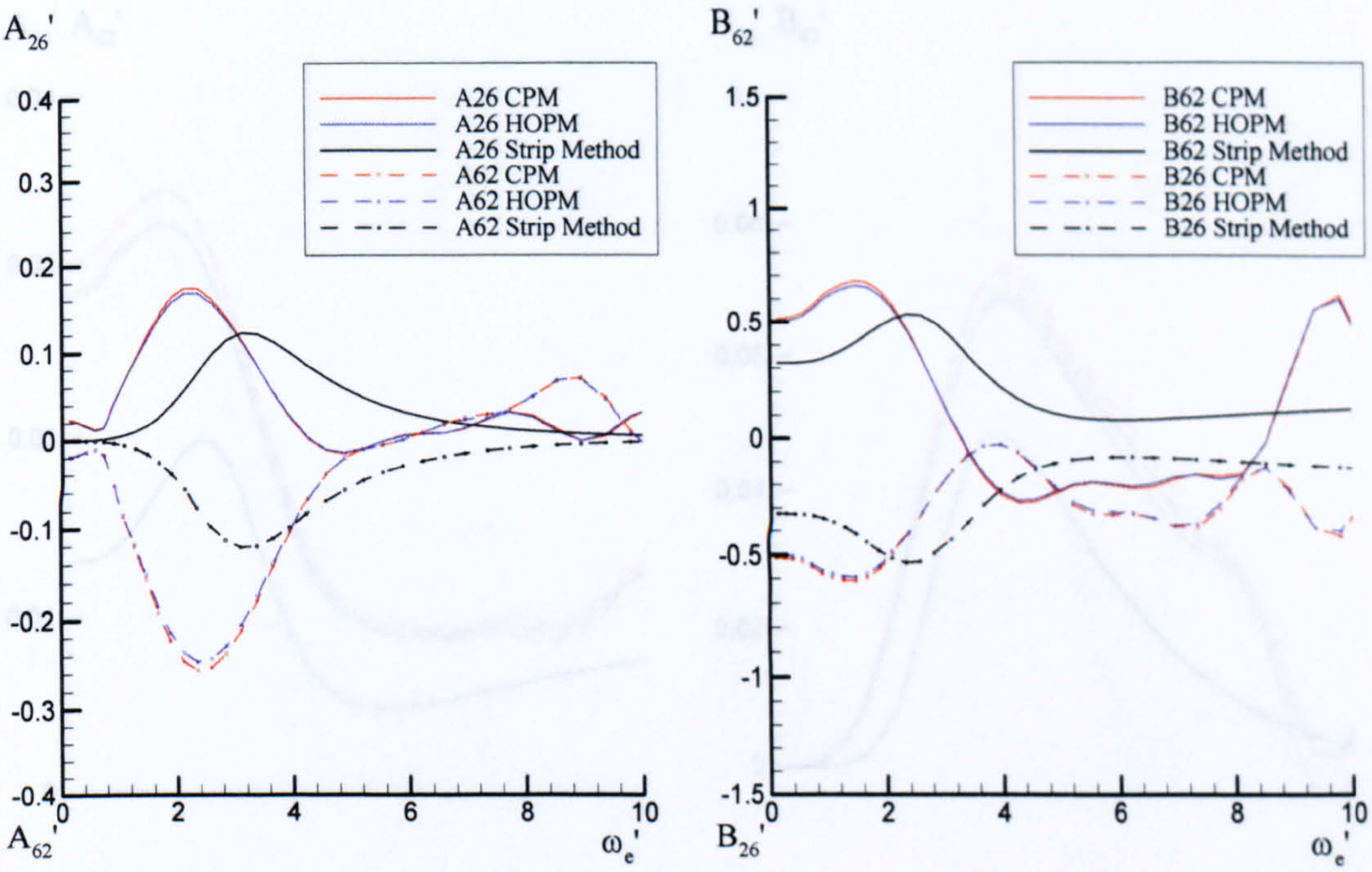

Figure B.4 Non-dimensional coupled added mass and damping coefficients in sway and yaw modes for Wigley hull travelling at Froude number 0.3

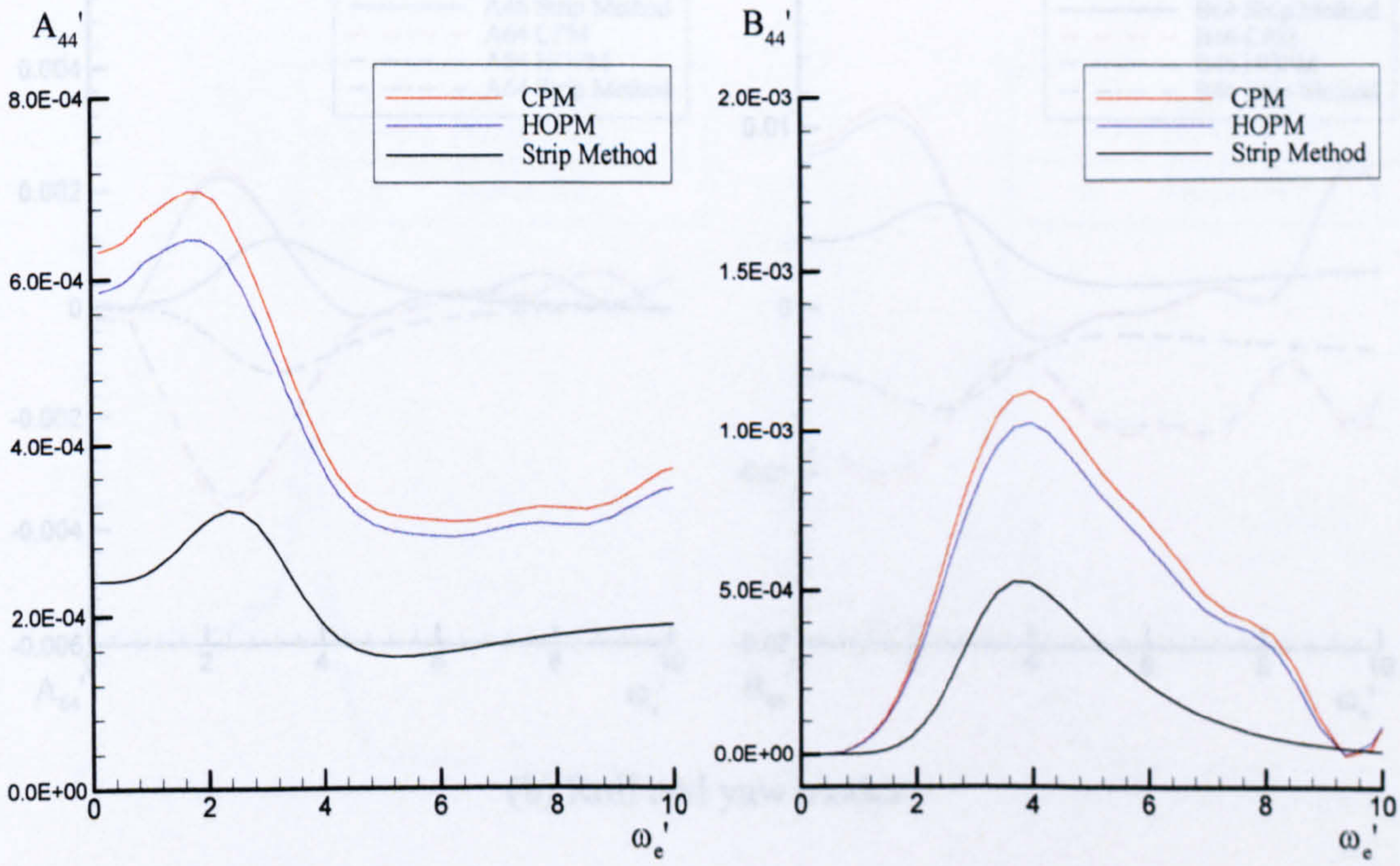

Figure B.5 Non-dimensional added mass and damping coefficients in roll mode for Wigley hull travelling at Froude number 0.3

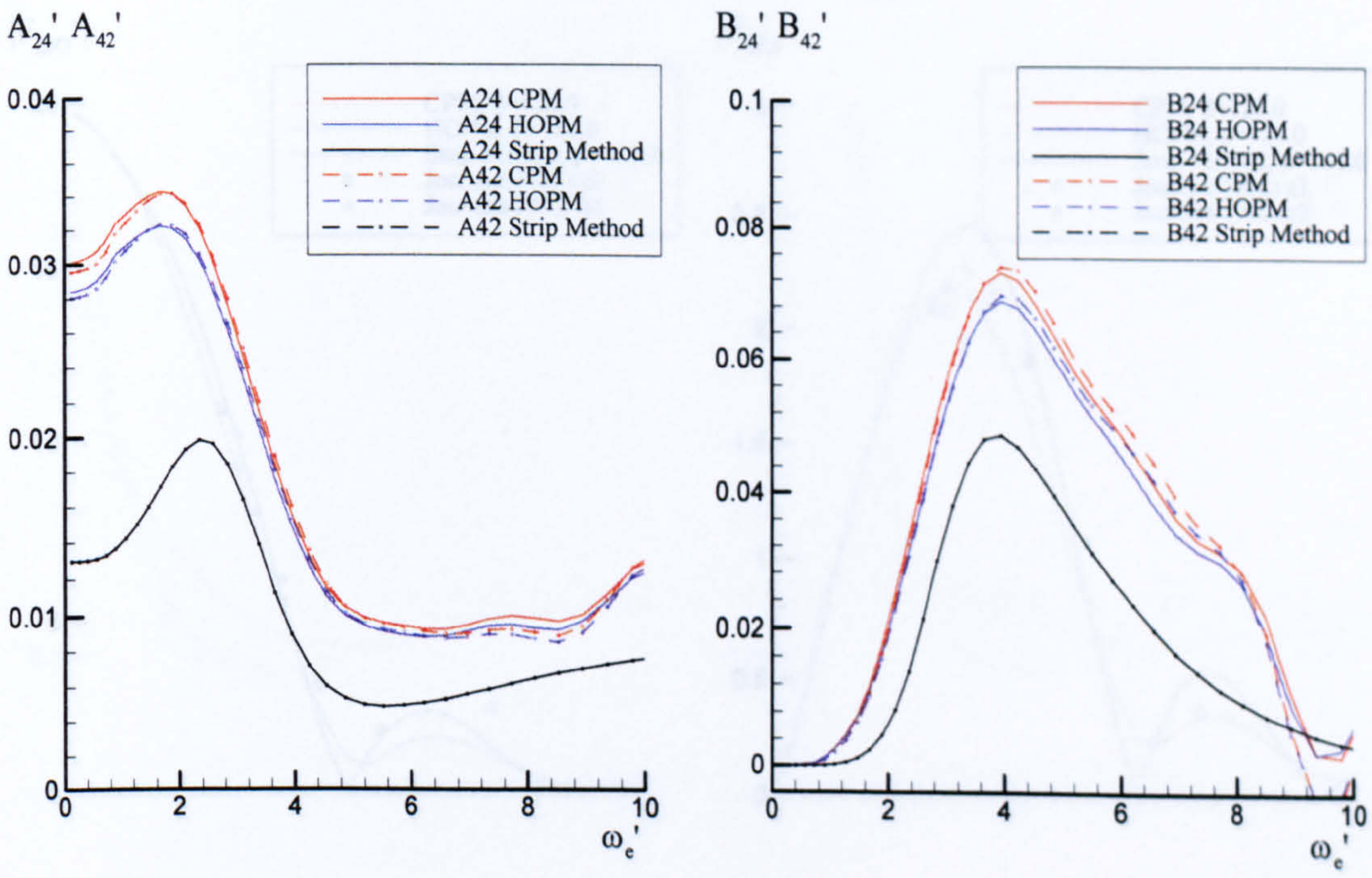

(a) Sway and roll modes

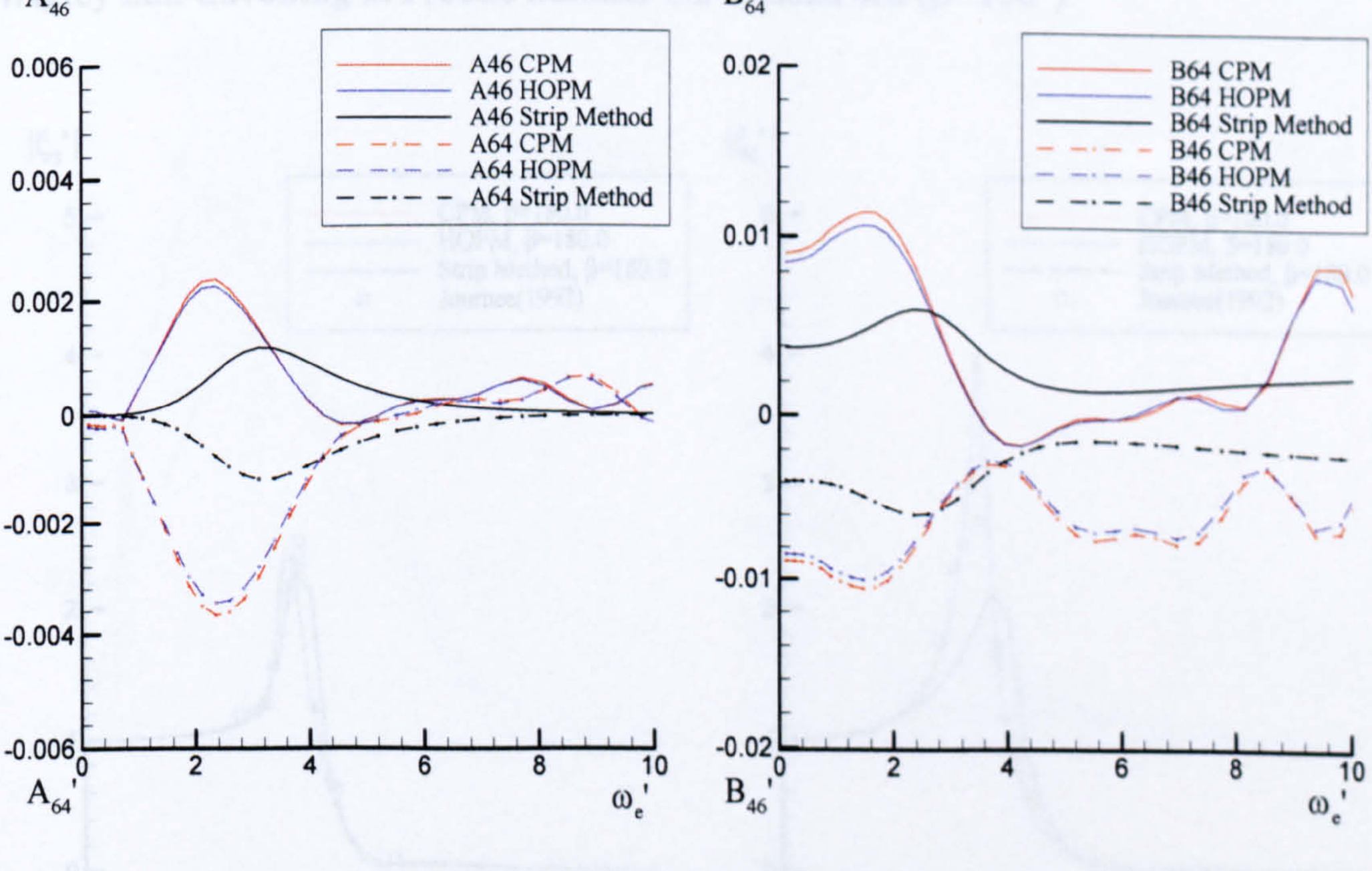

(b) Roll and yaw modes

Figure B.6 Non-dimensional coupled added mass and damping coefficients in sway-roll and roll-yaw modes for Wigley hull travelling at Froude number 0.3

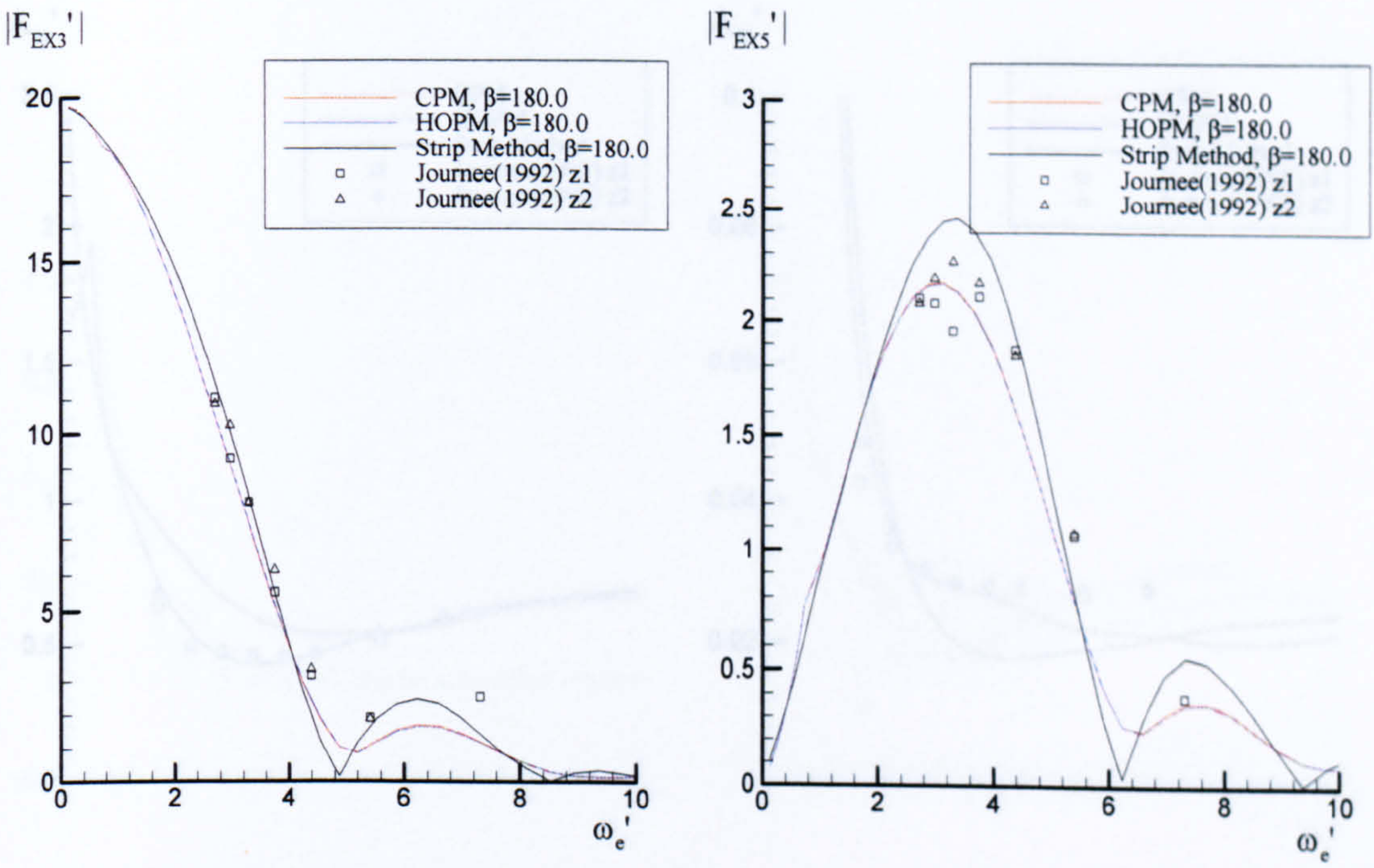

Figure B.7 Non-dimensional heave and pitch wave exciting force and moment for Wigley hull travelling at Froude number 0.3 in head sea (β=180°)

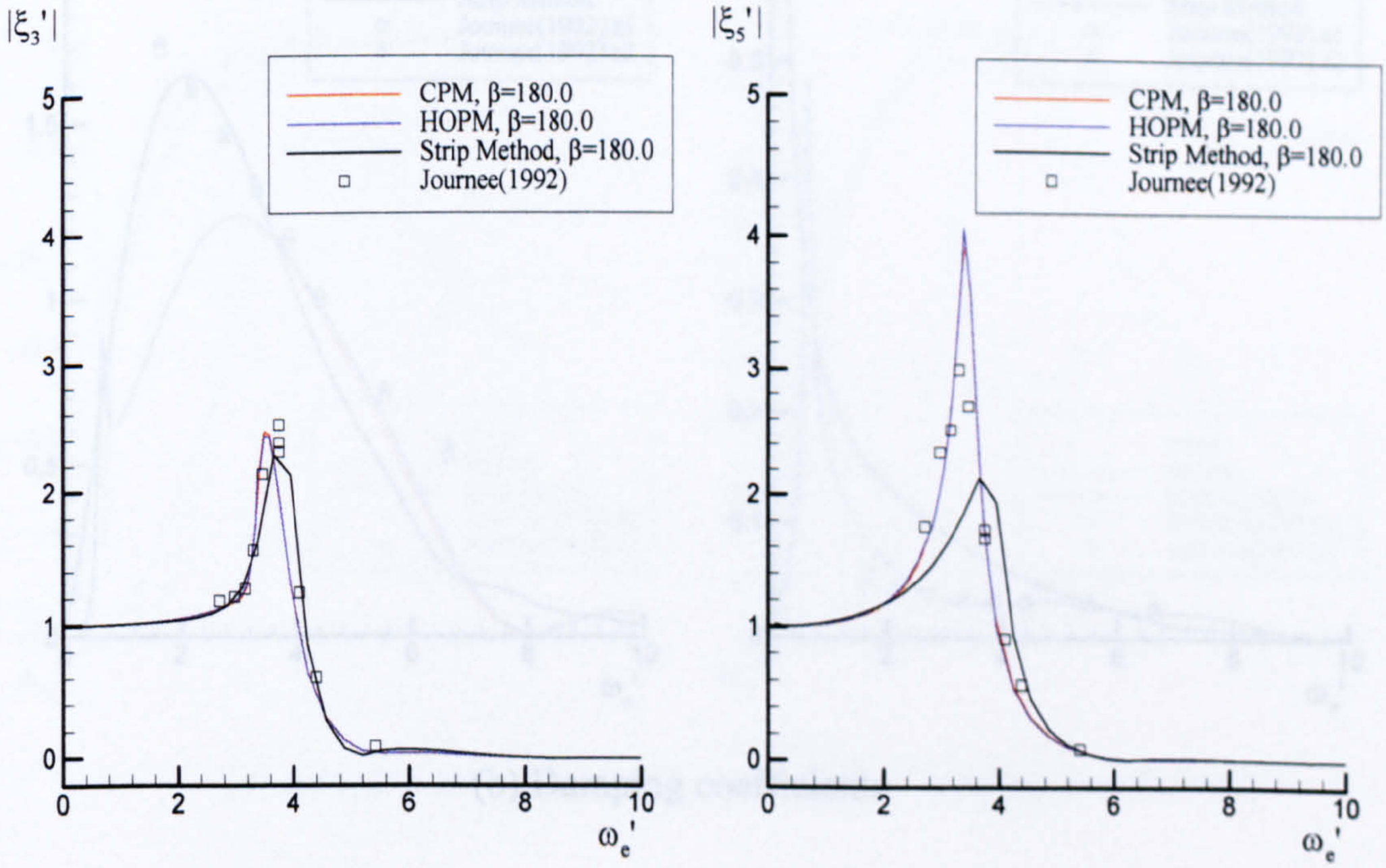

Figure B.8 Non-dimensional heave and pitch motion responses for Wigley hull travelling at Froude number 0.3 in head sea (β=180°)

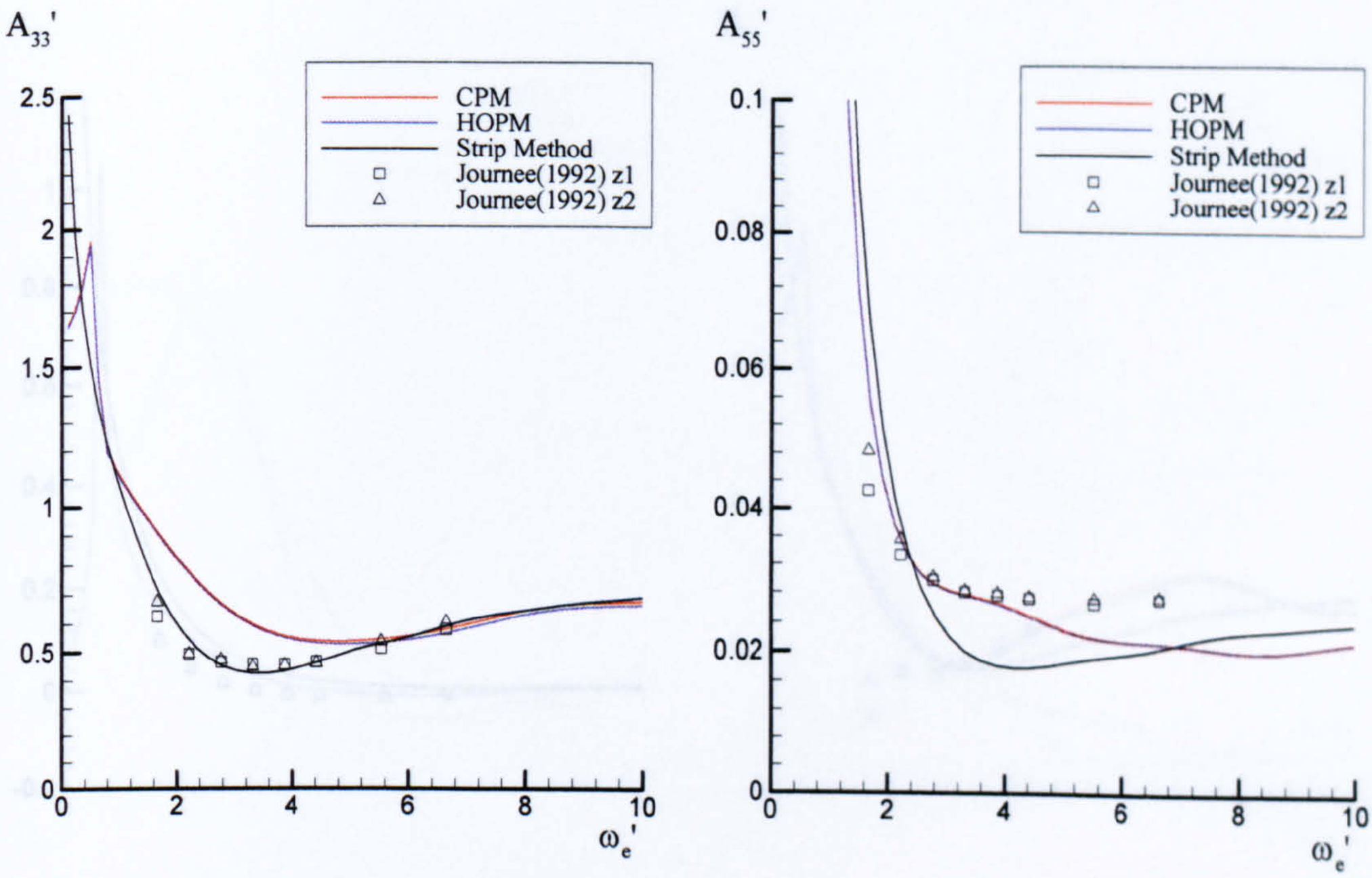

(a) Added mass

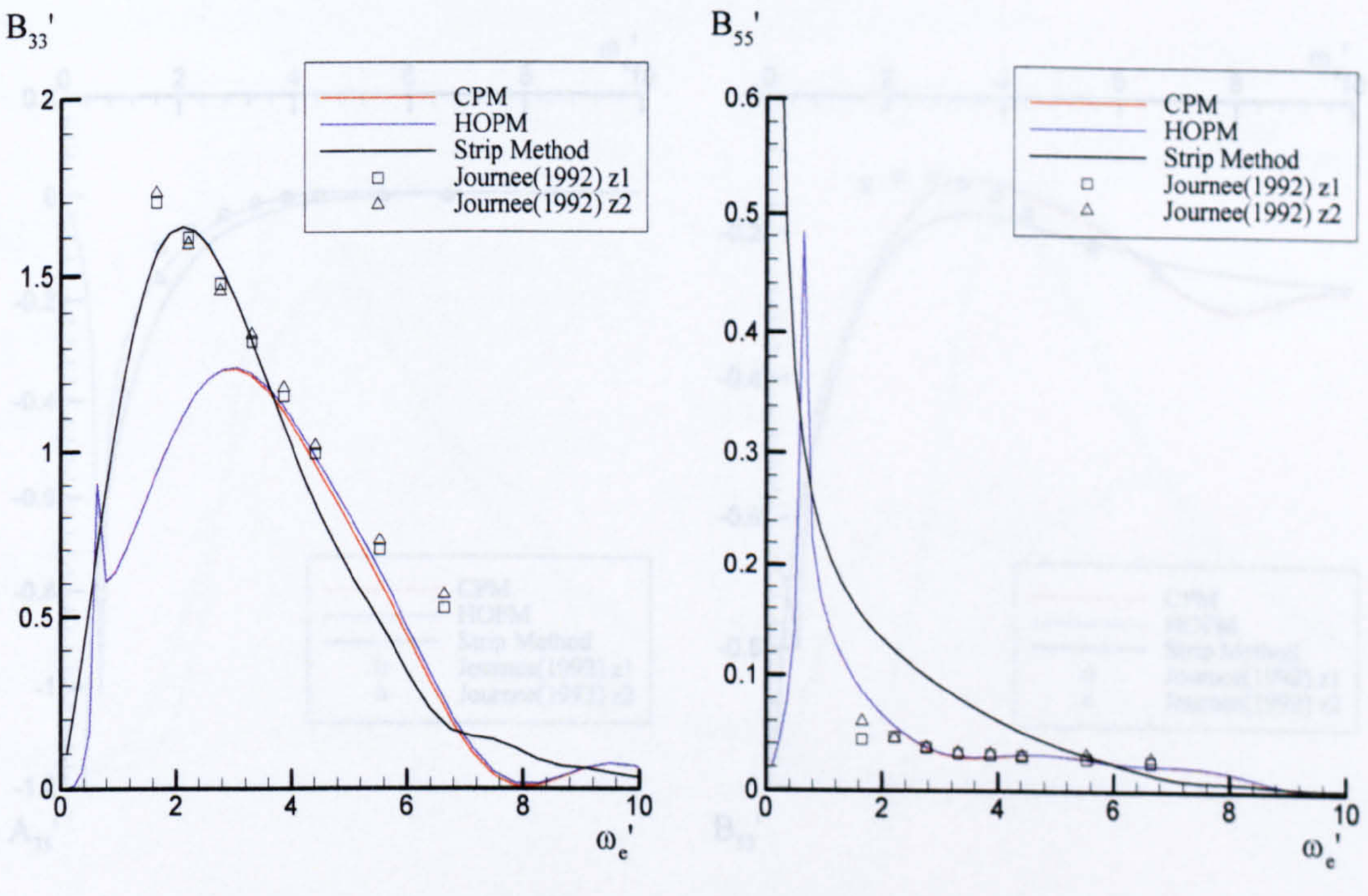

(b) Damping coefficients

Figure B.9 Non-dimensional added mass and damping coefficients in heave and pitch modes for Wigley hull travelling at Froude number 0.4

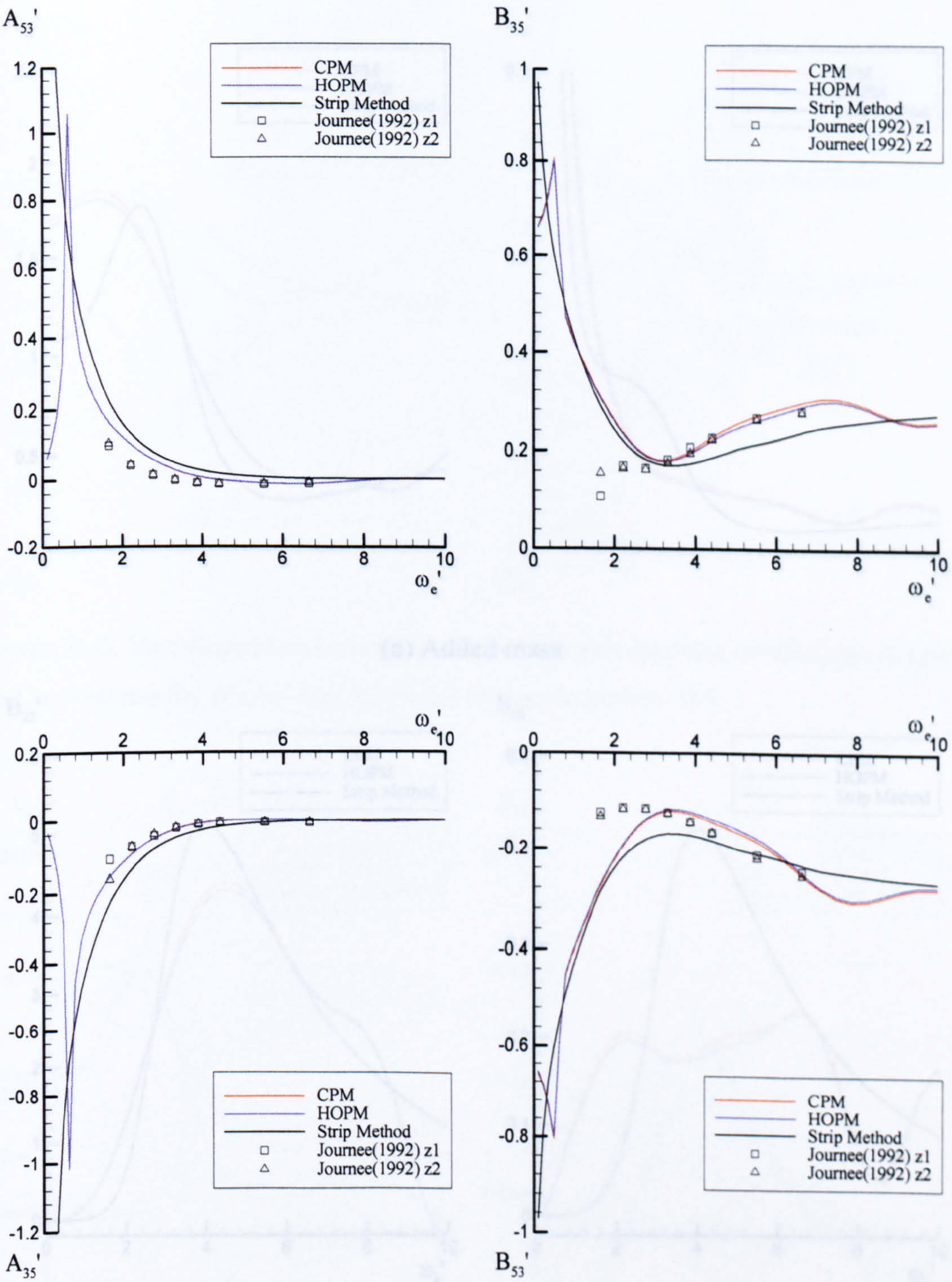

(a) Added mass (b) Damping coefficients

Figure B.10 Non-dimensional coupled added mass and damping coefficients in heave and pitch modes for Wigley hull travelling at Froude number 0.4

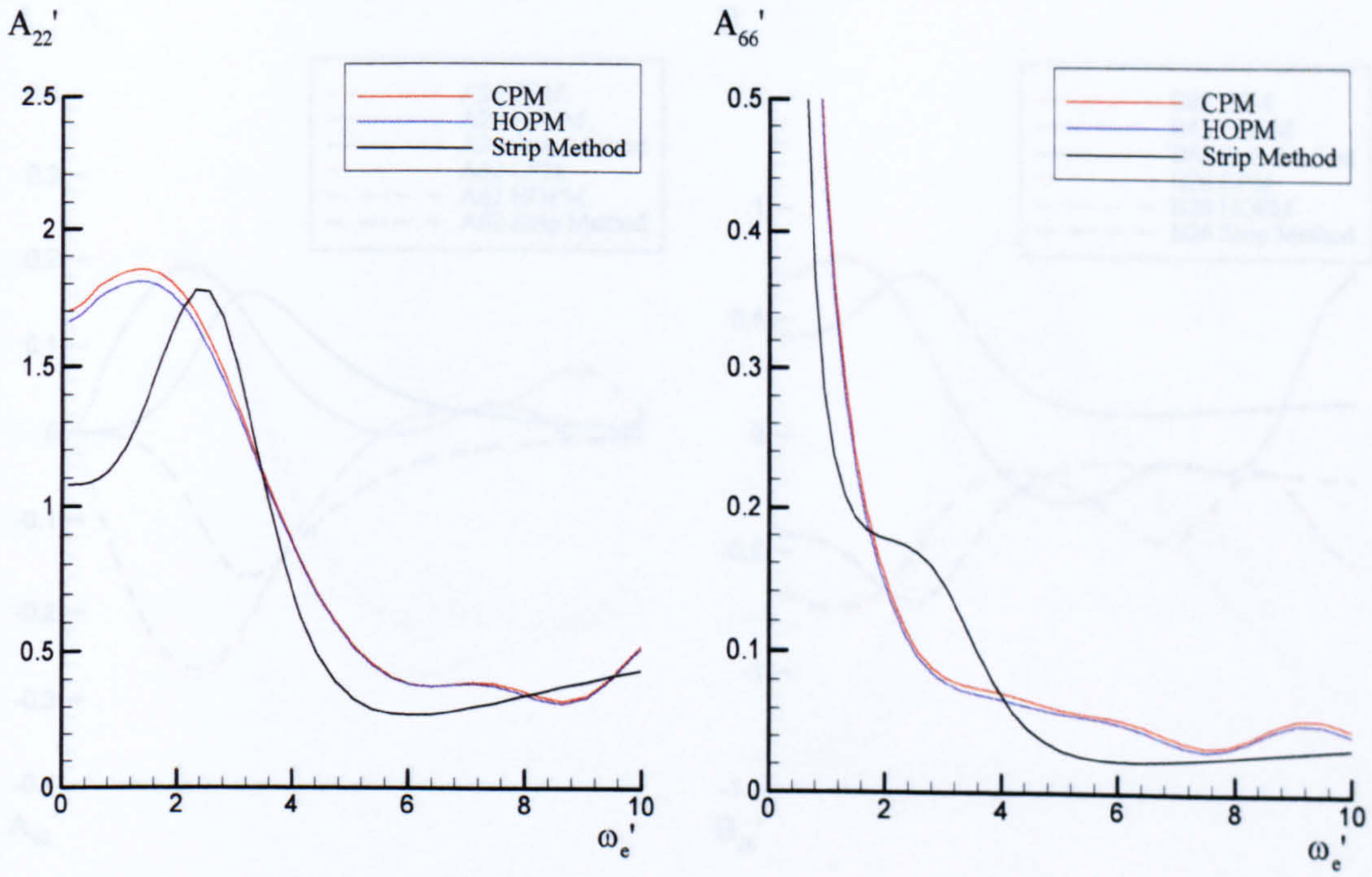

(a) Added mass

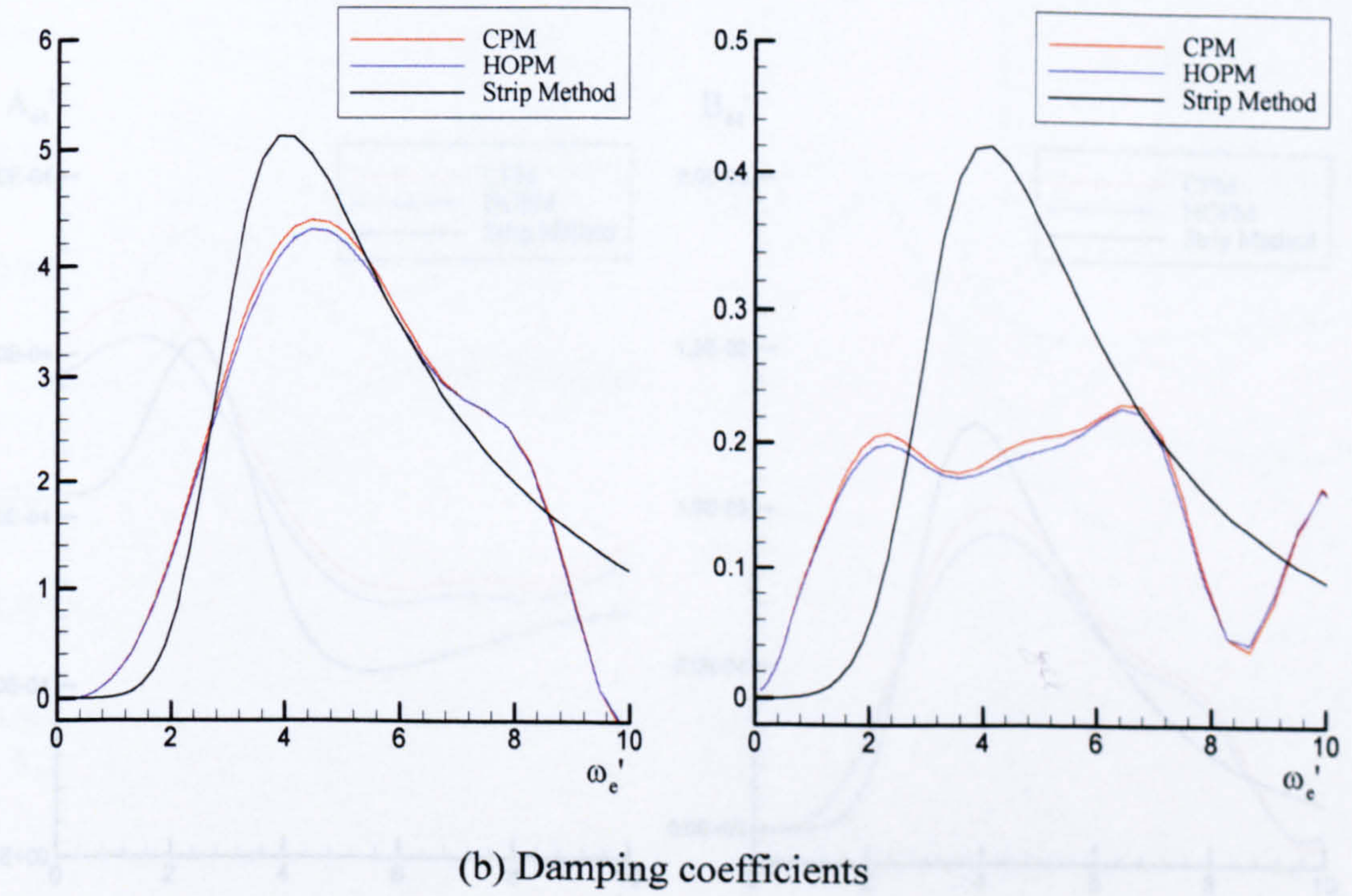

(b) Damping coefficients

Figure B.11 Non-dimensional added mass and damping coefficients in sway and yaw modes for Wigley hull travelling at Froude number 0.4

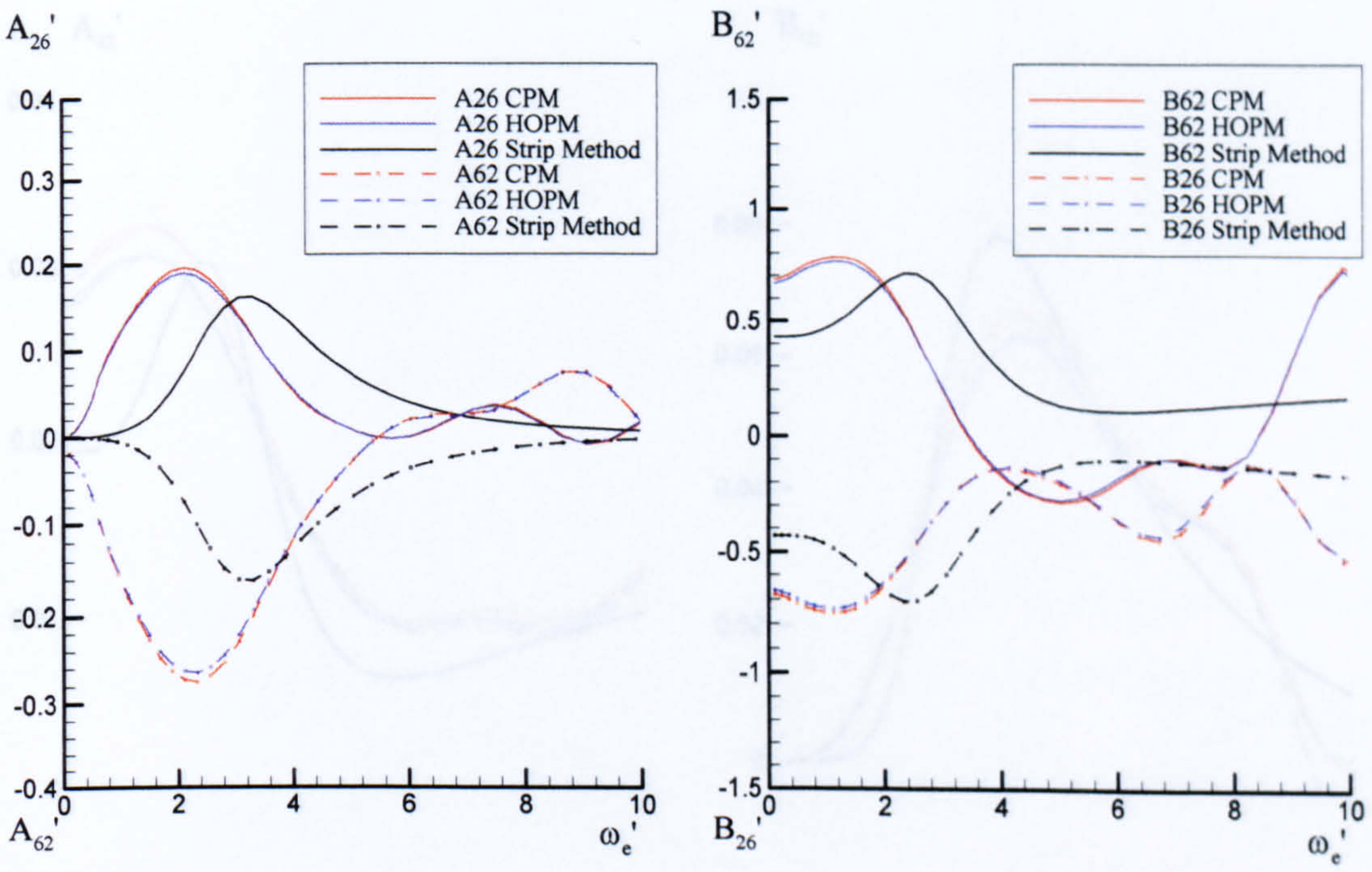

Figure B.12 Non-dimensional coupled added mass and damping coefficients in sway and yaw modes for Wigley hull travelling at Froude number 0.4

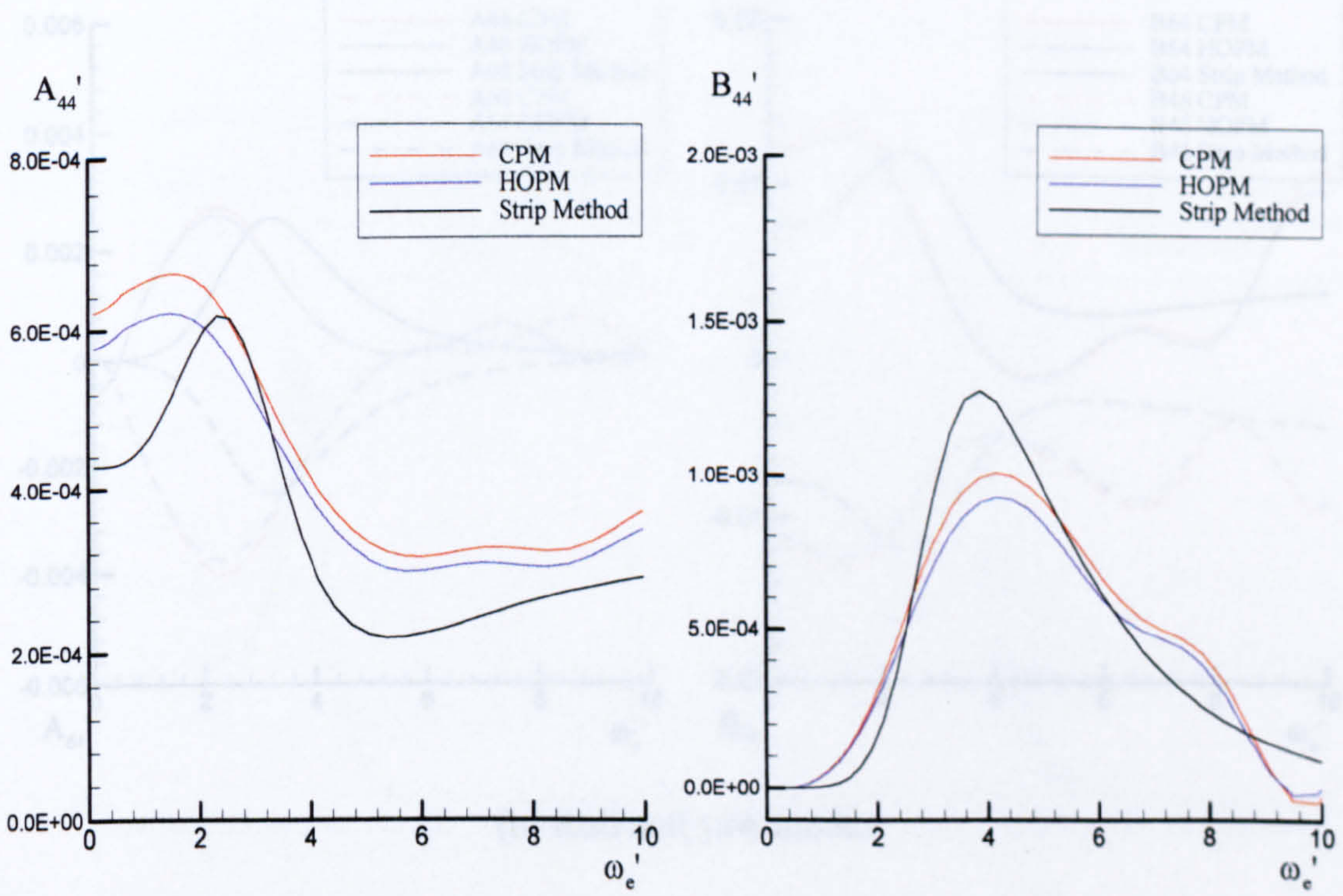

Figure B.13 Non-dimensional added mass and damping coefficients in roll mode for Wigley hull travelling at Froude number 0.4

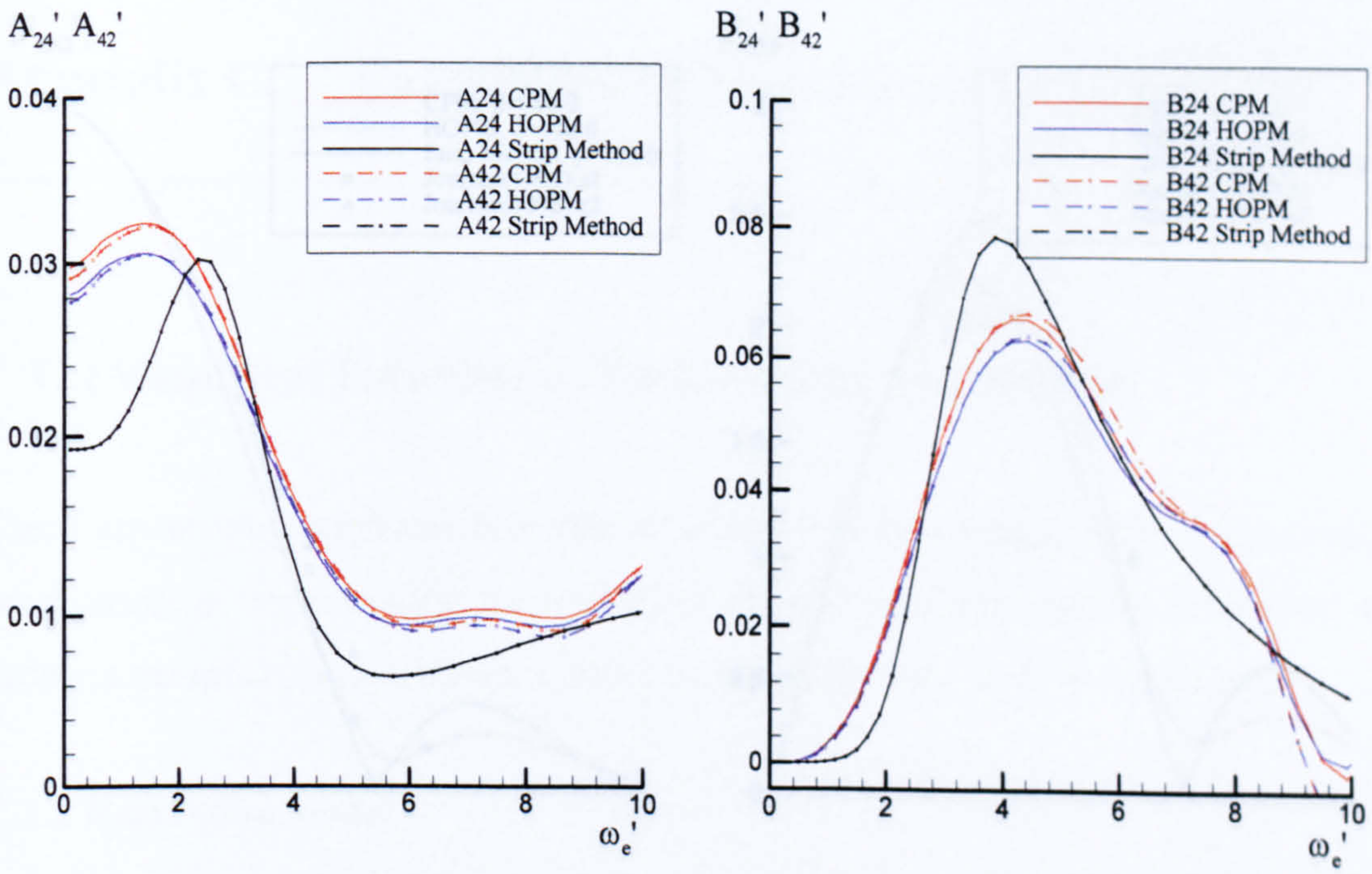

(a) Sway and roll modes

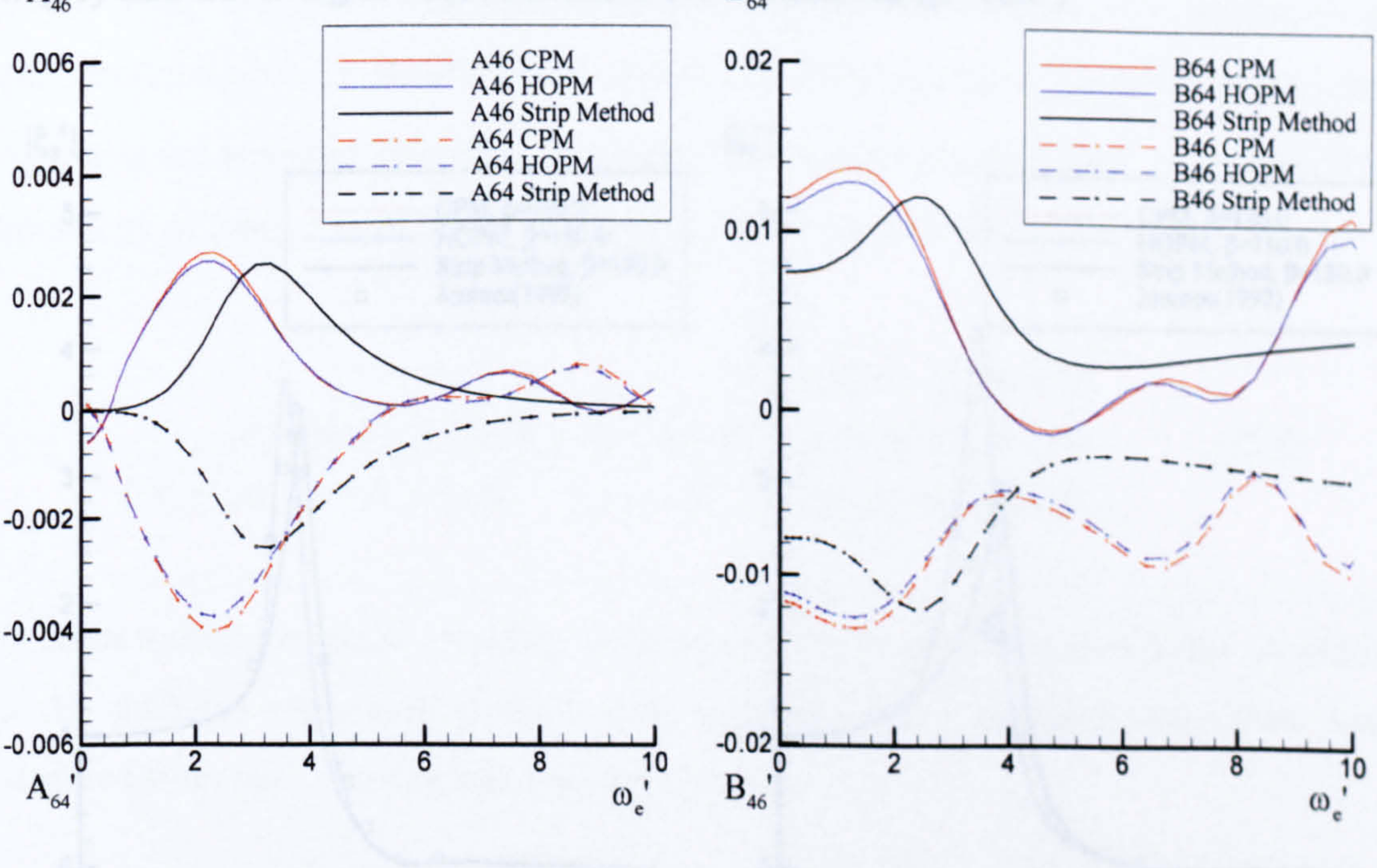

(b) Roll and yaw modes

Figure B.14 Non-dimensional coupled added mass and damping coefficients in sway-roll and roll-yaw modes for Wigley hull travelling at Froude number 0.4

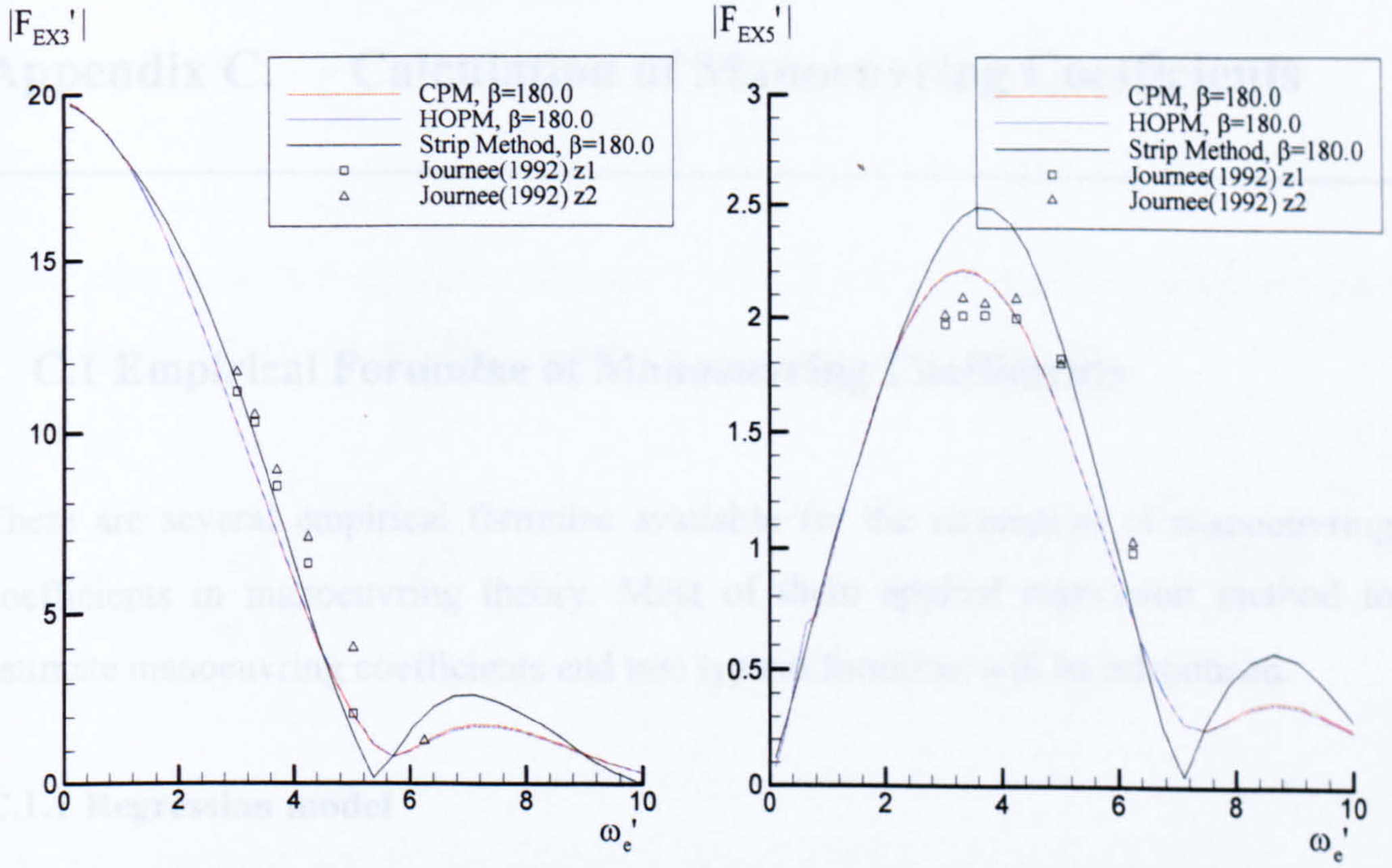

Figure B.15 Non-dimensional heave and pitch wave exciting force and moment for Wigley hull travelling at Froude number 0.4 in head sea (β=180°)

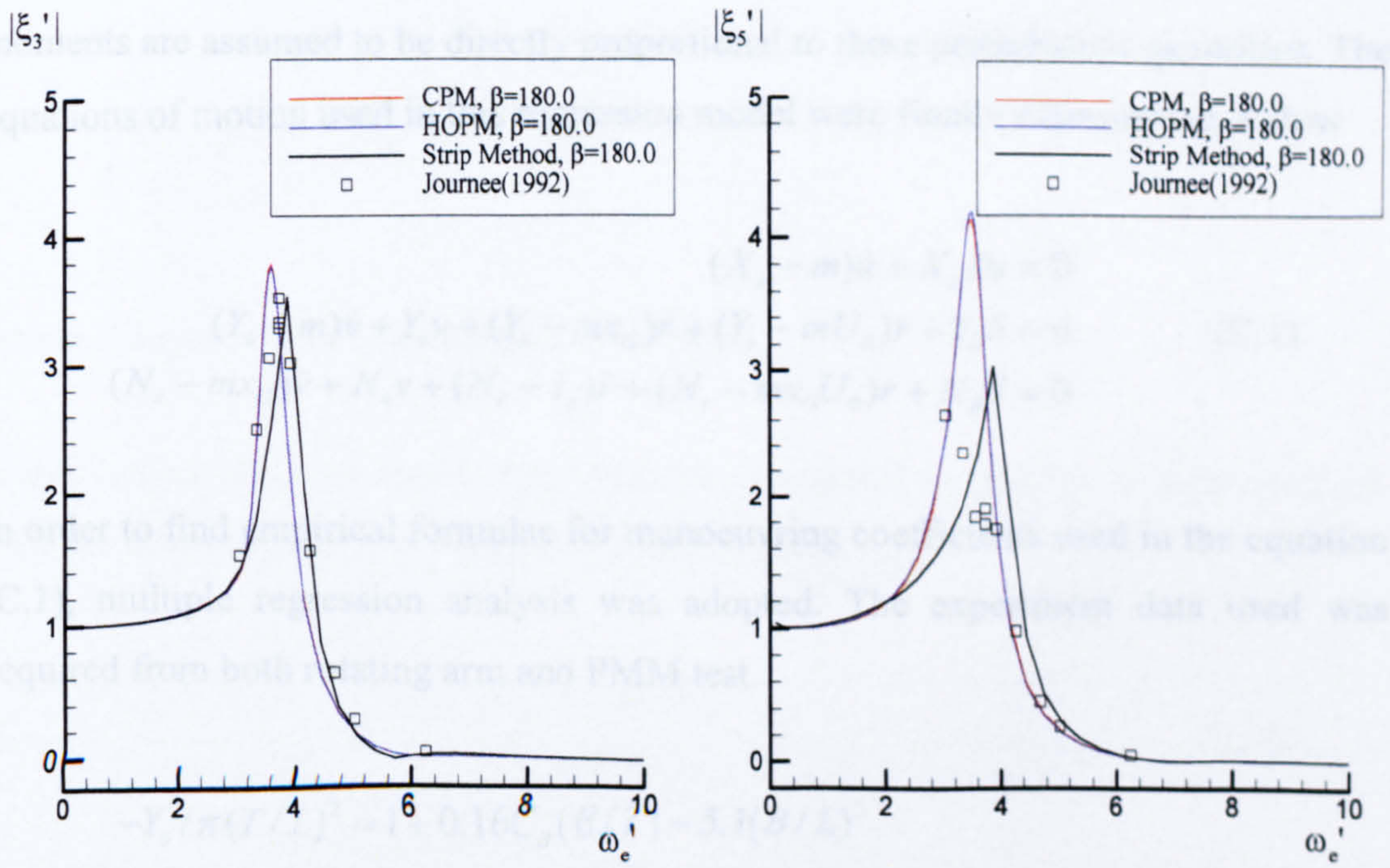

Figure B.16 Non-dimensional heave and pitch motion responses for Wigley hull travelling at Froude number 0.4 in head sea (β=180°)

Appendix C. Calculation of Manoeuvring Coefficients

C.1 Empirical Formulae of Manoeuvring Coefficients

There are several empirical formulae available for the estimation of manoeuvring coefficients in manoeuvring theory. Most of them applied regression method to estimate manoeuvring coefficients and two typical formulae will be introduced.

C.1.1 Regression model

Clarke et al. (1983) used linear equations of motion with three degrees of freedom, in surge, sway and yaw. The hydrodynamic forces and moments are expressed as perturbations about a steady ahead speed U_0. Then the hydrodynamic forces and moments are assumed to be directly proportional to these perturbation quantities. The equations of motion used in this regression model were finally expressed as follow

$$\begin{aligned}(X_u - m)\dot{u} + X_u \Delta u &= 0\\ (Y_{\dot{v}} - m)\dot{v} + Y_v v + (Y_r - mx_G)\dot{r} + (Y_r - mU_0)r + Y_\delta \delta &= 0\\ (N_{\dot{v}} - mx_G)\dot{v} + N_v v + (N_r - I_z)\dot{r} + (N_r - mx_G U_0)r + N_\delta \delta &= 0\end{aligned} \qquad \text{(C.1)}$$

In order to find empirical formulae for manoeuvring coefficients used in the equation (C.1), multiple regression analysis was adopted. The experiment data used was acquired from both rotating arm and PMM test.

$$\begin{aligned}-Y'_{\dot{v}}/\pi(T/L)^2 &= 1 + 0.16C_B(B/T) - 5.1(B/L)^2\\ -Y'_{\dot{r}}/\pi(T/L)^2 &= 0.67(B/L) - 0.0033(B/T)^2\\ -N'_{\dot{v}}/\pi(T/L)^2 &= 1.1(B/L) - 0.041(B/T)\\ -N'_{\dot{r}}/\pi(T/L)^2 &= 1/12 + 0.017C_B(B/T) - 0.33(B/L)\end{aligned} \qquad \text{(C.2)}$$

$$
\begin{aligned}
-Y_v^{'}/\pi(T/L)^2 &= 1+0.40C_B(B/T) \\
-Y_r^{'}/\pi(T/L)^2 &= -1/2+2.2(B/L)-0.080(B/T) \\
-N_v^{'}/\pi(T/L)^2 &= 1/2+2.4(T/L) \\
-N_r^{'}/\pi(T/L)^2 &= 1/4+0.039(B/T)-0.56(B/L)
\end{aligned}
\tag{C.3}
$$

The rudder force in sway direction is calculated on the basis that the rudder acts like a low aspect ratio wing, so that

$$
\begin{aligned}
Y_\delta^{'} &= \left(\frac{A}{LT}\right)\left(\frac{T}{L}\right)\left(\frac{\partial C_L}{\partial \delta}\right)\left(\frac{c}{u}\right)^2 \\
N_\delta^{'} &= -0.5Y_\delta^{'}
\end{aligned}
\tag{C.4}
$$

where c is water speed past the rudder, A the rudder area, and C_L the lift coefficient. The yaw moment due to the rudder is approximated half the ship length aft of amidships. Although the lift curve slope of the rudder $\partial C_L/\partial\delta$ and the velocity ratio $(c/u)^2$ are variables which are different for every ship, their product could be assumed constant, so that

$$
\left(\frac{\partial C_L}{\partial \delta}\right)\left(\frac{c}{u}\right)^2 = 3.0 \tag{C.5}
$$

which is a typical value for single screw ships.

If derivatives given in above equations are considered to be bare hull derivatives, then the following fin effects must be added to them:

$$
\begin{aligned}
Y_{v_{fin}}^{'} &= -\gamma Y_\delta^{'} & N_{v_{fin}}^{'} &= -1/2Y_{v_{fin}}^{'} \\
Y_{r_{fin}}^{'} &= -1/2Y_{v_{fin}}^{'} & N_{r_{fin}}^{'} &= 1/4Y_{v_{fin}}^{'}
\end{aligned}
\tag{C.6}
$$

where γ is a flow straightening coefficient, taken to be $\gamma = 0.3$.

The non-dimensionalised quantities used in equations (C.3) and (C.4) are defined as

$$
\begin{aligned}
Y'_{\dot{v}} &= \frac{Y_{\dot{v}}}{1/2\rho L^3} & Y'_{v} &= \frac{Y_{v}}{1/2\rho L^2 u} & Y'_{\delta} &= \frac{Y_{\delta}}{1/2\rho L^2 u^2} \\
Y'_{\dot{r}} &= \frac{Y_{\dot{r}}}{1/2\rho L^4} & Y'_{r} &= \frac{Y_{r}}{1/2\rho L^3 u} & N'_{\delta} &= \frac{N_{\delta}}{1/2\rho L^3 u^2} \\
N'_{\dot{v}} &= \frac{Y_{\dot{v}}}{1/2\rho L^4} & N'_{v} &= \frac{N_{v}}{1/2\rho L^3 u} & & \\
N'_{\dot{r}} &= \frac{Y_{\dot{r}}}{1/2\rho L^5} & N'_{r} &= \frac{N_{r}}{1/2\rho L^4 u} & &
\end{aligned}
\qquad \text{(C.7)}
$$

C.1.2 MMG model

Kijima et al. (1990) used drift angle β to express equations of motion as follows

$$
\begin{aligned}
&(m' + m'_x)\left(\frac{L}{U}\right)\left(\frac{\dot{U}}{U}\cos\beta - \dot{\beta}\sin\beta\right) + (m' + m'_y)r'\sin\beta = X' \\
&-(m' + m'_y)\left(\frac{L}{U}\right)\left(\frac{\dot{U}}{U}\sin\beta + \dot{\beta}\cos\beta\right) + (m' + m'_x)r'\cos\beta = Y' \qquad \text{(C.8)} \\
&(I'_{zz} + J'_{zz})\left(\frac{L}{U}\right)\left(\frac{\dot{U}}{L}r' + \frac{U}{L}\dot{r}'\right) = N'
\end{aligned}
$$

where

m' : Mass of ship

m'_x, m'_y : x and y axis components of added mass of ship respectively

I'_{zz}, J'_{zz} : Moment of inertia and added moment of inertia around z axis

L : Ship length

d : Draft

U : Ship's speed

The non-dimensionalised quantities used in the equation (C.8) are defined as

$$
\begin{aligned}
m', m'_x, m'_y &= m, m_x, m_y \Big/ \tfrac{1}{2}\rho L^2 d \\
I'_{zz}, J'_{zz} &= I_{zz}, J_{zz} \Big/ \tfrac{1}{2}\rho L^4 d \\
X', Y' &= X, Y \Big/ \tfrac{1}{2}\rho L d U^2 \\
N' &= N \Big/ \tfrac{1}{2}\rho L^2 d U^2 \\
r' &= rL/U
\end{aligned}
\tag{C.9}
$$

If we consider surge and sway velocity instead of ship's speed and drift angle

$$
\begin{aligned}
u &= U\cos\beta, & \dot{u} &= \dot{U}\cos\beta - \beta U\sin\beta \\
v &= -U\sin\beta, & \dot{v} &= -\dot{U}\sin\beta - \dot{\beta}U\cos\beta
\end{aligned}
\tag{C.10}
$$

Then rewritten forms of the dimensionalised equations of motion and hull forces and moments are found as

$$
\begin{aligned}
(m' + m'_x)\left[\frac{1}{2}\rho L^2 d\right]\dot{u} - (m' + m'_y)\left[\frac{1}{2}\rho L^2 d\right]vr &= X \\
(m' + m'_y)\left[\frac{1}{2}\rho L^2 d\right]\dot{v} + (m' + m'_x)\left[\frac{1}{2}\rho L^2 d\right]ur &= Y \\
(I'_{zz} + J'_{zz})\left[\frac{1}{2}\rho L^4 d\right]\dot{r} &= N
\end{aligned}
\tag{C.11}
$$

The external forces in equation (C.11) can be decomposed as

$$
\begin{aligned}
X &= X_H + X_P + X_R \\
Y &= Y_H + Y_R \\
N &= N_H + N_R
\end{aligned}
\tag{C.12}
$$

where the subscripts H, P and R represent hull, propeller and rudder components respectively. The hull forces X_H, Y_H and N_H can be further decomposed in terms of manoeuvring coefficients as follow

$$X_H = \frac{1}{2}\rho L d U^2 (X'_{\beta r} r' \sin\beta + X'_{uu} \cos^2\beta)$$

$$Y_H = \frac{1}{2}\rho L d U^2 (Y'_\beta \beta + Y'_r r' + Y'_{\beta\beta} \beta|\beta| + Y'_{rr} r'|r'| + Y'_{\beta\beta r} \beta^2 r' + Y'_{\beta rr} \beta r'^2)$$

$$N_H = \frac{1}{2}\rho L^2 d U^2 (N'_\beta \beta + N'_r r' + N'_{\beta\beta} \beta|\beta| + N'_{rr} r'|r'| + N'_{\beta\beta r} \beta^2 r' + N'_{\beta rr} \beta r'^2) \quad \text{(C.13)}$$

For surge direction, $X'_{\beta r}$ was suggested by Hasegawa (1980) as follows

$$X'_{\beta r} = (-1.66 C_B + 1.5) \times m'_y \quad \text{(C.14)}$$

and X'_{uu} is regarded to be related with resistance force. In order to obtain other manoeuvring coefficient data, various types of ships with general hull geometry are used in the captive model tests and following results are suggested.

- Even trimmed case:

$$Y'_\beta = \frac{1}{2}\pi k + 1.4 C_B B/L$$

$$Y'_r - (m' + m'_x) = -1.5 C_B B/L$$

$$Y'_{\beta\beta} = 2.5 d (1 - C_B)/B + 0.5 \quad \text{(C.15)}$$

$$Y'_{rr} = 0.343 d C_B/B - 0.07$$

$$Y'_{\beta rr} = 5.95 d (1 - C_B)/B$$

$$Y'_{\beta\beta r} = 1.5 d C_B/B - 0.65$$

$$N'_\beta = k$$

$$N'_r = -0.54k + k^2$$

$$N'_{\beta\beta} = -0.96 d (1 - C_B)/B + 0.066 \quad \text{(C.16)}$$

$$N'_{rr} = 0.5 C_B B/L - 0.09$$

$$N'_{\beta rr} = -(0.5 d C_B/B - 0.05)$$

$$N'_{\beta\beta r} = -\{57.5 (C_B B/L)^2 - 18.4 (C_B B/L) + 1.6\}$$

where $k = 2d/L$

It should be noticed that the foregoing formulae were valid in the application for conventional ship's body, especially with the conventional stern shape. The model tests were carried out on different loading conditions, therefore more expressions regarding trim conditions are also available. In a trimmed condition, the corresponding expressions with parameter $\tau'(=\tau/d_m)$, where τ is trim quantity and d_m is mean draught, are given as follow

- Trimmed case:

$$
\begin{aligned}
Y'_\beta(\tau) &= Y'_\beta(0)\{1+(25C_BB/L-2.25)(\tau/d_m)\} \\
Y'_r(\tau)-(m'+m'_x) &= \{Y'_r(0)-(m'+m'_x)\} \\
&\quad\times\{1+[571\{d(1-C_B)/B\}^2-81d(1-C_B)/B+2.1](\tau/d_m)\} \\
Y'_{\beta\beta}(\tau) &= Y'_{\beta\beta}(0)\{1-(35.7C_BB/L-2.5)(\tau/d_m)\} \\
Y'_{rr}(\tau) &= Y'_{rr}(0)\{1+(45C_BB/L-8.1)(\tau/d_m)\} \\
Y'_{\beta rr}(\tau) &= Y'_{\beta rr}(0)[1+\{40d(1-C_B)/B-2\}(\tau/d_m)] \\
Y'_{\beta\beta r}(\tau) &= Y'_{\beta\beta r}(0)[1+\{110d(1-C_B)/B-9.7\}(\tau/d_m)]
\end{aligned}
\qquad \text{(C.17)}
$$

$$
\begin{aligned}
N'_\beta(\tau) &= N'_\beta(0)\{1-(\tau/d_m)\} \\
N'_r(\tau) &= N'_r(0)\{1+(34C_BB/L-3.4)(\tau/d_m)\} \\
N'_{\beta\beta}(\tau) &= N'_{\beta\beta}(0)[1+\{58(1-C_b)/B-5\}(\tau/d_m)] \\
N'_{rr}(\tau) &= N'_{rr}(0)\{1-(30C_BB/L-2.6)(\tau/d_m)\} \\
N'_{\beta rr}(\tau) &= N'_{\beta rr}(0)[1+\{48(C_BB/L)^2-16C_BB/L+1.3\}\times10^2(\tau/d_m)] \\
N'_{\beta\beta r}(\tau) &= N'_{\beta\beta r}(0)\{1+(3C_BB/L-1)(\tau/d_m)\}
\end{aligned}
\qquad \text{(C.18)}
$$

The dimensionalised forms of manoeuvring coefficients are expressed as follow

$$
\begin{aligned}
X'_{\beta r} &= X_{\beta r}\Big/\tfrac{1}{2}\rho L^3 d & X'_{uu} &= X_{uu}\Big/\tfrac{1}{2}\rho L d \\
Y'_\beta &= Y_\beta\Big/\tfrac{1}{2}\rho L d U^2 & Y'_{\beta\beta} &= Y_{\beta\beta}\Big/\tfrac{1}{2}\rho L d U^2 \\
Y'_r &= Y_r\Big/\tfrac{1}{2}\rho L^2 d U & Y'_{rr} &= Y_{rr}\Big/\tfrac{1}{2}\rho L^3 d \\
Y'_{\beta\beta r} &= Y_{\beta\beta r}\Big/\tfrac{1}{2}\rho L^2 d U & Y'_{\beta rr} &= Y_{\beta rr}\Big/\tfrac{1}{2}\rho L^3 d
\end{aligned}
\qquad \text{(C.19)}
$$

$$N'_{\beta} = N_{\beta} \Big/ \tfrac{1}{2}\rho L^2 dU^2 \qquad N'_{\beta\beta} = N_{\beta\beta} \Big/ \tfrac{1}{2}\rho L^2 dU^2$$
$$N'_{r} = N_{r} \Big/ \tfrac{1}{2}\rho L^3 dU \qquad N'_{rr} = N_{rr} \Big/ \tfrac{1}{2}\rho L^4 d \qquad \text{(C.20)}$$
$$N'_{\beta\beta r} = N_{\beta\beta r} \Big/ \tfrac{1}{2}\rho L^3 dU \qquad N'_{\beta rr} = N_{\beta rr} \Big/ \tfrac{1}{2}\rho L^4 d$$

To explain the influence of the shape of aft body on the overall manoeuvring performance and yaw stability, particularly for the container vessels whose aft hull forms were drastically changed from the propulsion consideration, Mori (1995) proposed prediction formulas with additional four parameters such as e_a, e'_a, σ_a, K to express characteristics of aft hull shape.

- Fullness of aft run:

$$e_a = \frac{L}{B}\left(1 - C_{pa}\right), \qquad e'_a = e_a \Big/ \sqrt{\frac{1}{4} + \frac{1}{(B/d)^2}} \qquad \text{(C.21)}$$

- Aft sections fullness metric:

$$\sigma_a = \frac{1 - C_{wa}}{1 - C_{pa}} \qquad \text{(C.22)}$$

- Form factor:

$$K = \left(\frac{1}{e'_a} + \frac{1.5}{L/B} - 0.33\right)\left(0.95\sigma_a + 0.40\right) \qquad \text{(C.23)}$$

where C_{wa} and C_{pa} denote the water plane area coefficient and prismatic coefficient for the aft half hull respectively.

Kijima et al. (2000) modified the original expressions of Kijima et al. (1990) using the aft hull shape parameters and again presented approximate formulas particularly for aiming the difference of stern hull shape. The expressions of linear manoeuvring coefficients in even keel situation, where newly introduced parameters are combined with other hull parameters, are given as follow,

- Even trimmed case:

$$
\begin{aligned}
Y'_{\beta} &= \frac{1}{2}\pi k + 1.9257(C_B B/L)\sigma_a \\
Y'_r - (m' + m'_x) &= \frac{1}{4}\pi k + 0.052e'_a - 0.457 \\
Y'_{\beta\beta} &= -1.199C_b\sigma_a + 1.05 \\
Y'_{rr} &= 0.225(dC_b/B)e'_a - 0.12 \\
Y'_{\beta rr} &= 7.1256\{d(1-C_b)/B\} \\
Y'_{\beta\beta r} &= 10.443[\{d(1-C_b)/B\}e'_a]^2 \\
&\quad -9.374\{d(1-C_b)/B\}e'_a + 1.227
\end{aligned}
\tag{C.24}
$$

$$
\begin{aligned}
N'_{\beta} &= k[150.668\{d(1-C_B)/B\cdot e'_a K\}^2 \\
&\quad -23.819\{d(1-C_B)/B\cdot e'_a K\} + 1.802] \\
N'_r &= -0.54k + k^2 - 0.0477e'_a K + 0.0368 \\
N'_{\beta\beta} &= 43.857\{d(1-C_b)/B\cdot e'_a K\}^2 \\
&\quad -3.671\{d(1-C_b)/B\cdot e'_a K\} + 0.086 \\
N'_{rr} &= 0.15K - 0.068 \\
N'_{\beta rr} &= -0.4086C_b + 0.27 \\
N'_{\beta\beta r} &= -0.826\{d(1-C_b)/B\}e'_a - 0.026
\end{aligned}
\tag{C.25}
$$

- Trimmed case:

$$
\begin{aligned}
Y'_{\beta}(\tau) &= Y'_{\beta}(0)\{1 + (26.059(dC_b/B)\cdot\sigma_a - 2.425)(\tau/d_m)\} \\
Y'_r(\tau) - (m' + m'_x) &= Y'_r(0) - (m' + m'_x)\} \times \{1 - 0.307(\tau/d_m)\} \\
Y'_{\beta\beta}(\tau) &= Y_{\beta\beta}(0)[1 - \{71.404(dC_b/B)\sigma_a - 6.533\}(\tau/d_m)] \\
Y'_{rr}(\tau) &= Y_{rr}(0)[1 + \{0.572(B/d)e'_a - 14.23\}(\tau/d_m)] \\
Y'_{\beta rr}(\tau) &= Y_{\beta rr}(0)\{1 - (82.8kC_b - 3.6)(\tau/d_m)\} \\
Y'_{\beta\beta r}(\tau) &= Y_{\beta\beta r}(0)\{1 + (7.747C_b e'_a K - 3.508)(\tau/d_m)\}
\end{aligned}
\tag{C.26}
$$

$$
\begin{aligned}
N'_{\beta}(\tau) &= N'_{\beta}(0)\{1 - 0.935(\tau/d_m)\} \\
N'_r(\tau) &= N'_r(0)[1 + \{0.917C_b e'_a - 2.5625\}(\tau/d_m)] \\
N'_{\beta\beta}(\tau) &= N'_{\beta\beta}(0) \\
N'_{rr}(\tau) &= N'_{rr}(0)\{1 + 0.173(\tau/d_m)\} \\
N'_{\beta rr}(\tau) &= N'_{\beta rr}(0)[1 - \{1.98(e'_a)^2 - 14.648e'_a + 27.311\}(\tau/d_m)] \\
N'_{\beta\beta r}(\tau) &= N'_{\beta\beta r}(0)\{1 - 0.39(\tau/d_m)\}
\end{aligned}
\tag{C.27}
$$

C.2 Propeller and rudder force

Mathematical mode for the propeller thrust force can be written as

$$X_P = (1-t)T = (1-t)\rho n^2 D_P^4 K_T \tag{C.28}$$

For the calculation of propeller thrust coefficient K_T and relating terms in equation (C.28) Kijima et al. (1990) proposed following expressions

$$K_T = J_0 + J_1 J_P + J_2 J_P^2 \tag{C.29}$$

and

$$\begin{aligned} J_P &= U\cos\beta\left(1-w_P\right)/\left(nD_P\right) \\ w_P &= w_{P0}\exp\left(-4.0\beta_P'^2\right) \\ \beta_P' &= \beta - x_P' \cdot r' \end{aligned} \tag{C.30}$$

where

J_P : Propeller advance ratio

J_0, J_1, J_2 : Constants

w_P : Effective wake fraction at propeller location

w_{P0} : Effective wake fraction at propeller location in straight forward motion

β_P' : Effective drift angle at propeller location

x_P' : Non-dimensionalised location of propeller ($= x_P / L \approx -0.5$)

r' : Non-dimensionalised yaw angular velocity ($= r \cdot L / U$)

Mathematical model for rudder is given as

$$\begin{aligned} X_R &= -(1-t_R)F_N \sin\delta \\ Y_R &= -(1+a_H)F_N \cos\delta \\ N_R &= -(x_R + a_H x_H)F_N \cos\delta \end{aligned} \tag{C.31}$$

Following expressions are assumed for the normal force acting on rudder F_N with normal force coefficients C_N which is proposed by Kijima et al. (1990):

$$F_N = \frac{1}{2}\rho A_R C_N U_R^2 \sin\alpha_R \tag{C.32}$$

and

$$\begin{aligned} C_N &= 6.13\Lambda/(2.25+\Lambda) & s &= 1.0-(1-w_P)U\cos\beta/nP \\ U_R^2 &= (1-w_R)^2\{1+C\cdot g(s)\} & w_R &= w_{R0}\cdot w_P/w_{P0} \\ g(s) &= \eta K\{2-(2-K)s\}s/(1-s)^2 & \alpha_R &= \delta-\gamma\cdot\beta_R' \\ \eta &= D_P/H_R & \beta_R' &= \beta-2x_R'\cdot r' \\ K &= 0.6(1-w_P)/(1-w_R) & x_R' &\approx -0.5 \end{aligned} \tag{C.33}$$

where

A_R : Rudder area

H_R : Rudder height

Λ : Aspect ratio of rudder

U_R : Effective rudder inflow speed

α_R : Effective rudder inflow angle

C : Coefficients for starboard and port rudder

w_R : Effective wake fraction at rudder location

w_{R0} : Effective wake fraction at rudder location in straight forward motion

γ : Flow straightening coefficient

P : Propeller pitch

C.3 Filon's Method

An integral that occurs in the computation of impulse response function is one in which the integrand consists of a function, say $M(x)$ or $x \cdot M(x)$, multiplied by a sine or cosine function of x. If one must consider high frequencies in the sine or cosine function, a very fine mesh is required when evaluating the integral by the usual numerical approximation such as Simpson's Rule. [See example of sway impulse response function in equation (C.34).]

$$\begin{aligned} y_v(\tau) &= \frac{2}{\pi}\int_0^\infty Y_v(\omega)\cos(\omega\tau)d\omega \\ &= -\frac{2}{\pi}\int_0^\infty \omega Y_v(\omega)\sin(\omega\tau)d\omega \end{aligned} \tag{C.34}$$

To avoid this inconvenience Filon has suggested a procedure in cases where the function $M(x)$ varies smoothly with x. It is assumed that the function $M(x)$ is linear between two integration points, which is a reasonable assumption for small interval dx. To illustrate this method, we consider the following integral:

$$\begin{aligned} I(\tau) &= \int_0^\infty M(x)\cos\tau x dx \\ &= \sum_{i=1}^{N-1}\int_{x_i}^{x_{i+1}} (a_i + b_i x)\cos\tau x\, dx \\ &= \sum_{i=1}^{N-1} I_i \end{aligned} \tag{C.35}$$

The coefficients are given

$$\begin{aligned} a_i &= \frac{M(x_i)x_{i+1} - M(x_{i+1})x_i}{x_{i+1} - x_i} \\ b_i &= \frac{M(x_{i+1}) - M(x_i)}{x_{i+1} - x_i} \end{aligned} \tag{C.36}$$

and the incremental value of the integral is found analytically

$$I_i = a_i\left[\frac{\sin\tau x_{i+1} - \sin\tau x_i}{\tau}\right] + b_i\left[\frac{\cos\tau x_{i+1} - \cos\tau x_i}{\tau^2}\right] + b_i\left[\frac{x_{i+1}\sin\tau x_{i+1} - x_i\sin\tau x_i}{\tau}\right] \tag{C.37}$$

Suppose that the following integral must be determined $I' = I_{i-1} + I_i + I_{i+1}$. Combining terms for $M(x_{i-1})$, $M(x_i)$, etc., results in similar expressions for each these quantities, facilitating the numerical integration.